Motion Analysis of FPSO in Multidirectional Seas: The West African Offshore Region

By

Orji Charles Ugochukwu

A thesis submitted for the degree of Doctor of Philosophy

School of Agriculture, Geography and Engineering

(Marine Science and Technology)

NEWCASTLE UNIVERSITY

July 2019

ABSTRACT

The use of experiment remains the most accurate method in the prediction and evaluation of roll damping. Several models ranging from CFD to analytical and empirical techniques and tools have been developed over the years for this purpose. However, the issue of accurately capturing the adherent multilinear behaviour for hulls with sharp edges and bilge keels remains a challenge until date. The elaborate works of Oliveira and Fernandes (Oliveira and Fernandes ,2006,2010,2014) identified and characterized the existence of two regimes using the bilinear model, later modified to the hyperbolic model. Following their work, and identifying this gap, an enhancement in their formation lead to the introduction of a third damping term, which represented the transition between the large angle side and the small angle regions. A modified hyperbolic model has been proposed and tested against existing models with reasonable agreement in terms of regenerating the measured decay. The model's capture of the transition region was validated using the rigorous procedure of the bilinear methodology. The relative uncertainty associated with the predictive model was evaluated to fall within 3.5% to 5.9% .The decay data were used to modify the regression model of Oliveira and Fernandes and the enhanced model reduced the predictive error in the model parameters from second to first order range. The extracted damping coefficient and model where implemented in a code to study the influence of directionality and spectrum type on the roll motion response of the free-floating unit (typical FPSO) in real sea environment. Interactive contour plot representation was used to capture the sensitivities of spectrum type, directionality and the multidirectional wave streams summation techniques developed prior to roll motion response simulation. A barred region for the number of regular waves to be used was established using the maximum spectra energy density and the estimated significant wave height as the indicators. A 6dof code was developed using simplified methods and techniques. The novel frequency-spectra weighted technique was proposed for the estimation of the excitation force components of the equation of motion in irregular short crested seas from regular wave formulations. The method was validated by running similar scenarios in HydroD and the irregular wave test on scaled model. The roll motion response from the proposed method compared favourably within first order error range against the HydroD simulations and the irregular wave experiment conducted for

JONSWAP spectrum for the targeted significant wave heights. Similar error margins were also observed for the measured as well as the estimated wave elevations and all other motion modes. The interactive results from the contour plots when translated into roll motion was very evident in the estimated magnitudes in different sea state spectra combinations (type and directions). The use of the suggested spectra form (lognormal or triangular for the swell sea and JONSWAP-Glenn for the wind sea) for the West African region identified variations in the roll response of between 1-23% or more than 5.5^{o}. This goes to further show the need to use site or region specific spectrum for the determination of design and operational parameters for offshore structures and associated units and for personnel seakeeping comforts.

ACKNOWLEDGEMENTS

My appreciation goes to my Supervisors Dr YongChang Pu and Dr Hu ZhinQiang who saw me through when all hopes of getting this far seemed eroded, their wealth of experience, mentorship, advice were the key weapons used in this battle. I immensely thank you. I also thank Prof. Michael Woodward, Prof. Mehmet Atlar, Dr Francesca Taglliaferi and Prof. Tao Longbin for their supervisory supports at some point in this project. Loads of love to my father (Pa G.A.Orji) and great inlaws (Pa and Ma Azubuine).

I also acknowledge the Niger delta development commission (NDDC) in Nigeria for the scholarship. Great Thanks to Sir Dr Christopher Obor the then MD. Prof Itolima Ologadein, Prof Ayotamuno, Sir Dr. I. E.Douglas, Sir. K.T Johnson, Prof Igoni, Prof Akpa Jackson, Prof. Akpilla, Dick Ibitoru, Rev. Nitonye, Dr and Mrs. Bennett Okoni, Dr Igwe Aleruchi, Dr. Ekwulo, Dr Dennis Budume, Dr Solomon Eliozu, Dr Solomon Nyeche, Ayerite Tonye for their support while leaving the shores of Nigeria Not to forget Sir Dr. Boisa Ndokiari, who made sure I settled down in record time. My gratitude goes to Dr Davis Davidson Dimabo (D4) and wife Mrs Ubile Davis for their hospitality while in Newcastle and thereafter. Favour Davis Dimabo of blessed memory, we love you. My sincere gratitude goes to Tom Cunnell and Chris Pistolus for their immense support and contributions during the experiment, and the Towing tank crew most especially Kieran Oliver of blessed memory. May your gentle soul find solace with our creator.

Most importantly, my wonderful wife, a rare gem, novel breed, Mrs Gladys Nneoma Charles-Orji, whose support both emotionally and financially was of inestimable value during the travail: I owe you ALL Nneoma (aka Best Mother). My lovely kids, Master Reuel CJ and his sisters Confidence Nwachukwu, Godiva Nmesomachukwu Charles-Orj & Davina Munachimso Chimamanda Charles-Orji whose birth crowned the joy of our mission abroad. My friends and well-wishers and their spouses, Dr Ibekwe Achinike, Dr Nwamaka, Dr Musa Bashir, Dr Emovon, Dr Michael, Emmanuel Irimagha, Emmanuel Johnson, Islam Muhamed, Abam , Pereowei, Lucky Bebs, Vera, Prafula, Yakubu, Chima, Azubuike and a host of others for their support and encouragement during the most difficult times. Thank you so much Prof. Tim Gray. Finally, to JEHOVAH God Almighty, the Alpha and Omega, the giver of life I owe ALL acknowledgement.

DEDICATION

This thesis is dedicated to God Almighty, the creator of the immeasurable Universe who gave me life and energy to persevere, knowledge and wisdom to carry out this research to an accomplished end.

TABLE OF CONTENTS

LIST OF FIGURES

LIST OF TABLES

NOMENCLATURE

Xi	Displacement in i^{th} direction or degree of freedom mode
Fi, Mi	Excitation Forces & Moment in i^{th} direction or degree of freedom mode
t	time
th	Time duration
FPSO	Floating production Storage and offloading
ω	Regular wave frequency (rad/s)
S(T), S(ω,)	Longcrested spectra energy density
S(ω,θ)	Short crested spectra energy density in m2-s
θ, θi	Direction of secondary wave stream and experiment wave
T	Wave frequency in s
f	Wave frequency in Hz
Hs, Hss,Hsw	Significant wave height, Sig. wave height (Swell sea, Wind sea)
m_{ij}, I_{ij}	Mass and Inertial terms of unit
B_{ij}	Damping coefficient of unit
C_{ij}	Restoring coefficient of unit
Aij, aij	Added mass and added inertial terms (3d and 2d)
L_{bk}, w_{bk},	Length and width of bilge keel
d, df	Vessel Draft and experiment draft
Cb	Block coefficient
Cwap	Water plane area coefficient
Caw	Wetted surface area coefficient
Td,Tn	Roll natural period (s)
ωd, ωn	Roll natural period (rad/s)
δ	Local decrement
θn	Roll amplitude at station n along free decay curve
N	Number of regular wave frequency forming irregular wave
ζij	Wave amplitude for secondary wave with frequency ωi, direction θj

nomenclature continued

ξ	Local damping coefficient
k_{44}	Roll gyration radius
Δ	Mass displacement
β	Damping ratio
βeq	Linearized damping ratio
Pe	Energy dissipated per cycle in roll decay
α, $\alpha 1$	Slope control parameters for hyperbolic modelling
β_{bs}, β_{bl}, β_{bT}	Damping ratios in small, large and transition region respectively
k_i	Wave number for wave frequency ωi
εij	Random phase angle for wave with frequency ωi, direction θj
Wij,	Frequency/wave spectra dependent weighting parameter
D (ω,θ)	Directional spreading function
W(θ)	Directional weight
mo, σ	Standard deviation or area under the spectra curve
H	Transfer function
φ	Yaw angle
ψ	Roll angle
Sws, Sss	Spectra energy density for: wind sea, swell sea respectively
ζ_s, ζ_l, ζ_T	Damping coefficient in large, small and transition region respectively for roll hyperbolic models.

nomenclature continued

SSER	Sea state energy ratio
IMD	Intermodal distance
σ_{nd}	Standard deviation for a lognormal distribution
W_{cw}, W_{cs}, W_{ss1}, W_{ss2}	Weight coefficients for directions (wind sea, swell sea, swell 1, swell 2 respectively)
H_{ss1}, H_{ss2}, H_{sw},	Significant wave height for swell sea1, swell sea 2 and wind sea respectively.
mov	Volume under the shortcrested spectra plot
V_w	Wind velocity
V_c	Current velocity
ζ_{DK}	Water elevation above the keel
ζ	Water elevation above the mean water line (MWL)
d	Mean draft of ship
MWL	mean water line
A_{aw}	Hull area above water line (unwetted area)
A_{uw}	Hull area under water line (unwetted area)
r_c, r_{co}	Current angle of attack; instantaneous and initial respectively
r_w, r_{wo}	Wind angle of attack; instantaneous and initial respectively
q_w,	Wind dynamic pressure respectively
q_c	Current dynamic pressure respectively
T_{air}	Atmospheric temperature
V_{w10}	Wind velocity at standard reference 10m height above sea level.
V_0	Tidal current velocity at water surface
ρ_{air}	Air density
V_{wstd}	wind velocity standard deviation

Nomenclature continues

V_{mean}	wind velocity mean
[M]	Mass matrix
[B]	Damping matrix
[C]	Restoring coefficient matrix
[F]	Force matrix
ψ	total velocity potential
v_x, v_y and v_z	are the component fluid velocities in x, y and z.
Φ	Double body potential
$\emptyset$	been the steady potential of a source density distribution over the body surface
$\boldsymbol{S_b}$	body surface
G^*_{pq}	Double body Green function
$\vec{r}_{pq}$.	distance between potential point p and source q
$G^*_{pq_s}$	Elementary singularity
σ_p	source density distribution
φ	Unsteady part of the total potential
φ_0	incident wave velocity potential
φ_i	Radiation potential problem
$\boldsymbol{X}$	Non-dimensionalised radius
$\boldsymbol{Y}$	Non-dimensionalised vertical displacement vector
J_0, Y_0, H_0	The zero order Bessel function of first and second kind and the zero order Struve function respectively

Ps	steady (Ps) pressure fields
Pu	unsteady pressure fields
φ_7	diffraction velocity potential
$Z_k(\omega,\theta)$	complex response amplitude operator
$S_{\xi k}(\omega)$	the spectrum of the k^{th} motion mode is related to the incident wave spectrum by the equation below
R_{Fk}	reduction factor
u_A,	Standard uncertainty
U_A	Expanded uncertainty
U_R	Relative uncertainty
c_i	Sensitivity
k_f	Coverage factor
$(\Delta\theta)_{s1}$	Direction interval for sea swell 1
$(\Delta\theta)_{s2}$	Direction interval for sea swell 2
$(\Delta\theta)_w$	Direction interval for wind sea
u_x	Water particle velocity in x-direction
u_y	Water particle velocity in y-direction
u_z	Water particle velocity in z-direction
a_x	Water particle acceleration in x-direction
a_y	Water particle acceleration in y-direction
a_z	Water particle acceleration in z-direction

1 Chapter One: Introduction: Background and Rationale

1.1 Introduction

The first sets of Floating Production Storage and Offloading Structures (FPSO) unit concept were introduced in 1974 at the Ardjunal oil field (water depth of 43m) in Indonesia and in 1976 at the Garoupa and Castellon fields in Brazil and Spain respectively to cater for water depths of less than 150m. Recent applications have seen FPSO units in use in depths of 1400m-3000m (Shimamura, 2002; Lopez-Cortijo *et al* 2003). The demand for FPSO continues to rise; with about 113 FPSO units operating as at 2007, currently over 165 are operational worldwide and about 40 on request. Fourteen FPSO units are presently working for oil/gas companies in Nigeria amongst the over 40 operating in the West African Offshore fields. This structure has the capability of carrying out oil production activity through processing plants which get the production fluids from sea bed wells via risers while remaining afloat as a conventional vessel. In addition, it has enough designated storage tanks to keep the produced oil (different grades) which are subsequently offloaded onto shuttle tankers to export locations offshore, onshore or ashore. These functions distinguish it from other offshore structures and thus makes it more economical and flexible to use in deep water operations where the cost of laying pipelines if at all possible is very unrealistic according to (Roger et al 2001; Su *et al.*, 2005). FPSO technology is necessitated by the fast depletion of giant oil and gas fields in onshore and shallow water regions (<150m deep). With the emergence of giant oil/gas fields and small remote oil field clusters in deep and ultra-deep (1400-3000m) water, FPSO units offer the best forms of production units for field development with minimum economic field size using the flexibility of the unit (Shimamura, 2002). Some of these advantages the FPSO unit enjoys over the other offshore structures include but not limited to; adaptability for water depth; early deployment to work station as a complete unit; self-containment; easily movable and relocatable; segregated storage to avoid oil type contaminations; provision of expanded crude oil market and variable combinations with other facilities.

FPSO units are built by conversion of existing large oil tankers(VLCC) or purpose built from scratch to stay in location, weathering the harsh and calm environmental conditions throughout the life of the reservoir, in most cases beyond 20years field life as reported in (Turan and Zhao, 2001). They do not have the luxury of onshore maintenance like other shuttle vessels hence the need to incorporate this limitation into the design. Offshore structures represent huge investment and thus require more accurate predictions of their design loads. Traditional design of offshore

units based on long crested or two dimensional unidirectional seas underestimates the safety (limit or extreme motions and structural integrity) compared to designs based on a short crested multidirectional sea which represents an actual sea. As far back as 1976, (Marshall,1976) showed that the multidirectional component of the wave has a significant influence on the load, thus reducing fabrication cost for low load estimate. A recognition of this, lead to the construction of sizable and equipped wave basins capable of generating directional waves in some parts of the world, e.g. the MARINTEK lab in Norway in 1981;the Hydraulic Research Station in Wallingford UK in 1980; Edinburgh University in 1978; the Offshore Tech Corporation in USA in 1983;. The absence of a well-defined directional model partly contributed to the use of the longcrested idealization for designs (Okey ,1983). It is imperative to compare the differences between the responses experienced by the structure in both long and short crested sea to ascertain the effect of directionality. In the presence of linear relationship between the excitations and motions, linear superposition can be employed to determine the motion transfer function; however, in nonlinear situations like a typical roll motion, the nonlinear approach will be adopted to compute this function for the FPSO unit concerned.

The motion response or behaviour of the FPSO unit entails the interaction between the forces of excitation from the water environment (wave, current, wind, etc.) and the body structure defined by its principal dimensions and characteristics. It defines the extent to which the hydrodynamic and hydrostatic parameters i.e. inertial, damping, stiffness coefficients combine linearly or non-linearly or both, with dynamic or static parameters (velocity, acceleration and displacement) of the system to generate restoring forces or moments against the exciting forces or moments to sustain a pure or coupled motion of the ship.

Mooring systems are used to keep the unit steady while at work station, responding to disturbances from, wave, wind, current, motion of fluid up the risers, production and offloading operations, helicopter motions, and other operations within it. The type of mooring used depends on the characteristic of the location. The common types available are spread mooring and single point mooring buoy type using turret systems. The turret type allows the unit to weathervane by rotating around the turret position depending on the degree of rotation flexibility of the drag chain attached to the turret. A rotational movement of 360^{o} is possible. Systems which are used to maintain positions statically or dynamically are designed based on the response of the unit to these external and environmental excitations. These excitations (forces or moments) coming from the wave, wind and current cause the unit to move in six degrees of freedom (6 dof)

(Bhattacharyya, 1978**)**, the net effect depends on the most predominant motion mode(s). There are three vertical plane or symmetrical motions (surge, heave and pitch) and three lateral plane or anti-symmetrical motions (sway, roll and yaw). Lloyd (Lloyd, 1989) in his book categorized the degree of freedom as rotational (roll, pitch and yaw); translational (surge, sway and heave), and oscillatory (heave, roll and pitch)**.** This study is primarily limited to roll motion of the unit as it encounters the prevalent environmental conditions.

Ship hydrodynamics play a very important role in getting the response of a ship in sea. The pioneering work of Weibull and St. Dennis in 1950 on the motion of ships set the pace for the past and recent developments in this area of ship motion response study. (Salvesen, et al 1979; Grim 1960; Frank 1970) using the closed fit method established the strip theorem developed by B.V. Korvin-Kroukovsky and W.R. Jacobs in 1957 for the determination of two-dimensional added mass and damping hydrodynamic coefficients, which are significant parameters for the determination of ship motion response. These results were later validated by (Vugts,1968) through experiment.

1.2 Motivation and Justification to research

In the Niger Deltaic region of Nigeria, which is regarded as the chief economic host of the Nigerian State as at today, the inevitable youth restiveness as a result of acclaimed negligence, disregard and perceived poor governance over the years has led to incessant disruption of production time, regular vandalization of inland and onshore oil facilities including land rigs, platforms, well heads, pipelines etc. This has left the operators with a choice to search for and do business with other reservoir preferably at remote deep offshore regions within the operational mandate and region of the oil companies operating in Nigeria and other West African nations. The development in the deep oil exploration is also necessitated by the desire to protect the geographical health of the local communities and the region at large against artificial earthquakes, landslides and environmental pollution. Oil exploration started in the region since 1950's and has witnessed tremendous growth in terms of the number of offshore structures operating in the deep-water region of the country. Amongst the several offshore structures in operation, the FPSO unit has been found as a reliable structure for operation in the deep-water regions primarily because of its mobility and flexibility. Because of this drift in oil and gas exploration into deeper and harsher water environment, the demand for more precise and friendly

assessment of the motion behaviour of the FPSO unit is gaining adequate attention. Another impetus is the increasing interest for the oil from these regions by the developed nations.

The motion response of FPSO vessels can be used to predict critical motion amplitudes (Global and local) for typical West African region where unidirectional long period swell wave conditions predominate (Shimamura, 2002) for the purposes of proper seakeeping performance, assessment of safety level, design of associated structures like mooring lines, risers, stabilizers, bilge keels, etc. It is true that predictions for operational environmental conditions can be done, but the uncertainties caused by the ever-changing global climate cannot also be swept under the carpet, for instance the destruction of offshore facilities caused by Hurricane Katrina and others along her path is still fresh in our memories. Rather than attribute danger to sea structures to situations of rough sea states, low sea states have been recorded as responsible for damage events with an indication that rapid development of the sea state and particular combination of Wind Sea and swell might have played an important role (Toffolli et al, 2004). Predictions can also be done for arbitrary sea states, wave conditions etc. in preparation for these emergencies, by extrapolation. Another key motivation is the availability of a rich library of numerical techniques and tools that can be tested.

1.3 Aim and Objective of Study

The aim of this research is to investigate work station roll motion of the free floating FPSO unit in multidirectional sea states, by exploring numerical and experiment means. The objective is to establish a procedure to predict roll motion response based on simplified methods. The study will capture the water environmental conditions attainable in offshore West African region sandwiched around the North/South Atlantic Ocean, where Nigeria is a major player in the oil and gas exploration. The laid out objectives are;

- To investigate the feasibility of existing models in roll damping estimation.
- To suggest and develop an improved model based on above investigation.
- To develop a quick tool in the form of a 6dof motion solver for use in studying different variable impacts on the roll amplitude of a floating unit.
- To incorporate an appropriate non-linear roll damping model in a quasi 6dof equation of motion solver (developed above) to study the effects of non-linearity in models.

- To use routine developed to study the significance of sea state selection on the roll amplitude of the free floating unit.
- As part of the pursuit, the developed procedure will lay down the required numerical foundations for expanded study of unit in wind, current and moored situations.

1.4 Scope

It is imperative to establish a scope to constrain the research into a single PhD piece. Thus, the application is mainly limited to couple of real problems with simplifying assumptions made because of limited time and funding availability. The research revolves typically around the items below;

- Typical West African wave spectra shape (Multimodal spectrum) as recommended by the West African Swell Project (WASP)
- Wave excitation from the wave frequency
- Roll motion mode of the free floating unit

1.5 Novelties and Contributions to Knowledge from Identified gaps

The study of the response of a vessel depends greatly on the hydrodynamic parameters and the way they are determined. Over the years, the roll damping behaviour has been modelled only to be a bilinear characterization connecting the large and small angle sides and hence used for the estimation of roll response in a one degree of freedom system as well as when the roll is coupled to other motions. This follow from the various works of (Oliveira and Fernandez ,2010,2011,2014) on roll damping characterization. Identifying this gab, which suggest a possible trilinear behaviour with the third characterization signifying the transition region, it was possible to develop a modified hyperbolic roll damping model (trilinear model) which captured the three zones characterized by different damping coefficients. The trilinear model of the roll damping is a novelty in this area for estimating the roll damping coefficient used as input in response estimates. It is also a contribution to knowledge particularly in the realization that the complete characterization of the roll damping behaviour for a typical FPSO hull with flat bottom is trilinear and not the ideal bilinear formulation in existence.

Further gab following the work of Oliveira and Fernandez, in using their regression model to capture the estimation of the roll damping coefficients for the large as well as the small angle

regions was also studied. In their work, they suggested an improvement on the predictive model based on the expansion of their data source. Relying on this, the data from this work was used to enhance the original data which was then used to recalculate the coefficients and better results were obtained. The enhanced regression formulation remain as another novelty in this work and also as a contribution to knowledge.

Another significant aspect of this research is on the sea state characterization. The formulation of an equivalent sea state spectrum description for the West African sea region was developed by the (WASP,2004) which stands as an equivalent work as the JONSWAP project. However, it has been discovered that the implementation of the recommended lognormal or triangular spectra types for modelling the swell sea with the addition of the JONSWAP-Glenn spectrum for the associating wind sea has remained unattended to since the recommendations. This was identified as a gap, and thus attempts has been made in implementing this sea state spectrum which were used as input in determining the response of the unit when compared to other conventional spectra forms. It interesting to note that significant variations were observed in the roll response of the unit resulting from the application of the formulated spectrum in-line with the recommendations of the WASP. This is yet another contribution to knowledge.

Relying on the addition of separated seas using the square rule according to (Boukhanovsky and Soares, 2009), two novel techniques were developed. The first involved considering the swell seas as single units including their directional spreads against the wind sea. The second addition technique individually considered the swells and wind seas as different streams with their respective direction spreads. This formulation resulted in new combined spectra description for the west African region. These combined formulations were tested against conventional models and the variations estimated. No research has used this method to combine seas defined by the lognormal spectrum for swells and the JONSWAP-Glenn spectrum for the wind sea. These spectra formulation techniques as well as the formed spectrum stand as novelties and contribution to knowledge in the area of sea state representations. Another significant contribution is the provision of a further insight in the effect of the combining techniques on the overall response observed by the unit. As part of the effect, the variation of the sea state energy distribution was captured for the same seas when added using the different techniques.

With the spectrum formulated, a generic procedure was developed to approximate the Froude-Krylov and diffraction forces from existing regular wave formulations using the spectrum as a

weighting parameter. The forces are used as part of the overall excitation for the estimation of the motion responses. The estimates compared favourably in the determination of the overall motion response. Hence the spectrum weighting technique is another novelty and the ability to estimate these forces from regular wave formulations for short crested seas remain another contribution.

1.6 Approach adopted / Methodology

A comprehensive approach ranging from physical model preparations, experimentation, modelling in SESAM and development of a motion solver in MATLAB were used to achieve the set objectives. The procedures are nested and connected to one another as data were exchanged between different major blocks either as input for a model-the-model approach, or determination of other variables and also for validation and verification purposes for other block(s) of activities. The figure 1.1, captures the flow chart of the blocks of activities involved.

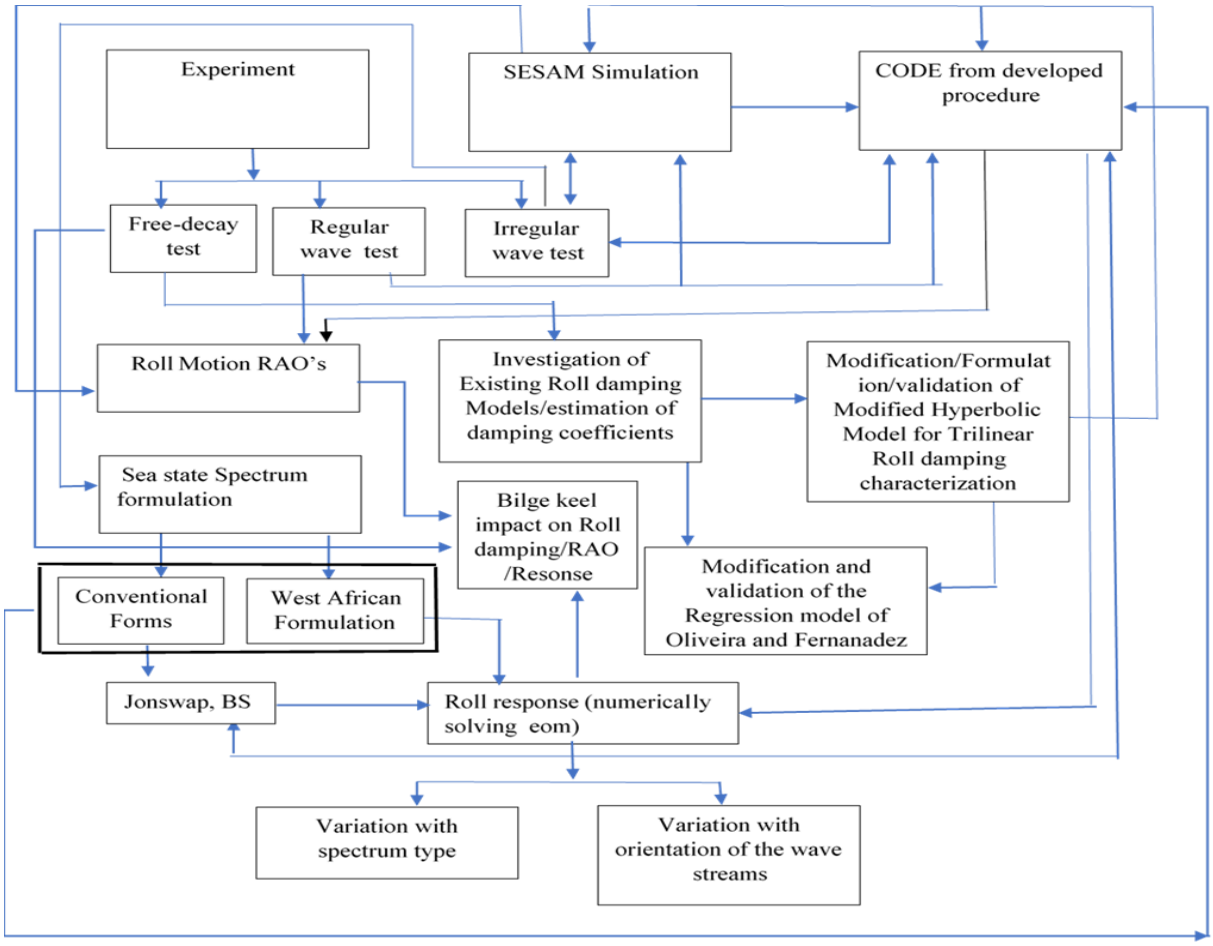

Figure 1.1. Flow chart illustrating task and procedure linkages for achieving Objectives

In-line with the laid down objectives, firstly, the investigation of existing roll damping models was achieved by conducting experiments using a scaled model of a typical FPSO. Three sets of experiments were performed (free decay, regular and irregular wave test) using two bilge keel configurations and the bare hull as well. The model was ballasted to the required draft line in the ballasting tank and the inclining test was carried out to determine the KG. The model dynamic ballasting or swing test was performed to estimate the roll, pitch and yaw radius of gyration.

Motion data were collected using a Qualysis camera method at data acquisition frequency of 200Hz. The motion data collected was used to estimate damping coefficients using the model-the mode approach with existing damping models and the modified version of the hyperbolic models as well. The developed modified hyperbolic model, as a means of validation was compared with the other methods including the original hyperbolic model as well. The enhancement of the regression equation of Oliveira and Fernandez from their original hyperbolic model was done, by estimating appropriate hull form and bilge dimensions which was used to improve their data for further regression analysis. The model was validated using experimental data and then compared with that of Oliveira and Fernandez.

The general equation of motion of the floating unit was developed using the standard Newtons laws of motion in the 6DoF. The various elements in the mass, damping and restoring added coefficients matrix were estimated using standard equations formulated using the strip theory approach were the 2d coefficients, estimated from the Lewis conformal mapping technique are integrated over the hull. The excitation force was determined using the regular wave formulations which was modified by a spectra weighted technique.

The equation of motion was solved using the Runge-Kutta numerical method. Spectra analysis was then carried out on the generated motion time series for the estimation of the significant values for different sea states and hull form (bilge keel configurations).

The model was also developed in SESAM-Genie and transported into SESAM-HydroD were different scenarios between the Code, SESAM were validated against experiment for the significant values for a JONSWAP spectrum in irregular sea. The SESAM numerical simulation was also validated using the RAO from the regular wave test.

Different scenarios using the formulated West African spectrum was carried out using the Code for the different bilge keels and comparison made against conventional spectra formulations.

At this point, it was necessary to also carry out a repeatability test to check the effect of the repeat experiment resulting in the variation of the damping coefficient, as it affects the overall output for few of the scenarios.

In addition, in other to show the effect of the bilge keel on the significant response, the variations in bilge keel damping from the different configuration was used and the generated roll significant responses investigated. This analysis introduces a new aspect of study, where the triple effect of bilge keel, sea state type and the method of wave stream combination was investigated.

Finally, a further validation based on the generated overall roll response values was also done by comparing the modified hyperbolic roll damping model with the original hyperbolic model of Oliveira and Fernandez to see the level of over prediction or under prediction with respect to the later.

1.7 Organization of the Thesis

Chapter1, highlights the basic background knowledge of the research work. It captures the justification or driving motive behind the research. Research aims and objectives as well as the scope restriction of studies were also mentioned.

Having discussed and introduced the background of study including the rationale, this thesis is in seven additional chapters with a comprehensive list of all referred works presented at the tail before the appendices. Chapter 2 brings to fore the extent of work already done in the subject area, both at specifics and extended disciplines as it relates to the entire research interest. The areas listed are discussed in terms of technicalities and history from contributors' contributions, content and limitations as well.

Chapter 3, as it is captioned, 'Experimental determination of roll damping', investigates in detail the experiment performed in the towing tank facility of Newcastle University. It further highlights the FPSO model in basin preparation and set up. The model loading was also carried out using the ballast tank to estimate the displacements associated with the different draft used. Three bilge keel configurations were prepared for attachment to hull during different scenario of experiment. Three types of experiment were carried out, free decay, regular wave and irregular wave runs for the different hull/bilge keel configurations. The results from the decay test were used to estimate the roll natural period for the different arrangements, and the various approaches as captioned in content were also applied to estimate the roll damping coefficients.

The least square optimization technique was then applied to carry out linearization of the non-linear roll damping formulations based on the different methods examined. The measured data were also tested using existing equations from leading authors like (Oliveira and Fernandez, 2000,2006,2010) in this area of research. Another attempt was made in studying the effect of introducing a small perturbation in the viscous term in the hyperbolic model leading to the modified hyperbolic model by author (a first attempt on this idea has already been published and presented in IMDC, Japan 2015 international conference). A second attempt was also made in other to establish a trilinear model for roll damping coefficient for a hull with bilge keel. Results were extracted and used as input to the simulation routine in subsequent chapters, thus a further comparison of response variations between roll damping estimating methods was not done beyond this stage. A concise uncertainty analysis was carried on the modified hyperbolic model. The results from this chapter thus formed input values for chapters 6 and 7.

This Chapter 4 was developed to capture the simplified mathematical formulations adopted in representing the sea state using the standard wave spectrum forms (Jonswap, Bretchneider, and Ochu-Hubble, Torsethagen) and other recommended forms (Lognormal, Triangular and the Jonswap –Glenn) for the West African region of interest. A MATLAB code was developed at this stage which was used to carry out sensitivity studies to show the extent of influence directionality has on the overall sea wave spectrum formulation. The different combinations and summation techniques for the standard forms were compared with the recommended forms for the West African regions. This was done for the different direction's combination cases. This part of the work generated results which were used as input to the HydroD Simulations. The code also formed part of the overall proposed method which was written into a 6dof code.

In Chapter 5, the amalgamation of simplified techniques to form the simulation routine was developed. A SESAM numerical example of model was demonstrated. The capabilities of SESAM was demonstrated in this chapter. The proposed theory adopts the part representation of the unit as a rectangular box in order to estimate the sea surface and hull surface projections. These surface points or swells were used as basis to estimate some parameters for the excitation forces. It is important to also note that some form coefficients between the box shape and the actual ship were used at some points to modify some vessel parameters from the standard rectangular representation. In other to determine the added mass and damping, the Lewis conformal mapping was applied to the actual hull form. The weighting technique developed was applied to estimate the Froude Krylov and the diffraction forces at every time step from

standard regular wave formulations. These estimates were then used to compute the motions time history using the Runge-Kutta method. The code has the flexibility of taking in different spectrum combinations for the seas (swell and wind) and the directionalities (spread) to do rough estimates of motion parameters and sensitivities as well. Methods to extract significant values from the time series (motion, force, velocity and acceleration) generated are also documented under this chapter. The numerical example in SESAM was used to validate part of the proposed method. The method was also developed to incorporate the effect of current, wind and mooring lines, however only the roll motion resulting from the impact of wave force at wave frequency was validated and captured in this research.

Chapter 6 captures the validation of the proposed method (Code) using experimental as well as SESAM simulations. The results from the regular and irregular wave test were presented in this chapter. The regular wave test was used to partly validate the SESAM simulation. The irregular wave (Jonswap spectrum) test results was used as a benchmark for validation of the proposed method. Comparisons which formed part of the validation process was done between results from the proposed method and that from the SESAM. A quick verification of the SESAM numerical example to study the influence of the wave random seed generator seed was also performed.

In Chapter 7, the influence of the impact of input wave spectrum on the roll motion amplitude was studied using different simulation cases with the proposed method. The effect of collinearity as well as non-collinear arrangements of wave streams were investigated. This chapter converts the variations observed for the sea spectrum from chapter 4 into proportional variation in the roll motion amplitude using the proposed method as an input /output system or a black box machine.

Chapter 8, is the last chapter, it is dedicated to concluding the entire research by summarizing the significant research findings and contributions to knowledge. The limitations encountered leading to recommendations for further study as part of the knowledge development process were also looked at in this chapter.

2 Chapter Two: Literature Review

This chapter captures a state-of-the-art review of different sections of the research. The operations of Floating structures around the globe particularly within the West African region was reviewed. Methods used for wave data gathering and analysis are reviewed, specifically the techniques involved in spectra modelling of sea wave techniques. In order to study the roll motion, roll damping is of essence and hence the different methods used in its estimation are x-rayed through relevant literatures. The methods used in motion response analysis are also captured in addition to the review of developments in the motion simulation models and formulations.

2.1 The West African (WA) offshore region

According to the world map shown in figure 2.1, the WA countries and its offshore region which is seated within the Atlantic Ocean, is bounded by lines stretching; 15^{o} east and 20^{o} west of the Greenwich meridian (0^{o} latitude) on the latitude scale and 10^{o} south ,20^{o} north of the equator (0^{o} longitude) on the longitude scale. Majority of the region is within the enclave of area 58 and 68 on the map with area subdivisions as shown in figure 2.2 (Hogben et al, 1984).

Figure 2.1 West Africa region, (United Nations Cartographic section)

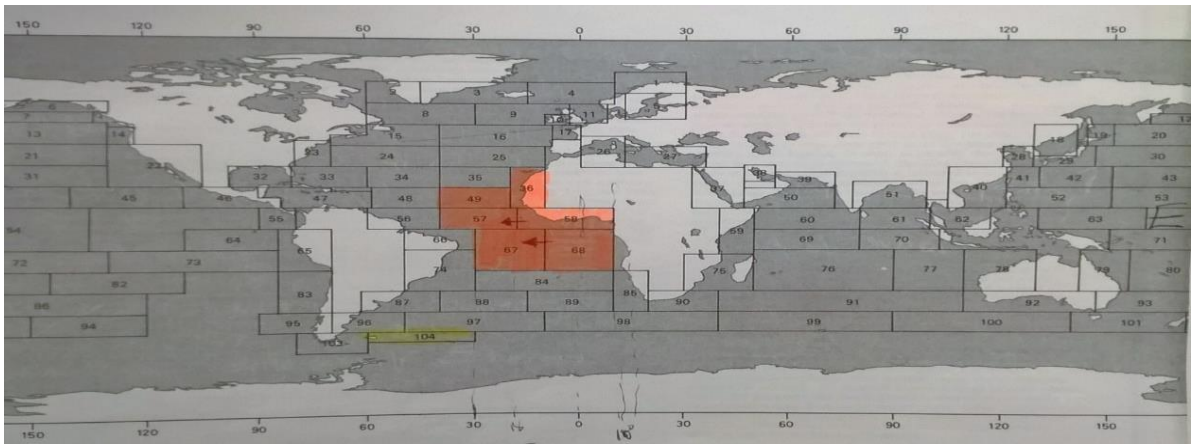

Figure 2.2 Deep offshore zone of West African region (BMT,2001)

The envelop coordinate shown in figure 2.2 is; Latitude 20^{O}S -10^{O}N, Longitude 15^{O}E- 40^{O}W, which stands as the Prospect zone. However, the present range of operating FPSO units in region is Latitude 3.4^{O}N – 5.5^{O}N, Longitude 4.6^{O}E- 7.9^{O}E. The desire to go deeper into the Atlantic may extend the regions operations to part of areas 67 and 57 according the (BMT, 2001) map in years to come. Under the National Data Buoy Centre (NDBC) area subdivision, the WA region is classified as Atlantic (Tropical) and with a number of buoys labelled; 31001(11.46 ^{o}N, 22.9 ^{O}W), 31006(4.03^{o}N, 22.97^{O}W), 31007(0.0, 22.97^{o}W), 15002(0.01^{O}N, 9.87^{O}W), 15006(6.03^{O}S, 9.99^{O}W), 15001(9.9^{O}S, 9.97^{O}W), 13010(3.51^{O}S, 0.7^{O}E), 15007(6^{O}S, 8^{O}E) stationed to gather data, as shown in Figure 2.3. The region is endowed with enormous amount of oil and gas reservoirs with a lot of offshore structures operating presently around the continental shelf deep offshore with Nigeria and Angola playing lead roles (Daniel, 2005). A data collation for FPSO units operating currently in the region is captured in appendix A.

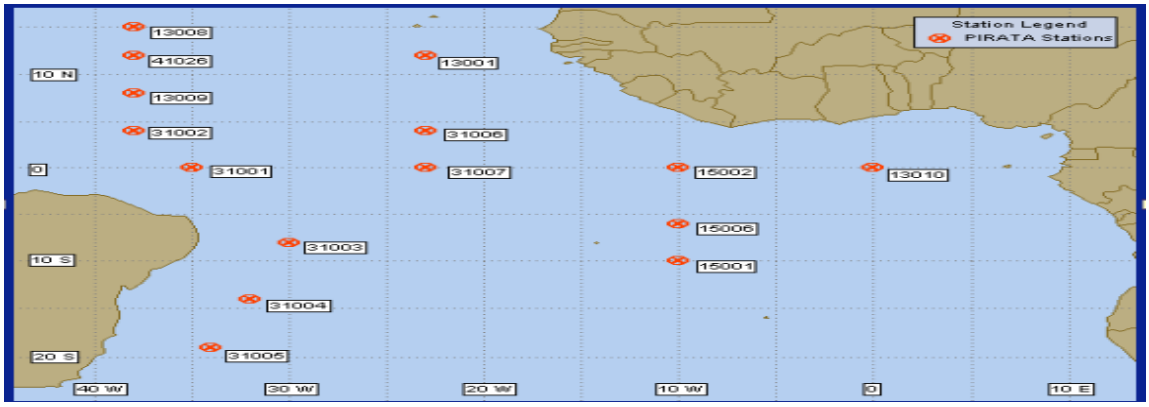

Figure 2.3 NDBC Data buoys stationed at the Atlantic (Tropical). (NDBC)

2.2 Sea State Modelling Approaches

The understanding of a vessel's behaviour in calm water is important, but a vessel's natural environment is far from being still with the major contributing disturbance coming from waves. As captured in (Yoshiyuki and Islam, 1999) waves are generated by wind blowing across the surface of the water (air-water interface), underwater rock movements, rainfall, current and seasonal variations etc. Ocean waves with periods of 3-25secs are primarily generated by wind and are regarded as surface gravity waves. For many years, the characterization of the irregular and confused sea state or sea water surface as viewed by an observer eluded the world of oceanography and science. In 1905, R.E.Froude (Tupper, 2004) theorized the irregular sea state as composition of multiple regular waves locally having small amplitudes and covering a range of periods. His further postulation that the impact of the observed irregular wave pattern is the cumulative effect of the individual regular wave forms became the foundation for all modern studies of waves and ship motion. Regular waves are defined as waves with constant height and period, whereas irregular waves which are typically 3-D in nature, exhibit unsteady variation of height and period leading to an unsteady time changing sea surface. Prior to early 1950, these postulates could not be advanced because of the absence of the necessary mathematical theories, thus the breakthrough started after then.

Motion response study entails the understanding of the true nature of the operational water environment (wave height, period, wind speed, direction, steepness, persistence etc.) for the structure. Proper capture of Ocean waves is of basic interest to the coastal and offshore structure designers to ensure safe designs against extreme conditions (Yingguang and Yiqing, 2013; Teena et al, 2012). Ocean waves are primarily irregular in nature because of the randomness experienced in their heights, shape, length, period and speed of propagation and hence require a random wave model for appropriate description (DNV-RP-H103, 2011). To corroborate the forgoing, (Hanne, 2003) described the surface elevation as highly non- deterministic and thus the need to fit good statistical models which give acceptable parameter predictions and associated uncertainty estimates for data. The essence of the uncertainty estimate suggest that waves are more frequent than statistical predictions as supported by (Dean,1990; Sand et al,1990; Hopkin, 2004; Broad,2006; Solli et al,2007) as evidenced by the presence of rogue and freak waves**.** This modelling which could be linear or nonlinear (depending on application and desired accuracy) is achieved by the application of statistical principles such as; Raleigh distribution, Weibull probability function, Gamma function, Gaussian distribution, Generalized Pareto distribution (GPD), Generalized extreme value (GEV), Gumbel function,

Exponentiated functions, and many other distribution and functions on randomly observed or measured wave properties over a reasonable time period (Yoshimi et al, 2010). The pioneering work of (Longuet-Higgins, 1952) introduced the Raleigh distribution for the prediction of the wave amplitude in a narrow banded random sea. The Work of (Cartwright and Longuet-Higgins,1956) included the spectra bandwidth parameter to modify the Raleigh distribution to capture behaviour of a broader sea. The study carried out by (Longuet-Higgins,1980) in fitting of wave data generated in the Gulf of Mexico to Raleigh distribution by adjusting the root-mean square wave height by 7.5% lower correlated strongly with those of (Forristall ,1978) using the Weibull distribution instead. Fitting of wave data using Weibull or Raleigh distributions in different occasions enabled the quantification of the randomness and subsequent determination of these critical extreme values. Characterization of the randomness can be approached by transforming the sea surface into summation of simple sine waves using the Fourier theorem and then defining the wave properties in terms of its spectrum. Another method involves the description of the variability of the wave field in terms of the marginal probability of individual wave while describing a point in the wave record as comprising of sequence of individual waves with distinct heights and periods. The later provides the possibility of studying the waves in terms of period and direction.

The aim of wave data analysis is to extract long-term and short term (few hours) statistics which are used to determine the rate of occurrence, exceedance, persistence, expectance rates of a characteristic property or properties of a given amplitude and sense. Long term statistics of irregular seaway involves the gathering of data for a longer period span (week, months, years) to include the time variations experienced by the seaway energy (Falttinsen,1998). Short term Seaway data can be used to determine the long-term statistics, like return periods of feasible extreme values in the seaway throughout the operational life of structures offshore. Extreme values analysis with the pioneering credence given to (Gumbel, 1958) involves the fitting of long-term statistics data to theoretical probability distributions. This theory has since seen remarkable improvement over the years (Davidson and Smith, 1990). Wave data gathering are also used in the development of wave surface models like the Airy, Stokes etc. formulations of sea surface.

Ocean conditions data collection used to be accomplished by voluntary observers working in voluntary observing fleet (VOF) or voluntary observing ships (VOS). The procedure, mode, quality and quantity of data gathering are regulated and standardized by participating

organizations. Information from (Hogben et al, 1984) reveals that over 55million marine meteorological observations made since 1854 -1984 by different countries on dedicated sea areas under the supervision of World Meteorological Organization (WMO) is stored in computerized archives in the Marine Data Bank. British sailors working in British ships however pioneered the gathering of ocean data through observations. The sea regions were divided into 104 areas and shared amongst 8-nations for data gathering and archiving. By this arrangement, the West African region is under the mandate of the Federal Republic of Germany. Processed data from this archive is used in this work to describe the water environment and establish extreme values of characteristic wave parameters within the West African sub region. Apart from well controlled visual observations, recent data gathering techniques employ the use of location moored buoys, fitted with measuring instruments for real time data acquisition. Notable amongst this organization is the National Oceanic and Atmospheric Administration (NOAA) through its National Data Buoy Centre (NDBC) unit and other partners operate a variety of buoys that measure wind speed, wave height, sea surface temperature, sea level pressure, air temperature, wave spectra, (Cardone, 1989; Goda, 1993). Some regions also have their unique observations. For instance, the hydrographic institute of the republic of Croatia has 43,274 complete ship meteorological observations from 1957-1971 (Josko et al, 2011). Data collated from these sources are normally coded and sent to the WMO marine data bank archives (Bridget et al,2005)**.** Fugro OCEANOR is also a major actor in the collation of global wave data with a claim of having the most reliable data of highest quality available in 0.5^{O} grids at 6 hourly intervals from 1996 to date**.** Data from the VOS and buoys sometimes contain some inconsistence coming from; observational errors, averaging and approximating methods, equipment calibration and location, errors in calculation of true wind from relative wind, (Cardone, 1989; Lindau, 1995; Chen, 2004). The identification of the existence of random and systemic errors and their nature has been studied by (Chen et al, 2004). The water environmental envelope of the West African region is described in the preceding section.

2.2.1 *Wave data analysis methodology and Spectra types.*

Wave data from (BMT, 2001), Fugro OCEANOR, NDBC and West African Swell Project WASP, by (Kelvin et al 2004), showed that the sea state for the West Africa region is predominantly benign, to moderate (sea state code 0-4) with significant wave height of 0.0m-4m. Predominant peak period <8s. The spectra description is multimodal, (multiple swell and

wind sea combined), and multidirectional 3D spectrum and swell dominated with a sea swell energy ratio (SSER) <<1, (Olagnon et al, 2014) with data from the BMT global statistics online used in determining the extreme values for the region. The analysis method which is tagged the NMINET analysis procedure, was developed by the BMT and NMI. The method summarily involves the use of joint probability distribution function of the wind and wave data. There are three categories of data set present.

(a). The 2-group wind/wave data set used for deriving model parameters captures periods when sea wave (H1) and swell wave (H2) groups were reported since 1949.

(b). All wind data, more in number which are used as inputs for long term statistics, captures periods when winds were reported (1854-1983).

(c). All wind/wave includes all cases when both waves and winds were reported post 1949.

The data base is frequently updated as reliable measurements are received (Hogben et al,1984). In dealing with the issue concerning the effect of directionality and seasonality, the separate season approach described by (Cook, 1983; Coles,1994, Cook and Craig, 1999) was adopted. During the development of the software program by NMIMET using the mathematical procedures adopted, they recognized and treated some of the possible sources that may lead to result invalidation. For instance, the bias between the number of all wind and 2- group data was reduced by adopting a wave height enhancement methodology. The reliability of the method is prefixed on the validity of the methodology and the quality and quantity of controlled observed data used. further clarification can be seen in the work of (Kuwashima and Hogben, 1986).

2.2.1.1 *Approach used by NIMET and others*

For a set of observation for a wind class of Beaufort scale 1-12, the resultant wave height is obtained by combining the swell and wind sea wave heights using the square law according to (Boukhanovsky, and Guedes, 2009).

Note that for Beaufort 0 the sea is assumed to be calm with a defining flat surface (zero wave height), zero wind speed, no direction. See (BMT, 1986) for further details. In dealing with summation of complex seas, (Evans et al, 2006) compared the methods of (Hanson and Philips, 2001) to that of (Guedes Soares, 1984) and adopted the method of Guedes in many cases. The method was used in this work. In dealing with the estimation of Persistence of Storms and

Calms the NMI adopted the procedure developed by (Kuwashima and Hogben,1986), which is a modified version of that developed by (Graham,1982). Apart from the numerical rigours prone to errors in the computation of the shape parameters, the Graham's method failed to predict the effect of seasonality and other sources of variation in the shape of the exceedance probability distribution. Persistence as the name implies, quantifies the duration for which a specified sea situation is likely to persist. Persistence is obtained by fitting the wave height data to a 3-parameter Weibull distribution which is another form of the GEV distribution for a shape parameter k<0 which is called the Fisher-Tippet Type III distribution (Teena et al, 2012) and as FT-type II or Fretchet distribution in (Yoshimi,2010)**.** This classification contradicts that of (Palutikof et at,1999), where Weibull was classed as FT-Type I with k=0**.** It is widely accepted that the Weibull distribution is a good model for wind speed distribution (Joseph, 1977) and the wind speed contributes greatly to the determination of the wave height vis a vis the significant wave height. Fitting can also be achieved using a 2-parameter Weibull form for the modelling of the distribution of the duration of storm or calm as the case may necessitate. For details of mathematical procedure involved in the estimation of the storm or calm duration, see (BMT, 1986).

There are three basic ways of quantifying the persistence probability of storm or calm:

Exceedance probability of a given threshold Hs' based on the duration, the Number of Occurrence in each period and the Proportion of time. This first index (exceedance probability) is to primarily determine the probability of exceedance, P, of the wave record above a pre-determined level called the threshold significant wave height Hs'. The threshold must be high enough to ensure that the excess over it converges to a General Pareto distribution (GPD) and leaves enough data points for satisfactory determination of the GPD parameters (Teena et al, 2012; Palutikof et al, 1999). See (Davison et al, 1990 and Jan, 2002) for modelling exceedance over high thresholds. Methods such as, probability weighted moment (PWM) of (Greenwood et al, 1978), L-moments by (Hosking, 1989), maximum likelihood, least square method, method of moments (MOM) are available for the fitting of distributions to data sets (Yoshimi, 2010)**.** Fitting can also be performed by the program routine WAFO in Matlab developed by the Lund University in Sweden (Teena et al, 2012) and the GRG solver engine in excel for solving non-linear least square optimization problems. The threshold wave height is used to differentiate between storm and calm for a given time record.

The number of occurrence (N) is a measure of the number of appearances made by a given interest wave height value (x) in each period $N(\geq x)$. This is related to the mean duration probability distribution $P(\geq x)$, as $N(\geq x) = N.P(\geq x)$

The Proportion of time is another form of measure of persistence, which quantifies the proportion of time which the storm persisted (exceedance above threshold Hs') or the persistence of calm (non-exceedance above a threshold) during the entire mean duration of the time record.

These statistical quantities give very important information concerning how sensitive down-time estimates are to operational lag and lead times of offshore structures in water environment. The longer the duration of calm experienced for a given threshold wave condition, the better it is for operational time.

2.2.1.2 *Extreme Value Estimation (Wave height and Period)*

Accurate estimation of extreme values is important to achieve a balance between safety and cost coming from over design of offshore structures. The damage caused by storm is dependent on both the peak and total number of waves in the storm within the duration of persistence (Sheng Yue, 2002). This involves the use of the principles explained above to study the extreme or maximum values of data sets divided into epochs of specified separation time bands. These extreme values are called quantiles (X_i) and are attached to a return period (T) through the probability density function $P(\geq x)$ defining the data set. (Palutikof et al, 1999), and (Klara, 2007) defined the quantile value, as a maximum wave parameter exceeded once on the average every return period of T years. The classical extreme value theory (GEV) of Von Misses in 1936 (Palutikof et al,1999) describes how a sufficiently long sequence of independent and identically distributed random variables, the maximum of samples of size n, can be fitted to any of the three basic family of probability distribution functions: Fisher-tippet I (Gumbel), Fisher-tippet II (Frechet), Fisher-tippet III (Weibull).

The expression for the return period ($T_{X_{Ti}}$:usually in years) of a given wave of magnitude X_{Ti}, having a probability of exceedance $P(\geq x_{Ti})$, joint return time, are all captured in (BMT,1986) $i = 1,2$ describes the independent and identically distributed random variates.

The dilemma on extreme wave height analysis lies on whether to use the GEV or GPD series.

The GEV approach considers only a single maximum within an epoch, neglecting other extreme events that may have occurred within the epoch. The method of r-largest values by (Weissman,1978) used more than one extremal value within an epoch (traditionally taken as one year) to improve the accuracy of the prediction. The method of independent storm (MIS) developed by (Cooks,1982,1985) further increased the modelling precision by increasing the number of extremal values or r-largest values by subdividing the epoch into smaller epochs of independent storms and used the maximal from each sub epoch. Improvements of the MIS was carried out by (Harris, 1999) by modifying the plot method and finding a better fit for the Liebein BLUE (best linear unbiased estimators) thereby cutting off the need for data reduction. (Coles, 2001) provided the statistical details of predicting extreme values based on annual maximum and a more robust Point over Threshold Technique (POT). The POT was improved by (Fernando et al 2006, Melanissa 2009) by making its parameters time dependent. An advantage of the GPD is the use of a threshold and the application of the more current and better predictive model of peaks over threshold (POT) technique unlike the classical GEV which makes use of a single annual extreme value.

The NMINET method uses the moment matching technique to fit the wave data to a 3-parameter Weibull distribution (GEV). The distribution coefficients A, B, and k obtained for every data set are stored in the British Maritime Technology (BMT) data base for every data set, also taking into consideration seasonality and directionality. The NMIMET program provides these distribution coefficients to be used for other calculations.

For a given Probability P and return period the most probable maximum possible wave height (H_m) associated with the significant wave height H_s in a storm of duration D_s, with the mean period T_m of N number of waves in the storm can be obtained.

The return period (T_{Hs}) which is significant in design is represented by the equation 2.1

$$\boldsymbol{T_{H_s}} = \frac{\boldsymbol{D_s}}{\boldsymbol{8760.P((\geq H_s).N}} \qquad (2.1)$$

for cases of both annual and all directions data set and the effect of seasonality (proportion of the year represented by the season) and directionality (proportion of the time the wind blows from that directional sector).

2.2.2 *Sea State Spectrum*

The World Meteorological Organization (WMO) sea state codes have often been used in reporting wave height and period against more precise estimates for describing the sea conditions. It classifies the sea state from code 0-9, for significant wave height range from 0m to 14m, signifying calm sea through moderate to phenomenal like the type found in North Sea. Every typical sea, representing the water environment is described by a distribution which is obtained by using the parameters obtained from the various methods reviewed above. This distribution is often called the energy spectra for the sea state intended to be established. The pioneer work of (Phillip, 1958) on the energy balance and exchange during wind wave generation set the pace for breakthrough in spectra formulation. An equilibrium frequency range, within which this happens was introduced by Phillip. The foundational spectra formulations developed throughout the years have robust application in offshore designs. They range from single peaked spectra shapes for developing and fully developed seas with single defining parameter to multiple peaked shapes having as much as six parameters. Seas are composed of random combinations of swells (waves entering location from other areas) and wind sea (waves generated by local wind), (Walter 1999), thus use of spectra models developed in this manner have always been hit by the suspicion that the integrity of the estimate may be invalidated because of the simplifications applied according to (Torsethaugen, 2004). Part of the simplification involve the definition of the spectra shape using averaged significant wave height and peak periods. Using averaged parameters or averaged spectra shapes (in forming the bigger spectrum), significant source of randomness is neglected. A possible generalized approach has been to use a family of spectra shapes defining each sea state with pre-assigned occurrence probability, this technique was also adopted in the WASP 2004. Thus, at this junction, a review of the available spectra shapes is undertaken up to the approved shape for the West African sea area.

As posited earlier, the sea is represented in the form of an energy spectrum, the most widely recognized theoretical formulation of this kind is the *2-parameter* spectrum by Bretchneider in 1959. The expression is universally given as

$$S_{(T)} = \alpha . T^{5} . e^{-\beta T^{4}} \qquad (2.2)$$

Where α, β are functions of independent parameters, such as significant wave height and any of these characteristic periods (peak, modal, mean, or zero up crossing). However, the modal period is more commonly used for computations. The fitting distribution was the Rayleigh

distribution. Based on this postulation, with the availability of data from specific regions, expressions were fitted to define relationships for α & β thus giving rise to other formulations: see mathematical expressions for various spectrum formulations in appendix B.

The ISSC and ITTC spectrum were developed in 1964 and 1978 respectively. Following the work of Neumann, (Pierson and –Moskowitz, 1964) the Pierson-Moskowitz (P-M) spectrum was derived. This P-M spectrum became the favourite choice until a realization that it was limited in application to only fully developed sea generated by relatively moderate winds over very wide fetches. To account for situations where the spectrum covering a range of lower periods for a given significant wave height is generated from impact of high winds on short fetches, a two-parameter form was required. This led to the development of the Modified P-M spectrum. However, it does not differ so much from the already formulated Bretchneider spectrum.

Another significant spectrum was the JONSWAP spectrum. The JONSWAP was developed through a joint project from England, USA, Holland and Germany, which targeted at generating enough and reliable wave data for establishing an empirical formulation for adequately defining a sea state given the significant wave height and period (Hasselmann et al, 1973). This project was viewed as an extension of pioneering works of (Snyder and Cox, 1966; Barnett and Wilker-son, 1967). Data was collated from 168km into the North Sea westward from Sylt from sensors, which were arranged to act quasi-continuously for about 10 weeks. The spectrum has the robustness of accommodating a range of spectra shapes from those representing the fully developed P-M limit to those that are sharply peaked. The need to modify the spectrum to achieving this feature came from the fact that, as the fetch increased, there was no tendency for the JONSWAP to settle down to original P-M. The JONSWAP parameters are site specific. However general values exist in the absence of such data. It is worthy of noting that the JOSWAP spectrum, which is made up of five parameters (including the defining 2-parameter) is a P-M spectrum multiplied with a peak enhancement function.

The multi-parameter equivalent of equation 2.2., can be expressed in a standard form as;

$$S_{(T)} = \alpha . T^{r} . e^{-\beta T^{q}} \qquad (2.3)$$

Specific coefficients for the parameters α, β, r and q are obtained through fitting of data to equation 2.3. With r=5, and q=4 fixed, the model reduces to the standard 2-parameter spectrum discussed earlier. A 3-parameter form can be established if data is fitted while considering any

one of ‘r’ and ‘q’, as independent variable while the other is dependent. Using the same approach, considering both as dependent variables leads to a 4-parameter spectra formulation. (Ochi, 1978) formulated a 3-parameter spectrum by holding q as constant at 4 while r was made a variable. According to (Walter, 1999), the essence of multi-parameterization in defining a sharply peaked spectrum over a 2-parameter spectrum was validated. The Ochi 3-parameter spectrum was seen to have represented the actual sea better than the 2 or 4 parameter models. This however, also suggests that increasing the number of parameters does not necessarily translate to better accuracy in terms of sea state capture.

The sea is composed of a high frequency wind sea and low frequency swell wave, one is likely to expect the presence of at least two visible peaks. This explains why a double peaked spectrum is a better representation compared to single peaked spectrum for this purpose (Ochi & Hubble, 1976; Guedes Soares, 1984, 1992; Torsethaugen, 1993, 1996). Predominantly, low frequency swell waves can propagate at much faster rate compared to the generating wind field and thus portray the ability of getting to areas yet to be influenced by the wind. These swell waves add up locally with the wind to thus create double peaked spectra forms. For several years the Torsethaugen double peaked spectra (TS) has found frequent use for design and motion response estimates at the Norwegian continental shelf for numerical as well as model testing. The original TS was developed by fitting two JONSWAP shaped models to averaged measured spectra from the Norwegian shelf. JONSWAP was formulated from data from North Sea, and research has shown that geographical parameters play very significant role in properly defining spectra shapes for different areas. However, the Ochi-Hubble double peaked spectrum model (OHS) is more frequently applied outside the Norwegian shelf. The Ochi-Hubble spectrum is a 6-parameter spectra developed by the addition of two 3-parameter distribution. Each of the components are represented by unique gamma distribution and are then combined. The double peaked models have been adjudged a better representation of the real sea compared to the single peaked ones. However, during designs utilizing the 100-10000yrs return sea states, because extrapolations are unavoidable, model accuracy is associated with uncertainties, much lesser for the double peaked formulations though. Conclusively, the double peaked spectra are adequate representations for moderate seas, as this fails when the seas become more intense. For such intense conditions, the 3-parameter single, sharp formulation performs the better.

2.2.2.1 *West African Spectra shape*

From the forgoing, the double peaked spectra is a suitable representation for the West African sea state, which is moderate or benign in nature. It is characterised by the presence of multiple swells and wind sea components, and thus minimally bimodal in nature. The WASP was sponsored by Shell to conduct a research like the JONSWAP for developing and characterizing the West African offshore region sea states. A robust data collation campaign was taken, with data spanning from the coast of Cote d'Ivoire through Nigeria to Namibia. This data was collated and contributed by different participants. See figure 2.4 for region data spread.

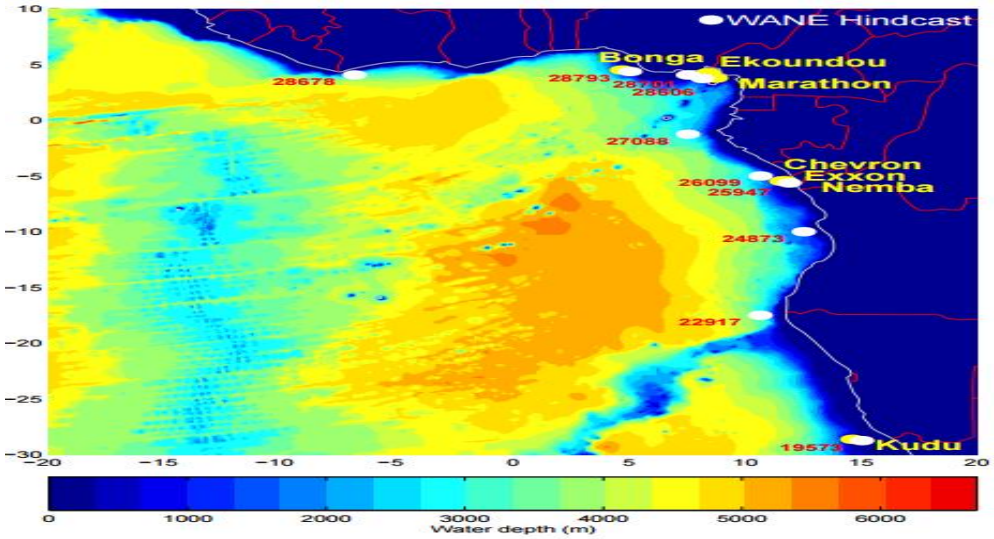

Figure 2.4 WASP data base locations (Final report, WASP, 2004)

Within the program framework, work done by Kevin and Olagnon adapting four spectra (JONSWAP-Glenn, Triangular, Lognormal and Gaussian) to data, could suggest better spectra characterization for West African. This was significant, because existing spectra shapes (assumed generalized), which were validated with data from North Sea or in semi closed regions such as Gulf of Mexico, should be applied to other regions with caution, particularly in regions with predominant swell seas. Remarkable difference in responses between measured spectra and simplified models have been observed (Van Iseghem et al, 2001). In dealing with data from the different areas the JONSWAP-Glenn was used for the wind sea and the swell was modelled using all four spectra models. The total sea obtained by combining these components suggest that the lognormal as well as the triangular models were best suited for defining the swell obtainable in the region. A wrapped normal distribution was suggested for

the directional spectrum (Olagnon, 2014). According to (DNV RP H103, 2011) the gamma spread function is a better representation compared to the cosine square spread distribution of (Haring and Heideman, 1978) obtained by modifying the equations of (Longuet-Higgins, 1961). This research work adopted the gamma spread function and the West African Sea state that is thus predominantly multimodal and multidirectional as well.

2.2.2.2 *Multidirectional, multimodal sea states*

The estimation of wave induced loads in both the frequency and directional domain of the wave is critical in the motion study and subsequently design of offshore structures. The directional wave form is an indication of the energy balance between the local wind on sea surface, interaction between swells coming from distant areas and the wind waves.

Ideally, not all sea states have unimodal wave spectra and narrow (or finite) spectra bandwidths. In real sense, local wind waves sometime develop in the presence of some low frequency swell coming from distant storms and the resulting mixed sea state will have bimodal wave spectra shape, i.e. two distinct peaks each at the low and high frequency regions (Yingguang and Yiqing, 2013). It has been found that low and moderate sea states often consist of swell and wind seas and consequently are better modelled or described as bimodal or two peak energy spectra (Petya and Guedes,2011). Bimodal sea states mainly occur in sea states which do not take place at the hike of severe storm (Felice and Guedes, 2009). They occur in about 40% in low and moderate sea states compared to 5% in high sea states. However, observations have been made of this kind of spectra in phenomenal seas with significant wave heights of 9-13.3m (Guedes, 1984). Evidence of the existence of this kind of sea states are recorded mainly in the North Atlantic: 16% for open North Sea and 22% for North Atlantic which confirms the observation of 25% in the North Sea made by (Ferreira and Guedes, 2000). Some attempts have been made to categorize the bimodal sea according to the dominant component based on the sea swell energy ratio (SSER) parameter (Petya and Guedes, 2011, 2011; Yingguang and Yiqing, 2013), which is defined as the ratio of the low frequency energy of the swell(s) sea to that of the high frequency wind sea component.

Observations by (Boukhanovsky,2009) suggest that studies in wave modelling have concentrated their effort in dealing with unimodal spectra, thus as old as the Ochi-Hubble modified spectrum in 1976 (Ochi and Hubble,1976), it is used as the bases for modelling the

shape of a bimodal sea state in 2D. It involves the statistical modelling of the entire bimodal spectrum to account for both the low and high frequency regions. The approach linearly combines two 3-parameter gamma spectra (modified Pierson-Moskowitz spectrum) to form a 6-parameter single 2D Ochi-Hubble spectrum. A re-parameterization of the coefficients to limiting it to 4, yielded a 4-parameter spectra model by (Guedes Soares, 1984; Guedes and Nolasco, 1984). The frequency spectra is then combined with a directional spread to give the complete multidirectional, short crested sea which is the actual representation of a real sea condition.

The Pierson-Moskowitz spectrum been almost the most accepted spectrum for a fully developed sea with an infinite forth spectra moment m4, making the narrow bandwidth proposition questionable. In regions of limited fetch, modification of P-M is thus required to fit properly to real data.

Guedes Soares in 1984 following the ideas of (Strekalov and Massel, 1971) by representing a double peak with the sum of a low and high frequency spectra, used two JONSWAP spectra instead, to develop a 4P spectra. The argument was pinned on the fact that the wind sea side of the spectrum is always still at the developing stage and as such can better be described by a JONSWAP spectrum (Guedes, 1984). It follows systemically that with the knowledge of the two adjoining spectra as explained above, the shape of the summation can be ascertained.

The distribution coefficients which are obtained by numerical integration of the PM and JONSWAP spectrum by (Ewing, 1971) are constant correction coefficients for the difference in peak period and area of both spectra. The values of coefficients for different peak enhancement factors γ are contained in (Guedes, 1984). Another important parameter used for defining double peak spectra is the ratio of the spectra ordinates of both spectra at the peak frequencies (S_R) (Guedes and Nolasco, 1984)**.** It is straight forward to find the two spectra peaks (H_{sw}, H_{ss} and S_{sp} and S_{wp}) from a measured spectra, and thus obtained the combined Hs, T_Z to enable the spectra to be modelled.

(Torsethaugen, 1993) leaning on the proposal of Guedes Soares developed a 7P bimodal spectrum using JONSWAP Spectrum for each system. There have been quite few recent works in this area, such as the works of (Fedele and Arena, 2005; Aziz and Fedele, 2006), which modified the linear quasi-deterministic theory of (Boccotti, 1989) to account for some degree

of non-linear nature of large sea waves in deep waters. Most modifications are made in the probability function describing the wave heights of the sea surface (Petya and Guedes, 2009).

At some location like the North Sea, spectrums are simply modelled with energy concentrating around a single or at most two modal frequencies and defined directions. The West African offshore region is faced with moderate but complex wave conditions of several swells with at least a wind sea at every instance. These patterns have their frequencies and directions with an implication of multiple number of parameters required to properly model it. This is evidenced in the WASP of 2004 as reported in (Kelvin et al, 2004; Olagnon et al, 2014). The WASP pointed out some possible limitations of the existing bimodal spectra for application in the West African Offshore region. Some of these included the unreasonably high value of shape parameter of about 70 for swell periods above 8s in northern Gulf of Guinea and 10s in Angola when JONSWAP was used. This value is about 10times bigger than the maximum of 7 expected for a JONSWAP spectrum. Again, the propagation of swell does not provide energy outside of a finite frequency range. The underlying reason is that these spectrums were developed for sea wind and not for swells. This suggests that proper modelling of the West African offshore region will involve in partitioning of the spectrum into its several swell components and the wind components and treating each of them differently. The swell component was modelled using the triangular and lognormal distributions and the modified JONSWAP called JONSWAP-Glenn was used for the wind component. (Marie-Aurelle et al,2007; Nerzic et al, 2007) affirmed the significant improvement in the prediction of responses by partitioning the entire spectrum into components. The triangular and lognormal spectra when applied to a data set from the West African region fitted comparatively better. Upon reconstruction of the time series from spectrum used for structural fatigue computation for a FPSO, the results were satisfactorily reproduced. The proposed simplified spectra are captured in the appendix B.

2.2.2.3 *Identifying Patterns in a Spectrum Defining a Multidirectional Sea State.*

It took a long time for the shipping industry to acknowledge the significance of combined sea conditions in assessing of wave induced loads. The work of (Toffoli et al,2004) on the analysis of about 270 ship mishaps revealed the presence of mixed or combined or crossing seas (wave trains travelling along different directions), which may undermine the safety of marine operations. This is so because mixed seas with relatively narrow angle between the spectra

peaks produce wave crest which deviate significantly from that of a single peaked sea state. The practice has always been to use any of the idealized unimodal spectra to describe a sea state of (Hs, T, θ), and with the help of wave atlas determine the occurrence probabilities. Better understanding of the wave loads requires not just the estimates based on (Hs, T, θ) for a particular primary wave direction but also a knowledge of the directional wave energy spread spectrum S (w, θ). This procedure can also be expanded to capture the real sea situations of multi-modal peaks. (Boukhanovsky, 2009) showed that the swell patterns in sea states can be identified by understanding the spatial distribution of the relative frequencies of the spectra. Prior to this, (Rodriguez and Guedes, 1999) developed a simple procedure to identify unimodal, bimodal and multimodal sea states from the raw data based on the logarithmic transformation of their spectrum estimates.

Looking at a representative generalized sea condition as swell and wind waves from different directions, with associated functional spread, as (Boukhanovsky and Guedes, 2009). In addition to a modal frequency (ω_p) exist a modal angle ,θ_p because of the overlapping (summation and subtraction) of secondary wave from the different primary patterns meeting at some undefined directions and frequency domain within their spread limits. The mathematical derivations associated with this are captured in the work of (Boukhanovsky and Guedes, 2009; Ochi and Hubble, 1978). This is done to determine the maximum or peak values of the overall multi-peaked spectrum values. The integration can be performed using Simpson's or Trapezoidal method. The explicit presentation of this method is captured in appendix C.

Going by the weighting factors (W_i) from the spread functions, it is observed that the secondary waves closer to the primary direction contribute comparatively bigger energy to overall spectrum as close to the primary wave pattern itself. It is therefore ideal and logical to concentrate on the region where secondary wave patterns from both individual spectra are closer to their respective primary wave direction (closed in zone). This zone is used to define the region were the largest dissipation of wave energy is observed within the overall spread. Hence, the highest possible will be thus achieved if the two patterns are closest to their primary direction, i.e. an extreme case will result when both waves are exactly on the same primary direction (collinear orientation). For design safety, it is then best to use the aligned direction and the resulting combined spectra for response analysis. Although research has also shown that the magnitude of impact by wave does not necessarily depend on the wave height but also on the frequency of advance which has the potency of causing resonant excitation of the ship.

In this work, attempt will be made to identify the wave parameters within the closed in zone for a given system of waves.

2.3 Roll Damping Assessment

Early FPSO designs with weathervane capabilities gave a misconception that roll motion was not of serious consequence, if the local sea condition is wind dependent or driven. This assumption, however, contradicts observation from real life field operations, as swell waves may also be observed. The smooth operations of FPSO's in harsh regions like the North Sea, Brazil offshore and the Gulf of Mexico are strongly influenced by roll motion amplitude; which affects both crew and equipment. Even in benign regions like the West African deep offshore, the combination of swell seas with characteristic long waves together with wind seas can put a FPSO unit in situations of discomfort. This may compromise the entire production process, due to possible shut downs which lead to unproductive downtimes. Sometimes the weathervane mode of a FPSO around the turret does not completely remove excitations coming from the multidirectional sea environment, which may include wave, wind and current. According to ISO 19901-01, API RP2-MET (Washington Monthly, 2012) the West African 100yr return period significant wave height (Hs) and peak period (Tp) are for the main swell; Hs=4-5m, Tp=14-15s, secondary swell; Hs=2-3m, Tp=11-13s and wind sea component has Hs=2-2.5m, Tp=8-9s. The associated 1 hr wind speed measured at 10m above MWL is 12-13m/s and a mean surface current of 2.0m/s. In the presence of multiple and multidirectional waves interacting-, it is still possible a FPSO to have a beam sea which is the most critical heading for excessive roll motions (El-Bassiouny, 2007). Roll stabilization is however well studied. To minimize roll motion in unfavourable situations, technologies can be used such as: anti-roll stabilization tanks (active and passive); U-tank; bilge keels; motion azimuthal thrusters; mooring lines. These systems either try to increase the roll damping or attempt to reposition the FPSO to a less critical heading relative to the excitation. Bilge keels, in addition to their economic advantage, work in a passive mode, and could reduce, the amplitude of roll near the resonance. Bilge keels are also very effective for vessels with no forward speed, such as on stationed FPSOs. (Vassilopoulus ,1971; Cox et al ,1977 as reported in Jose, 2002), have contributed immensely in the study of roll motion damped by bilge keels. Detailed studies of roll motion have also been carried out by (Salvesen, et al 1970; Haddara,1980, 1984; Bass and Haddara,1988; Wu and McCue, 2008).

FPSOs can, by design, be obtained by the conversion of very large crude carriers (VLCC). Alternatively, they may be newly built; in which case they would typically have a predominantly flat bottom, approximately squared mid-ship sections with large bilge keels and be wall sided. Non-linear roll motion, which is more apparent when using bilge keels, is predominantly dependent on viscous damping. This aspect of roll damping, which is specifically nonlinear because of vortices (Gustavo and Juan, 2013) is not captured by the predominant potential flow theory applied in most motion modelling tools for floating units. As such, the 19th century postulates by William Froude could not effectively explain the physics involved for such hull forms. (Ikeda et al 1977, 1978, Himeno 1981, Ikeda 2004, Chakrabati 2001) produced some explanations to non-linear roll damping physical background by dividing the viscous damping into various components. Using this they developed empirical expressions for approximately predicting the damping values and coefficients for rounded hull vessels at forward and zero speed. This corroborated with the quadratic behaviour and dependence from Froude postulate which could not predict correctly the behaviour of FPSO hull due to dominant vortex shedding influence over the hull (Downie et al, 1988; Wanderly et al, 2007; Kinnas, 2004).

In the polynomial method, the damping term is decomposed into distinct components, each term, describing to an approximate extent the physics surrounding the phenomenon. The method uses curve fitting technique to model the damping evolution in the form of a polynomial with variable represented by the roll rate. The coefficients of the polynomial are described as: the linear damping moment which is the linear viscous damping coefficient; the non-linear quadratic damping (eddy) moment, the non-linear cubic damping moment, the surface tension effect or Coulomb damping (but not significant in this case).

Research has been done using varying permutations of these components for studying roll damping. Prominent amongst these are the energy methods of Froude and Faltinsen, which rely on the fitting of quadratic polynomial and linear fit to the extinction data respectively. These methods however are limited in their explanations of the conspicuous two distinct plateaus resulting from vortex shedding which exist in a free roll decay for typical FPSO hulls with bilge keel and flat bottom (Antonio and Allan, 2009). For this kind of hulls, the roll damping behaviour between the large angle side and small angle side which defines the two distinct plateaus are quite distinct. Conclusively, standard methods could not correctly represent and predict the damping behaviour for significant number of cases (Oliveira and Fernandes, 2014;

Souza et al 2014). The vortex shedding, which modifies the flow around the bilge keel region, could not be efficiently predicted by the polynomial methods, even at increased order for instance the cubic technique (capturing dependence on amplitude and velocity as well). This highlighted the need for developing numerical approaches to model data from experimental test (Oliveira and Fernandes, 2014). From visualizations of experimental data and CFD simulations of hulls with bilge keels or sharp edges vortices are sent away after every rolling motion. This happens in such a manner that they affect the successive vortex generated afterwards. Thus, this interaction differentiates the two vortex modes, and results in a bilinear behaviour, which cannot be correctly modelled by the conventional polynomial methods. In dealing with this, a bilinear methodology, which recognizes two distinct regimes, was implemented. The bilinear method as the name correctly implies characterized the damping evolution of the two distinct plateaus observed with two (bi) linear behaviour. However, (Oliveira and Fernandes, 2009, 2011) and Fernandes and (Oliveira, 2009) adapted the bilinear model to smoothly fit the intermediate area connecting the two plateaus visible from several decay tests. This methodology could recognize the observed stoppage in the increase of the damping coefficient after some critical or transition angle or point. The model idea was based on the behaviour of the hyperbolic tangent curve. A careful observation on the data sets, suggest that, although as postulated, there may be saturation to a constant value, but the spread in the region may be better modelled by adjoining straight lines rather than a line with a constant value or zero slope. The modified Bilinear model, which is tagged the Hyperbolic model by (Oliveira and Fernandes, 2014) captures the transition from small angle to large angle and gives an indication that the damping coefficient saturates to a constant value. A close observation of the use of grouped data set has proven to be better in explaining some of these phenomena not visible in single data. It suggests that although there may be saturation at some point, the behaviour of the hyperbolic tangent function curve upon which the transition is modelled predicted a direct approach to this point.

The coefficients of the polynomial are solved by fitting experimental data from a decay test using the energy methods first described by William Froude in the 19^{th} century. This approximation is obtained by reducing the polynomial to a quadratic form.

By integrating the resulting truncated polynomial fit over a half cycle and equating work done by restoring moment to energy dissipated due to damping, the roll decrement and mean roll angle is obtained. The fit coefficients are obtained from polynomial fitting of roll extinction

data from decay test. The method could be applied to both crest and trough values from the decay test or to the combined data set.

Faltinsen evaluated the loss of energy during the cycle with a linear equivalent equation. This approach is however the standard industry approach but does not have the potential of explaining the distinct zones or plateaus observed in real data for flat bottom, wall sided, and sharp edges characterized by vortices. Faltinsen's approach can lead to over prediction of damping in large angles which is unsafe for floating platforms.

In other to overcome the limitation of these approaches, a bilinear method was developed (Oliveira and Fernandez,2014). This was a non-polynomial technique; however, it was considered rigorous and yielded a non-continuous formulation which was limited in application. Fernandez and Oliveira further modified the bilinear technique by utilising the behaviour of a hyperbolic tangent curve. This resulted in a hyperbolic model which was less rigorous and continuous in form than the original but performed better for application in simulations.

The non-polynomial Models or Hyperbolic Model, (Oliveira and Fernandes ,2014) which is a follow up from the bilinear method, is rooted in the surrounding physics of vortex shedding behavior noticed during model test. It considers the large energy dissipation region caused by the effect of big vortices on the water dynamic pressure over the FPSO bottom side. This phenomenon is commonly developed around bilge keels and sharp edges. The name bilinear is due to the existence of a dual linear behavior in the damping evolution observed between the small and large angle decay regions during roll decay; (Oliveira and Fernandes, 2006; Fernandes and Kroft, 2000).

The modified bilinear model proposed by (Oliveira and Fernandes,2009) gave a better prediction for both small and large angles, with a better capture of the vortex shedding due to bilge keel and bare hull motions. The envelope function from bilinear method representing the damping ratio was further modified using a continuous function dependent on the roll angle and roll velocity as well. Replacing the envelope function in the original bilinear model; yielded the modified bilinear model or the Hyperbolic Model. This model was built on the behavior of hyperbolic tangent which clearly, in a continuous mode captures the normalized damping coefficients for the two linearly assumed regions of the decay: large angle and small angle

respectively. The overall normalized linear equivalent damping coefficient can then be easily deduced.

(Oliveira and Fernandes,2012) have also made attempt in establishing a nonlinear analytical formulation by using dimensional analysis technique while considering aspects which have strong influence on viscous damping, loading conditions, hull form and bilge keel characteristics. A regression formulation was developed afterwards.

Some of the methods above, however, are fantastic in the prediction of the damping coefficient and behavior for hulls with sharp edges, they can only locate a point rather than the regions with possible transition occurring. Capability of identifying this transition region rather than a transition point is still needed. This thus is likely to give birth to a trilinear modeling of roll damping from decay data. This research attempts to abridge this gap, by modifying the proposed hyperbolic model by studying the behaviour of a small perturbation using an additional hyperbolic tangent term as well as a transition damping coefficient to represent the region.

2.4 Motion response analysis methods

The motion study of any floating unit in a seaway is undertaking by considering the degree at which the unit is assumed to move freely in the influence of originating external excitations. Two principal degrees are attainable in this respect, the single degree and the more generalized case of multi-degree considerations. In the single degree, the unit is assumed to move freely in one defined direction, say roll or yaw or sway etc. depending on the physics of the interactions being studied. However, the more generalized nature of a typical floating unit, whether restricted or not is for the unit to move in all six degrees or even more if multiple units are involved. Two methods, the frequency and the time domain techniques, have been developed over the years to model these motions. This section looks at the developments so far in these regards.

There are various procedures for determining the functions needed for the calculation of motion response. (Fukuda ,1967) initially proposed the usual basic assumptions that the ship responses are linear with respect to the exciting waves together with the Gaussian characteristic postulate for the sea state. On these premises, linear spectra analysis can be applied to derive simple statistics of the sea state and ship responses alike. This has been applied by (Guedes Soares and

Moan, 1991) and several others. (Guedes Soares et al, 2008) used this linearity approach to simulate the ship responses which compared favourably with the non-linear methods.

2.4.1 *Frequency and Time Domain Approach*

Two major approaches which can be used in predicting motion of FPSO unit are Frequency domain or Time domain analysis methods. FPSO motions are either studied as free-floating units or together with its mooring and riser units. Research has shown that the response amplitude in coupled states are always lower than those in uncoupled states (Das and Das, 2005), an indication that this ancillary units or appendages help in reducing the response amplitude. It is interesting to note that the solution in time domain and frequency domain are related by the Fourier transform (Beck and King, 1989). The analysis of ship motion in time domain was first reported by W.E. Cummins and T.F. Ogilivie in the early 1960's. Because of this discovery, time domain solutions making use of transient Green functions evolved over time. In applying the time domain method, the responses at each time interval is solved and used to derive the response time history which can then be used to ascertain the wave frequency response system parameter. (Holappa and Falzarano, 1998) while considering frequency dependent hydrodynamic coefficient used time domain in analysing roll motion. M. Taylan in 1999 as reported by **(**Das and Das, 2005) studied roll motion of ship using the generalized Krylov-Bogoliiubov asymptotic method in time domain. The Generalized Duffing's method was also used in frequency domain by (Taylan, 2000) to study ship roll motion. Similarly Surendran in **(**Holappa and Falzarano, 1998) and Reddy in (Wu and McCue, 2008) were able to investigate the influence of various parameters on ship capsize in beam sea by modelling the ship motion response in frequency domain. Group of researchers as reported in (Taghipour *et al.*, 2008) made use of hybrid frequency-time domain approach to analyse dynamic response in marine structures. In frequency domain, the general equation of motion describing the response is decoupled and solved independently for the mean, low and wave frequency responses which are then mathematically combined or superimposed under conditions of linearity to obtain the final response **(**Luo and Baudic, 2003**).** The time domain is adjudged the better of the two in terms of prediction, however it is also more time consuming and thus computationally expensive.

2.4.2 *Reviewed works on Ship Motion Simulation Techniques*

The actual study of ship motion comprises the solution of the entire behaviour of the structure in response to the external environment (wind, wave, current and resistance contributions from appendages) in the six degree of freedom states. The degree of freedom simply defines the possible modes in which the structure can move freely as it reacts to excitations. The motion modes include three translations (Surge, Sway and Heave) and three rotational (Pitch, Roll and Yaw). It is quite a huge task to accurately predict the motion of ships in seaway (moving or stationary) in their coupled 6dof, thus simplifications range from solving its single or 1-dof (sdof) or partial coupling of some of the modes. However, the predictions from fully coupled motions enjoy high level of comparative accuracy compared to sdof or reduced dof (Aung et al, 2015). Motion analysis which is used for design and operational studies (crew and equipment), seakeeping and manoeuvring is performed via well planned experiment (model or full-scale trials), numerical and approximated analytical expressions based popularly on strip theory (Korvin-Kroukovsky, 1957; Salvesen et al, 1970). Each method suffers its demerit ranging from cost, rigorousness, over approximations of real characteristics e.g. fluid-hull interactions or combination of these. Some however are robust in applicability within engineering precision. The presence of high speed computers has caused enhanced development of available but expensive software packages validated based on costly experimentations. Motion estimates are obtained by applying frequency or time domain techniques which involve the application of the fundamental Newton's law in balancing forces on the body. The generalized equation of motion (eom) is stated below

$$\sum_{j=1}^{6}\left((m_{ij} + A_{ij}).\ddot{x}_j + B_{ij}.\dot{x}_j + C_{ij}.x_j\right) = F_i \quad (i = 1 \text{ to } 6) \qquad (2.4)$$

This involves the balance of the inertial forces ($m_{ij}.\ddot{x}_j$), radiation forces ($A_{ij}.\ddot{x}_j + B_{ij}.\dot{x}_j$), restoring and buoyancy ($C_{ij}.x_j$) and external excitations (F_i) from wave, current and wind.

Because the task of estimating all coupled coefficients is huge, for floating structures with lateral symmetry (shape and weight distribution) the six dof are reduced to two sets of 3dof equation (grouped as; 'surge, heave, pitch' and 'sway, roll, yaw'). For roll motion study, if the entire 6dof is not solved, the latter is dealt with instead. (Aung et al, 2015) however developed mathematical model which captured the anti-symmetric coupled motion for roll-yaw (2dof) and sway-roll-yaw (3dof). Because of the difficulty in estimating the hydrodynamic coefficients, he tactically adopted values from experiments conducted by (Vughts,1968) and close fit curves from (Frank and Salvesen,1970). His results were in-line with real observations,

however he did not include other excitations from wind and current. In this work, the data for a VLCC from (OCIMF, 1994) was reconstructed and appropriate fit equations developed for the estimation of time varying current and wind coefficients with respect to the changing ship relative path.

Fundamentally, the development of motion simulation codes and tools extends from the need to gain accuracy against cost, computational time. This can be achieved by the application of modern techniques in the estimation of the various constituent components of the equation of motion in fully coupled state or partial combinations of the interest dof(s). In terms of component estimates, (Tristan and Thor, 2006) used frequency response function (FRF) of ship with the sea spectrum to simulate the wave forces as a multi-sine time series for a 4dof manoeuvring simulation model. Limited to handling ship near harbour, (Zhang et al 2004) developed a 3dof (surge, sway and yaw) model by first estimating the forces acting on ship, after which a first order differential eom from Newton's law was solved for the motion using Runge-Kutta method. Because the wave force estimate is dependent on the wave model adopted, (Cieutat et al, 2001) relied on the work of (Fournier and Reeves, 1986) to estimate wave forces using the sea surface swell beneath the ship. This however was limited in application since the estimated response for different ships in the same wave environment was the same. (Shyh-Kuang et al, 2008) using the height field technique implemented it to accommodate various shape of ships. (Zhao et al, 2004) adopting a memory storage or recording technique developed a short-term motion predictor using minimum component analysis and Eigen value approach. (Triantafyllou et al, 1983) utilised the Kalmer filter technique which required the knowledge of the ship and thus was improved upon for less reliability on such knowledge by (Lainiotis et al, 1992) since their target was for computer games. (D Spanous et al, 1997) attempted to formulate the entire 6dof motion, however in estimating the forces required, he neglected the distortion of free surface by diffraction of incident wave and radiation when carrying out the integration of the hydrostatic and incident wave pressure over wetted surface for force estimates. He also computed the added mass and potential damping terms using the NEWDRIFT program of (Papanikolaou, 1988), thus making the approach not independent. However, the conformal mapping technique, though very accurate for typical ship shape, it has found valid application in the determination of added mass and potential damping of arbitrary structures over the years (Ciobanu and Anghel, 2008). This technique simplifies to a large extent the estimation of the hydrodynamic mass and damping coefficients.

2.4.3 *Roll motion analysis*

Excessive roll motion and accelerations are one of the major considerations in FPSO unit response analysis since they have direct impact on operational down time. The Units roll motion is significant from many aspects including safety, stability and operational limits of on board equipment, therefore important in defining the operational window when exposed to varying environmental conditions (Babak and Nuno,2016; Gustavo and Juan, 2012). Even in moored situations, excessive roll motions can result when the unit is conditioned to an unfavourable beam sea situation (El-Bassiouny, 2007) as a result of single or combinations of environmental conditions. When the unit is exposed to other sea states the amplitude of roll motion may not be as high as that experienced in a beam sea. However, theoretically it is expected that FPSO unit with transverse symmetry in pure head or following sea states do not experience significant roll motion (Chang, 2008). The pitch excitation from the coupling between the roll and pitch motion, results in a sudden roll motion called parametric roll which may lead to pure loss of stability and thus serious Seakeeping and safety problems (Chang, 2008; Surendran *et al.*, 2007). Severe roll is the most dangerous motion mode to ship capsizing. Other consequences of roll motion include but not limited to discomfort on board, effects on topside equipment and personnel, green water, and effect on risers. Detail studies of roll motion has been carried out by (Salvesen, et al 1970; Haddara, 1980, 1984; Bass and Haddara 1988, Wu and McCue, 2008).

The assessment of the roll motion response of the FPSO unit and other vessels can be achieved either using techniques such as CFD, numerical solution of developed empirical expressions or model testing in a towing tank or even full-scale trial test. The techniques are formulated either in frequency or time domain as earlier mentioned. Study and use of Statistical data from the environment also forms an integral path to understanding the behaviour. In some instances, combination of these techniques is used to come up with better results due to complexities and peculiarities in the actual system being investigated. There are also situations in which the result from one technique is used to validate or improve or modify the results from another technique. For example, by adopting the 'model the model' approach (Luo and Baudic, 2003), results generated from CFD and/or model experiments can be used to modify the coefficients or calibrate the analytical and empirical model solved numerically. It is true to know that several CFD packages and codes, experimental fluid mechanics (EFD) methods, numerical

techniques and model test procedures have evolved over the years but the window for developments and suggestions for improvement is still open, since techniques and methodologies are based on some certain assumptions and approximations thus opening them up for continuous modifications.

3 Chapter Three: Experimental determination of Roll Damping

This chapter is dedicated to the determination of the global damping coefficient for roll motion of the FPSO unit. Critical amongst the outcomes of this chapter is the possible estimation of the damping coefficient and natural periods from the decay curves (Zhao WenHua et al, 2013). The experiment was carried out at the Newcastle University Towing tank. The dimension of the FPSO used are shown in table 3.1. The procedure was divided into four segments, where different activities were performed. The primary objective was to develop a continuous nonlinear roll viscous damping model and its linearized equivalent, which could be used in simulation of the roll motion. Two basic approaches were used in the analysis of the free decay data. In dealing with this, the separate use of crest and trough values has been dealt with in the paper (Orji and Woodward, 2015) presented at the 2015 IMDC conference in Japan. This work concentrates on the other approach which involves the use of the combined data and the combination of the entire data in group recommended by (Oliveira and Fernandez, 2014) as a better procedure in capturing the damping nature for a FPSO, with sharp edges. It should be noted that the experimental approach remains the best means of predicting damping for hull forms even in the presence of high quality CFD simulations.

3.1 Test Facility and Model preparation

3.1.1 *The Towing Tank*

The towing tank is 36m X 3.8m X 1.2m. Two hull forms were used, one with a bilge keel, and the other without the bilge keel. On each hull form, three draft lines, with each using three different initial angles were considered. The initial angle is the angle in which the model is tilted to in tank before being released. A regular wave test as well as a standard JONSWAP spectrum irregular wave test was also performed. The model is ballasted to the desired level as predetermined with the balls mounted atop and positioned within the range of the Qualysis camera. The model is lightly kept in position by tethered lines attached to body of hull to the sides of the towing tank. The tether lines however do not produce any significant damping or restoring to the model and thus do not contribute significantly to the motion of the model. The water is allowed to settle for about 20 minutes to maintain a calm state, to reduce the influence of external excitation coming from the environment.

Once the rigid body mode of the model is captured, the hull is slightly tilted to the desired initial angle using the digital protractor and released to perform free roll. Figure 3.1 shows the entire set-up in the towing tank. At the instance of release, the system is simultaneously triggered, and motion recorded at 200Hz. The possible sources of observable errors and their remediation are listed in Appendix D.

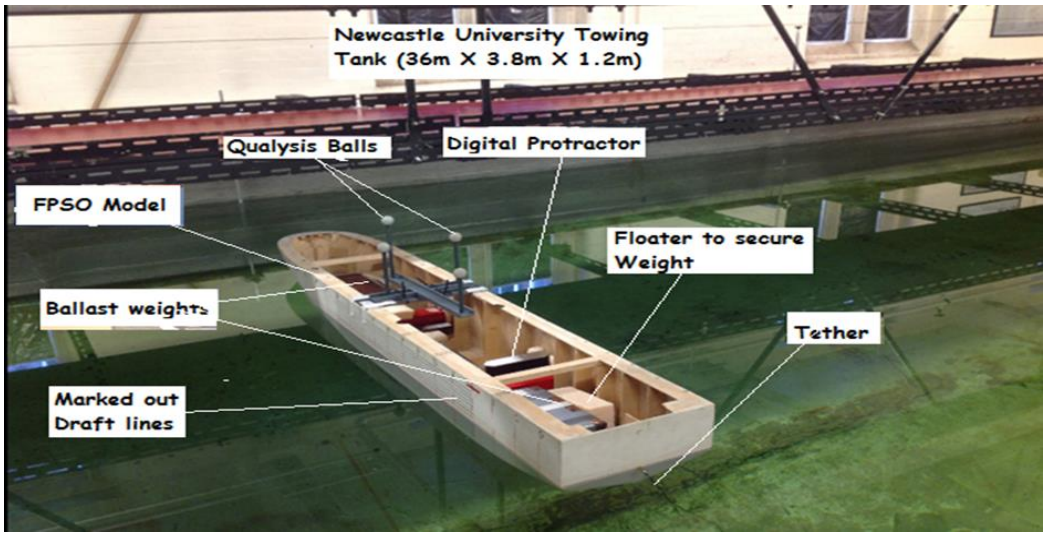

Figure 3.1 FPSO mounted transversely across tank, to minimize wave reflection from wall.

3.1.2 *The FPSO Model Preparation*

The model which is shown in figure 3.2, is a typical North Sea FPSO Prototype scaled to 1:128. The principal dimensions of the Unit are summarised in table 3.1. The vessel lines form is contained in appendix E. This model has been used by (Oliver and Longbin, 2014) for single draft line assumed to be the design draft. However, this experiment was conducted for three different draft lines shown in table 3.3 signifying instances of full load, ballast loading and possible overloaded conditions as it is typified in a practical field operation. The hull form was marked out at draft intervals of 1cm above and below the design draft. The draft line designated as 9, is at 12.5cm above the keel and 11cm freeboard at model scale. A total of seventeen lines were marked, equally spaced above and beneath the draft line 9. Draft lines 6 (9.5cm from keel, 14cm freeboard), 12 (15.5cm keel, 8cm freeboard).

This in conjunction with the digital protractor enabled the easy identification of the angle of heel in free decay test. Bilge keel is attached to the hull using adhesive to enable removal during the next set of runs for hull without bilge keels. Two sets of bilge keels were used in combination to ideally two draft lines. This experiment was done for free decay, regular and irregular waves as well.

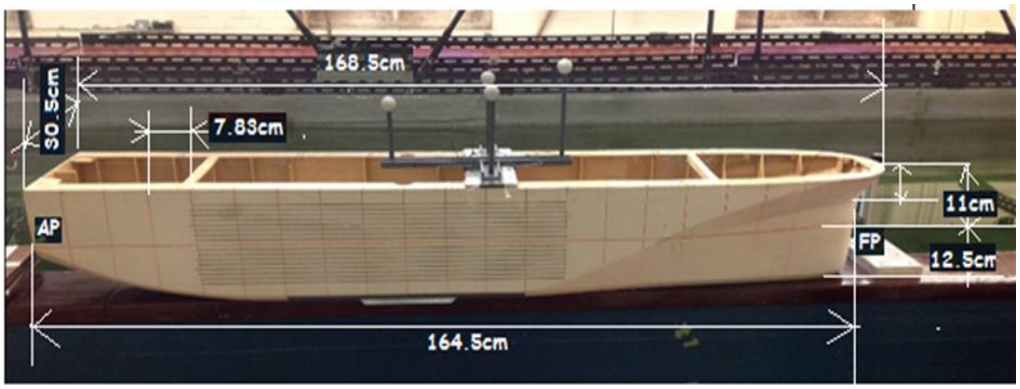

Figure 3.2 Marked FPSO Model with bilge keel, showing principal dimensions with Qualysis balls mounted.

Table 3.1 Principal Dimension of FPSO.

			Actual FPSO	MODEL
s/n	Item	Unit	Value	Value
1	length btw perpendicular	m	210.56	1.645
2	Breadth	m	38.4	0.305
3	Draft (design)	m	16	0.125
4	Displacement (@ draft line 9)	kg	109370671.1	50.88
5	Bilge Keel dimensions (Polymer Frame+10mm steel sheet extending 90^{o} out of frame)	mm	BK0:0X0 BK1:60.16X1.28 BK2:60.16X0.64	BK0:0X0 BK1:470X10 BK2:470X5
6	Vertical centre of Gravity	m	8.832	0.069
7	Transverse Centre of Gravity	m	0	0
8	Longitudinal centre of Gravity	m	96	0.75
9	Transverse metacentric height (GM)	m	4.191	0.0327
10	Radius of Gyration (Roll) Kxx	m	13.51, 9.15(ITTC)	0.09 (ITTC)
11	Radius of Gyration (Pitch) Kyy	m	60.76	0.475
12	Radius of Gyration (Yaw) Kzz	m	61.41	0.48
13	Natural periods (Roll) T44n	s	9.27s	0.85s

3.2 Experimental set up

The experiment was predesigned to capture possibilities that ensured minimal interference from wall in order to get reasonable length of time histories.

3.2.1 *Model set up*

A schematic arrangement of the model in the towing tank of Newcastle University is shown below in figure 3.3. The model is positioned vertically across the tank to reduce interference from reflecting waves from the walls. A light tether arrangement was used to ensure that the unit was held in position before the interaction with waves or unit set into free decay by a gentle tilt. The wave probe was positioned such that the waves breaking point happens at some point away from the unit, that is after the unit from the direction of the incoming wave. As shown in the figure 3.1 or 3.2, the motions are measured using the Qualysis system mounted strategically at the top of the unit using a platform which is accounted for as part of the mass of the unit. Data was acquired at frequency of 200hz.

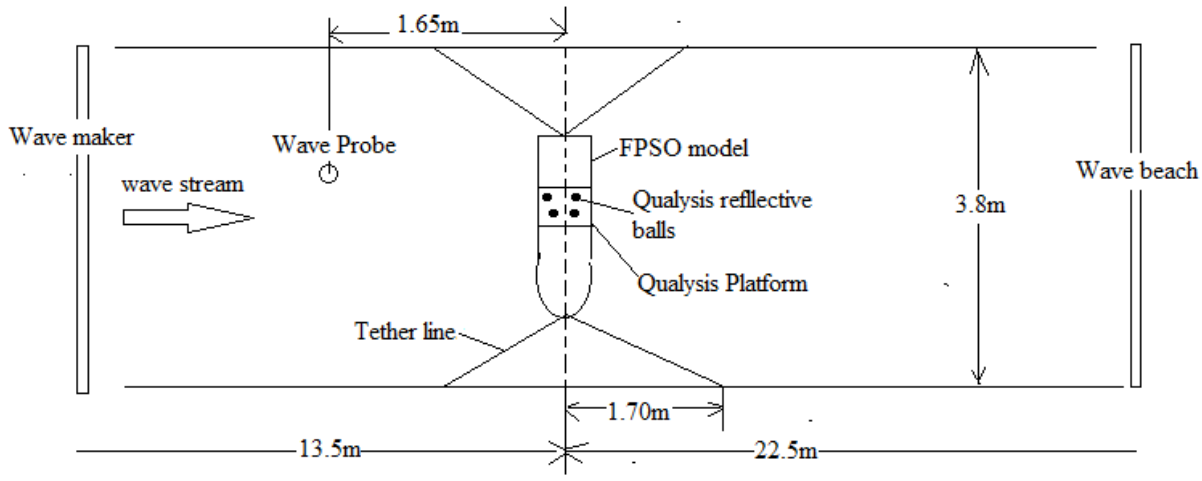

Figure 3.3 Model layout in towing tank (not drawn to scale)

The direction of the unit is altered according to the wave direction of interest, this is achieved by simply moving the unit to align in the set angle, and the tether anchor point are correctly adjusted to accommodate the lines to keep the unit in position. The head sea direction was then obtained by turning the unit 90^{o} with the bow facing the wave maker.

3.2.2 *Test Matrix*

As mentioned earlier, three categories of test were performed on the free-floating Unit. The free decay, regular and irregular wave tests. These tests were performed for cases of hull with and without bilge keels. In order to capture the bilinear damping behaviour observable in hull forms like the FPSO from a free decay data, (Oliveira and Fernandez, 2014) suggested the use of group data during the estimation of the damping coefficient. This concept was applied in designing the test matrix, thus three initial angles of tilt were used and the combined data used during the parameter estimations. Due to tank limitation, the irregular wave test was scoped to JONSWAP spectrum. However, the significant wave heights used depicted ranges from mild to harsh sea state. A description of the variables and their values used for the different test cases are given below. The test matrix is then followed. However, a comprehensive table of the test matrix capturing the experiments, parameters and designation are captured in appendix E2.

The Bilge keel configuration are giving in table 3.2. The actual dimensions are used in the estimation of the actual values of the damping coefficients. Bilge keel 0 (BK0) signifies a case were the hull is simply without a bilge keel.

Table 3.2 The Bilge keel configuration and its dimension

	Model		Actual	
	Length, L_{bk} (mm)	Width, w_{bk} (mm)	Length, L_{bk} (m)	Width, w_{bk} (m)
BK0	0	0	0	0
BK1	470	10	60.16	1.28
BK2	470	5	60.16	0.64

Load lines indicating different loading conditions have been marked out on the model from the design load line. The displacement values for the three draft lines of interest are captured in table 3.3.

Table 3.3 Draft (load condition):

Draft	**Load Lines**	**Displacement (kg) (model)**	**Displacement (ton) (Actual)**
d1	6 (ballast loading)	36.675	78758.543
d2	9 (design load line)	50.863	107806.196
d3	12 (over load line)	64.103	135650.083

In addition to the parameters in tables 3.2, and 3.3 above, for the Free Decay Test (T1), another significant input data is the target Initial angle (ai) which is the same for both actual ship and model). Three values where targeted, a1=6^o, a2= 12^o, a3 = 18^o, which signified small angle region, medium angle and large angle regions respectively.

The test matrix for the free decay test is shown in table 3.4 below.

Table 3.4 Free decay test matrix

	d1			d2			d3		
ai	a1	a2	a3	a1	a2	a3	a1	a2	a3
Bk									
0	√	√	√	√	√	√	√	√	√
1	√	√	√	√	√	√	√	√	√
2	√	√	√	√	√	√	-	-	-

The regular wave test (T2) was performed for two directions beam (90^o) and head (180^o) sea designated as Q2 and Q1 respectively. Six sets of waves were generated and used for the different configurations of bilge keel and draft. See table 3.5 for the wave generated at the model scaled which attempted to estimated feasible sea states in actual situations.

Table 3.5 Wave parameters for regular wave test

s/no	Model				Actual ship			
	Amplitude (m)	frequencies			Amplitude (m)	frequencies		
		f(Hz)	ω (rad/s)	T(s)		f(Hz)	ω (rad/s)	T(s)
ws1	0.02	0.7	4.398	1.429	2.56	0.062	0.389	16.162
ws2	0.0234	0.85	5.341	1.176	2.944	0.075	0.472	13.31
ws3	0.0254	1	6.283	1	3.2	0.088	0.555	11.314
ws4	0.0273	1.15	7.226	0.87	3.456	0.102	0.639	9.838
ws5	0.0293	1.3	8.168	0.769	3.712	0.115	0.722	8.703
ws6	0.0313	1.45	9.111	0.69	3.968	0.128	0.805	7.803

Based on the nomenclature of the table 3.5 above, the test matrix for the regular wave test conducted was designed as shown in table 3.6.

Table 3.6 Regular wave test matrix

	df1						df2					
Qi	Q1			Q2			Q1			Q2		
Bk	0	1	2	0	1	2	0	1	2	0	1	2
w												
ws1	√	√	√	√	√	√	√	√	√	√	√	√
ws2	√	√	√	√	√	√	√	√	√	√	√	√
ws3	√	√	√	√	√	√	√	√	√	√	√	√
ws4	√	√	√	√	√	√	√	√	√	√	√	√
ws5	√	√	√	√	√	√	√	√	√	√	√	√
ws6	√	√	√	√	√	√	√	√	√	√	√	√

In a similar vein, for the irregular wave test (T3) the three significant wave heights used captured sea states like that obtained in the West African sea region for the swell and wind sea components. The values used as input to the towing tank wave generator for JONSWAP spectrum are enumerated in table 3.7. The test was mapped, and experiment conducted according to the matrix of table 3.8 below.

Table 3.7 Input parameters for towing tank wave generator

Test case	Model			Actual ship		
	H_s (m)	Ts (s)	Freq (Hz)	H_s (m)	Ts (s)	Freq(Hz)
Hw1	0.015	0.764	1.2	1.92	8.644	0.106
Hw2	0.025	0.942	0.92	3.2	10.658	0.081
Hw3	0.035	1.1	0.77	4.48	12.445	0.068
JONSWAP spectrum user defined Input parameters in tank						
g	g	MaxFreq(rad/s)	MinFreq(rad/s)	σ(alpha)	σ(beta)	α
9.81	3.3	2	0.1	0.07	0.09	0.0081

Table 3.8 Irregular wave test matrix

	df1						df2					
Qi	Q1			Q2			Q1			Q2		
Bk	0	1	2	0	1	2	0	1	2	0	1	2
Hs												
Hs1	√	√	√	√	√	√	√	√	√	√	√	√
Hs2	√	√	√	√	√	√	√	√	√	√	√	√
Hs3	√	√	√	√	√	√	√	√	√	√	√	√

3.2.3 *Model loading conditions (ballasting experiment)*

Based on the lines of interest already marked out on the hull of the unit, a simple ballast experiment was carried out to estimate the corresponding loads used to ensure even keel positions. Figure 3.4 shows the model in the ballasting tank at the Newcastle university hydrodynamic lab. The essence was to determine the volume/mass displacement and some hull coefficients at the designated draft lines for other relevant calculations. The loads were arranged in patterns which ensured that the centre of gravity was as low as possible, thus flat but heavy weights were used to achieving this. The ballasting was done by placing the loads in four principal stations spanning from AP through FP. The stations are positioned at distances from the AP of the vessel, (Section A: 325.35mm, Section B: 587.25mm, Section C: 978.75mm,

Section D: 1291.95mm) and at distances from the keel which depended on the height of the parked load. However, load shifts were also done to ensure that even keel position was attained in all scenario. An inclining test was also undertaken to ensure that the centre of gravity was in the correct position. The swing test in the relevant motion modes were done to ensure that the right weight distribution resulted in the scaled down KG and radius of gyration as well. Starting with an initial weight distribution plan as stated above, the weights were moved into positions to ensure that the measured pendulum period estimated the required gyration radius.

Figure 3.4 Ballast set up Newcastle University Hydrodynamic lab ballast tank.

The results and estimates for the coefficients are captured in table 3.9 shown below.

Table 3.9 Hull form coefficient estimation from ballast experiment and

line	Draft		mass		Actual Unit					box			form coeff		
	model	actual	Exp	Sesam	Vol	Aw	Awp	Lwl	Beam	Vol	Aw	Awp	Cb	CAw	CAwp
	(cm)	(m)	(kg)	(kg)	(m^3)	(m^2)	(m^2)	(m)	(m)	(m^3)	(m^2)	(m^2)	(-)	(-)	(-)
1	4.5	5.76	32841400	33989532.25	33160.519	8066	6580	202.8	38	44388.864	10480.416	7706.4	0.747	0.770	0.854
2	5.5	7.04	41739616	42738919.07	41696.506	8690	6760	206.8	38	55323.136	11305.184	7858.4	0.754	0.769	0.860
3	6.5	8.32	50375688	51698728.66	50437.784	9342	6900	206.8	38	65381.888	11931.872	7858.4	0.771	0.783	0.878
4	7.5	9.6	59691237	60825647.43	59342.095	9972	7010	206.8	38	75440.64	12558.56	7858.4	0.787	0.794	0.892
5	8.5	10.88	68627202	70078109.09	68368.887	10530	7092	206.8	38	85499.392	13185.248	7858.4	0.800	0.799	0.902
6	9.5	12.16	78758543	79422979.15	77485.833	11110	7156	206.8	38	95558.144	13811.936	7858.4	0.811	0.804	0.911
7	10.5	13.44	87256203	88839421.88	86672.607	11710	7200	206.8	38	105616.896	14438.624	7858.4	0.821	0.811	0.916
8	11.5	14.72	97127498	98304897.6	95907.217	12310	7231	206.8	38	115675.648	15065.312	7858.4	0.829	0.817	0.920
9	12.5	16	1.08E+08	107807890.7	105178.430	12900	7256	206.8	38	125734.4	15692	7858.4	0.837	0.822	0.923
10	13.5	17.28	1.17E+08	117342605.7	114480.591	13460	7279	206.8	38	135793.152	16318.688	7858.4	0.843	0.825	0.926
11	14.5	18.56	1.27E+08	126908474.4	123813.146	14020	7303	206.8	38	145851.904	16945.376	7858.4	0.849	0.827	0.929
12	15.5	19.84	1.36E+08	136507248.7	133177.804	14610	7330	206.8	38	155910.656	17572.064	7858.4	0.854	0.831	0.933
13	16.5	21.12	1.46E+08	146150557	142585.909	15210	7365	207.2	38	166290.432	18230.848	7873.6	0.857	0.834	0.935
14	17.5	22.4	1.54E+08	155844987.4	152043.890	15810	7413	207.9	38	176964.48	18916.52	7900.2	0.859	0.836	0.938
15	18.5	23.68	1.66E+08	165613959.5	161574.595	16380	7476	208.8	38	187886.592	19622.848	7934.4	0.860	0.835	0.942
16	19.5	24.96	1.72E+08	175463819.2	171184.214	16980	7540	209.9	38	199085.952	20351.368	7976.2	0.860	0.834	0.945
17	20.5	26.24	1.85E+08	185395159.9	180873.327	17600	7603	210.9	38	210292.608	21076.472	8014.2	0.860	0.835	0.949
Awp: Water plane area, Aw: Wetted surface area												**Mean Val**	**0.823**	**0.813**	**0.915**

Figure 3.5 shows the ballast weights at different depths corresponding to different draft lines. There is generally a linear relationship between depth and the ballast weight. Using basic hydrostatic equations, computation of the form coefficients was carried out and the result compared with the hydrostatic parameter generated from the different draft levels.

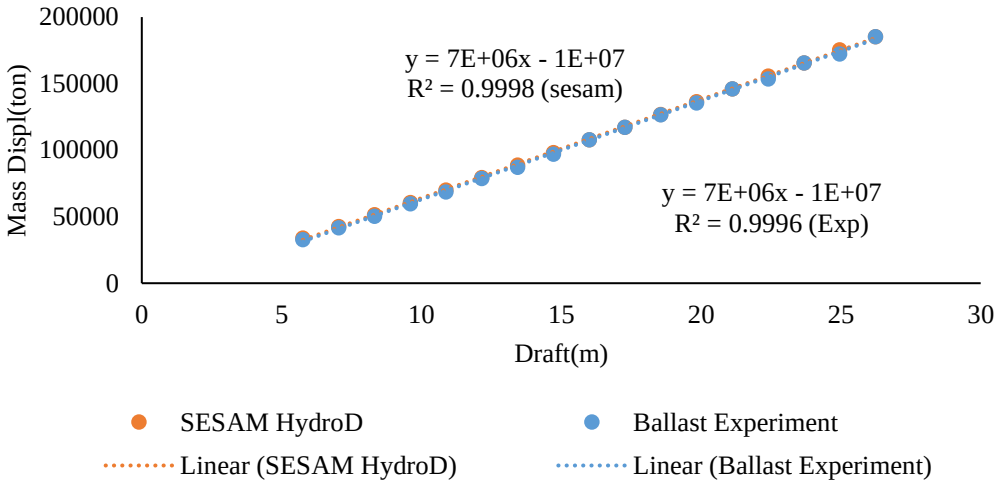

Figure 3.5 Graph of ballast weight to the draft line for actual FPSO.

From the figure 3.5, values between the ballast experiment and the SESAM calculations agree. Similarly, the depth variation of the hull form coefficients was also modelled as can be seen from figure 3.6. These equations were adopted in the formulation of the 6dof code developed. They were used in the estimation of actual hull form parameters from its box shape equivalent.

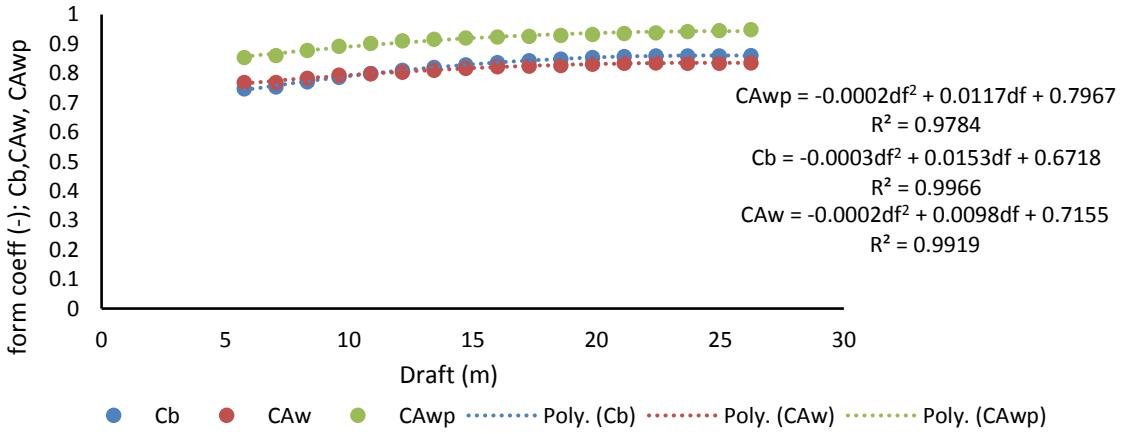

Figure 3.6 Form Coefficient variation with draft

Table 3.10 Comparison between linear and quadratic models for hull form/draft variations.

Form coeff.	Trend lines	R^2
C_{Awp}	$C_{Awp} = 0.0042\ df + 0.8476$	0.8924
	$C_{Awp} = -0.0002df^2 + 0.0117df + 0.7967$	0.9784
C_b	$C_b = 0.0053\ df + 0.7396$	0.8976
	$C_b = -0.0003df^2 + 0.0153df + 0.6718$	0.9966
C_{Aw}	$C_{Aw} = 0.0034\ df + 0.7592$	0.8934
	$C_{Aw} = -0.0002df^2 + 0.0098df + 0.7155$	0.992

3.3 Preliminary estimations for roll damping coefficients

The time history of the roll motion was investigated for the extraction of peak values (trough and crest). This was done for all experimental cases. See the collated peak values in appendix G. A sample of the typical decay curves and its associated extinction curves for cases T1Bk0df1a1 and T1Bk1dfa2 are shown in figure 3.7.

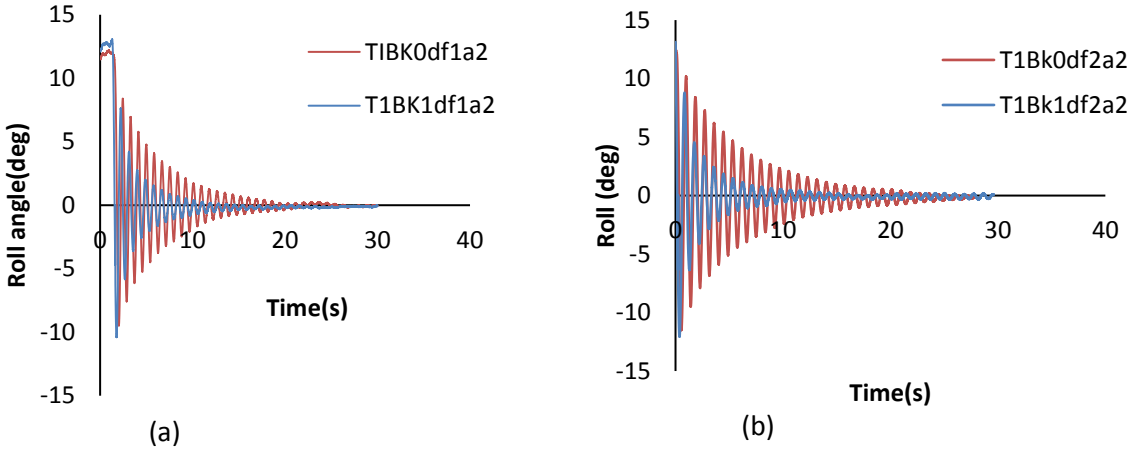

Figure 3.7 Roll angle decay curve for experiment cases; (a) T1Bk0df1a2 and T1Bk1df2a2, (b) T1Bk0df2a2 and T1Bk1df1a2

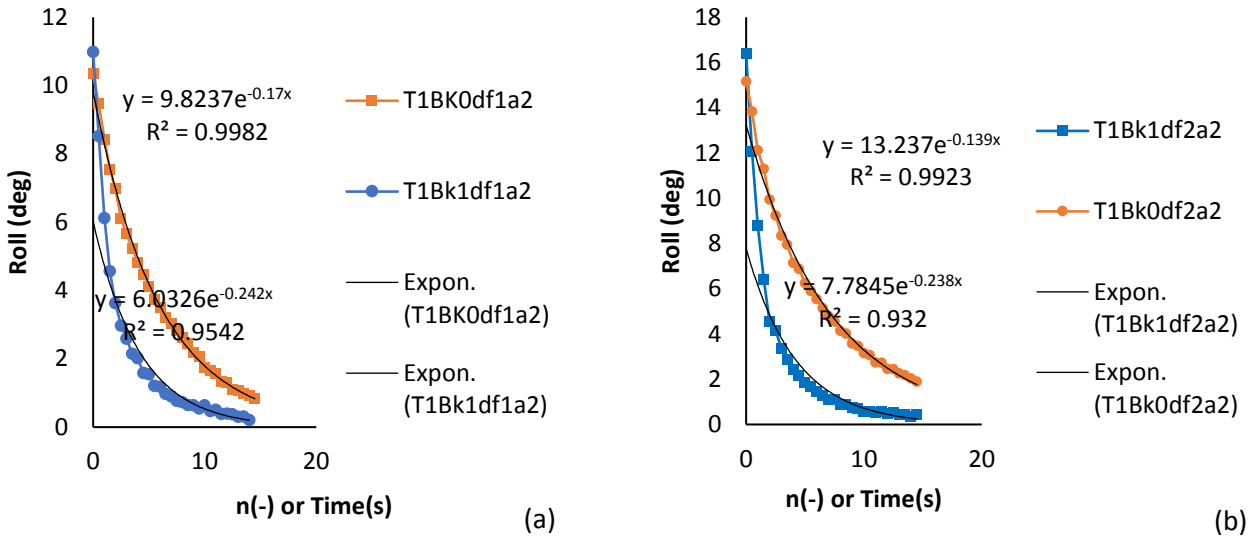

Figure 3.8 Extracted roll peaks for crest and trough values for experiment cases; (a)T1Bk0df1a2 and T1Bk1df2a2, (b) T1Bk0df2a2 and T1Bk1df1a2

From the decay data, preliminary estimations which include the natural period, the local damping as well as the fitting parameters are carried out. The behaviour of the trough and crest values for a linear damping system are very similar in magnitude. Some parameters, such as the local log decrement, local damping coefficient and even the damped natural period are estimated to be equal if the crest and trough data are used independently. Some research however prefers to combine both data in order to capture, to great extent, the associated non-linearity in the data. This may be deficient at some points at which the successive absolute value of a trough becomes greater than successive peak crest value. This is characteristic of real decay data, thus to avoid this, and enhance the computation of all possible non-linearity, the peak and trough data are treated separately and the average value of primary parameters, e.g., the log decrement which are in turn used to compute the other secondary parameters are used instead. This approach has been demonstrated in (Orji and Woodward, 2015). However, the approach adopted in this presentation used both data as a single unit but carried out estimate through one complete cycle, while maintaining the values in their absolute forms.

For a given data set, the damped natural period is estimated as

$$T_d = \frac{t_{end} - t_{start}}{N(cycles)} \tag{3.1}$$

$$\omega_d = \frac{2\pi}{T_d} \tag{3.2}$$

To approximate the undamped natural frequency using the mean damping coefficient, the computed log decrement across each oscillation, yields;

$$\delta = \frac{1}{m-n} \ln\left(\frac{\theta_n}{\theta_m}\right) \quad (3.3)$$

Where m and n are the numerical positions of the peak values θ_m to θ_n respectively;

The associated mean local damping coefficient (ξ) is thus estimated as

$$\xi = \sqrt{\frac{\delta^2}{4\pi^2 + \delta^2}} \quad (3.4)$$

and the natural frequency (ω_n) estimated from the local damping and as;

$$\omega_n = \frac{\omega_d}{\sqrt{1-\xi^2}} \quad (3.5)$$

See values of computed averages for the test set carried out in Appendix G.

To determine the damping coefficients, for each experiment set, the combined data for both crest and trough were used, then the preliminary fitting parameters computed independently from all initial angles for experiment case were then grouped according (Oliveira and Fernandez, 2014) for the overall damping coefficient estimation. A typical extraction for the data set of figure 3.7b is shown in table 3.11.

Table 3.11 Typical preliminary calculations of fitting parameters

s/n	n	t	θi	θi	θm	$(\theta m)^2$	$X_{=16.\theta m/3.Tn}$	δθ	θvel	δi	ζi	Pe	Xhm
	(-)	(s)	(deg)	(rad)	(rad)	(rad^2)	(rad/s)	(rad)	(rad/s)	(-)	(-)		
1	0	0	16.31	0.285									
2	0.5	0.455	12.081	0.211	0.219	0.048	1.297	0.131	0.142	0.619	0.098	1.375	0.04837
3	1	0.925	8.783	0.153	0.161	0.026	0.955	0.099	0.108	0.637	0.101	1.416	0.02622
4	1.5	1.375	6.388	0.111	0.116	0.013	0.688	0.074	0.082	0.662	0.105	1.470	0.01364
5	2	1.835	4.531	0.079	0.092	0.008	0.545	0.039	0.042	0.431	0.068	0.957	0.00850
6	2.5	2.3	4.152	0.072	0.069	0.005	0.407	0.021	0.022	0.302	0.048	0.670	0.00474
7	3	2.755	3.351	0.058	0.061	0.004	0.363	0.022	0.025	0.366	0.058	0.814	0.00378
8	3.5	3.2	2.879	0.050	0.050	0.003	0.299	0.016	0.018	0.323	0.051	0.718	0.00255
9	4	3.65	2.426	0.042	0.044	0.002	0.260	0.013	0.014	0.287	0.046	0.637	0.00194
10	4.5	4.11	2.161	0.038	0.037	0.001	0.220	0.010	0.011	0.281	0.045	0.624	0.00138
11	5	4.56	1.832	0.032	0.033	0.001	0.198	0.009	0.009	0.257	0.041	0.571	0.00112
12	5.5	5.01	1.671	0.029	0.029	0.001	0.171	0.006	0.007	0.221	0.035	0.491	0.00083
13	6	5.445	1.469	0.026	0.026	0.001	0.153	0.007	0.007	0.253	0.040	0.562	0.00067
14	6.5	5.89	1.298	0.023	0.023	0.001	0.133	0.006	0.007	0.280	0.045	0.622	0.00051
15	7	6.34	1.110	0.019	0.021	0.000	0.124	0.003	0.004	0.157	0.025	0.349	0.00044
16	7.5	6.8	1.109	0.019	0.018	0.000	0.107	0.003	0.003	0.152	0.024	0.337	0.00032
17	8	7.2	0.954	0.017	0.017	0.000	0.102	0.004	0.005	0.250	0.040	0.556	0.00030
18	8.5	7.68	0.864	0.015	0.015	0.000	0.087	0.004	0.004	0.263	0.042	0.585	0.00022
19	9	8.13	0.733	0.013	0.014	0.000	0.081	0.003	0.003	0.203	0.032	0.450	0.00019
20	9.5	8.585	0.705	0.012	0.012	0.000	0.073	0.001	0.001	0.077	0.012	0.170	0.00015
21	10	9.035	0.679	0.012	0.011	0.000	0.066	0.002	0.003	0.197	0.031	0.437	0.00013
22	11	9.455	0.579	0.010	0.011	0.000	0.065	0.002	0.002	0.160	0.025	0.355	0.00012
23	11	9.87	0.579	0.010	0.010	0.000	0.058	0.001	0.001	0.083	0.013	0.183	0.00009
24	12	10.35	0.534	0.009	0.009	0.000	0.056	0.001	0.001	0.149	0.024	0.330	0.00009
25	12	10.81	0.499	0.009	0.009	0.000	0.052	0.001	0.001	0.141	0.022	0.313	0.00008
26	13	11.25	0.463	0.008	0.008	0.000	0.049	0.001	0.001	0.114	0.018	0.253	0.00007
27	13	11.71	0.445	0.008	0.008	0.000	0.046	0.001	0.001	0.086	0.014	0.191	0.00006
28	14	12.12	0.425	0.007	0.008	0.000	0.045	0.000	0.000	0.048	0.008	0.107	0.00006
29	14	12.55	0.424	0.007	0.004	0.000	0.022	0.007	-0.001	-	-	-	0.00001

It is pertinent that the behaviour of the independent data and the grouped data for a given experiment set is similar and thus the concept of grouping as a single data for parameter identification is correct. The characteristics of the hull with bilge keel suggest strongly that the bilge keel modifies the roll motion by reducing the amplitude of roll at any given instance as compared to the hull without the bilge keel. It is common knowledge observable from figures 3.7 and 3.8, this observation is in tandem with existing phenomenon. There is a greater decrease in roll angle from one peak to the other as can be seen. This phenomenon is further explained by the higher decay rate for the T1Bk1df1a2. The comparative reduction in amplitude is necessitated by the increase in the viscous damping, as the FPSO rolls in water. Note that the trend line equations are not models but simply for illustrations to show the distinct regions between the hull types. An exponential decay value of 0.17 for the bare hull compared with that of 0.242 for draft line 1, and 0.139 against 0.238 for draft line 2 is an indicator of the influence on damping from the bilge keel. The steep demarcation observed in figure 3.7, shows a higher tendency for non-linear roll damping behaviour for hulls with bilge keel. This is due to the modification of the flow field and vortex shedding around the keel as the hull radiates energy to surrounding water mass. There is thus a distinct behaviour observable between the large and small angle regions which can best be modelled using a minimum of two linear regions as against the linear fits used by polynomial methods.

3.4 Roll damping theoretical development from free decay test

In order to extract the damping coefficient, a slightly different approach in the handling of the free decay data is applied here as compared to the method adopted in the paper by (Orji and Woodward, 2015). Both the crest and trough data are taken as continuum and thus the tendency for the process to capture damping properties as the vessel rolls from the crest to trough regions and vice versa.

A standard and generally accepted roll equation, derivable from the fundamentals of the Newton's law of motion for a 1DOF system can be expressed as:

$$(I_{44} + i_{44})\ddot{X}_{44} + B\left(X_{44}, \dot{X}_{44}\right)\dot{X}_{44} + C(X_{44})X_{44} = M_4(t) \quad (3.6)$$

Representing the roll amplitude as; $X_{44} = \theta$,

Thus:

$$(I_{44} + i_{44})\ddot{\theta} + B\left(\theta, \dot{\theta}\right)\dot{\theta} + C(\theta)\theta = M_4(t, \omega) \quad (3.7)$$

The virtual moment of inertial can be calculated as

$$(I_{44} + i_{44}) = \Delta * g * GM_T/{\omega_n}^2 \quad (3.8)$$

With, ω_n estimated from equations 3.5.

This value can also be approximated by using the ITTC-7.-02-07-02(2002) approximation for the radius of gyration

$$k_{44} \approx (0.3\ to\ 0.35) * B \quad (3.9a)$$

$$(I_{44} + i_{44}) \approx \Delta * {k_{44}}^2 \quad (3.9b)$$

Depending on application, the damping, restoring term are treated as linear or non-linear terms. Particularly for roll motion, the nonlinearity in the damping term cannot be easily neglected, however for small amplitude roll, the restoring coefficient can be approximated with a linear model.

(Robert ,1985) showed that the coefficients derivable from the restoring moment can be represented as

$$C(\theta)\theta = \Delta.\,\mathrm{g}.\sum_{j=i}^{m} C_j\theta^{2j-1} = \Delta.\,\mathrm{g}.\,GZ(\theta) \quad (3.10)$$

For j=1, m=1,

$$GZ(\theta) = C_1\theta \quad (3.11)$$

And (linear restoring moment)

$$C(\theta)\theta = \Delta * g * C_1\theta\ = \Delta * g * GM_T \quad (3.12)$$

i.e. $C_1 = GM_T$

Generally, j= 1,2, 3, 4 ……m, non-linear restoring moment/coefficients

$$GZ(\theta) = C_1\theta + C_2\theta^3 + C_3\theta^5 + C_4\theta^7 + \cdots \quad (3.13)$$

This has gained wide acceptance in terms of applicability as can be seen in (Taylan ,2000).

3.4.1 *Polynomial method in damping coefficients estimation:*

In this method, the damping term is decomposed into distinct components, each term, describing to an approximate extent the physics surrounding the phenomenon.

Where

$$B(\theta,\dot{\theta})\dot{\theta} = B_{44L}.\dot{\theta} + B_{44NLQ}.|\dot{\theta}|.\dot{\theta} + B_{44NLC}.\dot{\theta}^3 + B_4.\dot{\theta}/|\dot{\theta}| + \ \ldots \quad (3.14)$$

$B_{44L}.\dot{\theta}$ = linear viscous damping

$B_{44NLQ}.|\dot{\theta}|.\dot{\theta}$ = non − linear quadractic damping(eddy)

$B_{44NLC}.\dot{\theta}^3$ = non − linear cubic damping

$B_4.\frac{\dot{\theta}}{|\dot{\theta}|}$ = surface tension effect or coulomb damping (not significant for large body in water)

Approximately,

$$B_{44Leq} = 2 * \xi.\omega_n.(I_{44} + i_{44}) \quad (3.15)$$

Were ξ is assumed to be the linearized equivalent of the global damping ratio which can be obtained by running a least square optimization on the nonlinear damping formulation

The critical damping coefficient is given as,

$$B_{44crit} = 2 * \sqrt{(I_{44} + i_{44}) * \Delta * g * GM_T} \quad (3.16)$$

Different research had been done using varying permutations of these components for studying roll motion. Prominent amongst these are the energy methods of Froude and Faltinsen which relied on the fitting of quadratic polynomial and linear fit to the extinction data respectively. These methods however are limited in their explanation of the conspicuous two distinct plateaus (large and small angle regions) resulting from vortex shedding which exist in a free roll decay for a typical FPSO hull particularly with bilge keel and flat bottom (Antonio and Allan, 2009). The modified Bilinear model, which is tagged the Hyperbolic model by (Oliveira and Fernandez, 2014) captured a possible transition from small angle to large angle and gives an indication that the damping coefficient saturates to a constant value. Observation of the grouped data set has proved to be better in explaining some of these phenomena, which are not visible in single data. The hyperbolic model suggests that although there may be saturation at some point, the behaviour of the **tanh (a.x)** curve upon which the model was formed did not capture a clear transition zone. Virtual inspection of the data suggests the presence of a transition zone before saturation is reached. To achieve the characterization of this observation, the inclusion of a second **tanh a*** term, showed a tendency to predict this reduced rate as observed.

Substituting equations 3.13 and 3.14 into 3.7, and dividing across by the virtual moment, yields

$$\ddot{\theta} + \beta_1.\dot{\theta} + \beta_2.|\dot{\theta}|.\dot{\theta} + \beta_3.\dot{\theta}^3 + \alpha_1\theta + \alpha_2\theta^3 + \alpha_3\theta^5 + \cdots = f_4(t,\omega) \quad (3.17)$$

Were;

$$\beta_j = \frac{B_j}{(I_{44}+i_{44})},\ j = 1-3;\ \alpha_i = \frac{C_i}{(I_{44}+i_{44})} = \frac{C_i}{mk^2} \qquad for\ \ i = 1,2,3,4\ldots\ldots \tag{3.18}$$

$$B_1 \equiv B_{44L};\ B_2 \equiv B_{44NLQ};\ B_3 \equiv B_{44NLC}$$

$$f_4(t,\omega) = \frac{M_4(t,\omega)}{(I_{44}+i_{44})}, \tag{3.19}$$

Especially, $\alpha_1 = \frac{(C_1=C_{44}=\Delta*g*GM_T)}{(I_{44}+i_{44})} = {\omega_n}^2$ (3.20)

ω_{nat} is the roll natural frequency of the FPSO

The damping coefficients in the equation 3.17 are solved by fitting experimental data from a decay test using the energy method.

3.4.1.1 *William Froude's (19TH Century) and the Cubic approach*

For the Froude approximation, $\beta_3 = 0$; reducing the polynomial of equation 3.17 to equations 3.21 and 3.22

$$\ddot{\theta} + \beta_1.\dot{\theta} + \beta_2.\left|\dot{\theta}\right|.\dot{\theta} + {\omega_n}^2.\theta = f_4(t,\omega) \tag{3.21}$$

$$\ddot{\theta} + 2v.\dot{\theta} + \beta_2.\left|\dot{\theta}\right|.\dot{\theta} + {\omega_n}^2.\theta = f_4(t,\omega) \tag{3.22}$$

Where, $v = k.\omega_n = \frac{B_{44L}}{B_{44crit}}.\omega_n$ (3.23)

$$\beta_1 = 2 * k.\omega_n \tag{3.24}$$

By integrating the equations 3.21 or 3.22 over half cycle and equating work done by restoring moment to energy dissipated due to damping, the equation 3.25 or 3.26 for the roll decrement and mean roll angle is obtained.

k is the fraction of critical damping and *v* is the damped natural frequency.

$$\delta\theta = \frac{\pi\beta_1}{2.\omega_n}\theta_m + \frac{4\beta_2}{3}\theta_m^2 + \frac{3\pi\beta_3}{8}\theta_m^3 + \cdots \qquad \text{(Polynomial fit)} \tag{3.25}$$

$$\delta\theta = \pi k.\theta_m + \frac{4\beta_2}{3}\theta_m^2 + \frac{3\pi\beta_3}{8}\theta_m^3 + \cdots \tag{3.26}$$

The coefficients k, β_1, and β_2 are obtained from polynomial fitting of roll extinction data from the decay test data. See figure 3.9 for the sample for a grouped data TIBk0df1.

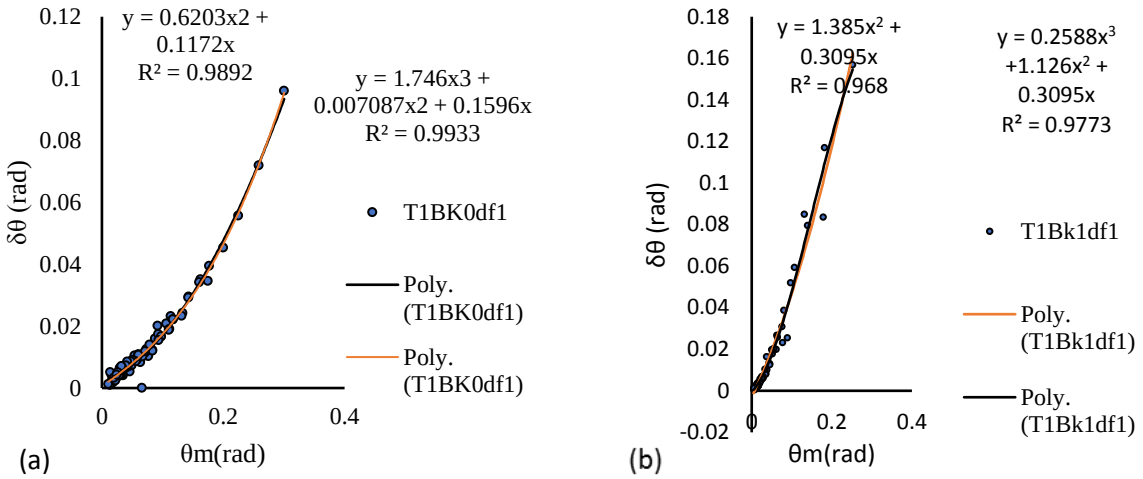

Figure 3.9 Froude and Cubic Polynomial technique for (a) bare hull (b) hull with bilge keel
The values are estimated thus:

$\beta_1 = a1 * \frac{2.\omega_{nat}}{\pi}$; $\beta_2 = a2 * \frac{3}{4}$; $\beta_3 = a3 * \frac{8}{3\pi}$ were a1, a2 and a3 are directly obtained from the fitting.

The method was applied to the combined crest and trough values from the decay test. See table 3.11 for estimated data for the hull with bilge keel, designated as exp. T1BK1df1a2. The comprehensive presentation is captured in appendix H**,** where individual estimates are grouped for all angles used.

The linear hydrostatic restoring coefficient $\alpha_1 \; or \; C_1$(see equations 3.13,3.20) are used in this calculation. The other non-linear restoring coefficients ($\alpha_2 \; or \; C_2, \; \alpha_3 \; or \; C_3, \; \alpha_4 \; or \; C_4 \ldots\ldots$) can be obtained from equation 3.13, by fitting an odd power polynomial to a transverse $GZ(\theta)$ curve. (Hamid et al, 2010; Taylan, 2000; Holappa and Falzarano, 1998).

The cubic fitting rather than truncating the equation at the quadratic term, includes the cubic term, thus $\beta_3 \neq 0$ is the full polynomial as represented by equations 3.25 and 3.26 are implemented. However studies have shown that the inclusion of the third term does not necessarily mean an improvement of the prediction compared to the complexity carried along.

For both the Froude and cubic methods, the equivalent linearized damping coefficient is obtainmed by optimizing the value of (β_{eq}) while minimizing the the least square error $\boldsymbol{E}(\beta_{eq})$ between the assummed linear damping β_{eq} and the non-linear configuration as shown below in equations 3.27 and 3.28.

$$\beta_{eq} = \beta_1 + \beta_2 * |\dot{\theta}| + \beta_3 * \dot{\theta}^2 \quad (3.27)$$

$$\boldsymbol{E}(\beta_{eq}) = \left[\beta_{eq} - (\beta_1 + \beta_2 * |\dot{\theta}| + \beta_3 * \dot{\theta}^2)\right]^2 \quad (3.28)$$

With the global equivalent linearized damping coefficient , from equation 3.21 obtained as

$$B_{eq} = \beta_{eq} * (I_{44} + i_{44}) \quad (3.29)$$

3.4.1.2 *Faltinsen's Approach (most used by industries is based on small angles):*

The loss of energy during the cycle (Pe) was evaluated with an equivalent linear model of equations 3.25 or 3.26.

$$P_e = \frac{2.\ln\left(\frac{\theta_i}{\theta_{i+2}}\right)}{T_n} = \beta_1 + \left[\frac{8}{3\pi}.\beta_2.\omega_n\right]\theta_{m,i} \quad (3.30)$$

$$P_e = \frac{2.\ln\left(\frac{\theta_i}{\theta_{i+2}}\right)}{T_n} = \beta_1 + \left[\frac{16}{3T_n}.\theta_{m,i}\right].\beta_2 \quad (3.31)$$

$\theta_{m,i}$ is the mean roll amplitude station i.

The resulting roll equation, after the determination of the coefficients remains as equations 3.21 **or** 3.22.

The optimized values of β_1 and β_2 are obtained by fitting a linear model to the plot of $P_e\ vs\ \frac{16}{3T_n}.\theta_{m,i}$ as it is shown in figure 3.10 below

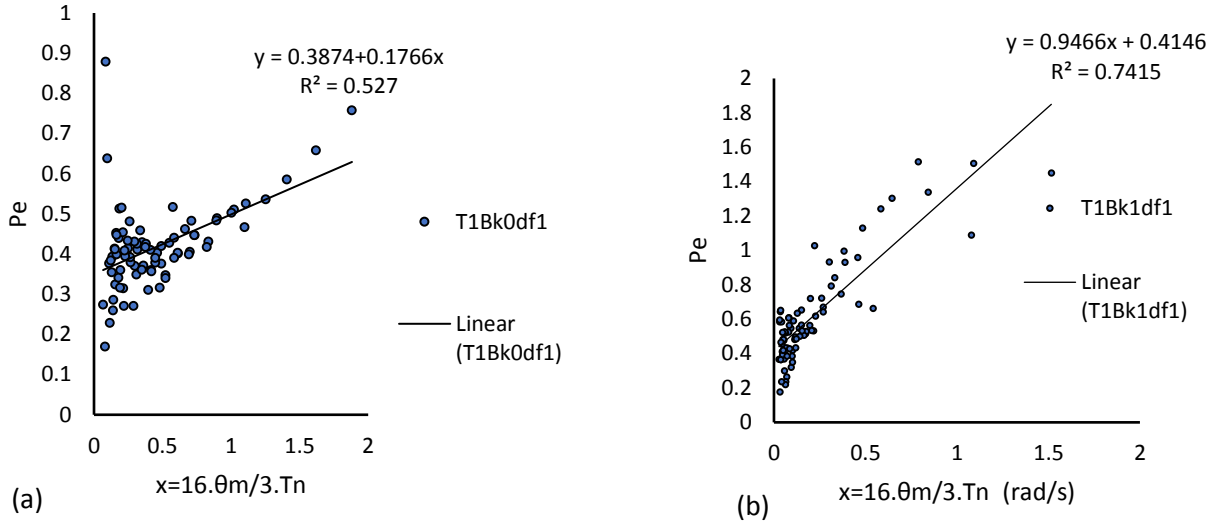

Figure 3.10 Faltinsen Polynomial technique for (a) bare hull (b)hull with bilge keel

The equivalent linearized damping coefficient is also obtained by similar minimization as represented in equations. 3.27 and 3.28, with $\beta_3 = 0$.

3.4.2 *Non-polynomial models:*

Non-polynomial methods do not rely on truncation of a polynomial series to formulate the model relationship. The Hyperbolic model and its modification are presented in this section.

3.4.2.1 *Hyperbolic model, (Oliveira and Fernandez 2014).*

This approach which is an extension of the bilinear method, is rooted in the surrounding physics of vortex shedding behavior noticed during model test, which considers the large energy dissipation region caused by the effect of big vortices on the water dynamic pressure over the FPSO bottom side. This phenomenon is commonly developed around bilge keels and sharp edges. The name bilinear is due to the existence of a dual approximate linear behavior in the damping evolution observed in between the small and large angle decay regions during roll decay. (Oliveira and Fernandez, 2006; Fernandez and Kroft, 2000)

The modified Bilinear model proposed by (Oliveira and Fernandez, 2009) gave a better prediction for both small and large angles, with a better capture of the vortex shedding due to bilge keel and bare hull motions. The damping ratio is expressed as a continuous function dependent on the roll angle and velocity as given in equation 3.31.

$$\beta_{BL}(\theta,\dot{\theta}) = \beta_{bS} + (\beta_{bl} - \beta_{bS}).tanh\left[\alpha\,.\left(\theta^2 + \frac{\dot{\theta}^2}{\omega_n^2}\right)\right] \qquad (3.32)$$

Replacing the envelope function in the original bilinear model with equation 3.32, yields the modified bi-linear model referred to as hyperbolic model.

Thus: substituting

$\beta_{BL}(\theta_e(t)) = \beta_{BL}(\theta,\dot{\theta})$ into equation 3.21

$$\ddot{\theta} + 2\beta_{BL}(\theta_e(t)).\omega_n\,\dot{\theta} + \omega_{nat}^2\,.\theta = f(\omega_n,\zeta) \qquad (3.33)$$

Yields:

$$\ddot{\theta} + 2\left(\beta_{bS} + (\beta_{bl} - \beta_{bS}).tanh\left[\alpha\,.\left(\theta^2 + \frac{\dot{\theta}^2}{\omega_n^2}\right)\right]\right)\omega_{nat}\,\dot{\theta} + \omega_{nat}^2\,.\theta = f(\omega_n,\zeta) \qquad (3.34)$$

Equation 3.34 was built on the behavior of hyperbolic tangent as in figure 3.18. Note that the $\beta_{bl}\ and\ \beta_{bS}$ are the normalized damping coefficients for the two linearly assumed regions of the decay; for large angle and small angle regions respectively. These parameters are estimated by fitting the model of equation 3.32 and implementing the optimization technique adopted for other procedures. The typical curve for the example samples are captured in figures 3.11 below.

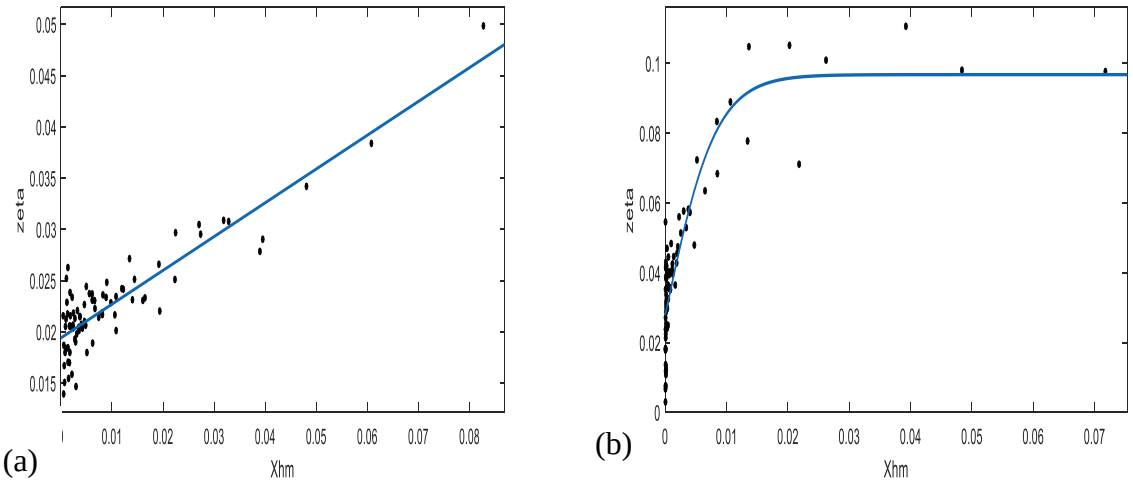

Figure 3.11 (a) Hyperbolic model for T1Bk0df2 showing1-region: (b) Hyperbolic model for T1Bk1df2 showing 2-regions: (TR same as LVM algorithm)

β_{BL} is the overall local damping coefficient. This parameter is obtained by minimizing as usual the error represented by the equation below;

$$\boldsymbol{E}(\beta_{eq}) = \left[\beta_{BL} - \left(\beta_{bS} + (\beta_{bl} - \beta_{bS}).\, tanh\left[\alpha\,.\left(\theta^2 + \frac{\dot{\theta}^2}{\omega_n^2}\right)\right]\right)\right]^2 \qquad (3.35)$$

The global linearized damping is again then estimated according to equation 3.29 as;

$$B_{eq} = 2 * \beta_{eqhm} * (I_{44} + i_{44}) * \omega_n \qquad (3.36)$$

3.4.2.1 *Regression model of Oliveira and Fernandez via dimensional analysis*

As follow up from the recommendations that their regression model can be expanded to possibly increase its accuracy by including other FPSO data from test (Oliveira and Fernandes, 2012), this section examines the sensitivity of the prediction by this model when additional data from the test conducted from this research was included. The regression model was built based on the combination of different dimensionless ratios obtained from hull and bilge keel dimensions. the following dimensionless ratios defined below were used in the regression procedure.

$$\left[x1 = \frac{d}{B}; x2 = \frac{b_{bk}}{B}; x3 = \frac{l_{bk}}{B}; x4 = \frac{g.T_n^2}{B}\right]$$

The generalized equations are shown below

$$\xi_L = g1[x1, x2, x3, x4] \qquad (3.37)$$

$$\xi_S = g2[x1, x2, x3, x4] \qquad (3.38)$$

$$\alpha = g3[x1, x2, x3, x4] \qquad (3.39)$$

The final equation is expressed as:

$$\xi_L = a0 + a1(x1.x2.x3.x4) + a2(x1.x2.x4) + a3(x2.x3.x4) + a4(x2.x4) + a5(x1.x3.x4) + a6(x1.x4) + a7(x2.x4) + a8(x4) + a9(x1.x2.x3) + a10(x1.x2) + a11(x2.x3) + a12(x2) + a13(x1.x3) + a14(x1) + a15(x3.) + a16(x1.x2.x3.(x4)^2) \qquad (3.40)$$

Similar equations were also used to represent ξ_S *and* α , with the coefficients been b0 to b16, and c0 to c16 respectively. Estimates resulting from this method are presented in the subsequent sections 3.4.3 and 3.4.4.

3.4.2.2 *Modified Hyperbolic Model:*

By careful observation of the free decay data used for the determination of the coefficients, research has shown that there are at least two regions characterizing the small and the large angle roll regimes. This property is very conspicuous for hulls with sharp edges or bilge keels where vortex effect is predominant. The hyperbolic model has been used to successfully model the two regimes for a motion with inherent vortex. However, the transition from the small angle motion to the large angle motion is still elusive, even though the cumbersome bilinear method approach can be used to identify the transition point rather than the region. It is thus significant to attempt to identify this region by also introducing a damping value associated to it. To achieve this, a first attempt was made where the existing hyperbolic model was perturbed by an additional hyperbolic tangent term as shown in figure 3.13 below, this was done in consonance with the observable scatter or trend in data at the large angle side.

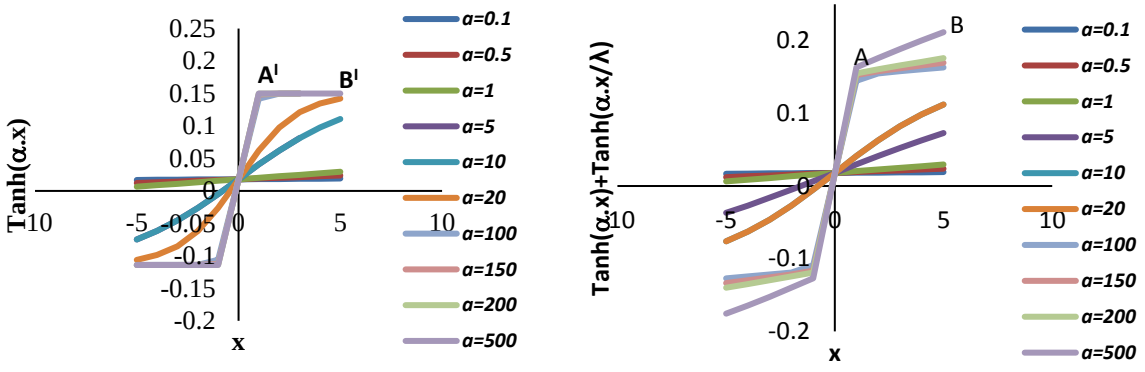

(a) (b)

Figure 3.12 The behaviour of the hyperbolic tan function wrt to α (a) tanh(αx) function (b) sum of tanh(αx).

Relying on the behavior of the additional hyperbolic tangent '***tanh***' term from figures 3.12b, the general model was represented by equation. 3.41

$$\beta_{BL}(\theta,\dot{\theta}) = \beta_{bS} + (\beta_{bl} - \beta_{bS}).\left\{tanh\left[\alpha\,.\left(\theta^2 + \frac{\dot{\theta}^2}{\omega_n^2}\right)\right] + \tanh\left[\frac{\alpha}{\lambda}\,.\left(\theta^2 + \frac{\dot{\theta}^2}{\omega_n^2}\right)\right]\right\} \tag{3.41}$$

Testing the behavior of the parameter $\boldsymbol{\lambda}$ (regarded as a scale parameter) on data, to the overall model, it was observed that as the value increases, the model approached the original hyperbolic model. $\boldsymbol{\lambda}$ is a scaling parameter introduced for purpose of tuning to ensure better damping fitting resulting from the influence of the addition of the tanh term on the original hyperbolic model. However, at some values, the change in $\mathbf{R^2}$ values became constant. Thus, it was necessary to choose a reasonable value around 100, to test this model. The value of the entire addition represented a small perturbation which tried to shift the line $\mathbf{A^IB^I}$ as in figure 3.12a to AB in figure 3.12b, which represented the visually observed trend in the grouped data set. (see also data in Allan and Fernandez, 2010).

With

$$Xhm = \theta^2 + \frac{\dot{\theta}^2}{\omega_n^2} \tag{3.42}$$

$$\beta_{BL}(\theta,\dot{\theta}) = \beta_{BL}(Xhm) = \beta_{bS} + (\beta_{bl} - \beta_{bS}).\{\tanh[\alpha\,.\,(Xhm)]\} \tag{3.43}$$

Incorporating the perturbation term,

$$\beta_{BL}(Xhm) = \beta_{bS} + (\beta_{bl} - \beta_{bS}).\left\{tanh[\alpha\,.\,(Xhm)] + \tanh\left[\frac{\alpha}{100}\,.\,(Xhm)\right]\right\} \tag{3.44}$$

$$\beta_{BL}(Xhm) = \beta_{bS} + (\beta_{bl} - \beta_{bS}).\left\{tanh[\alpha\,.\,(Xhm)] + \tanh\left[\frac{\alpha}{100}\,.\,(Xhm)\right]\right\} \tag{3.45}$$

The optimization can be performed by either using a 3D plot of $(\theta^2, \dot{\theta}^2, \beta_{BL})$ or a 2D fitting of (Xhm, β_{BL}), were Xhm is used to linearize the quadratic terms used in the 2D fit. However, both procedures yielded the same values for the optimized equation coefficients sorted.

The simulated roll decay curve, for the proposed equations 3.41 and 3.45 was tested against traditional methods like the differential equation fitting (DEFT) (limited to Froude's approach and an inclusion of the cubic term) and Energy methods (restricted to Faltinsen methods) and that of the original Hyperbolic Model.

The Hyperbolic model was built based on behavior of the hyperbolic Tanh curve, however the addition of a second hyperbolic term, which could capture the region after the rapidly increasing damping coefficient with a rather slowly reducing damping rate as against the rapid decay to a saturation value could be tracked. The region AB is associated with the beginning part of the roll decay, i.e. the large angle region of the decay data. The motion gradually decreases during the early portion of the decay, this continues as the vessel continue to dissipate its energy, at some point there is a commencement of rapid decrease of local damping coefficient as the motion gradually dies out. Both methods were tested using the Levenberg-Marquardt, non-linear least square algorithm of the MATLAB. The prediction using simulated roll decay from the Runge-Kutta method of MATLAB, showed reasonable agreement between the proposed method, the original hyperbolic model and the industry based Faltinsen (see Orji and Woodward, 2015). There were discrepancies in the Froude method which showed its comparative limitation for hulls with bilge keels. This modification however failed to yield the desired result of identifying the transition region in a parametric sense.

Thus, relying on simple formulation of Oliveira and Fernandez, the equation of 3.32, was applied with the assumption that there are in existence 3-regions, the small angle side, the transition and the large angle region defined by different damping rates $\beta_{bS}, \beta_{bT}, and\ \beta_{bL}$, respectively. There are also two slope control parameters α and α1, which are used to model the connecting linearities in such a way as to obtain a least square error fit between the data and the formulation.

The resulting mathematical equation 3.46 was derived:

$$\beta_{BL}(Xhm) = \{\beta_{bS} + (\beta_{bT} - \beta_{bS}).tanh[\alpha\ .(Xhm)]\} + \{\beta_{bL} - (\beta_{bS} + (\beta_{bT} - \beta_{bS}).tanh[\alpha\ .(Xhm)]\}.tanh[\alpha 1\ .(Xhm)] \quad (3.46)$$

Equation 3.46 was reduced to equation 3.47 using a quick regression test which confirmed the generation of similar results for parameters and including the goodness of fit between them.

$$\beta_{BL}(Xhm) = \beta_{bS} + (\beta_{bT} - \beta_{bS}).tanh[\alpha\ .(Xhm)] + (\beta_{bL} - \beta_{bT}).\ tanh[\alpha 1\ .(Xhm)] \quad (3.47)$$

The equation 3.47 was tested on the T1Bk1df2 data set, the regression performed using Levermberge-Marqaudt, Trust region and the Gauss-Newton Technique to carry out least square procedure for parameter identification. See figure 3.13 where a conspicuous 3-regions was identified by model as against the normal hyperbolic model in figure 3.11 for the same data set.

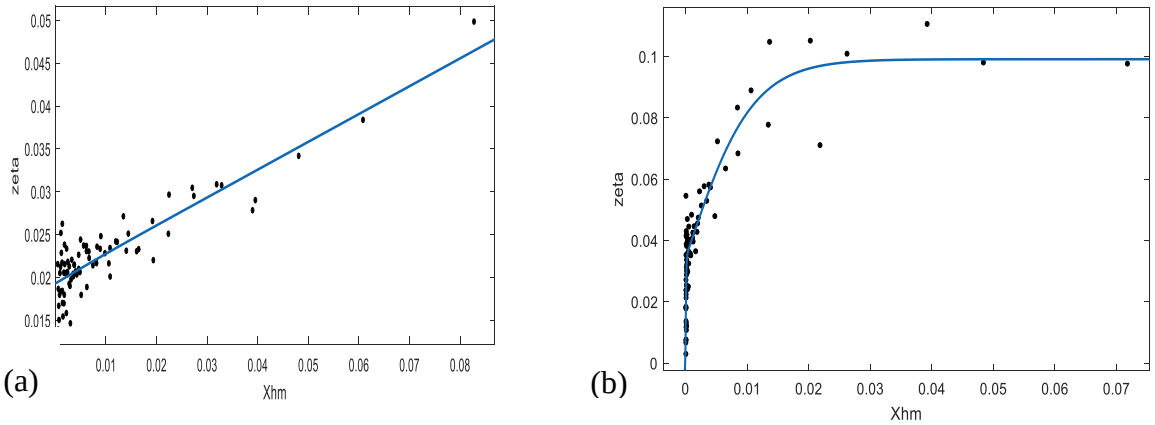

Figure 3.13 (a) Modified Hyperbolic model for T1Bk0df2 showing1-region: (b) Modified Hyperbolic model (equation 3.47) for T1Bk1df2 showing 3-regions: (TR same as LVM algorithm)

Table 3.12 presents the sample results obtained from test data of T1Bk0df2, T1Bk1df1, and T1Bk1df2 test cases.

Table 3.12 Sample application of the modified hyperbolic model

	T1Bk0df2												
Optim. meth	β_{bL}	β_{bs}	α	R^2	β_1	β_2	R^2	β_{bL}	β_{bT}	β_{bS}	α	α 1	R^2
LVM	1.223	0.0194	0.274	0.794	0.229	0.1924	0.7304	1.372	0.0196	0.01931	95.56	0.24	0.7942
TRSreg	0.1198	0.01957	3.133	0.7902	0.229	0.1924	0.7304	0.1019	0.02517	0.01817	96.91	1.483	0.794
G-N	0.3479	0.019473	0.746167	-	0.22904	0.1924	0.730	0.08868	0.02701	0.08119	5.7744	8363.12	-
	T1Bk1df1												
Optim. meth	β_{bL}	β_{bs}	α	R^2	β_1	β_2	R^2	β_{bL}	β_{bT}	β_{bS}	α	α 1	R^2
LVM	0.09526	0.03092	121.6	0.7746	0.4063	0.9616	0.7316	0.09833	0.04355	0.02732	956.8	78.73	0.7833
TRSreg	0.09531	0.03093	121.6	0.7746	0.4063	0.9616	0.7316	0.09832	0.04353	0.02732	958.4	78.8	0.7833
G-N	0.096	0.023	117.773	-	0.4146	0.9466	0.7415	0.0938	0.04455	0.02934	712.89	77.2426	-
	T1Bk1df2												
Optim.meth	β_{bL}	β_{bs}	α	R^2	β_1	β_2	R^2	β_{bL}	β_{bT}	β_{bS}	α	α 1	R^2
LVM	0.09648	0.02726	124.3	0.8058	0.3535	0.9936	0.7532	0.0989	0.03353	0.002707	11520	95.46	0.8607
TRSreg	0.09651	0.02727	124.1	0.8058	0.3535	0.9936	0.7532	0.0989	0.03354	0.002739	11490	95.42	0.8607
G-N	0.09676	0.027875	120.831	-	0.3608	0.9819	0.7575	0.09955	0.03472	0.01461	6586.34	90.682	-

Using the regression coefficient to assess the goodness of fit of the model for the design draft df2, the modified model with a R^2 value of about 6% above that of the hyperbolic model shows a better performance in the data capture for the hull with the bilge keel. However, no significantly enhanced performance was noticed for hulls without bilge keels. This results from the fact that such hulls display damping characteristics that are largely linear and thus does not have zones with varying characterization or a possible transition regime as well. The transition region can further be validated using the rigorous bilinear method in which the transition point was observed to fall within the predicted transition region. The pattern is significantly consistent for the other configurations which can be seen in appendix I.

3.4.3 *Model coefficient estimates using least square optimization*

The data set from appendix I was used to carry out the optimization to estimate the local as well as the global damping coefficient for the different experiment configurations used. Critical amongst the derivable results using equation 3.1 are the local natural frequencies presented in table 3.13.

Table 3.13 Roll natural frequencies of experiment cases

	model		actual Ship	
Configuration	T_n (s)	w_n(rad/s)	T_n (s)	w_n (rad/s)
T1bk0df1	0.850	7.392	9.617	0.653
T1bk0df2	0.871	7.214	9.855	0.638
T1bk1df1	0.880	7.142	9.953	0.631
T1bk1df2	0.898	6.998	10.158	0.619
T1bk2df1	0.878	7.160	9.928	0.633
T1bk2df2	0.876	7.170	9.914	0.634
T1bk0df3	0.987	6.366	11.166	0.563
T1bk1df3	1.008	6.234	11.402	0.551

The summary of the results obtained from different methods are presented below in the tables 3.14-3.23.

Table 3.14 Estimates from Froude method (model)

Configuration	Model coefficient						$I_{44}+i_{44}$	B_{44}	B_{44crit}	ξ_{crit}
	a1	a2	β_1	β_2	R^2	β_{44}	(kgm^2)	(Nsm)	(Nsm)	(-)
T1bk0df1	0.117	0.620	0.552	0.465	0.989	0.581	0.240	0.140	3.553	0.039
T1bk0df2	0.073	0.701	0.335	0.526	0.978	0.363	0.321	0.116	4.624	0.025
T1bk1df1	0.310	1.385	1.407	1.039	0.968	1.524	0.257	0.392	3.677	0.107
T1bk1df2	0.333	1.248	1.484	0.936	0.970	1.599	0.341	0.545	4.766	0.114
T1bk2df1	0.235	1.223	1.073	0.917	0.963	1.173	0.256	0.301	3.668	0.082
T1bk2df2	0.237	1.182	1.082	0.887	0.968	1.169	0.324	0.379	4.651	0.082
T1bk0df3	0.020	1.086	0.080	0.815	0.988	0.127	0.544	0.069	6.928	0.010
T1bk1df3	0.130	1.439	0.517	1.079	0.976	0.678	0.567	0.385	7.075	0.054

Table 3.15 Estimates from Froude method (actual ship)

			$I_{44}+i_{44}$	B_{44}	B_{44crit}	ξ_{crit}
Configuration	β_{44}	β_{44} %	(kgm^2)	(Nsm)	(Nsm)	(-)
T1bk0df1	0.0514	5.137	8.258E+09	4.242E+08	1.079E+10	0.039
T1bk0df2	0.0321	3.207	1.101E+10	3.531E+08	1.404E+10	0.025
T1bk1df1	0.1347	13.47	8.846E+09	1.191E+09	1.117E+10	0.107
T1bk1df2	0.1413	14.13	1.170E+10	1.654E+09	1.447E+10	0.114
T1bk2df1	0.1037	10.37	8.802E+09	9.128E+08	1.114E+10	0.082
T1bk2df2	0.1033	10.33	1.114E+10	1.152E+09	1.413E+10	0.082
T1bk0df3	0.0112	1.124	1.870E+10	2.101E+08	2.104E+10	0.01
T1bk1df3	0.0599	5.993	1.950E+10	1.168E+09	2.149E+10	0.054

Table 3.16 Estimates from cubic method (model)

	Model coefficient								B_{44}	B_{44crit}	ξ_{crit}
Config	a1	a2	a3	β_1	β_2	β_3	R^2	β_{44}	(Nsm)	(Nsm)	(-)
T1bk0df1	0.160	0.007	1.746	0.751	0.005	0.201	0.993	0.905	0.181	3.553	0.051
T1bk0df2	0.140	-0.291	2.980	0.643	-0.219	0.351	0.991	0.700	0.203	4.624	0.044
T1bk1df1	0.159	4.091	-9.087	0.723	3.068	-1.080	0.977	2.141	0.271	3.677	0.074
T1bk1df2	0.109	4.955	-11.77	0.487	3.716	-1.428	0.987	2.244	0.313	4.766	0.074
T1bk2df1	0.084	3.715	-7.735	0.384	2.786	-0.917	0.977	1.774	0.173	3.668	0.047
T1bk2df2	0.079	4.012	-9.459	0.360	3.009	-1.120	0.984	1.749	0.208	4.651	0.045
T1bk0df3	0.070	0.489	1.335	0.285	0.367	0.178	0.970	0.764	0.167	6.928	0.024
T1bk1df3	0.087	2.007	-1.374	0.344	1.505	-0.187	0.980	1.361	0.292	7.075	0.041

Table 3.17 Estimates from cubic method (actual ship)

			B_{44}	B_{44crit}	ξ_{crit}
Configuration	β_{44}	β_{44} %	(Nsm)	(Nsm)	(-)
T1bk0df1	0.067	6.651	5.492E+08	1.079E+10	0.0509
T1bk0df2	0.056	5.596	6.162E+08	1.404E+10	0.0439
T1bk1df1	0.093	9.292	8.219E+08	1.117E+10	0.0736
T1bk1df2	0.092	9.198	1.076E+09	1.447E+10	0.0743
T1bk2df1	0.06	5.971	5.256E+08	1.114E+10	0.0472
T1bk2df2	0.057	5.673	6.323E+08	1.413E+10	0.0448
T1bk0df3	0.027	2.711	5.068E+08	2.104E+10	0.0241
T1bk1df3	0.045	4.543	8.857E+08	2.149E+10	0.0412

Table 3.18 Estimates from Faltinsen method; (model)

					B_{44}	B_{44crit}	ξ_{crit}
Configuration	β_1	β_2	R^2	β_{44}	(Nsm)	(Nsm)	(-)
T1bk0df1	0.350	0.148	0.264	0.360	0.086	3.553	0.024
T1bk0df2	0.229	0.192	0.730	0.239	0.077	4.624	0.017
T1bk1df1	0.405	0.947	0.732	0.514	0.132	3.677	0.036
T1bk1df2	0.354	0.994	0.753	0.476	0.162	4.766	0.034
T1bk2df1	0.396	0.646	0.545	0.466	0.119	3.668	0.033
T1bk2df2	0.498	0.487	0.192	0.545	0.177	4.651	0.038
T1bk0df3	0.148	0.251	0.274	0.162	0.088	6.929	0.013
T1bk1df3	0.263	0.532	0.451	0.500	0.284	7.075	0.040

Table 3.19 Estimates from Faltinsen method; (actual ship)

			B_{44}	B_{44crit}	ξ_{crit}
Configuration	β_{44}	β_{44} %	(Nsm)	(Nsm)	(-)
T1bk0df1	0.032	3.181	2.626E+08	1.079E+10	0.024
T1bk0df2	0.021	2.114	2.328E+08	1.404E+10	0.017
T1bk1df1	0.045	4.546	4.021E+08	1.117E+10	0.036
T1bk1df2	0.042	4.205	4.919E+08	1.447E+10	0.034
T1bk2df1	0.041	4.122	3.628E+08	1.114E+10	0.033
T1bk2df2	0.048	4.819	5.370E+08	1.413E+10	0.038
T1bk0df3	0.014	1.436	2.684E+08	2.104E+10	0.013
T1bk1df3	0.044	4.422	8.621E+08	2.149E+10	0.04

Table 3.20 Estimates from Hyperbolic model; (model)

	Model coefficient						B_{44}	B_{44crit}	ξ_{crit}
configuration	ζl	ζs	α	R^2	ζ_{bl44}	β_{44}	(Nsm)	(Nsm)	(-)
T1bk0df1	0.076	0.025	6.136	0.550	0.028	0.408	0.098	3.553	0.028
T1bk0df2	0.122	0.019	0.274	0.790	0.020	0.284	0.091	4.624	0.020
T1bk1df1	0.095	0.031	121.600	0.790	0.043	0.609	0.157	3.677	0.043
T1bk1df2	0.097	0.027	124.300	0.815	0.042	0.593	0.202	4.766	0.042
T1bk2df1	0.084	0.031	58.390	0.581	0.040	0.569	0.146	3.668	0.040
T1bk2df2	0.080	0.029	74.180	0.648	0.038	0.543	0.176	4.651	0.038
T1bk0df3	0.062	0.047	11.410	0.291	0.018	0.226	0.123	6.929	0.018
T1bk1df3	0.097	0.025	20.420	0.475	0.032	0.396	0.225	7.075	0.032

Table 3.21 Estimates from Hyperbolic model (actual unit)

			B_{44}	B_{44crit}	ξ_{crit}
configuration	β_{44}	β_{44} %	(Nsm)	(Nsm)	(-)
T1bk0df1	0.036	3.604	2.976E+08	1.079E+10	0.028
T1bk0df2	0.025	2.51	2.763E+08	1.404E+10	0.02
T1bk1df1	0.054	5.381	4.760E+08	1.117E+10	0.043
T1bk1df2	0.052	5.243	6.134E+08	1.447E+10	0.042
T1bk2df1	0.05	5.029	4.426E+08	1.114E+10	0.04
T1bk2df2	0.048	4.798	5.347E+08	1.413E+10	0.038
T1bk0df3	0.02	1.998	3.735E+08	2.104E+10	0.018
T1bk1df3	0.035	3.503	6.829E+08	2.149E+10	0.032

Table 3.22 Estimates from Modified Hyperbolic model; (model unit)

	Model coefficient								B_{44}	B_{44crit}	ξ_{crit}
Configuration	ζl	ζlT	ζs	α	α1	R^2	ζ_{bl44}	β_{44}	(Nsm)	(Nsm)	(-)
T1bk0df1	0.081	0.030	0.027	367	6.225	0.550	0.031	0.463	0.111	3.553	0.031
T1bk0df2	0.089	0.027	0.081	8363	5.774	0.790	0.023	0.327	0.105	4.624	0.023
T1bk1df1	0.098	0.044	0.027	956.8	78.730	0.783	0.042	0.605	0.156	3.677	0.042
T1bk1df2	0.099	0.034	0.003	11520	95.460	0.861	0.043	0.597	0.203	4.766	0.043
T1bk2df1	0.088	0.054	0.031	99.75	33.000	0.583	0.040	0.569	0.146	3.668	0.040
T1bk2df2	0.083	0.038	0.027	331.2	51.730	0.681	0.037	0.536	0.174	4.651	0.037
T1bk0df3	0.094	0.017	0.010	298.8	5.587	0.521	0.018	0.226	0.123	6.928	0.018
T1bk1df3	0.109	0.038	0.025	94.56	12.140	0.480	0.032	0.396	0.225	7.075	0.032

Table 3.23 Estimates from Modified Hyperbolic model (actual ship)

			B_{44}	B_{44crit}	ξ_{crit}
configuration	β_{44}	β_{44} %	(Nsm)	(Nsm)	(-)
T1bk0df1	0.041	4.095	3.382E+08	1.079E+10	0.031
T1bk0df2	0.0289	2.891	3.184E+08	1.404E+10	0.023
T1bk1df1	0.0534	5.344	4.727E+08	1.117E+10	0.042
T1bk1df2	0.0528	5.278	6.175E+08	1.447E+10	0.043
T1bk2df1	0.0503	5.029	4.426E+08	1.114E+10	0.04
T1bk2df2	0.0474	4.737	5.279E+08	1.413E+10	0.037
T1bk0df3	0.02	1.997	3.734E+08	2.104E+10	0.018
T1bk1df3	0.035	3.504	6.831E+08	2.149E+10	0.032

From the application of the regression model on the estimated parameters from the hyperbolic model, the resulting optimized coefficients (a0-a16, b0-b16 and c0-c16) obtained from the data of Oliveira and Fernandez and the enhanced data set are in appendix J**.** The comprehensive result obtained using the unenhanced coefficient and the enhanced coefficients are captured in appendix K. The summary of the relevant results obtained is shown below in table 3.24. When this model was used to estimate the damping parameters of the experimental data, the results shown in table 3.24 were obtained.

Table 3.24 Damping parameter estimate from Regression method

								oliveira and Fernandez						Enhanced data set					
	input (non-dimensionalized)				output (measured)			predicted			error			predicted			error		
CASE	T/B	b_{bk}/B	L_{bk}/B	gT_n^2/B	ζ_L	ζ_s	α	ζ_L	ζ_s	α	$\zeta_{L\,er}$	$\zeta_{s\,er}$	α_{er}	ζ_L	ζ_s	α	$\zeta_{L\,er}$	$\zeta_{s\,er}$	α_{er}
T1bk0df1	0.317	0	0	23.602	0.0762	0.025	6.136	-0.267	-0.064	302.08	450.15	356.03	4823.1	0.0709	0.0242	32.54	6.912	3.103	430.37
T1bk0df2	0.417	0	0	24.784	0.1223	0.0194	0.274	-0.795	-0.208	1101	750.24	1170.3	401723	0.1083	0.0296	17.41	11.48	52.51	6253
T1bk1df1	0.317	0.0326	1.5667	25.282	0.09526	0.0309	121.6	-0.008	0.0025	196.71	108.41	91.944	61.767	0.092	0.0288	151.7	3.391	6.793	24.715
T1bk1df2	0.417	0.0326	1.5667	26.332	0.09648	0.0273	124.3	-0.099	-0.025	128.58	203.04	191.24	3.447	0.0968	0.0265	91.03	0.374	2.744	26.765
T1bk2df1	0.317	0.0163	1.5667	25.157	0.08441	0.0311	58.39	0.0594	0.0223	190.27	29.666	28.402	225.85	0.0731	0.0255	123.4	13.39	18.1	111.32
T1bk2df2	0.417	0.0163	1.5667	25.082	0.08024	0.029	74.18	0.0675	0.028	252.54	15.823	3.4353	240.44	0.058	0.0276	75.95	27.69	4.607	2.3845
T1bk0df3	0.467	0	0	31.82	0.06195	0.0465	11.41	-0.693	-0.181	962.74	1217.9	488.78	8337.7	0.0786	0.0341	21.66	26.85	26.59	89.814
T1bk1df3	0.467	0.0326	1.5667	33.18	0.09726	0.0254	20.42	-0.063	-0.015	57.385	165.16	160.56	181.02	0.0896	0.0265	38.31	7.838	4.336	87.62

The sum of square error obtained from the original model of Oliveira and Fernandes for the ξ_L , ξ_S and α is 1.61, 0.116 and 2312817.29 respectively poorly compared to values of 0.005984, 0.00901 and 70265.06 from the model when the data was enhanced. It is very conspicuous to observe that the parameters are poorly predicted, presenting unrealistic values for the instance when the data was not enhanced before the regression procedure. This shows the dependence of the method on the uniqueness and the size of data used in the procedure. A further inspection on the average percent error for the estimates are 75.81%, 67.831 % and 9693.86% against those of 12.13%, 14.94% and 195.9% from the original model and the model from the enhanced data. It can also be observed that the largest set of errors are in the gradient parameter α, this however did not affect the global estimate of the damping coefficient in the same order of observed error proportion in α for the hulls with bilge keels.

3.4.4 *Models Comparison based on damping prediction*

The models were compared based on the prediction obtained for the damping coefficients, which stands as the critical parameter of interest derivable from this chapter. To achieve this with a glance, a direct compilation of the predicted values for the global damping coefficient and the critical damping ratio are plotted in figures 3.14 and 3.15 for the different cases according to the various methods.

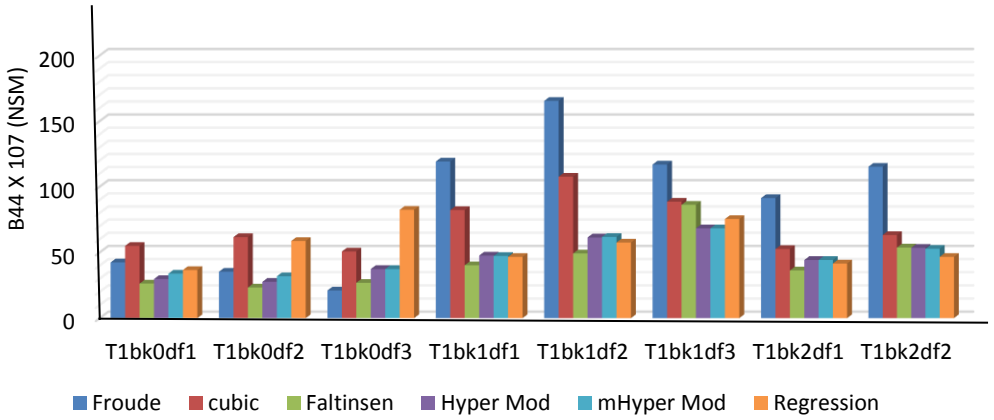

Figure 3.14 Global damping coefficients for different methods/ experiment cases

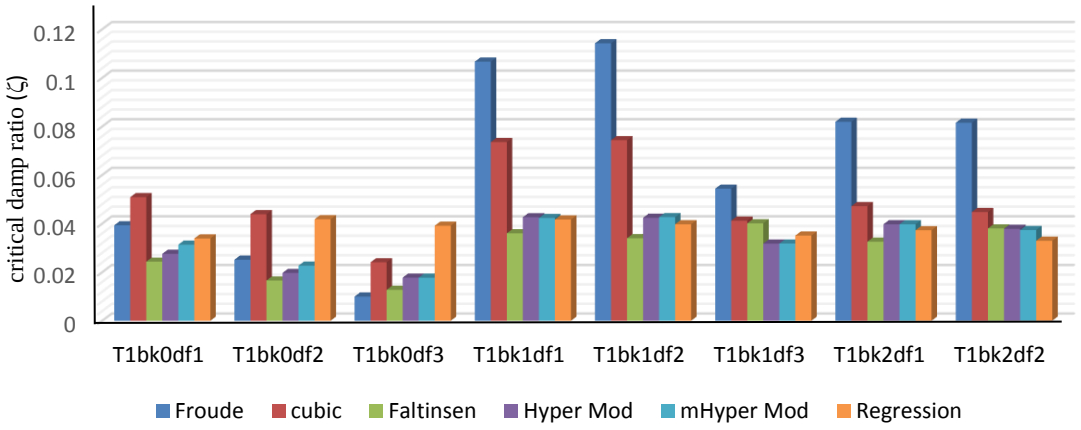

Figure 3.15 Critical damping ratio for different methods/experiment cases

It is evident that the general trend of prediction for both the global damping and the critical damping ratio are similar irrespective of the difference in the critical damping coefficient for each case**.** The critical damping coefficients were obtained by making use of the local natural frequencies from each experiment case**.** The performance of the hyperbolic and the modified hyperbolic are very similar across all cases particularly for the hulls with bilge keels. This is so because, the fundamental formulations are based technically on the same principles and they are best suited for hulls with sharp edges like the present hull in use. The Faltinsen method known as the industry method predicts the damping within reasonable differences as compared to the Froude and cubic methods. The two later methods are particularly handicapped in the prediction of such hulls because of their inability to capture the effect of vortices. Thus, there is always the tendency for these models to over predict the values which translates to an under estimation of the resulting roll amplitude when used for motion predictions. The regression model however, a product of the hyperbolic extrapolation compares favorably with the other methods except for Froude and cubic for hulls with bilge keels. See figure 3.16 for the increase in damping resulting from the effect of bilge for the different methods.

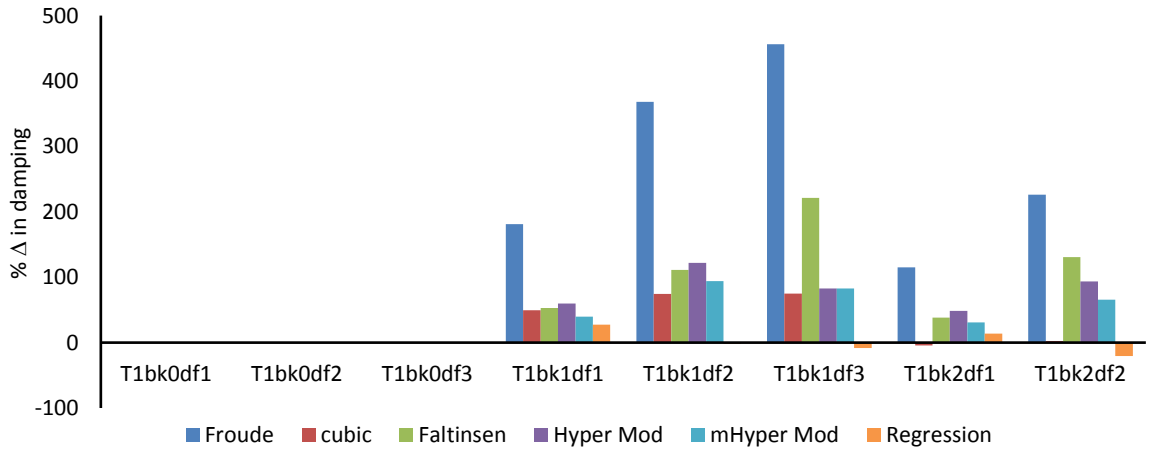

Figure 3.16 Percentage increase in damping due to bilge keel from various methods

The percentage increase predicted from methods are used comparatively to validate the usability of predictions. An engineering approximating model according to (Christopher C et al, 2011) estimates roll damping contribution from bilge keels in the range of 30-60%. From figure 3.16, the Froude method predicts a consistent high increase ranging from 115.2% for T1bk2df1 to 456% for T1bk1df3. The prediction of cubic method depicts a valid procedure;

however, the reduction in damping for T1bk2df1 and T1bk2df2 indicts the methods acceptability. The regression method failed in this respect as its prediction of -20.7%, -8.48% and -2.04% for cases T1bk2df2, T1bk1df3 and T1bk1df2 respectively does not correlate with existing facts. The other methods are reasonably within limits, with the best verification coming from hyperbolic model and the modified form. Hence, it is instructive to state that, the values derivable from either model is used as input data for future simulations in subsequent chapters. Because of the size of simulation required, the case T1bk1df2 with the highest % increase in damping from the modified hyperbolic model was used as the test data for all simulations. Note importantly that this is also the design draft line for the FPSO used.

3.4.5 *Model comparison based on simulated roll decay using Runge-Kutta method.*

Using the optimized fit equation parameters obtained for the data set T1bk1df2a2 as shown in table 3.25., with the appropriate model equations 3.16 for Froude and cubic fit, equation 3.20 for Faltinsen and equation 3.32 for the Hyperbolic models, the Runge-Kutta Cash-Karp technique was coded in Matlab and used to solve the resulting roll equation of motion in order to simulate the roll decay data. The simulated data was validated using the measured experiment data as shown in figure 3.17 below

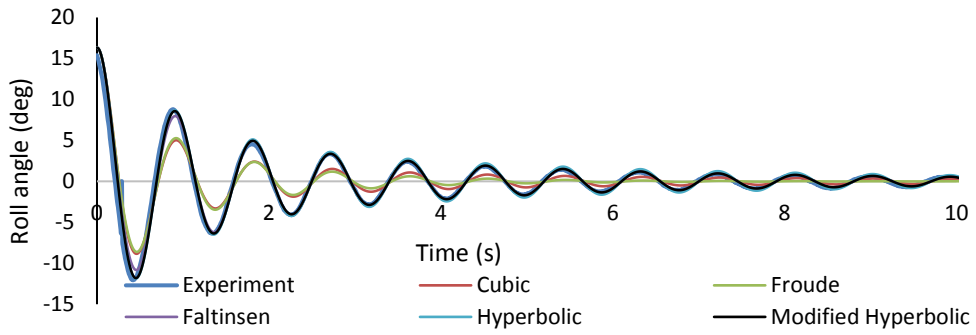

Figure 3.17 Simulated vs measured Roll angle for T1BK1df2a2

Table 3.25 Simulation parameters for T1BK1df2a2

	Fit coeff					Regress Coeff. (s-single, g-group, e-exp)			
	β_1	β_1	β_1			$R^{2\,(s)}$	$R^{2\,(e\text{-}s)}$	$R^{2\,(e\text{-}g)}$	$R^{2\,(s\text{-}g)}$
Froude	1.330	1.171	-			0.9738	0.7888	0.7918	0.9996
Cubic	0.122	5.076	-2.306			0.9927	0.8225	0.8088	0.9964
Faltinsen	0.304	1.095	-			0.8193	0.9498	0.9535	0.9996
	ξ_L	ξ_T	ξ_s	α	$\alpha 1$				
Hyperbolic	0.101	-	0.025	79.1	-	0.8707	0.9591	0.9621	0.9974
ModHypB	0.103	0.033	0.002	7699	85.84	0.9248	0.9759	0.9779	0.9994

The fit regression $R^{2\,(s)}$ is obtained from the local fitting equation used for the respective methods for single data set. This parameter gives a false indication of the extent of the overall fit. A virtual inspection of the graph of the simulated decay (figure 3.17) shows clearly that the Froude and cubic method, though having higher $R^{2\,(s)}$ values could not adequately predict the actual decay as compared to the other methods. This is very conspicuous particularly at the large angle region of the decay. The modified hyperbolic model better predicted the roll decay as it is evident from the $R^{2\,(s)}$ and $R^{2\,(e\text{-}s)}$ values of 0.9248 and 0.9759 respectively. The $R^{2\,(e\text{-}s)}$ is obtained from carrying out a linear regression between the simulated data and the measured data. When the grouped data was implemented, the trend of model performance did not change significantly compared to the single data as can be seen from the $R^{2\,(e\text{-}g)}$ and $R^{2\,(e\text{-}s)}$ values. There were slight improvements for all methods except the reduction from the cubic method. A comparison of the regression coefficient $R^{2\,(s\text{-}g)}$ obtained by comparing the simulated data from single and grouped data indicates that the grouped data is a justified means for estimating a more generalized coefficient. The plot for the calibration for modified hyper model is shown in figure 3.18. The plot for the other methods are in appendix L.

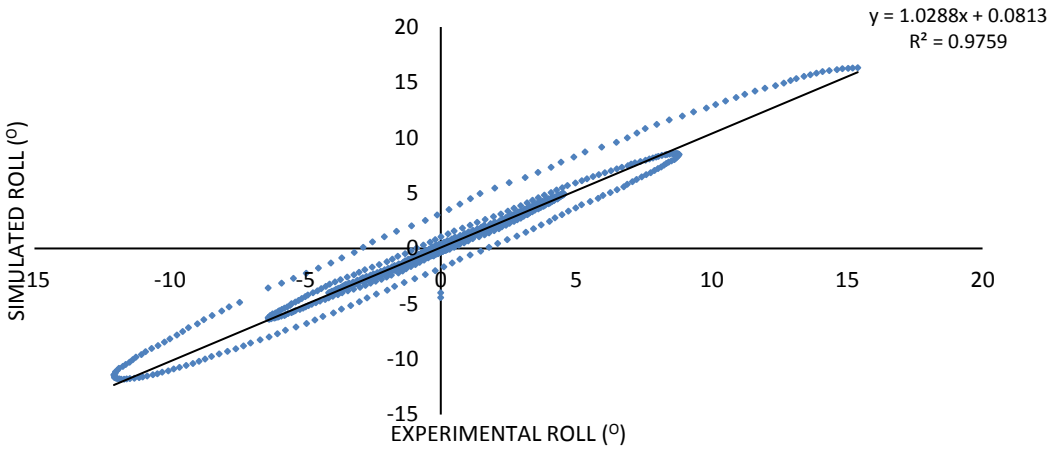

Figure 3.18 Calibration for Modified Hyper model

3.5 Transition region : Modified Hyperbolic model vs the Bilinear method of Oliveira and Fernandez

The bilinear method according to (Oliveira and Fernadez, 2006,2010) suggest that the transition point is the point with the lowest global sqaure error of possible solution. The R^2 diffrence between two consecutive fits (exponential or Linear) of the large angle and the small angle regions is then investigated for the most adherent solution. The method was applied to data set T1Bk1df2a2 for this purpose. The fits is progressively done and the table below captures the values obtained.

Table 3.26 Results of R^2 diffrenec from exponential and linear fit to data.

T1bk1df2a2				regression coeff (R^2)					
				Exponential			Linear		
s/no	t (s)	n(cycles)	θi (deg)	large angle	small angle	R^2 diff	large angle	small angle	R^2 diff
1	0	0	16.312	-	-	-	-	-	-
2	0.455	0.5	12.08132	1	0.9448	0.0552	1	0.6075	0.3925
3	0.925	1	8.78342	0.9997	0.9544	0.0453	0.9949	0.6672	0.3277
4	1.375	1.5	6.38752	0.9998	0.9632	0.0366	0.9848	0.7351	0.2497
5	1.835	2	4.53089	0.9995	0.9689	0.0306	0.9739	0.7906	0.1833
6	2.3	2.5	4.15216	0.9842	0.9684	0.0158	0.9334	0.7958	0.1376
7	2.755	3	3.35139	0.9805	0.9714	0.0091	0.9047	0.8269	0.0778
8	3.2	3.5	2.8785	0.9754	0.9723	0.0031	0.8768	0.8443	0.0325
9	3.65	4	2.42556	0.9733	0.9733	0	0.0853	0.8628	0.7775
10	4.11	4.5	2.16087	0.9688	0.9728	0.004	0.8288	0.8718	0.043
11	4.56	5	1.83186	0.9678	0.9733	0.0055	0.8086	0.8872	0.0786
12	5.01	5.5	1.67112	0.9641	0.9714	0.0073	0.7878	0.8896	0.1018
13	5.445	6	1.46865	0.962	0.9713	0.0093	0.0769	0.9005	0.8236
14	5.89	6.5	1.29776	0.9608	0.9706	0.0098	0.7517	0.0909	0.6608
15	6.34	7	1.11002	0.962	0.9688	0.0068	0.7366	0.9136	0.177
16	6.8	7.5	1.10929	0.957	0.962	0.005	0.7194	0.8984	0.179
17	7.2	8	0.95369	0.9559	0.9682	0.0123	0.7045	0.9227	0.2182
18	7.68	8.5	0.86378	0.9551	0.9691	0.014	0.6905	0.9334	0.2429
19	8.13	9	0.73283	0.9569	0.9735	0.0166	0.6782	0.9556	0.2774
20	8.585	9.5	0.7054	0.9562	0.9649	0.0087	0.6654	0.9414	0.276
21	9.035	10	0.67883	0.9535	0.9533	0.0002	0.6525	0.9263	0.2738
22	9.455	10.5	0.57947	0.9539	0.9622	0.0083	0.6411	0.9536	0.3125
23	9.87	11	0.57854	0.9514	0.9512	0.0002	0.6292	0.9357	0.3065
24	10.345	11.5	0.53356	0.9494	0.9413	0.0081	0.6178	0.9298	0.312
25	10.81	12	0.49867	0.9475	0.9206	0.0269	0.6069	0.9112	0.3043
26	11.245	12.5	0.46339	0.9458	0.9105	0.0353	0.5964	0.9086	0.3122
27	11.705	13	0.44501	0.9435	0.9892	0.0457	0.5862	0.7883	0.2021
28	12.115	13.5	0.42519	0.9408	1	0.0592	0.5761	0.0001	0.576
29	12.545	14	0.42412	-	-	-	-	-	-

The actual point is obtained by solving the resulting least R^2 difference equations. On this instance, the transition points vary slightly with values obtained being (3.146cycle, 2.2098^o) and (4.0904 cycle, 2.0466^o) for linear and exponential respectively.

Graphs from various fitting at the optimum points are captured below.

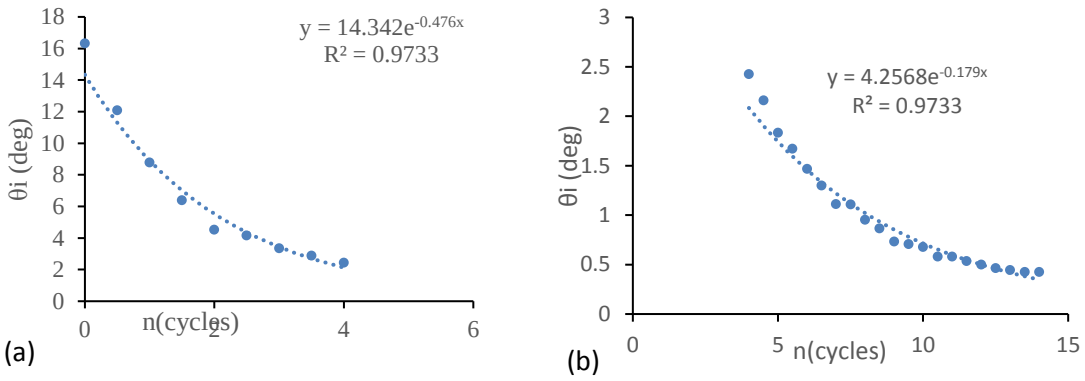

Figure 3.19 Graph of optimum point for exponential fit @n=3.5 (a)Large angle (b) Small angle

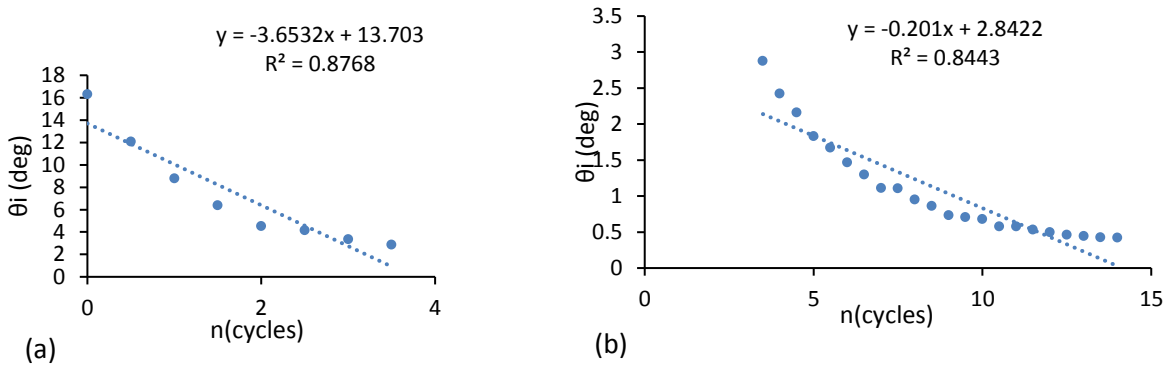

Figure 3.20 Graph of optimum point for linear fit @n=3.5 (a)Large angle (b) Small angle

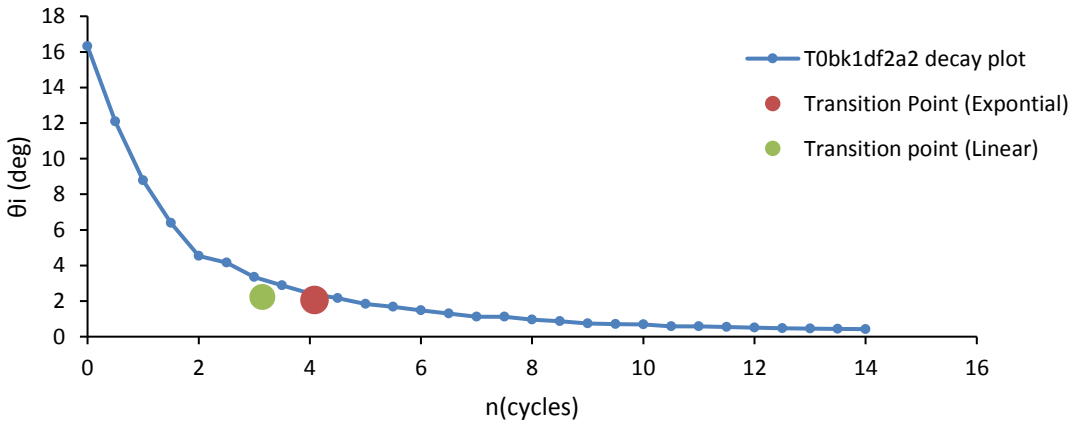

Figure 3.21 Graph showing transition points estimated from linear and exponential fits for T0Bk1df2a2

For the data, the transition points as estimated by the two fitting procedures, fall within the predicted transition range as predicted by the modified hyperbolic model for data sample.

From the optimized data for the data set, the transition region has a damping ratio of about β_{bT} =0.0335 and the saturation is at about β_{bL} =0.0989, solving the modified hyperbolic model equation for Xhm and then the corresponding cycles of occurrence. An estimated value of 7.65 cycles correspond to 0.0335 suggest that the transition occurs up till this value before possible saturation may begin to set in.

The graph of figure 3.22 below shows the suggested region commencement point to a value of (<= 7.65 cycles) which captures the values of 3.1 and 4 cycles as predicted by the bilinear methods.

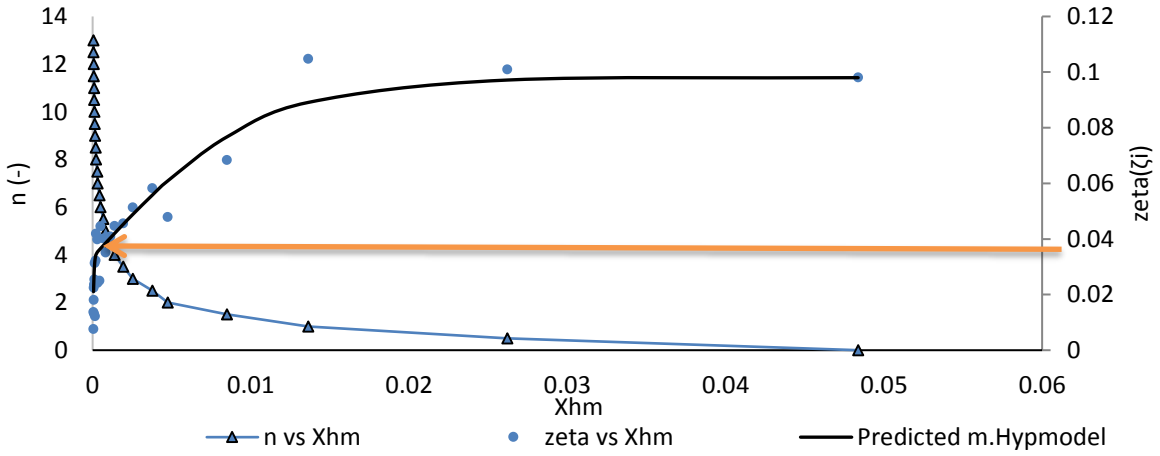

Figure 3.22 Bilinear vs modified hyperbolic model showing transition point in region.

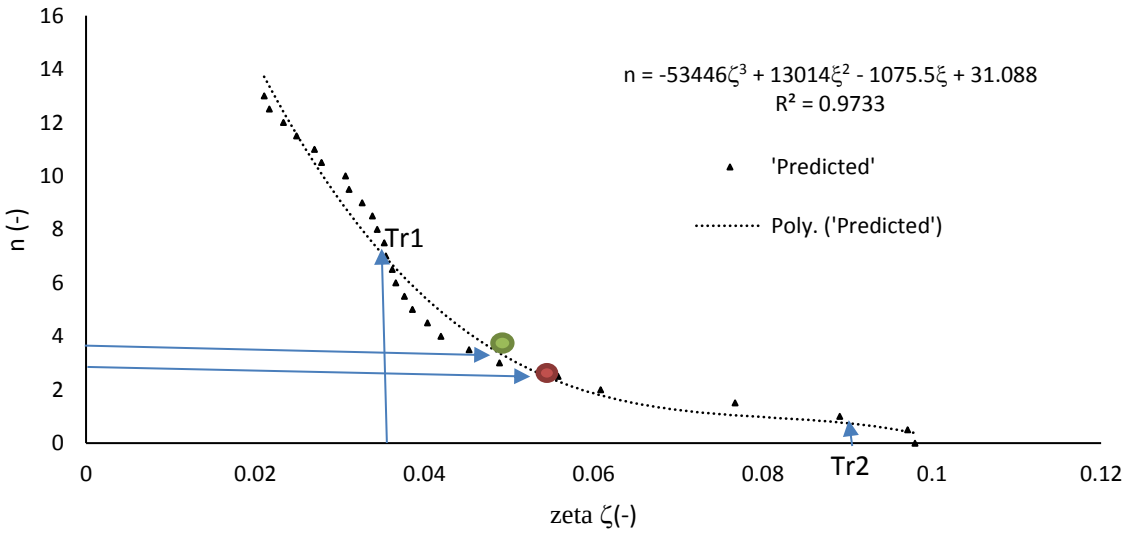

Figure 3.23 Predicted region showing Transition points by Bilinear methods within Transition region (Tr1 to Tr2) by the Modified Hyper Model

3.6 Uncertainty analysis of the Hyperbolic model estimate of mean roll damping coefficient from free decay test.

Measurement is an important aspect of our everyday life. In engineering, numerical data is used to quantify a parameter. This can be achieved either by direct measurement of the parameter (y) or by combining measurements of other parameters (x_i) upon which the primary parameter depend on. The parameter Y is termed the dependent variable and is related to the independent variable with some arbitrary function $\boldsymbol{g}$

$$Y = g(x_i) \tag{3.48}$$

In reality, no value of a parameter can be measured exactly to obtain a true value. This is because there are a lot of factors associated with the measurement process ranging from skill of operator, calibration of equipment, point to point variation, parallax in taking reading, environmental conditions, equipment scaling and resolution, procedure adopted during the exercise, repeatability and reproducibility, etc. These factors introduce errors in the parameter such that it is then only reasonable to define a measured value as composed of a best approximation within a range of possible capture. This defines a condition in which a measurand is closest to the best approximation (numerical value) but lies within a range of values (degree of uncertainty) around that value. Thus, a measurement process is not an exercise to only determine the true value of a measurand but simply an attempt to establish a reasonable range between which the true value lies. This range of values with an associated level of confidence is termed the uncertainty. The measurement can also be obtained through simulations.

Uncertainty estimate characterizes a measurand with the inclusion of the associated error terms within a confidence level. The analysis of which refers to a process of estimating the extent of impact the uncertainties in individual measurements have on the calculated result (Robert 1988). The error measures the difference between a measured value and the 'accepted' true value. There are basically two categories of errors encountered in measurement: firstly, is the Systematic error which tends to shift all measurements in a particular pattern, such that the mean is constantly displaced or changes predictably. Secondly is the random error unlike the systematic error which causes measurements to vary in an unpredictable manner. The most common way to assess random uncertainties is by replication or repeat of experiment which may not be possible particularly for very expensive experiments. Like in hydrodynamics. The combination of both errors gives the total error in the measurand.

There are basically two kinds of evaluation standards which make use of probability distribution functions in describing the characteristic of the measurand (Type A and B). Type A uncertainty analysis is carried out on repeated measurements and it allows the use of statistical analysis for evaluation. It involves the use of mean and standard deviation of the sample for the computation of the uncertainty which is taken as the standard deviation of the mean. The standard deviation of the mean indicates the amount a value averaged from several readings is expected to change from the accepted true mean. Unlike the type A, type B estimate is mainly used for system where repeatability may not be possible, thus single values are involved. If for a type A process, the repeated measurements show very poor scatter, the data is assumed to be a single value and evaluated as type B. So, for experimentation that are bounded by the type B, the standard uncertainty are evaluated based on scientific and available information on the variates, previous knowledge and properties of materials and instruments used, specified uncertainties to referenced data from handbooks, data from calibration and other reports including manufacturers specifications.

Uncertainty generally emanate from several sources not limited to: Model scaling**,** Digital signal measurement (random error)**,**Measurement equipment(s) (systematic)**,** Operator (systematic). **S**everal terms including but not limited to True value, Accuracy, Error, Trueness, Bias, Precision, Repeatability ,Reproducibility, Standard Uncertainty and Expanded uncertainty,

In this instance demonstration of uncertainty based on Repeatability is made: A measure of the precision of measurement carried out using the same methods, equipment and operator. This enables amongst other merits, easy platform for uncertainty evaluation through statistical means. It also enables the arithmetic mean to be computed which is viewed as the best estimate for the true value, identification of variations in measurement and equipment. The details of the regulations are explicitly contained in ISO guide in (JCGM,2008)**.** See **(**JCGM,2008; Stephanie,1999; ASME,1998; Fred et al,1999) for in-depth explanations of procedure).

Recall equation 3.48, let the number of independent variates be i,

for each variate, with j possible sources of uncertainty, using the quadrature rule to combine the individual uncertainties

$$u^2(x_i) = \sum_1^j u_j^2(x_i) \qquad (3.49)$$

The uncertainty $(u(x_j)$ is evaluated base on the group (type A or B) of the data set x_i.

The overall combined uncertainty for the measurand, from equation 3.48 can be written as:

$$dY = \sum_i^j \frac{\partial Y}{\partial x_i} dx_i \quad (3.50)$$

equation 3.50 can be written for small finite changes as:

$$\Delta Y = \sum_i^j \frac{\partial Y}{\partial x_i} \Delta x_i \quad (3.51)$$

With sensitivity coefficient c_i computed from equation 3.52

$$c_i = \frac{\partial Y}{\partial x_i}\Big|_{x_1, x_2, x_3, \ldots\ldots x_j} \quad (3.52)$$

Then, the total finite change in Y can be viewed as the sum of all the individual changes from the independent variables, thus:

$$\Delta Y = \sum_i^j \Delta Y_i \quad (3.53)$$

Equating equation 3.51 and equation 3.53

$$\Delta Y_i = \sum_i^j c_i \Delta x_i \quad (3.54)$$

If the change Δx_i, is caused by uncertainty $u(x_i)$ in parameter x_i, then the corresponding change in Y will be

$$u(Y_i) = u_i(Y) = c_i u(x_i) \quad (3.55)$$

Using the quadrature law, the combined uncertainty can be found to be

$$u_A^2(Y) = \sum_i^j u_i^2(Y) = \sum_i^j [c_i u(x_i)]^2 \quad (3.56)$$

For a data with a set of N_s samples of x (ensemble), the standard uncertainty associated with this kind of measurement can best be modelled using the segment method. The standard uncertainty associated with the individual test block is represented as equation 3.37

$$u_i = \frac{\sigma_i}{\sqrt{N_s}} \quad (3.57)$$

Where σ_i is mean sample standard deviation of sample set i.

The sensitivity coefficient can be determined experimentally or by direct calculation if the function is differentiable or with the use of numerical means. Uncertainty analysis of data based on repeatability can be subjected to the segment method for each of the samples, the expected variations (if any) in the standard uncertainty from each sample can convey an information regarding the contributory uncertainties from the individual repeat processes and procedures.

Equation 3.57 is multiplied by the coverage factor (k) to determine the expanded uncertainty U_A. The coverage factor is estimated by using the (=TINV(alpha, df) in excel. In this instance, for a 95 % confidence interval (alpha=0.05), and df=2, it is 4.3027.

$$U_A = k.\ u_A \qquad (3.58)$$

In this uncertainty analysis, the estimated values of the different parameters are used as the mean value, representing each sample. Hence the standard uncertainty of the mean value is estimated and used as the uncertainty to predict the extent of the effect of repeatability on the experimental procedure. Note that, in most hydrodynamic experiments, repeatability of high numbers is avoided because of cost and time. So, only three samples are presented for each of the hull/draft configurations. The optimum values of the equation parameters were obtained by applying the methods for the estimation of these values from the modified hyperbolic roll damping formulation to the time series data from the three samples (two repeats) of free decay test. Recall from equation 3.47;

$$\beta_{BL} = \beta_{bS} + (\beta_{bT} - \beta_{bS}).\, tanh[\alpha\,.(Xhm)] + (\beta_{bL} - \beta_{bT}).\ tanh[\alpha 1\,.(Xhm)] \qquad (3.59)$$

Thus; $\beta_{BL} = f(\beta_{bS}, \beta_{bT}, \beta_{bL}, \alpha, \alpha 1, \theta, \dot{\theta}, \omega_n)$ (3.60)

Since $Xhm = g(\theta, \dot{\theta}, \omega_n)$ (3.61)

Applying the quadrature law of equation 9 above. The total standard uncertainty u_{BL} of the dependent variable (β_{BL}) is;

$$u_{BL} = \sqrt{\begin{array}{c}\left(\frac{\partial \beta_{BL}}{\partial \beta_{bS}} * u_s\right)^2 + \left(\frac{\partial \beta_{BL}}{\partial \beta_{bT}} * u_T\right)^2 + \left(\frac{\partial \beta_{BL}}{\partial \beta_{bL}} * u_L\right)^2 + \left(\frac{\partial \beta_{BL}}{\partial \alpha} * u_\alpha\right)^2 + \left(\frac{\partial \beta_{BL}}{\partial \alpha 1} * u_{\alpha 1}\right)^2 \\ + \left(\frac{\partial \beta_{BL}}{\partial \theta} * u_\theta\right)^2 + \left(\frac{\partial \beta_{BL}}{\partial \dot{\theta}} * u_{\dot{\theta}}\right)^2 + \left(\frac{\partial \beta_{BL}}{\partial \omega_n} * u_{\omega_n}\right)^2\end{array}} \qquad (3.62)$$

The expanded uncertainty

$$U_{BL} = k_f * u_{BL} \qquad (3.63)$$

Where the coverage factor kf=4.3027 in this circumstance.

The sensitivities are estimated by partially differentiating equation 3.59;

Thus:

$$\frac{\partial \beta_{BL}}{\partial \beta_{bS}} = 1 - \tanh\left[\alpha\left(\theta^2 + \frac{\dot{\theta}^2}{\omega_n^2}\right)\right] \tag{3.64}$$

$$\frac{\partial \beta_{BL}}{\partial \beta_{bT}} = \tanh\left[\alpha\left(\theta^2 + \frac{\dot{\theta}^2}{\omega_n^2}\right)\right] - \tanh\left[\alpha 1\left(\theta^2 + \frac{\dot{\theta}^2}{\omega_n^2}\right)\right] \tag{3.65}$$

$$\frac{\partial \beta_{BL}}{\partial \beta_{L}} = 1 + \tanh\left[\alpha\left(\theta^2 + \frac{\dot{\theta}^2}{\omega_n^2}\right)\right] \tag{3.66}$$

$$\frac{\partial \beta_{BL}}{\partial \alpha} = (\beta_T - \beta_S)\left(\theta^2 + \frac{\dot{\theta}^2}{\omega_n^2}\right) sech^2\left[\alpha\left(\theta^2 + \frac{\dot{\theta}^2}{\omega_n^2}\right)\right] \tag{3.67}$$

$$\frac{\partial \beta_{BL}}{\partial \alpha 1} = (\beta_L - \beta_T)\left(\theta^2 + \frac{\dot{\theta}^2}{\omega_n^2}\right) sech^2\left[\alpha 1\left(\theta^2 + \frac{\dot{\theta}^2}{\omega_n^2}\right)\right] \tag{3.68}$$

$$\frac{\partial \beta_{BL}}{\partial \theta} = 2\alpha\theta\,(\beta_T - \beta_S)\left(\theta^2 + \frac{\dot{\theta}^2}{\omega_n^2}\right) sech^2\left[\alpha\left(\theta^2 + \frac{\dot{\theta}^2}{\omega_n^2}\right)\right] + 2\alpha 1\theta\,(\beta_L - \beta_T)\left(\theta^2 + \frac{\dot{\theta}^2}{\omega_n^2}\right) sech^2\left[\alpha 1\left(\theta^2 + \frac{\dot{\theta}^2}{\omega_n^2}\right)\right] \tag{3.69}$$

$$\frac{\partial \beta_{BL}}{\partial \dot{\theta}} = 2\alpha\dot{\theta}\,(\beta_T - \beta_S)\left(\theta^2 + \frac{\dot{\theta}^2}{\omega_n^2}\right) sech^2\left[\alpha\left(\theta^2 + \frac{\dot{\theta}^2}{\omega_n^2}\right)\right] + 2\alpha 1.\dot{\theta}\,(\beta_L - \beta_T)\left(\theta^2 + \frac{\dot{\theta}^2}{\omega_n^2}\right) sech^2\left[\alpha 1\left(\theta^2 + \frac{\dot{\theta}^2}{\omega_n^2}\right)\right] \tag{3.70}$$

$$\frac{\partial \beta_{BL}}{\partial \omega_n} = -2\alpha\frac{\dot{\theta}^2}{\omega_n^3}(\beta_T - \beta_S)\left(\theta^2 + \frac{\dot{\theta}^2}{\omega_n^2}\right) sech^2\left[\alpha\left(\theta^2 + \frac{\dot{\theta}^2}{\omega_n^2}\right)\right] - 2\alpha 1.\frac{\dot{\theta}^2}{\omega_n^3}(\beta_L - \beta_T)\left(\theta^2 + \frac{\dot{\theta}^2}{\omega_n^2}\right) sech^2\left[\alpha 1\left(\theta^2 + \frac{\dot{\theta}^2}{\omega_n^2}\right)\right] \tag{3.71}$$

3.6.1 *Effect of repeatability on the estimated roll damping model coefficients*

Relying on the formulation of the model roll damping coefficient of equation 3.59 according to modified hyperbolic model formulation, the error from repeatability and the uncertainty associated with the mean damping coefficient are estimated and discussed. The summary results in table 3.27 was obtained. The tabulated results are captured in figures 3.24 to 3.26.

Table 3.27: Table of estimated modified hyperbolic roll damping model coefficients from different repeat test.

Test cases	w(n)	βl	βsT	βs	α	α1	R2	βbl	b44	B44(Nsm)	% Δ B44
T1bk0df1	0.8500	0.0805	0.0295	0.0272	3.6696E+02	6.2250	0.5498	0.0313	0.0410	3.3817E+08	
T1bk0df1 (r1)	0.8404	0.0789	0.0292	0.0269	3.6309E+02	6.0064	0.5362	0.0309	0.0408	3.2933E+08	
T1bk0df1 (r2)	0.8486	0.0815	0.0302	0.0277	3.7598E+02	6.4617	0.5455	0.0321	0.0420	3.4598E+08	
T1bk0df2	0.8710	0.0887	0.0270	0.0212	8.3631E+03	5.7744	0.7904	0.0305	0.0389	4.2820E+08	
T1bk0df2 (r1)	0.8584	0.0875	0.0266	0.0209	8.1689E+03	5.6849	0.7813	0.0300	0.0388	4.1525E+08	
T1bk0df2 (r2)	0.8732	0.0889	0.0271	0.0212	8.5730E+03	5.9194	0.7850	0.0307	0.0391	4.3230E+08	
T1bk1df1	0.8797	0.0983	0.0436	0.0273	9.5680E+02	78.7300	0.7833	0.0423	0.0534	4.7268E+08	39.7732
T1bk1df1 (r1)	0.8648	0.0962	0.0430	0.0269	9.4184E+02	77.4616	0.7631	0.0415	0.0533	4.5536E+08	38.2668
T1bk1df1(r2)	0.8834	0.0990	0.0438	0.0274	9.6323E+02	79.0651	0.7742	0.0426	0.0536	4.7769E+08	38.0685
T1bk1df2	0.8978	0.0989	0.0335	0.0271	1.1520E+04	95.4600	0.8607	0.0427	0.0528	6.1748E+08	44.2056
T1bk1df2(r1)	0.8879	0.0972	0.0332	0.0268	1.1276E+04	93.4530	0.8471	0.0443	0.0554	6.2444E+08	47.9705
T1bk1df2(r2)	0.9032	0.0999	0.0342	0.0273	1.1598E+04	97.4738	0.8560	0.0459	0.0564	6.2815E+08	45.3058
T1bk2df1	0.8776	0.0881	0.0542	0.0308	9.9750E+01	33.0000	0.5831	0.0397	0.0503	4.4262E+08	30.8858
T1bk2df1(r1)	0.8583	0.0861	0.0531	0.0304	9.8710E+01	31.9378	0.5613	0.0390	0.0504	4.2455E+08	28.9119
T1bk2df1(r2)	0.8793	0.0883	0.0543	0.0309	1.0193E+02	33.9195	0.5778	0.0400	0.0505	4.4604E+08	28.9224
T1bk2df2	0.8763	0.0830	0.0381	0.0271	3.3120E+02	51.7300	0.6810	0.0374	0.0474	5.2786E+08	23.2746
T1bk2df2(r1)	0.8490	0.0820	0.0373	0.0264	3.2355E+02	50.1218	0.6320	0.0365	0.0477	4.9924E+08	20.2281
T1bk2df2(r2)	0.8868	0.0839	0.0386	0.0274	3.3522E+02	52.3554	0.6775	0.0379	0.0475	5.4156E+08	25.2747

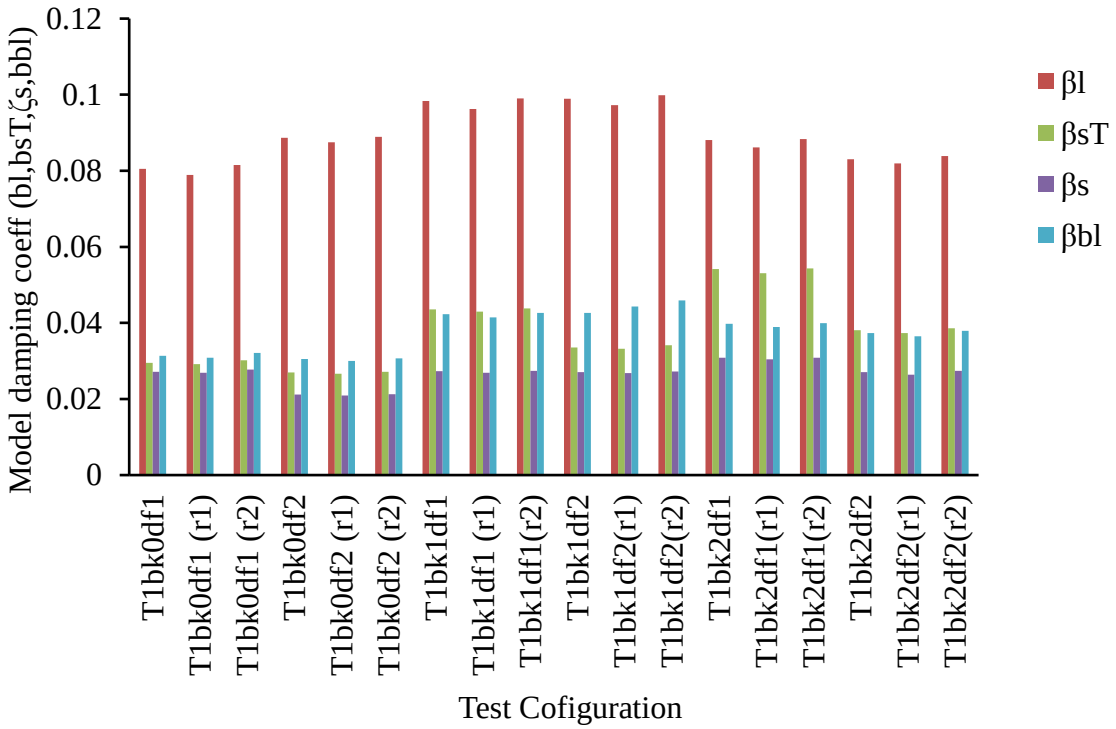

Figure 3.24: Effect of repeated test on roll model damping coefficients

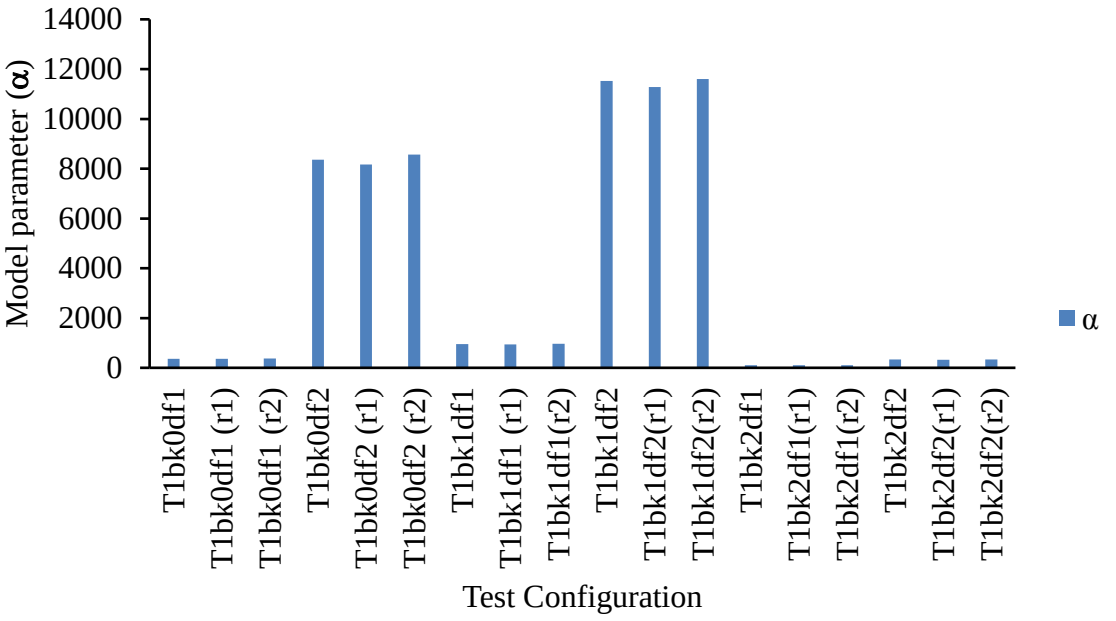

Figure 3.25: Effect of repeated test on roll model α parameters

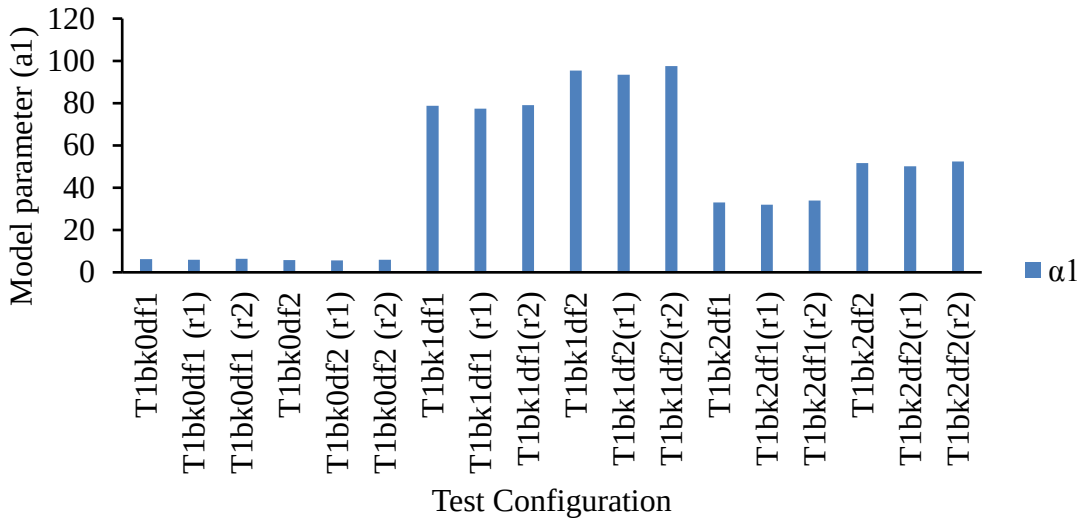

Figure 3.26: Effect of repeated test on roll model α1 parameters

According to figures 3.24 to 3.26., the observed trends in terms of order of magnitude for all the model variables were similar except for slight variations in actual estimated magnitudes. For the hull without bilge keels at draft 1, (T1bk0df1) the natural frequencies was approximated for both the first and second repeat test at variations of about 1.13 and 0.45%. The large angle damping coefficient (βl) showed a variation of 2.0 and 1.4 % resulting from repeat test. Whilst for the hull with bilge keel (T1bk1df1) the estimate varied from 2.15% and 0.69% for the (βl) parameter. Similar percentage variations of first order were experienced by the other model parameters as well. The % variations of model coefficient did not change significantly between hulls with bilge keels when compared to hulls without bilge keels. This is an indication that the repeat test did not have any significant effect on the parameters and as such may also not propagate any serious errors towards secondary parameters. The observed scatter resulting from the repeat test were also similar from the R^2 values for data analysis for each test. The effect of the repeat on the approximated mean roll damping coefficient B_{44} is captured in the chart of figure 3.27.

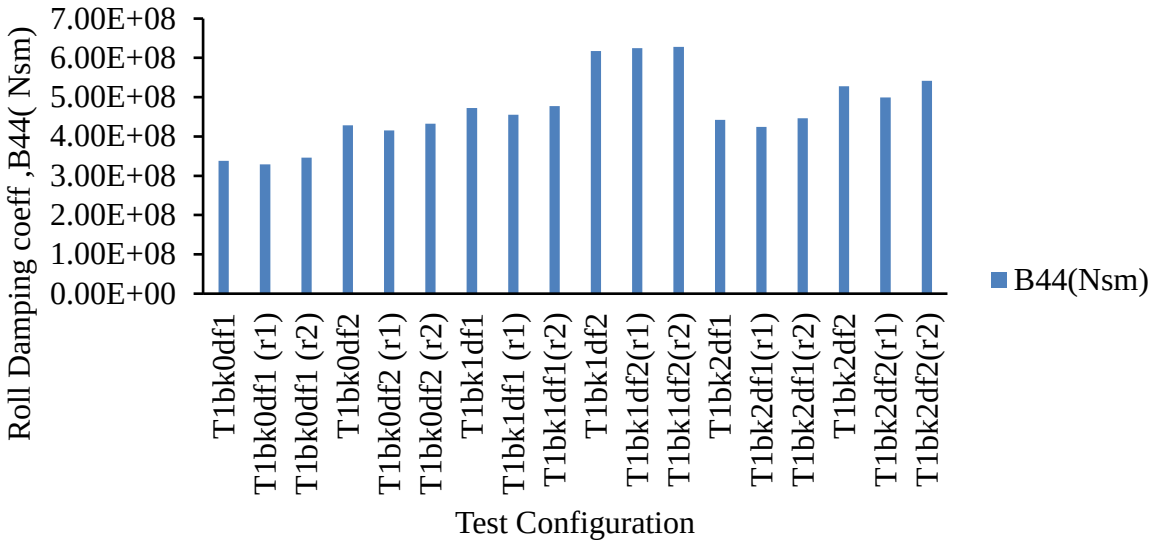

Figure 3.27: Effect of repeated test on roll damping coefficient for actual FPSO

The percentage contribution from bilge keel varied from 25% for T1bk2df2 (r2) to as high as 48% for T1bk1df2(r1). However, when values where compared within the same test scenario, the recorded difference in estimating the contribution ware not more than 5.42% the highest recorded for the repeat test in T1bk2df2(r1). Estimation difference as small as 0.77% was observed in test T1bk2df1(r2). The uncertainty analysis carried out o ascertain the extent of uncertainty using the standard uncertainty analysis for the test samples is reported in the next session.

3.6.2 *Uncertainty variation on mean roll damping coefficient from different test blocks*

From table 3.28 and 3.29 shows the values of the mean values and standard uncertainties estimated for the different parameters for the modified hyperbolic model using the equations 3.57, 3.55 and 3.63to 3.71 for the estimations of the various sensitivities of the independent model variables. The uncertainty analysis was carried on the developed mathematical model used for the estimation of roll damping coefficient as shown in equation 3.62. The standard uncertainties were estimated as the normalized standard deviation of each of the data sets for each parameter. The sensitivities estimated for the different repeat test did not vary significantly from the assumed first test.

Table 3.28: Table showing mean (assumed true value), standard deviation and the standard uncertainty for the different test blocks.

Test Group	Property	**w(n)**	**βl**	**βsT**	**βs**	**α**	**α1**	**θm (rad)**	**θvel (rad/s)**
T1bk0df1	mean	0.8463	0.0803	0.0296	0.0272	368.6764	6.2310	0.0720	0.0165
	std(σ)	0.0042	0.0011	0.0004	0.0004	5.4036	0.1859	0.0572	0.0181
	u_A	0.0025	0.0027	0.0011	0.0009	13.4233	0.4618	0.1421	0.0449
T1bk0df2	mean	0.8675	0.0883	0.0269	0.0211	8368.3191	5.7929	0.0834	0.0153
	std	0.0065	0.0006	0.0002	0.0002	164.9995	0.0966	0.0546	0.0153
	u_A	0.0038	0.0004	0.0001	0.0001	95.2625	0.0558	0.0315	0.0089
T1bk1df1	mean	0.8760	0.0978	0.0434	0.0272	953.9551	78.4189	0.0350	0.0158
	std	0.0081	0.0012	0.0003	0.0002	8.9628	0.6906	0.0444	0.0293
	u_A	0.0047	0.0007	0.0002	0.0001	5.1746	0.3987	0.0256	0.0169
T1bk1df2	mean	0.8963	0.0987	0.0336	0.0270	11464.5504	95.4623	0.0409	0.0191
	std	0.0063	0.0011	0.0004	0.0002	137.3077	1.6415	0.0509	0.0346
	u_A	0.0036	0.0006	0.0002	0.0001	79.2746	0.9477	0.0294	0.0200
T1bk2df1	mean	0.8717	0.0875	0.0539	0.0307	100.1313	32.9525	0.0444	0.0170
	std	0.0095	0.0010	0.0005	0.0002	1.3432	0.8097	0.0485	0.0284
	u_A	0.0055	0.0006	0.0003	0.0001	0.7755	0.4675	0.0280	0.0164
T1bk2df2	mean	0.8707	0.0830	0.0380	0.0270	329.9894	51.4024	0.0418	0.0159
	std	0.0159	0.0008	0.0005	0.0004	4.8430	0.9408	0.0462	0.0259
	u_A	0.0092	0.0005	0.0003	0.0002	2.7961	0.5432	0.0267	0.0149

Table 3.29 : Table showing the sensitivities of the different roll model parameters for the various test case to estimate mean roll damping coefficient

	Sensitivities							
Test case	**w(n)**	**βl**	**βsT**	**βs**	**α**	**α1**	**θm (rad)**	**θvel (rad/s)**
T1bk0df1	-0.0004	0.5149	0.6146	0.3339	4.03E-06	4.03E-05	0.0683	2.69E-04
T1bk0df1 (r1)	-0.0003	0.4973	0.6143	0.336	3.95E-06	3.95E-05	0.0652	2.51E-04
T1bk0df (r2)	-0.0003	0.5333	0.6174	0.3293	4.04E-06	4.04E-05	0.0716	2.81E-04
T1bk0df2	-0.0002	0.565	0.9435	0.0178	2.38E-07	5.85E-04	0.058	2.03E-04
T1bk0df2 (r1)	-0.0002	0.5565	0.9443	0.2145	3.41E-07	2.93E-05	0.0564	1.91E-04
T1bk0df2 (r2)	-0.0002	0.5787	0.9421	0.145	1.68E-06	2.89E-05	0.0595	2.09E-04
T1bk1df1	-0.0027	0.1433	0.2977	0.5591	8.67E-05	2.92E-05	0.0467	2.67E-03
T1bk1df1 (r1)	-0.0025	0.1419	0.2966	0.5615	8.72E-05	5.59E-04	0.0455	2.52E-03
T1bk1df1(r2)	-0.0027	0.1436	0.2983	0.5581	8.69E-05	5.72E-04	0.0472	2.73E-03
T1bk1df2	-0.0026	0.1924	0.6958	0.1118	5.14E-06	3.26E-04	0.0486	2.56E-03
T1bk1df2(r1)	-0.0025	0.1904	0.6948	0.1148	5.28E-06	3.25E-04	0.0476	2.45E-03
T1bk1df2(r2)	-0.0027	0.1944	0.6947	0.1109	5.45E-06	3.23E-05	0.0505	2.67E-03
T1bk2df1	-0.0012	0.1103	0.1112	0.7785	6.28E-04	5.14E-04	0.0683	2.69E-04
T1bk2df1(r1)	-0.0011	0.1077	0.1125	0.7798	6.14E-04	5.08E-04	0.0683	2.69E-04
T1bk2df1(r2)	-0.0012	0.1125	0.1116	0.7759	6.20E-04	5.06E-04	0.0683	2.69E-04
T1bk2df2	-0.0014	0.1383	0.2332	0.6285	5.18E-05	7.87E-04	0.2519	1.43E-03
T1bk2df2(r1)	-0.0013	0.1355	0.2325	0.6321	5.21E-05	7.96E-04	0.2449	1.31E-03
T1bk2df2(r2)	-0.0015	0.1394	0.234	0.6266	5.19E-05	7.88E-04	0.2564	1.49E-03

Table 3.30 : Estimation of the standard and relative uncertainties for different test blocks or groups.

	Mean sensitivities for each test group								U_A in βl	βbl	U_R=
Test Group	**w(n)**	**βl**	**βsT**	**βs**	**α**	**α1**	**θm (rad)**	**θvel (rad/s)**		**(mean)**	**U_A/ βbl (%)**
T1bk0df1	-0.0003	0.5151	0.6154	0.3330	4.0039E-06	4.0039E-05	0.0684	0.0003	0.0016	0.0314	4.9545
T1bk0df2	-0.0002	0.5667	0.9433	0.1258	7.5447E-07	2.9132E-05	0.0580	0.0002	0.0011	0.0304	3.5497
T1bk1df1	-0.0026	0.1429	0.2975	0.5595	8.6924E-05	5.6703E-04	0.0464	0.0026	0.0022	0.0421	5.3391
T1bk1df2	-0.0026	0.1924	0.6951	0.1125	5.2904E-06	2.2773E-04	0.0489	0.0026	0.0022	0.0443	4.9886
T1bk2df1	-0.0011	0.1102	0.1118	0.7781	6.2096E-04	5.0921E-04	0.0683	0.0027	0.0024	0.0396	5.9830
T1bk2df2	-0.0014	0.1377	0.2332	0.6290	5.1905E-05	7.9042E-04	0.0251	0.0014	0.0021	0.0372	5.6095

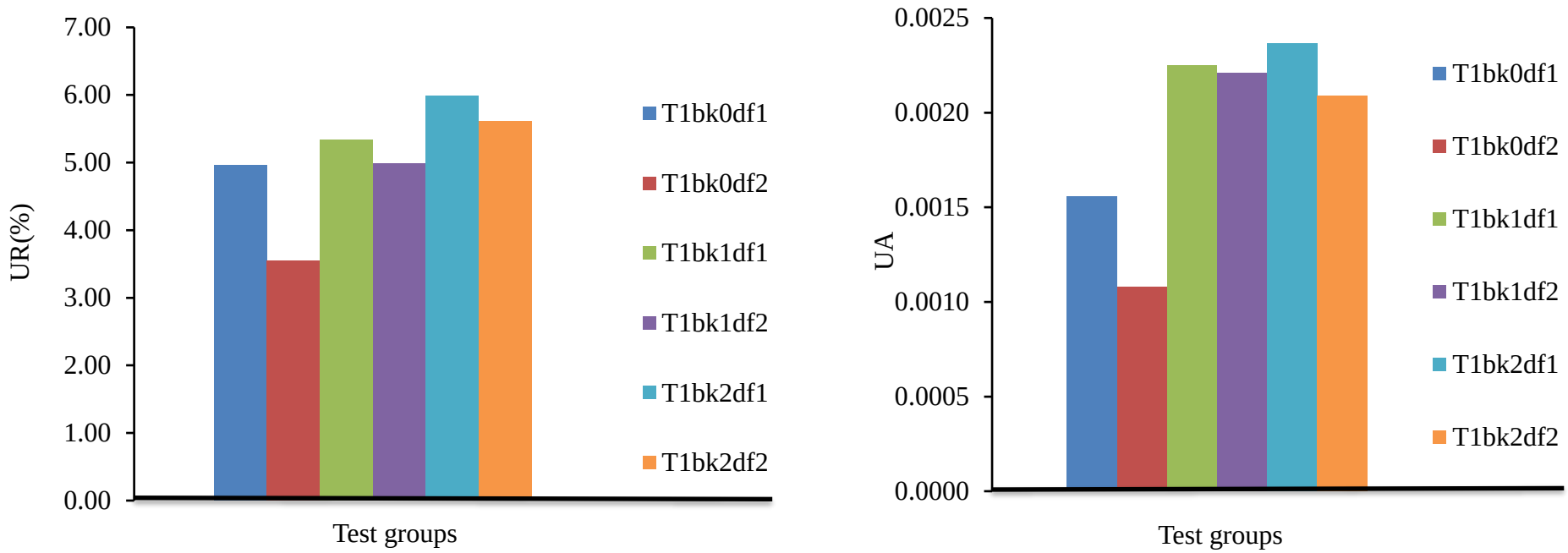

(a) (b)

Figure 3.28: Comparison between different test blocks showing the effect of bilge keel on the uncertainty of roll damping (a) Relative Uncertainty (b) Standard uncertainty.

The estimated expanded uncertainty of the mean damping coefficient using equation 3.63 with a coverage factor of 4.303 at a 95% confidence interval were presented in table 3.30. Figures 3.28 shows that the lowest uncertainties were observed for the hull without bilge keel (3.49% for T1bk0df2 and 4.95% for T1bk0df1**)** compared to the hulls with bilge keels. Relative uncertainties of about 5.9% were observed for the hull with bilge keel and at draft configuration 2 (T1bk0df1). The reason could be attributed to the uncertainty associated with vortex field experienced as a result of the sharp edge from the bilge keel. A cross examination of the uncertainties amongst bilge keels indicate that for the same draft line, the relative uncertainty associated with the bigger bilge keel (bk2) are more compared to those with the smaller bilge keels (bk1). For the draft configuration 1, there was an upward change of about 0.6439% which is 12.06% increase between the two bilge keels. Similar values of 0.6209% indicating a 12.44% increase was observed for the draft configuration 2. This is an indication that the scale of the bilge keel affects the uncertainty of the measurement however at a minimal level. Thus, it is possible to have larger relative uncertainties associated to bigger bilge keels which could be in correlation to the earlier observation between the bare hull and the hull with bilge keels.

3.7 Conclusion:

It is pertinent to conclude that the effect of bilge keels to the overall roll motion is significant in determining the roll damping and thus the associated response behaviour of the unit to environmental excitations. The results obtained from the different trials on the modifications made with reference to the original hyperbolic models are not in significant variation; this shows that the proposed 'Modified Hyperbolic' method is workable as realized. However, the significance thus is on the parameterization of the transition region with the transition-damping variable, obtainable through least square routine, and the function is easy to implement as a continuous function in a time domain motion code. The transition region as predicted by the modified hyperbolic model was validated using the rigorous bilinear method. The capture of the transition points within the region showed a significant representation of the transition region. As part of the deliverables from this section, the damping coefficients, roll natural period as well as some form relationship have been obtained which will form part of the input parameters for subsequent chapters. The uncertainty analysis conducted on the predictive hyperbolic model showed a standard uncertainty of about 0.0011Nsm to 0.0024 Nsm and a relative expanded uncertainty of 3.5% to 5.9 % associated with the model. However, the uncertainties are affected by the presence of bilge keels, which tend to slightly increase the uncertainties. It was observed that the repeatability in test did not alter the estimations significantly.

4 Chapter Four: Sea State Modelling

The pattern of ocean waves is highly irregular in nature and 3D or shortcrested too, and thus significant to carry out response studies based on this understanding. The idealization of a longcrested formulation is only an assumption used for design purpose which has limitations in terms of predications. As early as 1976, (Marshall,1976) reported more than twice estimated fatigue life of a structure when shortcrested sea was used instead of the longcrested idealization. The significant difference between the two ideals is the recognition of a directional spread representing other secondary waves propagating from different directions in combination to the primary waves forming the mean sea state observed. The inclusion of directionality has shown to be a good way of estimating effects like excessive rolling and yawing motions, torsional loads etc. on floating structures (Okey, 1989). The availability of wave tanks with the capacity of producing high quality short crested seas has changed a great deal the way in which design of structures are carried out; directionality in wave spectra has become a part of the design process for offshore structures.

Generally, sea state modelling starts with measurements of water surface elevations, orthogonal water surface slopes, horizontal orthogonal water particle velocities etc. at single or multiple locations. The data are fitted to standard formulations derivable from the study of the wave energy by methods such as maximum entropy method (MEM), maximum likelihood method (MLM) and Fourier series as well. This chapter looked at the various existing standard sea spectra formulations, and how they are combined for separated seas to form a standard sea state for the typical West African sea condition. Comparisons where done to find out the influence of directionality on the spectra shape, which can be translated into motion as well.

4.1 Spectra representations

This section does not intend to go through the fundamentals of deriving the spectra forms from raw sea water surface data. Rather already derived forms are adopted for analysis. Following (St. Denis and Pierson, 1953), the irregular sea state wave elevation may be represented by infinite number of harmonic waves. Each harmonic component is defined

by a bin of wave frequency and random phase angle. Considering an inertial reference system moving with the ship mean forward velocity. The orientation of the system has its origin at the mean waterline coinciding at the vertical of the centre of gravity. The y-axis pointing to port side, the vertical axis pointing downward, and +ve x-axis pointing to the mean bow direction. The generalized Airy linear water surface (ζ) elevation model for longcrested wave can then be written as equation 4.1. This form is adopted for this research.

$$\zeta(x,y,t) = \sum_{j=1}^{N} a_i(cos(k_i\, x\, .cos\theta + k_i\, y.sin\theta - \omega_i\, t + \epsilon_i) \qquad (4.1)$$

The wave, with amplitude a_i is moving in direction θ relative to the ship path. For a regular longcrested sea (N=1), for an irregular longcrested sea (N>>>1) with all wave traveling in the same direction. Extending this to represent a shortcrested sea state, involves the addition of several regular wave sets with amplitude a_{ij} coming from different directions θ_j . The shortcrested formulation of equation 4.1 is written as the equation 4.2 (Ching Tong Choi & Ling Chang, 2007).

$$\zeta(x,y,t) = \sum_{i=1}^{N}\sum_{j=1}^{M} a_{ij}(cos(k_i\, x\, .cos\theta_j + k_i\, y.sin\theta_j - \omega_i\, t + \epsilon_{ij}) \qquad (4.2)$$

The equation 4.1 is assumed a homogenous, stationary, ergodic random Gaussian process, with zero mean. Because the relative amplitude of expected wave to water depth is very small, the assumptions are satisfactory for the localization of the model within the West African region.

Recall the generalized spectra representation of sea state from equation 2.1, the formulated standard equations for S (ω) are already presented in appendix B.

For a generalized longcrested sea, the spectrum is represented as:

$$S(\omega_i) = f1(Hs, \omega_o, \omega_i) \qquad (4.3)$$

The wave amplitude of every regular frequency is computed as:

$$a_i = \sqrt{2.S(\omega_{i,})\Delta\omega_i} \qquad (4.4)$$

Whilst for the Shortcrested Sea, the inclusion of the directional spread formulates the equation to that in equation 4.5

$$S(\omega_i, \theta_j) = f2(H_s, \omega_o, \omega_i, \theta_j) \qquad (4.5)$$

With the associated regular wave amplitude given as

$$a_{ij} = \sqrt{2.S(\omega_{i,}\theta_j)\Delta\omega_i \,.\, \Delta\theta_j} \quad (4.6)$$

The relationship between the two states are

$$S(\omega_i, \theta_j) = S(\omega_i) * W(\theta_j) \quad (4.7)$$

The weighted functions W(θj) for given frequency/direction containing (i, j) bin can thus be obtained for any wave system of interest.

The weighting $W(\theta_j)$ function is calculated thus:

$$W(\theta_j) = D(\omega_i, \theta_j) \ * \ \Delta\theta \quad (4.8)$$

D (ω,θ) is the directional spreading function and the domain containing all element combinations of $(\omega_{i,}\theta_j)$ i.e**., i * j** number of elements. Δθ is the directional interval and is measured typically in radian.

The weighting function is normalized such that at all time

$$\sum_{j=1}^{M} W(\theta_j) = 1 \quad (4.9)$$

The generalized form of the directional spread function according to (Longuet-Higgins, 1961), is

$$D(\omega, \theta) = \begin{cases} k_m . cos^{2m(\omega)}(\theta_j - \theta_o) & \theta_j - \theta_o < 90^0 \\ 0 & \theta_j - \theta_o \geq 90^0 \end{cases} \quad (4.10)$$

θ_o is the mean direction of the primary wave system

Where:

$$k_m = \frac{\Gamma(m(\omega)+1)}{2\sqrt{\pi}\,\Gamma(m(\omega)+1/2)} \quad (4.11)$$

Is a normalizing parameter, such that equation 4.8 is true.

With the power of angular spreading given as

$$m(\omega) = m_p \left(\frac{\omega}{\omega_p}\right)^{\beta} \quad (4.12)$$

$$\begin{cases} m(\omega) = m_p \left(\frac{\omega}{\omega_p}\right)^{5} & \text{if } \omega \leq \omega_p \\ m(\omega) = m_p \left(\frac{\omega}{\omega_p}\right)^{-2.5} & \text{if } \omega > \omega_p \end{cases} \quad (4.13)$$

And accordingly, for:

$m_p \rightarrow \infty$, narrow bandedness, the waves are longcrested and for $m_p \rightarrow 0$, broad bandedness, the waves are shortcrested; θ_j is the azimuth measured counter-clockwise from the principal wave direction and θ_p is the direction of the primary wave w.r.t. to the ships path. (Cummins and Bales, 1980) suggested that the cosine squared spreading distribution of (Haring and Heideman, 1978) is best suited to model this function. Thus, within a spread of 180^0 $(\pm 90^0)$

$$D(\omega, \theta) = \begin{cases} \frac{2}{\pi}.cos^2(\theta - \theta_0) & \theta_j - \theta_p < 90^0 \\ 0 & \theta_j - \theta_p \geq 90^0 \end{cases} \quad (4.14)$$

However, according to DNV report (pg. 35, DNV-RP-C 205, 2007) the directional spread was estimated as follows;

$$D(\theta_j) = \begin{cases} \frac{\Gamma(1+\frac{n}{2})}{\sqrt{\pi}\Gamma(\frac{1}{2}+\frac{n}{2})}.cos^n(\theta_j - \theta_p) & \theta_j - \theta_p < 90^0 \\ 0 & \theta_j - \theta_p \geq 90^0 \end{cases} \quad (4.15)$$

Where $n \geq 6\ (Swell);\ n = 2\ to\ 4\ (Wind\ Sea)$

A later report from (DNV RP H103, 2011) as reviewed, did not alter significantly the parameter as estimated. Relying on equations 4.10 and 4.11 values of m (ω) =1 to 2, $m(\omega) \geq 3$ recommended for wind sea and swell sea respectively.

In estimating the weighting function, the relative angle (θj- θp= 0) gives the maximum W(θj) which coincides with the observed primary direction of system. The spectra ordinate at each frequency and directional bin can then be estimated, such that the amplitude at the bin co-ordinate within the entire spread ($\pm 90^0$) with the primary wave system at the centre. At this stage, two approaches adopted in combining the Swell and Wind Sea which are assumed to be separated already: note that the significant height can be estimated from the spectra density curve by using equation 4.16

$$H_s = 4 * \sqrt{mo} \quad (4.16)$$

Where mo is the variance or the area under the spectra density curve (S (ω) vs ω).

4.2 Multidirectional sea: The West African situation

The sea state is modelled relying on the WASP (WASP, 2004) project conducted for the West African sea region. Different techniques in dealing with the combination of the already partitioned seas (swells and wind sea) are presented. In this work, in order to model the shortcrested sea, the method was developed using various spectra shapes for the longcrested sea which was combined with the appropriate directional spread function. Some of the equations for the Long crested spectra used are already presented in appendix B. For the West African sea as recommended, the swell sea is modelled using the Lognormal or the Triangular spectra shapes in equations 4.17 and 4.18 respectively.

$$S(f) = \frac{mo}{f*\sigma*\sqrt{2\pi}}.e^{-(\frac{-[\ln(f)-\bar{\mu}]^2}{2\sigma^2})} \quad (4.17)$$

Where:

$$\sigma = \sqrt{ln\left[\left(\frac{\sigma_{nd}}{f_o}\right)^2 + 1\right]}$$

With $\sigma_{nd} = \frac{a}{{T_o}^b}$; a, b are location dependent variables (pg. 113, DNV-RP-C205, 2011) recommendation for values)

$\bar{\mu} = \ln(fo) + \sigma^2$

mo is obtained from equation 4.16.

$$\left\{\begin{array}{c} S(f) = Sp * \left[m * \frac{f}{f_o} - (m-1)\right] \quad (\text{for } f > fc * f_o \text{ and } f < f_o) \\ S(f) = Sp * \left[m - (m-1) * \frac{f}{f_o}\right] \quad (\text{for } f >= fc \text{ and } f < f_o/fc) \\ S(f) = 0 \qquad\qquad (\text{elsewhere}) \end{array}\right\} \quad (4.18)$$

Where;

m=6 (DNV recommendation)

$Sp = \frac{2m(m-1)*mo}{(2m-1)*f}$

$fc = \frac{(m-1)}{m}$ (Width of triangular family to ensure good fit)

$fr1 = fc * f_o; \quad fr2 = (1/fc) * f_o; \quad$ (in Hz)

$wr1 = fc * \omega_o; \quad wr2 = (1/fc) * \omega_o; \quad$ (in rad/s)

The wind sea is formulated using the JONSWAP-Glenn spectrum(JSG) in equation 4.19, this is a modified version of the JONSAP spectrum(JSS).

$$S(\omega) = C_{jm} * \left(\frac{\omega}{\omega_o}\right)^{-5} * C_j * e^{(-1.25*\left(\frac{\omega}{\omega_o}\right)^{-4})} \quad (4.19)$$

With

$\lambda = 3.3$

$J = e^{-(\frac{(1-\frac{\omega}{\omega_o})^2}{2\sigma^2})}$

$\sigma = 0.07 \ for \ \omega < \omega_o \ ; \ \sigma = 0.09 \ for \ \omega > \omega_o$

$C_j = \lambda^J$

$C_{jm} = \frac{5*mo}{f_o} / \left(1.15 + 0.1688 * \lambda - \left\{\frac{0.925}{1.909+\lambda}\right\}\right)$

The directional spread function in accordance with equation 4.15 is implemented.

The sea state according to ISO 19901-01, API RP2-MET (Washington Monthly, 2012) for the West African sea condition for 100yr return period is used. Recall;

*Main swell (Sss1); H_{ss1}=4-**5m**, T_{oss1}=14-**15**s,*

*Secondary swell (Sss2); H_{ss2}=2-**3**m, T_{oss2}=11-**13**s*

*Wind sea component has H_{sw}=2-**2.5**m, T_{osw}=8-**9**s.*

The associated 1 hr wind speed measured at 10m above MWL is 12-13m/s and a mean surface current of 2.0m/s.

4.2.1 *Mean Single wave stream approach*

In a partitioned sea with separated wave streams, the resultant wave in magnitude (significant wave height and period) as well as direction is obtained for the purpose this analysis. This involves the use of the square law method according to (Boukhanovsky and Soares, 2009) for the combination of wave streams that are fully separated.

The entire three separated streams (two Swells and a Wind Sea) are added to obtain a single significant wave height H_s and direction θ_s . The procedure is shown below.

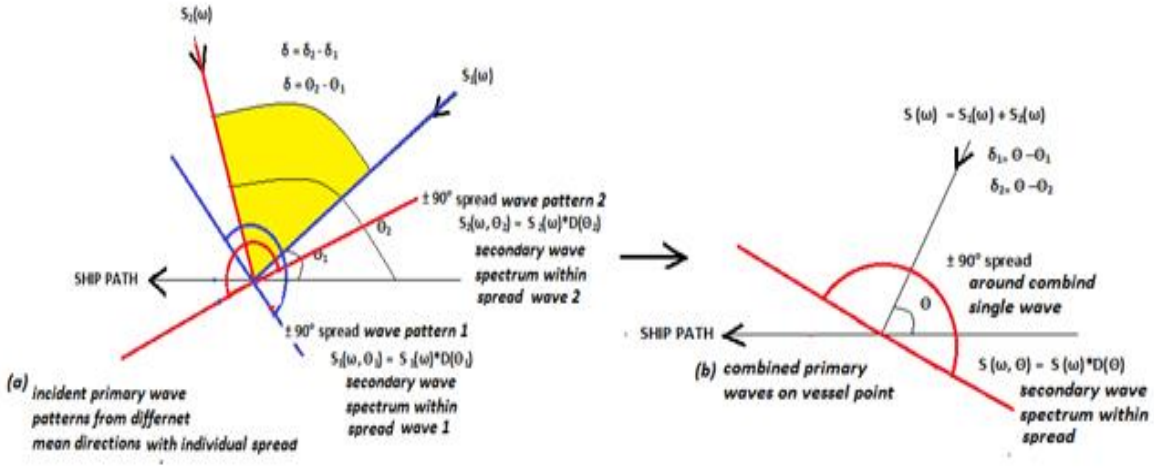

Figure 4.1 Wave streams and equivalent approaching a measurement point on water plane

In Figure 4.1, the two swell streams are initially added.

$$H_{ss} = \sqrt{{H_{ss1}}^2 + {H_{ss2}}^2} \tag{4.20}$$

Compute the weight coefficients for directions for individual swells (W_{ss1} and W_{ss2})

$$W_{ss1} = {H_{ss1}}^2 / {H_{ss}}^2 \tag{4.21}$$

$$W_{ss2} = {H_{ss2}}^2 / {H_{ss}}^2 \tag{4.22}$$

Compute combined swell modal period;

$$T_{oss} = T_{oss1} * T_{oss2} / \sqrt{{T_{oss1}}^2 * W_{ss2} + {T_{oss2}}^2 * W_{ss1}} \tag{4.23}$$

Compute combined swell wave direction;

$$\theta_{ss} = tan^{-1}\left[\frac{W_{ss1}*\sin(\theta_{ss1}) + W_{ss2}*\sin(\theta_{ss2})}{W_{ss1}*\cos(\theta_{ss1}) + W_{ss2}*\cos(\theta_{ss2})}\right] \tag{4.24}$$

Having obtained the combined swell parameter, it is then appropriate to combine this with the wind sea following the same procedure:

The overall combined significant wave height H_s then becomes

$$H_s = \sqrt{{H_{ss}}^2 + {H_{sw}}^2} \tag{4.25}$$

In addition, the weight coefficients for wind sea (W_{cw}) and swell sea (W_{cs}) for directions are computed thus;

$$W_{cw} = {H_{sw}}^2 / {H_s}^2 \tag{4.26}$$

$$W_{cs} = {H_{ss}}^2/{H_s}^2 \quad (4.27)$$

Computing the combined wave modal period yields;

$$T_{oc} = T_{osw} * T_{oss}/\sqrt{{T_{osw}}^2 * W_{cs} + {T_{oss}}^2 * W_{cw}} \quad (4.28)$$

The overall combined wave direction is then readily obtained;

$$\theta_{ss} = tan^{-1}\left[\frac{W_{cw}*\sin(\theta_{sw})+W_{cs}*\sin(\theta_{ss})}{W_{cw}*\cos(\theta_{sw})+W_{cs}*\cos(\theta_{ss})}\right] \quad (4.29)$$

The sea-state-energy ratio (SSER) and the intermodal distance (IMD) which are significant parameters used in assessing the degree of dominance by the wave streams are thus estimated

$$SSER = (\frac{H_{sw}}{H_{ss}})^2 \quad (4.30)$$

$$IMD = \frac{wosw-wocs}{wosw+wocs} \quad (4.31)$$

For SSER<<1 is indicative of a swell dominated sea, whereas for a wind-sea dominated sea SSER>>1. The value of SSER approximately 1 is used to describe a sea that is of comparable energy, mixed wind and swell sea are comparatively equal in energy contributions. The intermodal distance is always between 0 and 1.

With the Hs and Toc as the new combined sea state, one can then proceed to treat it either as Longcrested or Shortcrested sea. Appropriate long crested sea spectrum equations are applied for the Longcrested sea and together with the cosine square directional spread of equation 4.14, the shortcrested sea is formulated. For the Shortcrested sea, a predetermined directional interval $\Delta\theta$ is also used. The directional spread coefficient $D(\theta_j)$ is computed for every wave stream, with that of the primary being the maximum since($\theta_j - \theta_p = 0\ ;\ \ cos^2 0 = 1$). From equation 4.8, the weight contribution is estimated thus. Therefore, the shortcrested ordinate for every combination of frequenc and direction bin is computed in-line with equation 4.7; Figure 4.1b shows diagrammatically the wave spread of the combined stream around ±90^o.

4.2.2 *Separated Wave streams approach*

Like the approach adopted in estimating the resultant sea as a mean or averaged sea referred to as the mean single approach, this approach treats the swells as combined and separated from the wind sea. In handling this aspect, the swell seas were applied

individually to their mean direction, with a spread of ($\pm 90^0$); this implies that the resultant system comprises of two co-linear swells acting along the mean direction and a wind sea coming from another direction.

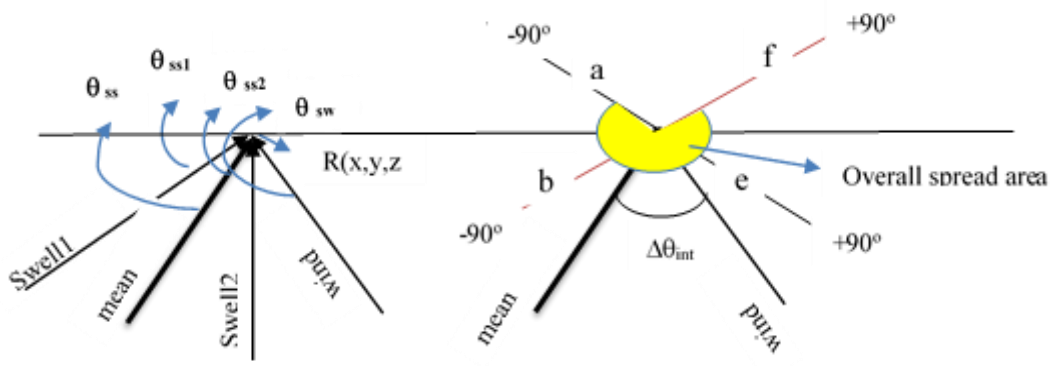

Figure 4.2 Wave system and its equivalent wind sea showing overall spread region

To compute the total spectra ordinate, use is made of equations 4.32 or 4.33 below,

$$\boldsymbol{S(\omega,\theta)} = \sum_{k=1}^{nw}[S_k(\omega_{i,}) * W_k(\theta_j)] \qquad [m^2/(\text{rad/sec})] \qquad (4.32)$$

$$S(\omega_i,\theta_j) = [S_{ss1}(\omega_{i,}) * W_{ss1}(\theta_j)] + [S_{ss2}(\omega_{i,}) * W_{ss2}(\theta_j)] + [S_{sw}(\omega_{i,}) * W_{sw}(\theta_j)] \qquad (4.33)$$

The overall spread area is subdivided into 'n' directional bins using the difference between the mean swell direction and the wind sea interval $\Delta\theta_{int}$,

The interval of the directional bin is;

$$\Delta\theta = \frac{\Delta\theta_{int}}{n^*} \qquad (4.34)$$

n* is a conveniently selected whole number.

However, in computing the weighting function using the equations. (4.15), for the swell systems,

$W_{ss}(\theta_j) = 0$, for any $\theta_j = a, e, and\ out\ side\ its \pm 90°$ within the overall spread region;

And for the wind sea;

$W_{ws}(\theta_j) = 0$ for any $\theta_j = b, f, and\ out\ side\ its \pm 90°$ within the overall spread region;

Since the research interest is for the West African region, in-line with the findings of the (WASP, 2004, Kelvin et al, 2013) the spectra are represented as $S_{ss1,2}(\omega_i)$ using equations 4.17 or 4.18, and the wind sea $S_{sw}(\omega_i)$ with equation 4.19.

4.2.2.1 *Separated A for combining swell waves and wind sea streams*

The approach used by considering the streams as being separated is divided into two categories with nomenclatures as separated A and separated B. The separated A approach as an alternative would be to use the combined swell wave system in significant wave height, direction and period, thus equation 4.32 will then be written as;

$$S(\omega_{i,}\theta_j) = [S_{ss}(\omega_{i,}) * W_{ss}(\theta_j)] + [S_{sw}(\omega_{i,}) * W_{sw}(\theta_j)] \quad (4.35)$$

The above methodologies are adopted in order to overcome the difficulty of finding common directional lines for all three systems if treated uniquely separated.

4.2.2.2 *Separated B for combining swell waves and wind sea streams*

Another pragmatic and more robust approach to achieve the combined sea would be to ensure that the angular difference between the streams are either the same or multiples of a given value, e.g. 5°, 10° 15° or 20°. By this, the directional lines can then be assigned to capture the primary waves and all their secondary streams within the expanded spread region.

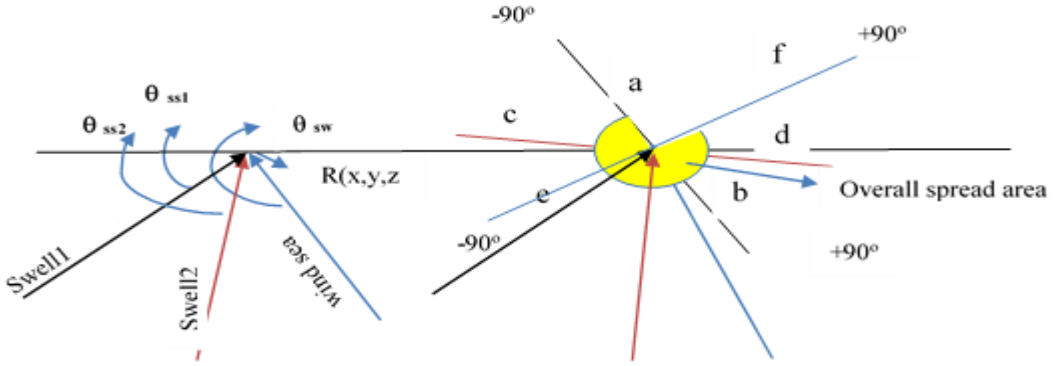

Figure 4.3: Wave system combined overall spread region

Assuming the difference between the primary swell streams is

$$\theta_{s1} - \theta_{s2} = diff \quad (4.36)$$

And this difference is a factor of the difference between $\theta_{s1} - \theta_{ws}$ and $\theta_{ws} - \theta_{s2}$

The overall spread region can be designated as falling within the min (a, b, c, d, e, f) to max (a, b, c, d, e, f) around the region housing the primary directions of the streams. If the difference is ascertained, then the directional spread region is given as equation 4.37

$$\theta_{dirspread} = \theta_{min} : diff : \theta_{max} \quad (4.37)$$

Note that this range contains all the wave streams both primary and secondary at their specified direction. The total spectra ordinate can be formulated as given in equation 4.32 Apply equations. 4.17- 4.19 for the longcrested spectra ordinates; apply equations 4.10 or 4.15 and 4.8 for the directional spread and weight contributions respectively.

The technique picks each wave stream at a time. Within the overall spread, the active secondary waves within its $\pm 90°$ range are considered and all the others outside are computed using zero weighting contributions.

The procedure is repeated for the other swell and wind sea. The above procedure which captures the shortcrested sea form can be modified to represent Longcrested Sea by;

(a) Removing the directional spread from the equation 4.33 and implemented using the appropriate spectrum equations. This computation is done within the selected frequency range.

(b) A better approach would be to normalize the weight function and make only the corresponding value of the primary wave as 1, while others are assigned 0. Also, the value of the interval $\Delta\theta$ in equation 4.6 and 4.8 is also made automatically to 1.

Generally, the normalization is done using the equation 4.38 below.

$$W(\theta_j) = W(\theta_j) / \sum_{j=i}^{j=N} W(\theta_j) \qquad (4.38)$$

This is done to ensure that the condition of equation 4.9 is met. With this technique, it is easy to convert a shortcrested sea to long crested sea just by ensuring that every value of the normalized $W(\theta_j)$ is made 0, except for the maximum which corresponds to that of the primary wave, i.e. single wave and direction is achieved. This value is made equal to 1,

Thus, for the longcrested sea, taking a step further;

$$W(\theta_j) = W(\theta_j) / \max[W(\theta_j)] \qquad (4.39)$$

The above routine of equation 4.39 converts the primary wave $(\theta_j) = 1$, thus standing as the only contributing wave stream for estimation of the spectra ordinate.

To further convert every other $(\theta_j) = 0$, we simply apply the equation below

$$W(\theta_j)[(W(\theta_j) \neq 1)] = 0 \qquad (4.40)$$

This means technically that every secondary wave does not contribute any value to the combined spectra ordinate thus making it equivalent to a longcrested sea.

4.2.2.3 *Mathematical form of the West African Sea state spectrum*

Based on the formulations and the mathematical analysis for the addition of the separated seas described above, three compound spectrum formulations were obtained for the region as recommended by the (WASP,2004). Relying on the equations 4.8, 4.15,4.17, 4.19 and 4.32, the following compound spectrum were formulated for the region. Note that only the lognormal spectrum for swell is considered in this case.

(a) Combining all separated seas as single stream with common directional spread

$$S(\omega,\theta)=\left[\frac{mo}{2\pi\omega*\sigma*\sqrt{2\pi}}.e^{-\left(\frac{-[\ln(2\pi\omega)-\bar{\mu}]^2}{2\sigma^2}\right)}\right]* \begin{cases} \frac{\Gamma\left(1+\frac{n}{2}\right)}{\sqrt{\pi}\Gamma\left(\frac{1}{2}+\frac{n}{2}\right)}.cos^n\left(\theta_j-\theta_p\right) & \theta_j-\theta_p<90^0 \\ 0 & \theta_j-\theta_p\geq 90^0 \end{cases} *\Delta\theta \quad (4.41)$$

Were

$mo=\frac{{H_{SS1}}^2+{H_{SS2}}^2+{H_{SW1}}^2}{16}$

And $\omega_o\ \sigma,\bar{\mu}$ are estimated using equations 4.21-4.29.

(b) Combining the swell seas as one unit and adding to a wind sea with different spectrum and directional spread

$$S(\omega,\theta)=\left[\frac{mos}{2\pi\omega*\sigma_s*\sqrt{2\pi}}.e^{-\left(\frac{-[\ln(2\pi\omega)-\bar{\mu}_s]^2}{2\sigma_s^2}\right)}\right]* \begin{cases} \frac{\Gamma\left(1+\frac{n_s}{2}\right)}{\sqrt{\pi}\Gamma\left(\frac{1}{2}+\frac{n_s}{2}\right)}.cos^n\left(\theta_j-\theta_p\right)_s & \left(\theta_j-\theta_p\right)_s<90^0 \\ 0 & \left(\theta_j-\theta_p\right)_s\geq 90^0 \end{cases} *(\Delta\theta)_s+\left[C_{jm}*\left(\frac{\omega}{\omega_{ow}}\right)^{-5}*C_j* e^{\left(-1.25*\left(\frac{\omega}{\omega_{ow}}\right)^{-4}\right)}\right]* \begin{cases} \frac{\Gamma\left(1+\frac{n_w}{2}\right)}{\sqrt{\pi}\Gamma\left(\frac{1}{2}+\frac{n_w}{2}\right)}.cos^{n_w}\left(\theta_j-\theta_p\right)_w & \left(\theta_j-\theta_p\right)_w<90^0 \\ 0 & \left(\theta_j-\theta_p\right)_w\geq 90^0 \end{cases} *(\Delta\theta)_w \quad (4.42)$$

Were

$mos=\frac{{H_{SS1}}^2+{H_{SS2}}^2}{16}$,

And $\omega_{os}\ \sigma_s,\bar{\mu}_s$ are estimated using equations 4.21-4.29.

$C_{jm}=\frac{2\pi*5*mow}{\omega_{ow}}/\left(1.15+0.1688*3.3-\left\{\frac{0.925}{1.909+3.3}\right\}\right)$, $mow=\frac{{H_{SW1}}^2}{16}$

$$C_j = 3.3^{e^{-\left(\frac{(1-\frac{\omega}{\omega_{ow}})^2}{2\sigma^2}\right)}} \quad \sigma = 0.07 \ for\ \omega < \omega_{ow} \quad ; \quad \sigma = 0.09 \ for\ \omega > \omega_{ow}$$

(c) Combining all streams as separated seas with different spectrum and associated directional spreads

$$S(\omega,\theta) = \left[\frac{mos1}{2\pi\omega * \sigma_{s1} * \sqrt{2\pi}} . e^{-(\frac{-[\ln(2\pi\omega)-\bar{\mu}_{s1}]^2}{2\sigma_{s1}^2})}\right] *$$

$$\left\{\begin{matrix} \frac{\Gamma\left(1+\frac{n_s}{2}\right)}{\sqrt{\pi}\Gamma\left(\frac{1}{2}+\frac{n_s}{2}\right)} . cos^{n_s}\left(\theta_j - \theta_p\right)_{s1} & \left(\theta_j - \theta_p\right)_{s1} < 90^0 \\ 0 & \left(\theta_j - \theta_p\right)_{s1} \geq 90^0 \end{matrix}\right\} * (\Delta\theta)_{s1} +$$

$$\left[\frac{mos2}{2\pi\omega * \sigma_{s2} * \sqrt{2\pi}} . e^{-(\frac{-[\ln(2\pi\omega)-\bar{\mu}_s]^2}{2\sigma_{s2}^2})}\right] * \left\{\begin{matrix} \frac{\Gamma\left(1+\frac{n_s}{2}\right)}{\sqrt{\pi}\Gamma\left(\frac{1}{2}+\frac{n_s}{2}\right)} . cos^{n}\left(\theta_j - \theta_p\right)_{s2} & \left(\theta_j - \theta_p\right)_{s2} < 90^0 \\ 0 & \left(\theta_j - \theta_p\right)_{s2} \geq 90^0 \end{matrix}\right\} *$$

$$(\Delta\theta)_{s2} + \left[C_{jm} * \left(\frac{\omega}{\omega_{ow}}\right)^{-5} * C_j * e^{\left(-1.25*\left(\frac{\omega}{\omega_{ow}}\right)^{-4}\right)}\right] *$$

$$\left\{\begin{matrix} \frac{\Gamma\left(1+\frac{n_w}{2}\right)}{\sqrt{\pi}\Gamma\left(\frac{1}{2}+\frac{n_w}{2}\right)} . cos^{n_w}\left(\theta_j - \theta_p\right)_{w} & \left(\theta_j - \theta_p\right)_{w} < 90^0 \\ 0 & \left(\theta_j - \theta_p\right)_{w} \geq 90^0 \end{matrix}\right\} * (\Delta\theta)_w \qquad (4.43)$$

Where,

$mos1 = \frac{{H_{ss1}}^2}{16}, mos2 = \frac{{H_{ss1}}^2}{16}, mow = \frac{{H_{sw}}^2}{16}$, subscript (s or ss) and (w or sw) denote swell and wind sea respectively.

4.3 The effect of Multi-directionality on spectra shape

In order to study the effect of directionality on the response, the effect is first studied on the overall spectra obtained from the confused sea state. To do this, an array of possible cases from the combinations of the waves with the intention of formulating them with the different spectrum are presented below in table 4.1. The total estimates of the swell and wind sea in magnitude and directions obtained from the principle highlighted above from equations 4.20-4.29. The upper limit values (main swell; Hs=5m, To =15s, primary swell;

Hs=3m, To =13s and wind sea; Hs=2.5m, To=9s) according to the range established by ISO 19901-01, API RP2-MET (Washington Monthly, 2012) used. Value of 6.34m for overall significant wave height correlate with the moderate sea classification according to (Halvor Lie e al, 2007). This gave a SSER of 0.1838 indicating a swell dominated sea state and Intermodal distance (ID) of 0.2302.

Table 4.1 Cases for sensitivity studies

case	Swell Dir (deg)		combined swell			Wind sea	combined sws+ws		
	swell 1	swell 2	Hss (m)	Tos (s)	θ (deg)	(deg)	Hs (m)	To (s)	θ (deg)
All colinear									
CaseS_1	0	0	5.831	14.3825	0	0	6.344	12.9	0
CaseS_2	45	45	5.831	14.3825	45	45	6.344	12.9	45
CaseS_3	90	90	5.831	14.3825	90	90	6.344	12.9	90
CaseS_4	135	135	5.831	14.3825	135	135	6.344	12.9	135
CaseS_5	180	180	5.831	14.3825	180	180	6.344	12.9	180
CaseS_6	30	30	5.831	14.3825	30	30	6.344	12.9	30
CaseS_7	60	60	5.831	14.3825	60	60	6.344	12.9	60
non colinear									
CaseS_8	90	45	5.831	14.3825	78.5	180	6.344	12.9	89.1
CaseS_9	180	45	5.831	14.3825	161.1	90	6.344	12.9	151.8
CaseS_10	45	90	5.831	14.3825	56.5	180	6.344	12.9	66.2
CaseS_11	90	180	5.831	14.3825	109.8	45	6.344	12.9	106.8
CaseS_12	180	90	5.831	14.3825	160.2	45	6.344	12.9	150
CaseS_13	45	180	5.831	14.3825	63.9	90	6.344	12.9	67.9
CaseS_14	90	135	5.831	14.3825	101.5	180	6.344	12.9	111.4
CaseS_15	60	90	5.831	14.3825	67.8	30	6.344	12.9	62.2
CaseS_16	60	30	5.831	14.3825	52.2	90	6.344	12.9	57.8
CaseS_17	90	60	5.831	14.3825	82.2	30	6.344	12.9	74.8
swell1,2 col									
CaseS_18	45	45	5.831	14.3825	45	90	6.344	12.9	51.6
CaseS_19	90	90	5.831	14.3825	90	45	6.344	12.9	83.4
swell1,ws col									
CaseS_20	45	90	5.831	14.3825	56.5	45	6.344	12.9	54.7
CaseS_21	90	45	5.831	14.3825	78.5	90	6.344	12.9	80.3
swell2,ws col									
CaseS_22	90	45	5.831	14.3825	78.5	45	6.344	12.9	73.5
CaseS_23	45	90	5.831	14.3825	56.5	90	6.344	12.9	61.5

A common observation of the table above, with the estimated combined directions suggest that the main swell has a strong influence on the resultant composition in

magnitude and direction as well. To capture the variation effect of directionality on the response via the spectra ordinate, a contour plot was used. The colour map indicates the spectra density or ordinate or the associated energy (m^2-s). A clear representation for the energy cluster is shown within the effective spread area in terms of direction and frequency. The Matlab script flow chart presented below was used to carry out this analysis for the different parameters investigated.

4.3.1 *Matlab code for investigation of the impact of number of regular frequency and sea state combination methods*

The code was developed by using the equations highlighted and derived in this chapter. The code however forms an integral part of the overall method for the motion simulation**.** The flow chart representation of the relevant blocks is captured in figure 4.4.

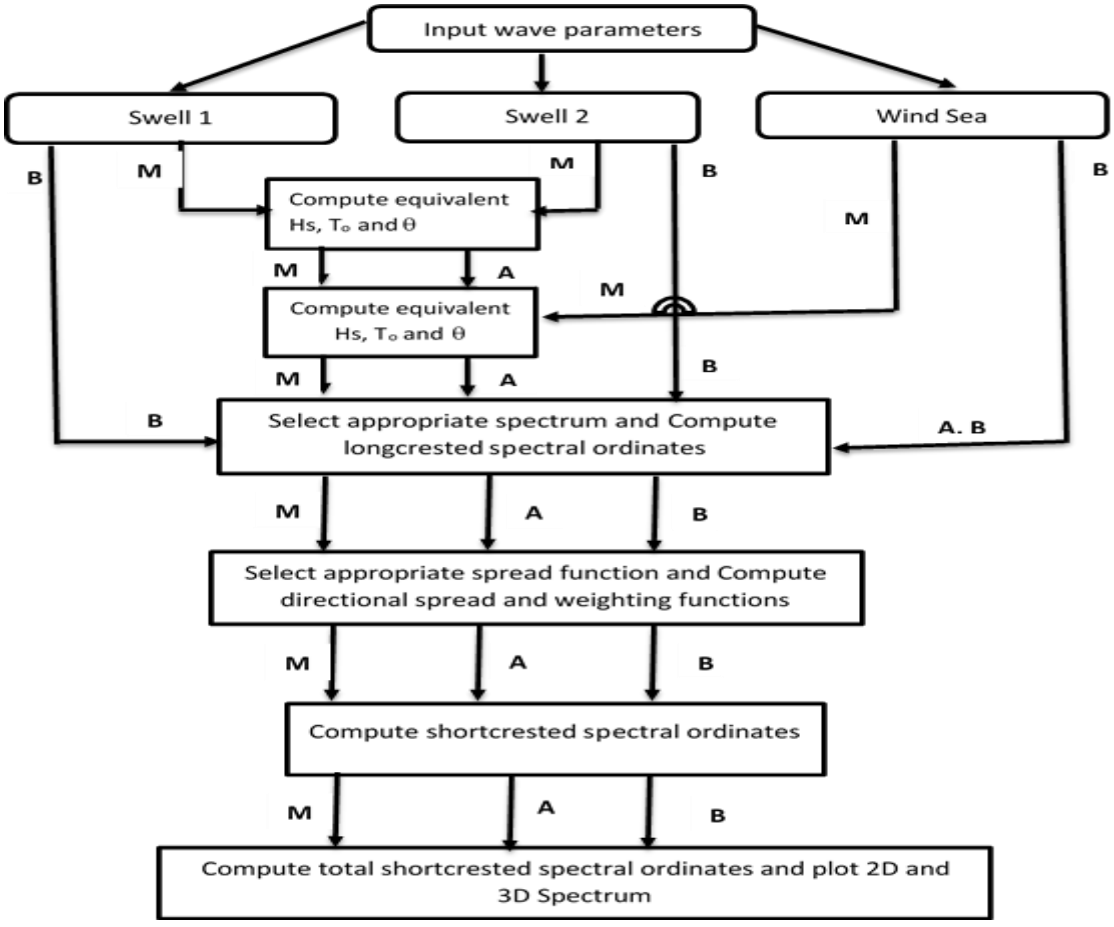

Figure 4.4 Script flow chart for spectra summation routine (*M: meansingle, A: separate A technique, B: separate B technique)*

4.3.2 *Sensitivity of spectrum variation on overall sea state*

To carry out this analysis, two wave arrangements (collinear; case 3 and noncollinear case 8, 16;) used. The different summation modes ran and their contour plots comparatively examined**.** A first observation from the Meansingle approach runs indicate that all spectra used estimated the significant wave height using equation 4.136 as compared to the square law estimate of 6.3443m for the summation of wave streams according to equation 4.26. Using the Meansingle technique, the errors observed -0.11664%, 0.08512%, -0.11664%, 0%, 0%, 1.4785% and 0% for the spectrum Bretchneider(BS), JSS, Pierson Moskowitz (PM), Lognormal, Triangular, Torsethaugen and Ochu-Hubble respectively. Similar trend of (-0.1324%, -1.8662%, -0.06147%, -0.06935% and -0.06147%) observed when the combined swell was represented using BS), Pierson Moskowitz (PM), Lognormal, Triangular, Ochu-Hubble with the wind sea using the Jonswap-Glenn spectrum respectively. The use of Ochu-Hubble for both waves gave an error of -0.01419%.
Below are typical shortcrested sea, Longcrested Sea and the contour plots from different spectra application for the cases 3 and 8, applying the mean single technique.

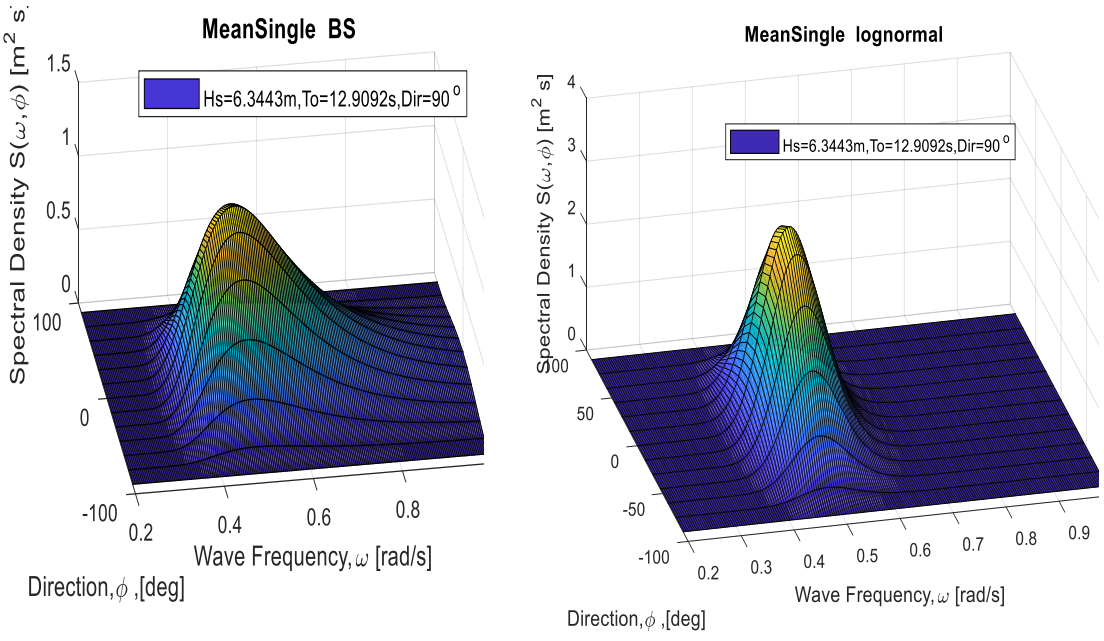

Figure 4.5 Shortcrested spectrum for Meansingle application to case 3

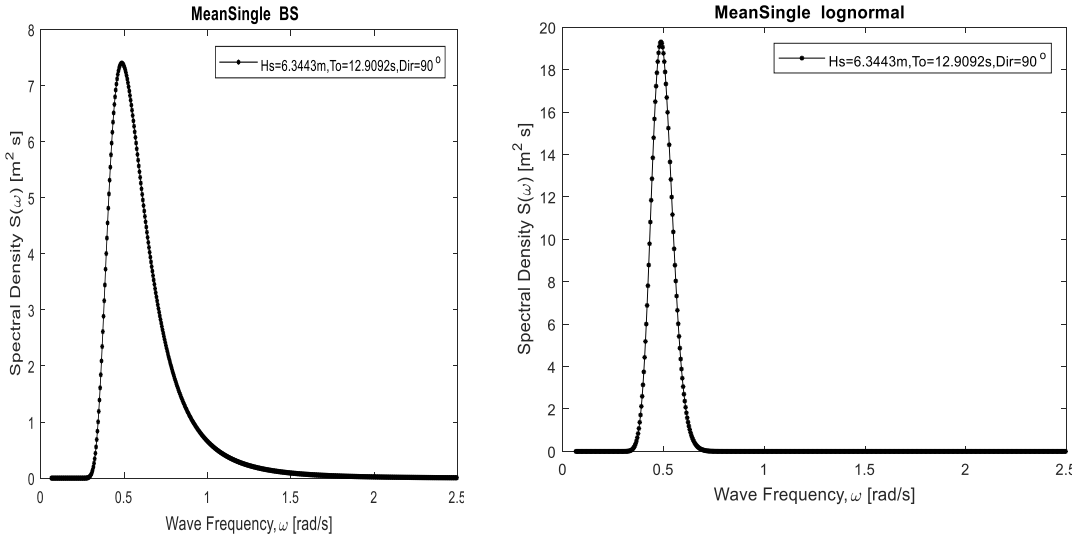

Figure 4.6 Longcrested spectrum from Meansingle application to case 3;

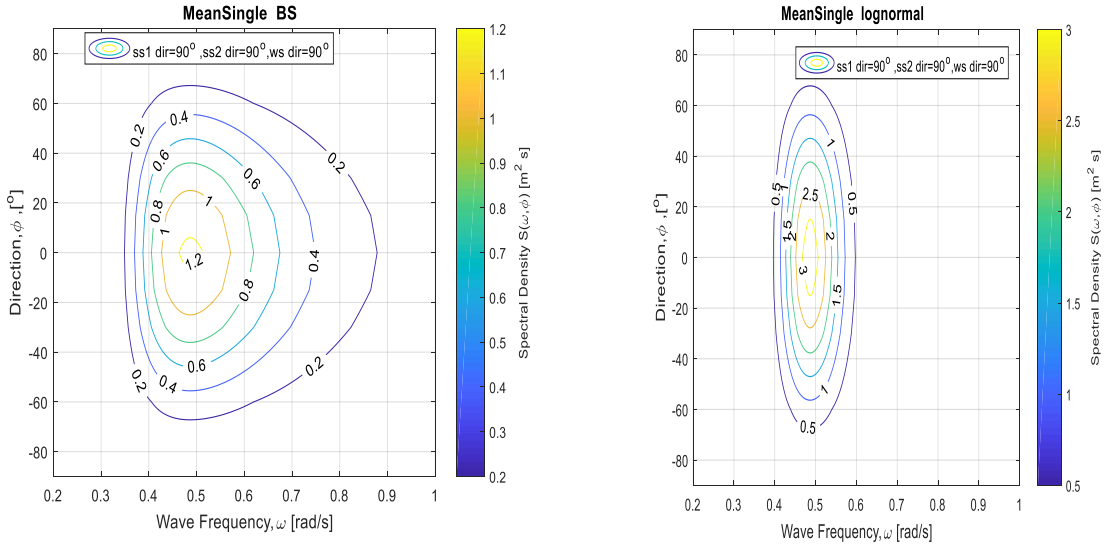

Figure 4.7 Contour plot for shortcrested spectrum from Meansingle application to case 3 (frequency in rad/s)

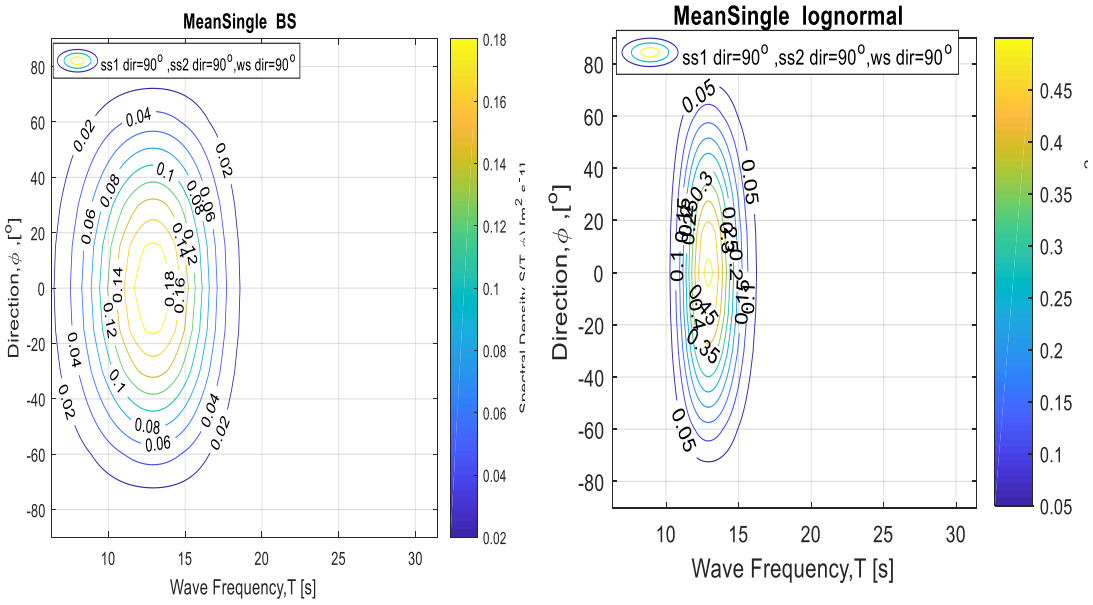

Figure 4.8 Contour plot for shortcrested spectrum from Meansingle application for case 3 (frequency in s)

The case above depicts an instance of collinearity for all the streams. The shortcrested spectrum of figure 4.5 for BS shows a more broad-banded energy distribution compared to the lognormal representation. This is also evident in the longcrested spectrum for both cases. However, the contour plots give visual capture of the influence of the type of spectrum used. From the diagrams of figure 4.7, it can be deduced that spectrum variation is critical in defining the energy distribution of the represented sea state from the spectra density magnitude as well as its spread particularly along the frequency bin. The same trend observed for each of the spectra cases when the non-collinear case in case 16 was used. This however was the case even though the resultant direction of the combined sea changed from 90º to 57.8º. Thus, different sets of spectra were used to further expand the study. Below are representations obtained from Triangular and Torsethaugen spectra.

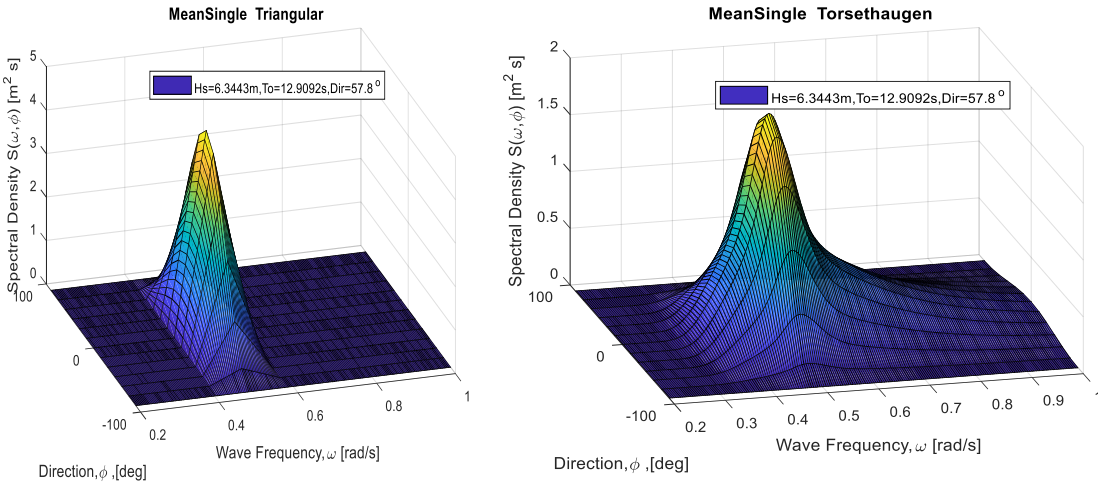

Figure 4.9 Shortcrested spectrum for Meansingle application to case 16

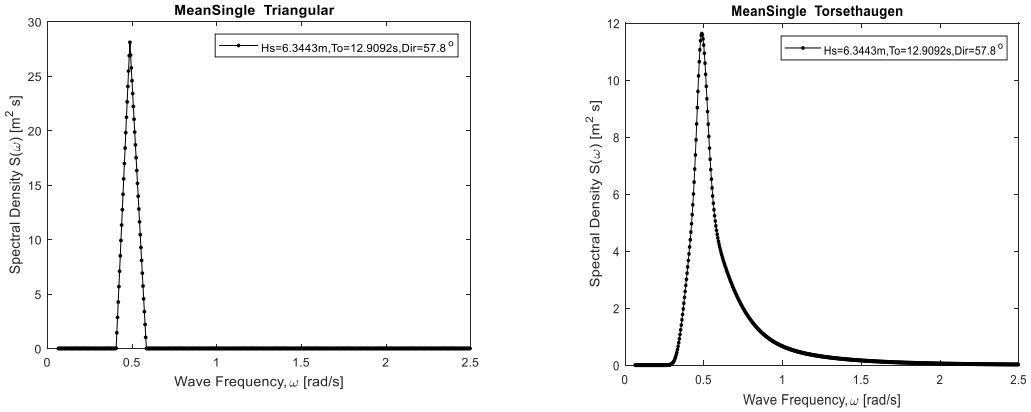

Figure 4.10 Longcrested spectrum for Meansingle application to case 16

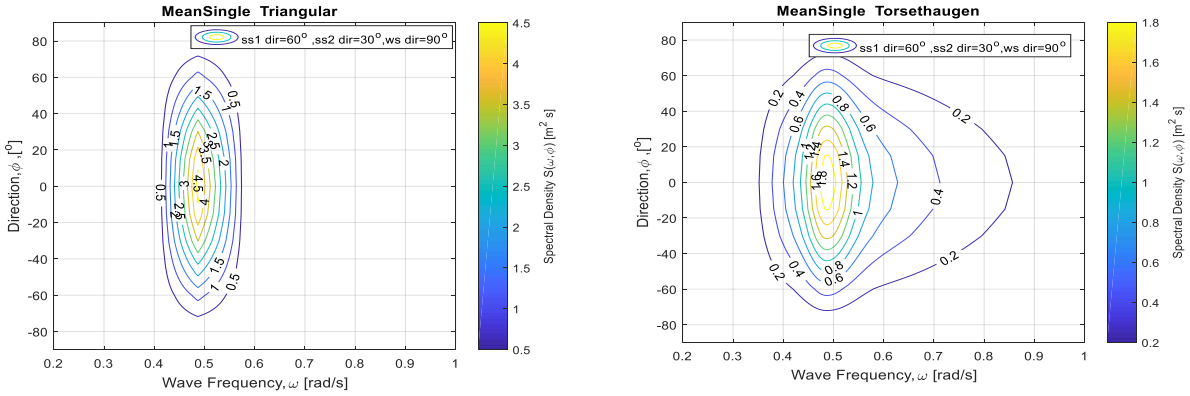

Figure 4.11 Contour plot for shortcrested spectrum from Meansingle application to case 16 (frequency in rad/s)

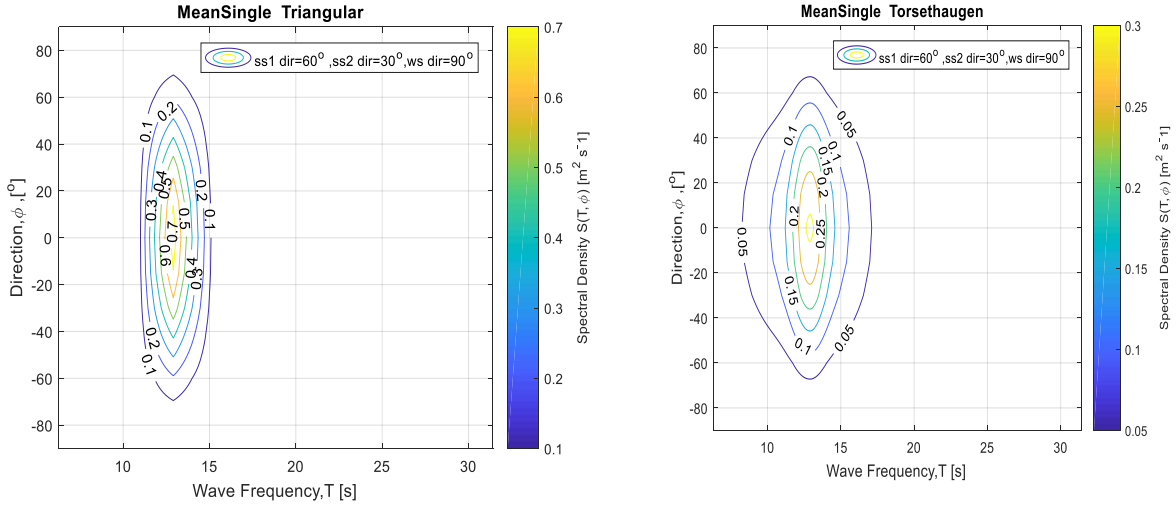

Figure 4.12 Contour plot for shortcrested spectrum from Meansingle application to case 16 (frequency in s)

Observation explained for the case of BS vs Lognormal are very conspicuous from the above diagrams of figure 4.9-4.12. However, as earlier posited, the WASP suggest the use of either the Lognormal or the Triangular for the region, this can also be seen from the shapes and magnitudes displayed above amongst them.

4.3.3 *Sensitivity of sea state combination method variation on overall sea state*

Further analysis was performed to ascertain the extent of influence the method employed in the summation process has on the overall spectra energy and the spread as well. In this instance, the cases 3 and 16 were run using the Separated-A and B techniques. See diagrammatic representations from the runs.

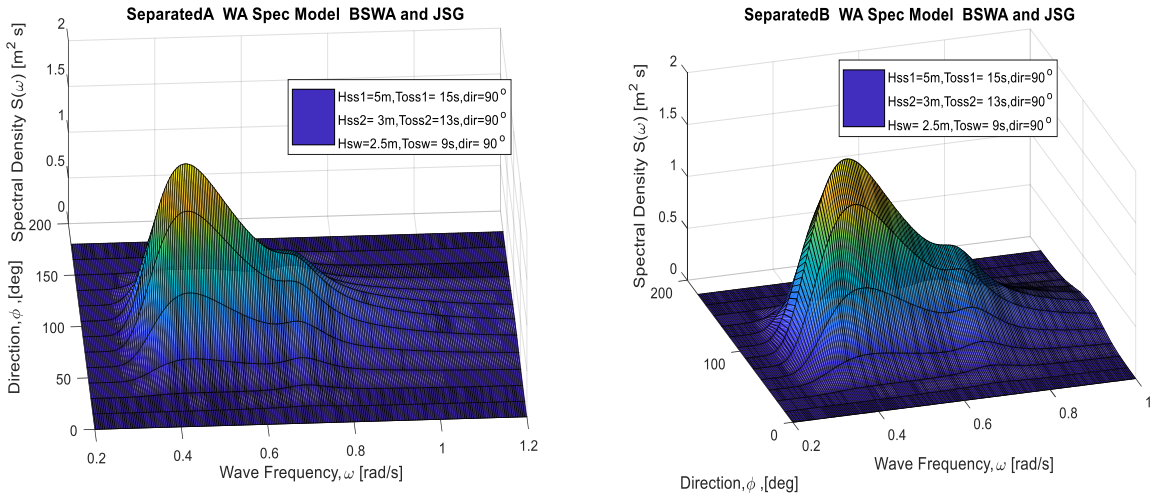

Figure 4.13 Shortcrested spectrum from Separated A and B technique to case 3; BS+JSG

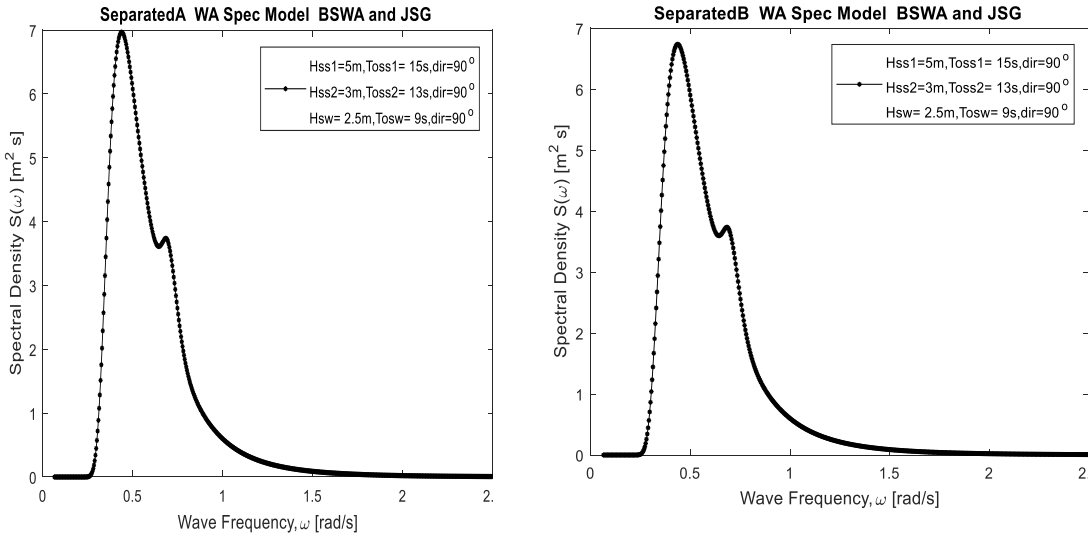

Figure 4.14 Long crested spectrum from Separated A and B technique to case 3: BS+JSG

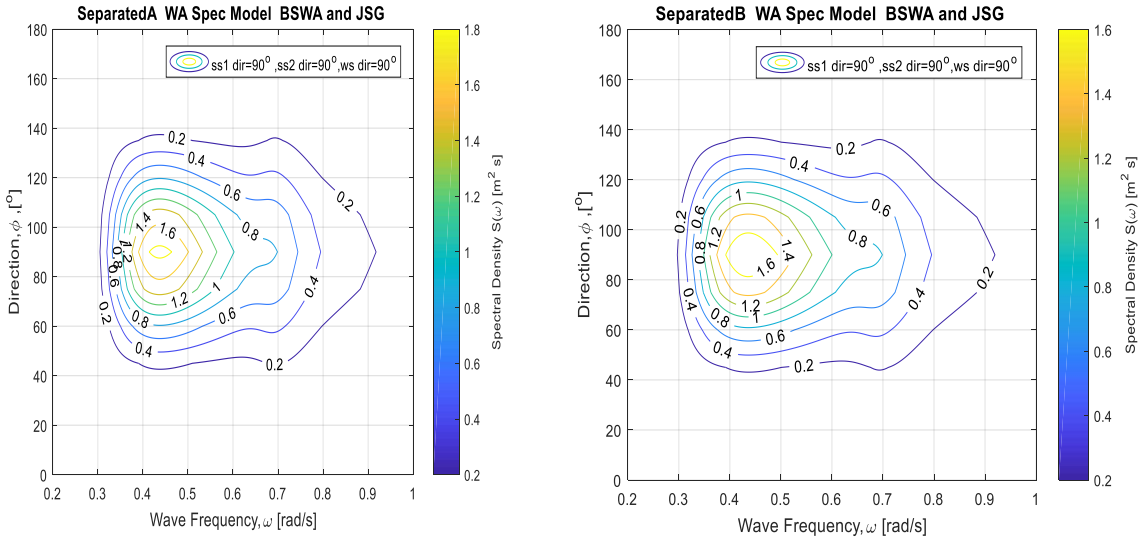

Figure 4.15 Contour plot for shortcrested spectrum from Separated A & B techniques; case 3 BS+JSG (frequency in rad/s)

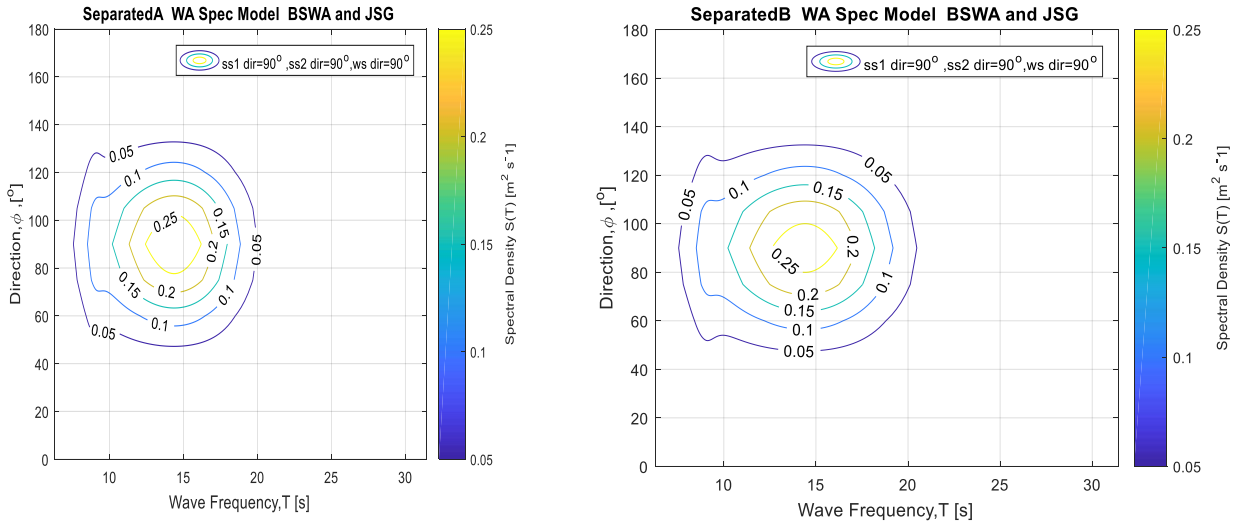

Figure 4.16 Contour plot for shortcrested spectrum from Separated A & B techniques; case 3 BS+JSG (frequency in s)

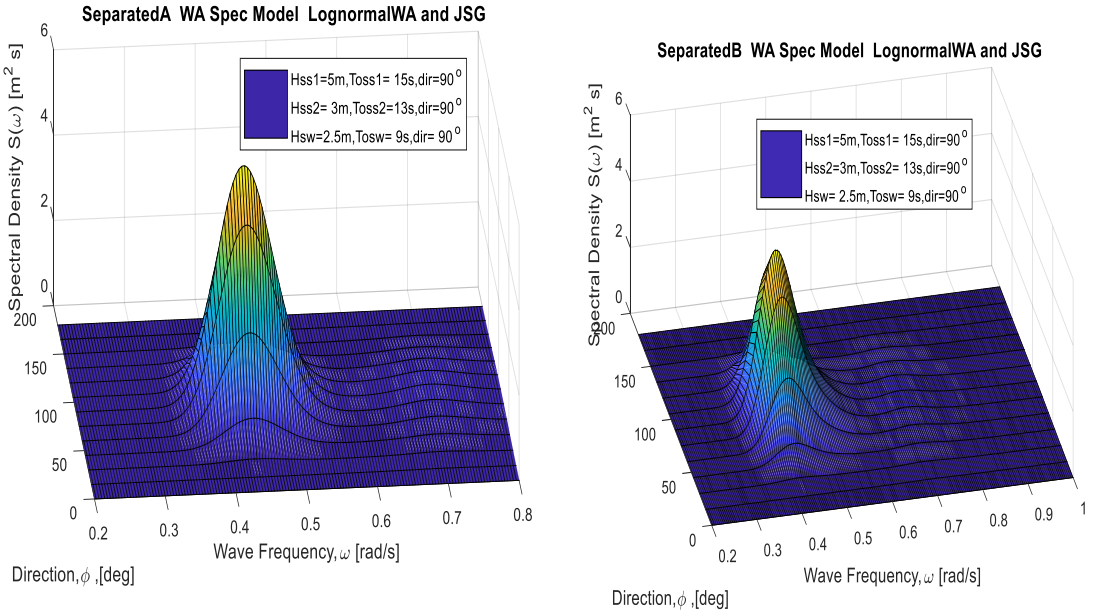

Figure 4.17 short crested spectrum from Separated A and B techniques; case 3, LN+JSG

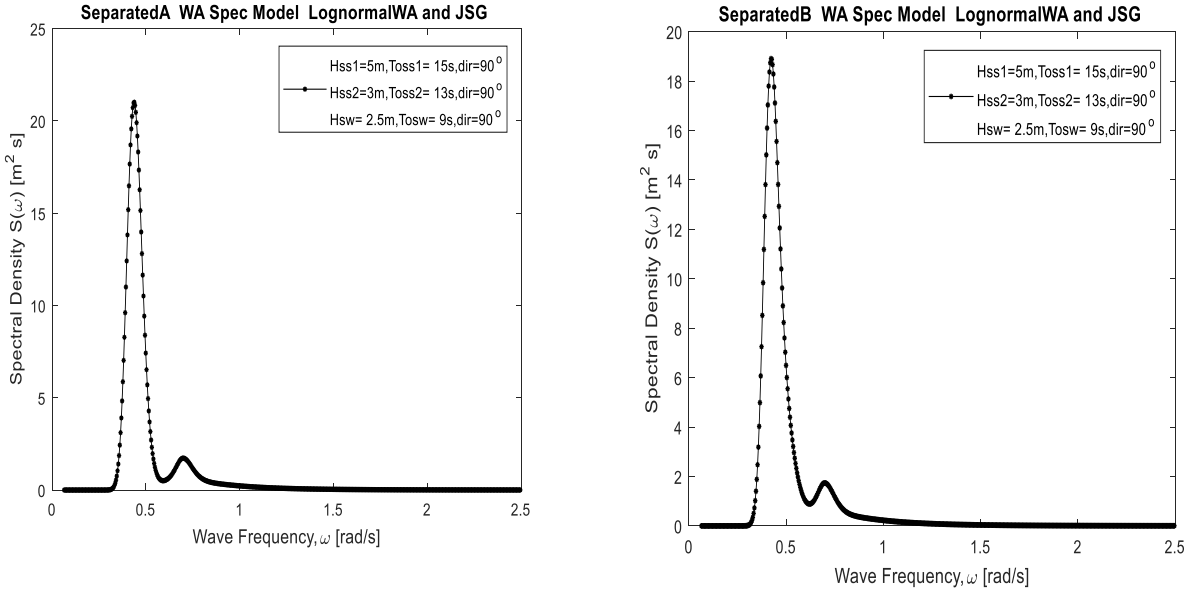

Figure 4.18 Long crested spectrum from Separated A and B techniques; case 3, LN+JSG

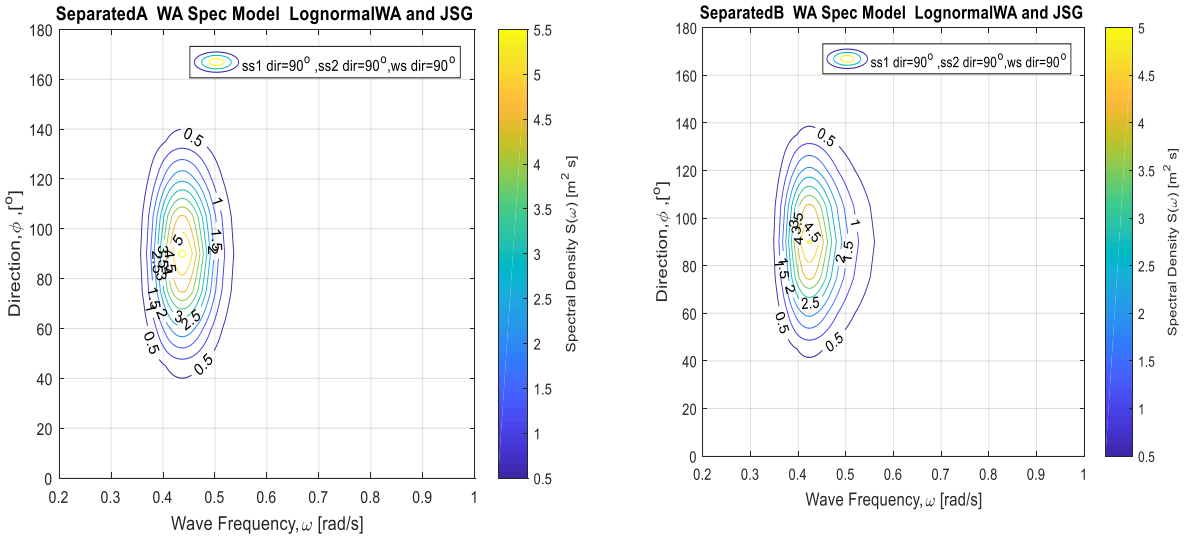

Figure 4.19 Contour plot for shortcrested spectrum from Separated A & B techniques; case 3 LN+JSG (frequency in rad/s)

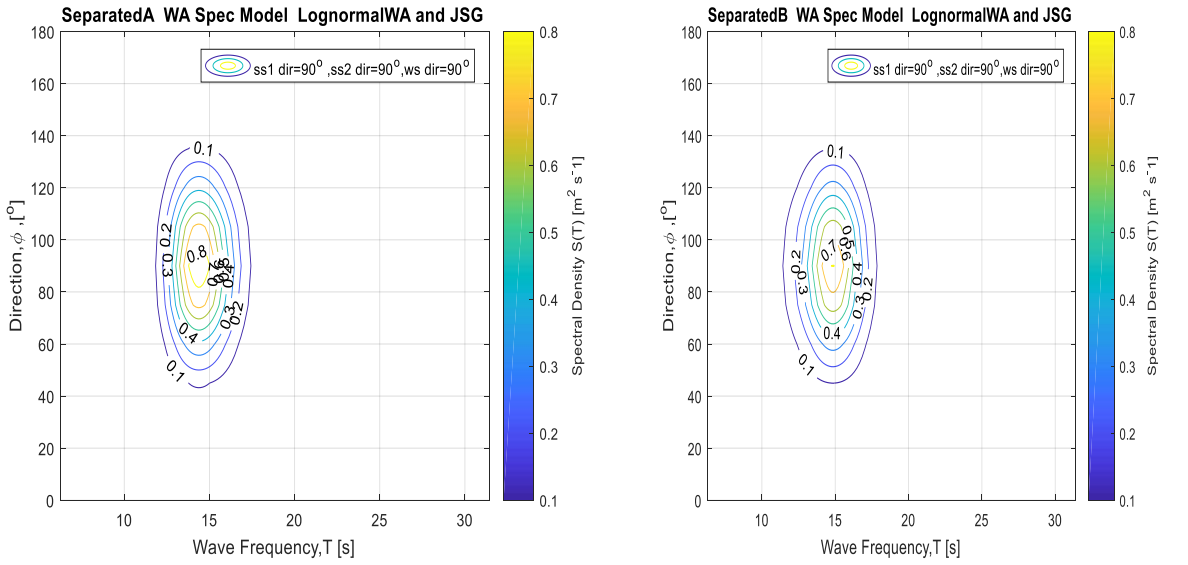

Figure 4.20 Contour plot for shortcrested spectrum from Separated A & B techniques; case 3 LN+JSG (frequency in s)

Similar plots for case 16 and Ochu-Hubble is contained in appendix M. It may appear that the techniques are not very different in concept, however, an investigation of the methods for a wind dominated sea (SSER=1.2426, and IMD=0.3685) resulted in the figures of 4.21-26 below.

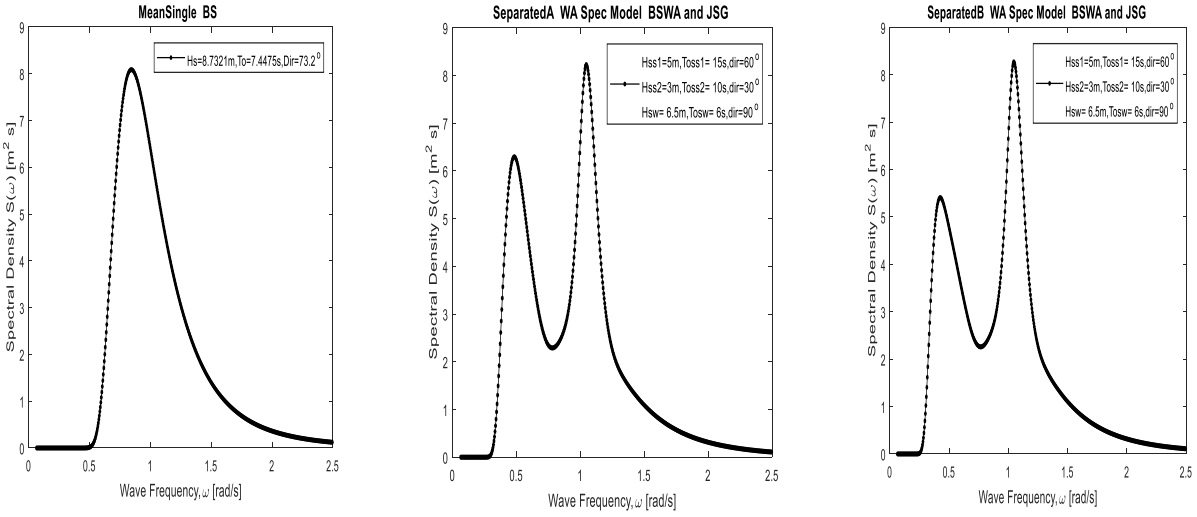

Figure 4.21 Longcrested sea spectrum for wind dominated sea (SSER=1.2426, IMD=0.3685) all technique: BS

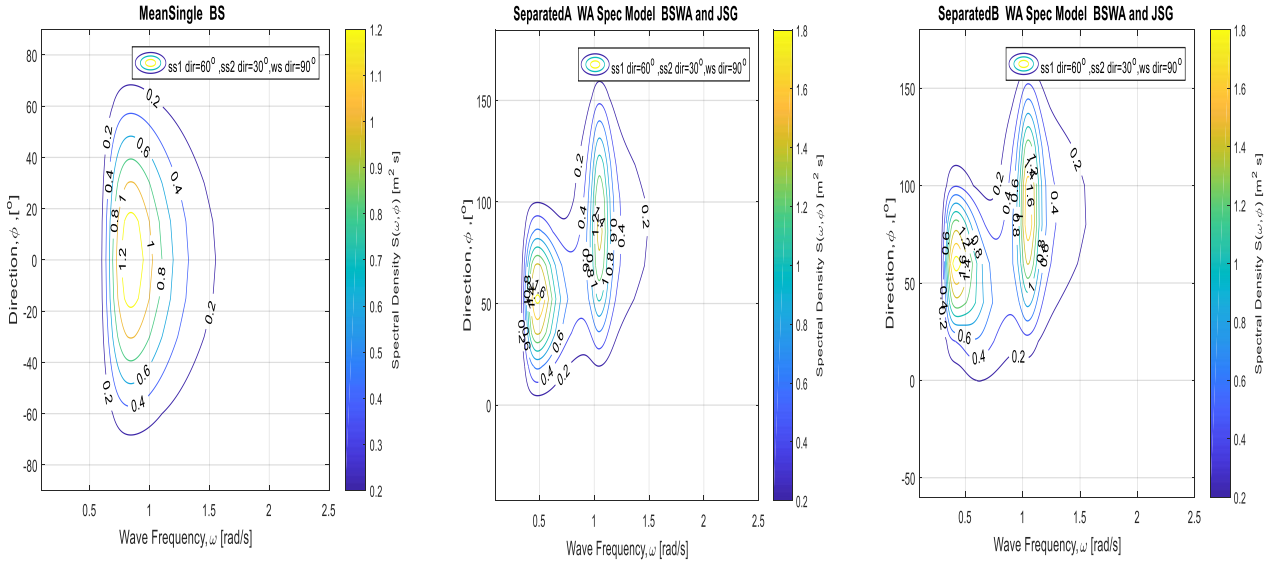

Figure 4.22 Contour plot for wind dominated sea (SSER=1.2426, IMD=0.3685) all technique: BS

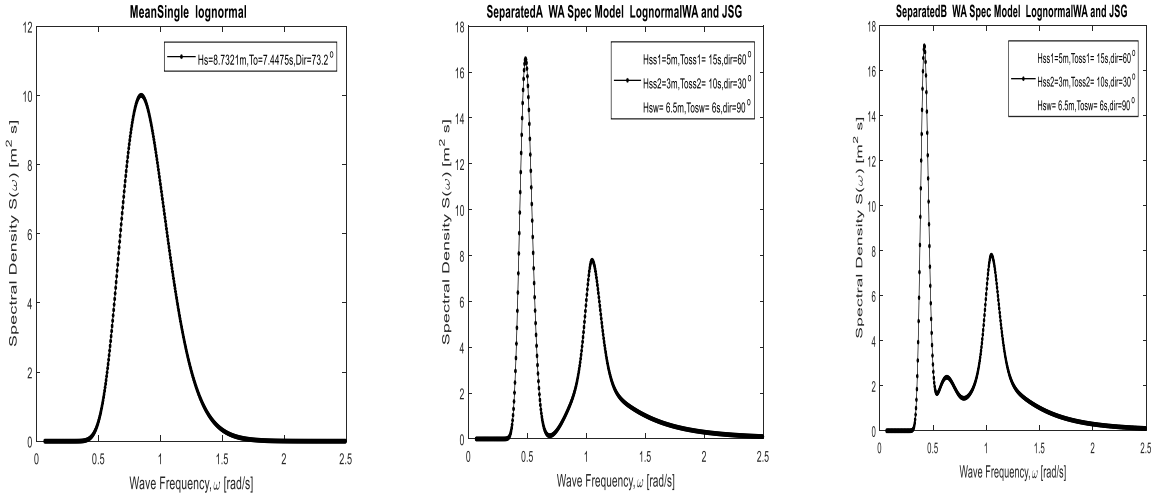

Figure 4.23 Longcrested sea spectrum for wind dominated sea (SSER=1.2426, IMD=0.3685) all technique: Lognormal

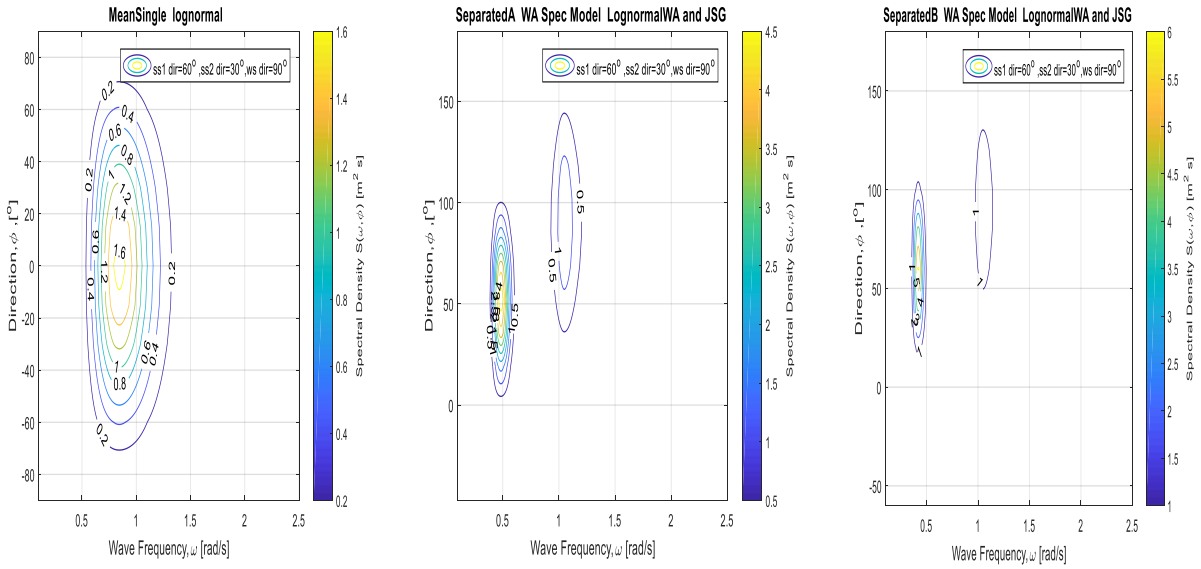

Figure 4.24 Contour plot for wind dominated sea (SSER=1.2426, IMD=0.3685) all technique: Lognormal

The multi-peaks are clearly represented for the separated A and B techniques, which is not present in the meansingle approach the streams are well separated in terms of frequency. Depending on the method adopted, there is likelihood of misinterpreting the resonance from the number of wave frequencies, which might cause possible excitation. From the typical plots of figure 4.23, for the meansingle approach, the expected resonance

may likely occur at a single wave frequency as indicted by the single peak. Whereas for the separated-A technique two instances of such phenomenon are expected compared to three in the separated-B method.

4.3.4 *Sensitivity of stream directions on overall sea state*

Because the separated B technique considers the unique directional orientations of the individual streams, it is instructive to conduct this analysis using it as the yardstick method. The Lognormal spectrum for the swells and the JSG for the wind sea were implemented for this sensitivity study. All the directional combinations in table 4.1 were performed. It is common knowledge to infer that the directionality of the streams would result in a variation of the overall spread, which implies a variation in the distribution of wave energy around the region. For the case 3 [90^o, 90^o, 90^o], the spread spans from 0^o to 180^o with an effective spread area of 180^o. For the case 8 [90^o, 45^o, 180^o], the spread area is -45^o to 270^o with an effective spread region of 315^o. This is also not the same for the case 16 [60^o, 30^o, 90^o], the region spans from -60^o to 180^o, with its effective region been 240^o. The figure 4.25 shows the maximum spectra density obtained from various combinations of the wave streams. This quantity which represents the energy present in the wave is being used as an indicator to tract the influence of directions from the wave streams.

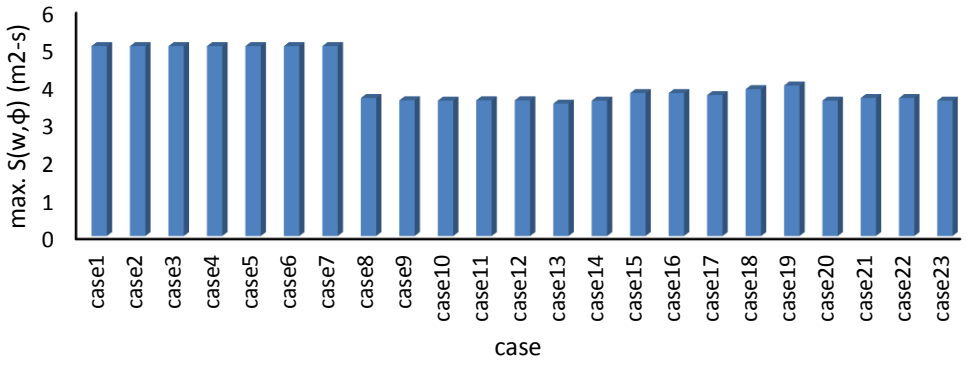

Figure 4.25 Maximum spectra density for varying combinations of wave directions

The figure 4.25, shows that for collinear cases, the spectra energy is practically unaltered, with a relatively constant value of 5.0416 m^2-s. This deduction may be misleading attempting to remove the effect of directionality for collinear cases. A further observation from the contour plot shown in figures 4.26 below, gave a significant variation in the overall spread within which the energy is distributed.

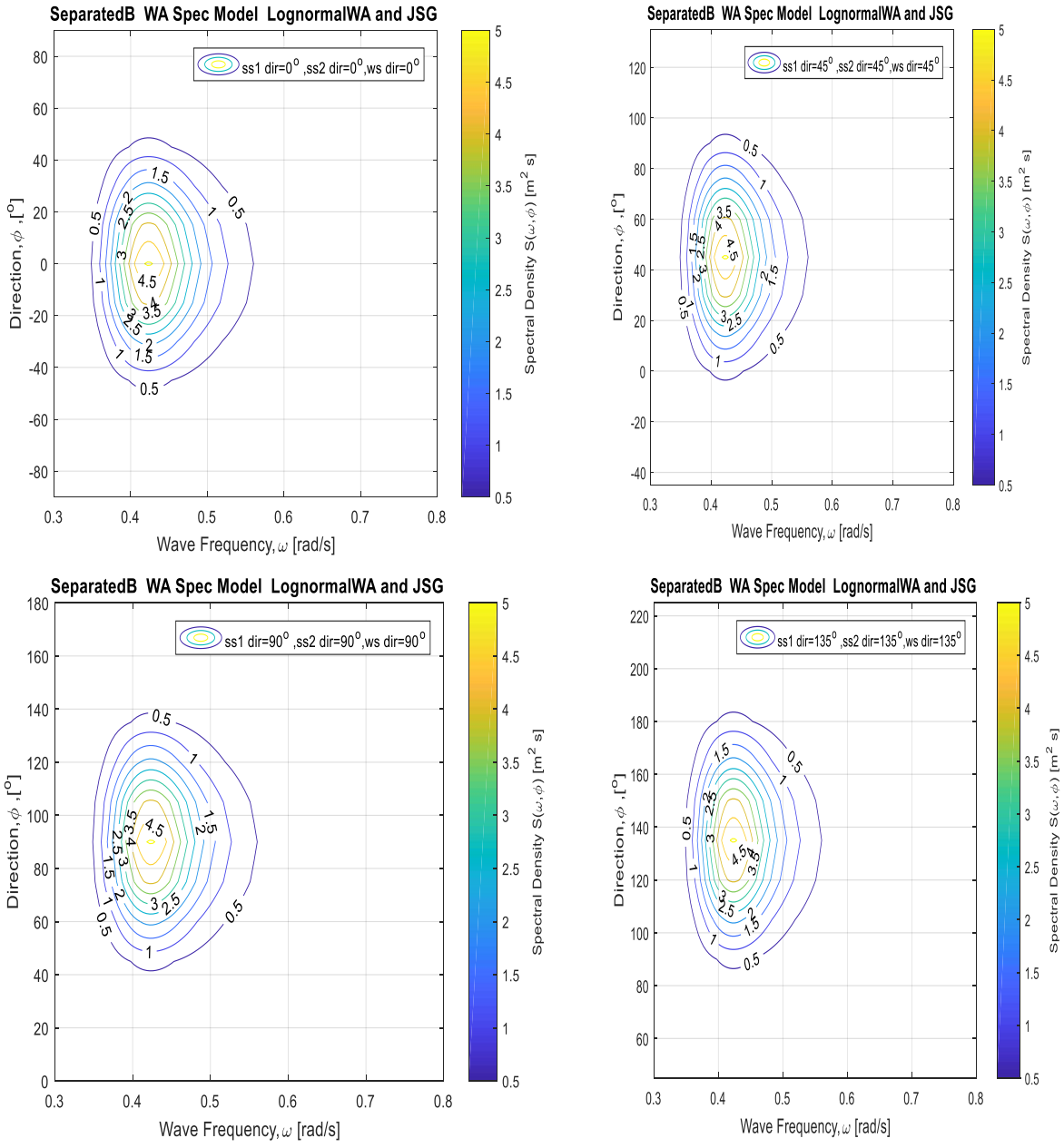

Figure 4.26 Contour plot showing Sω(ω,φ) distribution w.r.t. to (ω,φ) bin for collinear cases 0º, 45º, 90º and 135º

Whilst the energy is the same, the directional span of influence is around (-50º to 50º), (-5º to 95º), (40º to 140º) and (85º to 185º) for collinearity 0º, 45º, 90º and 135º respectively. The frequency range of about 0.35rad/s (18s) to 0.57rad/s (11s) appears the same for these cases as well. This observation is also similar for the collinear cases of 180º (130º to 230º), 30º (-20º to 80º) and 60º (-15 º to 75 º).

This however is not true for instances of non-collinearity as indicated from figure 2.26 for case 8 to case 23. There are variations ranging from 4.001 m^2-s for case 19 to 3.51 m^2-s for case 13. However, the estimated significant wave height from all cases are significantly the same at 6.3404m, it is then concluded that the reduction in the spectra density observed is because of the presence of other significant peaks with the ability of adequately redistributing the spectra density. The figure 4.27 below are plots for cases 18, to 23. This was the phenomenon noticed in the contour plots scenario of cases 13 and 14.

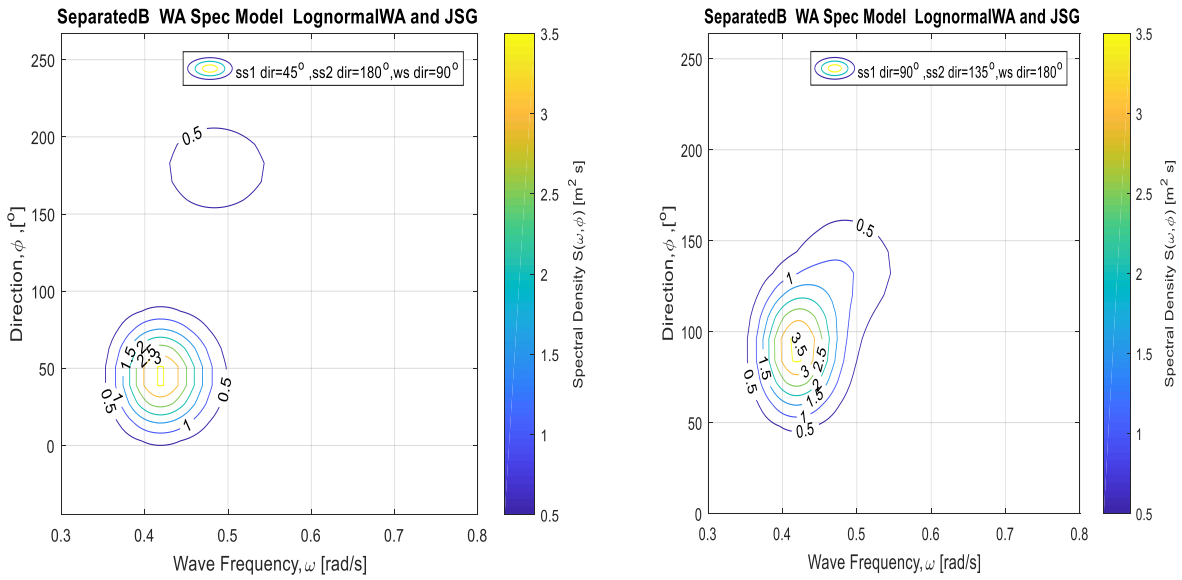

(a) (b)

Figure 4.27 Contour of non-collinear cases showing possible multi-peaks (a) case 13(b) case 14

From figure 4.25, comparing case 2 and case 18, a change in direction from 45º to 90º for the wind sea component produced a reduction of 1.1392 m^2-s (22.59%), similarly,

comparing case 3 and case 19, an associated change from 90° to 45° resulted 1,0416 m^2-s (20.66%) reduction in spectra density. However, when case 8, 20 and 22 where compared for the wind sea changing direction from 180° to 90° and 45°, the change in spectra density was remarkably insignificant (≈ 0%). This further illustrates the swell dominance of the sea state in use.

Comparing the case 2 and case 20, a 1.4426 m^2-s (28.61%) reduction was estimated for a direction change of 45° to 90° for the main swell. Similarly, for case 11 and 19, for a direction change of 180° to 90°, a 28.44% reduction was computed. Similar variation was observed for the secondary swell when cases 2 and 22, and cases 3 and 23 were compared, reduction of 1.3732, (27.24%) and 1.443 m^2-s (28.62%) estimated respectively. Unlike the case of the wind sea, a comparison within the non-collinear combination for the main swell, looking at cases 12 and 19, and case 9 and 18 yielded increase of 0.3924 m^2-s (10.88%, for 180° to 90°) and 8.17% (0.2947 m^2-s, 8.17%, for 180° -45°) respectively. For the secondary swell, changing from 180° -90°, from case 13 and 23 yielded an increase of 0.079236 m^2-s (2.25%) of the spectra density.

4.3.5 *Sensitivity of number of regular frequency on overall sea state*

The Separated B technique was used while varying the number of regular wave frequencies. The runs for the different cases are plotted below.

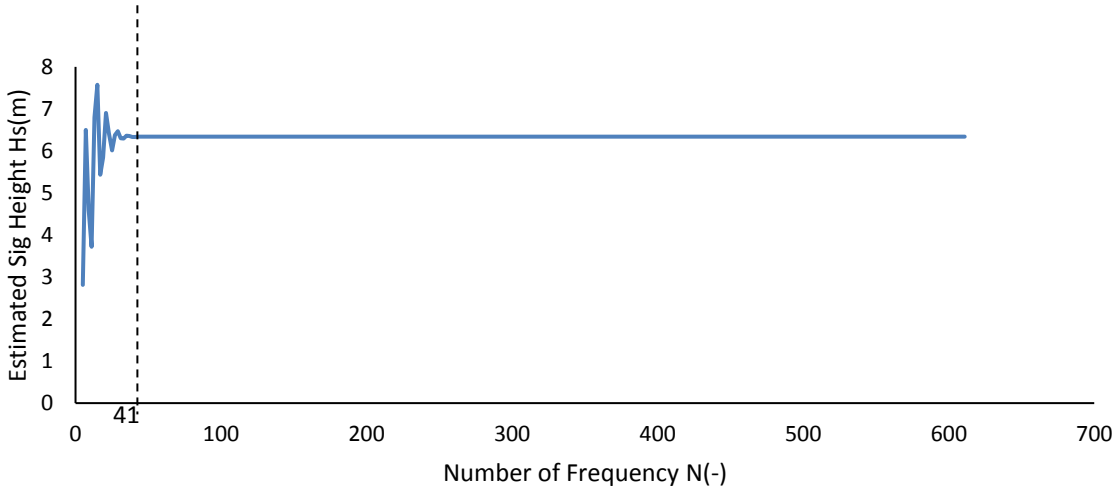

Figure 4.28 Estimated significant wave height against number of regular frequencies

The equation 4.13a was used in estimating the significant wave height from the total spectra curve obtained for the different directional combinations. The run was conducted for various pre-selected number of regular waves from 5 to 610 at intervals of 2. From figure 4.28, the values inconsistently estimated from an under estimated 2.813m for N=5, at an error 55.66%, to an over estimated value of 7.5837m at N=15 with an error of 19.54%. At N≈ 41, the estimated value was 6.3358m at a reasonable error margin of 0.137%. The stable estimation obtained from that point suggest that, any value less that 41 is invalid in carrying out this analysis. However, it is not enough to justify the use of this value based on just the significant wave height as the only estimator. The maximum spectra density was investigated with the wave height. From the figure 4.29, the spectra density estimation was found to be very unsteady after N=41, however normalizes to some point around N=199. It is instructive to note that, a minimum of 1000 regular waves are needed to generate a reasonable irregular sea even for short periods (Faltinsen, 2000**).** Thus, with about 13 directions for 41 waves, i.e. 533 waves cannot be sufficient for this purpose. For N (199) gives 2587 waves, thus after this point, for both the collinear (figure 4.29) and non-collinear (figure 4.30) cases, the estimation became reasonably stable. It can be inferred that after N=199, the number of frequencies used may not be very significant in determining other secondary parameters associated with the wave.

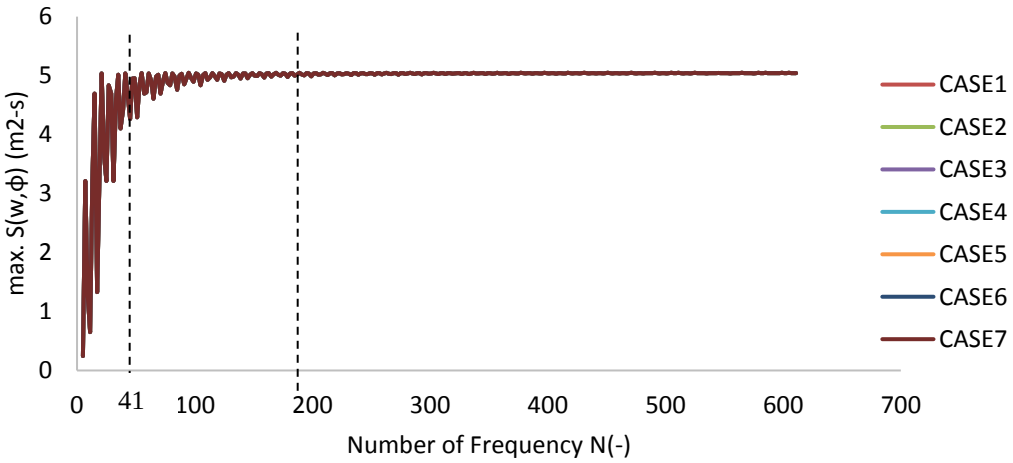

Figure 4.29 Curve of maximum spectra density against N for collinear cases

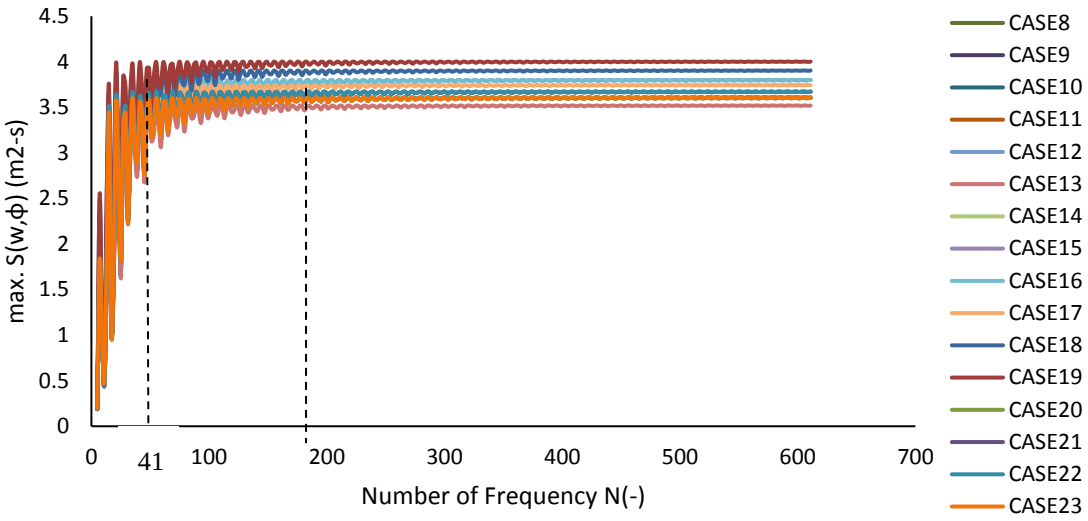

Figure 4.30 Curve of maximum spectra density against N for non-collinear cases

At this point, it is the choice of the programmer to either use higher value for clarity of the 3D Spectrum against computational time.

4.4 Generalized Weighted Technique Approach to Estimate Exciting Forces from Regular Wave Formulations

It has been demonstrated that the fundamental principle behind the determination of irregular wave formulations are based on regular wave extractions. This section presents a generalized presentation of a novel technique premised on the fact that, wave excitations are products of the sea wave. The sea wave is primary defined by the spectrum which is frequency dependent. Rather than adopt the principle of direct supposition of the regular wave forces, it uses a weight modified formulation and through a black box approach (input/output), combines the individual contributions from the individual waves. The weight is estimated from the existing spectra density, based on the contribution from the individual wave frequency on the entire spectrum. (Spanos et al,1997) used a similar approach in the determination of the diffraction force through frequency–dependent diffraction coefficient not based on the spectrum. The coefficient was used to modify the instantaneous wave elevation instead.

Let the generalized force from the regular wave formulation be represented as

$$F = f(\omega, \theta, \epsilon) \tag{4.36}$$

Where;

ω represents the frequency of regular wave, θ represents the direction and ε is for other independent variables.

For a regular wave, with a single stream the force F can be determined. Assuming the sea is composed of 'N' number of regular waves, the generalized force from each stream, can be interpreted as follows.

$$F_i = f(\omega_i, \theta_i, \epsilon) \tag{4.37}$$

The total force can be mathematically represented as

$$F = \sum_{i=1}^{N} W_i * F_i \tag{4.38}$$

It is logical to argue that, since the sea is composed of different regular waves in varying proportions as it is evident from the spectrum. The weight W_i is a measure of this energy contribution from a stream 'i' within its bandwidth $d\omega$ on the overall energy (mo).

Mathematically;

$$W_i = \frac{\delta(mo_i)}{mo}; \tag{4.39}$$

Where;

$$\delta(mo_i) = S_\zeta(\omega_i) * \delta(\omega_i) \tag{4.40}$$

$$mo = \sum_i^N S_\zeta(\omega_i) * \delta(\omega_i) \tag{4.41}$$

Equation 4.37 is applied on the condition that

$$\sum_i^N W_i = 1 \tag{4.42}$$

The above equations can then be extended to a generalized shortcrested sea; thus, for an individual secondary wave stream of frequency ω_i and direction θ_j, the force can be idealized as;

$$F_{ij} = f(\omega_i, S_\zeta(\omega_i, \theta_j), \theta_j, \epsilon) \quad (i=1\text{-}N, j=1\text{-}M) \tag{4.43}$$

The total force can be mathematically represented as,

$$F = \sum_{i=1}^{N} \sum_{J=1}^{M} [W_{ij} * F_{ij}] \tag{4.44}$$

Similarly;

$$W_{ij} = \frac{\delta(mo_{ij})}{mov}; \tag{4.45}$$

Where;

$$\delta(mo_{ij}) = S_\zeta(\omega_i, \theta_j) * \delta(\omega_i) * \delta(\theta_j) \tag{4.46}$$

$$mov = \sum_{i=1}^{N} \sum_{J=1}^{M} [S_\zeta(\omega_i, \theta_j) * \delta(\omega_i) * \delta(\theta_j)] \tag{4.47}$$

Equation 4.44 is also applied on the condition that

$$\sum_{i=1}^{N}\sum_{j=1}^{M}\left[W_{ij}\right] = 1 \qquad (4.48)$$

Whereas mo signifies the area under the longcrested spectra, mov represents the volume under the shortcrested spectrum.

4.5 Conclusion

By extending the wave summation technique of (Boukhanouvsky and Soares, 2009), three approaches were successfully adopted in developing the representative seaway for the West African region. The meansingle approach applies the summation technique by assuming the existence of a single wave stream with the energy equivalent to the supposed overall sea state. A limitation of this method is that peak frequencies play major roles in the determination of the magnitude of response experienced when a structure encounters the sea way. Because the real sea is multi-peaked, the other smaller peaks are most times supressed alongside the larger ones. Unlike the meansingle technique, the Separated-A approach considers the swell seas as single stream and then combines them with the independent wind sea component with different directional spreads. In this approach, there is also the likelihood of supressing a weaker swell component, and thus the peak characterization of the separated swell streams is not well represented. These limitations lead to the extension of the technique (Separated-B) to consider independently the separated wave streams, and the spreads as well. For seas with the streams well separated from the value estimated from the IMD, the presence of the three distinct peaks signifies a better characterization of the actual sea. The formation of these streams is geographically dependent, as such the need to use an appropriate spectrum model when characterizing a specific region is significant. From the WASP, like the JONSWAP, it is recommended that the benign region of the West African deep offshore be represented by a Lognormal or Triangular spectrum distribution for the multiple swells. Whilst the JONSWA-Glenn (modified JONSWAP) is used for the wind sea component. Visual inspection, as well as quantifying of the spectra energy density and the spread area, has shown that the spectrum has a strong influence on the overall shape of the seaway. Another significant extraction is the influence exhibited by the directions of approaching wave streams. However, this directional effect is not significant for cases in which all the

streams are collinear, but significant in cases where streams generated, travel to structure from different or non-collinear directions. Significant variations of over 20% in spectra density were estimated for all streams when collinearity was compared to non-collinear arrangements. In assessing the adequate number of wave frequencies to form the irregular surface, the sensitivity study performed using the significant wave height simultaneously with the estimated maximum spectra density, suggest a region of acceptability for values of N>=199. Although, this was not captured in the sensitivity for the significant wave height, but it gave a clue of the phenomenon of unsteady estimation encountered during the iteration. The estimate was random from the N=5 up to 41, and then became steady. The findings defined an appropriate value for N to represent the sea way. The N values above the minimum threshold may also be selected with the consideration of chart clarity against computational time.

The contour plots present a good visual interactive platform for the easy identification of patterns in parameters variations and influence on the sea state energy distribution. This was also used extensively by (Boukhanovsky and Soares, 2009) In line with the set objective for this chapter, some outputs such as, the spectra shape, the summation technique, the number of frequencies are used to develop the motion simulation code.

The concept of estimating the forces for a real sea state (irregular shortcrested sea) is pined on the superposition of the forces obtained from the regular longcrested wave formulation. Fundamental principles upon which hydrodynamic tools works are explicitly obtained in tool's user manuals. A new approach using a weighted technique based on the spectra density has been presented for the estimation of the Froude Krylov and Diffraction forces from regular wave formulation. The generalized equation was presented in this chapter, this equation was used in expanded form in chapter five.

5 Chapter Five: Numerical Development of Motion Simulation Routine (SESAM and Proposed method (Code))

5.1 Introduction

The real motion description of any unit exposed to the ocean environment is typically in six degrees, three translational (surge, sway and heave) and three rotational (roll, pitch and yaw). For design and operational considerations of the unit, these motions must be estimated. In other to avert the limitations involved in several complex and cost intensive techniques which are not feasible for preliminary studies, this research uses simplified methods to approximate every component of the 6 dof equation of motion (eom) for a simply shaped unit tautly moored to the sea bed. However, the actual FPSO is formulated using form coefficients to modify some of the parameters.

The unit is partially represented as a rectangular box, which is compliant with the need for ease of construction and for enhanced storage capacity. The actual hull form and its associated characteristics are obtained by using the form coefficients as transfer functions on the rectangular form. This is recommended since the unit is not a mobile structure but is built to operate at a specific region over a very long period ranging from 15 to 35 years.

FPSO's are typically known to have large top side areas, hence the top sides are modelled using rectangular vertical plane walls across the four sides (Port Sides (PS), Starboard Side (SB), After side (AF), Forward side (FP)). It also has a predominantly flat bottom.

The location of interest is the West African deep offshore region, where the water is generally assumed to be benign with modal significant waves of up to 2m to 5m in height. It is also a multimodal sea with multiple swells, combining with wind seas to form the sea surface.

Because it is a benign region, most FPSO's presently operating are moored to the sea bed using steel catenary systems ranging from 8 to 18 lines (see Appendix A), spanning from the tether point at the Turret, i.e. the fairlead down to the anchor points at the sea bed. However, as the need for safe and economic operations increases, steel catenary mooring lines are being gradually replaced by Taut Polyester lines. The major advantage being the massive reduction of overall mooring line weight and length. This also is good for the

subsea equipment should in case of failure of any of the lines during operations. The restoring capability between these two systems also differ. While the steel catenary lines carry out restoring via their weight, the taut or pre-tensioned polyester lines do restoring using their elastic properties instead. Figure 5.1 and 5.2 a & b below is a schematic layout of the FPSO in location;

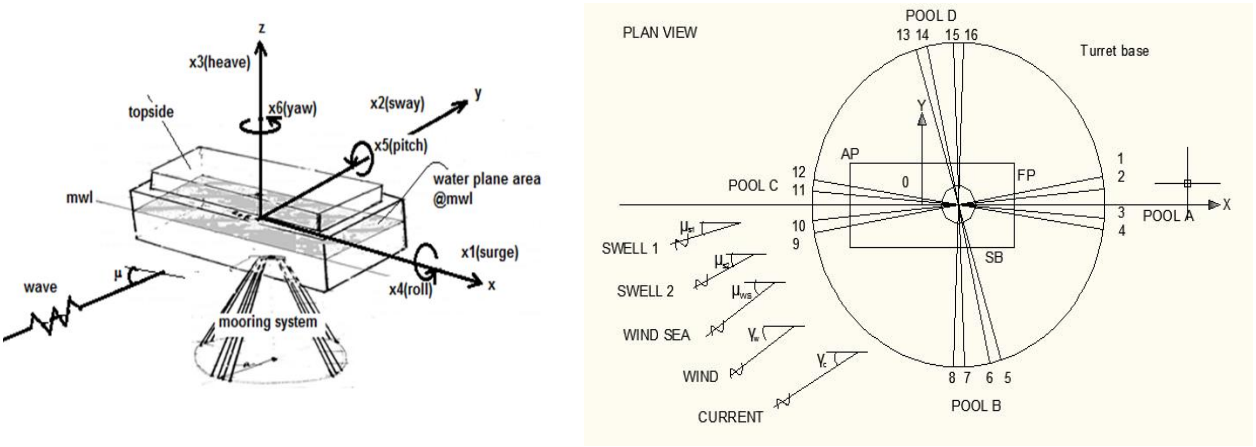

(a) (b)

Figure 5.1 (a) Schematic diagram of moored FPSO (b) Plan View of FPSO;

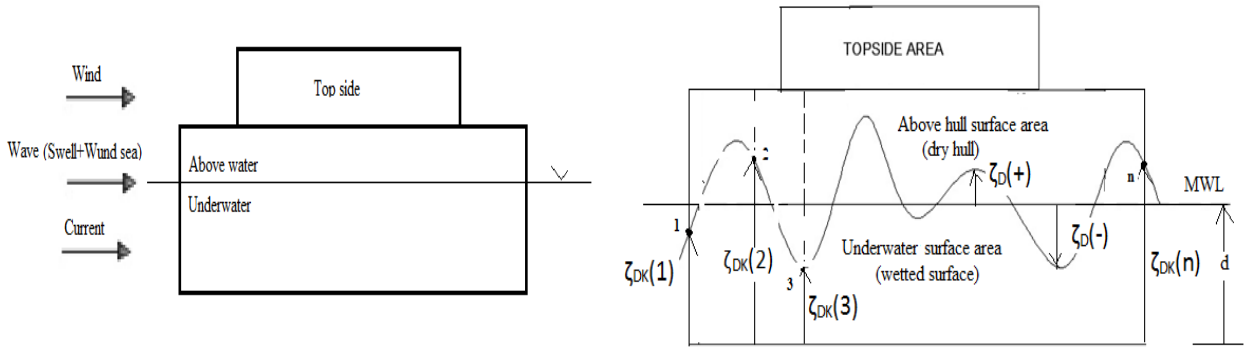

(a) (b)

Figure 5.2 Free Floating unit (a) Side view in calm sea;(b) Side view in wave

The analysis procedure benefits from the convenience of the Froude-Krylov assumption, in which the hull is assumed to be transparent. This enables an approximation to be made for the elevations at every grid point within the rectangular water plane area of the mean floating unit at any given time. Secondarily, the excitation forces are estimated using the

pressure integration over the wetted surface and the formulated wave frequency-spectra density weighted technique. The drift forces are estimated from simple approximations while the instantaneous current and wind forces are computed from the OCIMF VLCC data for the coefficients.

5.1.1 *The Equation of Motion and its components*

The equation of motion resulting from the balancing of forces acting on floating unit using the popular Newton's law of motion is re-represented as the primary problem. The components are as described in equation 5.1. This constitute the primary problem as represented by equation 5.1 to be solved.

$$\left[M_{ij} + A_{ij}\right] * \{\ddot{X_j}\} + \left[B_{ij} + B_{ij}^{v}\right] * \{\dot{X_j}\} + \left[C_{ij} + K_{ij}\right] * \{X_j\} = \{F_J\} \qquad (5.1)$$

With $i, j = 1{:}6$

And the excitation force vector dependent on the defining parameters of the unit's geometry, the sea state and the wind, current condition.

$$\{F_J\} = f_1(\mathrm{S}(\omega, \theta), V_w, V_c) \qquad (5.2)$$

The sea state S(ω,θ) has been robustly dealt with in the preceding chapter 4. V_w and V_c are the instantaneous wind and current velocities respectively.

5.1.2 *Estimation of the Surface Elevation*

In order to apply the technique, the instantaneous surface elevation around the water plane is estimated for each grid point. It commences with the proper discretisation of the plane, in line with the number of sections intended for use for the estimation of the added mass and potential damping using the strip theory approach.

5.1.2.1 *Discretization of the water plane area and hull*

The water plane area in calm water condition is discretized into bins. A reasonable number of grids are taken to reduce the effect of the internal points which are used in subsequent computations. The grid points are also chosen such that reasonable number of points along wave profile are randomly captured.

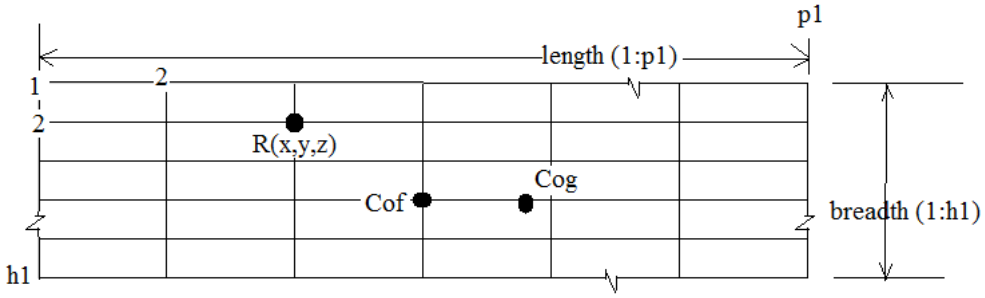

Figure 5.3 Discretized rectangular water plane

The length is divided into h1 points and the breadth into p1 points. This gives a total of (h1 X p1) number of grid points on the water plane surface. The values of h1 and p1 are kept as odd numbers to enable the application of Simpson's rule during integration.

The selected wave system is imposed on each grid point, and the elevation approximated using the water surface elevation equation 4.1 or 4.2. for whether regular or irregular wave formations.

Note that at every time step, the resulting motion of the FPSO causes the water plane to move onto new grid points with respect to the global origin which is initially fixed at the centre of floatation (CoF) of the water plane at the geometric centre of the rectangular water plane. Every subsequent movement is computed relative to this position, not the moving cof of the FPSO itself. The method takes advantage of the moving water plane to re-compute a fresh Froude-Krylov surface at every time step. Because of this procedure, the technique is referred as moving Froude-Krylov mean water plane area. However, the forces are computed based on the body fixed coordinate system and transformed onto the body moving coordinate system via the transformation matrix before the computation of the next time step commences (Fossen, 2011).

At every grid point in each time t, R (x, y, t) the elevation (z) above the mean water line(MWL) ζ and that above the keel ζ_{Dk} can be approximated from equations 4.1 and 5.3; see diagram in figure 5.2b above.

$$\zeta_{Dk} = \zeta + d \tag{5.3}$$

Note that the MWL draft 'd', changes with time due to the mean heave motion or mean sinkage or floatation.

5.1.2.2 *Regular Wave Frequency Estimation Procedure:*

A reasonable frequency range which captures the natural periods of the entire 6dof motion states is selected.

$$\omega_{range} = \omega_{max} - \omega_{min} \tag{5.4}$$

This ensures that the modal frequency of all constituent waves falls within this bound. A reasonable number of regular frequency 'N' is chosen, (pg. 28 of DNV –RP-C205, 2007) recommends $N \geq 1000$ for the formation of an irregular short-term sea surface. However, for time integration, the value could be reduced to a manageable size, particularly for shortcrested seas were directionality is included but on the optimum value obtained by minimizing the error between the mean combined significant wave height 'Hs' and the estimated value $H_{1/3}$ from a regenerated spectrum from the elevation time series is desirable.

$$minimize\ (error = \left|H_s - H_{\frac{1}{3}}\right|) \tag{5.5}$$

Where $H_{1/3}$ is giving by equation 4.13a

The frequency as well as the direction interval is estimated either as a constant or randomly varying value. The essence of randomization is to avoid a possible repeat of sequence in the time histories during simulation (Lloyd, 2004) after a given repeat time equivalent to

$$T_{repeat} = \frac{2\pi}{\Delta\omega} \tag{5.6}$$

The intervals can be constant or varied accordingly.

(a) Constant interval

$$\Delta\omega = \frac{\omega_{range}}{N-1} \tag{5.7}$$

With ($\omega_{range=\omega_{max}-\omega_{min}}$) another approach to select a reasonable frequency bin, is to stretch the modal frequencies of the primary waves to the left and right sides of the band using predetermined factors a, b such that;

$$\left\{\begin{matrix}\omega_{min} = a * \omega_{o,min} \\ \omega_{max} = b * \omega_{o,max}\end{matrix}\right\} \quad (5.8)$$

Where

$\omega_{o,min}$ and $\omega_{o,max}$ are the smallest and largest modal frequency between the streams.

(b) Varying random interval

As earlier stated this is necessary in other to avoid possible repetition of the series after a given time. The quickest technique will be to adopt the procedure of (pg. 208-209, Thor Forsen,2011). In this case the two extreme values $\omega_{min}\ and\ \omega_{max}$ are removed and a new range of frequency obtained as follows

$$\omega_i = \omega_{min} + i * \Delta\omega\ ;\ (i = N - 2) \quad (5.9)$$

A random number (0 to 1), uniformly distributed is used to select a value between $\omega_i\ and\ \omega_{i+1}$, such that the new frequency lies close to ω_i but not necessarily the same value. We can obtain boundary frequencies equally spaced on both sides, thus;

$$\left\{\begin{matrix}\omega_{i1} = \omega_i - \Delta\omega/2 \\ \omega_{i2} = \omega_i + \Delta\omega/2\end{matrix}\right\} \quad (5.10)$$

The new value of random frequency becomes;

$$\omega_i = \omega_{i1} + (\omega_{i2} - \omega_{i1}) * randN \quad (5.11)$$

Similarly, the random frequency interval becomes;

$$\Delta\omega_i = \omega_{i+1} - \omega_i \quad (5.12)$$

The same technique above, can be applied to the values of the directional spread angles as well as its intervals. Thus, with a constant interval $\Delta\theta$, we can obtain constant directional values θ_j as well as random directional intervals $\Delta\theta_j$. This makes available four different options in selecting the type of frequency/directional spread to use in the simulations carried out in this work;

- Constant frequency and constant directions
- Random frequency and random directions
- Constant frequency and random directions
- Random frequency and constant directions

5.1.2.3 *Random Phase generation:*

The random phase which describes the phase lead or lag with which the regular wave approaches the measurement or estimation point is easily modelled using a random number uniformly distributed from 0 to 2π (360^o), and simply estimated as;

$$\varepsilon_{ij} = a + (b - a) * runif; \quad (5.13)$$

Were a=0; b=2π, i, j corresponds to the size of $\omega_{i,}$and θ_j respectively, *runif* is a random number uniformly selected between 0 and 1.

With this known, the surface elevation across an area equivalent to the rectangular water plane can then be approximated.

5.1.3 *Estimation of the Excitation Forces/Moments*

The time varying excitation forces are estimated using simplified formulations from regular waves. The formulations are modified using a weighting technique from the spectra density defining the sea state. The area and volume of the underwater (wetted) and above water (dry) regions for the regular rectangular hull form are estimated. The form coefficients used as continuous functions dependent on draft or section displacement or constants are then used to modify these values to represent the actual hull form.

5.1.3.1 *Computation of Underwater Volume and Buoyancy Force;*

With the elevations above mean water line (MWL) and keel estimated for all grid points in Figure 5.3, the Riemann water plane or surface is obtained in discrete form.

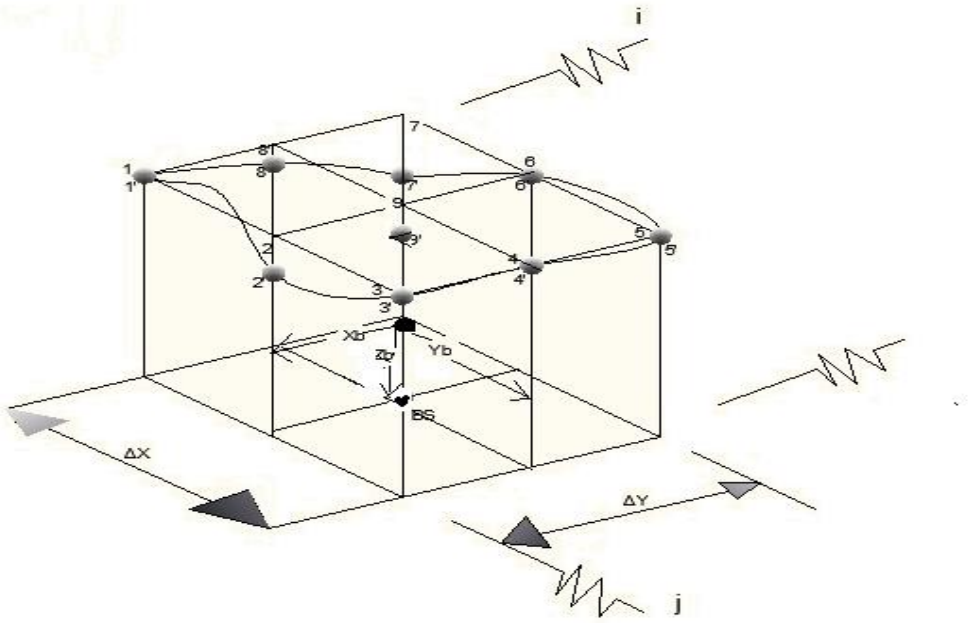

Figure 5.4 Elemental volume of underwater hull

From Figure 5.4 above, the MWL grid surface is represented by points [1,2,3……9], Whilst the Riemann surface ($= f(\,)$) is represented by points [1',2',3'…….9'];

Note;

$$\left.\begin{aligned} f(1') &= \zeta_{Dk}(1) \\ f(2') &= \zeta_{Dk}(2) \\ f(3') &= \zeta_{Dk}(3) \\ &\vdots \\ f(9') &= \zeta_{Dk}(9) \end{aligned}\right\} \tag{5.14}$$

$\zeta_{Dk}(9)$ is the measurement for the central grid point for the 9 neighbouring points used. i.e. distance from keel to water surface approximated.

Using the Riemann approach (Kreyszig, 2010), the elemental volume is approximated as

$$\delta vol = f(9') * \delta a \tag{5.15}$$

$$\delta a = \Delta x * \Delta y \tag{5.16}$$

Whilst using a modification of the Riemann approach which guarantees that all points contribute to approximation, particularly in instances when the grids are not large, the elemental volume is estimated as;

$$\delta vol = mean[f(1'), f(2'), f(3'), \dots \dots \dots f(9')] * \delta a \quad (5.17)$$

i.e.

$$\delta vol = \frac{\sum_{i=1}^{9} f(i')}{9} * \delta a \quad (5.18)$$

The total under water volume at time 't' can then be estimated across the surface for 'nv' number of such combinations of points possible;

$$vol(t) = \sum_{i=1}^{nv} \delta vol \quad (5.19)$$

Instantaneous change in under water volume leading to buoyancy effect is thus estimated as

$$\Delta vol(t) = vol(t) - vol(t = 0) \quad (5.20)$$

Were volume at the start of simulation is

$$vol(t = 0) = Ls * Bs * d(t = 0) \quad (5.21)$$

The Buoyancy Force is then approximation adequately as;

$$F_B(t) = \rho . g . vol(t) \quad (5.22)$$

The volumes and areas where modified using appropriate form coefficients to estimate the values for the actual unit.

5.1.3.2 *Estimation of the center of buoyancy;*

Let the centroid of the approximated elemental volume be $(x_b(i), y_b(j), z_b(k))$. The centroid is obtained by computing all elemental moments moving systematically along the x-direction, and then y- direction. This will then involve double integral, in discrete form;

$$X_B(t) = \frac{\sum_{i=1}^{n}\sum_{j}^{m}\delta vol(t).y_b(j,t)}{vol(t)} \tag{5.23}$$

$$Y_B(t) = \frac{\sum_{i=1}^{n}\sum_{j}^{m}\delta vol(t).x_b(i,t)}{vol(t)} \tag{5.24}$$

$$Z_B(t) = \frac{\sum_{i=1}^{n}\sum_{j}^{m}\delta vol(t).z_b(k,t)}{vol(t)} \tag{5.25}$$

The value of x_b and y_b depends on the grid intervals and the position or index of the surface panel under consideration. The z-ordinate can be approximated as the midpoint of the forming small rectangular box using Riemann or the modified value as it may be necessary.

$$\left\{\begin{array}{l} z_b(k,t) = \frac{f(9')}{2} \\ \qquad = \frac{\frac{\sum_{i=1}^{9} f(i')}{9}}{2} \end{array}\right\} \tag{5.26}$$

Note that the index i, j, k picks only the even grid points following the pattern used in the discretization.

With the centre of buoyancy determined, the turning moment due to buoyancy force is then computed from the diagram of Figure 5.5 using equation 5.27.

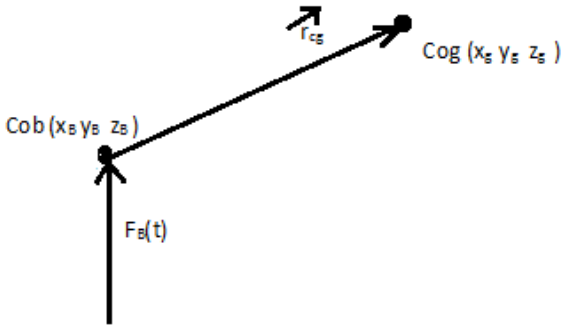

Figure 5.5 Buoyancy force/moment arm diagram

$$M_B(t) = \overrightarrow{r_{Cg}}(t)\ \mathbf{X}\ \overrightarrow{F_B}(t) \tag{5.27}$$

With $\overrightarrow{F_B}\ (t)$ pointing vertically upwards towards the mwl;

$\overrightarrow{r_{Cg}}$ is the displacement vector between the instantaneous CoB and the fixed Cog.

5.1.3.3 *Determination of hull wetted surface area and hull area above water surface*

The surface areas above and below the water line serve as transfer function for the input total pressure from wave and dynamic pressures from the wind and current as well for the estimation of forces and moments. The areas are computed using Simpson's rule applied per face, i.e. (PS, SB, AF, FP). Only one of the sides will be demonstrated as the procedure is the same for other sides.

Applying Simpson's rule with multipliers 'SM', the underwater area available for current attack is

$$A_{uw(s)}(t) = \frac{\Delta x}{3} \sum_{i=1}^{n} SM(i).\zeta_{Dk}(i,t) \tag{5.28}$$

And the area above water becomes;

$$A_{aw(s)}(t) = A_{o(s)}(0) - A_{uw(s)}(t) \tag{5.29}$$

Where the area at start of simulation or in calm water is

$$A_{o(s)}(0) = Ls * d(0) \tag{5.30}$$

The total area above water available for wind attack is;

$$A_{s(s)}(t) = A_{Ts(s)} - A_{aw(s)}(t) \tag{5.31}$$

The subscript (s) denotes the side of the hull under consideration (s-starboard, p-portside, Fp-forward side, Ap-aft side).

However, it is significant to note that the current and wind dynamic pressure act only on projected surfaces of the available area. This area is projected onto the surface perpendicular to the relative direction of the wind or current at every time step. This relative angle, also called the angle of attack is greatly dependent on the yawed position of the unit. Thus, it is instantaneous in nature.

5.1.3.4 *Estimation of varying hull projected areas as functions of angle of attack*

The hull projected area available for the wind attack is dependent on the angle of attack which in turn is dependent on the instantaneous yawed position of the unit. For the above water plane, with the diagram of Figure 5.6,

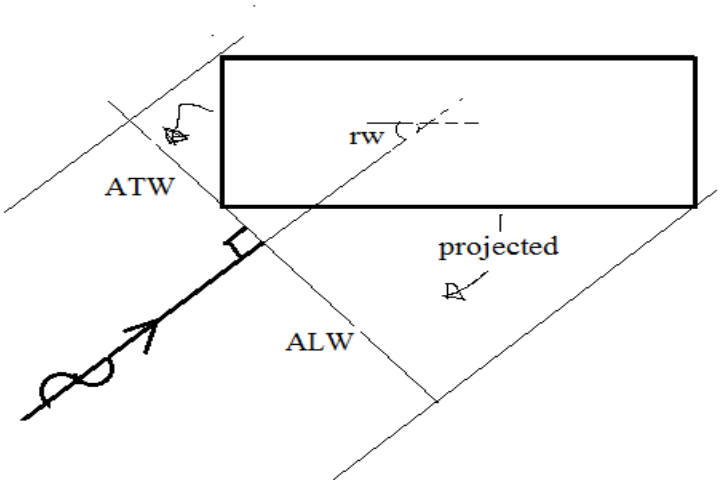

Figure 5.6 Wind or Current line of action and its projected plane

for the wind consideration; with rw representing the updated angle of attack by including the yawed angle to the original angle of attack '*rwo*';

$$rw = rwo + yaw; \tag{5.32}$$

For $0 \leq rw \leq 90°$

$$\left\{ \begin{matrix} ATw = A_{s(AF)} * cos(rw) \\ ALw = A_{s(SB)} * sin(rw) \end{matrix} \right\} \tag{5.33}$$

For $90 \leq rw \leq 180°$

$$\left\{ \begin{matrix} ATw = A_{s(FP)} * cos(180 - rw) \\ ALw = A_{s(SB)} * sin(180 - rw) \end{matrix} \right\} \tag{5.34}$$

For $180 \leq rw \leq 270°$

$$\left\{ \begin{matrix} ATw = A_{s(FP)} * cos(rw - 180) \\ ALw = A_{s(SB)} * sin(rw - 180) \end{matrix} \right\} \tag{5.35}$$

For $270 \leq rw \leq 360°$

$$\left\{ \begin{array}{l} ATw = A_{s(AF)} * cos(360 - rw) \\ ALw = A_{s(PS)} * sin(360 - rw) \end{array} \right\} \quad (5.36)$$

All the estimated areas are time variant.

For under water current application, the equations obtained are similar, replacement is made of the angle of attack (rw with rc; rwo with rco). The appropriate areas are adequately replaced as well (As(s) with Aaw(s); ALw with ALc; ATw with ATc).

5.1.4 *Estimation of Wind and Current Forces and Moments.*

This section presents the method used in the calculation of the wind and current force/moment coefficients. A continuous function, relating the instantaneous ship path with the coefficients are established. This thus introduces the concept of constantly varying coefficients together with the varying attack areas to improve the fidelity of the estimation of these forces.

FPSO are very large fixed structures, without specific available data, use was made of the data of a very large crude carrier (VLCC) from oil companies international marine forum (OCIMF) (1994) documentation. VLCC are very similar to FPSO and thus can exhibit similar characteristics in these regards. The charts were digitised and curves fitted to generate a relationship between the angle of attack (rw and rc) and the coefficients C (for current: *CXc, CYc, CNc;* for wind*: CXw, CYw, CNw*). Two fitting equations, the Fourier and sum of sines were used to capture the trend with very high values of regression coefficient R^2 achieved. Other methods from Isherwood and Blendermann (94) according to Fossen (2011) are also available.

5.1.4.1 *Reconstructed data fit for Coefficient estimates (VLCC, OCIMF (1994)):*

The whole method is centred on careful extraction of the data from the graphs for the VLCC in (OCIMF, 1994) booklet. The coefficients are obtained by using a least square

optimization method. The sum of square error between the reconstructed data (assumed measured) and the fit predicted data is minimized.

The fit models adopted are the Fourier and sum of sines models, to define a continuous function for the relationship between dependent coefficients C as defined above and independent angle of attack (α) values, i.e.

$$C = f(\alpha) \quad [with\ \alpha = rw\ or\ rc] \tag{5.37}$$

The generalized Fourier fit model is given below;

$$C = a0 + \sum_i^n a_i * \cos(\alpha + w) + b_i * \sin(\alpha + w) \tag{5.38}$$

The equivalent Sum of sines fit model is given below:

$$C = \sum_i^n a_i * \sin(b_i * \alpha + w) \tag{5.39}$$

The reconstruted data as well as their optimized coeficients are presented in appendix N and appendix O for wind and current respectively.

i. Wind Coefficient fitted curves:

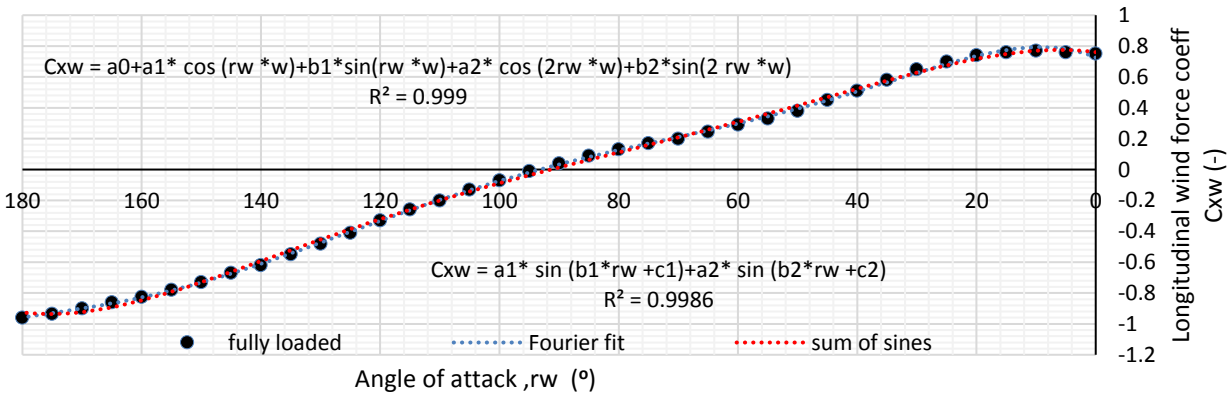

Figure 5.7 CXw vs angle of attack (Reconstructed from OCIMF, VLCC)

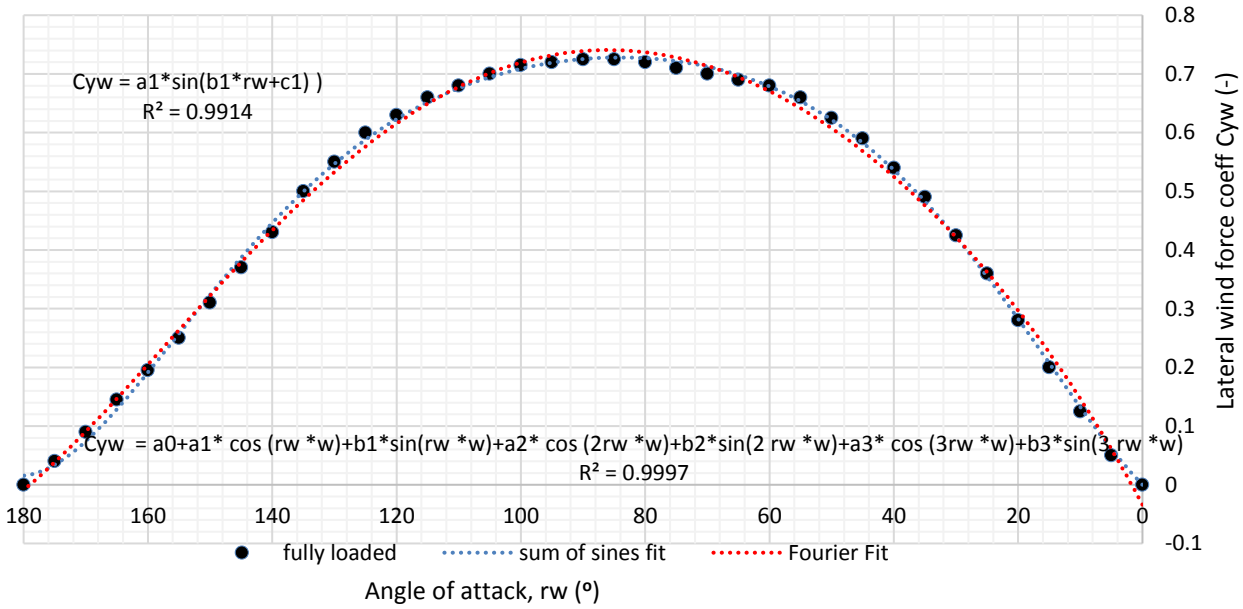

Figure 5.8 Cyw vs angle of attack (Reconstructed from OCIMF, VLCC)

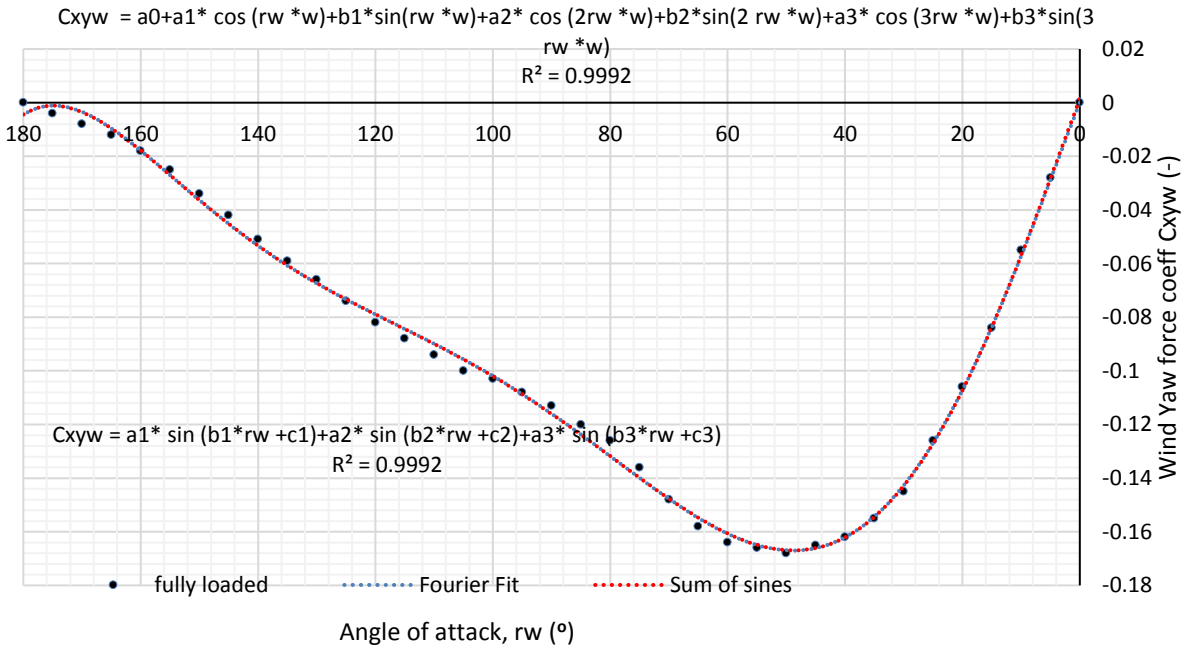

Figure 5.9 Cxyw vs angle of attack (Reconstructed from OCIMF, VLCC)

ii. Current coefficient fitted curves:

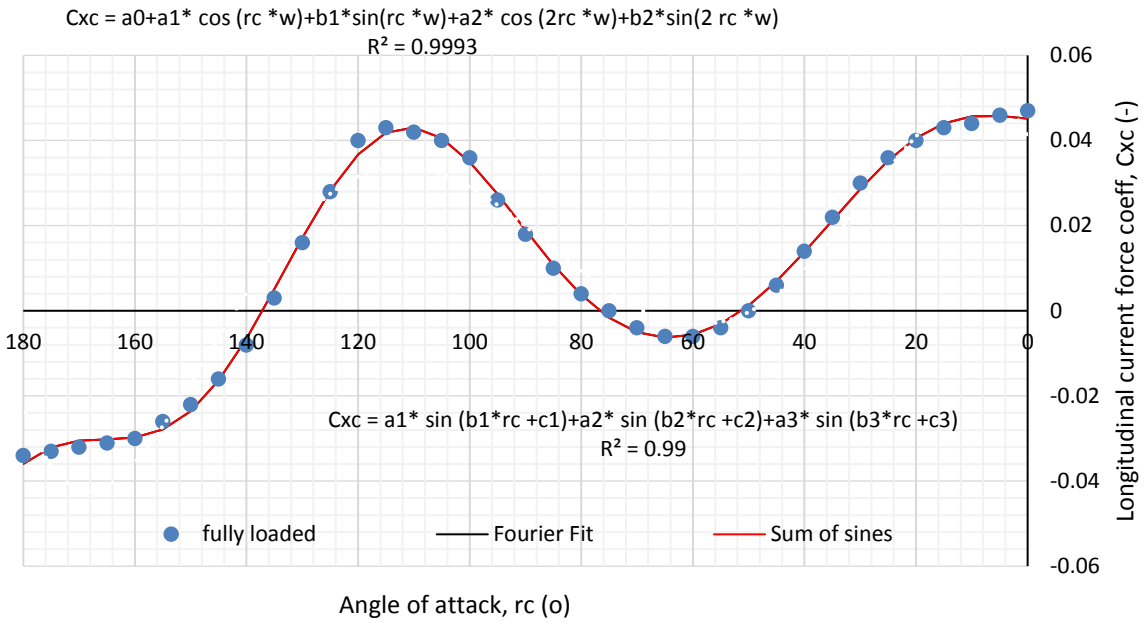

Figure 5.10 Cxc vs angle of attack (Reconstructed from OCIMF, VLCC)

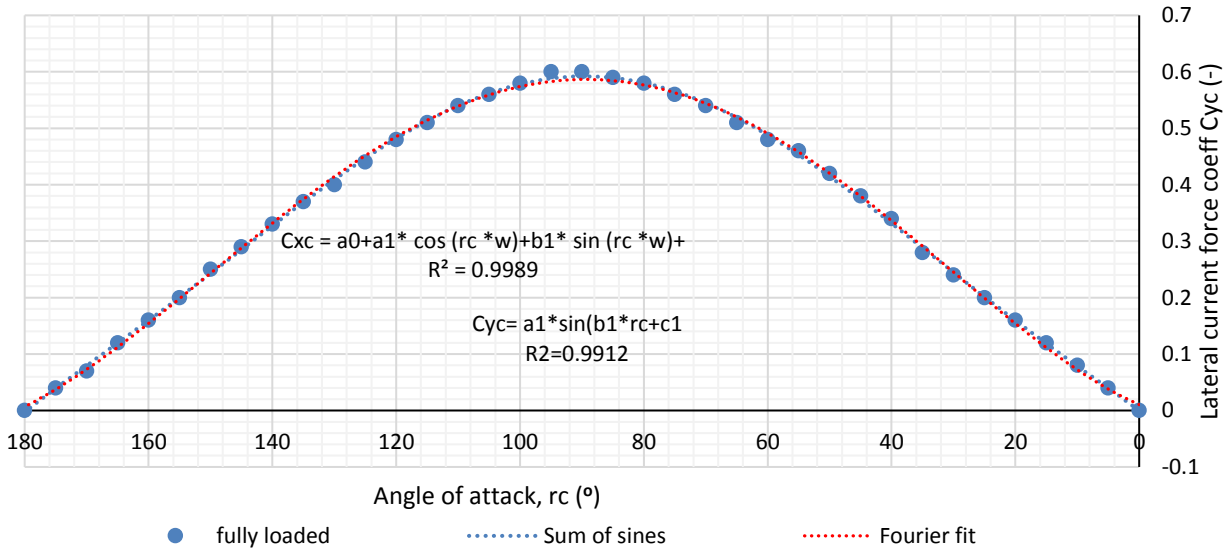

Figure 5.11 Cyc vs angle of attack rc, (Reconstructed from OCIMF, VLCC)

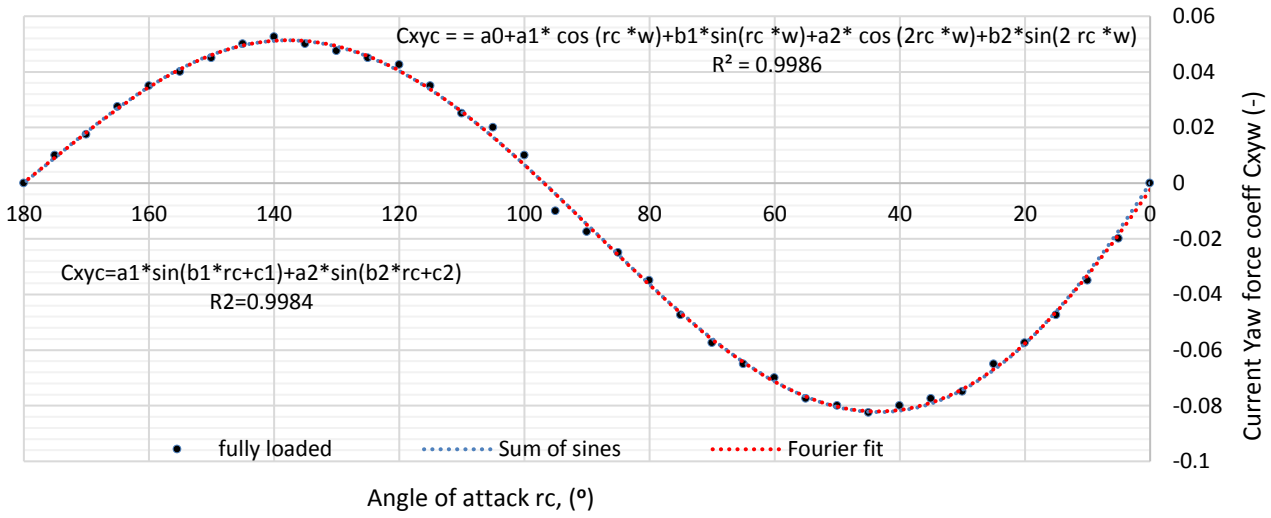

Figure 5.12 Cxyc vs angle of attack (Reconstructed from OCIMF, VLCC

5.1.4.2 *Wind Force Estimate*

Using empirical equations from (Thor Forsen,2011); Wind Force and Moment are computed using equations 5.40,5.41 and 5.42 below;

$$F_{xw} = qw(t) * (1/3.8) * CXw * ATw \quad (5.40)$$

$$F_{yw} = -qw(t) * \left(\frac{1}{3.8}\right) * CYw * ALw \quad (5.41)$$

$$M_{zw} = -qw(t) * (1/3.8) * CNw * ALw * Ls \quad (5.42)$$

With the dynamic pressure(qw) estimated for a given height and air temperature T_{air}.

$$qw = \frac{1}{2} * \rho_{air} * {V_w}^2 \quad (5.43)$$

$$\rho_{air} = 2 * 10^{-5} * {T_{air}}^2 - 0.0048 * T_{air} + 1.2925 \quad (5.44)$$

Equation 5.44 was obtained by fitting a second order polynomial to an online data, to make density a function of temperature.

The wind speed (V_w) is computed at a specified height using the 1/7th law relative to the standard 10m height value. However, the wind was defined as a stochastic model using a

normal distribution. The standard deviation (V_{wstd}) and mean (V_{wmean}) values are selected such that the wind speed values are within the storm value throughout the simulation period. From the normal distribution spectrum,

$$V_{w10} = V_{wmean} \pm \sqrt{\frac{2 * {V_{wstd}}^2}{\ln(V_{wstd} * f(V_{w10}) * \sqrt{2\pi}}} \quad (5.45)$$

$f(V_{w10})$ is the random, normally distributed probability distribution function generating values from (0 to 1).

The actual wind speed at actual wind mean height (*he)*, is estimated as shown below

$$V_w = V_{w10} \left\{\frac{he}{10}\right\}^{1/7} \quad (5.46)$$

At this point, it was necessary to recognize instances when the wind speed will be zero, thus a window or time span was created where this condition can be implemented within the routine. Thus;

$$V_w(th1 : th2) = 0 \quad (5.47)$$

Where

th1 is the start of wind shot off and th2 is the end of wind shot off; however it is desirable that in studying storm durations, the wind is applied all through a reasonable length of the simulated time frame.

5.1.4.3 *Current force Estimate*

Similarly, for current:

$$F_{xc} = qc(t) * \left(\frac{1}{2}\right) * CXc * ATc \quad (5.48)$$

$$F_{yc} = -qc(t) * \left(\frac{1}{2}\right) * CYc * ALc \quad (5.49)$$

$$M_{zc} = -qc(t) * \left(\frac{1}{2}\right) * CNc * ALc * Ls \quad (5.50)$$

With the dynamic pressure estimated at a current velocity and air temperature *T* given below

$$qc = \frac{1}{2} * \rho_{air} * V_c^{\,2} \tag{5.51}$$

Three models of the current velocity are considered therein;

If it is tidal driven; then

$$V_c = V_0 \left\{\frac{y}{\mathrm{hd}}\right\}^{1/7} \tag{5.52}$$

Were *y* is the instantaneous distance measured in meters from seabed, hd is the water depth, and *Vo* is the tidal current at the surface of the water.

For wave driven current;

$$V_c = V_0 \left\{\frac{y}{\mathrm{hd}}\right\}^{1} \tag{5.53}$$

(See pg. 25, Srinivasan, 2015)

However, a third option which considers the *Vc* as a constant value equal to the surface current velocities V_0 can be used for extreme considerations.

5.1.5 *Wave Excitation Estimate*

The wave excitation force can be approximated from simplified techniques presented below. Starting with an elemental coarse pressure integration around the wetted regions of the hull, the force is obtained by summing all elemental forces/moments adequately.

5.1.5.1 *Pressure Integration over Wetted Surface*

With the elevations around the immersed portion of the hull estimated above the keel, the force due to the wave is estimated by carrying out a coarse pressure integration over the wetted surface area, taking each side of the unit at a time. The total pressure on the panel is estimated by summing the hydrostatic pressure (resulting from an instantaneous static pressure head from the free surface to the keel) and the dynamic portion is approximated

using the water particle velocity computed at the centre of pressure of the panel under consideration. It may however be useful to use an averaged value of the velocities computed from the water surface to the keel over each panel. This may give a slightly different value, but its effect on overall pressure is not significant compared to the added computation complexity and time.

Consider a panel of a given face of FPSO, as shown below in figure 5.13.

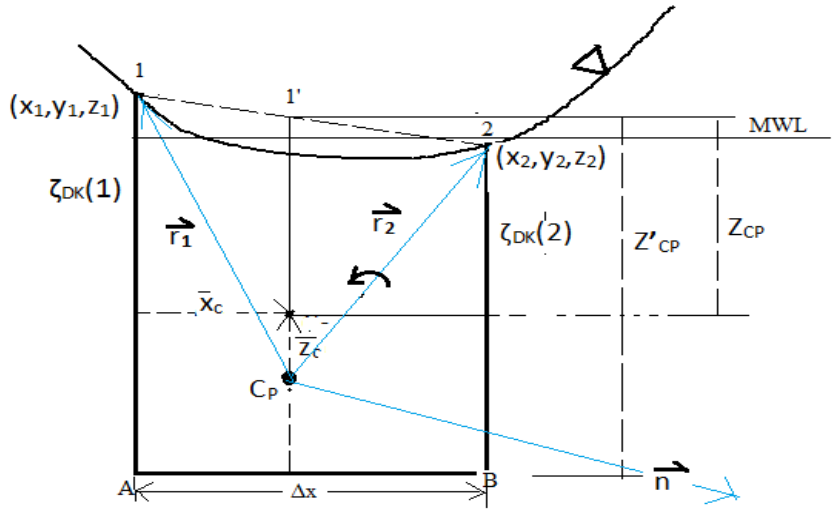

Figure 5.13 Under water trapezoidal panel approximation with normal vector at cp

Assume panel to be a simple trapezium '12BA' and entirely underwater as described by the free surface boundary;

5.1.5.2 *Determination of the Centre of Pressure of a Panel* $[Cp(\overline{x_c}, z_{cp})]$;

From the panel in

Figure 5.13 the procedure starts with the estimation of elemental area δA represented by equation 5.54

$$\delta A = \frac{1}{2}\left(\zeta_{Dk}(1) + \zeta_{Dk}(2)\right) * \Delta x \qquad (5.54)$$

The centre of trapezoidal panel plane $Cp(\overline{x_c}, \overline{z_c})$ is then computed as shown below

$$\bar{z_c} = \frac{1}{3}\left(\frac{\left(\zeta_{Dk}(1)^2+\zeta_{Dk}(1)*\zeta_{Dk}(2)+\zeta_{Dk}(2)^2\right)}{\zeta_{Dk}(1)+\zeta_{Dk}(2)}\right. \quad (5.55)$$

$$\bar{x_c} = \frac{\Delta x}{3}\left(\frac{\left(\zeta_{Dk}(1)+2*\zeta_{Dk}(2)\right)}{\zeta_{Dk}(1)+\zeta_{Dk}(2)}\right. \quad (5.66)$$

Using $\bar{x_c}$, linear interpolation is done between 1 and 2 to get the point 1', i.e. $\bar{z_c}'$.

$$\overline{z_c'} = \frac{\zeta_{Dk}(1)-\zeta_{Dk}(2)}{\Delta x}[\Delta x - \bar{x_c}] + \zeta_{Dk}(2) \quad (5.67)$$

In general, for any indexed point i,

$$\overline{z_c'}(i) = \frac{\zeta_{Dk}(i)-\zeta_{Dk}(i+1)}{\Delta x}[\Delta x * i - \bar{x_c}(i)] + \zeta_{Dk}(i+1) \quad (5.68)$$

With the point $\overline{z_c'}$ obtained, we can then assume the trapezium to be equivalent to a rectangular plane of height $\overline{z_c'}$, this enables the easy determination of the vertical centre of pressure from the mwl.

Thus, the vertical centre of pressure is simply estimated using equation 5.69 below

$$z_{cp} = \frac{2}{3} * \overline{z_c'} \quad (5.69)$$

Generally, for an indexed form;

$$z_{cp}(i) = \frac{2}{3} * \overline{z_c'}(i) \quad (5.70)$$

5.1.5.3 *Water Particle Velocity;*

The equations according to (Pablo et al, 2013) for irregular sea is modified to suit our purpose.

Since the FPSO is not moving, vessel steady velocity was taken to be zero and the Froude number term is viewed with regards to a moving water relative to the FPSO. Thus, it was possible to reduce the equations to the forms as shown below;

$$U(x,y,z,t) = \sum_{i=1}^{N}\sum_{j=1}^{M}\frac{\zeta_{ij}}{Fr}.\sqrt{k_i} * e^{k_i * Z}(cos(k_i\, x\, .cos\theta_j - k_i\, y.sin\theta_j - \omega_i\, t + \epsilon_{ij})\, cos\theta_j \quad (5.71)$$

$$V(x,y,z,t) = \sum_{i=1}^{N}\sum_{j=1}^{M}\frac{\zeta_{ij}}{Fr}.\sqrt{k_i} * e^{k_i * Z}(cos(k_i\, x\, .cos\theta_j - k_i\, y.sin\theta_j - \omega_i\, t + \epsilon_{ij})\, sin\theta_j \quad (5.72)$$

$$W(x,y,z,t) = \sum_{i=1}^{N}\sum_{j=1}^{M}\frac{\zeta_{ij}}{Fr}.\sqrt{k_i} * e^{k_i * Z}(sin(k_i\, x\, .cos\theta_j - k_i\, y.sin\theta_j - \omega_i\, t + \epsilon_{ij}) \quad (5.73)$$

Note that with the assumption made, the ratio was modified accordingly to yield;

$$\frac{\sqrt{k_i}}{Fr} \equiv \omega_i \sqrt{\frac{2\pi}{g}} \quad (5.74)$$

The technique uses the water wave as the moving reference at velocity equivalent to the celerity, with the characteristic length represented with the wavelength. With ($z = z_{cp}$) already approximated, x, y, are the coordinates as defined by the boundaries of the instantaneous water plane.

Net velocity can then be estimated using the square law;

$$\bar{V}_m = \sqrt{U^2 + V^2 + W^2} \quad (5.75)$$

An estimate of the pressure acting at point Cp due to water waves is obtained as;

$$P = -\rho_{water} * \overline{z_c{}'} * g + \frac{1}{2}\rho_{water} * \bar{V}_m{}^2 \quad (5.76)$$

Note that the static head used is the overall estimated water height from the instantaneous free surface to the keel along point 1' for the panel, however this pressure acts at a point z_{cp} from the water surface and normal to the plane as well.

5.1.5.4 *Computing unit normal vector to surface;*

From above, the normal unit vector on any panel acting at the centre of pressure and pointing outwards is

$$\vec{n} = \frac{\vec{r}_{nc}}{|\vec{r}_{nc}|} \quad (5.77$$

$\vec{r}_{nc}$ is the vector defining the normal to the surface of the panel

$$\vec{r}_{nc} = \vec{r}_2 \, \boldsymbol{X} \, \vec{r}_1 \tag{5.78}$$

$\boldsymbol{X}$ signifies the vector product, and $\vec{r}_1 \; and \; \vec{r}_2$ are represented by equations 5.79 and 5.80

$$\vec{r}_1 = (x_1 - x_c)i + (y_1 - y)j + (z_1 - z_c)k \tag{5.79}$$

$$\vec{r}_2 = (x_2 - x_c)i + (y_2 - y)j + (z_2 - z_c)k \tag{5.80}$$

Note that the vector $\vec{r}_{nc}$ is obtained by vector cross product of $\vec{r}_2$ against $\vec{r}_1$ to ensure that its direction is outward to the surface (pointing into the fluid domain) when the right-hand screw rule is applied.

5.1.5.5 *The Pressure Force and Moment estimate;*

For an elemental area δA, with the pressure P acting normal to its surface estimated, the elemental normal force to surface is calculated as thus;

$$d\vec{F}_{w(s)} = (P \, \boldsymbol{X} \, \vec{n}) * \delta A \tag{5.81}$$

Total force from all such contributions, over the entire wetted surfaces becomes

$$\left\{ \begin{array}{c} \vec{F}_{w(s)} = \sum_i^{np} d\vec{F}_{w(s)} \\ \vec{F}_{w(s)} = \sum_i^{np} (P \, \boldsymbol{X} \, \vec{n}) * \delta A \end{array} \right\} \tag{5.82}$$

(s) Signifies the part of FPSO under consideration and np is the number of panels involved.

The moment due to the elemental force is thus found by taking moment of elemental forces about the centre of gravity of the unit. With the moment arm $\vec{r}_{cpc}$ from panel pressure centre to cog known, the moment is estimated as;

$$\vec{M}_{w(s)} = \sum_i^{np} \vec{r}_{cpc} \, \boldsymbol{X} \, d\vec{F}_{w(s)} \tag{5.83}$$

The Total Pressure Force over the wetted surface most times referred to as the Froude Krylov force and moment are approximated by repeating the procedure from equations 5.54 to 5.83 for all other parts and then added vectorially to obtain an approximated total Froude-Krylov excitation due to wave motion according to the pressure integration method.

5.2 Application of the Weighting Technique to estimating the Froude Krylov and Diffraction Force:

Use is made of the equations presented in (Araki, 2004) and (Ming-Chung, 2005) to develop a methodology for estimating the Froude Krylov force in all 6dof modes and diffraction force in 5 dof modes except the surge mode which is not significant since the body is considered a slender body. The equations are further modified to suit a case of irregular sea for both the Longcrested and shortcrested seas. Dimensional consistency of equations was ensured before use. The basic concept of strip theory was applied in this case since the condition that (L/B>5) is consistent with the hull in use. The developed generalized concept of a weighting technique in chapter 4, equations 4.94 to 4.105 is applied in this section to estimate the Froude Krylov as well as the diffraction force. The technique averts the tedious computing involved in the retardation functions and convolution integrals which would take extra development time. The approach is outlined below for the Froude-Krylov and the Diffraction forces.

5.2.1 *Froude-Krylov Force*

Using the cordinate system shown in Figure 5.14

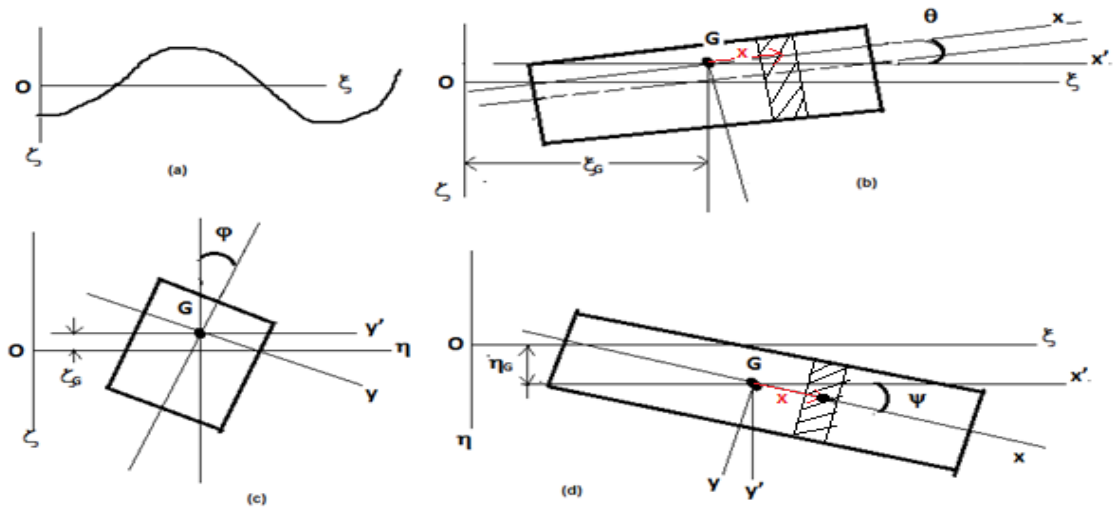

Figure 5.14 Cordinate system showing a strip at section x from unit cog:

The original equations given by (Ming-Chung fang et al, 2005) are;

Surge:

$$X_{FK} \cong \rho g\theta . \int_L A(x).dx - \rho g.\cos(\varphi).\int_L F(x).A(x).\sin(\xi_G + x.\cos(\varphi) - c.t)\,.dx \quad (5.84)$$

Sway:

$$Y_{FK} \cong \rho g.\sin(\varphi).\int_L F(x).A(x).\sin(\xi_G + x.\cos(\varphi) - c.t)\,.dx \quad (5.85)$$

Heave:

$$Z_{FK} \cong -\rho g.\int_L A(x).dx - \rho g.\int_L F(x).A(x).\cos(\xi_G + x.\cos(\varphi) - c.t)\,.dx \quad (5.86)$$

Roll:

$$K_{FK} \cong -\rho g.\int_L y'_B(x).A(x).dx - \rho g.\sin(\varphi).\int_L F(x).A(x).z'_B(x).\sin\{k.(\xi_G + x.\cos(\varphi) - c.t)\}.dx \quad (5.87)$$

Pitch:

$$M_{FK} \cong \rho g.\int_L A(x).x.dx - \rho g.\int_L F(x).A(x).x.\cos\{k.(\xi_G + x.\cos(\varphi) - c.t)\}.dx \quad (5.88)$$

Yaw:

$$N_{FK} \cong \rho g.\sin(\varphi)\,.\int_L F(x).A(x).x.\sin\{k.(\xi_G + x.\cos(\varphi) - c.t)\}.dx \quad (5.89)$$

With

$$F(x) = \zeta_\omega . k.\frac{sin\left(k.\frac{B(x)}{2}.\sin(\varphi)\right)}{k.\frac{B(x)}{2}.\sin(\varphi)}.e^{-k\left(\xi_G - x.\theta + \frac{A(x)}{B(x)}\right)} \quad (5.90)$$

A(X), B(x) are the wetted area and the breadth of each strip at each instant of time respectively.

y'_B and z'_B are the coordinate of the centroid of the instantaneous wetted hull strip.

$c = \frac{\omega}{k}$ or $\sqrt{\frac{g}{k}}$ (the wave celerity);

k= wave number and a= wave amplitude.

ψ is the instantaneous roll angle

θ is the instantaneous pitch angle

φ is the instantaneous yaw angle

5.2.2 *Modified equations to estimate the Froude-Krylov forces:*

To estimate the Froude-Krylov force from existing regular wave formulations, the equations are modified to accommodate the specific sea type, in this regard the irregular longcrested as well as shortcrested sea. Consider the diagram of a barge in a shortcrested sea, in figure 5.15

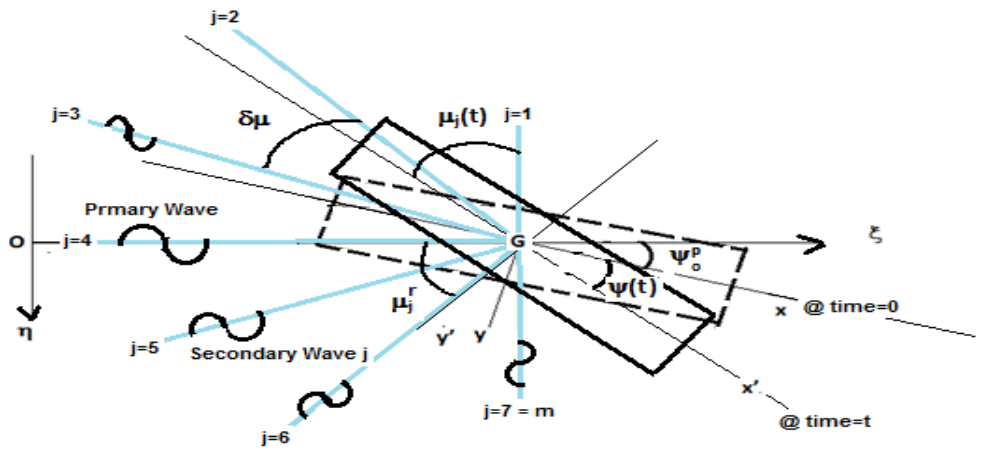

Figure 5.15. Schematic diagram of a yawing unit in a shortcrested sea

5.2.2.1 *Dealing with the Surge Froude-Krylov(FK) Force:*

For a given time t, with θ, φ, ψ, A(X), B(x), ξ_G, y'$_B$ and z'$_B$ all time dependent, then the instantaneous Froude Krylov force in surge can be written as:

$$X_{FK}(t) \cong \rho g\theta(t).\int_L A(x,t).dx - \rho g.\cos\big(\varphi(t)\big).\int_L F(x,t).A(x,t).\sin(\xi_G(t)+x.\cos(\varphi(t))-c.t).dx \tag{5.91}$$

Thus:

$$F(x,t) = \zeta_\omega.k.\frac{sin\left(k.\frac{B(x,t)}{2}.\sin(\varphi(t))\right)}{k.\frac{B(x,t)}{2}.\sin(\varphi(t))}.e^{-k\left(\xi_G(t)-x.\theta(t)+\frac{A(x,t)}{B(x,t)}\right)} \tag{5.92}$$

Again, it is worthy of note that $X_{FK}(t)$ is frequency dependent, therefore, for a given frequency ω, the Froude-Krylov force in surge can be further written as:

$$X_{FK}(\omega,t) \cong \rho g\theta(t).\int_L A(x,t).dx - \rho g.\cos(\varphi(t)).\int_L F(x,\omega,t).A(x,t).\sin\big(\xi_G(t)+x.\cos\big(\varphi(t)\big)-c(\omega).t\big).dx \tag{5.93}$$

With $F(x,\omega,t)$ further modified thus:

$$F(x,\omega,t) = \zeta_\omega(\omega).k(\omega).\frac{sin\left(k(\omega).\frac{B(x,t)}{2}.\sin(\varphi(t))\right)}{k(\omega).\frac{B(x,t)}{2}.\sin(\varphi(t))}.e^{-k(\omega)\left(\xi_G(t)-x.\theta(t)+\frac{A(x,t)}{B(x,t)}\right)} \tag{5.94}$$

Were, wave amplitude

$$\zeta_\omega(\omega) = \sqrt{2.S(\omega).d\omega} \text{ (for long crested sea)} \tag{5.95}$$

$$\zeta_\omega(\omega,\mu) = \sqrt{2.S(\omega,\mu).d\omega.d\mu} \text{ (for short crested sea)} \tag{5.96}$$

In general, re-writing equations 5.91 and 5.92 for a secondary wave of frequency index i, and direction index j, i.e. ω_{ij},

Thus replacing $\varphi(t)\ with\ \varphi_{ij}(t)$, and considering $\varphi(t)$ henceforth as the yaw angle measured relative to the initial position

$$X_{FK}(\omega_{ij},t) \cong \rho g\theta(t).\int_L A(x,t).dx - \rho g.\cos(\varphi_{ij}(t)).\int_L F\left(x,\omega_{ij},t\right).A(x,t).\sin\left(\xi_G(t) + x.\cos\left(\varphi_{ij}(t)\right) - c(\omega_{ij}).t\right).dx \quad (5.97)$$

Again, with

$$F\left(x,\omega_{ij},t\right) = \zeta_\omega(\omega_{ij}).k(\omega_{ij}).\frac{sin\left(k(\omega_{ij}).\frac{B(x,t)}{2}.\sin(\varphi_{ij}(t))\right)}{k(\omega_{ij}).\frac{B(x,t)}{2}.\sin(\varphi_{ij}(t))}.e^{-k(\omega_{ij})\left(\xi_G(t)-x.\theta(t)+\frac{A(x,t)}{B(x,t)}\right)} \quad (5.98)$$

The first approximation was made in the value of the $F\left(x,\omega_{ij},t\right)$ considering the fact that term $\frac{sin\left(k(\omega_{ij}).\frac{B(x,t)}{2}.\sin(\varphi_{ij}(t))\right)}{k(\omega_{ij}).\frac{B(x,t)}{2}.\sin(\varphi_{ij}(t))} = infinity$ for possible case of $\varphi_{ij}(t) = 0$;

this might result in computational instabilities; thus, the Taylor series was used to approximate the term, truncating it at the 20th term which gave good accuracy.

With

$$A = k(\omega_{ij}).\frac{B(x,t)}{2}.\sin\left(\varphi_{ij}(t)\right) \quad (5.99)$$

$$\frac{sin\left(k(\omega_{ij}).\frac{B(x,t)}{2}.\sin(\varphi_{ij}(t))\right)}{k(\omega_{ij}).\frac{B(x,t)}{2}.\sin(\varphi_{ij}(t))} = \frac{sin(A)}{A} = 1 + \sum_{j=1}^{20}\left|(-1)^j * \frac{A^{2j}}{(2j+1)!}\right| \quad (5.100)$$

Note that the instantaneous direction $\varphi_{ij}(t)$ is that associated with the secondary wave stream been considered, thus it is written as

$$\varphi_{ij}(t) = \varphi_0^p + \mu_j(t) \quad (5.101)$$

$$\mu_j(t) = \varphi(t) + {\mu_j}^r \quad (5.102)$$

$${\mu_j}^r = \left[j - \frac{m+1}{2}\right].\delta\mu_j \quad (5.103)$$

φ_0^p is the instantaneous mean ship path measured w.r.t the primary wave direction at time t=0, and ${\mu_j}^r$ is the angle interval between a secondary wave j, and the primary wave with

($\mu_j{}^r = 0$) for the mean path of primary wave stream. $\varphi(t)$ is the current yaw angle of the unit.

Numerical integration using Simpsons rule can then be applied to equation 5.97 above to compute the FK force due to a given secondary wave stream ω_{ij}, to obtain

$$X_{FK}(\omega_{ij},t) \cong \rho g\theta(t).\frac{\Delta x}{3}\sum_{x=1}^{x=ns} SM(x).A(x,t) - \frac{\Delta x}{3}\sum_{x=1}^{x=ns} SM(x).F(x,\omega_{ij},t).A(x,t).\sin\left(\xi_G(t) + x.\cos\left(\varphi_{ij}(t)\right) - c(\omega_{ij}).t\right) \quad (5.104)$$

Were SM(x) is the Simpson multiplier for a given section x.

At this stage, the weighting technique is then applied to estimate the net Froude-Krylov force from all the secondary waves making up the irregular wave. Simply put;

$$X_{FK}(t) = \sum_{\substack{i=1\ to\ N \\ j=1\ to\ M}} X_{FK}(\omega_{ij},t) \quad (5.105)$$

$$X_{FK}(t) = \sum\{W_{ij} * X_{FK}(\omega_{ij},t)\} \quad (5.106)$$

On the condition that ($\sum W_{ij} = 1$) as in equation 5.105

N, M are the number of regular wave frequencies and directions used respectively.

The technique is based on assumption of linearity as proposed by (Spanos et al,1997) such that the individual force contributions from respective regular waves components composing the wave train can be added linearly. However, this technique further modifies the previous by using a weighting model based on the spectra formulation instead. Elementary wave weights are obtained using their contribution in the formation of the irregular wave train energy spectrum. It is common knowledge to argue that energy is a form of force, therefore the wave energy spectra upon which the weights are computed can be used as a measure of the force impact which a given wave trapped within the irregular wave may have. For the sake of simplifying the technique, it is worthy to note that difference as well as sum frequencies resulting from instantaneous random interactions amongst the regular waves from second order were not considered.

For the longcrested sea, were only a primary wave or one wave stream is considered for a given frequency, without directional spread, then

$$\left.\begin{array}{c} \omega_i \equiv \omega_{ij} \\ W_i \equiv W_{ij} \\ W_i = \frac{S(\omega(i)).d\omega}{m_o} \\ \sum W_i = 1 \end{array}\right\} \tag{5.107}$$

Where m_o is as described in chapter 4.

$$m_o \cong H_S^2/16 \tag{5.108}$$

Or the area under the wave energy spectra curve. The coordinate $S(\omega(i))$ maybe readily computed and used as discrete values or the continuous function representation of the spectra is used instead.

Following the same procedure, the other motion modes can be estimated thus;

Sway:

$$Y_{FK}(\omega_{ij}, t) \cong \rho g.\sin(\varphi_{ij}(t)).\frac{\Delta x}{3}\sum_{x=1}^{x=ns} SM(x).F(x, \omega_{ij}, t).A(x,t).\sin\left(\xi_G(t) + x.\cos\left(\varphi_{ij}(t)\right) - c(\omega_{ij}).t\right) \tag{5.109}$$

$$\left.\begin{array}{c} Y_{FK}(t) = \sum_{\substack{i=1\ to\ n \\ j=1\ to\ m}} Y_{FK}(\omega_{ij}, t) \\ = \sum\{W_{ij} * Y_{FK}(\omega_{ij}, t)\} \end{array}\right\} \tag{5.110}$$

Heave:

$$\begin{aligned} Z_{FK}(\omega_{ij}, t) \cong & -\rho g.\frac{\Delta x}{3}\sum_{x=1}^{x=ns} SM(x).A(x,t) - \\ & \rho g.\frac{\Delta x}{3}\sum_{x=1}^{x=ns} SM(x).F(x, \omega_{ij}, t).A(x,t).\cos\left(\xi_G(t) + \right. \\ & \left. x.\cos\left(\varphi_{ij}(t)\right) - c(\omega_{ij}).t\right) \end{aligned} \tag{5.111}$$

$$\left.\begin{array}{c} Z_{FK}(t) = \sum_{\substack{i=1\ to\ n \\ j=1\ to\ m}} Z_{FK}(\omega_{ij}, t) \\ = \sum\{W_{ij} * Z_{FK}(\omega_{ij}, t)\} \end{array}\right\} \tag{5.112}$$

Roll:

$$K_{FK}(\omega_{ij},t) \cong -\rho g.\frac{\Delta x}{3}\sum_{x=1}^{x=ns} SM(x).y'_B(x,t).A(x,t) - \rho g.\sin(\varphi_{ij}(t)).\frac{\Delta x}{3}\sum_{x=1}^{x=ns} SM(x).F(x,t).A(x,t).z'_B(x,t).\sin\left\{k(\omega_{ij}).\left(\xi_G(t) + x.\cos\left(\varphi_{ij}(t)\right) - c(\omega_{ij}).t\right)\right\} \quad (5.113)$$

$$\left.\begin{aligned} K_{FK}(t) &= \sum_{\substack{i=1\ to\ n \\ j=1\ to\ m}} K_{FK}(\omega_{ij},t) \\ &= \sum\{W_{ij} * K_{FK}(\omega_{ij},t)\} \end{aligned}\right\} \quad (5.114)$$

Pitch:

$$M_{FK}(\omega_{ij},t) \cong \rho g.\frac{\Delta x}{3}\sum_{x=1}^{x=ns} SM(x).A(x,t).x - \rho g.\frac{\Delta x}{3}\sum_{x=1}^{x=ns} SM(x).F(x,t).A(x,t).x.\cos\left\{k(\omega_{ij}).\left(\xi_G(t) + x.\cos\left(\varphi_{ij}(t)\right) - c(\omega_{ij}).t\right)\right\} \quad (5.115)$$

$$\left.\begin{aligned} M_{FK}(t) &= \sum_{\substack{i=1\ to\ n \\ j=1\ to\ m}} M(\omega_{ij},t) \\ &= \sum\{W_{ij} * M_{FK}(\omega_{ij},t)\} \end{aligned}\right\} \quad (5.116)$$

Yaw:

$$N_{FK}(\omega_{ij},t) \cong \rho g.\sin\left(\varphi_{ij}(t)\right).\frac{\Delta x}{3}\sum_{x=1}^{x=ns} SM(x).F(x,t).A(x,t).x.\sin\left\{k(\omega_{ij}).\left(\xi_G + x.\cos\left(\varphi\varphi_{ij}(t)\right) - c(\omega_{ij}).t\right)\right\} \quad (5.117)$$

$$\left.\begin{aligned} N_{FK}(t) &= \sum_{\substack{i=1\ to\ n \\ j=1\ to\ m}} N_{FK}(\omega_{ij},t) \\ &= \sum\{W_{ij} * N_{FK}(\omega_{ij},t)\} \end{aligned}\right\} \quad (5.118)$$

5.2.2.2 *Application of the weighting technique to estimate the Sway Diffraction force*

Some of the time changing parameters in equation 5.109 as it affects the entire system include

$\psi(t), m_{ii}(x), b_{ii}(x),$, these values are thus used within the time loop and are recomputed at every time step.

For a regular wave of frequency ω , the equations 5.109-5.118 can be easily solved for the appropriate values of the respective diffraction forces at every time step, hence a time varying diffraction force is obtained which is then added to form the total force before solving the motion equation.

For a rectangular hull form, at every instantaneous mean water depth, d (t), the sectional draft d (j) are the same, thus;

$$d(j) = d(t) \tag{5.119}$$

Also, the centre of gravity Cog is a fixed point on the body fixed coordinate system but varies relative to the assumed global origin. The added mass or inertial are estimated using a simple Lewis conformal mapping technique. The frequency dependent 2D damping coefficients may be estimated from a continuous function obtained by reconstructing the experimental data by (Vugths,1968). However, for the sake of simplicity, may be to consider the infinite or zero frequency values as '0' in user manual of SEAWAY by (Journée, 2001). In this work, a rigorous technique using the weighting technique was employed to carry out the force estimate in all the other modes of motion.

The original equations given by (Ming-Chung et al, 2005):

Sway:

$$Y_{DF} = \int_L \left[m_{22}(x) \frac{d\bar{w}_H}{dt} + b_{22}(x)\bar{w}_H \right] dx \tag{5.120}$$

Heave:

$$Z_{DF} = \int_L \left[m_{33}(x) \frac{d\bar{w}_V}{dt} + b_{33}(x)\bar{w}_V \right] dx \tag{5.121}$$

Roll:

$$K_{DF} = \int_L \left[m_{44}(x) \frac{d\bar{w}_R}{dt} + b_{44}(x)\bar{w}_R \right] dx \quad (5.122)$$

Pitch:

$$M_{DF} = \int_L \left[m_{33}(x) \frac{d\bar{w}_V}{dt} + b_{33}(x)\bar{w}_V \right] (-x) dx \quad (5.123)$$

Yaw:

$$N_{DF} = \int_L \left[m_{22}(x) \frac{d\bar{w}_H}{dt} + b_{22}(x)\bar{w}_H \right] (x) dx \quad (5.124)$$

With

$$\bar{w}_H = a.k.c.\sin(\varphi).e^{-k(\xi_G - x.\theta + z'_B(x))}.\cos\{k.(\xi_G + x.\cos(\varphi) - y'_B(x).\sin(\varphi) - c.t)\} \quad (5.125)$$

$$\bar{w}_V = a.k.c.\sin(\varphi).e^{-k(\xi_G - x.\theta + z'_B(x))}.\sin\{k.(\xi_G + x.\cos(\varphi) - y'_B(x).\sin(\varphi) - c.t)\} \quad (5.126)$$

$$\bar{w}_R = -a.k^2 2.c.\sin(\varphi).e^{-k(\xi_G - x.\theta + z'_B(x))}.\cos\{k.(\xi_G + x.\cos(\varphi) - y'_B(x).\sin(\varphi) - c.t)\} \quad (5.127)$$

Differentiating to get the corresponding accelerations;

$$\frac{d\bar{w}_H}{dt} = a.k^2.c^2.\sin(\varphi).e^{-k(\xi_G - x.\theta + z'_B(x))}.\sin\{k.(\xi_G + x.\cos(\varphi) - y'_B(x).\sin(\varphi) - c.t)\} \quad (5.128)$$

$$\frac{d\bar{w}_V}{dt} = -a.k^2.c^2.\sin(\varphi).e^{-k(\xi_G - x.\theta + z'_B(x))}.\cos\{k.(\xi_G + x.\cos(\varphi) - y'_B(x).\sin(\varphi) - c.t)\} \quad (5.129)$$

$$\frac{d\bar{w}_R}{dt} = -a.k^3 2.c^2.\sin(\varphi).e^{-k(\xi_G - x.\theta + z'_B(x))}.\sin\{k.(\xi_G + x.\cos(\varphi) - y'_B(x).\sin(\varphi) - c.t)\} \quad (5.130)$$

For the Sway diffraction force:

Following the approach adopted in dealing with the Froude-Krylov Force, the necessary equations can be modified thus for a given section x;

The Velocities from equation 5.125 to 5.127 are modified accordingly to;

$$\bar{w}_H(\omega_{ij},t) = \zeta_\omega(\omega_{ij}).k(\omega_{ij}).c(\omega_{ij}).\sin\left(\varphi_{ij}(t)\right).e^{-k(\omega_{ij})\left(\xi_G(t)-x.\theta(t)+z'_B(x,t)\right)}.\cos\left\{k(\omega_{ij}).\left(\xi_G(t)+x.\cos\left(\varphi_{ij}(t)\right)-y'_B(x,t).\sin\left(\varphi_{ij}(t)\right)-c(\omega_{ij}).t\right)\right\} \quad (5.131)$$

$$\bar{w}_V(\omega_{ij},t) = \zeta_\omega(\omega_{ij}).k(\omega_{ij}).c(\omega_{ij}).\sin\left(\varphi_{ij}(t)\right).e^{-k(\omega_{ij})\left(\xi_G(t)-x.\theta(t)+z'_B(x,t)\right)}.\sin\left\{k(\omega_{ij}).\left(\xi_G(t)+x.\cos\left(\varphi_{ij}(t)\right)-y'_B(x,t).\sin\left(\varphi_{ij}(t)\right)-c(\omega_{ij}).t\right)\right\} \quad (5.132)$$

$$\bar{w}_R(\omega_{ij},t) = -\zeta_\omega(\omega_{ij}).k(\omega_{ij})^2.c(\omega_{ij}).\sin\left(\varphi_{ij}(t)\right).e^{-k(\omega_{ij})\left(\xi_G(t)-x.\theta+z'_B(x)\right)}.\cos\left\{k(\omega_{ij}).\left(\xi_G(t)+x.\cos\left(\varphi_{ij}(t)\right)-y'_B(x,t).\sin\left(\varphi_{ij}(t)\right)-c(\omega_{ij}).t\right)\right\} \quad (5.133)$$

In a similar approach, the modification of the corresponding accelerations are given as equations 5.128 to 5.130

$$\frac{d\bar{w}_H}{dt}(\omega_{ij},t) = \zeta_\omega(\omega_{ij}).k(\omega_{ij})^2.c(\omega_{ij})^2.\sin\left(\varphi_{ij}(t)\right).e^{-k(\omega_{ij})\left(\xi_G(t)-x.\theta(t)+z'_B(x,t)\right)}.\sin\left\{k(\omega_{ij}).\left(\xi_G(t)+x.\cos\left(\varphi_{ij}(t)\right)-y'_B(x,t).\sin\left(\varphi_{ij}(t)\right)-c(\omega_{ij}).t\right)\right\} \quad (5.134)$$

$$\frac{d\bar{w}_V}{dt}(\omega_{ij},t) = -\zeta_\omega(\omega_{ij}).k(\omega_{ij})^2.c(\omega_{ij})^2.\sin\left(\varphi_{ij}(t)\right).e^{-k(\omega_{ij})\left(\xi_G(t)-x.\theta(t)+z'_B(x,t)\right)}.\cos\left\{k(\omega_{ij}).\left(\xi_G(t)+x.\cos\left(\varphi_{ij}(t)\right)-y'_B(x,t).\sin\left(\varphi_{ij}(t)\right)-c(\omega_{ij}).t\right)\right\} \quad (5.135)$$

$$\frac{d\bar{w}_R}{dt}(\omega_{ij},t) = -\zeta_\omega(\omega_{ij}).k(\omega_{ij})^3.c(\omega_{ij})^2.\sin\left(\varphi_{ij}(t)\right).e^{-k(\omega_{ij})\left(\xi_G(t)-x.\theta(t)+z'_B(x,t)\right)}.\sin\left\{k(\omega_{ij}).\left(\xi_G(t)+x.\cos\left(\varphi_{ij}(t)\right)-y'_B(x,t).\sin\left(\varphi_{ij}(t)\right)-c(\omega_{ij}).t\right)\right\} \quad (5.136)$$

The sway diffraction force of equation 6.120 can then be adequately modified to

$$Y_{DF}(t) = \int_L \left[m_{22}(x,t)\frac{d\bar{w}_H}{dt}(\omega_{ij},t) + b_{22}(\omega_{ij},x,t)\bar{w}_H(\omega_{ij},t)\right]dx \tag{5.137}$$

For a given wave of frequency index i and direction j, the diffraction force assuming it is to act alone is

$$Y_{DF}(\omega_{ij},t) = .\frac{\Delta x}{3}\sum_{x=1}^{x=ns} SM(x).m_{22}(x,t)\frac{d\bar{w}_H}{dt}(\omega_{ij},t) + \frac{\Delta x}{3}\sum_{x=1}^{x=ns} SM(x).b_{22}(\omega_{ij},x,t).\bar{w}_H(\omega_{ij},t) \tag{5.138}$$

Applying the weighting technique, the cumulative sway diffraction force is thus;

$$\left.\begin{aligned} Y_{DF}(t) &= \sum_{\substack{i=1\ to\ n \\ j=1\ to\ m}} Y_{DF}(\omega_{ij},t) \\ &= \sum\{W_{ij} * Y_{DF}(\omega_{ij},t)\} \end{aligned}\right\} \tag{5.139}$$

The next challenge is to compute the 2D damping coefficient (b_{22}) usable in equation 5.120, 5.138.

Similar procedure is adopted to estimate the diffraction force for the other motion modes.

Heave:

$$Z_{DF}(\omega_{ij},t) = .\frac{\Delta x}{3}\sum_{x=1}^{x=ns} SM(x).m_{33}(x,t)\frac{d\bar{w}_V}{dt}(\omega_{ij},t) + \frac{\Delta x}{3}\sum_{x=1}^{x=ns} SM(x).b_{33}(\omega_{ij},x,t).\bar{w}_V(\omega_{ij},t) \tag{5.140}$$

$$\left.\begin{aligned} Z_{DF}(t) &= \sum_{\substack{i=1\ to\ n \\ j=1\ to\ m}} Z_{DF}(\omega_{ij},t) \\ &= \sum\{W_{ij} * Z_{DF}(\omega_{ij},t)\} \end{aligned}\right\} \tag{5.141}$$

Roll:

$$K_{DF}(\omega_{ij},t) = .\frac{\Delta x}{3}\sum_{x=1}^{x=ns} SM(x).m_{44}(x,t)\frac{d\bar{w}_R}{dt}(\omega_{ij},t) + \frac{\Delta x}{3}\sum_{x=1}^{x=ns} SM(x).b_{44}(\omega_{ij},x,t).\bar{w}_R(\omega_{ij},t) \tag{5.142}$$

$$\left.\begin{aligned} K_{DF}(t) &= \sum_{\substack{i=1\ to\ n \\ j=1\ to\ m}} K_{DF}(\omega_{ij},t) \\ &= \sum\{W_{ij} * K_{DF}(\omega_{ij},t)\} \end{aligned}\right\} \tag{5.143}$$

Pitch:

$$M_{DF}(\omega_{ij},t) =. \frac{\Delta x}{3}\sum_{x=1}^{x=ns}\left[SM(x).m_{33}(x,t)\frac{d\bar{w}_V}{dt}(\omega_{ij},t)\right]*(-x) + \frac{\Delta x}{3}\sum_{x=1}^{x=ns}\left[SM(x).b_{33}(\omega_{ij},x,t).\bar{w}_V(\omega_{ij},t)\right]*(-x) \quad (5.144)$$

$$\left.\begin{aligned} M_{DF}(t) &= \sum_{\substack{i=1\ to\ n \\ j=1\ to\ m}} M_{DF}(\omega_{ij},t) \\ &= \sum\{W_{ij} * M_{DF}(\omega_{ij},t)\} \end{aligned}\right\} \quad (5.145)$$

Yaw:

$$N_{DF}(\omega_{ij},t) = \frac{\Delta x}{3}\sum_{x=1}^{x=ns}\left[SM(x).m_{22}(x,t)\frac{d\bar{w}_H}{dt}(\omega_{ij},t)\right]*(x) + \frac{\Delta x}{3}\sum_{x=1}^{x=ns}\left[SM(x).b_{22}(\omega_{ij},x,t).\bar{w}_H(\omega_{ij},t)\right]*(x) \quad (5.146)$$

$$\left.\begin{aligned} N_{DF}(t) &= \sum_{\substack{i=1\ to\ n \\ j=1\ to\ m}} N_{DF}(\omega_{ij},t) \\ &= \sum\{W_{ij} * N_{DF}(\omega_{ij},t)\} \end{aligned}\right\} \quad (5.147)$$

5.2.3 *Estimating the 2D and 3D damping coefficient (b_{ij}):*

A generalized approach was to use the method according to (Ciobanu and Anghel,2008) which was modified to implement the weighting technique. Use is made of the equations presented in (Edward ,1989) by applying the frequency spectra density weighting technique adopted in dealing with the Froude-Krylov and diffraction problem. The two-dimensional potential damping coefficients which is frequency dependent is approximated using the Lewis conformal mapping technique, the strip theory is then applied to estimate the 3d coefficients. The equations are further modified to suit a case of irregular sea for both the Longcrested and shortcrested seas. Dimensional consistency of equations was ensured before use.

However, another approach would be to fit models to the experimental data from Vughts hydrodynamic test for a rectangular section or actual ship sections in non-dimensionalized forms. This is to enable the continuous estimation of the sectional 2d

coefficients. The multi-parameter conformal mapping when employed to estimate the added mass and damping coefficients did not give significantly enhanced accuracy of overall output compared to the simplified Lewis form over computational time (Rajendran et al, 2015).

Original equations developed for regular waves for the 2d damping coefficients (Ciobanu and Anghel, 2008);

Sway;

$$b_{22} = \rho.\omega.I_{22}.{D_s}^2 \tag{5.148}$$

Heave;

$$b_{33} = \rho.\omega.I_{33}.{B_s}^3 \tag{5.149}$$

Roll;

$$b_{44} = \rho.\omega.I_{44}.{D_s}^4 \tag{5.150}$$

Sway-Roll;

$$b_{24} = \rho.\omega.I_{24}.{D_s}^3 \tag{5.151}$$

Were $I_{ij,}\ D_s, B_s$ are the non-dimensional mass coefficient of the ship form, the Lewis form draft and beam respectively.

For a regular wave of frequency, some of the time changing parameters in the equation as it affects the entire system include $D_s(t), B_s(t), I_{ii}(t)$. These values are thus used within the time loop and are recomputed at every time step.

For the regular wave scenario, the equations 5.148 to 5.151 can be easily solved for the appropriate values of the respective 2D damping coefficients at every time step, hence time varying value is obtained. The non-zero 3D damping coefficient can then be approximated using a predetermined odd number of mid-ship sections equally spaced at Δx . These values are then added to other damping coefficients to form the total damping matrix before solving the final motion equation. Note that for a stationary unit, like the

FPSO, *U≈0*. This reduces the equation as presented by (Camelia Ciobanu & Anghel, 2008) and (pg. 56 of Principle of Naval Arch, Vol.1) to those of equation 5.152 below.

$$\left.\begin{aligned} B_{33} &= \sum b_{33}\Delta x \\ B_{35} &= \sum x.\, b_{33}.\, \Delta x \\ B_{53} &= \sum x.\, b_{33}.\, \Delta x \\ B_{55} &= \sum x^2.\, b_{33}.\, \Delta x \\ B_{22} &= \sum b_{22}.\, \Delta x \\ B_{24} &= B_{42} = \sum b_{24}\Delta x \\ B_{26} &= B_{62} = \sum x.\, b_{22}.\, \Delta x \\ B_{44} &= \sum b_{44}.\, \Delta x \\ B_{46} &= B_{64} = \sum x.\, b_{24}.\, \Delta x \\ B_{66} &= \sum x^2.\, b_{22}.\, \Delta x \end{aligned}\right\} \qquad (5.152)$$

Combining the elements of equation 5.148-5.151 and 5.152, the non-zero potential damping coefficient matrix of the eom can be estimated at any given time step.

5.2.3.1 *Modifying equation for an irregular longcrested sea.*

For simplicity, let $\varphi(t)$, represent the mean wave-ship path. Every other parameter that is time invariant is kept constant. $(u = 0)$;

For an irregular wave stream consisting of N number of regular waves, the method computes parameters from equation 5.148 to 5.151 for each wave 'i', and modifies it using a weighting technique with weights estimated from the wave spectra energy density curve like the Froude Krylov or diffraction cases.

Thus, for a regular monochromatic wave $\omega(i)$, at station jand time t, the 2D damping coefficient according to equation 5.148,

$$b_{22\omega i}(j,t) = \rho.\, \omega(i).\, I_{22}.\, {D_s}^2 \qquad (5.153)$$

If the wave is irregular, then the 2d damping modifies according to the weight Wi as

$$b'_{22\omega i}(j,t) = W_i * \rho.\, \omega(i).\, I_{22}.\, {D_s}^2 \qquad (5.154)$$

For all the damping contributions from all wave streams, their contributions are dependent on their weight contributions, then, the total 2d damping at station j, time t becomes

$$b_{22}(j,t) = \sum_{i=1}^{i=N} W_i *. b_{22wi}(j,t) \qquad (5.155)$$

To estimate the 3D damping coefficient ($B_{22}(t)$), using equation 5.152, use is made of Simpson's rule to integrate across the length of ship, from station j=1 to M, running from FP to AP;

Thus

$$\left.\begin{aligned} B_{22}(t) &= \frac{\Delta x}{3}\sum_{j=1}^{i=ns}[SM(j) * b_{22}(j,t)] \\ &\quad or \\ &= \frac{\Delta x}{3}\sum_{j=1}^{i=ns}\{SM(j) * \sum_{i=1}^{i=M}[W_i *. b_{22wi}(j,t)]\} \end{aligned}\right\} \qquad (5.156)$$

The weighting parameter W_i for each contributing regular wave (i) is estimated according to equation 4.97 to 4.100;

Note that $b_{22}\,(j)\ or\ b_{22}(j,t)$ is the same as $b_{22}(\omega_i, x, t)$

With the elemental damping coefficient estimated from equation 5.155, the total diffraction force can be estimated assuming linearity by using the weighting contributions from relevant equations above.

Also, the centre of gravity Cog is a fixed point on the body fixed coordinate system but varies relative to the assumed global origin. The Lewis form draft and beam are estimated using a simple Lewis conformal mapping technique.

5.2.3.2 *Attempt to extend method to Shortcrested irregular sea with directional spread*

The modification is made simply by the introduction of the directional spread or secondary wave streams to the original formulation for the irregular longcrested sea.

With $\theta(k)$ as the angle between primary wave and the secondary waves, such that $(\theta(k) = 0\ )$ for the primary wave. And k denoting the index of the number of directions

used from the mean path of each secondary wave is thus included in the expressions of equation 5.153

Thus, for a regular monochromatic wave $\omega(i)$, at station *j* and time *t*, the 2D damping coefficient according to equation 5.152,

$$b_{22\omega ik}(j,t) = \rho.\omega(i,k).I_{22}.{D_s}^2 \tag{5.157}$$

If the wave is irregular, then the 2D damping modifies according to the weight W_{ik} as

$$b'_{22\omega ik}(j,t) = W_{ik} * \rho.\omega(i,k).I_{22}.{D_s}^2 \tag{5.158}$$

For all the damping contributions from all wave streams, their contributions dependent on their weight contributions, then, the total 2D damping at station j, time t becomes

$$b_{22}(j,t) = \sum_{\substack{k=1 \\ i=1}}^{\substack{k=M \\ i=N}} \{W_{ik} *. b_{22wik}(j,t)\} \tag{5.159}$$

To estimate the 3D damping coefficient ($B_{22}(t)$), using equation 5.152, use is made of Simpson's rule to integrate across the length of ship, from station *j*=1 to *M*, spanning across FP to AP;

Thus

$$\left.\begin{aligned} B_{22}(t) &= \frac{\Delta x}{3}\sum_{j=1}^{i=ns}[SM(j) * b_{22}(j,t)] \\ &\quad or \\ &= \frac{\Delta x}{3}\sum_{j=1}^{i=ns}\left\{SM(j) * \sum_{\substack{k=1 \\ i=1}}^{\substack{k=M \\ i=N}} \{W_{ik} *. b_{22wik}(j,t)\}\right\} \end{aligned}\right\} \tag{5.160}$$

The weighting parameter W_{ik} for each contributing regular wave (i) is estimated according to equation 4.97 to 4.100;

Note that $b_{22}\,(j)\ or\ b_{22}(j,t)\ \ is\ the\ same\ as\ b_{22}(\omega_{ik},x,t)$

This equation 5.160 gives the impression that the 2D damping coefficient is not dependent on the directional spread, anyway, the effect of the directional spread is introduced by the weights from the weighting technique. It also implies that the 2D values for all directions having the same frequency is the same.

Following the same procedure; equivalent equations are obtained for the other motion modes.

$$\left.\begin{aligned} b_{33}(j,t) &= \sum_{\substack{k=1\\ i=1}}^{\substack{k=M\\ i=N}} \{W_{ik} *. b_{33wik}(j,t)\} \\ b_{44}(j,t) &= \sum_{\substack{k=1\\ i=1}}^{\substack{k=M\\ i=N}} \{W_{ik} *. b_{44wik}(j,t)\} \\ b_{24}(j,t) &= \sum_{\substack{k=1\\ i=1}}^{\substack{k=M\\ i=N}} \{W_{ik} *. b_{24wik}(j,t)\} \end{aligned}\right\} \quad (5.161)$$

Applying equation 5.160 and 5.161 into equations 5.139 to 5.147 with the 2D added mass known, the diffraction forces are estimated.

In a similar manner, values for the other coefficients $B_{ij}(t)$ can be obtained from equations 5.160 and 5.161. The application of the weighting technique to estimating these values for irregular seas is a novel technique.

5.2.4 *Munk Moment estimate*

It is important to understand that the yaw moment has an additional inviscid part called the Munk moment (Mc). The moment is estimated using a simplified empirical formula

according to (DNV RP H103, 2011)

$$M_c = {V_c}^2 . \cos(rc) . \sin(rc) * (A_{11} - A_{22}) \quad (5.162)$$

$V_c \; and \; rc$ are the mean current velocity and direction respectively; $A_{11} \; and \; A_{22}$ are the added masses in the surge and sway directions. The surge added mass is estimated using the method proposed by (Bishops and Prize, 1979).

5.2.5 *Slow Drift Force approximated using methods from (DNV RP H103, pg. 108; Remery & Hermans 1971)*

The equation 5.163 is implemented in estimating the drift force which is proportional to the square of the wave elevation, as represented by the significant wave height.

$$F_{wd} = \frac{1}{8} \rho_{water} * g * R * Bs * {H_{1/3}}^2 \quad (5.163)$$

The unit in this sense is considered as a towing unit, significant enough is that the speed of the towing boat according to this assumption is zero which simplifies to the FPSO at work station. The reflection coefficient *R* is entered as an input value obtained from table contained in (DNV RP H103, 2011). Two methods are employed in dealing with this since we have a sea with multiple wave systems.

5.2.5.1 *Dealing with the waves as separated systems*

The Drift force contributions from the different wave systems are estimated as it is shown below;

For the Wind Sea;

$$F_{wdws} = \frac{1}{8}\rho_{water} * g * R * Bs * {H_{sw}}^2 \quad (5.164)$$

Resolved components;

$$F_{wdwsX} = F_{wdws} * \sin(\theta_{sw1}) \quad (5.165)$$

$$F_{wdwsY} = F_{wdws} * \cos(\theta_{sw1}) \quad (5.166)$$

For the swell sea represented as Swell 1;

$$F_{wdss1} = \frac{1}{8}\rho_{water} * g * R * Bs * {H_{ss1}}^2 \quad (5.167)$$

Resolved components;

$$F_{wdss1X} = F_{wdss1} * \sin(\theta_{ss1}) \quad (5.168)$$

$$F_{wdss1Y} = F_{wdss1} * \cos(\theta_{ss1}) \quad (5.169)$$

And for the swell sea designated as Swell 2;

$$F_{wdss2} = \frac{1}{8}\rho_{water} * g * R * Bs * {H_{ss2}}^2 \quad (5.170)$$

Resolved components;

$$F_{wdss2X} = F_{wdss2} * \sin(\theta_{ss2}) \quad (5.171$$

$$F_{wdss2Y} = F_{wdss2} * \cos(\theta_{ss2}) \quad (5.172)$$

The total drift force in X-direction (surge) and Y-direction (sway) are then obtained;

$$F_{wdX} = F_{wdwsX} + F_{wdss1X} + F_{wdss2X} \quad (5.173)$$

$$F_{wdY} = F_{wdwsY} + F_{wdss1Y} + F_{wdss2Y} \quad (5.174)$$

5.2.5.2 *Dealing with wave system as a single unit;*

The principle of (Bhoukanouvsky and Soares, 2004) is applied to add up the entire wave system to obtain the cumulative significant height (Hs) and mean direction. Applying equations 4.17 and 4.22 to find the combined significant wave height of combined sea. The total drift force from equation 5.155 with $H_{1/3}$ equivalent to H_s is;

$$F_{wd} = \frac{1}{8}\rho_{water} * g * R * Bs * {H_s}^2 \quad (5.175)$$

Resolving onto the surge (X) and Sway(Y) components, yields;

$$F_{wdX} = F_{wd} * \sin(\theta_s) \quad (5.176)$$

$$F_{wdY} = F_{wd} * \cos(\theta_s) \quad (5.177)$$

On investigation, the two methods gave virtually the same result with an error (measured discrepancy between methods) range of about 10^{-10}.

5.2.6 *Estimation of the Virtual Mass Matrix*

The virtual mass matrix [M], is composed of the actual mass and inertial 'm' of the unit and the added mass and inertial 'A' components resulting from motions.

$$[M]_{ij} = [m]_{ij} + [A]_{ij} \quad (5.178)$$

Using the standard form for the actual mass matrix;

$$[m]_{ij} = \begin{bmatrix} m_{11} & 0 & 0 & 0 & z_g * m_{11} & -y_g * m_{11} \\ 0 & m_{11} & 0 & -z_g * m_{11} & 0 & x_g * m_{11} \\ 0 & 0 & m_{11} & y_g * m_{11} & -x_g * m_{11} & 0 \\ 0 & -z_g * m_{11} & -y_g * m_{11} & I_{xx} + dI_{xx} & -I_{xy} & -I_{xz} \\ -z_g * m_{11} & 0 & -x_g * m_{11} & -I_{xy} & I_{yy} + dI_{yy} & -I_{yz} \\ -y_g * m_{11} & -x_g * m_{11} & 0 & -I_{zx} & -I_{zy} & I_{zz} + dI_{zz} \end{bmatrix}$$

(5.179)

For moored FPSO with large number of initially taut or tensioned tethers, the values of the mass of the unit changes slightly by taking up the adherent mass of the slacked polyester lines which eventually lose their taut state and hence become lump masses attached to the unit. At any instant in time, as the FPSO moves, altering the tensioned length of the lines, while some remain in tension, others are converted into lump masses and added to the FPSO mass to update the mass used inside the $[m]_{ij}$ matrix. The update is achieved by implementing equation 5.180.

$$m_{11u} = m_{11} + n_l * \delta m \tag{5.180}$$

n_l is the number of tension loosened cables and δm is the apparent mass of one cable line.

5.2.6.1 *Approximating the Inertia Tensor:*

The region at the bottom right of $[m]_{ij}$ matrix of equation 5.179 are the inertia terms contained in the mass matrix. The tensor is approximated either from input values of the radius of gyrations in x, y, and z axis, i.e. *Kxx, Kyy* and *Kzz* or from the geometry of the FPSO under water.

Theoretically;

$$[I]_{ij} = \begin{bmatrix} I_{xx} + dI_{xx} & -I_{xy} & -I_{xz} \\ -I_{xy} & I_{yy} + dI_{yy} & -I_{yz} \\ -I_{zx} & -I_{zy} & I_{zz} + dI_{zz} \end{bmatrix} \tag{5.181}$$

i, j=4:6 or x, y, z;

From standard equations

$$I_{xx} = I_{44} = \frac{m}{12} * ({B_s}^2 + {D_s}^2) \quad (5.182)$$

or

$$I_{xx} = m * {K_{xx}}^2 \quad (5.183)$$

$$I_{yy} = I_{55} = \frac{m}{12} * ({L_s}^2 + {D_s}^2) \quad (5.184)$$

or

$$I_{yy} = m * {K_{yy}}^2 \quad (5.185)$$

$$I_{zz} = I_{66} = \frac{m}{12} * ({L_s}^2 + {B_s}^2) \quad (5.186)$$

or

$$I_{zz} = m * {K_{zz}}^2 \quad (5.187)$$

The change in inertia because of the slack lines can be approximated as;

$$dI_{xx} = dI_{44} = \frac{n_l * \delta m}{12} * ({B_s}^2 + {D_s}^2) \quad (5.188)$$

$$dI_{yy} = dI_{55} = \frac{n_l * \delta m}{12} * ({L_s}^2 + {D_s}^2) \quad (5.189)$$

$$dI_{zz} = dI_{66} = \frac{n_l * \delta m}{12} * ({L_s}^2 + {B_s}^2) \quad (5.190)$$

These changes are used as corrections to the parameters being estimated over time.

The other terms for which $i \neq j$ are taken to be zero, due to hull symmetry.

5.2.6.2 *Determination of the Added Mass and Inertia Matrix;*

The standard simplified Lewis Conformal Mapping was adopted in this regard to estimate the non-zero terms in the added mass and inertial matrix. The 2D Strip theory is used in this form, to estimate the 2D added mass and inertial coefficients which are then integrated over the length to determine the 3D Coefficients. The procedure according to

(Camelia Ciobanu & Anghel, 2008) was adopted to compute the scale factor μ_s , and Lewis coefficients a_1 and a_3. These values are then used as input values in the computation of 2D added mass for some of the motion states. See equations below;

Sway

$$\mu_{22} = \frac{\pi\rho}{2}\mu_s{}^2\,[(1-a_1)^2 + 3a_3{}^2] \tag{5.191}$$

Sway –Roll

$$\mu_{24} = 4\rho\mu_s{}^3\,[\tfrac{1}{3}a_1(1-a_1)(1+a_1) + a_3[\tfrac{3}{5}(1+a_3) + \tfrac{4}{15}a_3(1-a_1) - \tfrac{6}{7}a_3]] \tag{5.192}$$

Heave;

$$\mu_{33} = \frac{\pi\rho}{2}\mu_s{}^2\,[(1+a_1)^2 + 3a_3{}^2] \tag{5.193}$$

Roll;

$$\mu_{44} = \pi\rho\mu_s{}^4\,[a_1{}^2(1+a_1)^2 + 2a_3{}^2] \tag{5.194}$$

The non-zero added mass/inertial can then be approximated using 21 mid-ship sections equally spaced at Δx . Note that for a stationary unit, like the FPSO, *U=0*. This reduces the equation as presented by (Camelia Ciobanu & Anghel, 2008) and pg. 56 of Principle of Naval Arch, Vol. III by (Edward,1989) to those of equation 5.195 below.

$$\left.\begin{aligned}
A_{33} &= \sum \mu_{33}\Delta x \\
A_{35} &= \sum x.\mu_{33}.\Delta x \\
A_{53} &= \sum x.\mu_{33}.\Delta x \\
A_{55} &= \sum x^2.\mu_{33}.\Delta x \\
A_{22} &= \sum \mu_{22}.\Delta x \\
A_{24} &= A_{42} = \sum \mu_{24}\Delta x \\
A_{26} &= A_{62} = \sum x.\mu_{22}.\Delta x \\
A_{44} &= \sum \mu_{44}.\Delta x \\
A_{46} &= A_{64} = \sum x.\mu_{24}.\Delta x \\
A_{66} &= \sum x^2.\mu_{22}.\Delta x
\end{aligned}\right\} \tag{5.195}$$

Combining the elements of equation 5.136 and 5.152 the virtual mass matrix of equation 5.135 can be estimated at the given time step.

Other methods may also be applied to determine the diagonal elements of the added mass matrix. See Bishops and Prize, 1979 for elaborate procedure.

The cross-sectional areas where obtained from the generalized form of the trapezium rule for unequal intervals applied to the offset points for each section.

5.3 Restoring Coefficient Matrix;

Restoring coefficient matrix resulting from the free floating FPSO (CC_{ij}) is modified by the restoring introduced from the mooring lines stiffness K_{ij} to give the final restoring coefficient matrix (C_{ij})

$$C_{ij} = CC_{ij} + K_{ij} \tag{5.196}$$

Using standard equations with parameters given, the non-zero elements of the CC_{ij} matrix can easily be approximated thus;

$$\left.\begin{array}{c} CC_{33} = \rho g S_O \quad or \quad \rho g \int B_S(x)dx \\ CC_{35} = \rho g x_f S_O \quad or \quad -\rho g \int x.B_S(x)dx \\ CC_{55} = \rho g I_y \quad or \quad \rho g \int x^2.B_S(x)dx \\ CC_{44} = \rho g.\nabla.\overline{GM_T} \end{array}\right\} \tag{5.197}$$

5.3.1 *Approximating the Restoring Coefficient contribution from Taut Tethers;*

Unlike a steel catenary mooring system which involves the use of heavy steel lines to produce the required restoring through its weight, the taut polyester lines are comparatively very light, and produce their restoring via a pre-tension applied to it. They have more advantages in terms of economy and safety of operations. The method adopted is found in pg. 2/98-99 of (Nina, 1990). The restoring is principally due to the elastic nature of the material having elastic stiffness λ .

The overall stiffness resulting from the entire mooring lines is represented by

$$K_{ij} = \sum_{q=1}^{q=Nm} k_{ij}^{q} \tag{5.198}$$

Where

k_{ij}^{q} is the stiffness matrix for a single mooring line.

Nm is the number of mooring lines used.

For a single mooring line, with a pre-determined pre-tension T,

$$T = \frac{MBL}{SF} \tag{5.199}$$

MBL – maximum breaking load of polyester material

SF – recommended safety factor

Two attachment points (the fairlead and anchor points) are established or approximated using the depth of water D and the attachment angle at the sea bed.

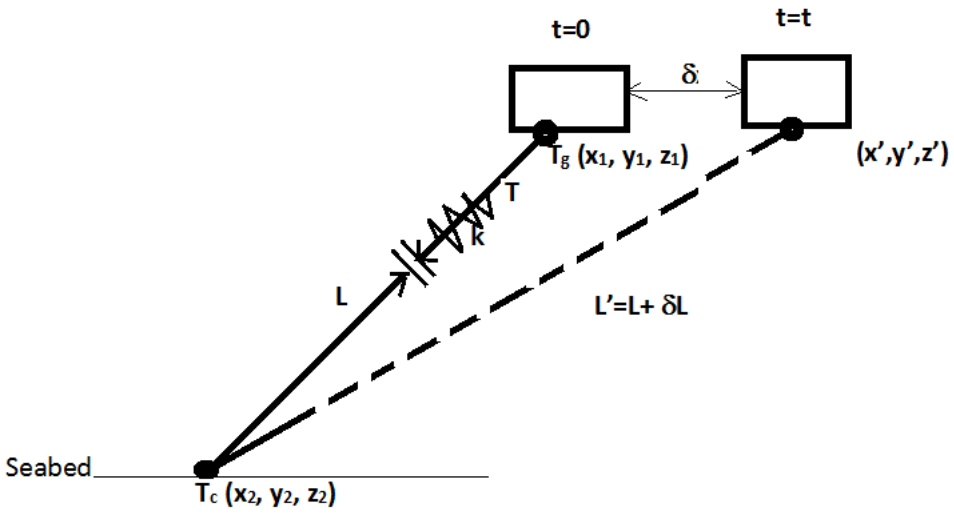

Figure 5.16 Mooring line motion resulting from moving FPSO

At the initial position (t=0), when all lines are taut, the restoring force is defined by the direction cosines. All these calculations steps captured below are performed for a single line index 'q'

With

$$\left.\begin{aligned} a_T &= x_2 - x_1 \\ b_T &= y_2 - y_1 \\ c_T &= z_2 - z_1 \end{aligned}\right\} \tag{5.200}$$

$$\left.\begin{aligned} l_x &= \cos(\alpha) = \frac{a_T}{L} \\ l_y &= \cos(\beta) = \frac{b_T}{L} \\ l_x &= \cos(\gamma) = \frac{c_T}{L} \end{aligned}\right\} \tag{5.201}$$

Initial length of taut tether is;

$$L = \sqrt{{a_T}^2 + {b_T}^2 + {c_T}^2} \tag{5.202}$$

Due to the small motion δx, new tether length to 1st order estimate yields;

$$L' = L + \delta L = L + \frac{a_T}{L}.\delta x \tag{5.203}$$

This will create additional tension, that can be evaluated as shown below;

$$\delta T = \lambda.\delta L = \lambda.\frac{a_T}{L}.\delta x \tag{5.204}$$

Thus, the resulting restoring force component in x-direction can be represented as;

$$\delta T_x = (T + \delta T)\cos(\alpha') - T\cos(\alpha) \tag{5.205}$$

Where the direction cosine in new position (2) is then obtained

$$\cos(\alpha') = \frac{a_T + \delta x}{L'} \tag{5.206}$$

$$\therefore\ T_x = (T + \delta T)\frac{a_T}{L'}\left[\frac{1 + \delta x/a_T}{1 + \delta L/L}\right] - T\ \frac{a_T}{L} \tag{5.207}$$

$$T_x = T cos(\alpha).\{\frac{\delta x}{a_T} - \frac{\delta L}{L} + \frac{\delta T}{T}\} \tag{5.208}$$

Approximating to first order, with the change in length given as;

$$\delta L\ \approx \delta x.l_x \tag{5.209}$$

$$\delta T_x = \frac{T}{L}l_x[\frac{L.\delta x}{a_T} - l_x.\delta x + \frac{\lambda.a_T}{T}.\delta x] \tag{5.210}$$

$$\delta T_x = \lambda.{l_x}^2 + \frac{T.\ sin^2(\alpha).\delta x}{L} = \lambda.{l_x}^2 + \frac{T.\ (1 - {l_x}^2).\delta x}{L} \tag{5.211}$$

The first stiffness term is defined as the limit expression of equation 5.212

$$k_{11}^{q} = \lim_{\delta x \to 0} \left[\frac{\partial T_x}{\partial x}\right] \tag{5.212}$$

This is then approximated as;

$$k_{11}^{q} = \lambda . {l_x}^2 + \frac{T}{L} \tag{5.213}$$

Other terms are estimated accordingly following similar procedure, thus;

$$\left.\begin{aligned} k_{21}^{q} &= \left[\lambda + \frac{T}{L}\right] . l_x . l_y \\ k_{12}^{q} &= k_{21}^{q} \\ k_{31}^{q} &= [\lambda + \frac{T}{L}] . l_x . l_z \\ k_{13}^{q} &= k_{31}^{q} \\ k_{22}^{q} &= \lambda . {l_y}^2 + \frac{T}{L}[1 - {l_y}^2] \\ k_{32}^{q} &= \left[\lambda + \frac{T}{L}\right] . l_y . l_z \\ k_{23}^{q} &= k_{32}^{q} \\ k_{33}^{q} &= \lambda . {l_z}^2 + \frac{T}{L}[1 - {l_z}^2] \end{aligned}\right\} \tag{5.214}$$

The remaining terms in the *6 X 6* matrix are computed as functions of the ones already estimated above;

$$\left.\begin{aligned} k_{41}^{q} = k_{14}^{q} &= k_{31}^{q} * y_2 - k_{21}^{q} * z_2 \\ k_{51}^{q} = k_{15}^{q} &= k_{11}^{q} * z_2 - k_{31}^{q} * x_2 \\ k_{61}^{q} = k_{16}^{q} &= k_{21}^{q} * x_2 - k_{11}^{q} * y_2 \\ k_{52}^{q} = k_{25}^{q} &= k_{21}^{q} * z_2 - k_{32}^{q} * x_2 \\ k_{62}^{q} = k_{26}^{q} &= k_{22}^{q} * x_2 - k_{21}^{q} * y_2 \\ k_{43}^{q} = k_{34}^{q} &= k_{33}^{q} * y_2 - k_{32}^{q} * z_2 \\ k_{53}^{q} = k_{35}^{q} &= k_{31}^{q} * z_2 - k_{33}^{q} * x_2 \\ k_{63}^{q} = k_{36}^{q} &= k_{32}^{q} * x_2 - k_{31}^{q} * y_2 \\ k_{44}^{q} &= k_{33}^{q} * {y_2}^2 - 2k_{32}^{q} * y_2 . z_2 + k_{22}^{q} * {z_2}^2 \\ k_{54}^{q} = k_{45}^{q} &= k_{31}^{q} * y_2 . z_2 - k_{21}^{q} * {z_2}^2 + k_{33}^{q} * y_2 . x_2 + k_{32}^{q} * x_2 . z_2 \\ k_{64}^{q} = k_{46}^{q} &= k_{32}^{q} * y_2 . x_2 - k_{22}^{q} * z_2 . x_2 - k_{31}^{q} * {y_2}^2 + k_{21}^{q} * y_2 . z_2 \\ k_{55}^{q} &= k_{11}^{q} * {z_2}^2 - 2k_{31}^{q} * x_2 . z_2 + k_{33}^{q} * {x_2}^2 \\ k_{65}^{q} = k_{56}^{q} &= k_{21}^{q} * z_2 . x_2 - k_{32}^{q} * {x_2}^2 - k_{11}^{q} * y_2 . z_2 + k_{31}^{q} * y_2 . x_2 \\ k_{66}^{q} &= k_{22}^{q} * {x_2}^2 - 2k_{21}^{q} * y_2 . x_2 + k_{11}^{q} * {y_2}^2 \end{aligned}\right\} \tag{5.215}$$

The above procedure is repeated for all other lines (q=1: Nm). It is important to note that the fairlead position is radially spaced around the turret base radius for all the lines, the anchor point at the sea bed varies for each line as well. To calculate the total stiffness, equation 5.196 is used.

A. Modification 1:

However, to capture a sense of dynamic interaction between the tether and the FPSO in the water, wind and current environment, the tether fairlead position is updated by the relative instantaneous or time varying surge X (1, t), Sway X (2, t), and the heave X (3, t) motions; thus, at every time step 't', for a given line q,

$$T_g(t) = [x_1 + X(1,t), y_1 + X(2,t), z_1 + X(1,t),] \quad (5.216)$$

This is then used to re-compute the stiffness matrix K_{ij}.

It is significant to note that the fairlead position is different for each mooring line due to the spread around the perimeter of the turret base where connection is made to each line. This thus implies that the above equation 5.216 is applied to each line (since x_1, y_1, z_1 are not the same for all lines.)

Therefore equation 5.216 can be modified to

$$T_g(q,t) = [x_1(\mathrm{q,t}) + X(1,t), y_1(\mathrm{q,t}) + X(2,t), z_1(\mathrm{q,t}) + X(1,t),] \quad (5.217)$$

With q signifying the mooring line index number.

A. Modification 2;

Another modification to the analysis was introduced to establish a minimum threshold in percentage (% P_T) of length of the cable ensuring line tautness. This will ensure that the cable is still under tension and supporting the restoring capability of the unit. Once the difference between the original length and the straight line distance of the connecting points (fairlead and sea bed) for any cable falls below the threshold on the negative side,

the cable is assumed to have slacked and hence regarded as having lost its taut state. This automatically converts that cable into a lump mass together with the Unit.

New taut length at position 2 is;

$$L' = \sqrt{(T_{gx} - x_2)^2 + (T_{gy} - y)^2 + (T_{gz} - z_2)^2} \tag{5.218}$$

Change in straigth line length becomes;

$$\Delta L = L' - L \tag{5.219}$$

For any cable 'q', at any given time t,

$$k_{ij}^{q} = 0 \quad (if\ \Delta L \quad < -\left[P_T * \frac{L}{100}\right]) \tag{5.220}$$

This brings the total stiffness to a value less than what could be obtained from equation 5.196

$$K_{ij} = \sum_{q=1}^{q=(Nm-nl)} k_{ij}^{q} \tag{5.221}$$

nl is the number of slacked cables. The overall mass of the unit is updated accordingly from equation 5.130 above.

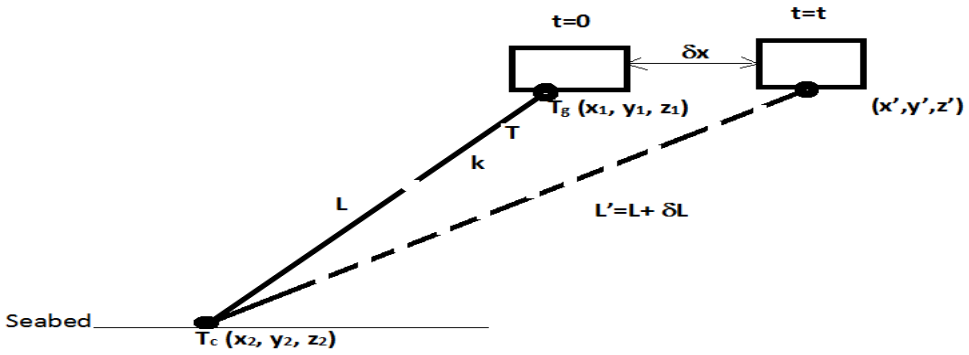

Figure 5.17 Mooring line slackness/tautness resulting from FPSO motion

5.4 Approximating the Damping Matrix $[B]_{ij}$;

Because of the rigours involved in estimating the damping matrix which is frequency dependent, a simplified way to approximate the damping value is adopted. The damping coefficient *Bij* for a given motion state was pre-applied by using a constant damping ratio ξ together with an estimated critical damping $B_{crit.}$ It is pertinent to know that damping is dependent on the added mass, frequency and stiffness of the system;

$$B = f(A, \omega, C) \tag{5.222}$$

For this analysis, the zero frequency value was used. This is the value of the damping at a calm sea condition or frequency independent part of the damping term. Thus;

$$B_{ij} = \xi * [B_{ij}]_{crit} \tag{5.223}$$

$$[B_{ii}]_{crit} = 2 * \sqrt{M_{ii} * C_{ii}} \tag{5.224}$$

To keep the computation reasonably simple, only the diagonal elements maybe considered. This implies that all the non-diagonal elements are made equal to 0.

$$B_{ij} = 0 \ \ for\ i \neq j \tag{5.225}$$

However, it is also possible to use a rough estimate of the entire damping matrix relying on equation 5.225. Different options for the application of the critical damping exist in the code.

Because most times it is easier to obtain the damping from a model test, it is then necessary to use the dimensional factor or linear scaling ratio for the damping parameter in order to get the actual approximate damping for the actual ship. The ratio according to (ITTC recommendation 7.5-02.07-02.6 pg5, 2002)

$$\xi_{actual} = \xi_{model} / \sqrt{\frac{\lambda}{c}} \tag{5.226}$$

Were λ and c are the linear scale ratio and density ratio respectively. The damping coefficient for a given damping ratio is time variant since it changes with other time varying parameters.

Another consideration was made in attempting to estimate the potential damping using the Lewis conformal mapping. This was applied in the computation of the Diffraction force using the weighting technique. See section 5.2.2.2 for this.

5.4.1 *Modifying the Roll Damping term B_{44}*

Depending on the model of roll damping used in developing the eom, the code allows for the modification using five options of model. However, the interest of this work is exploring the new modified hyperbolic model which is compared to the standard linear model. For this procedure, the model is such that the roll damping is dependent on the instantaneous roll velocity as well as the amplitude ($B_{44} = f(\dot{X}_{44}, X_{44})$)

Generally, from the uncoupled eom for roll;

$$M_{44}\ddot{x} + B_{44}\dot{x} + C_{44}x = F(t) \tag{5.227}$$

For free decay representation, since the coefficients are easily obtained via a free decay test;

$$m_{44}\ddot{x} + \beta_{44}\dot{x} + c_{44}x = 0 \tag{5.228}$$

i. For linear;

$$B_{44} = \beta_{44} * M_{44} \tag{5.229}$$

ii. Faltinsen and Froude;

$$B_{44} = (\beta_{441} + \beta_{442} * |\dot{X}_{44}|) * M_{44} \tag{5.230}$$

iii. Hyperbolic models

$$B_{44} = 2 * \beta_{44} * \omega_{44} * M_{44} \tag{5.231}$$

If not given; $$\omega_{44} = \sqrt{M_{44} * C_{44}} \tag{5.232}$$

a. **Fernandez and Oliveira;**

$$\beta_{44} = \beta_{bs} + (\beta_{ls} - \beta_{bs}) * tanh\left[\alpha.(X_{44}{}^2 + \frac{\dot{X}_{44}{}^2}{\omega_{44}{}^2})\right] \tag{5.233}$$

b. **Modified Hyperbolic model**

$$\beta_{44} = \beta_{bs} + (\beta_{Ts} - \beta_{bs}) * \left\{ tanh\left[\alpha.\left({X_{44}}^2 + \frac{{\dot{X}_{44}}^2}{{\omega_{44}}^2}\right)\right] + \beta_{Ts} + (\beta_{ls} - \beta_{Ts}) * tanh\left[\alpha 1\left({X_{44}}^2 + \frac{{\dot{X}_{44}}^2}{{\omega_{44}}^2}\right)\right]\right\} \quad (5.234)$$

The coefficients, $\beta_{44}, \beta_{441}, \beta_{442}, \beta_{bs}, \beta_{ls}, \alpha, \lambda$ are obtained via a free decay test. The approximated fitting parameters are contained in appendix H. The damping matrix can then be modified before solving the 6dof eom. If the parameter is obtained directly from experiment and unscaled to that of the actual structure at this point, the equation 5.226 is used before it is implemented in the eom.

Another section used the least square optimization technique to estimate the equivalent linear damping coefficient, this value is intended to be tested with the non-linear arrangement for comparison.

5.5 Solving the Equation of Motion

With all the terms in the typical 6dof eom estimated, at the given time t, the resulting rigid body eom can then be solved.

$$[M]\{\ddot{x}\} + [B]\{\dot{x}\} + [C]\{x\} = \{F(t)\} \quad (5.235)$$

With [*M*], [*B*], [*C*] and [*F*] being the overall mass, damping, restoring coefficient and excitation force matrices respectively.

It is also significant to point out that the force vector is transformed before carrying out computation. The Froude-Krylov force could be modified to account to a large extent for the diffraction component of the total excitation force vector by using a tuning parameter. Because of the uncertainty associated with selecting reasonable percentage to use as the tuning parameter, the Froude-Krylov was estimated using the coarse integration of the pressure on wetted surface as well as the weighting technique. The Diffraction forces were estimated using the weighting technique.

5.5.1 *Transformation of the Force Vector*

It is significant to transform the force computed on the fixed body coordinate system to the moving body coordinate system. This is achieved by using the transformation matrix which is dependent on the rotational motions of the center of gravity of unit. The transformation is done separately for the two types of motions, the translational forces and the rotational moments. However, use is made only of the transformed translational forces in this work.

The force vector computed at a given time step is

$$\{F^*\} = \begin{Bmatrix} F^*_{trans} \\ M^*_{rot} \end{Bmatrix} \tag{5.236}$$

The transformed force vector at the same time step is

$$\{F_T\} = T * \{F^*_{trans}\} \tag{5.237}$$

$$\{M_T\} = T * \{M^*_{rot}\} \tag{5.238}$$

Thus, the resulting force vector becomes

$$\{F\} = \begin{Bmatrix} F_T \\ M_T \end{Bmatrix} \text{ (If Moment is transformable)} \tag{5.239}$$

or

$$\{F\} = \begin{Bmatrix} F_T \\ M^*_{rot} \end{Bmatrix} \text{ (If Moment is not transformed)} \tag{5.240}$$

This force is in-turn used for the computation of the motion for the next time step.

The expression for the transformation matrix is given below

$$T = \begin{bmatrix} T_{11} & T_{12} & T_{13} \\ T_{21} & T_{22} & T_{23} \\ T_{31} & T_{32} & T_{33} \end{bmatrix} \tag{5.241}$$

Were:

$$\left.\begin{aligned}
T_{11} &= \cos\big(X(6,t)\big) * \cos\big(X(5,t)\big) \\
T_{12} &= -\sin\big(X(6,t)\big) * \cos\big(X(4,t)\big) + \cos\big(X(6,t)\big) * \sin\big(X(5,t)\big) * \sin\big(X(4,t)\big) \\
T_{13} &= sin\big(X(6,t)\big) * sin\big(X(4,t)\big) + cos\big(X(4,t)\big) * cos\big(X(5,t)\big) * sin\big(X(5,t)\big) \\
T_{21} &= \sin\big(X(6,t)\big) * \cos\big(X(5,t)\big) \\
T_{22} &= cos\big(X(6,t)\big) * cos\big(X(4,t)\big) + sin\big(X(4,t)\big) * sin\big(X(5,t)\big) * sin\big(X(6,t)\big) \\
T_{23} &= cos\big(X(6,t)\big) * sin\big(X(4,t)\big) + sin\big(X(5,t)\big) * sin\big(X(6,t)\big) * cos\big(X(4,t)\big) \\
T_{31} &= -\sin\big(X(5,t)\big) \\
T_{32} &= cos\big(X(5,t)\big) * sin\big(X(4,t)\big) \\
T_{33} &= cos\big(X(5,t)\big) * cos\big(X(4,t)\big)
\end{aligned}\right\}$$

(5.242)

5.5.2 *Numerical Schemes adopted to solve Equation of Motion*

Three numerical methods were tested for implementation.

1. Newmark-Betta method
2. Runge-Kutta 4th order
3. Runge-Kutta Carskarp multistep method

The methods solution algorithm is designed for fixed time step to allow for the introduction of updated parameters which occur at pre-selected times due to the fixed time interval used. For the Runge-Kutta methods, the 6dof 2nd ODE was first converted into two 1st ODEs using the state space technique, after which they are numerically solved. At this point, it is important to highlight that the initial conditions are constantly updated using newly computed values of the immediate past time step as bases to compute those of the new time step. The methods are demonstrated in appendix P.

With the eom simply expressed in equation 5.235

Write equation into two first order ODE, state variable $y(y1, y2)$ for integration coefficient calculations

$$\left.\begin{aligned}
\dot{X} &= \frac{dX}{dt} = y1; \\
\ddot{X} &= \frac{dy1}{dt} = y2
\end{aligned}\right\} \qquad (5.243)$$

$$\therefore\ dy1/dt = (F(t) - B * Xvel - C * X)/M; \qquad (5.244)$$

Note: $y1 = Xvel;\ dy1/dt = Xaccl;$

n =6; Dof;

Initial position in the 6 dof motion directions are all set to 0

HORIZONTAL PLANE MOTIONS to be applied at the same time with the FPSO Heading relative to the wave primary direction since they are all on the same plane.

$F(:,0) = 0;$ No Net force at calm sea t=0

$X(1,0) = 0;$ Surge (m)

$X(2,0) = 0;$ Sway (m)

$X(3,0) = 0;$ Heave (sinkage or floatation) (m)

VERTICAL PLANE MOTIONS

$X(4,0) = 0;$ Roll (Heel) angle, starboard (-), Portside (+),'deg'

$X(5,0) = 0;$ Pitch (List) Forward (+), After (-),'deg'

$X(6,0) = 0;$ Yaw angle will affect the relative ship path (deg), (+ve towards ps, (-ve) towards sb) 'deg'

$\ddot{X}(:,0) = M\backslash(F(:,0) - B * \dot{X}(:,0) - C * X(:,0));$ Approximated Initial

updated INITIAL CONDITONS at time th=th(t) during th(t):th(t+1) Integration of eom.

$Xi(:,0) = X(:,t);\ \dot{X}(:,0) = \dot{X}(:,t);$

Use current force (F (:, t) to compute acceleration at the start of the new time step (t)

$\ddot{X}(:,t) = M\backslash(F(:,t) - B * \ddot{X}(:,t) - C * X(:,t));$

$\ddot{X}i(:,0) = \ddot{X}(:,t);$

Re-assign for internal iteration via selected method for integration of eom

Updated initial conditions $\ddot{X}$ (:,0) at time t for (t):(t+1) integration of eom.

Integration of eom within a time step is carried out with updated parameters, X, Xvel & Xaccl. for tnm= (1: length(tnb)-1).

5.6 Motion Time history of any point on the body of the Ship

Once the motion time history of the centre of gravity of the unit has been estimated, the corresponding relative motion of any point P(Xp,Yp,Zp) on the body of the unit can be determined, given the unit as a solid body exhibiting the computed motion about its cog. The relative motion which depends on the distance of that point from the cog (Xg,Yg, Zg).

$$X = \begin{Bmatrix} X_{trans} \\ X_{rot} \end{Bmatrix} \tag{5.245}$$

$$\left.\begin{aligned} X_{trans} &= \begin{Bmatrix} X_1 \\ X_2 \\ X_3 \end{Bmatrix} \\ X_{rot} &= \begin{Bmatrix} X_4 \\ X_5 \\ X_6 \end{Bmatrix} \end{aligned}\right\} \tag{5.246}$$

If unit is assumed a solid body, all points have the same rotational motion X_{rot} at every time.

Let the motion of point P be X_{Pg}, thus

$$\left.\begin{aligned} X_{Pg.trans} &= \begin{Bmatrix} X_{Pg1} \\ X_{Pg2} \\ X_{Pg3} \end{Bmatrix} \\ X_{Pg.rot} &= \begin{Bmatrix} X_4 \\ X_5 \\ X_6 \end{Bmatrix} \text{(rigid body)} \end{aligned}\right\} \tag{5.247}$$

Mathematically

$$X_{Pg.trans} = X_{trans} + (X_{rot}\ \mathbf{X}\ \vec{\boldsymbol{r}}_{\boldsymbol{pg}}) \tag{5.248}$$

Were**;**

$$\vec{r}_{pg} = \vec{x}_{pg}i + \vec{y}_{pg}j + \vec{z}_{pg}k \tag{5.249}$$

$$\left.\begin{aligned}\vec{x}_{pg} &= x_g - x_p\\ \vec{y}_{pg} &= y_g - y_p\\ \vec{z}_{pg} &= z_g - z_p\end{aligned}\right\} \tag{5.250}$$

Solving equation 5.248 above, yields the translational displacement of the point P.

$$\left.\begin{aligned}X_{Pg1} &= X_1 + \left(X_5 * \vec{\boldsymbol{z}}_{\boldsymbol{pg}} - X_6 * \vec{\boldsymbol{y}}_{\boldsymbol{pg}}\right)\\ X_{Pg2} &= X_2 + \left(X_6 * \vec{\boldsymbol{x}}_{\boldsymbol{pg}} - X_4 * \vec{\boldsymbol{z}}_{\boldsymbol{pg}}\right)\\ X_{Pg3} &= X_3 + \left(X_4 * \vec{\boldsymbol{y}}_{\boldsymbol{pg}} - X_5 * \vec{\boldsymbol{x}}_{\boldsymbol{pg}}\right)\end{aligned}\right\} \tag{5.251}$$

Carry out differentiation to find the velocity and acceleration of the point

$$\left.\begin{aligned}\dot{X}_{Pg1} &= \dot{X}_1 + \left(\dot{X}_5 * \vec{\boldsymbol{z}}_{\boldsymbol{pg}} - \dot{X}_6 * \vec{\boldsymbol{y}}_{\boldsymbol{pg}}\right)\\ \dot{X}_{Pg2} &= \dot{X}_2 + \left(\dot{X}_6 * \vec{\boldsymbol{x}}_{\boldsymbol{pg}} - \dot{X}_4 * \vec{\boldsymbol{z}}_{\boldsymbol{pg}}\right)\\ \dot{X}_{Pg3} &= \dot{X}_3 + \left(\dot{X}_4 * \vec{\boldsymbol{y}}_{\boldsymbol{pg}} - \dot{X}_5 * \vec{\boldsymbol{x}}_{\boldsymbol{pg}}\right)\end{aligned}\right\} \tag{5.252}$$

$$\left.\begin{aligned}\dot{X}_{Pg.trans} &= \begin{Bmatrix}\dot{X}_{Pg1}\\ \dot{X}_{Pg2}\\ \dot{X}_{Pg3}\end{Bmatrix}\\ \dot{X}_{Pg.rot} &= \begin{Bmatrix}\dot{X}_4\\ \dot{X}_5\\ \dot{X}_6\end{Bmatrix}\end{aligned}\right\} \tag{5.253}$$

Acceleration;

$$\left.\begin{aligned}\ddot{X}_{Pg1} &= \ddot{X}_1 + \left(\ddot{X}_5 * \vec{\boldsymbol{z}}_{\boldsymbol{pg}} - \ddot{X}_6 * \vec{\boldsymbol{y}}_{\boldsymbol{pg}}\right)\\ \ddot{X}_{Pg2} &= \ddot{X}_2 + \left(\ddot{X}_6 * \vec{\boldsymbol{x}}_{\boldsymbol{pg}} - \ddot{X}_4 * \vec{\boldsymbol{z}}_{\boldsymbol{pg}}\right)\\ \ddot{X}_{Pg3} &= \ddot{X}_3 + \left(\ddot{X}_4 * \vec{\boldsymbol{y}}_{\boldsymbol{pg}} - \ddot{X}_5 * \vec{\boldsymbol{x}}_{\boldsymbol{pg}}\right)\end{aligned}\right\} \tag{5.254}$$

$$\left.\begin{aligned}\ddot{X}_{Pg.trans} &= \begin{Bmatrix}\ddot{X}_{Pg1}\\ \ddot{X}_{Pg2}\\ \ddot{X}_{Pg3}\end{Bmatrix}\\ \ddot{X}_{Pg.rot} &= \begin{Bmatrix}\ddot{X}_4\\ \ddot{X}_5\\ \ddot{X}_6\end{Bmatrix}\end{aligned}\right\} \tag{5.255}$$

5.7 Motion Time history Analysis Techniques

The output from a motion simulator is primarily the time histories of the displacements (translational and rotational), forces or moments. Time series data are treated differently from the other conventional data sets. The schematic diagram below depicts the analysis procedure employed in this research to deal with the output from the different simulation channels. Brief review of the methods is carried out and the results from the regular and irregular test conducted are presented afterwards.

The diagram below shows the analysis scheme

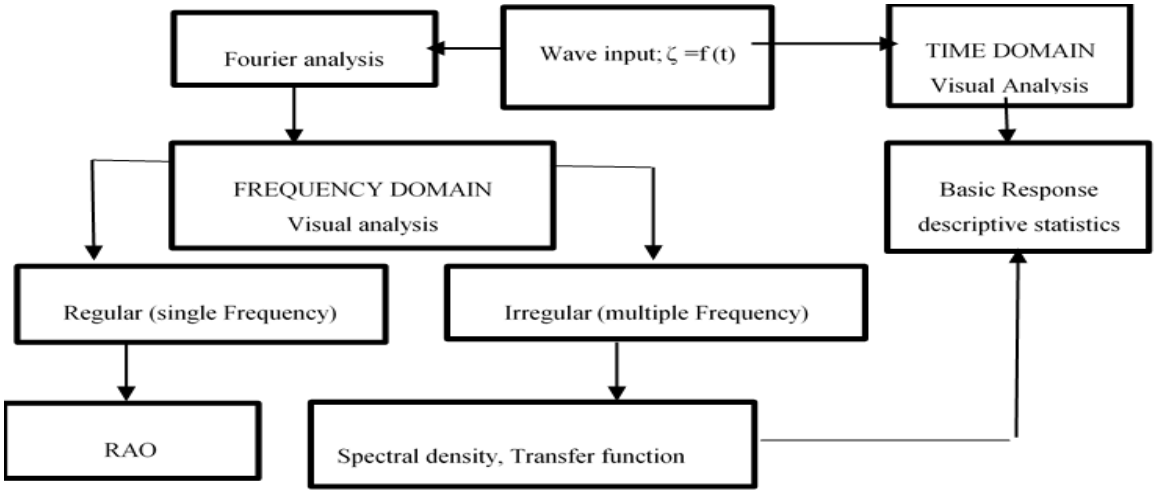

Figure 5.18 Motion time history analysis procedure

The wave input as well as the generated response are produced as time series from the various simulation channels. The raw data can be directly visualized from the time history or Fourier analysis carried out on them to enable conversion into the frequency domain for visualization. It is recommended that the data are filtered or cleaned from inherent systemic noise before this may be performed. The direct first-hand visualization of the time series is significant for use in assessing the global validity of the simulation or test, in which the amplitude and critical periods are estimated. In a similar manner, the visualized frequency domain data is used to decide the possibility of using a filter with the knowledge of the response frequencies and perhaps the noise level also.

Some of the descriptive statistics obtainable directly from the time series or the spectra density curve used for the evaluation of the response include the average (a_o), maximum (x_{max}) and minimum (x_{min}), i.e. range (x_{max}-x_{min}), the variance (mo) or standard deviation(σ). In addition to these statistics, the spectra moments (m_n) in equation 5.249 is also required from the spectra density curve. The significant value ($y_{1/3}$), average period (T_1), and average zero crossing period (T_2) of response are estimated thus.

$$m_n = \int_0^{\infty} \omega^n S(\omega).d\omega \tag{5.256}$$

(n=0,1,2,4)

$$\left.\begin{array}{c} \sigma = \sqrt{m_o} \\ y_{1/3} = 4\sigma \\ T_2 = \sqrt{\frac{m_o}{m_2}} \\ T_1 = \frac{m_o}{m_1} \end{array}\right\} \tag{5.257}$$

For a regular wave, the gain and phase of RAO is estimated by extracting the coefficients of the Fourier transforms on both the input (ζ =f (t)) and the response (y =g (t)) as shown below; for fg(t) representing either f(t) or g(t);

$$fg(t) = a_o + \sum_{i=1}^{\infty}[a_i \cos\left(\frac{2\pi.i}{T}.t\right) + b_i \sin\left(\frac{2\pi.i}{T}.t\right)] \tag{5.258}$$

$$\left.\begin{array}{c} a_o = \frac{1}{T}\int_o^T fg(t)dt \\ a_i = \frac{2}{T}\int_o^T fg(t)\cos\left(\frac{2\pi.i}{T}.t\right)dt \\ b_i = \frac{2}{T}\int_o^T fg(t)\sin\left(\frac{2\pi.i}{T}.t\right)dt \end{array}\right\} \tag{5.259}$$

$$\left.\begin{array}{c} RAO_{(gain)} = \frac{G_y}{G_\zeta} \\ RAO_{(phase)} = Ph_y - Ph_\zeta \end{array}\right\} \tag{5.260}$$

If parameters are obtained from the model, then the conversion to that actual vessel is presented below

$$[RAO]_{actual} = \frac{[RAO]_{model}}{\lambda} \tag{5.261}$$

The gain of response (G_y) and amplitude (G_ζ) and the phases are estimated from equation 5.262 for the respective data by using the appropriate coefficients a_i, b_i. (i=1, for regular wave).

$$\left.\begin{aligned} G &= \sqrt{{a_1}^2 + {b_1}^2} \\ Ph &= tan^{-1}\left(\frac{b_1}{a_1}\right) \end{aligned}\right\} \tag{5.262}$$

It is a priority to ensure that the frequency ($\omega=2\pi/T$) is the same as the one obtained from the Fourier fit before values are used.

For the irregular wave and associated irregular time series, the spectra density can be obtained by using the power density function (PSD), according to (Newland,1993, Roberts and Spanos,1990). The power density for a given signal is obtained using the Fast Fourier transform algorithm (fft). The conditions w.r.t. to the number of sample size attached to the method are properly adhered to. The ensuing transfer function $H(\omega)$ which is the equivalent of RAO for regular frequency data is thus obtained as equation 5.256 (DNV-RP-F205,201; Wishers, 2013; Tian et al, 2010)

$$[H(\omega)]^2 = \frac{S_{yy}(\omega)}{S_\zeta(\omega)} \tag{5.263}$$

The S_{yy}, S_ζ may be obtained by using the 'pwelch' algorithm inbuilt in MATLAB.

Program flow chart

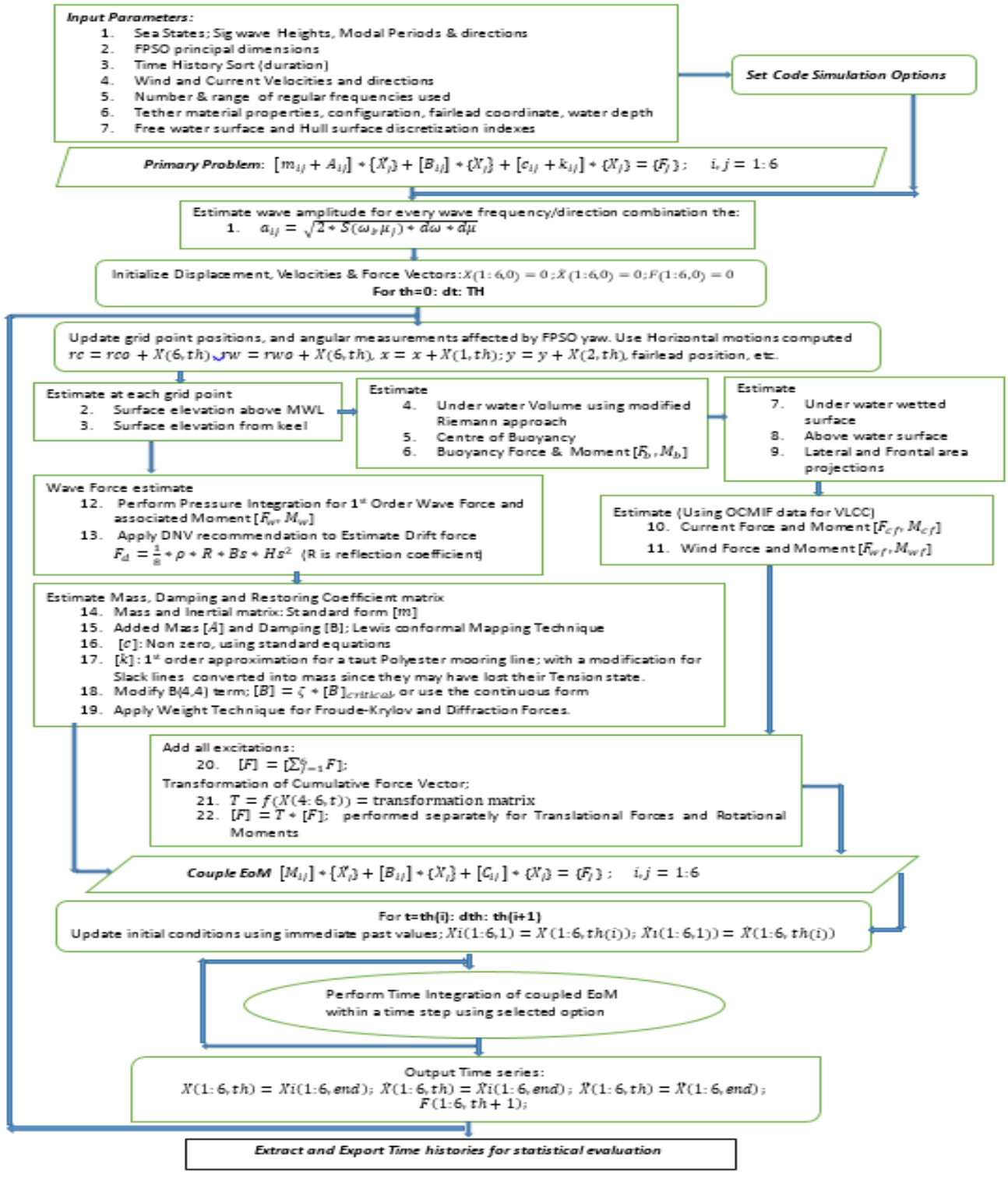

Figure 5.19 Flow chart showing major components in code

5.8 Numerical Simulation in SESAM HydroD

This section demonstrates the capability of the Sesam commercial tool employed in the research. A numerical example for the test cases simulated are also presented

5.8.1 *SESAM HydroD Modelling Capability and Technique*

SESAM is a robust tool for carrying out static and dynamic analysis of floating and fixed structures in a marine environment exposed to environmental forces (wind, wave and current). It is a patent software owned by DnV-GL for the purpose of carrying out hydrodynamic and other analysis related to offshore structures. In general, the package is basically divided into three separate independent and dependent analysis platforms namely; Genie, HydroD and DeepC. The Genie is used for developing the model (stored as a T1.FEM file) which serves as input to the HydroD. The HydroD is a specialised platform for hydrodynamic analysis. The third engine is the DeepC which receives result files (e.g., motion RAO's) from the HydroD and does the free motion, coupled analysis, fatigue analysis etc in specified water dept and environment. The wave load and motions are computed by Wadam or Wasim in the Sesam suite of programs. Wadam uses Morison's equation and first and second order 3D potential theory for the wave load calculations. Wasim uses Morison's equation and solves the 3D diffraction/radiation problem by a Rankine panel method. The incident wave potentials can either be defined by Airy linear or Stokes 5th order wave theory (Wasim only). Analysis can be performed in frequency domain or in time domain (Wasim only).

The package generates the following results: Hydrostatic and stability computations for intact and damage condition ,Hydrostatic data, Inertia properties ,Righting moment, Wind heeling moment, GZ curve, Still water sectional loads, analysis results checked against rules defined by internationally recognised codes, AVCG (Allowable Vertical Centre of Gravity) analysis, Global response, First order wave excitation forces and moments, Second order wave excitation forces and moments (used to model springing effects, low frequency forces etc), Hydrodynamic added mass and damping, First and second order rigid body motions, Sectional forces and moments, Steady drift forces and moments , Wave drift damping, Sectional load components (mass, added mass, damping and excitation forces), Panel pressures, Fluid particle kinematics (for gap calculations and free surface animation), calculation of selected global responses of a multi-body system ,

transfer of structural loads to a finite element model ,Inertia loads, Line loads on beam elements from Morison model , Point loads from pressure areas, anchor elements etc from Morison model , Pressure loads on plate/shell/solid elements. For details on the theory employed and calculation parameters in the wave load computation, the user is referred to the Wadam and Wasim user manuals. However, brief mathematical representations are captured in appendix Q.

The FPSO is generally described as a large volume floating structure. When it is in a real sea environment, it experiences first order motions due to excitations from the frequency(s) of the impacting wave(s). Because the waves are typically shortcrested, there are instances were secondary wave streams interact in difference as well as sum patterns to generate a new set of waves with difference and sum frequencies. These new resulting frequencies sometimes result in second order exciting forces, which are responsible for the second order motions experienced most times simultaneously by the structure. The forces (first and second order) are typically computed using the very well-developed potential flow theory for solving the velocity potential. The (Newmann,1963) approximation is mainly used by commercial packages including Sesam in the estimation of the quadratic transfer functions used for estimating second order forces and accompanying motions. The associated motions are very significant in the design of topside facilities, mooring lines, risers, as well as general sea keeping considerations for crew. This software package (Sesam) uses both the frequency and time domain approaches in tackling the equation of motion. The time domain representation is based on the inclusion of the memory effect or retardation function in the form of the convolution integral according to (Cummins, 1962).

The radiation force (i.e. the Added mass and potential damping coefficients) is obtained by solving the Radiation potential problem. The problem is subjected to the following boundary conditions (BC) (Laplace condition, free surface condition, body surface condition, body surface impermeability condition). The Froude-Krylov excitation which is due to the incident wave potentials is calculated by the direct integration of the incident wave pressure over the wetted surface area of hull. The diffraction potential problem is

first solved using the green function technique, were the potential is subjected to the BC similar to the radiation potential problem

Solving first order forces in irregular sea involves the solution of first order forces in regular longcrested sea formulations. This is currently done by the solution of the 3D diffraction-radiation problem of the floating body. The source density distribution method is a good approach to solving this boundary value problem on Rankine panels, to estimate the potentials. The resulting solution are then converted to irregular seas by the superposition theory for different regular wave streams, and also introduction of the directional spread for shortcrested formulation.

In modelling of the water environment, HydroD is limited in the available usable spectrum which are Jonswap, Bretchneider (2P Pierson-Mosquiwitz,) and Torsethagen. However, this thesis was based on a new set of combinable spectra as recommended by the (WASP,2004) for the West African region i.e., Jonswap-Glenn spectrum for the wind sea and Lognormal or Triangular for the swell components. Hence the need to develop a more spectrum flexible procedure to tackle this gap.

This section is designed to demonstrate the methods employed by the Hydrodynamic tool SESAM (HydroD) for estimating the forces and motions of a floating FPSO structure. The step by step capture of some of the methods applied are in Appendix P.

5.8.2 *Numerical Example with SESAM HydroD*

The hull model was developed by modifying an existing model to conform with the hull form under test. The Genie panel model has a total of 86 sections with over 1468 offset points from the FP to the AP. The hull was discretised to a total of 1408 panels. Trial runs where conducted to ensure that there were no areas of geometric discontinuities which may result in singularities during calculations. Figure 5.20 is the hull form with the discretised hydrodynamic panel model and the water surface in HydroD.

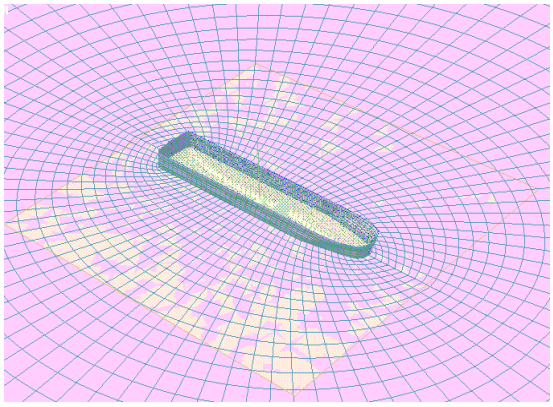

Figure 5.20 Hydrodynamic mesh of FPSO hull and water surface

The setup was executed from the Wasim solver in HydroD by initially creating the case file and the step by step input of required parameters. The step commences with the definition of the measurement units for parameters (basically: Force, time, temperature and length). The *location* describes the gravity term (g=9.1m/s2), the air and water densities as well as the depth of the operating region. In the *direction*, input of the directions used in defining the primary wave directions and the directional sets which defines the number of runs to be made if the frequency domain is selected. The *frequency set* is then applied to create the frequency points (period(s), wavelength (m) or frequency (Hz) forms) used in the RAO estimates. At this point, depending on the domain considered, for the frequency domain, the frequency domain condition is defined by selecting the already created direction set and frequency set. For the time domain (irregular), the *wave spectrum* is created at this point. Available spectrum includes, Jonswap 5, Bretchneider and Torsethaugen. The spectra are then created, and the directional *spreading* function also created by inputting appropriate power factor (n=6, 2 for swell and wind sea respectively), for the gamma spreading function in use. The irregular time condition is then created by selecting and adding appropriately.

The actual sea comprising of the wind sea and swell seas are combined with their representative spreading functions, mean directions. The random seed is also chosen for generating different epochs of the resulting time series, without significantly changing the statistical fidelity of the data. The algorithm selected to generate the wave components and the heading sectors, whether uniform or random, both ensures the conservation of the total wave energy corresponding to the spectrum and spreading function. The next

significant step is to create the *Hydro model*, *sectional model*, and sometimes the *structural model* for load transfers. The panel model is loaded adequately and the *loading condition* which defines the draft line is created. Initial positions of heeling, trimming, sinkage, etc. are defined. For this case, mean positions are assumed, so these values are entered as '0'. The mass model is then entered as an externally created model or the obtained from the panel model using the *homogenous density panel model* or *fill from buoyancy* technique. The product of inertial, centre of gravity and the gyration radii are updated. The issue of stability is ensured by making sure the distance between the cog and cob is within the limit through the *select location* dialog box. The mesh GUI is then used to discretize the water surface and the hull as shown in figure 5.20. The *motion control spring* is then set within range. This defines the natural frequency of the relevant motion modes where the spring are applied. The *damping coefficient or critical damping* is then defined. These values are added to the potential damping estimated for Wasim but overwritten in Wadam. The mass activity, setup activity is then built. This involves the combination of the already created sub modules of Hydro model, loading condition, location etc. to form a bigger module.

The pre-last stage involves the setting up of the solver run activity. The input interface is used to combine all the sub modules to form a problem executable block. The execution directory defines the simulation type sort for; free, forced or fixed. The time stepping is used to state the time history step, total duration and ramp length. Initial integration conditions for both displacement and velocities are stated in this interface. The first order time marching algorithm is used in this case since the vessel is not a high-speed type. The Neumann linearization scheme is adopted instead of the double body scheme because of better stability and absence of forward speed. It is also preferred for non-linear computations. The output directory is used for the display of the results. The results (displacements, velocities and accelerations time histories and Force/moment time histories) are appropriately stored and transferred for post processing. For frequency domain or time domain in which the Fourier activity is activated, the frequency dependent responses are also obtained. The last step termed the *Wizard* is the run GUI.

5.9 Conclusion

The methodology involved in the building of the simulation code for the floating structure has been elaborately presented. The different components of the equation of motion were obtained using simplified techniques. Starting with the added mass and damping, the 2D values were obtained using the Lewis conformal mapping and the 3D obtained from strip theory considerations. The restoring coefficient were estimated using standard equations. The wave excitation forces in the form of Froude-Krylov and Diffraction forces were estimated using standard regular wave formulations. A wave frequency-spectrum weighting technique was adopted to modify these equations and then implemented for short-crested sea states. However, the use of pressure integration over the instantaneous wetted surface of hull to estimate the Froude-Krylov force was also included. The entire method was developed and coded into a user friendly script. The capability of the employed commercial tool SESAM HydroD has also been demonstrated with the area of limitation in the flexible usage of the proposed west African spectra type highlighted.

6 Chapter Six: Verification and Validation of Numerical model and Code

6.1 Introduction

The numerical procedure from both the SESAM and the numerical tool proposed were validated against the regular and irregular test conducted for the free-floating unit. An aspect of the proposed method for the wave frequency motion was implemented for the free-floating unit. The numerical model was validated using the regular wave test and the proposed method was validated using the both the SESAM and the irregular experimental data.

6.2 Verification via sensitivity studies

A quick assessment of the workability of the numerical model was conducted using a sensitvity analysis of the random seed generator (seed) for the wave components. The response of the numerical scheme to changes in these parameters were quickly assessed from the estimated basic descriptive statistics of the resulting time series (Force and displacement) for all motion modes and elevations as well. The case 16 in table 4.1 was used as a common case for this analysis. For the random seed test, the sample time step used was 0.25 s for a 360s simulation length. Figure 6.1 shows a typical series (epochs) of the roll moment and amplitude and figure 6.2 for a wave surface elevation from three different seed combinations.

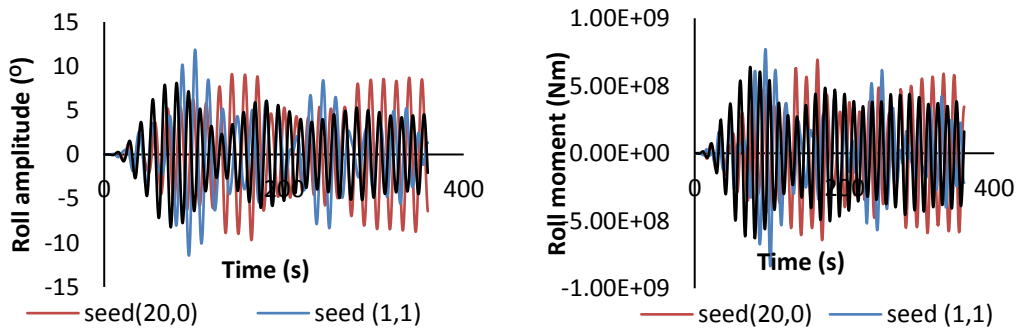

(a) (b)

Figure 6.1 Roll time series epochs from random seed variation (a) Roll amplitude (b) Roll moment

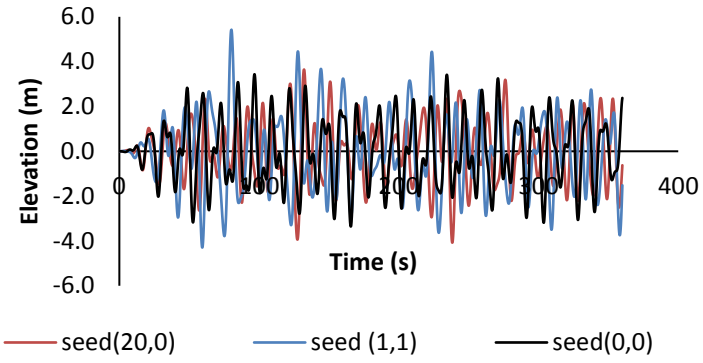

Figure 6.2 Water surface elevation Time series epochs from random seed variation

Table 6.1 Typical basic statistical evaluation for seed (1, 1)

Force/Moment	mean	STD	ampl	max	min	Range
surge	-1.234E+05	5.557E+06	2.223E+07	1.580E+07	-1.920E+07	3.500E+07
sway	-7.344E+04	2.483E+07	9.931E+07	7.970E+07	-6.160E+07	1.413E+08
heave	3.951E+05	3.899E+07	1.559E+08	1.200E+08	-1.360E+08	2.560E+08
roll	-4.289E+05	2.510E+08	1.004E+09	7.710E+08	-8.370E+08	1.608E+09
pitch	8.976E+06	1.160E+09	4.659E+09	2.880E+09	-3.310E+09	6.190E+09
yaw	-8.141E+06	8.190E+08	3.276E+09	1.590E+09	-1.820E+09	3.410E+09
Motion						
surge displ.	-0.25	0.25	1	0.305	-0.836	1.141
sway displ.	-0.063	1.031	4.123	2.64	-3.16	5.8
heave displ.	-0.015	1.554	6.215	4.97	-4.11	9.08
roll displ.	0.007	3.851	15.403	11.9	-11.4	23.3
pitch displ.	-0.838	0.493	1.971	0.608	-2.05	2.658
yaw displ.	-0.024	0.29	1.1603	0.769	-0.771	1.54
Wave Elevation	-0.01712	1.684329	6.734	5.42	-4.29	9.71

Results similar to those of table 6.1 for seed (1,1) for the other seeds are summarised with the charts shown in figure 6.3 to figure 6.9.

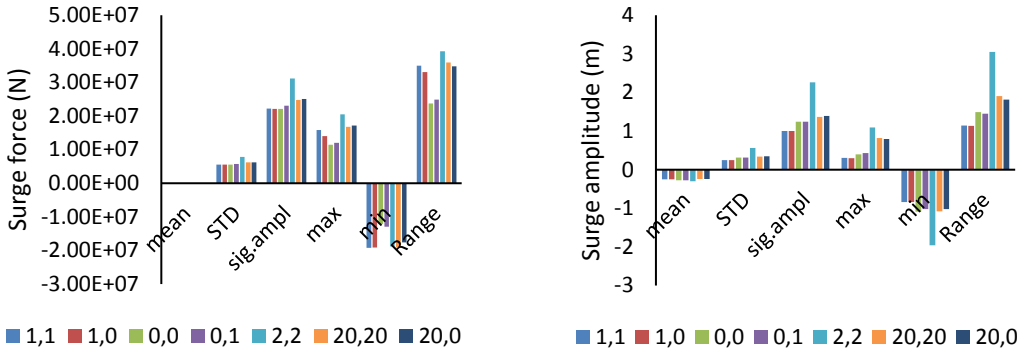

Figure 6.3 Impact of random seed variation on Surge force and Surge motion amplitude

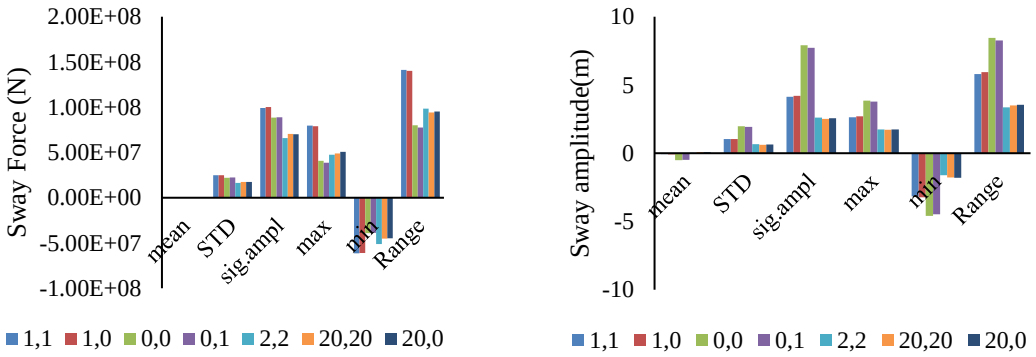

Figure 6.4 Impact of random seed variation on Sway force and Sway motion amplitude

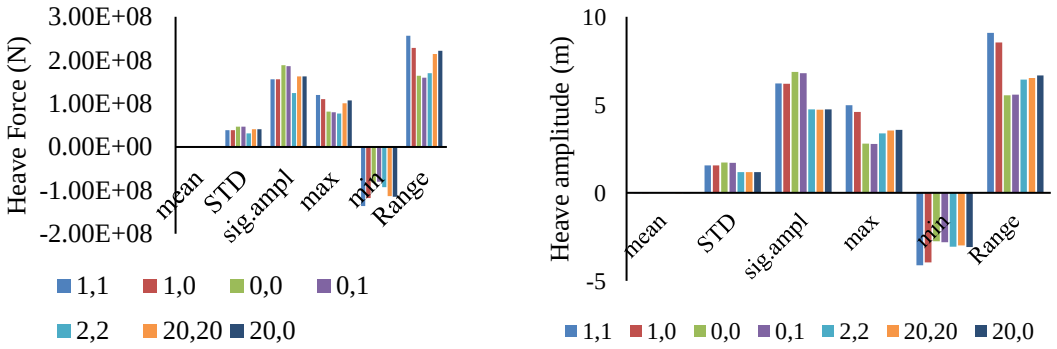

Figure 6.5 Impact of random seed variation on Heave force and Heave motion amplitude

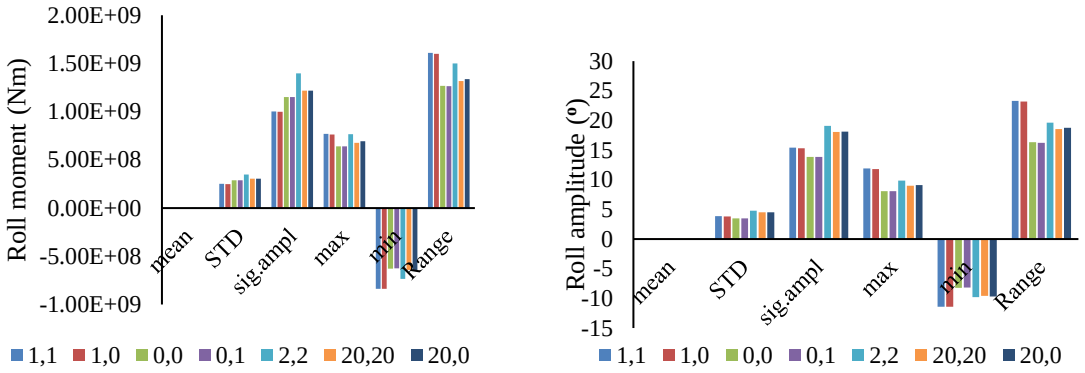

Figure 6.6 Impact of random seed variation on Roll force and Roll motion amplitude

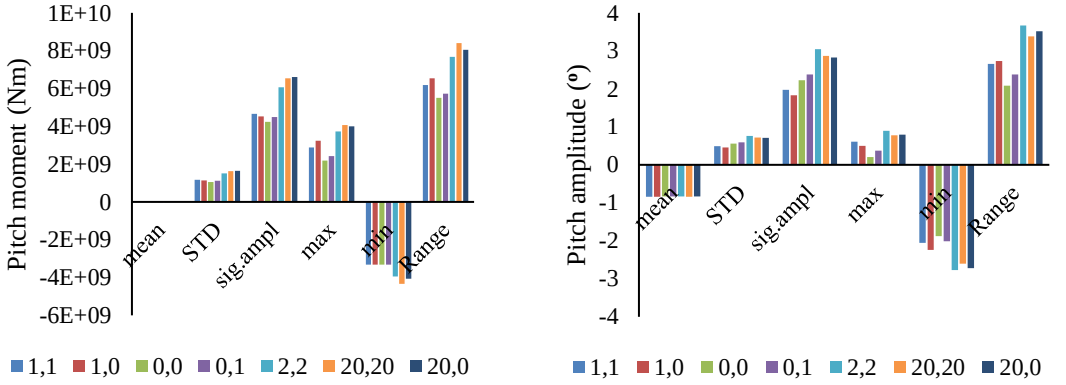

Figure 6.7 Impact of random seed variation on Pitch force and Pitch amplitude

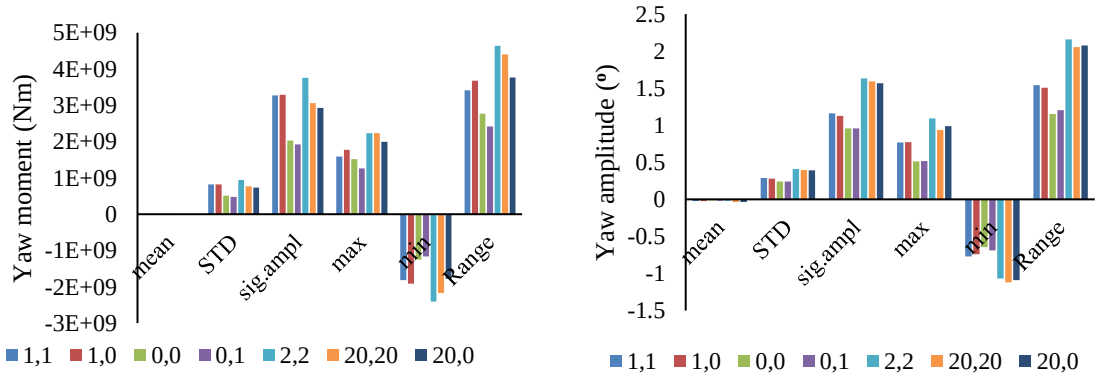

Figure 6.8 Impact of random seed variation on Yaw force and Yaw motion amplitude

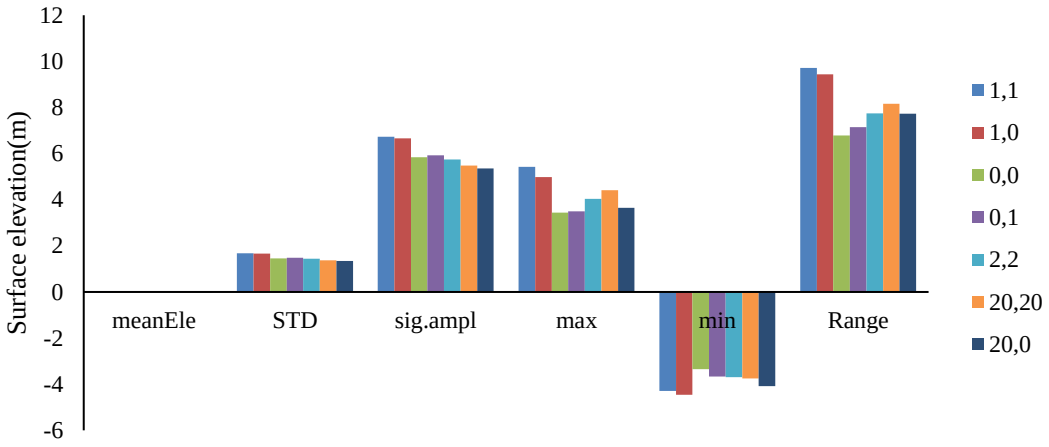

Figure 6.9 Impact of random seed variation on water surface elevation

The random seed selection played a significant role in the visual examination of the time series as can be seen from the different epochs from figure 6.1 and 6.2. The seed (i,j) is such that ‘i’ represents the swell formation and the ‘j’ is used for the wind sea component. However, it is expected that the overall statistical properties of the signal are holistically preserved, this is not true. The values from figures 6.3 for surge up to figure 6.9 for the elevation suggest that the measurements are affected by the seed chosen. The measured mean values are significantly the same across all motion mode cases irrespective of the seed used. This is not very correct for the other parameters. A quick cross examination of the coefficient of variation of the absolute values of the measurements captured in table 6.2, suggest that the variation is typically of second order.

Table 6.2 Coefficient of variation (CoV) for different seeds in (%)

Seed		1,1	1,0	0,0	0,1	2,2	20,20	20,0
Force	Surge	78.387	79.322	62.847	62.386	71.520	74.164	72.843
	Sway	78.773	77.552	56.507	56.594	80.047	76.768	76.110
	Heave	80.588	77.603	57.227	56.659	78.536	71.961	71.220
	Roll	87.172	87.133	62.840	62.410	65.976	69.299	69.155
	Pitch	68.804	73.166	59.520	59.014	71.838	71.000	69.067
	Yaw	61.735	62.978	74.801	74.455	75.575	75.637	74.392
Amplitude	Surge	72.845	75.411	74.713	75.518	80.262	72.243	71.507
	Sway	76.535	76.979	68.843	69.624	76.778	75.103	74.679
	Heave	78.517	77.874	56.942	56.761	73.773	80.863	79.792
	Roll	82.042	81.820	65.545	65.065	65.543	69.064	69.038
	Pitch	54.377	50.541	64.858	67.415	67.119	66.944	66.674
	Yaw	77.246	77.871	70.974	70.887	72.807	84.546	82.997
	Elevation	75.924	77.398	69.412	70.423	73.739	75.600	74.650

The maximum of 87.17% was observed when seed (1,1) was used in roll estimate compared to the minimum of 50.54% for pitch amplitude at seed (1,0). This is a strong indication of the extent of influence of the random seed selection. It is however noted that, no peculiar pattern could be traced in order to determine the best seed combination (see figure 6.10), it is instructive to point out that the seed combination should be clearly stated when results are presented.

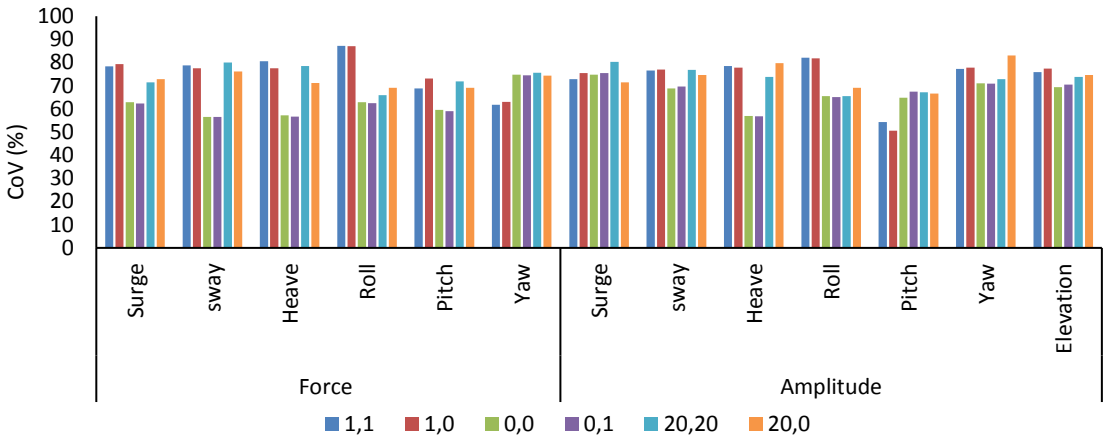

Figure 6.10 Coefficient of variation (CoV) for different seeds in (%)

6.3 Regular wave test vs numerical development with HydroD

The experimental matrix shown in table 3.5 and 3.6 for the beam sea condition was simulated in HydroD. The test was conducted to obtain an estimate of the RAO of the vessel and used as a validation tool for the numerical model. The test involved the generation of the regular wave from the tank for specific combination of frequency and wave amplitude as captured in the test matrix. The run was performed at a frequency of 200hz (time step of 0.005) and data collated for 40-45s. Figure 6.11 and figure 6.12 are typical captures of the time series of wave elevation and roll amplitude for two cases of T2bk1df2w3q2 and T2bk0df2w1q2 for hull with bilge keel (b1) and without bilge keel (b0) respectively.

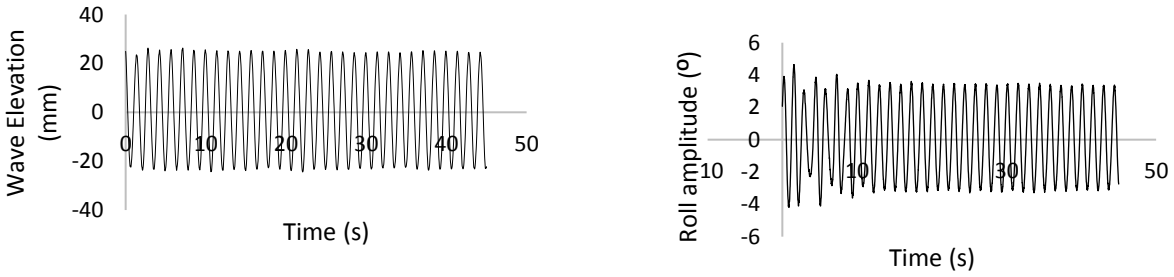

Figure 6.11 Regular wave elevation and roll amplitude time series for T2bk0df2w1q2

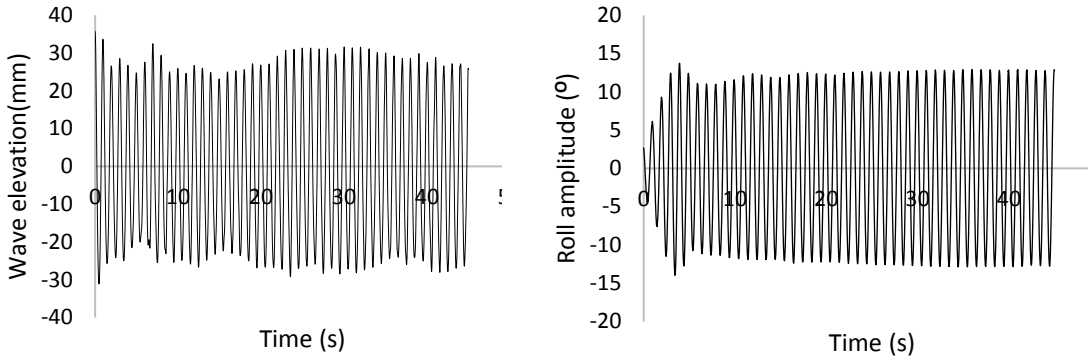

Figure 6.12 Regular wave elevation and roll amplitude time series for T2bk1df2w3q2

The Fourier analysis was applied to raw data using the Matlab cftool and the equation 5.255 used in estimating the RAO gain and phase. Table 6.3 below shows the estimated results. Similar scenario was also run in using the hydro model above and the results compared.

Table 6.3 Summary of estimates from Regular wave test and simulation for hull without bilge keel

exp.case	Model																		Actual				
	elevation(m)									roll response(rad)								RAO		RAO		w(a)	RAO (deg/m)	
	a0	a1	b1	w*	w^{fit}	% er w	R^2	gain	phase	a0	a1	b1	w^{fit}	% er w	R^2	gain	phase	gain	phase	gain	phase	rad/s	Exp	SESAM
T2b0d1w1q2	2.799E-04	0.001	0.024	4.398	4.398	-0.005	0.998	0.024	1.549	1.525E-03	-0.036	0.041	4.397	-0.028	0.983	0.055	-0.847	2.274	-2.396	0.018	-2.396	0.389	1.018	0.713
T2b0d1w2q2	1.192E-04	-0.025	0.004	5.341	5.341	0.005	0.989	0.025	-0.143	1.172E-03	0.088	-0.038	5.343	0.043	0.953	0.096	-0.411	3.806	-0.269	0.030	-0.269	0.472	1.704	1.152
T2b0d1w3q2	-5.376E-04	-0.016	-0.013	6.283	6.281	-0.035	0.931	0.021	0.664	1.823E-03	-0.183	0.036	6.278	-0.083	0.929	0.187	-0.196	8.923	-0.860	0.070	-0.860	0.555	3.994	1.079
T2b0d1w4q2	2.117E-04	-0.021	-0.006	7.226	7.227	0.019	0.972	0.022	0.278	-2.150E-03	0.048	0.305	7.170	-0.770	0.942	0.309	1.413	14.097	1.135	0.110	1.135	0.639	6.310	6.735
T2b0d1w5q2	-6.129E-04	-0.020	0.015	8.168	8.169	0.011	0.938	0.025	-0.635	-8.761E-03	0.020	-0.263	8.093	-0.920	0.779	0.264	-1.494	10.559	-0.859	0.082	-0.859	0.722	4.726	3.935
T2b0d1w6q2	-3.626E-05	0.001	0.022	9.111	9.084	-0.292	0.807	0.022	1.542	-1.801E-02	0.030	-0.089	9.046	-0.709	0.736	0.094	-1.249	4.339	-2.790	0.034	-2.790	0.805	1.942	0.230
T2b0d2w1q2	2.646E-04	0.023	-0.007	4.398	4.398	-0.005	0.998	0.024	-0.280	2.099E-04	0.051	0.027	4.398	-0.005	0.978	0.057	0.484	2.371	0.765	0.019	0.765	0.389	1.061	0.887
T2b0d2w2q2	6.536E-05	-0.023	0.010	5.341	5.340	-0.013	0.992	0.025	-0.425	3.188E-04	0.077	-0.066	5.343	0.043	0.960	0.101	-0.713	4.033	-0.288	0.032	-0.288	0.472	1.805	1.779
T2b0d2w3q2	-5.695E-04	-0.022	0.013	6.283	6.284	0.013	0.981	0.025	-0.525	4.034E-03	-0.015	0.210	6.283	-0.003	0.943	0.211	-1.498	8.459	-0.973	0.066	-0.973	0.555	3.786	0.333
T2b0d2w4q2	1.462E-05	0.016	-0.031	7.226	7.208	-0.244	0.953	0.035	-1.108	-8.611E-03	0.173	0.363	7.187	-0.535	0.945	0.402	1.126	11.478	2.234	0.090	2.234	0.639	5.138	5.817
T2b0d2w5q2	-1.134E-03	-0.015	0.021	8.168	8.126	-0.516	0.829	0.026	-0.960	-3.633E-03	-0.210	0.165	8.088	-0.981	0.762	0.267	-0.667	10.326	0.292	0.081	0.292	0.722	4.622	4.798
T2b0d2w6q2	-2.820E-04	0.018	-0.013	9.111	9.086	-0.270	0.869	0.022	-0.624	-5.415E-03	-0.082	-0.012	9.052	-0.643	0.638	0.083	0.146	3.717	0.770	0.029	0.770	0.805	1.664	0.922

Table 6.4 Summary of estimates from Regular wave test and simulation for hull with bilge keel configuration 1

exp.case	Model																		Actual				
	elevation(m)									roll response(rad)								RAO		RAO		w(a)	RAO (deg/m)	
	a0	a1	b1	w*	w^{fit}	% er w	R^2	gain	phase	a0	a1	b1	w^{fit}	% er w	R^2	gain	phase	gain	phase	gain	phase	rad/s	Exp	SESAM
T2b1d1w1q2	3.190E-04	0.016	0.018	4.398	4.399	0.018	0.997	0.024	0.852	3.798E-02	-0.036	0.044	4.400	0.040	0.971	0.057	-0.876	2.324	-1.728	0.018	-1.728	0.389	1.040	0.642
T2b1d1w2q2	3.240E-04	0.002	0.026	5.341	5.341	0.005	0.989	0.026	1.507	-2.567E-03	-0.003	-0.104	5.343	0.043	0.968	0.104	1.541	4.033	0.034	0.032	0.034	0.472	1.805	1.483
T2b1d1w3q2	-6.132E-04	-0.001	0.023	6.283	6.277	-0.098	0.964	0.023	-1.542	-9.418E-03	0.008	0.191	6.272	-0.178	0.961	0.191	1.528	8.153	3.070	0.064	3.070	0.555	3.650	4.177
T2b1d1w4q2	-1.544E-03	-0.021	-0.006	7.226	7.209	-0.231	0.877	0.022	0.278	-1.697E-02	0.219	0.064	7.180	-0.632	0.928	0.228	0.283	10.397	0.004	0.081	0.004	0.639	4.654	4.938
T2b1d1w5q2	-1.316E-03	0.023	-0.008	8.168	8.136	-0.393	0.744	0.024	-0.326	-1.992E-02	0.128	0.047	8.106	-0.761	0.848	0.136	0.355	5.690	0.682	0.044	0.682	0.722	2.547	2.925
T2b1d1w6q2	-1.111E-03	0.002	0.016	9.111	9.088	-0.248	0.788	0.017	1.441	-1.347E-02	0.018	-0.069	9.058	-0.578	0.834	0.071	-1.318	4.287	-2.760	0.033	-2.760	0.805	1.919	1.268
T2b1d2w1q2	7.805E-06	0.022	0.011	4.398	4.398	-0.005	0.998	0.024	0.489	-7.162E-03	0.016	0.056	4.399	0.018	0.978	0.058	1.290	2.399	0.801	0.019	0.801	0.389	1.074	0.527
T2b1d2w2q2	2.745E-05	0.019	-0.017	5.341	5.340	-0.013	0.993	0.025	-0.751	7.309E-03	-0.069	0.084	5.343	0.043	0.982	0.108	-0.885	4.247	-0.134	0.033	-0.134	0.472	1.901	2.268
T2b1d2w3q2	-5.060E-04	0.026	-0.008	6.283	6.274	-0.146	0.981	0.027	-0.289	-2.992E-03	0.169	-0.126	6.273	-0.162	0.981	0.211	-0.640	7.925	-0.351	0.062	-0.351	0.555	3.548	3.752
T2b1d2w4q2	-7.841E-04	-0.021	-0.006	7.226	7.196	-0.411	0.906	0.022	0.278	-7.306E-03	0.194	-0.134	7.171	-0.757	0.927	0.236	-0.606	10.750	-0.884	0.084	-0.884	0.639	4.812	5.017
T2b1d2w5q2	-2.561E-03	-0.014	-0.016	8.168	8.134	-0.418	0.762	0.021	0.855	-1.137E-02	-0.074	-0.131	8.097	-0.871	0.839	0.151	1.059	7.078	0.204	0.055	0.204	0.722	3.168	2.516
T2b1d2w6q2	4.191E-05	0.020	-0.010	9.111	9.066	-0.490	0.905	0.023	-0.468	-1.798E-03	-0.071	0.007	9.044	-0.731	0.852	0.071	-0.105	3.117	0.362	0.024	0.362	0.805	1.395	0.901

Table 6.5 Summary of estimates from Regular wave test and simulation for hull with bilge keel configuration 2

exp.case	Model																		Actual				
	elevation(m)									roll response(rad)								RAO		RAO		w(a)	RAO (deg/m)	
	a0	a1	b1	w*	w^{fit}	% er w	R^2	gain	phase	a0	a1	b1	w^{fit}	% er w	R^2	gain	phase	gain	phase	gain	phase	rad/s	Exp	SESAM
T2b2d1w1q2	-4.717E-04	-0.017	0.017	4.398	4.396	-0.051	0.997	0.024	-0.793	-1.793E-03	-0.058	-0.010	4.401	0.063	0.962	0.058	0.177	2.405	0.970	0.019	0.970	0.389	1.076	0.431
T2b2d1w2q2	-5.089E-04	0.000	-0.026	5.341	5.343	0.043	0.992	0.026	1.567	6.739E-04	0.001	0.100	5.355	0.268	0.952	0.100	1.564	3.844	-0.003	0.030	-0.003	0.472	1.721	1.408
T2b2d1w3q2	-8.793E-04	0.022	-0.013	6.283	6.284	0.013	0.979	0.025	-0.537	-3.686E-03	0.100	-0.166	6.279	-0.067	0.967	0.194	-1.027	7.591	-0.491	0.059	-0.491	0.555	3.398	3.188
T2b2d1w4q2	-1.564E-03	0.005	0.030	7.226	7.206	-0.272	0.956	0.030	1.392	-2.122E-03	-0.165	-0.199	7.160	-0.909	0.912	0.258	0.880	8.606	-0.512	0.067	-0.512	0.639	3.852	4.036
T2b2d1w5q2	-1.607E-03	0.019	0.014	8.168	8.190	0.268	0.826	0.024	0.627	-6.158E-03	0.200	0.025	8.048	-1.471	0.868	0.201	0.122	8.398	-0.505	0.066	-0.505	0.722	3.759	3.425
T2b2d1w6q2	-1.016E-03	0.004	0.019	9.111	9.034	-0.841	0.853	0.020	1.358	-6.246E-03	0.013	-0.083	8.985	-1.379	0.713	0.084	-1.418	4.233	-2.777	0.033	-2.777	0.805	1.895	1.618
T2b2d2w1q2	1.966E-04	-0.015	0.020	4.398	4.399	0.018	0.998	0.025	-0.929	-2.023E-03	-0.057	0.008	4.392	-0.142	0.970	0.058	-0.138	2.363	0.791	0.018	0.791	0.389	1.058	0.619
T2b2d2w2q2	2.095E-04	-0.023	0.015	5.341	5.343	0.043	0.991	0.027	-0.573	1.297E-03	0.089	-0.048	5.350	0.174	0.963	0.101	-0.491	3.748	0.082	0.029	0.082	0.472	1.678	1.871
T2b2d2w3q2	-3.422E-04	-0.018	0.016	6.283	6.298	0.236	0.947	0.024	-0.737	-5.347E-03	-0.070	0.155	6.273	-0.162	0.925	0.170	-1.149	7.034	-0.412	0.055	-0.412	0.555	3.148	3.088
T2b2d2w4q2	-1.714E-03	0.021	0.013	7.226	7.226	0.005	0.892	0.025	0.577	-6.372E-03	-0.257	0.003	7.150	-1.047	0.929	0.257	-0.010	10.423	-0.587	0.081	-0.587	0.639	4.665	5.330
T2b2d2w5q2	-2.049E-03	0.020	-0.001	8.168	8.178	0.121	0.711	0.020	-0.042	-1.641E-02	0.182	-0.084	8.058	-1.348	0.865	0.201	-0.432	10.046	-0.389	0.078	-0.389	0.722	4.497	4.394
T2b2d2w6q2	-7.441E-04	0.018	0.003	9.111	9.051	-0.654	0.814	0.018	0.183	-1.396E-02	-0.069	-0.047	8.988	-1.346	0.748	0.084	0.599	4.683	0.416	0.037	0.416	0.805	2.096	1.077

The highlight of the Fourier analysis was the percentage error observed between the target frequency w* and that (w) obtained from the fit. The regression coefficients are conveniently representative of a good fit.

The RAO curves obtained from the different bilge keel/draft arrangement for the tables 6.3.6.4 above are shown below.

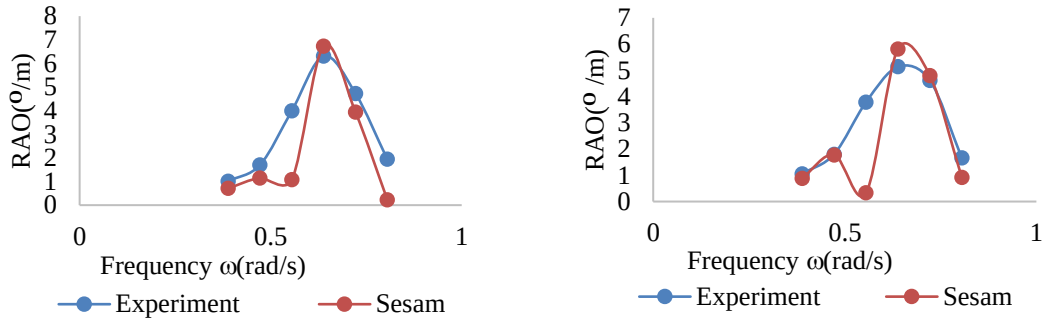

(a) (b)

Figure 6.13 RAO curve for hull without bilge-keel (a) draft 1: bk0df1q2

(b) draft 2 ; bk0df2q2

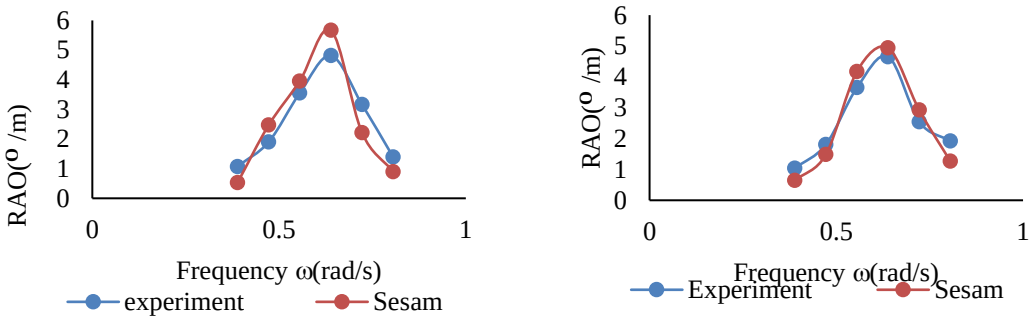

(a) ¬ (b)

Figure 6.14 RAO curve for hull with bilge-keel configuration 1 (a) draft 2: bk1df2q2

(b) draft 1: bk1df1q2

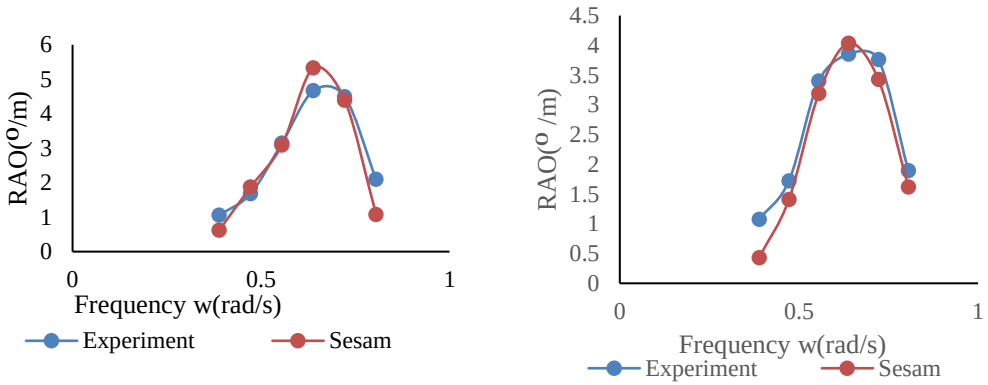

(a) (b)

Figure 6.15 RAO curve for hull with bilge-keel configuration 2 (a) draft 2; bk2df2q2 (b) draft 1; bk2df1q2.

The comparison between the experimental RAO and the simulated RAO was done using the coefficient of variation between the estimates as grouped according to the diagrams of figures 6.13 to 6.15 above. The summary result is captured in table 6.6 below.

Table 6.6 Coefficient of variation between estimates from Experiment and SESAM

Configuration	Experiment	SESAM	Difference (%)
bk0df1	62.695	109.572	46.877
bk0df2	57.086	95.125	38.039
bk1df1	51.128	67.141	16.013
bk1df2	54.347	67.981	13.635
bk2df1	45.660	59.558	13.898
bk2df2	52.505	68.695	16.191

It can be seen from the graphs, that the simulation overestimated the RAO around the peak frequency region. Though the resultant curve appears to be properly captured by visual verification, the coefficient of variation between the experimental value and the simulated values suggest otherwise. However, these discrepancies can be due to the

values of the damping coefficients used during the simulation. The values of 46.9% and 38.04% for the hull without bilge keel against the < 17% for hulls with bilge keels suggest the applicability of the damping model used. It is therefore possible that the model is better suited for hulls with bilge keels as it has been earlier postulated.

6.4 Irregular wave test vs numerical development with HydroD and Proposed method(code)

The experiment matrix of table 3.8 with input values from the table 3.7 were used to carry out the irregular wave test. Three sets of waves were tested, and the results adequately extracted for 20s test time. The short time was due to the averaged reflection time of about 18-25 s observed for the tank. For the purpose of validation of simulation, data from two beam sea test scenarios (T3bk1df2Hs1q2; Hs=0.015m, To=0.764s and T3bk1df2Hs3q2; Hs=0.035m, To=1.1s) at model scale were analysed. The JONSWAP spectrum with appropriate parameters was used in generating the wave and calibrated for both instances. Figure 6.16 is a typical time series of the wave elevation obtained for both cases.

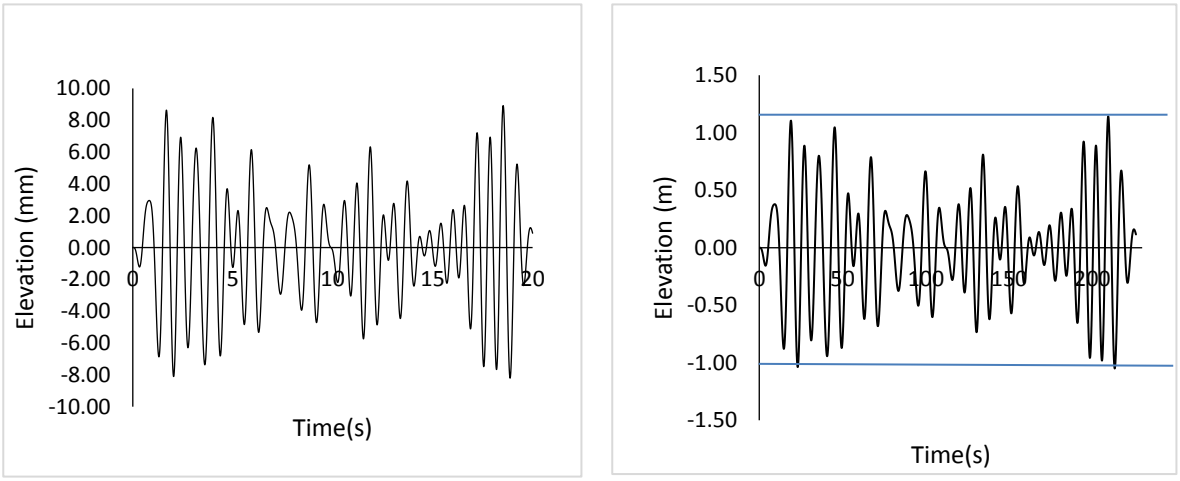

(a) (b)

Figure 6.16 Measured elevation time history for T3bk1df2Hs1q2; Hs=0.015m (a) Model (b) Scaled by 1:128

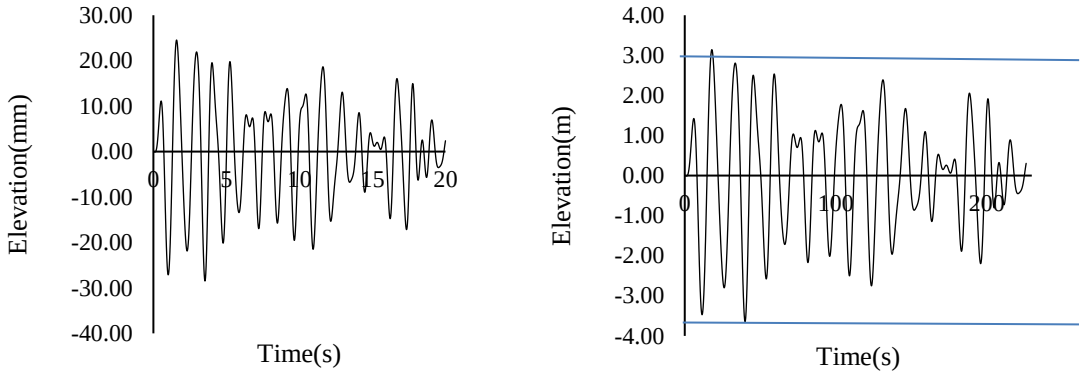

(a) (b)

Figure 6.17 Measured elevation time history for T3bk1df2Hs3q2; Hs=0.035m (a) Model (b) Scaled by 1:128

The corresponding simulation from SESAM and the proposed method for a longer period and larger time step are captured below for the two cases.

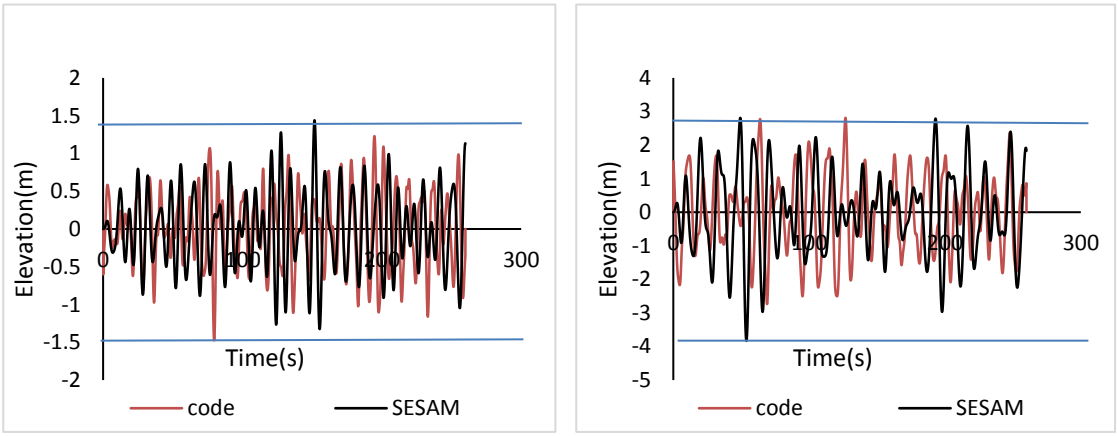

Figure 6.18 Elevation time history (method and SESAM) simulations; (a)Hs=1.92m (b) Hs=4.48m

It is visually observed that the time series are similar from the envelope values between simulations from SESAM and that from the proposed method. This is also significantly similar to the envelope value for the experiment from figures 6.16(b) and 6.17(b).

The target spectra for both cases are shown in figures below.

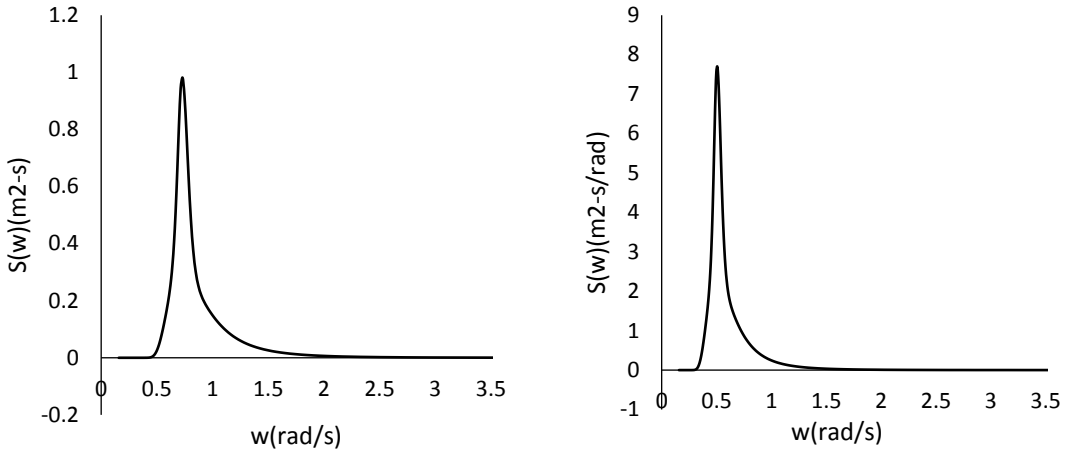

Figure 6.19 Target Jonswap Spectrum for both cases (a) T3bk1df2Hs1q2; Hs=1.92m, To=8.64s (b) T3bk1df2Hs3q2; Hs=4.48m, To=12.45s.

A quick approach of accessing the proximity of the data between the test and the simulations was to look at the descriptive statistics of the time series. The reproducibility for the spectrum using the code was high with a recomputed significant height of 1.917m against target 1.92m and 4.4833m against 4.48m. The comparative analysis of the three scenarios based on the descriptive statistics for the roll motion mode is captured below.

The roll motion time series obtained from the experiment and the numerical methods of Sesam and the proposed method (Code) for both test cases are presented in figures 6.20 and 6.21.

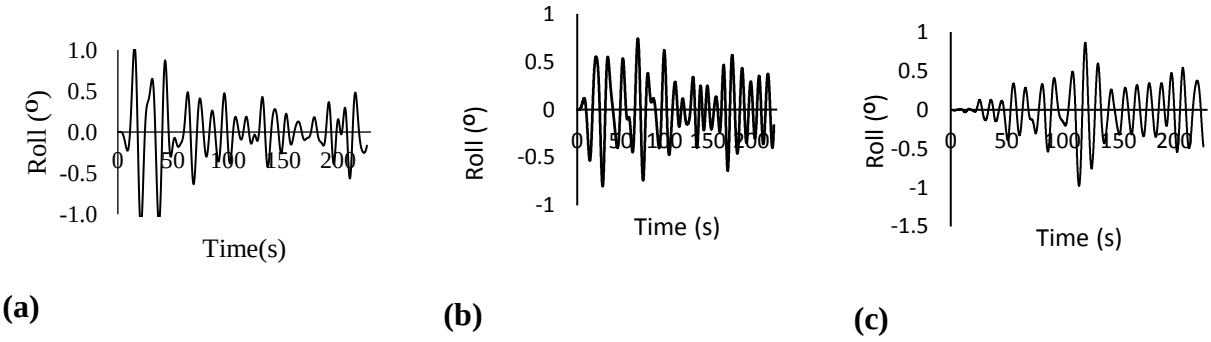

(a) **(b)** **(c)**

Figure 6.20: Roll time history for T3bk1df2hs1q2 (a) Experiment (b) Sesam (c) Code

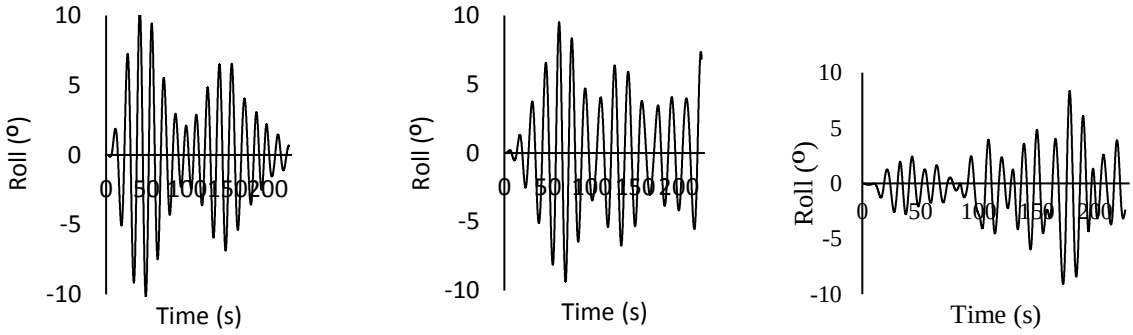

(a) **(b)** **(c)**

Figure 6.21: Roll time history for T3bk1df2hs3q2 (a) Experiment (b) Sesam (c) Code

Relevant response statistics for comparative analysis of the different methods are presented in table 6.8 and 6.9 for the time series obtained for the elevation as well as roll motion.

Table 6.7: Descriptive statistics for wave elevation time history

Hs=1.92m (case a1)			Sig.				% error			
	mean	Std.	Ampl.	Max	Min	Range	Ampl.	max	min	range
Exp. (model)	1.79E-05	0.004	0.014	0.009	-0.008	0.017				
Exp. (scaled)	2.29E-03	0.446	1.782	1.142	-1.05	2.191				
SESAM.	- 9.61E-04	0.505	2.018	1.44	-1.33	2.77	13.25	26.12	26.71	26.41
Code	-1.751E-03	0.491	1.963	1.229	-1.475	2.704	10.15	7.62	40.50	23.37
Hs=4.48m (case a2)										
Exp. (model)	-9.34E-05	0.011	0.044	0.025	-0.029	0.053				
Exp. (scaled)	-1.196E-02	1.411	5.643	3.136	-3.648	6.784				
SESAM.	-2.121E-03	1.233	4.933	2.81	-3.83	6.64	-12.58	-10.40	4.99	-2.12
Code	-9.588E-03	1.192	4.768	2.81	-2.737	5.547	-15.50	-10.39	-24.98	-18.23

Table 6.8: Descriptive statistics for Roll amplitude

Hs=1.92m (case a1)							% error			
	mean	Std.	Sig. Ampl.	Max	Min	Range	Ampl.	max	min	range
Exp. (model)	-0.002	0.257	1.035	0.817	-0.911	1.728				
Exp. (scaled)	-0.002	0.257	1.035	0.817	-0.911	1.728				
SESAM	0.003	0.299	1.196	0.742	-0.801	1.543	15.60	-9.18	-12.07	-10.71
Code	-0.007	0.223	0.893	0.721	-0.713	1.433	-13.66	-11.8	-21.75	-17.05
Hs=4.48m (case a2)										
Exp. (model)	-0.006	3.833	15.333	10.500	-10.200	20.700				
Exp. (scaled)	-0.006	3.833	15.333	10.500	-10.200	20.700				
SESAM	0.030	4.044	16.176	9.500	-9.340	18.840	5.498	-9.524	-8.431	-8.986
Code	-0.396	3.522	14.087	11.314	-11.478	22.792	-8.124	7.754	12.530	10.107

The percentage error obtained for the estimated significant amplitudes for the case a1 indicate an error of (wave elevation: 13.25% against 10.15% for SESAM and Code respectively. Similarly, for the roll response, error margins of 15.65% against 13.66%. However, the effective difference between the two simulations are 3.1% and 1.94% for elevation and roll response respectively. This difference in error margin is low within first order which is adequate for the purpose of comparison. Corresponding margin for the case a2 showed first order values of 2.92% and 2.63% as well for the elevation and roll response respectively. For the other indicators, the maximum difference was observed in the estimation of the minimum value (20%) for the wave elevation in the case a2 test. Error difference of 18.55 and 13.79% were also observed for the case a1 instance for the elevation, however the difference in the range which aggregates the maximum and minimum value was of single digit (3.04%). For the roll response the difference ranges from as low as 1.12% for range case a2 to as high as 9.68% for the minimum value case a1. An overall assessment validates the usability of code in comparison with to the others thus.

Estimates of the RAO obtained by dividing the significant amplitude of the roll response to the wave elevation for all scenarios were compared with the values obtained using Fourier analysis of the time series.

Table 6.9: RAO estimate from direct method and Fourier approximation

Hs=1.92m (case a1)	RAO (deg/m)		% error	
	Roll sig. value/ Elevation sig value	Fourier	Roll sig. value/ Elevation sig. value	Fourier
Exp.(scaled)	0.580	0.553		
SESAM	0.593	0.492	2.08	10.91
Code	0.455	0.471	21.61	14.84
Hs=4.48m (case a2)				
Exp.(scaled)	2.71	2.567		
SESAM	3.28	3.185	21.03	24.09
Code	2.95	3.058	8.86	19.11

The result shown in table 6.9 showed that the values from the code are intermediate between the experiment and the SESAM simulations. The observed error difference from the RAO estimate above for case a1 indicate values of 19.53% and 3.93% for the two methods used. And similarly, for case a2 12.17% and 4.98% were estimated for methods used. These values are like the error observed when the two simulations were compared; thus, for the case a1 23.21% and 4.41% were estimated against 10.01% and 4.01% for case a2.

Adopting a similar approach for the other motion modes, the time series for case 1 (T3bk1df2hs1q2) are presented in figures 6.22 to 6.26. The time series obtained for case 2 (T3bk1df2hs3q2) are captured in appendix R**.** Visual inspection of the time series asserts good correlation in terms of pattern for most of the motion modes except for the yaw motions. In the case of the surge motion for the code, the several undulation resulting from the simulation did not however distort the overall trend as it is evidenced from the smoothed trendline (red colouration) which conforms to those from the experiment and Sesam. Similar trend was also observed in the sway motion amongst the different techniques. In the overall comparative assessment using the visual technique, the range

values, which envelope the time series for corresponding motions are similar. However, it is expected that the time series vary in terms of epochs, since the entire system is a stochastic , hence no two series are expected to be exactly the same across the time span.

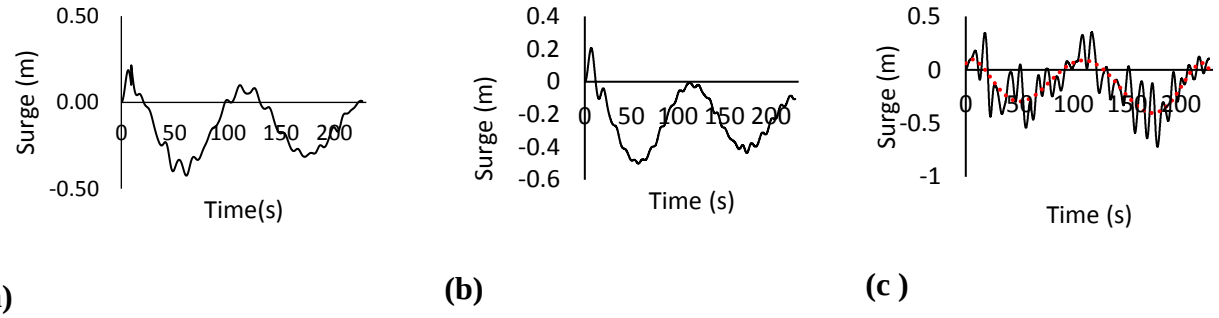

Figure 6.22 Surge motion time history for T3bk1df2hs1q2 (a) Experiment (b) Sesam (c) Code

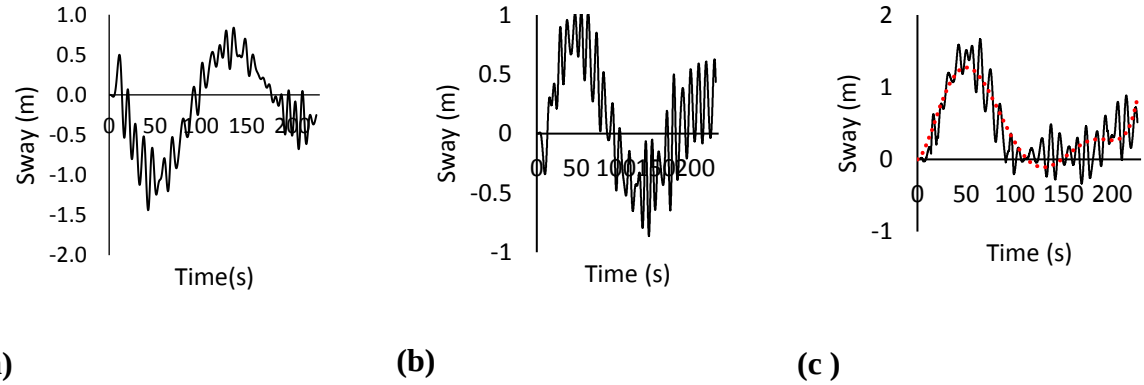

Figure 6.23: Sway motion time history for T3bk1df2hs1q2 (a) Experiment (b) Sesam (c) Code

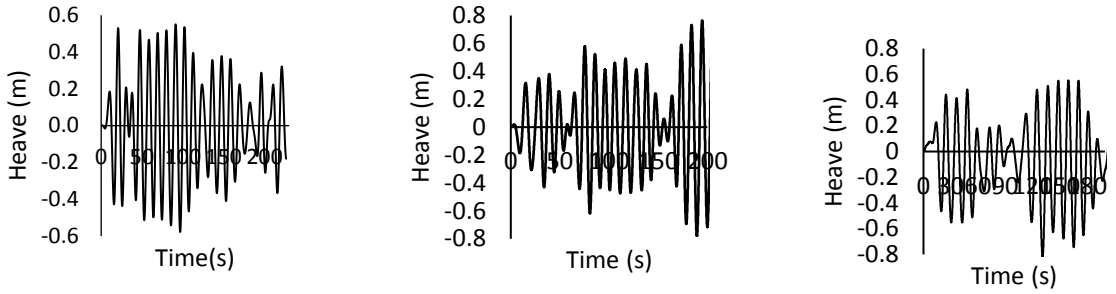

(a) **(b)** **(c)**

Figure 6.24: Heave motion time history for T3bk1df2hs1q2 (a) Experiment (b) Sesam (c) Code

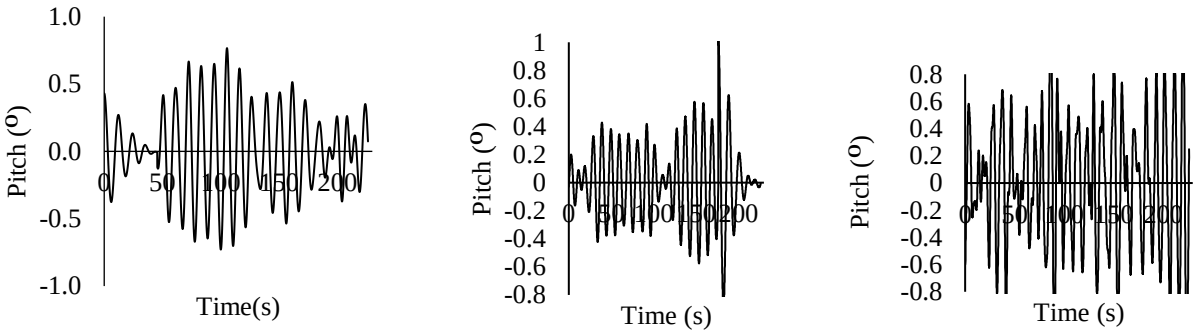

(a) (b) (c)

Figure 6.25; Pitch motion time history for T3bk1df2hs1q2 (a) Experiment (b) Sesam (c) Code

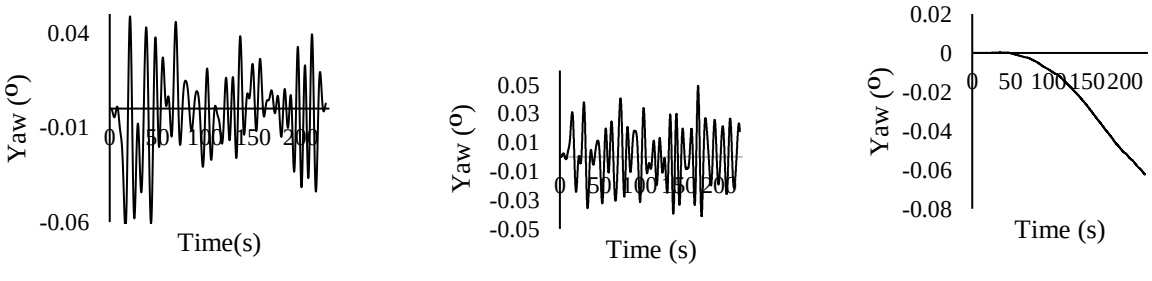

(a) **(b)** **(c)**

Figure 6.26: Yaw motion time history for T3bk1df2hs1q2 (a) Experiment (b) Sesam (c) Code

The statistical evaluation of the time series for all the motion modes are presented in tables S1 and S2 of Appendix S, with the associated chart for all analysed statistical parameters. The figures 6.28 to 6.30 captures the summary of the significant values of the time series estimated from the standard deviation of the data measured for the experiment and simulated for the other methods.

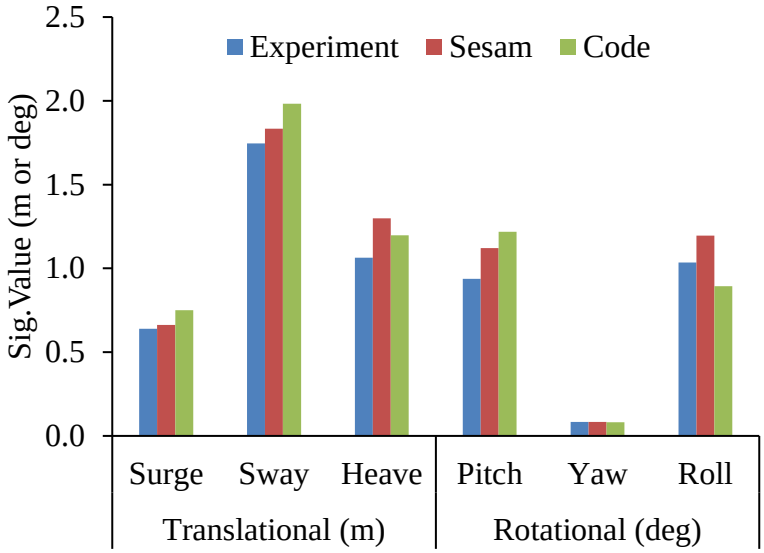

Figure 6.27: . Comparative analysis of the significant value of response for the different techniques (T3bk1df2hs1q2)

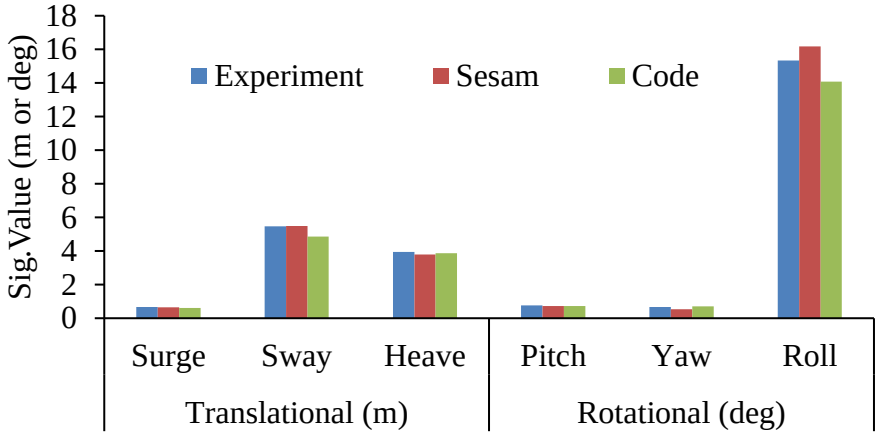

Figure 6.28: Comparative analysis of the significant value of response for the different techniques (T3bk1df2hs3q2).

Aa comparative analysis of the significant values suggest high values in the roll and sway motions compared to other motions because of the beam sea orientation of the unit in water. For the low significant wave case, variations as low as 0.94% for Yaw motion to 22% from the heave motion were observed between the experiment and the Sesam simulation. Similar variation of 2.1% for Yaw motion and 30% from the pitch motion were estimated between the experiment and Code. The comparative studies between the Sesam and Code showed minimum difference of 3% in the Yaw motion to that of 25% in roll motion, which was estimated at 13.7% variation by the Code. The averaged prediction variation from all motions for the Code is estimated to be 9.63% against the 11.16% captured for the Sesam simulation, recording a performance difference of about 1.5% in favour of the code.

For the simulated mild sea condition of significant wave height of 4.48m, i.e. case a2 (T3bk1df2hs1q2), the predictions performed better with an averaged prediction variation of 4.86% for the Sesam compared to 5.15% from the code for all motions. Interestingly, most of the variations fell below 10% for both Sesam and Code except in sway(11%) and yaw(22%) for Code and Sesam respectively. On the overall assessment, a rough estimated prediction average suggest a validation range of about -5.15% to 9.63% prediction capability for the Code as compared to the experiment for both cases. The range when compared to the commercial tool Sesame is however smaller falling within -1.02% to 1.09%. It was also necessary to look at the overall prediction pattern of motions between Sesam and Code, it can be adjudged to be similar in terms of overprediction (+ve) or under prediction (-ve) for the different motions.

Another criterial which involved the use of the ratio between the motion significant value and the wave elevation significant value were also estimated for all scenario and used as bases for validation. The table 6.10, 6.11,and figures 6.29 and 6.30 captures the estimated ratio.

Table 6.10: Ratio of significant motion response to wave significant amplitude (T3bk1df2hs1q2)

	RA ratio (xi/ζwave)			Comparative Error estimates		
	Experiment	**Sesam**	**Code**	**Exp/Sesam**	**Exp/Code**	**Sesam/Code**
Surge	0.3586	0.3267	0.3905	-8.89	8.92	19.55
Sway	0.9791	0.9042	1.0320	-7.65	5.40	14.14
Heave	0.5968	0.6405	0.6229	7.33	4.37	-2.75
Pitch	0.5262	0.5529	0.6339	5.07	20.46	14.65
Yaw	0.0467	0.0414	0.0424	-11.30	-9.21	2.36
Roll	0.5804	0.5925	0.4550	2.08	-21.61	-23.21

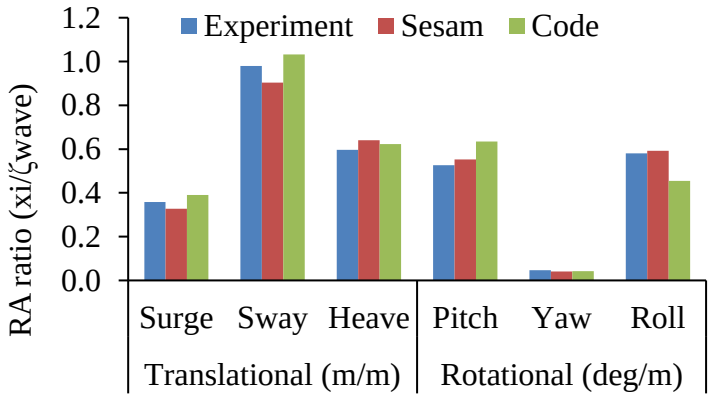

Figure 6.29 Comparison of estimated RA ratio for methods for (T3bk1df2hs1q2)

Table 6.11: Ratio of significant motion response to wave significant amplitude (T3bk1df2hs3q2)

	RA ratio (m/m or deg/m)			Comparative Error estimates (%)		
	Experiment	**Sesam**	**Code**	**Exp/Sesam**	**Exp/Code**	**Sesam/Code**
Surge	0.1172	0.1307	0.1264	11.53	7.86	-3.30
Sway	0.9694	1.1129	1.0209	14.80	5.32	-8.26
Heave	0.6979	0.7679	0.8121	10.02	16.35	5.75
Pitch	0.1362	0.1454	0.1505	6.71	10.46	3.51
Yaw	0.1200	0.1074	0.1498	-10.51	24.83	39.49
Roll	2.7100	3.2800	2.9500	21.03	8.86	-10.06

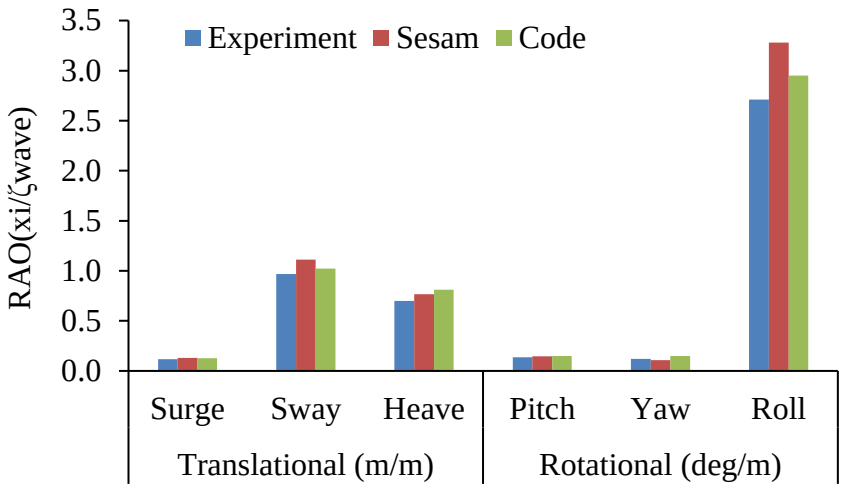

Figure 6.30: Comparison of estimated RA ratio for methods for (T3bk1df2hs3q2)

For case 1, the prediction witness as low as 4.37% variation for heave for the code against 7.33 % from the Sesam simulation, with an average prediction range of about 1.4% compared to that of 12.3% for case 2. For case 2, the heave motion was predicted at a variation of about 16% which is about 6% different from that of the Sesam. A comparative assessment of the code against the commercial tool (Sesame) suggest a uniform average of about 4% for both cases.

6.5 Conclusion

To validate the proposed method, similar scenarios were tested using the standard SESAM package. The simulation from SESAM was partly validated using the experimental test result for the regular wave as well as the irregular wave test. However, the simulation was partly verified by the random seed sensitivity test carried out. It was evident that the random seed affected the quantitative value of the response, however the order of impact was not significant to offset the overall meaning of the output. The RAO values of 2.95deg/m and 2.71deg/m obtained from the proposed method (code) and experiment respectively showed remarkable correlation between the experiment and method. About 13 to 16 % coefficient of variation in the result was observed for the hulls

with bilge keels. High coefficient of variation of about 48% was observed for the hulls without the bilge. The two cases adopted from the irregular wave test, was used to validate the roll motion response part of the proposed method and results were also compared with the simulation. The descriptive statistics obtained from the validation procedure for the three methods showed some level of % variation in the roll amplitude as well as the water surface elevation. For the elevation, 13% and 10% overestimations (against experiment) were recorded for the case of Hs=1.92m for the SESAM and the proposed method (code) respectively. However, an overall evaluation suggests insignificant deviations between methods. Similar values of 15.6% and 13.6% were observed for the second wave height case. In the aspect of estimated roll amplitude, (12.6% and 15.5%; case a1) and (5.5% and 8%; case a2) were observed for SESAM and proposed method respectively.

For other motion modes, relying on the two test cases a1 and a2 (T3bk1df2hs1q2 and T3bk1df2hs3q2 respectively), two comparative parameters; the significant amplitude estimated from the standard deviation of the time series and the response to wave significant amplitude ratio (RA ratio) from experiment, Sesam and the Code were compared. On the overall assessment, a rough estimate suggest a validation range of about -5.15% to 9.63% prediction capability for the Code as compared to the experiment for both cases. The range when compared to the commercial tool Sesame is however smaller falling within -1.02% to 1.09%. The response ratio comparative assessment of the code against the commercial tool (Sesame) with the experiment suggest a uniform average of about 4% for both cases. Also, the overall prediction pattern of motions between Sesam and Code, it can be adjudged to be similar in terms of overprediction (+ve) or under prediction (-ve) for the different motions with respect to the experiment. It significant to point out that the difference between results from Sesam and Code to the experiment are attributed to uncertainties in the real process of carrying out the test compared to ideal situations in numerical formulations. Issues related to scaling effect is also a source of variation. The commercial solvers most times implement potential theory in formulating and solving the flow problem which is not the case in a real experimental basin where viscous effect is a reality. Possible errors from operator's competence are also sources of variations.

The proposed method also incorporates an aspect which is designed to estimate the wind and current forces/moments on the structure. The wind coefficients were obtained by fitting a time variant function to regenerated points from the OCIMF curves for VLCC. The coefficients are obtained at every time step since the overall direction of the unit changes alongside with the yaw angle.

This chapter sets the foundation for the next chapter, where the proposed method was used to carry out simulations to study basically the impact of spectrum type and wave directions on the overall roll motion amplitude for a free-floating structure.

7 Chapter Seven: Impact of Input Sea State Spectrum on Roll Amplitude of free floating FPSO in the West Africa offshore region.

7.1 Introduction

This chapter is dedicated to using statistical tool to analyse the time histories obtained from the simulation for different wave orientation and spectrum applications. It buttresses the applicability of the developed method in capturing typical trend and phenomenon observable in practice. When varying sea spectrums are applied to a free floating FPSO, the. The West African sea state earlier described was simulated for duration of 3hrs. The extracted time histories of the displacements for the different cases were used for comparative investigation. Three scenarios were investigated, cases of all wave components been collinear, non-collinear and two components in collinear against the other in different direction. The times series were analysed using the Fourier analysis technique in Matlab and the significant value was extracted from the area under the energy spectra curve for the parameter for the roll motion mode. The method is used to transform this variation into amplitude by imposing the wave as a disturbance onto the free-floating vessel and the corresponding roll motion studied adequately.

7.2 Impact of wave directionality

The effect of directionality has long been studied by (Marshall, 1976 and Okey 1989) and response deviations in offshore units recorded. This is evident in the under estimation of the response parameters between the Longcrested Idealization when compared to the real Shortcrested spectra for sea representation. This section examines the impact of the directional orientation of the different wave streams forming the irregular sea state. Figure 7.1 to 7.3 shows typical input wave elevation spectrum for the three-different sea state spectrum representations for case 16 used.

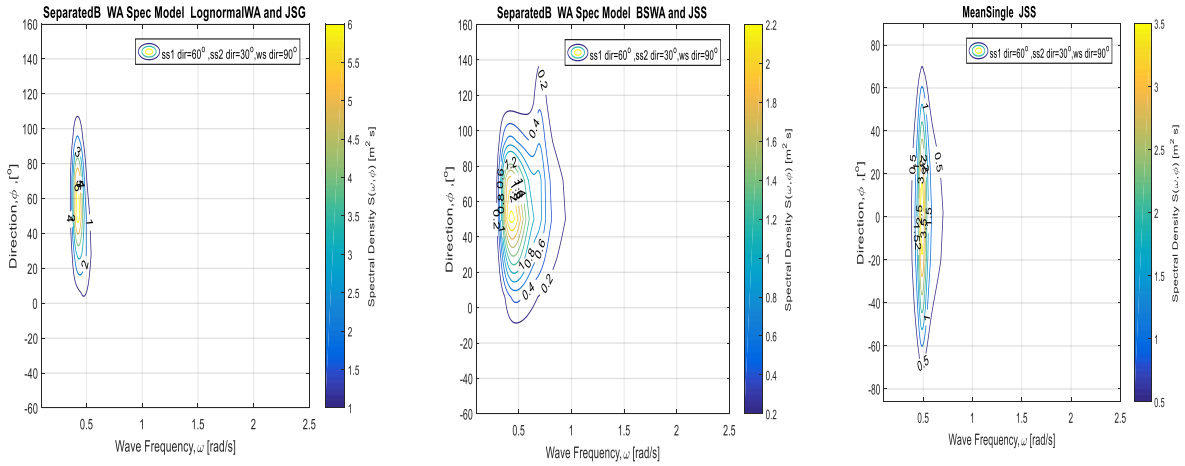

Figure 7.1 Contour plot showing spectra representation for 3-spectrum combinations (case 16)

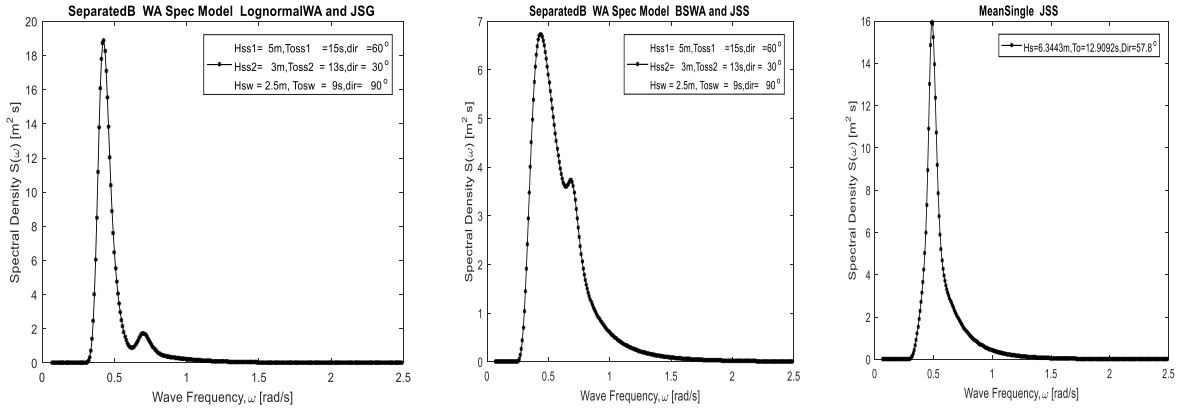

Figure 7.2 Longcrested representation for 3-spectrum combinations (case 16)

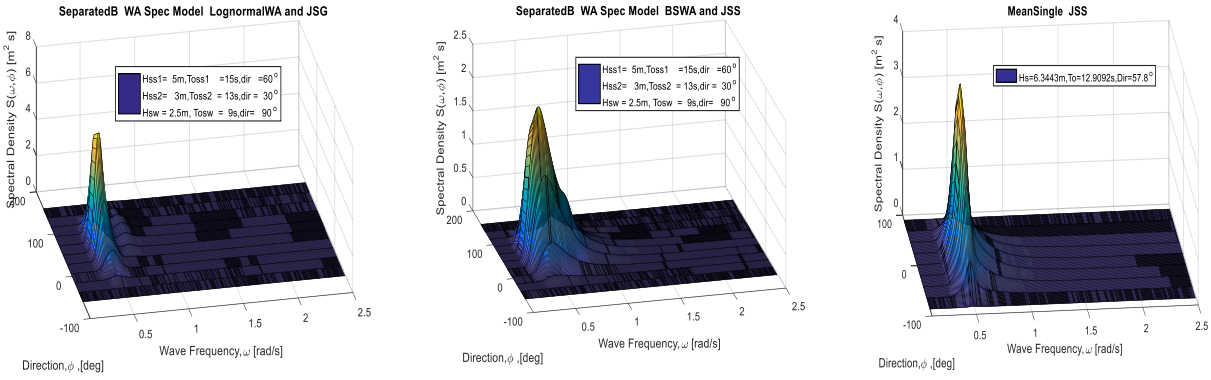

Figure 7.3 Shortcrested representation for 3-different combined spectrum (case 16)

7.2.1 *Waves in collinear orientation*

The table 7.1 shows the approximate estimation of the significant value of the roll response for the different wave combinations for three sets of sea spectra formation. The global direction is the mean direction of all the wave streams taking into consideration their various magnitudes and directions. However, in this instance, all the local primary waves are heading in the same direction except for cases 18-23 in which two streams are concurrent against the other.

Table 7.1 Significant roll amplitude for wave streams in collinear orientation

case	spectra combination					% error LogN vs		% error
	BS+JSS	BS+JSS (SESAM)	LogN+JSG	JSS	global Direct(°)	BS+JSS	JSS	BS+JSS/JSS
case 1	2.480	2.256	2.626	2.718	0	-5.590	3.510	9.639
case 2	16.289	17.104	14.989	16.736	45	8.678	11.683	2.765
case 3	27.312	30.316	23.379	28.944	90	16.823	23.785	5.959
case 4	14.579	15.614	14.427	16.714	135	1.050	15.879	14.674
case 5	2.350	2.564	2.500	2.612	180	-5.991	4.505	11.165
case 6	11.229	12.139	10.708	11.844	30	4.869	10.658	5.521
case 7	21.557	22.743	19.087	22.205	60	12.946	16.271	2.945
case18	16.431	17.663	15.011	17.323	51.6	9.463	15.335	5.364
case19	27.225	28.994	23.371	27.914	83.4	16.490	19.485	2.572
case20	20.384	20.609	18.197	21.644	54.7	12.018	19.035	6.264
case21	23.861	24.147	22.082	25.552	80.3	8.053	15.781	7.152
case22	23.787	24.025	22.652	24.718	73.5	5.014	9.133	3.922
case23	21.519	23.564	18.210	22.535	61.5	18.171	23.648	4.634

The results are graphically represented on the charts of figure 7.4 below. A study of the trend from the radar plot of figure 7.4b shows that the response is dependent on the type of spectra used. The plot also suggest that the pattern of prediction is similar independent of the spectrum combination. The use of the JSS for the entire mean stream gave relatively the highest values as compared to the other combination.

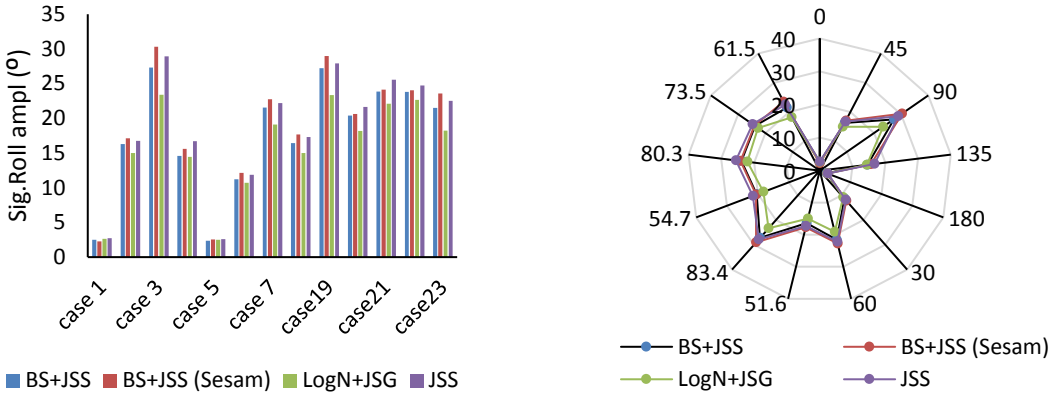

(a) (b)

Figure 7.4 Significant roll amplitude vs Spectrum type for collinear cases (a) Significant roll vs cases (b) Radar plot significant roll vs mean global direction

The LogN+JSG is below the two tested spectra formations. The percentage variation in estimation over the proposed spectra combination as observed, ranged from an average of 1% to 18% for the BS+JSS compared to 3.5% to as high as 23.8% for the single spectrum JSS model. Comparing LogN+JSG and BS+JSS in terms of the actual angle estimation, the value ranged from as low as 0.15^{o} for case 4 to as high as 3.3^{o} for the instance when the swell 2 and Wind Sea are beam sea wise against the swell 1 in 45^{o} direction. The overall observation follows standard predictions with the highest magnitude in the beam sea direction for the case 3 and the lowest at the head and following sea orientations where residual parametric roll is perhaps expected. Similar predictions were captured for the JSS formation in which case the lowest variation in case1 is 0.10^{o} against 5.5^{o} in beam sea. The overall envelope can thus be estimated to vary between 0.15^{o} - 5.5^{o} resulting from the use of the proposed spectra for the West African sea state.

7.2.2 *Waves in non-collinear orientation*

The essence of looking at the non-collinear arrangement is to identify the possibility of high amplitudes resulting from streams combining to form critical paths**.** It is most believed that the collinear cases are more critical in presenting higher magnitudes of response compared to the non- collinear cases. The results from the simulations are

presented in table 7.2 below. The pattern of predictions is like those observed for the collinear cases as can be seen from figures 7.5(a) and (b).

Table 7.2 Significant roll amplitude for waves in non-collinear orientation

case	Spectrum combination					% error LogN vs		% error
	BS+ JSS	BS+ JSS (SESAM)	LogN+ JSG	JSS	global Direct(°)	BS+ JSS	JSS	BS+ JSS/JSS
case 8	25.056	27.562	23.369	26.246	89.100	7.220	12.311	4.749
case 9	9.447	10.203	8.489	9.261	151.800	11.294	9.097	-1.974
case 10	5.653	6.049	5.299	5.592	66.200	6.676	5.533	-1.071
case 11	23.575	24.518	21.285	24.658	106.800	10.760	15.850	4.595
case 12	8.170	9.151	7.612	8.811	150.000	7.338	15.752	7.839
case 13	22.942	25.122	20.043	23.719	67.900	14.466	18.342	3.386
case 14	24.424	24.424	22.636	25.640	111.400	7.896	13.270	4.980
case15	22.190	24.143	20.882	23.122	62.200	6.266	10.730	4.202
case16	18.984	20.028	17.048	19.741	52.800	11.354	15.798	3.990
case17	24.218	26.083	23.028	25.490	74.800	5.167	10.691	5.253

Non- collinear combinations as those in cases 8, 11, 14 and 17 gave magnitudes close to the beam sea estimates. This observation is critical in understanding the severity of possible combinations leading to the beam sea condition. A common observation amongst the cases, points to the fact that the swell 1 (in 90°) has a considerable impact in the overall response. The observed envelope of variation in the estimation for the non-collinear arrangement is within the bracket of 5.2% to 18.4% or 1.2° to 3.7°.

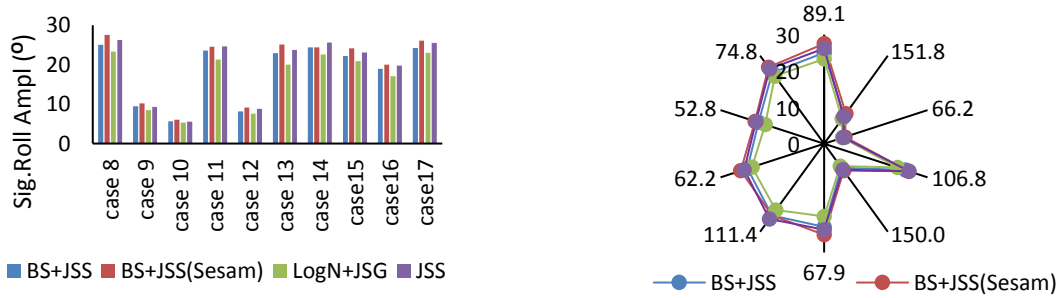

(a) (b)

Figure 7.5 Significant roll amplitude vs Spectrum type for Non-collinear cases (a) Significant roll vs cases (b) Radar plot significant roll vs mean global direction

7.2.3 *Impact of wave spectrum type*

The principal input excitation to a floating unit in any sea state is the wave. The wave is specifically defined by the spectrum representation. In direct linear analysis, once the RAO or transfer function is known, it is used with the wave spectrum to generate the response spectra. The spectra then become dependent on the input wave spectrum or the sea state. The same assumption of dependence was used in this research. Because the RAO are not directly known, the sea state was then used as input to the code to generate the response time series which was simply analysed for significant value extraction. The radar plots of figures 7.4 and 7.5 clearly extrapolates the level of dependence of roll response on the type of spectra used as input. Two critical deductions were reached (1). The over prediction from the BS+JSS combination could be because of the broad banded of the spectrum which was used to model the ordinarily benign sea state of West Africa. (2) The estimate from the JSS model, with the sea state viewed as a unimodal spectrum and a broad wind sea region or high frequency tail of the spectra, possibly resulted in the variation observed. The LogN+JSG spectra definition is comparatively narrow and heavily peaked at the swell region and most importantly was formulated with data specifically collated within the West African region as asserted by (WASP, 2004).

7.3 Bilge keel effect on roll motion response

Roll motion is significant in assessing the seakeeping performance of a vessel. The effect of roll damping on the roll motion has been extensively studied. Roll damping has great influence on the roll amplitude such that it may cause capsize if not well estimated for due consideration (Haddara, 1989). Roll damping prediction through model test remains the most accurate way of estimating its value and as such many research has been targeted to ensuring improved methods to accurately predict damping (Pesman et al 2007). This is so because the limitations and inaccuracies of the most accepted empirical formulations of (Ikeda, 1977, 1978, 2004) and the inability of potential theory to capture the effect of viscosity, wave and free surface hull interaction (ITTC, 2011; Bassler et al, 2011) has been identified. The potential theory thus underestimates the roll damping thereby over estimating the roll amplitude. The impact of bilge keels, thus; damping was studied using

CFD simulation by (Yang, 2012, Yue et al). The result shows the increased gain in damping resulting from bilge keel addition on to the bare hull. This results in reduction in the roll motion or amplitude. (Yue et al, 2015) also suggest that the best position for the bilge keel to offer effectively high damping was at the bilge compared to other locations. This collaborates the work of (Chakrabarti, 2001) based on Ikedas's method on the position effect of bilge keels. A generalized damping sensitivity study was performed, the graph of figure 7.6 shows a decline in the significant value as the damping increased up to a saturation region.

Table 7.3 Significant Roll amplitude for two wave stream combinations

	Sig. Roll amplitude (^{o})		Error compared to bk0		
Damping (Nms)*10^6	BS+JSS	LogN+JSG	% Δ BS+JSS	% Δ LogN+JSG	Δ in Damping (-)
(bk0) 318.401	22.554	19.863	0	0	0
527.856	21.400	18.735	5.116	5.682	0.658
617.482	20.577	17.981	8.765	9.478	0.939
1910.504	16.480	15.157	26.932	23.694	5.000
3203.526	13.639	12.804	39.525	35.541	9.061
4496.548	11.216	10.775	50.268	45.753	13.122
5789.570	9.778	9.333	56.648	53.013	17.183
8684.355	7.390	7.146	67.234	64.027	26.275
11579.140	5.912	5.655	73.788	71.529	35.367
14473.925	4.897	4.680	78.288	76.440	44.458
17368.709	4.177	3.965	81.481	80.038	53.550
20263.494	3.645	3.457	83.841	82.595	62.641
23158.279	3.230	3.098	85.680	84.406	71.733
26053.064	2.899	2.796	87.145	85.926	80.825
28947.849	2.630	2.532	88.339	87.253	89.916
31842.634	2.407	2.307	89.329	88.384	99.008
34737.419	2.218	2.117	90.165	89.343	108.100

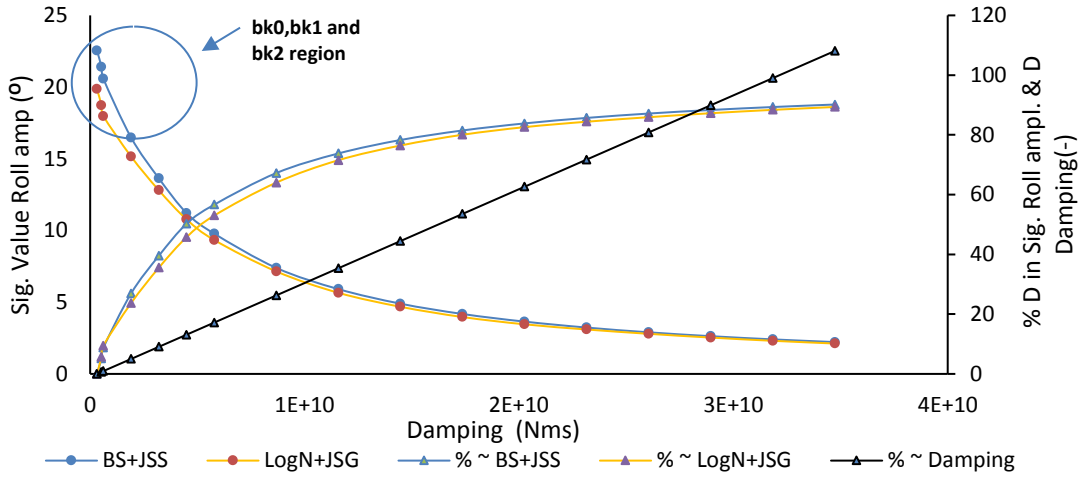

Figure 7.6 Sensitivity trail on damping/bilge keel effect on Sig. value of roll response (case 16)

The significant value is also dependent on the type of spectrum adopted in the formulation of the sea state. The encircled region is the superimposition of the approximations of the damping estimated for the bare hull configuration (bk0), and the bilge keel configurations (bk1 and bk2) for data set for design draft, the following observations were made. The response was estimated to reduce by 8.75% and 9.48% for the hull with similar damping to the bilge bk1 for BS+JSS and LogN+JSG respectively. Whereas a reduction in the damping as exemplified by the bilge keel configuration bk2 had correspondingly smaller roll amplitude reductions of 5.12% and 5.68% respectively. As the damping was increased, the observed roll amplitude diminished exponentially for both spectra combinations. A corresponding exponential gain in the % increase in the effect of increased damping was also observed. At some point around the damping value of 14.474GNms, the estimated gain in % resulting from additional damping reduced to a single digit value of < 7% and gradually saturates at some point and extends towards infinity. This explains the fact that, an increased damping via bilge keel does not necessarily guarantee a corresponding gain in the roll amplitude reduction. Thus, a comparative analysis between the costs of securing bigger bilge keels against the significance of reduction gained is important. This affirms to a summarised extent the impact of bilge keel on the response. The variation is similar across the different spectrum combinations.

7.3.1 *Comparison between roll damping linearization and the non-linear formulation*

A short simulation for the different experiment was done using the original non-linear coefficient against the linearized global damping coefficient. The non-linear representations are captured in chapter 3 and the estimated linear damping (B_{eq}) obtained equally through the least square method. The results are presented below in table 7.4.

Table 7.4 Summary of significant roll amplitude for linearized vs Non-linearized roll damping

BS+JSS		LogN+JSG	
Linearized	Non-linear	Linearized	Non-linear
18.018	20.074	16.433	18.134
18.859	25.039	16.698	18.102
16.657	19.682	16.130	17.976
16.737	19.687	16.211	18.057
17.003	19.878	16.211	18.058
17.3193	19.929	16.283	18.087

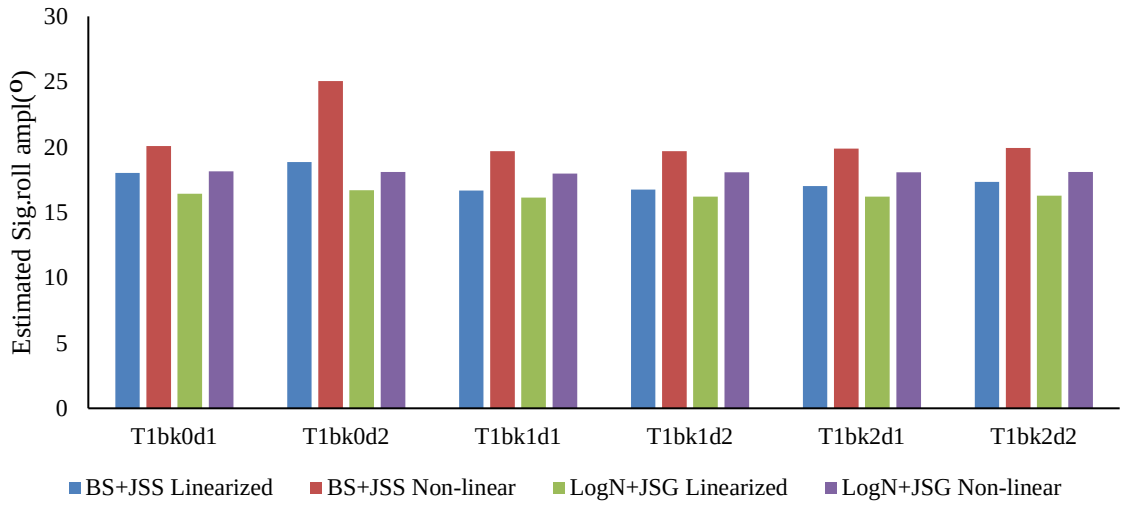

Figure 7.7 Significant roll amplitude for linear and non-linearized roll damping formulation

Irrespective of the input spectrum, the estimation from the non-linearized form of the damping parameter range from 9% to 24% compared to that estimated from the linearized damping ratio. The magnitude is in the region of between 2^o to 6^o between the non-linear

and linearized forms. This is attributed to the overestimation of the damping coefficient resulting from the linearization process.

7.4 Conclusion

The use of JONSWAP and Bretchneider when compared to the proposed lognormal and Jonswap-Glenn spectrum for the region resulted in the estimation of the responses in the order of 1-23% variation or more than 5.5^{o}. This thus can be directly translated to possible over design of unit dimensions and support equipment like the mooring lines, topside foundations, risers or their end fittings, crew wellness and comfort assessment etc. It also can affect helicopter operations as well as loading/unloading of supply vessels. The region is benign and as such the essence of considering this variation may not be critical particularly from environmental reasons, but it becomes significant from the long-term cost implication. Results from simulation attest to the fact that bilge keels are significant in the reduction of the overall amplitude of roll due to the increased damping they offer. It is pertinent to note that, the corresponding reduction in the amplitude is not linearly proportional to the associated linear increase in the damping added. There exists a saturation value beyond which there is a drop in the marginal gain of amplitude reduction achieved. It was also observed that at very high damping values, the variation in the roll amplitude becomes independent on the input wave spectrum.

The use of the linearized form of the damping suggest an averaged over estimation of the damping coefficient in an order which translates to a net reduction in the significant roll amplitude in the range of 9-24% or 2-6^{o}.

8 Chapter Eight: Conclusions, and Recommendations for Further Studies

8.1 Conclusions

Experimental determination of roll damping via model test remains the most accurate method for predicting the level of damping present. Conventional techniques are better suited for the prediction of roll damping for hulls without sharp edges where vortex plays a critical role. The Bilinear formulation or the hyperbolic model stretches the development towards identifying two damping plateaus or regions for sharp edged hulls, thus describing the phenomenon as a bilinear one. This is achieved by characterizing the regions with damping coefficients associated with the large angle and small angle sides. However, there is the suspicion that the behaviour for such hulls is rather trilinear as there exist a region between the two identified plateaus. As part of the objectives of this study, having recognized this gap, thus, relying on the method of (Oliveira and Fernandez,2006), this research has developed a model representation that captures the third region significantly. The regions are characterized using three specific damping terms for the large angle, small angle and the transition region. Unlike the bilinear representation, two slope control parameters are introduced. In addition to the trilinear representation, the non-linear characterization of the damping term is also conserved. This is important since roll motion is better studied as a non-linear phenomenon against the simplified linearization been used in some instances. It is significant to note that this model is better suited for hulls like the FPSO with sharp edges or with the presence of bilge keels for better roll reduction. The model-the model technique in parameter identification was used together with the least square optimization method in identifying the model coefficients. The model was validated against other models using experimental data and verified with the bilinear method. The uncertainty analysis carried out showed a 3.5% to 5.9% relative uncertainty in the roll damping predictive model. It also revealed a possible influence on the uncertainty resulting from sharp edge or bilge keel effect.

From the roll damping sensitivity trial carried out, a linear increase in the damping coefficient resulted in an exponential decrease in the roll amplitude estimated. The trend is such that the decrease saturates at some region off the initial damping coefficients. The reduction in roll amplitude resulting from the influence of bilge keels was 5.11% and

8.77% for bilge keels configurations bk1 and bk2 for BS+JSS respectively. These values are small because the motion does not coincide with the roll natural frequency of the hull. The percentage increase in the damping was estimated at 65.78% and 93.93% for bk1 and bk2 respectively. The same pattern was observed when the input spectra was varied to LogN+JSG (5.68%, 9.48%). It was also observed that at very high damping values, the variation in the roll amplitude becomes independent on the input wave spectrum.

The use of the linearized damping formulations against the global linearized damping suggest an averaged over estimation of the damping coefficient in an order which translates to a net variation in the significant roll amplitude in the range of 9-24% or 2-6^{o} in magnitude. The trend observed is independent of the spectra used when the two approximations are considered. However, the magnitudes estimated are dependent on the input sea spectrum.

The second objective was to establish a simulation routine, capable of generating roll motion amplitude in real sea way, with interest in the type obtainable in the West African (WA) region. Relying on the gap identified in the recommendations of (WASP, 2004) that the spectra representation for the WA region is not exactly like the conventional models being used, it was necessary to develop this routine with the capacity to implement this recommendation. The idea was to comparatively assess the roll amplitude estimates from the LogN+JSG spectrum to other conventional types. The WA region is a multiple swell dominated region with wind sea component(s) as well. Though benign in nature but the sea configuration which is typically irregular can be best described as complex and complicated. To overcome this challenge, a routine was developed to carry out the summation of the separated seas into a common stream. This was necessary since the SESAM package suffers a limitation in this aspect. It does not currently have this spectra type as part of the usable wave spectra. Secondly, the capability is limited to one swell sea against the minimum two swell (primary and secondary swells) observed for the WA region. Three different summation techniques were used by applying the work of (Bhoukanouvsky and Soares, 2009). The tool was validated by using the model test for irregular wave and SESAM simulation. The verification was done by carrying out a sensitivity studies on the number of regular wave frequency component used in the formulation of the irregular sea way. In assessing the adequate number of wave

frequencies to form the irregular surface, the sensitivity study performed using the significant wave height simultaneously with the estimated maximum spectra density, suggest a region of acceptability for values of N>=199. Although, this was not observed in the sensitivity for the significant wave height, but it gave a clue of the phenomenon of unsteady estimation encountered during the iteration. The estimate was random from the N=5 up to 41, and then became. The findings define an appropriate value for N, while considering chart clarity against computational time.

The first explicit technique captioned meansingle approach applies the summation technique by assuming the existence of a single wave stream with the energy equivalent to the supposed overall sea state. A limitation of this method lies in the fact that peak frequencies play major roles in the determination of the magnitude of response experienced when a structure encounters the sea way. Because the real sea is multi-peaked, the spectrum of the smaller peaks are most times supressed by the dominant spectra. Unlike the meansingle technique, the Separated-A approach considers the swell seas as single stream and then combines them with the independent wind sea component with different directional spreads. In this approach, there is also the likelihood of supressing a weaker swell component, and thus the peak characterization of the separated swell streams is not well represented. These limitations lead to the extension of the technique to a more implicit approach captioned as Separated-B technique which considers independently the separate wave streams, and their spreads as well. For seas with the streams well separated from the value estimated from the IMD, the presence of the three distinct peaks signified better characterization of the actual sea. The formation of these streams is geographical dependent, as such the need to use an appropriate spectra model when characterizing a specific region is significant. From the WASP, similar to the JONSWAP, it is recommended that the benign region of the West African offshore region be represented by a Lognormal or Triangular spectra distribution for the multiple swells. Whilst the JONSWAP-Glenn (modified JONSWAP) is used for the wind sea component. Visual inspection, as well as quantization of the spectra energy density and the spread area, has shown that the spectra combination technique has a strong influence on the overall characterization or shape of the seaway. Another significant extraction is the influence exhibited by the directions of approaching wave streams. The directional

variation is not significant for collinear cases as all the maximum recorded spectra density was about 5.04 m^2-s. This was not so in cases of non-collinear directions, values ranged from 3.67 m^2-s to 4.0 m^2-s, significantly due to the redistribution of the spectra energy by the different streams. The observed variations were between 20% to 27% reduction in maximum spectra energy was estimated between cases of collinearity compared to non-collinear arrangements. The contour plots from the routine present good visual interactive platform for easy identification of patterns in parameters variations and influence on the sea state energy distribution. It captures the variations in terms of energy concentration and distribution between the LogN+JSG and other combinations of spectra in the formulation of the sea state. In line with the set objective, outputs such as, the spectra shape, the summation technique, the number of frequencies are used as input in the following part of the proposed method.

The vessel motions hydrodynamic problems are tedious to solve resulting in the use of strip theory by most numerical algorithms. Other methods which include the panel method, with Green functions, boundary element are also available as implemented in commercial software like SESAM. The concept of estimating the excitation forces for a real sea state (irregular shortcrested sea) is based on the superposition of the forces obtained from the regular wave formulation. The search for simplified algorithms explores the advantage of using less ship information to carry out adequate motion predictions (Lainiotis et al, 1992). The robust application of these simplified techniques is evident in the virtual reality industry. Forces are estimated, and the equation of motion developed from Newton's laws are solved using the Runge-Kutta methods (Zhang et al, 2004). The work of (Cieutat et al, 2001; Shyh-Kuang et al, 2008) estimated the forces using sea surface height function and thus suffered the limitation of producing the same result for vessels of different hull form in the same wave condition. This was corrected by (Damitha et al, 2010) who combined the advantages derivable from (Shyh-Kuang et al 2008, and Gatis et al, 2007) to produce a better 6dof simulator. A new approach using a weighted technique based on the spectra density and regular wave frequency has been presented for the estimation of the Froude Krylov and Diffraction forces from available regular wave formulation. The diffraction and Froude-Krylov forces were estimated for all the individual regular waves, then weighted by their contribution towards the

formation of the sea state. The total force is then obtained by the superposition of the weighted components. The generalized method was robustly expanded to capture instances of irregular short crested sea with multiple swells and wind sea components.

The methodology involved in the building of the overall simulation routine for the free floating structure under the influence of wave frequency has been elaborately presented. The different components of the equation of motion were obtained using available simplified techniques. Starting with the added mass and damping, the 2D values were obtained using the simple form of the Lewis conformal mapping and the 3D obtained by integrating the 2D across the length of the hull. The restoring coefficient were estimated using standard equations. The wave excitation forces in the form of Froude-Krylov and Diffraction forces were estimated using standard regular wave formulations. A wave frequency-spectrum weighting technique was adopted to modify these equations and then implemented for short-crested sea states. However, the use of pressure integration over the instantaneous wetted surface of hull to estimate the Froude-Krylov force was also included. In order to validate the code, similar scenarios were tested using the standard SESAM package. The simulation from the SESAM was partially validated using the experimental test result for the regular wave as well as the irregular wave test. However, the SESAM numerical development was partly verified by the random seed sensitivity test carried out. It was evident that the random seed affected the quantitative value of the response, however the order of impact was not significant to offset the overall meaning of the output. The RAO values obtained showed remarkable correlation between the experiment and the numerical simulation. The averaged variation of the peak values for draft condition 1 were 13.22%, 6.10% and 14.23% for bare hull, bk1 and bk2 respectively. Similar variations of 6.7%, 4.26% and 4.78% were obtained for the draft condition 2. The two cases adopted from the irregular wave test, was used to validate the roll motion response part of the proposed method and results were also compared with the simulation. The descriptive statistics obtained from the validation procedure for the three methods showed some level of percentage variation in the roll amplitude as well as the water surface elevation. For the elevation, 13% and 10% overestimations (against experiment) were recorded for the case of Hs=1.92m for the SESAM and the proposed method respectively. However, an overall evaluation suggests insignificant deviations between

methods. Similar values of 15.6% and 13.6% were observed for the second wave height case. In the aspect of estimated significant roll amplitude, (12.6% and 15.5%; case a1) and (5.5% and 8%; case a2) were observed for SESAM and proposed method respectively.

With the method validated and verified accordingly within the estimated identified error range, the sensitivity of the impact of spectra type to the overall roll response for free floating unit in wave frequency was done. The extreme wave conditions of the seaway associated with the 100year return period for a typical WA region was simulated. For instances when all streams are collinear or two collinear against the other, the use of JONSWAP and Bretchneider when compared to the proposed lognormal and Jonswap-Glenn spectrum for the region resulted in the estimation of the significant roll responses in the order of 1-23% variation or in excess of 0.15^{o} to 5.5^{o}. Similar variation envelope of 5.2% to 18.4% or 1.2^{o} to 3.7^{o} were observed in cases when the streams are completely non-collinear in orientation. This thus can be directly translated to possible over design of unit dimensions and support equipment like the mooring lines, topside foundations, risers or their end fittings, crew wellness and comfort assessment etc. it also can affect helicopter operations as well as loading/unloading of supply vessels. It is general knowledge that the region is benign and as such the essence of considering this variation may not be critical particularly from environmental reasons, but from the long-term cost implication of the capex, it becomes significant.

The proposed method which has been rigorously transformed into an algorithm is novel in its application for determining the roll motion of free floating unit to wave frequency by adopting the novel non-linear roll model with the capability of identifying the transition zone. The ability to apply the weighted technique in combination with other numerous simplified empirical formulations to estimate the roll motion amplitude is a novel achievement. Given its simplistic approach, the method is computationally friendly with good potential for expansion. The sea state interactive routine provides a good tool to be used for demonstrations as well.

8.2 Limitations and Recommendations for future works

As it is with any research ending up in Theses, the inevitable constrain to desired objectives by time and availability of research tools, finance and the environment are common. These limitations present the research with a realistic scope to work within. The present research is thus not void of this reality and it has not been perfectly possible to exhaustively and comprehensively investigate all areas of concern and interest.

The free decay investigation carried out suggest the presence of three damping plateaus, the large damping side, small damping zone and a transition region between them. Careful observation suggests that the region with the large angle experiences the small damping compared to the less significant small angle region were the damping is observed to be larger. It is further recommended thus for an investigation to be carried out to study the dynamics of damping associated with the small angle region specifically.

The application of the overall proposed method has been limited in terms of verification and validation to the influence emanating from the wave force and wave frequency alone. Setting a platform for limitations and recommendations for further studies, the proposed method incorporates an aspect which is designed to estimate the wind and current forces/moments on the structure. The wind coefficients were obtained by fitting a time variant function to regenerated points from the OCIMF curves for VLCC. The coefficients are obtained at every time step since the overall direction of the unit changes alongside with the yaw angle. For estimating the coefficients, the resulting continuous functions obtained from the reconstructed data compared within the error of < 2% with the actual curves. The impact of mooring lines using the taut configuration which stands as the new trend in mooring has also been laid for the programme to be used in the study of the global effect of mooring on the roll amplitude of the unit. Mooring line dynamics are essential in the overall assessment of the absolute motion of a FPSO, however, the design of such unit follow from the study of the free motion of the unit which is the core interest of this research.

Relying on one of the findings of this research with respect to the influence of the input spectrum on the roll motion parameter, further work is thus required to assess the degree of overestimation or underestimation resulting from such variations on the dimensions of

the units and its support structures likewise. This is significant for possible recommendations to be made for modifications of the design status quo particularly as it concerns preliminary designs. It is in my opinion, that the standard conventional spectrum can be forced to adopt the recommended lognormal formulation by using advanced optimization technique for coefficient parameterization, the level of associated error is worth investigating. Significantly, the robustness of the procedure can be further enhanced by including a regular wave simulator to the code

Furthermore, because one of the objectives was to develop the method into an interactive tool, it is important to further develop the scripts into very friendly interactive user defined interfaces.

REFERENCES

Abhilash S. Somayajula and Jeffrey M. Falzarano (2014), 'Non-Linear Dynamics of Parametric Roll of Container Ship in Irregular Seas' [+] Author Affiliations, Texas A & M University, College Station, TX Paper No. OMAE2014-24186, pp, V007T12A018;10 pages doi:10.1115/ OMAE2014-24186

Abled, J., Andersen, E. Y. & Rosbjerg, D. (1992). 'The Climate of Extreme Winds at the Great Belt, Denmark'. *J. Wind Eng. Ind. Aerodyn*, 41–44**:** 521–532.

Allan C. de Oliveira, Antonio Carlos Fernandes, Anderson (2012), 'An empirical non-linear model to estimate FPSO with extended bilge keel roll linear equivalent damping in extreme seas', *Proceedings of the ASME, 31st International Conference on Ocean, and Artic Engineering*, OMAE2012. Brazil.

Allan C. de Oliveira, Antonio Carlos Fernandes, Anderson R.W. Soares (2014), 'A comparison among alternative to assess FPSO roll damping via model testing', *Proceedings of the ASME, 33rd International Conference on Ocean, and Artic Engineering*, OMAE2014. California:

Allan C. de Oliveira and Antonio Carlos Fernandes (2014), 'The Nonlinear Roll Damping of FPSO Hull' *J. of offshore Mechanics and Artic Engineering*, vol. 136, pp1-10, available online at: http://offshoremechanics.asmedigitalcollection.asme.org

Allan C. de Oliveira, and Antonio Carlos Fernandes, (2010), 'An alternative to model the non-linear roll damping of a FPSO hull', *Proceedings of the ASME, 29th International Conference on Ocean, and Artic Engineering*, OMAE2014. China:

ASME,(1998), An American National Standard, Test Uncertainty, ASME PTC 19.1-1998.

Antonio Carlos Fernandes and Allan C. de Oliveira and (2009), `The Roll Damping assessment via decay model testing (new ideas about an old subject' *Journal of Marine Science and Technology*, 8, pp. 144-150

Araki Motoki (2004),`Ship Manoeuvring Mathematical Model using System Identification Technique with Experimental and CFD free Running Trials in Calm Sea and Astern Waves', *Osaka University Knowledge Archive*, Online http://ir.library.osaka-u.ac.jp/dspace/

Aung Myat Thu, Ei Htwe, Htay Win, (2015),'Mathematical modelling of a ship motions in waves under coupled motions', *International Journal of engineering and applied science*, Vol. 2, issue 12.

Available online; https://cepprofs.civil.tamu.edu/mhkim/OE-673-MET-OCEAN.pptx

Aziz M. Tayfun, and Franceso Fedele, (2006),'Wave-Height Distribution s and Non linear effects A two peaked wave spectrum model', *Proc. of the 25th International Conference on Offshore Mechanics and Artic Engineering. OMAE, Hamburg, Germany.*

Babak Ommani and Nuno Fonseca (2016),`Bilge keel induced roll damping of an FPSO with Sponsons', *Proceeding of the ASME2016 International Conference on Ocean, Offshore and Artic Engineering*, OMAE 2016, Busan,South Korea.

Barnett, T. P., (1968),`On the generation, dissipation, and prediction of wind waves`. *J. geophys. Res*. 73, 513.

Bass, D. W. and Haddara, M. R. (1988) 'Nonlinear models of ship roll damping', *Int. Shipbuilding. Progress*, vol.35 (401),pp 5–24.

Bassler, C., Miller, R., Reed, A., Brown, A., (2011), 'Considerations for Bilge Keel Force Models in Potential Flow Simulations of Ship Manoeuvring in Waves', *Proceedings of 12th International Ship Stability Workshop.*

Beck, R.F. and King, B. (1989) 'Time-domain analysis of wave exciting forces on floating bodies at zero forward speed', *Applied Ocean Research*, vol.11(1), pp. 19-25.

Bhattacharyya, R., (1978) 'Dynamics of Marine Vehicles. Wigley, New York.

Bishops R.E.D., and Prize W.G.,(1979),' Hydroelasticity of Ships', Cambridge University Press, pg.126.

BMT Fluid mechanics (2001), 'Review of model testing requirements for FPSO's', *offshore technology report* 2000/123, United Kingdom

BMT, (1986), 'Global wave statistics', Published by Urwin Brothers ltd., England

Boccotti, P., (1989), 'On Mechanics of irregular gravity waves' Atti della Accademia Naionale dei Lincei, Memoire VIII, pp11-170.

Boccotti P., (2000). Wave Mechanics for Ocean Engineering. Elsevier, Oxford.

Boukhanovsky A.V., Guedes Soares C.,(2009), 'Modelling of multipeaked directional wave spectra', *J. Applied Ocean Research*, 31:132-141.

Boukhanovsky A.V., Leonid J. Lopatoukhin, Guedes C. Soares (2009), 'Spectra Wave Climate of the North Sea' *J. Applied Ocean Research vol 29*, pp146-154.

Bridget R. Thomas, Elizabeth C. Kent, Val R. Swail. (2005), 'Methods to Homogenize Wind Speeds from Ships and Buoys', *Int. J. Climatology*, vol.25, pp 979-995.

Broad W.J. (2006), 'Rogue Giants at sea', *The New York Times*, July 11. Available online: http//:www.mytimes.com

Brouwer J., Tukker J., Rijsbergen Van M.,(2013), `Uncertainty Analysis of Finite Length Measurement Signals',`*The 3rd International Conference on Advanced Model Measurement Technology for EU Marine Industry.*, Gdansk, Poland, 17-18 Sept.

Cardone V.J., Greenwood J.G., Mark A.C. (1989), 'On trends in Historic Marine Wind Data', *Journal of climate* 3, pp.113-127

Cartwright D. E. and M. S. Longuet-Higgins (1956), The Statistical Distribution of the Maxima of a Random Function', *Proc. of the Royal Society of London*. Series A, Mathematical and Physical Sciences, Vol. 237, No. 1209, pp. 212-232

Chakrabarti, S., 2001, "Empirical Calculation of Roll Damping for Ships and Barges," Ocean Eng., 28, pp. 915–932.

Chan H.S.Y. (1995),Xu Z., Huang W.L., 'Estimation of nonlinear damping coefficients from large-amplitude ship rolling motions', *Applied Ocean Research 17,* pp217-224.

Chan H.S.Y. (1995),Xu Z., Huang W.L., 'Estimation of nonlinear damping coefficients from large-amplitude ship rolling motions', *Applied Ocean Research 17,* pp217-224.

Chang, B.C. (2008), 'On the parametric rolling of ships using a numerical simulation method', *Ocean Engineering*, vol.35(5–6), pp. 447-457.

Chen G. (2004), 'An Inter-comparison of TOPEX, NSCAT, and ECMWF Wind speeds: illustrating and understanding systematic discrepancies, *Monthly weather review* vol. 132 780-792

Ching Tong Choi & Ling Chang, (2007),'Ships on real time rendering dynamics ocean applied in 6Dof platform motion simulator', *CACS International conference*, Taichun, Taiwan.

Christopher C. Bassler, Arthur M. Read and Alan J Brown ,(2011), `A piecewise model for the prediction of larg amplitude total ship roll damping', *Proc. of the ASME 30th International Conference on Ocean , Offshore and Artic Engineering*, OMAE, June 19-24 , Rotterdam, Netherlands.

Cieutat JM, Gonzato JC, Guitton P (2001), `A new efficient wave model for maritime training simulator', *IEEE spring conference on computer graphics*, pp. 202–209

Ciobanu Camelia and Anghel Arlene-Rabela,(2008),''The computing of the damping generalized coefficient'', *Proceedings of the Romania Academy*, Series A, vol.9, No.3.

Ciobanu Camelia, Arlette-Rabela Anghel (2008)," The Computing of the damping generalized coefficients", *Proceedings of the Romania Academy*, Series A, Vol. 9,No.3.

Ciobanu Camelia, Cata M.,Arlette-Rabela Anghel (2006) ,`Conformal Mapping in Hydrodynamic`, Bullettin of Transilvania University of Brasov, Vol 13(48).

Coles, S. (2001), `An Introduction to Statistical Modelling of Extreme Values`, Springer: London.

Coles, S. G. & Walshaw, D. (1994). Directional Modelling of Extreme Wind Speeds. *Appl. Stat*., 43**:** 139–157.

Cook, N. J. (1982). 'Towards Better Estimation of Wind Speeds'. *J. Wind Eng. Ind. Aerodyn*., 9**:** 295–323.

Cook, N. J. (1983), `Note on Directional and Seasonal Assessment of Extreme Winds for Design`, *J. Wind Eng. Ind. Aerodyn*., 12: 365–372.

Cook, N. J. (1985). *The Designer's Guide to Wind Loading of Building Structures. Part 1: Background, Damage Survey, Wind Data and Structural Classification*. Building Research Establishment, Garston, and Butterworths, London, 371 pp.

Cook, N. J. and Craig A.Miller (1999). Further note on Direction Assessment of Extreme Winds for Design' . *J. Wind Eng. Ind. Aerodyn*., 79: pp201–208.

Cummins W.E., (1962),'The impulse response function and ship motions', Schiffstechnik, vol.9, pp102-109.

Cummins W.E., Bales, S.L., (1980) 'Extreme value and rare occurrence wave statistics for northern hemispheric shipping lanes', The TRIS and ITRD database, *Supplemental notes from SNAME Meeting and STAR symposium "safety and marine environment*" Coronado, California. Available online at: http://trid.trb.org/view

D.Spanos, A.D.Papanikolaou, G.Zaraphonitis,(1997) 'On the 6DOF Mathematical model for the simulation of ship capsize in waves', Hellenic Institute of Marine Technology & Ship Design Laboratory, National Technical University of Athens Heroon Polytechniou 9, 15 773 Zografou, Athens Greece.

Damitha Sandaruwan, Nihal Kodikara, Chamath Keppitiyagama and Rexy Rosa (2010), 'A six Degree of Freedom Ship Simulation System for Maritime Education', *The International Journal of Advances in ICT for Emerging Regions*, 03(2), pp.34-47.

Daniel Morris (2005), ' The Chance to go Deep: U.S. Energy Interests in West African', *Journal of the National Committee On American Foreign Policy*, 28(3), pp.225-238

Das, S.N. and Das, S.K. (2005) 'Mathematical model for coupled roll and yaw motions of a floating body in regular waves under resonant and non-resonant conditions', *Applied Mathematical Modelling*, vol.29(1), pp. 19-34.

Davison A.C., and Smith R.L., (1990), 'Models for Exceedance Over High Thresholds', *J. Royal Statistical Society*, Series B, vol 52, 3,pp393-442.

Dean R. (2006), 'Freak Waves: A Possible Explanation', *Proc. Water Kinematics, Nato* ASI Series E, vol178, pp609-612.

DNV-RP C205, (2008),' Recommended Practice-Environmental Conditions and Environmental Loads.

DNV-RP-C 205 (2007) "Environmental Conditions and Environmental Loads". Available online: http:/rules.dnvgl.com/docs/pdf/DNV/codes/2007-10/RP-C205.pdf

DNV-RP-F205, 2010, ‘Global performance analysis of deep water floating structures’, Det Norsk Veritas, Norway.

DNV-RP-H103 (2011) “Modelling and Analysis of Marine Operations”. Available online: http:/rules.dnvgl.com/docs/pdf/DNV/codes/2011-04/RP-H103.pdf

DNV-RP-H205, (2004), ‘Recommended Practice: Modelling and Analysis of Marine Operations

Downie, M.J.,, Bearman, P. W., Graham, J.M.R.., (1988), ‘Effect of Vortex shedding on the coupled roll response of Bodies in waves’, *J.Fluid Mech.*,189,pp.243-264.

Edward V Lewis (ed), (1989), ’Principles of Naval Arch; motions in waves and controllability, vol.III, Published by SNAME, Jersy city, USA.

El-Bassiouny, A.F. (2007) ‘Nonlinear analysis for a ship with a general roll-damping model’, *Physica Scripta*, vol.75(5), pp. 691-709.

Erwin Kreyszig, (2010), ‘Advanced Engineering Mathematics’,

Ewing J. A., (1971): `A numerical wave prediction method for the North Atlantic Ocean`. *Dt. hydrogr. Z.* 24, 241.

Ewans K.C., Bitner-Gregerson EM, Guedes Soares C. (2006),’Estimation of wind sea and swell component in a bimodal sea state’, *J. Offshore Mechanics and Artic Engineering*, 128:265-270.

Faltinsen, O. M , and Michelsen, F. C , (1974), "Motions of Large Structures in Waves at Zero Froude Number," *Proceedings of the International Symposium on Dynamics of Marine Vehicles and Structures in Waves,* London, pp. 91-106

Falttinsen O.M., (1998), ‘Ocean Technology Series: Sea Loads on Ships and Offshore Structures’, Cambridge University Press, United Kingdom.

Fedele F., Arena F., (2005), ’Weakly nonlinear statistics of high random waves‘, *J. Physics of Fluid*, vol 17(2) pp1-10.

Felice Arena, Guedes C. Soares, (2009),’ Nonlinear Crest, Trough, and Wave Height Distributions in Sea States with Double-Peaked Spectra,’ vol.131,pp1-8.

Fernandes A.C. ,Kroft S.A.B., (2000),’Bi-linear Modelling of wider, longer an continuous bilge-keels for FPSO roll motion control’, ‘Proceedings of the 19TH International symposium on offshore mechanics and Artic Engineering, (ETCE/OMAE200 Joint Conference). New Orleans: Estados Unidos, February 14-17

Fernando J. Mendez, Melisa Menendez, Aalberto Luceno, Inigo J. Losada (2006),’ `Estimation of the Long Term Variability of Extreme Significant Wave Height using a Time-Dependent Peak Over Threshold (POT) model’, *J. Geophysical Research* vol 3, pp1-13.

Ferreira, C., Guedes Soares (2000),' Modelling distribution of significant wave height', *J. Coastal Engineering,* vol 40, pp361-374

Forristall, G.Z. (1978), On the Statistical Distribution of Wave Heights in a Storm, *J. Geophys. Res.,* 83**,** 2353-2358**.**

Fournier A, Reeves WT (1986),`A simple model of ocean waves`, *Proceedings of SIGGRAPH*'86, pp 75–84

FPSO World fleet.com, available online at: www.fpso.com/fpso

Frank W., Salvesen N.,(1970) 'The Frank close-fit ship motion computer program', Report 3289, NSRDC, Washington, DC, 1970.

Fred Stem, Maran Muste, Maria-Laura Beninati, and William E. Eichinger (1999),' Summary of Experimental Uncertainty assessment methodology with example.

Froude W., (1861), 'On the rolling of Ships', *RINA Transactions and Annual Report* 1861, London.

Fugro OCEANOR, 'integrated environmental monitoring systems', available online at: http///:www.pceanor.com

Fugro OCEANOR, 'World Wave Global Offshore Database'. Available online: http://www.oceanor.no/services/worldwaves/WW_database

Fukuda,J.(1967),'Theoretical determination of design wave bending moments', *Japan Shipbuilding and Marine Engineering,* vol.2,no. 3, pp12–22.

Gabriel Bulian, Alberto Francescutto, Fabio Fucile (2010),' An experimental investigation in the framework of the alternative assessment for the IMO weather criterion', *Proc. of the HYDRALAB III Joint User Meeting,* Hannover, February.

Gatis Barauskis, Peter Friis-Hansen. (2007), "Fast-Time Ship Simulator.' 2007. Safety at Sea.

Goda, Yoshimi, Hawkes, Peter, Mansard, Etienne, Martin, Maria Jesus, Mathiesen, Martin, Peltier, Eric, Thomson, Edward, Van Vledder, Gerbrant (1993),' Intercomparison of Extremal Wave Analysis Methods using Numerically Simulated Data', *Proc. 2nd International Symposium on Ocean Wave Measurement and Analysis;* New Orleans USA.

Graham C., (1982), 'The Parameterisation and Prediction of Wave Height and Wind Speed Persistence Statistics for Oil Industry Operation Planning Purposes', *Coastal Engineering,* vol.6,pp303-329.

Greenwood J.A., Landwehr and Matalas N.C.(1979), 'Probability Weighted Moments: Definition and Relation to Parameters of Several Distributions Expressible in Inverse form'; *J. Water Resources Research* 15(5) pp.1049-1064.

Guedes C. Soares, (1984),'Representation of Double-Peaked Sea Wave Spectra', *J.Ocean Engrg*. Vol 11(2),pp.185-207.

Guedes C. Soares, Nolasco M.C.,(1984),'Spectra Modelling of Sea State with Multiple wave systems', *J. Ocean Mechanics and Arctic Engineering*. Vol 114,pp.278-284.

Guedes Soares C, N. Fonseca, and R. Pascoal, (2008),' Abnormal Wave-Induced Load Effects in Ship Structures', *Journal of Ship Research*, Vol. 52, No. 1, March 2008, pp. 30–44.

Guedes Soares C.(2002), Weisse R, Alvarez E, Carretero J.C., A 40 years hindcast of wind sea level and waves in European waters', *Proceedings of the 21st International conference of offshore mechanics and artic engineering* (OMAE, 2002). NY (USA): ASME;2002(Paper OMAE2002-28604).

Guedes Soares C., and Moan, T. (1991), `Modern uncertainty in the long-term distribution of wave induced bending moments for fatigue design of ship structures', *Marine Structures*, Vol.4, pp294–315.

Guedes Soares, C., "Spectra Modelling of Sea States With Multiple Wave Systems", *Journal of Offshore Mechanics and Arctic Engineering*, vol.114 1992.

Gumbel, E.J. (1958), `Statistics of Extremes, Columbia University Press`, New York,. (375 pages).

Gunther F. Clauss, Janou Henning, Heike Cramer and Stefan Kruger (2003), 'Development of Safer Ships by Deterministic Analysis of Extreme Roll Motions in Harsh Seas', *Proc. 22nd Int. Conference on Offshore Mechanics and Artic Engineering*, vol2,pp135-143**.**

Gunther F. Clauss, Katja Stutz (2002),'Time domain analysis of floating bodies with forward speed*' J. Offshore Mechanics and Arctic Engineering,*' vol.124 pp66-73 .

Gustavo O. Guarniz Avalos and Juan B.V.Wanderley ,(2012),`A two dimensional numerical simulation of roll damping decay of FPSO using the upwind TVD scheme of ROE-SWEBY'`, *Proceeding of the ASME2012 International Conference on Ocean, Offshore and Artic Engineering*, OMAE 2013, Rio de Janeiro, Brazil.

Gustavo O. Guarniz Avalos and Juan B.V.Wanderley ,(2013),'Roll damping decay of a FPSO with bilge keel`, *Proceeding of the ASME2013 International Conference on Ocean, Offshore and Artic Engineering*, OMAE 2013, Nantes France.

Haddara, M. R. (1980), 'On the parametric excitation of non- linear rolling motion in random seas, *Int. Shipbuild. Progress*, vol.27(315), 290–293.

Haddara, M. R. (1984), 'A note on the effect of damping moment form on rolling response; *Int. Shipbuild. Progress*, vol.31(363), 285–290.

Haddara, M. R., & Bennett, P., 1989, "A Study of the Angle Dependence of Roll Damping Moment", *Ocean Engineering*, vol. 16(4), pp. 411-427.

Halvor Lie, Zhen Gao, Torgeir Moan, (2007),' Mooring line damping estimate by a simplified dynamic model**',** *Proceeding of the 26th International Conference on Offshore Mechanics and Arctic Engineering*,(OMAE2007), California USA.

Hamid Zeraatgar, Mohsen Asghari, Firooz Bakhtiari-Nejad (2010), 'A Study of the roll motion by means of a free decay test', *Offshore Mechanics and Artic Engineering. Vol 132 pp1-8.*

Hanne Therese Wist, (2003) 'Statistical Properties of Successive Ocean Wave Parameters', PhD Theses, Department of Marine Technology, Facultyt of Engineering and Technology, Nowegian University of Science and Technology, Trondheim. ISBN 82 771 5669 7. Available online at: www.diva-portal.org/smash/get/diva2:122564/FULLTEXT01.pdf

Hanson J L, and Philips O M (2001),`Automated Analysis of ocean surface directional spectra`, *J. Armos Oceanic Tecnol*; 18:277-93.

Haring R.R., and Heideman J.C. (1978),' Gulf of Mexico rare wave return periods,*'Proc., 10th Annual Offshore Technology Conference*., OTC 3229. Houston TEX., 1523-1536

Haring, R.E., Heideman, J.C., 1978, `Gulf of Mexico rare wave return periods`, *Proc. 10th Offshore Tech. Conf*., OTC 3230, pp. 1537-1550.

Harris R.I. (1999), 'Improvements to the Methods of Independent Storms', *J. Wind Engineering Industrial Aerodynamics*, 80, pp. 1-30.

Hasselmann, K. et.al. (1973) Measurements of Wind Wave Growth and Swell Decay during the Joint North Sea Wave Project. (JONSWAP), Deutsches Hydrographishe Institut Reihe A 12

Hewlett, C., Liles, E., Huddleston, W., McCabe, C., and Battacharjee, S.,(1997), ' Design, Conversion and Installation of an FPSO for Zafiro Field, *Offshore Technology Conference*, paper no. 8427, Houston, May.

Himeno Y., (1981), Prediction of ship roll damping, a state of the art@ Michigan Univ. An Arbor, Dept of Naval Architecture and Marine Technical Report.

Hogben N., Dacunha, N.M.C. and Oliver G.F. (1984) 'Global Wave Statistics' compiled and edited by British Maritime Technology Ltd., Published by Urwin Brothers ltd., England.

Holappa, K.W. and Falzarano, J.M. (1998) 'Application of extended state space to nonlinear ship rolling', *Ocean Engineering*, 26(3), pp. 227-240.

Hopkin M., (2004) 'Snap Shots will Map Frequency of Freak Waves' *Nature*, vol.430, pp 492.

Hosking J.R.M.,(1990), 'L-moments: Analysis and Estimation of Distribution using Linear Combinations of Order Statistics', *J. Royal Statistical Society*, Series B, vol 52,1, pp105-124.

Ikeda, Y., (2004), `Prediction Methods of Roll Damping of Ships and Their Application to Determine Optimum Stabilization Devices'. *Marine Technology*, vol. 41(2), pp. 89-93.

Ikeda Y., Himeno, Y., and Tanaka, N. (1977) 'On eddy making Components of roll damping Forces on Naked Hull', *J. of Japan Society of Naval Architects*, vol. 142.

Ikeda, Y., Himeno, Y., & Tanaka, N., (1978), `A Prediction Method for Ship Roll Damping`, *Report of the Department of Naval Architecture*, University of Osaka Prefecture.

Ikeda Y., Himeno, Y., and Tanaka, N. (1978) ''Components of roll damping of ships at forward speed'', *J. of Japan society of Naval Architects*, vol. 143, pp113-125: ISSN: 0514-8499.

Ikeda, Y., Komatsu, K., Himeno, Y., & Tanaka, N., (1977), "On Roll Damping Force of Ship, Effects of Hull Surface Pressure Created by Bilge Keels", *Journal of Kansai Society of Naval Architects*, vol. 165, pp. 31-40.

IMO,(2006) 'ANEX: Explanatory notes to the interim guidelines for alternative assessment of the weather criterion

Isaacson, M., and Sinha, S., 1986, "Directional Wave Effects on Large Offshore Structures," *Journal of Waterway, Port, Coastal, and Ocean Engineering,* ASCE, vol. 112(4), pp. 482-497.

Ishay Weissman, (1978), 'Estimation of Parameters and Large Quantiles Based on the K-Largest Observations', *J. American Statistical Association*, vol.73,(364),pp812-815.

ITTC-7.5-0207-0.21 (2002): `Recommendation Procedures, Testing and Extrapolation Methods, Loads and Responses, Sea keeping, Experiments`.

ITTC, 2011, "ITTC-Recommended Procedures: Numerical Estimation of Roll Damping", vol. 7.5-02-07-04.5, pp.1-33.

J.H. Vugts, 1968, 'The Hydrodynamic Coefficients for Swaying, Heaving and Rolling Cylinders in a Free Surface', *Report 194*, Laboratorium Voor Scheepsbouwkunde, Technische Hogeschool Delft,.

Jan Beirlant, Elisabeth Joossens, Johan Segers (2002), 'Modelling Excesses Over High Thresholds by Pertubed Generalized Pareto Distributions. Available online: www.eurandom.tue.nl/reports/2002

Jose A. Ferrari Jr. and Marcus Donato A. Ferreira (2002), 'assessment of the effectiveness of the bilge keel as an antiroll device in VLCC-sized FPSOs' ,*Proceedings of the 12th International Offshore and Polar Engineering Connference*. Japan:

Joseph P. Hennessey JR, (1977), 'Some Aspects of Wind Power Statistics', *J. Applied Meteorology*, vol16, 2, pp119-128

Josko P., Maro Corak, Marina P. (2011), 'Wave Height Statistics for Seakeeping Assessment of Ships in the Adriatic Sea', *J. of Ocean Engineering* 38, pp.1323-1330

Joint Committee for Guide in Meteorology JCGM, (2008), 'Evaluation of the measurement data-Guide to the expression of uncertainty in measurement', 1ST ed

Journée, J. M. J. (2001a). 'User Manual of SEAWAY (Release 4.19)'. *Technical Report 1212a*, Delft University of Technology, Ship Hydromechanics Laboratory, The Netherlands.(Internet:http://dutw189.wbmt.tudelft.nl/~johan or http://www.shipmotions.nl).

Kareem A., K.Gurly (1996),'Damping in structures: its evaluation and treatment of uncertainty', *J. Wind Engineering*, vol. 59,pp-157.

Ke Wang, Xi Zhang, Zhi-Qiang Zhang, Wang Xu (2012). 'Numerical analysis of added mass and damping of floating production storage and offloading system', *J. Acta Mechanica Sinica* ,vol28(3) pp870-876

Kelvin Ewans, George Z., Forristall, Olagnon Michael, Marc Prevosto,Sylvie Van Iseghem(2004), `West African Swell Project (WASP), Final report, sponsored by Shell International ,Exploration and Production`.

Kinnas S.A., (2004),'FPSO Roll Motions`, Texas A & M University, *Technical report* No. B157.

Klara Persson and Jesper Ryden (2007),' Exponentiated Gumbel Distribution for Estimation of Return Levels of Significant Wave Height' U.U.DM. Report,

Korvin-Kroukovsky BV, Jacobs WR (1957) Pitching and heaving motions of a ship in regular waves. *Trans Soc Nav Arch Mar Eng*r. 65:590–632.

Kuwashima S. and Hogben N., (1986), `The Estimation of Wave Height and W', *Coastal Engineering*, vol.6,pp303-329.

Lainiotis DG, Charalampous C, Giannakopoulos, Katsikas S (1992) `Real time ship motion estimation`. *Proc. OCEAN'92 conference*, pp. 283–287

Lighthill, J., (1978*)* `Waves in Fluids`, Cambridge University Press, pp. 221-228.

Lindau R. (1995), ‘A New Beaufort Equivalent Scale`, *Proceeding of international COADS and Workshop*s, may, Germany. Pp232-252

Lindsey Wilhoit, Chad Supan, E. Kurt Albaugh, PE of BHP Billiton, Chris (2010),’ World wide survey of Floating production, storage and offloading unit (FPSO), offshore magazine, available online at: www.offshore-mag.com/maps/posters

Lloyd, A.R.J.M. (1989) ‘Seakeeping; Ship Behaviour in Rough Weather`. Ellis Horwood, Chichester, Sussex, United Kingdom.

Longuet-Higgins M.S., Cartwright, D.E., and Smith N.D., (1961), ’On the Joint Distribution of wave Periods and Amplitudes in random sea waves.’ *Proc. 10th symp. on Naval Hydrogn.*, pp597-605.

Longuet-Higgins, (1975),’ On the Joint Distribution of the Periods and Amplitudes of Sea Waves.’ *J. Geophysical Research,* vol. 80(18), pp2688-2694.

Longuet-Higgins, M. S. (1952), On the Statistical Distribution of the Heights of Sea Waves, *J. Mar. Res.*, **11**, 245–266,.

Longuet-Higgins, M.S, Cartwright, D.E., and N.D. Smith,(1963): Observations of the directional spectrum of sea waves using the motions of a floating buoy. *Proceedings Conf of Ocean Wave Spectra conference,* 111-131, Prentice-Hall, Englewood Cliffs, New Jersey

Longuet-Higgins, Michael S. (1980),’ On the distribution of the heights of sea waves: some effects of nonlinearity and finite band *width’, Journal of geophysical research*, 85(C3) pp.1519-1523

Lopez-Cortijo, J., Duggal, A., van Dijk, R. and Dnv, S.M.(2003) 'A New Solution for Floating Production in Ultra Deep Waters'.

Luo, Y. and Baudic, S. (2003), *Proc Thirteenth Int Offshore Polar Eng Conf, Honolulu, Hawaii, USA.*

Marie-Aurelie Kerbiriou, Marc Prevosto, Christophe Maisondieu, Aurelien Babarti, Alain Clement (2007),’ Influence of an improved sea state description on a wave energy converter production’, *Proc. of the 26th international conference on offshore mechanics and artic engineering, California, USA, OMAE2007-29254.*

Marine traffic team, available online @ http://www.marinetraffic.com/users

Marshall P.W. (1976),’ Dynamic and fatigue analysis using directional spectra. *Proc. offshore Technology Conference*, Houston, Paper No. OTC 2537.

Maruo, H. (1960),’ The Drift of a Body floating o waves ,’ *Journal of ship Research* , vo.4, no. 3 pp1-10.

Mashall, P.W.,(1976),'Dynamics and Fatigue Analysis using directional Spectra', *Proc. offshore Technology Conference* , Houston, Paper No. OTC 2537

Melisa Menendez, Fernando J. Mendez, Cristina Izaguirre, Alberto Luceno, Inigo J. Losada (2009),' The Influence of Seasonality on Estimating Return Values of Significant Wave Height', *J. Coastal Engineering* vol 56, pp211-219.

Michael Olagnon, Agbeko Kpogo-Nuwoklo, Zakoua Guede (2014),' Statistical processing of West African wave directional spectra time –series into a climatology of swell events' *J. Marine Systems* vol. 130, pp101-108

Ming-Chung Fang, Jhih-Hong Luo and Ming –Ling Lee(2005),'A nonlinear Mathematical Model for Ship Turning Circle Simulation in Waves', *Journal of ship research* , vol 49,n0 2,pp69-79.

Mostafa M.D. and Mamoud M.W., (1964),' On the Problem of Estimation of the Bivariate Distribution', *Biometrical*, vol.51,3/4, pp522-527

Nathaniel B. Guttman, Hosking J.R.M., James R.Wallis, (1993),' Regional Precipitation Quantile Values for the Continental United States Computed from L-Moments', *J. of Climate,* vol.6,pp2326-2340.

National Oceanic and Atmospheric Administration's (NOAA), National Data Bouy Center (NDBC)', Available online at: http//:www.ndbc.noaa.gov/

Nayfeh, A. H. and Khdeir, A. A. (1986) 'Nonlinear rolling of ships in regular beam seas; *Int. Shipbuild. Progress*, vol.33(379), pp40–49.

Neal, E.,(1974),' Second Order Hydrodynamic Forces due to stochastic Excitation., Proc. 10th ONR SYMPOSIUM, Cambridge, Mass.

Nerzic R., Frelin C., Prevosto M,., Quiniou-Ramus V., (2007);' Joint Distribution Of Wind/Waves/Current In East African And Derivation of Multivariate Extreme I-FORM Contours' *Proceedings of the Seventeenth International Offshore and Polar Engineering Conference*, Portugal

Newland D.E.,(1993),'An introduction to random vibrations and spectra analysis', 3rd edition, Published by Longman, London.

Newman J.N. (1963), 'The exciting forces on fixed bodies in waves' hydrodynamics laboratory research and development report, report 1717: reprint of paper published in *J. Ship research*, SNAME, vol 6(3)

Newman, J.N. (1977),' Marine Hydrodynamics', MIT Press, Cambridge and London, England.

Newmann J.N., (1974),'Second Order Slowly varying Forces on vessels in irregular waves. *Proc. Int. Symp. on Dynamics of Marine Vehicles and Structures in waves*, pp 182-186, London.

Nina Morgan (1990),'Marine Technology Reference book', Butterworths, London.

Nwogu O., Isaacson M.(1991), 'Drift motions of a floating barge in random multidirectional waves,' *J. Offshore Mechanics and Arctic Engineering,*' vol.113 pp37-42.

O.A.Grim, (1960) 'A Method for a more Precise Computation of Heaving and Pitching motions Both In Calm Water And In Waves, *Proc. Symp. Nav. Hydodyn.,* 3rd ACR-65 Off. Nav. Res., Washington, DC, p.483.

Ochi, M., K., Hubble, E., N. (1976). On six-parameters wave Spectra, *Proc. 15th Coastal Eng. Conf.* Vol 1 pp 301-328.

OCIMF(1994),"Prediction of wind and current loads on VLCCs", Witherby and co, England.

Offshore Magazine; (2007) ''Worldwide Survey off Floating Production, Storage and Offloading (FPSO) Units, Houston, USA.

Okey Nwogu,(1989),''Analysis of fixed and floating structures in random multidirectional waves', PhD Thesis, Faculty of Graduate studies, Civil Engineering Department, University of British Columbia, Vancouver, Canada.

Olagnon, M. (2001),"Representativity of some standard spectra models for waves", *Proc. Int. Offshore and Polar Engineering Conf.*, ISOPE Vol. 3, Stavanger, pp. 92-99.

Olagnon, M. & Krogstad, H.E.(1998), "Observed short- and long-term distributions of wave steepness", *Proc. Int. Offshore and Polar Engineering Conf.*, Vol. 3, Montréal, pp. 63–70.

Oliveira A.C., Fernabdes A.C.,(2006), 'The Billinear Behaviour for the FPSO Rolling Motions', *Proceedings of the 9th International Conference on Stability of Ships and Ocean Vehicles*, Brazil.

Oliveira A.C., Fernabdes A.C.,(2010), 'Alternative to model the non-linear roll damping of a FPSO hull', *Proceedings of the ASME 2010 29th International conference on ocean , offshore and artic Engineering*.OMAE 2010, Shangai China.

Oliveira A.C., Fernabdes A.C., (2011), 'Roll damping of Flat bottom Hulls: critique of the quadratic reason'', *J. Marine Technology and Engineering*, Vol.1 Taylor and Frances Group, London Uk.

Oliveira A.C., Fernabdes A.C., (2014), 'The non linear roll damping of FPSO hulls'', *J. of offshore mechanis and artic engineering*, vol.136

Oliver A.S., and Longbin Tao, (2014), 'Experimental Determination of Roll Damping Coefficient for FPSO', *Proceedings of the 33rd International Conference on Ocean, and Artic Engineering*, OMAE2014. California.

Orji C.U., and Woodward M. 'Roll Motion Analysis of FPSO from Free Decay Data in Calm Sea', *Proceedings of the 12th International Marine Design Conference*, IMDC 2015, Tokyo, Japan. Vol 3, pp313-324.

Pablo M. Crrica, Farzad Ismail, Mark Hyman, Shanti Bhushan, Frederick Stern, (2013), "Turn and zigzag manoeuvres of a surface combatant using a URANS approach with dynamic overset grids", *J. Marine Science and Technology (2013),vol 18*,pp166-181.

Palutikof J.P., Brabson B.B., Lister D.H., Adcock S.T. (1999), 'A Review of Methods to Calculate Extreme Wind Speeds', *J. Meteorol. Appl*. vol.6(1), pp119-132

Papanikolaou, A.D. (1988),'NEWDRIFT: The six DOF three dimensional diffraction theory program of NTUA-SDL for the calculation of motions and loads of arbitrarily shaped bodies in regular waves', NTUA-SDL, *Internal Report*, Athens

Pesman, E., Bayraktar, D., & Taylan, M., 2007, "Influence of Damping on the Roll Motion of Ships", *The 2nd International Conference on Marine Research and Transportation* (ICMRT'07), pp. 28-30.

Petya G. Petrova and Guedes Soares C. (2009),' Probability distribution of wave heights in Bimodal seas in an offshore basin' *J. applied ocean research vol 31, pp90-100.*

Petya G. Petrova and Guedes Soares C. (2011),'Wave Height Distribution in Bimodal Sea States from offshore basins' *J. ocean engineering*, vol 38, pp658-672.

Phillips, O., M. (1958) The equilibrium range in the spectrum of wind generated waves. J. Fluid Mech. 4 426-434

Pierson, W., J., Moskowitz L. (1964). A proposed spectra form for fully developed wind sea based on the similarity Theory by Kitaigorodsksii. *J. Geophys. Res.* Vol 69(24) p 5181

Pinkster,J.A.(1976) Low Frequency second order forces on vessels moored at sea,' *Proc. 11th Symp. on Naval Hydrodynamics*, pp 603-615, London.

Remery, G.F.M and Hermans, A. J. (1971) " The Slow Drift 0scillations.of a Moored Object in Random Seas ". *Proc. 3rd Annual Offshore Technology Conference (OTC)*, Dallas, Texas. vol.2, pp829-238.

Robert F. Beck and Bradley King (1989),'Time domain analysis of wave exciting forces on floating bodies at zero forward speed,' *J. Applied Ocean Research*, vol. 11, pp19-25.

Roberts J.B and Spanos P.D., (1990),' Random vibration and statistical linearization', Published by John Wisley & Son's Ltd, England.

Roberts, J. B. and Dacunha N.M.C (1985) 'Roll motion of a ship in random beam waves: comparison between theory and experiment`, *J. Ship Res*., vol. 29(2), pp.112–126.

Roberts, J. B. (1985) 'Estimation of nonlinear ship roll damping from free-decay data`, *J. Ship Res*., vol. 29(2), pp.127–138.

Robert J. Moffat, (1988), 'Describing the Uncertainties in Experimental Results' *J. Experimental thermal and fluid science* vol.1,pp3-17

Rodriguez G., and Guedes Soares (1999),' A criterion for the automatic identification of multimodal sea wave spectra', *J. Applied Ocean Research,* vol.21,pp329-333.

S. Rajendran, N. Fonseca, C. Guedes Soares ,'Simplified body nonlinear time domain calculation of vertical ship motions and wave loads in large amplitude waves', *J. Ocean Engrg*., 107 (2015), pp. 157-177

Salvesen, N., Tuck, E. O., and Faltinsen, O. M. (1970)**,''**Ship motions and sea loads, *Trans. Soc. of Naval Architects and Marine Engineers*, vol.78, pp.250–287.

Sand, S.E., Ottesen Hansen N.E., Klining P., Gudmestad Ove T., Sterndorff Martin J.,(1990), 'Freak Wave Kinematics', *Proc. Water Kinematics, NATO ASI Series E,* vol178, pp535-550.

Selvam R. Panneer and Bhattacharyya (2006),' System Identification of a coupled two DOF moored Floating body in random ocean waves' *J. Offshore Mechanics and Arctic Engineering,*' vol.128, pp191-202.

Sheng Yue (2002),' The Bivariate Lognormal Distribution for describing Joint Statistical Properties of a Multivariate Storm Event', *J. Environmetrics ,* vol.13,pp811-819

Shimamura, Y. (2002) 'FPSO/FSO: State of the art', *Journal of Marine Science and Technology*, 7(2), pp. 59-70.

Shin Y.S., Belenky V.L., Weems K.M., Engle A.H., (2003),' Nonlinear Time Domain Simulation Technology for seakeeping and wave-load Analysis for Modern Ship design', *ABS Technical Papers*. Pp258-281.

Shyh-Kuang Ueng, David Lin, Chich-Hong Liu ,(2008), ''A ship motion simulation system'', Virtual reality.

Snyder, It. L. and C. S. Cox, .1966: A field study of the wind generation of ocean waves. *J. mar. Res. 2(1), 141.*

Solli, D.R., Ropers C., Koonath, P., and Jalali B., (2007) ,' Optical Rogue Waves' *Nature,* vol.450, pp1054-1058

Souza J.R. Jr, A. C. Fernandes, I. Q. Masetti, S. da Silva, S. A. B. Kroff (1998), '' Nonlinear rolling of an FPSO with larger-than-usual bilge keels'', *Proceedings of the 17TH international conference of offshore mechanics and artic engineering* ,OMAE,1998 Portugal.

Spouge, J. R. (1988) 'Non-linear analysis of large-amplitude rolling experiments; *Int. Shipbuild. Progress,* vol.35(403), pp271–320.

Srinivasan Chandrasekaran,(2015),'Dynamic Analysis and Design of Offshore Structures', Springer, New Delhi, India.

ST. Denis, M., and Pierson, W.J. (1953) 'On the motions of ships in confused seas'. *Transactions of the Society of Naval Architects and Marine Engineers*, vol.61, pp280–357

Stephanie Bell (1999),' A Beginner's Guide to Uncertainty of Measurement', *Measurement Good Practice* No.11(Issue2).

Strekalov S., Massel S.(1971),' On the Spectra Analysis of Wind Waves' *Arch. Hydot*., vol. 18,pp 457-85.

Su, H.S., Wang, J., Eleye-Datubo, A.G., Yang, J.B. and Liu, J. (2005), 'Safety assessment of FPSO turret-mooring system using approximate reasoning and evidential reasoning', *Marine Technology*, vol.42(2), pp. 88-102.

Surendran, S., Lee, S.K. and Sohn, K.H. (2007) 'Simplified model for predicting the onset of parametric rolling', *Ocean Engineering*, vol.34(3–4), pp.630-637.

Taghipour, R., Perez, T. and Moan, T. (2008) 'Hybrid frequency–time domain models for dynamic response analysis of marine structures', *Ocean Engineering*, vol.35(7), pp. 685-705.

Taylan, M. (2000) 'The effect of nonlinear damping and restoring in ship rolling', *Ocean Engineering*, vol.27(9), pp. 921-932.

Teena N.V., Sanil Kumar, K. Sudheesh, R. Sajeev (2012), 'Statistical Analysis on Extreme Wave Height', *J. National Hazards* vol 64, pp223-236.

Theory Manual: MAESTRO-Wave Theoretical Background, available on MAST computer Cluster, Newcastle University, UK

Thor I. Fossen (2012), 'How to Incorporate Wind, Waves and Ocean Currents in the Marine Craft Equations of Motion.

Thor I.Fossen, (2011),`Handbook of Marine Craft Hydrodynamics and Motion Control",

Tian X, Yang J., Lu H., 2010,' Development of data analysis program for the offshore engineering hydrodynamics model test,' *Research and exploratory in Laboratory* . vol 29(6)

Toffoli Alessandro, Lefevre Jean Michel, Monbaliu Jaak, Bitner-Gregersen Elzbieta (2004), 'Dangerous Sea-States for Marine Operations', *Proc. of the 14TH Int. Offshore and Polar Engineering Conference*, France, pp85-92.

Toffoli Alessandro, Lefevre Jean Michel, Monbaliu Jaak, Bitner-Gregersen Elzbieta (2004), 'Dangerous Sea-States for Marine Operations', *Proc. of the 14TH Int. Offshore and Polar Engineering Conference*, France, pp85-92.

Torsethaugen K. A., (1993),' A two peaked wave spectrum model', *Proc. of the 12th International Conference on Offshore Mechanics and Artic Engineering. OMAE, NewYork, USA ,Vol.2,pp175-180.*

Torsethaugen, K. (1994), `Model for a doubly peaked spectrum. Lifetime and fatigue strength estimation implications. International Workshop on Floating Structures in Coastal Zone, Hiroshima, November 1994.

Torsethaugen, K. (1996). `Simplified double peak spectra model for ocean waves`. *SINTEF report STF22 A96204*, paper no.2004, JSC 193.

Triantafyllou MS, Bodson M, Athans M (1983) Real time estimation of ship motions using Kalman filtering techniques. IEEE *J. Oceanic Engrg* 8(1):9–20.

Tristan Perez and Thor I. Fossen (2003),`A 4-Dof Simulink Model of a Coastal Patrol Vessel for Maneuvering In Waves, 2003.

Tupper E.C., (2004), 'Introduction to Naval Architecture, 4th ed., Elsevier Butteworth-Helnemann, UK., p89.

Turan, O. and Zhao, E. (2001) 'Stability of FPSOs in Extreme Environment; *Proceedings of the International Conference on Offshore Mechanics and Arctic Engineering*-OMAE, Rio de Janeiro. Available at:

United Nations Cartographic section, department of field support, map library. Available online: http//www.un.org/dept/cartographic

Van Iseghem, S., Deleuil, G. & Guérin, P. `Improved characterizations for design waves` *Proc. Int. Offshore and Polar Engineering Conf.*, ISOPE Vol.3, Stavanger (2001).

Veer van't R., and Fathi F., (2011), 'On the roll damping of an FPSO with Riser balcony and bilge keels', Trans. RINA,. vol 153, Part A2, pp.A125-A135, *International J. of Maritime Engineering,* April-June.

Voltera V. (1930), 'Theory of functionals', Dover Publications, New York.

Walter H. Michael(1999),'Sea Spectra revisited ', *J. Marine Technology*, vol 36,no.4, pp211-227.

Wanderly , J.B. V.., Ramiro, A., Reis, T., Fernades A.C., and Levi C.,(2007), 'Numerical simulation of roll damping of A FPSO', *26th International Symposium on Offshore Mechanics and Artic Engineering* (OMAE), .Paper no.OMAE2007-29017, San Diego.

Washington Monthly (2012) National, Texas A & M University,

Wave Introduction., Available online at: http://www.wamwatt.tmd.go.th/wave-intro.html

Wishers J., (2013), 'Guide to single point moorings`, Wmooring inc. Houston. Texas, USA.

Wu, W. and McCue, L. (2008) 'Application of the extended Melnikov's method for single-degree-of-freedom vessel roll motion', *Ocean Engineering*, vol.35(17-18), pp.1739-1746

Yang, B., Wang, Z.-c., & Wu, M., 2012, "Numerical Simulation of Naval Ship's Roll Damping Based on CFD", *Procedia Engineering*, vol. 37, pp. 287-293.

Yeung, R. W., and Ananthakrishman, P., (1992),' Oscillation of a Floating Body',J. Engineering Maths., 26,pp211-230.

Ying Min Low and Robin S. Langley (2008), 'Understanding the dynamic coupling effects in deep water floating structures using a simple model' *J. Offshore Mechanics and Arctic Engineering,*' vol.130, pp1-10.

Yingguang Wang and Yiqing Xia (2013),' Calculating Nonlinear Wave Crest Exceedance Probabilities using a Transformed Rayleigh Method' *J. Coastal Engineering* vol 78,pp1-12.

Yonghwan Kim, Kyong-Hwan Kim, Jae-Han Kim, Taeyoung Kim, Min-Guk Seo and Yooil Kim. (2011),'Time domain analysis of nonlinear responses and structural loads on ships and offshore structures: development of WISH programs', *J. Nav Architect Oc Engng*. vol.3, pp37-52.

Yoshimi Goda, Masanobu Kudaka, Hiroyasu Kawai (2010),'Incorporation of Weibul Distribution in L-Moments Method for Regional Frequency Analysis of Peaks-Over Threshold wave heights', *Proc. of 32nd International Conference on Coastal Engineering, China.*

Yoshiyuki Inoue and Islam M.R. (1999) 'Relative Motions of Multiple Floating Offshore Structures' *Proc. International Conference of Offshore Mechanics and Artic Engineering OMAE,* Newfoundland, Canada. pp 361-368.

Yoshiyuki Inoue and Kamruzzaman (2008), 'Analysis of hydrodynamic characteristics for arbitrary multihull ships advancing in waves', *J. Marine Sci. Technol.*, vol. 13, pp231-243.

Yue Gu, Sandy Day, Evangelos Boulougouris (2015) 'A Study of the effects of bilge keels on the roll damping coefficient' *Proc. International Conference of on stability of ships and ocean Vehicles,* 14-19 June, Glasgow, UK.

Yuki, Kawahara, Kazuya Maekawa, Yoshiho Ikeda (2009), 'A simple Formular of roll damping of conventional cargo ships on the basis of Ikeda's Method and its Limitation', *Proceedings of the 10th International Conference on Stability of Ships and Ocean Vehicles,* Russia. Vol 6,pp387-398.

Zhang X, Jin Y, Yin Y, Li Z (2004), `Ship-simulation using virtual reality technique. *In: ACM Siggraph International conference on virtual reality continuum and its applications in industry*, pp 282–285.

Zhao WenHua, Yang JianMin, Hu ZhiQiang, XIAO LongFei and PENG Tao (2013)' Experimental and numerical investigation of the roll motion behaviour of a floating liquefied natural gas system'. *Sci Chiina-Pys Mech Astron*, 56:629-644, doi:10.1007/s11433-012-4914-3.

Zhao X, Xu R, Kwan C (2004),' Ship-motion prediction: algorithms and simulation results'. *In: IEEE International conference on acoustics, speech, and signal processing*, pp 125–128.

APPENDICES

Appendix A Data Collated for FPSO Operating Around West African Region

s/no	country	vessel name	owner/operator	location(lat E/long. N	operating depth(m)	reserve/total wells (MMBOE)	max. prod.pday (MBOPD)	classification	length(oal(m)	lpp (m)	breadth(m)	depth (m)	max depth (m)	Freeboard(m)	Min. model scale req(k)	slenderness ratio(L/B)	slenderness ratio(L/D)	dead weight(TONNES)	gross tonnage(tonnes)	net tonnage (tonnes)	storage capcity(MBBLs)	mooring system/type	number of anchor legs
1	Cote D'voire	BAOBAB IVOIRIEN MV 10	MODEC/CAR international	4.971095E / -4.544778S	970	123/8	70	ABS	390	350.75	60	28.32	24	3.044	808.3333	6.5	13.77118644	344289	167349	138001	2000	ET/P	8
2		ESPOIR IVOIRIEN	PROSAFE/CNRL interntinal		120	105/12	40	DNV	269		54	20	15	5	100	4.981481	13.45	132500	77985		1100	IT/6	6
3	Ghana	KWAME NKRUMAH MV21 (JUBILE	MODEC/TULLOW	-2.55/ 4.38	1100		120		358.6	317.48	59	29.7		10.02	916.6667		12.07407407	240550.01	151542	76586	1600		
4	Nigeria	ABO	PROSAFE/ENI		550	82/6	44	ABS	280.422	268	54.6	20	15	4.692	458.3333	5.135934	14.0211	155612	80025	48091	932	SM/P	12
5		AGBAMI	CHEVRON/NNPC	3.462613 / 5.560596	1462	770/37	250	ABS	319.994	319.994	58.399	31.988	-	8.023	1218.333	5.479443	10.00356384	337859	198470	112355	1800	-	-
6		AKPO	TOTAL/TOTAL	3.139782 / 6.82248	1325	620/44	240	BV	310		61	31			1104.167	5.081967	10	345000	186448	116000	2000	SM/P	12
7		ARMADA PERKASA	BUMI ARMADA/AFREN AMNI	4.40481/7.829307	164	-/7	27	ABS	211		46	23	17	6	136.6667	4.586957	9.173913043	58557	32666		360	SM/P	10
8		ARMADA PERDANA	BUMI ARMADA/ENII	5.387987 / 4.591458	1100		45	ABS	298.275	283	46	22.55		5.203	916.6667	6.484239	13.22727273	159587.7	84065	60261	1000		
9		BERGE OKOLOBA TORU LPG	BW OFFSHORE/SHELL		134			DNV	216		34	19	13	6	111.6667	6.352941	11.36842105	55173			472	SM	
10		BONGA	SHELL/SHELL	4.557463 / 4.616295	1250	1000/16	170	LRS	305		58	32	23	9	1041.667	5.258621	9.53125	312500	174662		1400	SM	
11		ERHA	EXXON/MOBIL	5.356342 / 4.342041	1180	1000/25	250	DNV	285		64	33	24	9	983.3333	4.453125	8.636363636	375000	188758		2200	SM	
12		KNOCK ADOON	FRED OLSEN/ADAX PETROLEUM	4.222172 / 8.335898	37		70	DNV	207		54	26	19	7	30.83333	3.833333	7.961538462	239781	133940		1700	SM	
13		MYSTRAS	AENR/AGIP NINGERIA	3.991248/7.290635	72	240/10	100	ABS	271	260	44	22.4	17	5.409	60	6.159091	12.09821429	138930	76053	56710	1035	SM/P	12
14		SEA EAGLE	SHELL/SHELL	5.547928/5.724983	375	394/20	200	LRS	274		50	28	20	8	312.5	5.48	9.785714286	207000	112334		920	JSY/P	12
15		SENDJE BERGE	BW OFFSHORE/ADAX PETROLEUM	3.852367 / 6.9799	140	40/8	38	DNV	350		52	27	22	5	116.6667	6.730769	12.96296296	274333	133871		920	SM/P	12
16		TRINITY SPIRIT	ConocoPhillips/Shebah E&P	-	85	48/7	20	ABS	337.0539	319.9973	54.982	26.9992	18	6.007	70.83333	6.130259	12.48384767	274779	132995	99817	1700	SM/P	8
17		USAN	TOTAL/TOTAL	3.573412/7.3932	750	500/42	180	BV	320		61	32	25	7	625	5.245902	10	353200	199340		2000	SM/P	9
18	Equitorial guinea	ASENG	SBMO/NOBLE	3.37389 / 9.137212	1000	-/8	80		330.3	310	56	29.5	19.8	9.7	833.3333	5.898214	11.19661017	255502	144072	75629	1600	IT/P	
19		SENDJE CEIBA	BV OFFSHOR/ARMADA HESS	1.409333 / 9.228333	800	356/28	160	DNV	265		52	27	22	5	666.6667	5.096154	9.814814815	274473	133969		2000	SM/P	12
20		SERPENTINA	EXXON MOBIL/SBMO	3.801773 / 8.078613	475	994/20	110	DNV	362		56	29	22	7	395.8333	6.464286	12.48275862	307431	151123		1900	SM/P	12
21		ZAFIRO	EXXON MOBIL/EXXON MOBIL & GE PET.	N/A	180	993/38	80	ABS	331		56	27	20	7	150	5.910714	12.25925926	263933	133118		1900	SM/P	13
22	Gabon	KNOCK ALLAN	FRED OLSEN/CNRL international	-3.135895 /10.21237	100		35	DNV	274		44	24	17	7	83.33333	6.227273	11.41666667	145242	79902		1300	SM	
23		PETROLEO NAUTIPA	JV - Prosafe/Fred.Olsen/ Vaalco energy	-3.757005 / 10.52771	142		20	DNV	255		44	23	16	7	118.3333	5.795455	11.08695652	141330	71176		1080	SM/P	8
24	Congo	AZURITE FDPSO (royal viking)	PROSAFE /MURPHY	N/A	1400	75/10	40	DNV	322.22	311.77	56	29.5	19.667	9.833	1166.667	5.753929	10.92271186	259999	20240	58256	1400	SM/P	12
25		CONKOUATI	Perenco/Perenco	N/A	114	500/30	35	ABS	324.9686	310.893	48.1066	26.4658	20	6.074	95	6.755177	12.27881266	232922	112848	71334	1420	SM/P	12
26		N'KOSSA LPG FPU	Maersk/total	N/A	120		65	BV	219		37	20	11	9	100	5.918919	10.95	48924			1000	ET/P	9
27	Angola	ANGOLA PSVM	MODEC/BP	-6.240392/10.73273	1980	600/48	157	BV	333	314.76	57.5	31.5	22.22	9.28	1650	5.791304	10.57142857	296230	168674	93837	2000	ET	
28		DALIA	TOTAL/TOTAL	-7.685988 / 11.76194	1360	940/67	35	BV	300		59	32	23	9	1133.333	5.084746	9.375	329000	194665		916	ET/P	9
29		GIMBOA	Saipem/SONAGOL	-7.542833 / 12.16867	711	7 /7	60	ABS	337		54.5	27	21	6	592.5	6.183486	12.48148148	273777	134033		1800	SM	12
30		GIRASSOL	TOTAL/TOTAL		1410	700/40	60	BV	300		60	31	23	8	1175	5	9.677419355	343000	171959		525	IT/P	10
31		GREATER PLUTONIO	BP/BP	-7.84955 / 12.11152	1200	1166/43	155	BV	310		58	32	-		1000	5.344828	9.6875	360000	181173		950	IT/P	14
32		KIZOMBA "A"	EXXON MOBIL/EXXON MOBIL	14.6848 / -17.3975	1180	1000	250	DNV	285		63	32	24	8	983.3333	4.52381	8.90625	375000	187864		2200	SM	
33		KIZOMBA "B"	EXXON MOBIL/EXXON MOBIL	39.56237 / 2.628395	1016	1000	100	DNV	285		60	32	24	8	846.6667	4.75	8.90625	340660	188203		940	IT/D	9
34		KUITO	JV - SBMO/Partner/CHEVRON		373	/33	100	ABS	335	319	44	28	21	7	310.8333	7.613636	11.96428571	220000	112539		1400	SM/P	12
35		MONDO	JV - SBMO/Partner/EXXON MOBIL	-6.174109 / 11.32415	728	/17	100	ABS	337.0539	319.9973	54.4982	26.9992	21	6.006	606.6667	6.184679	12.48384767	262460	132206	103147	2100	ET/P	9
36		OCEAN PRODUCER	Oceaneering/SONAGOL	22.58957 / 120.3046	73	28/8	20	ABS	240	230	36	18	13	5	60.83333	6.666667	13.33333333	720250	42113		510	SM/P	8
37		PAZFLOR	TOTAL/TOTAL	-7.592669 / 12.11043	823	/49	160		325		61	30			685.8333	5.327869	10.83333333	346089	209116		2000	SM	
38		SANHA LPG FPSO	JV - SBMO/Partne/CHEVRON		58			ABS	264		49	29	13	16	48.33333	5.387755	9.103448276	92700	111246		362	ET/P	9
39		SAXI-BATUQUE (KIZOMBA C)	JV - SBMO/Partne/MOBIL	-6.32126 / 11.33311	760	/20	100	ABS	369		56	29	22	7	633.3333	6.589286	12.72413793	295000	150762		2000	ET/P	10
40		XIKOMBA	JV - SBMO/Partner/EXXON MOBIL	1.299475 / 103.6542	1300	/7	90	ABS	366.09	329.2	51.8	25.6	21	5.615	1083.333	7.067375	14.30039063	255920	124176	97756	1840	ET/P	9
41	UK (sim in Lab)	SCHIEHALLION	BP/BP	60.35674/ -4.06498	425	663/29	90	LRS	245		45	27	20	7	354.1667	5.444444	9.074074074	154000	85000		100	IT	12

Data source: **key** shallow <304.8m (1000') SALM-Single Anchor Leg Mooring CONSTRUCTION TYPE

ABS, available online at: www.eagle.org/safenet/record deep >304.8m(1000'), < 1532.9m(5000') JSY-Jacket Soft Yoke C-Conversion

Lindsey et al (2010) ultra deep > 1532.9m(5000'), < 3047.9m(10,000') SM-Spread Moored N-New build

FPSO World fleet.com MOORING SYSTEM TYPE RTM-Riser Turret Mooring slenderness ratio(L/B)(strip theory can be applied to >=2.5)

Marine traffic team, available online @ http://www.marinetraffic.com/users IT-Internal Turret ET-External Turret SALS-Single Anchor Leg System Min. model scale req(k), wrt ncl towing tank depth (1.2m)

CALM-Catenary Anchor Leg Mooring

Appendix B Spectra Representations

1. Bretchneider:

   $S(\omega) = \frac{A}{\omega^5} * e^{-(\frac{B}{\omega^4})}$

   $A = \frac{487.{H_s}^2}{{T_o}^4}$; $B = \frac{1949}{{T_o}^4}$ or

   $A = 2964.8892 * {H_s}^2 * {\omega_o}^4$; $B = 1.2505 * {\omega_o}^4$

   Note: $S(f) = 2\pi * S(\omega)$

2. JONSWAP (JSS)

   $\lambda = 3.3$

   $J = e^{-(\frac{(1-\frac{\omega}{\omega_o})^2}{2\sigma^4})}$

   $\sigma = 0.07 \ for \ \omega < \omega_o \quad ; \quad \sigma = 0.09 \ for \ \omega > \omega_o$

   $C_j = \lambda^J$

   $S(\omega) = 0.658 * C_j * \frac{A}{\omega^5} . e^{-(\frac{B}{\omega^4})}$

3. JONSWAP-Glenn (JSG)

   $\lambda = 3.3$

   $J = e^{-(\frac{(1-\frac{\omega}{\omega_o})^2}{2\sigma^2})}$

   $\sigma = 0.07 \ for \ \omega < \omega_o \quad ; \quad \sigma = 0.09 \ for \ \omega > \omega_o$

   $C_j = \lambda^J$

   $C_{jm} = \frac{5*mo}{f_o} / \left(1.15 + 0.1688 * \lambda - \left\{\frac{0.925}{1.909+\lambda}\right\}\right)$

   $S(\omega) = C_{jm} * \left(\frac{\omega}{\omega_o}\right)^{-5} * C_j * e^{(-1.25*\left(\frac{\omega}{\omega_o}\right)^{-4})}$

4. Lognormal (like Gaussian swell; ref Orkaflex manual)

   $\sigma_{nd} = \frac{a}{{T_o}^b}$; a, b are location dependent variables (see DNV recommendation)

   $\sigma = \sqrt{ln\left[\left(\frac{\sigma_{nd}}{f_o}\right)^2 + 1\right]}$

   $\bar{\mu} = \ln(fo) + \sigma^2$

$$mo = \frac{{H_s}^2}{16}$$

$$S(f) = \frac{mo}{f*\sigma*\sqrt{2\pi}} . e^{-(\frac{-[\ln(f)-\bar{\mu}]^2}{2\sigma^2})}$$

5. Triangular

   m=6 (see DNV recommendation)

   $$Sp = \frac{2m(m-1)*mo}{(2m-1)*f}$$

   $fc = \frac{(m-1)}{m}$ (Width of triangular family to ensure good fit)

   $fr1 = fc * f_o; \quad fr2 = (1/fc) * f_o;$ (in Hz)

   $wr1 = fc * \omega_o; \quad wr2 = (1/fc) * \omega_o;$ (in rad/s)

   $S(f) = Sp * \left[m * \frac{f}{f_o} - (m-1)\right]$ (for f > *fc*f_o and f < f_o*)

   $S(f) = Sp * \left[m - (m-1) * \frac{f}{f_o}\right]$ (for f >= *fc and f < f_o/fc*)

   $S(f) = 0$ (Elsewhere)

6. Ochi-Hubble six parameter spectrum

   $$S(\omega) = \sum_{j=1}^{2} S_j(\omega)$$

   $$S_j(\omega) = \left[\frac{4\lambda_j+1}{4} * \left(\frac{\omega_{oj}}{\omega}\right)^4\right]^{\lambda_j} * \frac{{H_{sj}}^2}{4\omega*\Gamma(\lambda_j)} * e^{\left[-\frac{4\lambda_j+1}{4}*\left(\frac{\omega_{oj}}{\omega}\right)^4\right]}$$

   j=1 for combined swell seas component

   j=2 for wind sea component

Appendix C Approach for short crested sea formulation

$$\boldsymbol{S(\omega,\theta)} = \sum_{\boldsymbol{k=0}}^{\boldsymbol{N}} \boldsymbol{S_k(\omega,\theta,\Xi_k)} \quad \text{(C.1)}$$

A more generalized spread function can be written as

$$f(\omega,\theta,m) = \begin{cases} k_m.cos^{2m(\omega)}(\theta) & \theta < 90^0 \\ 0 & \theta \geq 90^0 \end{cases} \quad \text{(C.2)}$$

Where: $k_m = \frac{\Gamma(m(\omega)+1)}{2\sqrt{\pi}\,\Gamma(m(\omega)+1/2)}$ (C.3)

Is a normalizing parameter such that

$\int_{-\pi/2}^{\pi/2} f(\theta)d\theta = 1$ is true (C.4)

With the power of angular spreading been

$$m(\omega) = m_p\left(\frac{\omega}{\omega_p}\right)^{\beta} \quad \text{(C.5)}$$

$$\begin{cases} m(\omega) = m_p\left(\frac{\omega}{\omega_p}\right)^{5} & \text{if } \omega \leq \omega_p \\ m(\omega) = m_p\left(\frac{\omega}{\omega_p}\right)^{-2.5} & \text{if } \omega > \omega_p \end{cases} \quad \text{(C.6)}$$

For

$m_p \to \infty$, narrow bandedness, waves are long crested

$m_p \to 0$ broad bandedness, waves are short crested

And $\theta\, is$ the azimuth measured counter-clockwise from the principal wave direction, which also represents

Which means,

For k=0:

$$S_0(\omega,\theta) = S(\omega,\theta,\Xi_0) = S_0(\omega).f_0(\theta) \quad \text{(C.7)}$$

For k=1: bimodal

$$S_1(\omega,\theta) = S(\omega,\theta,\Xi_1) = S_1(\omega).f_1(\theta) \quad \text{(C.8)}$$

For k>2: multimodal

$$S_k(\omega,\theta) = S(\omega,\theta,\Xi_k) = S_k(\omega).f_k(\theta) \quad \text{(C.9)}$$

Where the value of $S_k(\omega)$ is the one peaked spectrum for the k, computed using any of the best idealized spectra for the pattern and the element of the $\boldsymbol{\Xi_k}$ $domain.$ The sum of the individual targets using equation 38:

$$S^*(\omega,\theta) = \sum_{k=0}^{N} S_k{}^*(\omega,\theta,\Xi_k) \quad \text{(C.10)}$$

Used as a target spectrum for the minimization of equation A7.28, using the random linear search algorithm or least square method.

$$\boldsymbol{J^{(N)}(\Xi) = \sqrt{\int_0^{\infty}\int_0^{2\pi}[S^*(\omega,\theta) - S(\omega,\theta,\Xi)]^2 \; d\omega.d\theta}} \quad \text{(C.11)}$$

Subject to the constraint

$$\left|\omega_p^{(k)} - \omega_p^{(l)}\right| \geq \delta\omega \quad \text{(C.12)}$$

$$\left|\theta_p^{(k)} - \theta_p^{(l)}\right| \geq \delta\theta \quad \text{(C.13)}$$

$$k,l = 0,N \quad and \quad k \neq j$$

This is done to determine the maximum or peak values of the overall multi-peaked spectrum values. The integration can be performed using Simpson's or Trapezoidal rules within the total frequency and direction domain

$$\phi = \bigcap_{k=0}^{l} \phi_k \qquad : \; \omega,\theta \; \epsilon \; \phi_k \quad \text{(C.14)}$$

Defined by discretised values of $\omega \; and \; \theta$ forming constant interval grid points ($d\omega.d\theta$) for simplification,

Where k=0 represents the wind wave which could be modelled using any of the idealized spectra and k=N represents the number of swell components.

$$\Xi_k = \left(m_{0,}^k\, \omega_{p,}^k \theta_p^k, n_k, m_p^k, \mathrm{A}_\theta^k, \beta_k\right) \qquad \text{(C.15)}$$

are the set of parameters required for approximation of the given spectrum k. subscript p, depicts the value of parameter at the modal points of the wave spectrum. For each system of k=0,N set of $\Xi_k = \left(m_{0,}^k\, \omega_{p,}^k \theta_p^k, n_k, m_p^k, \mathrm{A}_\theta^k, \beta_k\right)$ is required for the solution. For dimensional pruning, we can consider independence of $m(\omega)$ in equation. C2 not dependent on frequency, this will reduce

$$m(\omega) = m_p\ ,\ \mathrm{A}_\theta^k = \beta_k = 0, \qquad \text{(C.16)}$$

Whereas,

$m_{0,}^k\, \omega_{p,}^k \theta_p^k$, are obtained from the spectra directly, $n_k, m_p, \gamma_{p\ ,,}$are fixed parameters defining the spectra used and the spreading function considered. If the simple cosine square spread is considered, $m_p = 1, k_m = 2/\pi,$, and for Pierson-Moskowithz spectrum $n_k = 5$, for JONSWAP , $\gamma_p = 3.3, etc.$

The algorithm of the random search technique is

$\Xi_{k+1} = \Xi_k + \varepsilon_k . \overrightarrow{e_k}$

$\varepsilon_{k+1} = \varepsilon_k . \varphi_1$ for $J^N(\Xi_{k+1}) < J^N(\Xi_k)$

$\overrightarrow{e_k} = \vec{e}_{k-1}$

IF k+1 iteration is successful

Else

$\Xi_{k+1} = \Xi_k$

$\varepsilon_{k+1} = \varepsilon_k . \varphi_2$ for $J^N(\Xi_{k+1}) \geq J^N(\Xi_k)\ and\ \Xi_{k+1} \in R$

$\vec{e}_{k+1} = rand(\vec{e}_l),$

$for\ l = 1\ to\ m$

See details of computation in (Boukhanovsky and Guedes, 2009; Ochi and Hubble, 1978)

Appendix D Possible error sources and remediation's.

1. Error from the mass measuring equipment, meter rule for distance measurement, digital protractor for angle of inclination during inclination test and actual experiment.

2. Accuracy of the ballasting to desired depth, error from reading parallax: however, counting on the accuracy level of the marked-out lines on both sides, this was reduced considerable

3. Error due to the convex nature of the water-hull surface**.**

4. Unsteady nature of the water surface to capture the solid body mode: time was allowed to enable a comparatively steady mode to be reached before capturing of solid mode was made. This timing was maintained between successive experiments, enabling waves to die out before commencing the nest run.

5. Reading/setting of initial angle of inclination before release is done: the accuracy of the digital protractor was employed to reduce error in this regard

6. Slight movement of the ballast weights during the roll motion of model: this was however mitigated to an appreciable extent using rubber strips and floaters to keep weight in stable position**.**

7. The time difference between the let-go-off model at initial angle position and the commencement of the reading by the equipment (human error: operator and the experimentalist).

8. Wave Reflection from the tank walls which subsequently interfere with the actual motion response. These waves are created by the motion of the hull form on the water mass and are tagged radiated waves. They travel outwards and return as reflected waves upon hitting a stationary, non-absorbing mechanism. If the distance is not appreciable and the model motion is still on, they interfere with the actual motion mode. To reduce this, the model is kept at the central location of the 3.8m towing tank, and the time of observed reflection was also taken into consideration. It however varied for the different depths and initial angle combinations, with an average range of 20-3

Appendix E Vessel line diagram

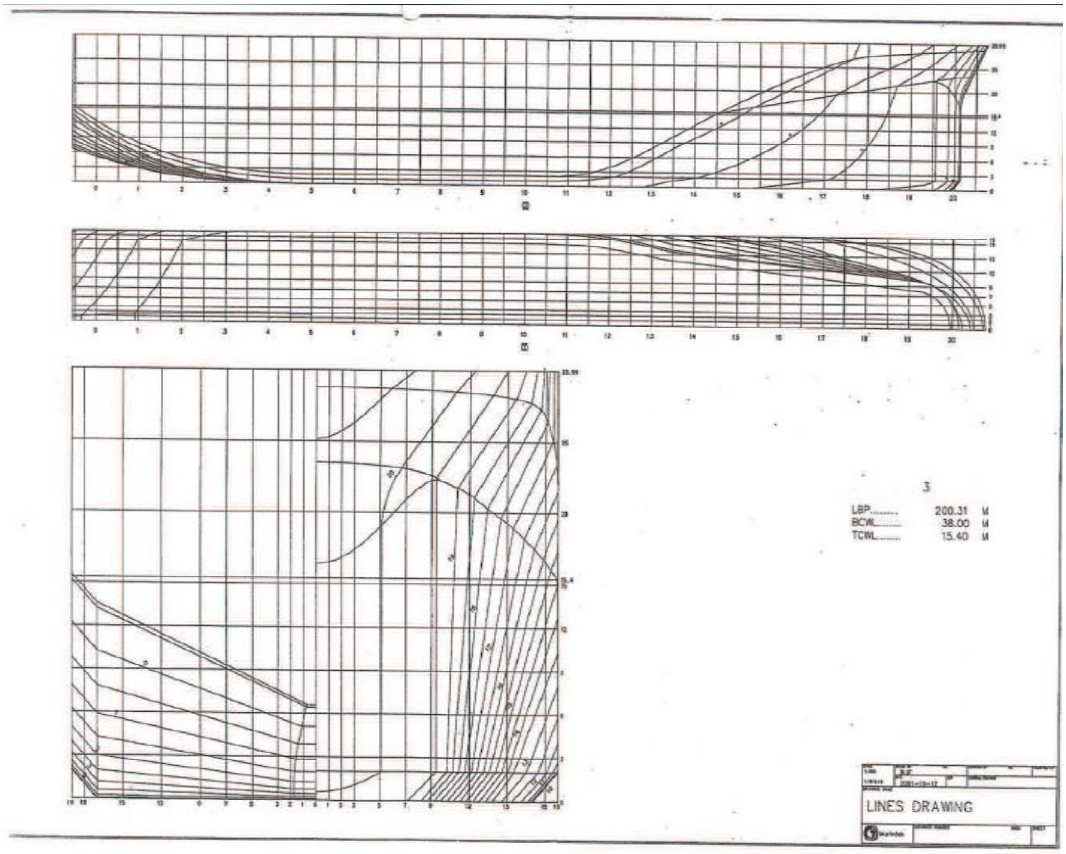

Appendix F Comprehensive test matrix

Free Decay (T1)

S/NO	Bilge keel	draft (load condition)	Initial Angle(a)	Designation
1	Bk0	df1	a1	T1Bk0df1a1
2			a2	T1Bk0df1a2
3			a3	T1Bk0df1a3
4		df2	a1	T1Bk0df2a1
5			a2	T1Bk0df2a2
6			a3	T1Bk0df2a3
7		df3	a1	T1Bk0df3a1
8			a2	T1Bk0df3a2
9			a3	T1Bk0df3a3
10	Bk1	df1	a1	T1Bk1df1a1
11			a2	T1Bk1df1a2
12			a3	T1Bk1df1a3
13		df2	a1	T1Bk1df2a1
14			a2	T1Bk1df2a2
15			a3	T1Bk1df2a3
16		df3	a1	T1Bk1df3a1
17			a2	T1Bk1df3a2
18			a3	T1Bk1df3a3
19	Bk2	df1	a1	T1Bk2df1a1
20			a2	T1Bk2df1a2
21			a3	T1Bk2df1a3
22		df2	a1	T1Bk2df2a1
23			a2	T1Bk2df2a2
24			a3	T1Bk2df2a3
25		df3	a1	T1Bk2df3a1
26			a2	T1Bk2df3a2
27			a3	T1Bk2df3a3

Regular wave (T2)

S/NO	Bilge keel	draft (load condition)	Wave freq. set	Direction (q)	Designation
1	Bk0	df1	w1	q1	T2Bk0df1w1q1
2				q2	T2Bk0df1w1q2
3			w2	q1	T2Bk0df1w2q1
4				q2	T2Bk0df1w2q2
5			w3	q1	T2Bk0df1w3q1
6				q2	T2Bk0df1w3q2
7			w4	q1	T2Bk0df1w4q1
8				q2	T2Bk0df1w4q2
9			w5	q1	T2Bk0df1w5q1
10				q2	T2Bk0df1w5q2
11			w6	q1	T2Bk0df1w6q1
12				q2	T2Bk0df1w6q2
13		df2	w1	q1	T2Bk0df2w1q1
14				q2	T2Bk0df2w1q2
15			w2	q1	T2Bk0df2w2q1
16				q2	T2Bk0df2w2q2
17			w3	q1	T2Bk0df2w3q1
18				q2	T2Bk0df2w3q2
19			w4	q1	T2Bk0df2w4q1
20				q2	T2Bk0df2w4q2
21			w5	q1	T2Bk0df2w5q1
22				q2	T2Bk0df2w5q2
23			w6	q1	T2Bk0df2w6q1
24				q2	T2Bk0df2w6q2
25	Bk1	df1	w1	q1	T2Bk1df1w1q1
26				q2	T2Bk1df1w1q2
27			w2	q1	T2Bk1df1w2q1
28				q2	T2Bk1df1w2q2
29			w3	q1	T2Bk1df1w3q1
30				q2	T2Bk1df1w3q2
31			w4	q1	T2Bk1df1w4q1
32				q2	T2Bk1df1w4q2
33			w5	q1	T2Bk1df1w5q1
34				q2	T2Bk1df1w5q2
35			w6	q1	T2Bk1df1w6q1

36				q2	T2Bk1df1w6q2
37		df2	w1	q1	T2Bk1df2w1q1
38				q2	T2Bk1df2w1q2
39			w2	q1	T2Bk1df2w2q1
40				q2	T2Bk1df2w2q2
41			w3	q1	T2Bk1df2w3q1
42				q2	T2Bk1df2w3q2
43			w4	q1	T2Bk1df2w4q1
44				q2	T2Bk1df2w4q2
45			w5	q1	T2Bk1df2w5q1
46				q2	T2Bk1df2w5q2
47			w6	q1	T2Bk1df2w6q1
48				q2	T2Bk1df2w6q2
49	**Bk2**	df1	w1	q1	T2Bk2df1w1q1
50				q2	T2Bk2df1w1q2
51			w2	q1	T2Bk2df1w2q1
52				q2	T2Bk2df1w2q2
53			w3	q1	T2Bk2df1w3q1
54				q2	T2Bk2df1w3q2
55			w4	q1	T2Bk2df1w4q1
56				q2	T2Bk2df1w4q2
57			w5	q1	T2Bk2df1w5q1
58				q2	T2Bk2df1w5q2
59			w6	q1	T2Bk2df1w6q1
60				q2	T2Bk2df1w6q2
61		df2	w1	q1	T2Bk2df2w1q1
62				q2	T2Bk2df2w1q2
63			w2	q1	T2Bk2df2w2q1
64				q2	T2Bk2df2w2q2
65			w3	q1	T2Bk2df2w3q1
66				q2	T2Bk2df2w3q2
67			w4	q1	T2Bk2df2w4q1
68				q2	T2Bk2df2w4q2
69			w5	q1	T2Bk2df2w5q1
70				q2	T2Bk2df2w5q2
71			w6	q1	T2Bk2df2w6q1
72				q2	T2Bk2df2w6q2

Irregular wave test (T3)

S/NO	Bilge keel	draft (load condition)	Wave set	Direction (q)	Designation
1	**Bk0**	df1	Hs1	q1	T3Bk0df1Hs1q1
2				q2	T3Bk0df1Hs1q2
3			Hs2	q1	T3Bk0df1Hs2q1
4				q2	T3Bk0df1Hs2q2
5			Hs3	q1	T3Bk0df1Hs3q1
6				q2	T3Bk0df1Hs3q2
7		df2	Hs1	q1	T3Bk0df2Hs1q1
8				q2	T3Bk0df2Hs1q2
9			Hs2	q1	T3Bk0df2Hs2q1
10				q2	T3Bk0df2Hs2q2
11			Hs3	q1	T3Bk0df2Hs3q1
12				q2	T3Bk0df2Hs3q2
13	**Bk1**	df1	Hs1	q1	T3Bk1df1Hs1q1
14				q2	T3Bk1df1Hs1q2
15			Hs2	q1	T3Bk1df1Hs2q1
16				q2	T3Bk1df1Hs2q2
17			Hs3	q1	T3Bk1df1Hs3q1
18				q2	T3Bk1df1Hs3q2
19		df2	Hs1	q1	T3Bk1df2Hs1q1
20				q2	T3Bk1df2Hs1q2
21			Hs2	q1	T3Bk1df2Hs2q1
22				q2	T3Bk1df2Hs2q2
23			Hs3	q1	T3Bk1df2Hs3q1
24				q2	T3Bk1df2Hs3q2
25	**Bk2**	df1	Hs1	q1	T3Bk2df1Hs1q1
26				q2	T3Bk2df1Hs1q2
27			Hs2	q1	T3Bk2df1Hs2q1
28				q2	T3Bk2df1Hs2q2
29			Hs3	q1	T3Bk2df1Hs3q1
30				q2	T3Bk2df1Hs3q2
31		df2	Hs1	q1	T3Bk2df2Hs1q1
32				q2	T3Bk2df2Hs1q2
33			Hs2	q1	T3Bk2df2Hs2q1
34				q2	T3Bk2df2Hs2q2
35			Hs3	q1	T3Bk2df2Hs3q1
36				q2	T3Bk2df2Hs3q2

Appendix G Collated peak values for all free decay test

G.1 Collated peak values for all free decay test

		T1bk0df1a1		T1bk0df1a2		T1bk0df1a3		T1bk0df2a1		T1bk0df2a2		T1bk0df2a3	
s/N	n(cycles)	t (s)	θi (deg)	t (s)	θi (deg)	t (s)	θi (deg)	t (s)	θi (deg)	t (s)	θi (deg)	t (s)	θi (deg)
0	0	0	7.163	0	11.008	0	19.956	0	7.205	0	12.294	0	19.023
1	0.5	0.435	6.672	0.430	10.322	0.450	16.875	0.485	6.392	0.430	11.382	0.470	15.814
2	1	0.860	5.834	0.855	9.030	0.855	14.456	0.910	6.075	0.870	10.320	0.905	13.902
3	1.5	1.275	5.482	1.280	8.312	1.280	12.756	1.345	5.516	1.305	9.380	1.335	12.422
4	2	1.735	4.683	1.715	7.336	1.705	11.267	1.795	5.262	1.740	8.521	1.765	11.213
5	2.5	2.120	4.571	2.130	6.923	2.125	10.155	2.230	4.814	2.175	7.784	2.200	10.350
6	3	2.550	4.095	2.555	6.070	2.550	9.008	2.660	4.600	2.600	7.419	2.640	9.235
7	3.5	2.980	3.852	2.970	5.829	2.975	8.201	3.080	4.148	3.045	6.734	3.065	8.597
8	4	3.400	3.513	3.405	5.119	3.405	7.333	3.515	3.962	3.475	6.336	3.510	7.886
9	4.5	3.825	3.376	3.840	4.835	3.825	6.866	3.960	3.635	3.910	5.783	3.940	7.274
10	5	4.270	2.928	4.245	4.418	4.245	6.064	4.390	3.487	4.345	5.583	4.375	6.811
11	5.5	4.675	2.778	4.685	4.122	4.680	5.794	4.835	3.202	4.770	4.993	4.815	6.289
12	6	5.100	2.502	5.085	3.763	5.095	5.109	5.255	3.035	5.210	4.813	5.240	5.852
13	6.5	5.515	2.476	5.530	3.543	5.525	4.907	5.685	2.801	5.655	4.320	5.670	5.489
14	7	5.980	2.116	5.960	3.141	5.945	4.421	6.135	2.646	6.070	4.163	6.100	5.006
15	7.5	6.390	2.077	6.390	3.026	6.390	4.104	6.555	2.535	6.510	3.859	6.550	4.785
16	8	6.815	1.886	6.805	2.639	6.800	3.744	7.010	2.325	6.955	3.611	6.980	4.352
17	8.5	7.235	1.817	7.240	2.610	7.225	3.447	7.430	2.264	7.390	3.387	7.415	4.249
18	9	7.660	1.517	7.650	2.247	7.645	3.135	7.870	2.110	7.815	3.175	7.850	3.733
19	9.5	8.065	1.508	8.075	2.210	8.080	2.957	8.300	2.034	8.250	2.991	8.285	3.732
20	10	8.505	1.322	8.510	1.901	8.500	2.616	8.750	1.827	8.695	2.813	8.720	3.262
21	10.5	8.925	1.265	8.925	1.858	8.935	2.462	9.195	1.736	9.135	2.632	9.155	3.260
22	11	9.335	1.118	9.330	1.631	9.365	2.132	9.610	1.606	9.565	2.473	9.570	2.974
23	11.5	9.775	1.088	9.770	1.625	9.785	2.047	10.070	1.551	9.990	2.298	10.030	2.893
24	12	10.185	1.015	10.215	1.377	10.195	1.757	10.480	1.461	10.430	2.223	10.465	2.612
25	12.5	10.615	0.927	10.640	1.341	10.630	1.644	10.910	1.396	10.885	1.948	10.905	2.498
26	13	11.050	0.774	11.035	1.220	11.065	1.520	11.340	1.299	11.295	1.939	11.335	2.249
27	13.5	11.495	0.638	11.465	1.201	11.485	1.359	11.785	1.279	11.705	1.736	11.760	2.195
28	14	11.910	0.720	11.910	1.037	11.905	1.276	12.220	1.135	12.175	1.697	12.205	2.003
29	14.5	12.335	0.568										

G.2 ;G con't

		T1bk1df1a1		T1bk1df1a2		T1bk1df1a3		T1bk1df2a1		T1bk1df2a2		T1bk1df2a3	
s/N	n(cycles)	t (s)	θi (deg)	t (s)	θi (deg)	t (s)	θi (deg)	t (s)	θi (deg)	t (s)	θi (deg)	t (s)	θi (deg)
0	0	0	5.81092	0	12.58722	0	18.9373	0	10.306	0	16.312	0	19.8486
1	0.5	0.405	5.16918	0.42	10.23943	0.495	13.749	0.475	8.2108	0.455	12.081	0.43	15.0812
2	1	0.855	4.34947	0.865	7.79497	0.945	9.94883	0.935	6.5857	0.925	8.7834	0.9	10.7144
3	1.5	1.295	3.39995	1.315	5.6821	1.395	7.04543	1.395	5.0301	1.375	6.3875	1.35	7.49408
4	2	1.74	2.81509	1.775	4.39247	1.845	5.07901	1.83	3.894	1.835	4.5309	1.815	5.51317
5	2.5	2.185	2.26308	2.225	3.45611	2.295	4.06194	2.3	3.1892	2.3	4.1522	2.28	4.27612
6	3	2.62	2.05269	2.66	2.91562	2.75	3.7447	2.74	2.7911	2.755	3.3514	2.715	3.6968
7	3.5	3.025	1.79291	3.09	2.43689	3.19	2.91649	3.19	2.2417	3.2	2.8785	3.175	2.98149
8	4	3.495	1.60457	3.535	2.1706	3.63	2.577	3.635	2.1325	3.65	2.4256	3.635	2.57145
9	4.5	3.935	1.4316	3.975	1.85695	4.07	2.1929	4.09	1.7469	4.11	2.1609	4.09	2.21224
10	5	4.37	1.20645	4.405	1.71503	4.515	1.63266	4.515	1.6577	4.56	1.8319	4.52	2.04441
11	5.5	4.815	1.1269	4.89	1.47058	4.93	1.5929	4.98	1.3952	5.01	1.6711	4.985	1.69305
12	6	5.255	0.97054	5.315	1.37172	5.395	1.28924	5.435	1.2934	5.445	1.4687	5.425	1.50801
13	6.5	5.695	0.87105	5.74	1.17987	5.83	1.23919	5.87	1.1375	5.89	1.2978	5.87	1.35571
14	7	6.125	0.76408	6.18	1.03747	6.275	1.03918	6.285	1.0063	6.34	1.11	6.335	1.1721
15	7.5	6.55	0.68074	6.595	0.95446	6.715	1.02238	6.79	0.9436	6.8	1.1093	6.76	1.0778
16	8	7.015	0.63245	7.06	0.8626	7.12	0.88928	7.2	0.7886	7.2	0.9537	7.22	0.90951
17	8.5	7.425	0.60652	7.46	0.82881	7.615	0.86122	7.63	0.7787	7.68	0.8638	7.66	0.80199
18	9	7.855	0.57041	7.93	0.6595	8	0.73523	8.103	0.6529	8.13	0.7328	8.07	0.72711
19	9.5	8.325	0.55104	8.36	0.65796	8.425	0.65781	8.535	0.6299	8.585	0.7054	8.55	0.6307
20	10	8.75	0.50031	8.825	0.55533	8.87	0.61973	8.98	0.5035	9.035	0.6788	9.02	0.60666
21	10.5	9.185	0.44754	9.2	0.54339	9.31	0.52216	9.42	0.4806	9.455	0.5795	9.455	0.58935
22	11	9.635	0.40539	9.71	0.47203	9.75	0.49037	9.9	0.4403	9.87	0.5785	9.905	0.47529
23	11.5	10.07	0.374	10.13	0.43939	10.18	0.43336	10.36	0.3851	10.345	0.5336	10.35	0.45348
24	12	10.51	0.36565	10.565	0.3969	10.65	0.38878	10.81	0.3791	10.81	0.4987	10.825	0.44139
25	12.5	10.98	0.31876	11	0.35983	11.11	0.33419	11.25	0.3431	11.245	0.4634	11.205	0.4326
26	13	11.345	0.27597	11.435	0.32339	11.53	0.29121	11.65	0.3389	11.705	0.445	11.66	0.37215
27	13.5	11.825	0.24688	11.91	0.30645	11.96	0.25643	12.13	0.3368	12.115	0.4252	12.1	0.30689
28	14	12.255	0.23499	12.3	0.29907	12.39	0.2966	12.61	0.3249	12.545	0.4241	12.565	0.40101

G.3 ;G con't

		T1bk2df1a1		T1bk2df1a2		T1bk2df1a3		T1bk2df2a1		T1bk2df2a2		T1bk2df2a3	
s/N	n(cycles)	t (s)	θi (deg)	t (s)	θi (deg)	t (s)	θi (deg)	t (s)	θi (deg)	t (s)	θi (deg)	t (s)	θi (deg)
1	0	0	8.07673	0	11.82456	0	19.6452	0	6.4209	0	11.535	0	17.9852
2	0.5	0.415	7.24021	0.42	9.89834	0.415	15.6894	0.44	5.7071	0.445	9.2041	0.415	15.3427
3	1	0.865	5.92666	0.875	7.93037	0.85	11.7031	0.88	4.8664	0.885	7.394	0.86	11.1949
4	1.5	1.31	4.92055	1.31	6.29996	1.31	8.41055	1.32	4.0262	1.325	6.0588	1.29	8.54548
5	2	1.74	4.15345	1.75	4.97358	1.745	6.82736	1.76	3.4533	1.755	4.8127	1.745	6.65334
6	2.5	2.19	3.62144	2.185	4.24263	2.185	5.24587	2.195	3.0189	2.2	4.3335	2.19	5.47407
7	3	2.635	3.07948	2.63	3.64828	2.62	4.64329	2.63	2.5586	2.645	3.4519	2.63	4.42271
8	3.5	3.065	2.78009	3.075	3.14629	3.06	3.76701	3.075	2.2598	3.075	3.2639	3.065	3.96162
9	4	3.5	2.6982	3.515	2.83058	3.495	3.5905	3.525	1.953	3.53	2.727	3.5	3.30691
10	4.5	3.945	2.29002	3.94	2.42078	3.935	2.84535	3.95	1.9131	3.96	2.6025	3.93	3.03985
11	5	4.4	1.80062	4.39	2.28845	4.395	2.76683	4.385	1.6813	4.385	2.1632	4.38	2.46737
12	5.5	4.82	1.72949	4.845	1.94439	4.83	2.43062	4.845	1.3834	4.84	2.1433	4.825	2.4181
13	6	5.255	1.48844	5.245	1.88419	5.26	2.15777	5.275	1.2394	5.27	1.7916	5.255	2.00596
14	6.5	5.7	1.45011	5.715	1.57446	5.705	1.99709	5.715	1.2365	5.735	1.7276	5.69	1.87368
15	7	6.135	1.40647	6.155	1.52093	6.125	1.65044	6.13	1.1913	6.155	1.5027	6.16	1.70322
16	7.5	6.595	1.19397	6.595	1.22457	6.585	1.59429	6.555	1.0653	6.615	1.3717	6.6	1.48258
17	8	7.01	1.06412	7.025	1.20624	7.02	1.33087	7.035	0.9894	7.02	1.3123	7.015	1.37673
18	8.5	7.445	1.02232	7.45	1.02168	7.475	1.3108	7.46	0.9076	7.465	1.2203	7.465	1.19853
19	9	7.87	0.9946	7.875	0.99694	7.905	1.15397	7.925	0.744	7.93	1.1541	7.91	1.11987
20	9.5	8.3	0.87073	8.335	0.91996	8.355	1.12256	8.345	0.716	8.37	0.9168	8.345	1.01494
21	10	8.76	0.79113	8.74	0.83921	8.765	0.9726	8.765	0.6779	8.775	0.7368	8.78	0.91381
22	10.5	9.18	0.66661	9.2	0.82463	9.225	0.95619	9.205	0.6189	9.21	0.7339	9.235	0.88384
23	11	9.61	0.60969	9.67	0.72201	9.66	0.8744	9.62	0.569	9.645	0.5649	9.655	0.75898
24	11.5	10.075	0.5206	10.105	0.63435	10.09	0.80387	10.1	0.413	10.13	0.4839	10.105	0.72467
25	12	10.49	0.50923	10.56	0.59685	10.51	0.59298	10.49	0.2741	10.57	0.4508	10.59	0.7106
26	12.5	10.94	0.4788	10.92	0.50408	10.98	0.4915	10.92	0.2639	11.01	0.378	10.975	0.56479
27	13	11.375	0.46298	11.415	0.40984	11.43	0.46808	11.38	0.1806	11.425	0.3524	11.38	0.52347
28	13.5	11.8	0.37795	11.85	0.39182	11.87	0.42891	11.83	0.1523	11.85	0.2677	11.835	0.50199
29	14	12.245	0.34762	12.275	0.52663	12.24	0.366	12.25	0.1239	12.28	0.2781	12.29	0.27171
30	14.5	12.705	0.33903	12.695	0.39073	12.72	0.34398	12.73	0.2923	12.74	0.6075	12.73	0.6229
31	15	13.135	0.31707			13.14	0.70618						

G.4 ;G con't

		T1bk1df3a1		T1bk1df3a2		T1bk1df3a2*		T1bk1df3a3		T1bk1df3a3*	
s/N	n(cycles)	t (s)	θi (deg)	t (s)	θi (deg)	t (s)	θi (deg)	t (s)	θi (deg)	t (s)	θi (deg)
0	0	0	5.5804	0	8.8836	0	13.66	0	20.63	0	27.62
1	0.5	0.445	5.1741	0.47	7.6918	0.47	11.365	0.465	16.36	0.46	19.319
2	1	0.97	4.5807	1.025	6.3934	1	9.3986	0.98	12.16	0.975	14.326
3	1.5	1.44	3.9023	1.5	5.4072	1.495	7.8658	1.5	9.563	1.465	10.707
4	2	2.02	3.5051	2.01	4.7598	2	6.5258	1.995	8.371	2.005	8.8138
5	2.5	2.49	3.372	2.535	4.3414	2.535	5.5486	2.5	7.129	2.53	7.617
6	3	3	2.8219	3.015	3.8686	3.04	5.0476	3.015	6.135	3.01	6.4828
7	3.5	3.47	2.5274	3.525	3.4117	3.55	4.4514	3.535	5.339	3.525	5.4906
8	4	4.04	2.2633	4.025	3.2094	4.04	4.0967	4.04	4.645	4.02	5.0611
9	4.5	4.48	2.2202	4.535	2.7798	4.545	3.6027	4.55	4.168	4.53	4.3817
10	5	5.02	2.155	5.085	2.6635	5.055	3.2983	5.07	3.935	5.055	3.7031
11	5.5	5.485	1.831	5.56	2.3184	5.56	2.8198	5.545	3.388	5.565	3.4427
12	6	6.025	1.8689	6.085	2.1698	6.08	2.5994	6.04	3.021	6.075	3.1128
13	6.5	6.555	1.5477	6.57	2.0211	6.575	2.3044	6.67	2.654	6.535	2.934
14	7	7.075	1.4661	7.055	1.8181	7.095	2.1059	7.06	2.559	7.05	2.5618
15	7.5	7.495	1.4067	7.58	1.615	7.555	1.9074	7.59	2.301	7.595	2.3292
16	8	8.02	1.3452	8.095	1.5312	8.125	1.8029	8.085	2.065	8.115	2.0966
17	8.5	8.51	1.0555	8.59	1.209	8.575	1.6984	8.555	1.968	8.575	2.0699
18	9	9.06	1.0378	9.08	1.1388	9.09	1.6733	9.07	1.912	9.09	1.9891
19	9.5	9.54	1.0318	9.53	1.0686	9.6	1.6482	9.59	1.797	9.6	1.8185
20	10	10.04	0.9733	10.11	0.995	10.155	1.4428	10.13	1.724	10.09	1.5395
21	10.5	10.52	1.0106	10.62	0.9214	10.605	1.287	10.625	1.652	10.63	1.5435
22	11	11.08	0.8133	11.1	0.9279	11.125	1.2381	11.04	1.561	11.13	1.4147
23	11.5	11.555	0.9393	11.61	0.8955	11.59	1.0441	11.63	1.373	11.58	1.2285
24	12	12.025	0.756	12.1	0.8547	12.14	0.9286	12.135	1.406	12.1	1.2075
25	12.5	12.545	0.8686	12.61	0.8138	12.645	0.8423	12.605	1.306	12.61	1.0575
26	13	13.03	0.6885	13.09	0.8111	13.095	0.6312	13.12	1.235	13.13	1.1404
27	13.5	13.525	0.7581	13.66	0.8083	13.605	0.6338	13.605	1.117	13.59	1.0083
28	14	14.08	0.6654	14.12	0.8065	14.13	0.5298	14.115	1.064	14.16	0.9639
29	14.5	14.55	0.5405	14.66	0.8047	14.52	0.5447	14.655	0.985	14.59	0.9834
30	15	15.075	0.5683	15.12	0.7976	15.16	0.4809	15.15	0.898	15.12	0.8254
31	15.5	15.585	0.3192	15.56	0.7877	15.53	0.5363	15.64	0.825	15.63	0.7679
32	16	16.015	0.4789	16.13	0.6935	16.135	0.404	16.155	0.752	16.14	0.7713
33	16.5	16.59	0.1294	16.56	0.6798	16.585	0.34	16.63	0.707	16.57	0.758
34	17	17.145	0.4316	17.16	0.6661	17.175	0.2761	17.13	0.662	17.06	0.7459
35	17.5	17.665	0.044	17.61	0.5408	17.51	0.3087	17.645	0.592	17.56	0.6875
36	18	18.085	0.3705	18.11	0.4746	18.08	0.3414	18.045	0.521	18.15	0.629
37	18.5	18.685	0.0104	18.6	0.4084		0.3859	18.7	0.46	18.66	0.594
38	19	19.035	0.3403		0.3625			19.045	0.399		0.5589
39	19.5	19.625	0.0077		0.2691			19.63	0.393		0.0481
40	20							20.08	0.388		
41	20.5							20.625	0.361		
42	21							21.145	0.333		
43	21.5							21.645	0.267		
44	22							21.98	0.2		
45	22.5							22.705	0.17		
46	23							22.975	0.139		
47	23.5								0.321		

G.5 ;G con't

		T1bk0df3a1		T1bk0df3a2		T1bk0df3a2*		T1bk0df3a3		T1bk0df3a3*	
s/N	n(cycles)	t (s)	θi (deg)	t (s)	θi (deg)	t (s)	θi (deg)	t (s)	θi (deg)	t (s)	θi (deg)
0	0	0	6.1935	0	8.8741	0	13.402	0	19.68	0	28.48
1	0.5	0.47	5.9953	0.475	7.8684	0.48	12.536	0.455	17.64	0.46	22.469
2	1	0.985	5.2197	0.975	7.3788	0.99	10.64	0.97	14.34	0.96	17.565
3	1.5	1.45	5.2201	1.443	6.9939	1.45	9.8966	1.425	13.04	1.415	14.982
4	2	1.935	4.7451	1.945	6.4892	1.975	8.9039	1.94	11.31	1.915	13.048
5	2.5	2.445	4.4833	2.42	6.1415	2.425	8.5604	2.395	10.44	2.415	11.182
6	3	2.91	4.1515	2.955	5.6808	2.965	7.2099	2.915	9.369	2.915	10.115
7	3.5	3.43	3.9129	3.425	5.4408	3.41	7.3457	3.38	8.764	3.37	9.3607
8	4	3.935	3.7193	3.925	5.1893	3.915	6.6453	3.885	8.004	3.91	8.3216
9	4.5	4.41	3.4783	4.395	4.9239	4.395	6.4368	4.37	7.521	4.37	7.6981
10	5	4.89	3.1516	4.935	4.355	4.905	5.7495	4.885	7.047	4.87	7.5003
11	5.5	5.405	3.1919	5.375	4.1538	5.405	5.6874	5.37	6.588	5.35	6.8907
12	6	5.955	2.8379	5.905	3.9526	5.89	5.2053	5.885	5.99	5.91	5.9769
13	6.5	6.38	2.8531	6.375	3.7112	6.365	5.2758	6.37	5.604	6.37	5.9142
14	7	6.915	2.6376	6.915	3.4699	6.91	4.6044	6.83	5.259	6.91	5.1235
15	7.5	7.35	2.5738	7.348	3.3309	7.345	4.0795	7.315	5.142	7.365	4.9569
16	8	7.835	2.5104	7.89	3.1919	7.895	4.1126	7.835	4.598	7.865	4.7076
17	8.5	8.335	2.3719	8.355	3.1573	8.35	3.7512	8.345	4.488	8.32	4.6003
18	9	8.865	2.4528	8.895	2.9711	8.885	3.5415	8.83	4.04	8.82	4.493
19	9.5	9.36	2.1791	9.335	2.7848	9.33	3.2104	9.315	3.885	9.32	4.2913
20	10	9.9	1.9839	9.87	2.6234	9.87	3.2371	9.8	3.731	9.86	3.8583
21	10.5	10.33	2.0192	10.31	2.3279	10.33	2.8706	10.29	3.637	10.29	3.4964
22	11	10.855	1.9098	10.84	2.2068	10.89	2.7249	10.8	3.543	10.86	3.0424
23	11.5	11.3	1.8242	11.32	2.0858	11.305	2.5843	11.285	3.409	11.32	2.9861
24	12	11.82	1.6654	11.85	2.0376	11.845	2.574	11.83	3.05	11.82	2.9297
25	12.5	12.34	1.7287	12.32	1.9894	12.27	2.3296	12.285	3.032	12.32	2.7615
26	13	12.745	1.3435	12.79	1.9398	12.83	2.5433	12.77	3.011	12.82	2.75
27	13.5	13.275	1.6156	13.3	1.8903	13.275	2.0464	13.24	2.73	13.28	2.695
28	14	13.87	1.2269	13.8	1.8232	13.785	2.3817	13.74	2.658	13.82	2.6401
29	14.5	14.28	1.5297	14.26	1.7666	14.29	1.8482	14.255	2.523	14.27	2.1309
30	15	14.895	1.0845	14.8	1.6072	14.74	2.1521	14.775	2.388	14.77	2.0963
31	15.5	15.24	1.3588	15.24	1.5735	15.255	1.7187	15.26	2.304	15.27	2.0617
32	16	15.85	1.0828	15.85	1.5147	15.74	1.9095	15.745	2.219	15.77	1.9322
33	16.5	16.275	1.2909	16.25	1.4558	16.265	1.6724	16.23	1.973	16.27	1.834
34	17	16.81	1.0171	16.82	1.4092	16.71	1.8275	16.75	1.956	16.81	1.7358
35	17.5	17.27	1.258	17.24	1.3626	17.245	1.5309	17.23	1.843	17.27	1.6831
36	18	17.655	0.9221	17.83	1.259	17.72	1.6587	17.72	1.731	17.73	1.6303
37	18.5	18.245	1.1256	18.24	1.1554	18.205	1.5099	18.2	1.489	18.23	1.4692
38	19	18.87	0.7446	18.8	1.0591	18.69	1.594	18.685	1.332	18.77	1.3081
39	19.5	19.3	0.8892	19.2	1.0534	19.175	1.3667	19.23	1.175	19.2	1.3077
40	20	19.79	0.7353	19.77	0.9994	19.695	1.5706	19.745	1.148	19.73	1.237
41	20.5	20.21	0.8819	20.21	0.9613	20.18	1.3582	20.2	1.12	20.22	1.0707
42	21	20.76	0.7024	20.78	0.8531	20.665	1.4329	20.72	1.092	20.72	1.1548
43	21.5	21.215	0.8069	21.2	0.7842	21.15	1.35	21.165	0.989	21.22	1.0507
44	22	21.67	0.7007	21.76	0.8211	21.635	1.3	21.72	0.886	21.8	0.9632
45	22.5	22.225	0.7309	22.19	0.6463	22.15	1.1904	22.155	0.881		
46	23	22.67	0.5812			22.68	1.0989	22.69	0.876		
47	23.5	23.195	0.5739			23.13	1.1616	23.09	0.881		
48	24	23.66	0.5482			23.655	1.0925	23.63	0.84		
49	24.5	24.17	0.4913			24.135	1.0188	24.175	0.878		
50	25	24.62	0.5383					24.63	0.751		
51	25.5	25.265	0.0834					25.135	0.769		
52	26	25.64	0.4032								
53	26.5	26.2	0.0663								

Appendix H : Computed parameters from free decay data used for parameterization

H.1 T1bk0df1

grouped	s/n	n (cycle)	t (s)	θi (deg)	θi (rad)	θm (rad)	$(\theta m)^2$	$X_{=16.\theta m^3.Tn}$ (rad/s)	δθ (rad)	θvel (rad/s)	δi (-)	ζi (-)	Pe	Xhm
	1	0	0	7.1631	0.1250									
1	2	0.5	0.435	6.6719	0.1164	0.1134	0.0129	0.7117	0.0232	0.0270	0.2052	0.0326	0.4828	0.0129
2	3	1	0.86	5.8343	0.1018	0.1061	0.0112	0.6655	0.0208	0.0247	0.1964	0.0312	0.4620	0.0113
3	4	1.5	1.275	5.4824	0.0957	0.0918	0.0084	0.5759	0.0201	0.0230	0.2198	0.0350	0.5172	0.0084
4	5	2	1.735	4.6830	0.0817	0.0877	0.0077	0.5505	0.0159	0.0188	0.1818	0.0289	0.4277	0.0077
5	6	2.5	2.12	4.5712	0.0798	0.0766	0.0059	0.4806	0.0103	0.0126	0.1342	0.0214	0.3159	0.0059
6	7	3	2.55	4.0947	0.0715	0.0735	0.0054	0.4612	0.0125	0.0146	0.1711	0.0272	0.4025	0.0054
7	8	3.5	2.98	3.8524	0.0672	0.0664	0.0044	0.4166	0.0101	0.0119	0.1531	0.0244	0.3603	0.0044
8	9	4	3.4	3.5134	0.0613	0.0631	0.0040	0.3958	0.0083	0.0098	0.1319	0.0210	0.3104	0.0040
9	10	4.5	3.825	3.3763	0.0589	0.0562	0.0032	0.3527	0.0102	0.0117	0.1823	0.0290	0.4290	0.0032
10	11	5	4.27	2.9278	0.0511	0.0537	0.0029	0.3370	0.0104	0.0123	0.1949	0.0310	0.4586	0.0029
11	12	5.5	4.675	2.7785	0.0485	0.0474	0.0022	0.2973	0.0074	0.0090	0.1574	0.0250	0.3703	0.0022
12	13	6	5.1	2.5015	0.0437	0.0459	0.0021	0.2877	0.0053	0.0063	0.1152	0.0183	0.2710	0.0021
13	14	6.5	5.515	2.4762	0.0432	0.0403	0.0016	0.2528	0.0067	0.0076	0.1674	0.0266	0.3940	0.0016
14	15	7	5.98	2.1158	0.0369	0.0397	0.0016	0.2493	0.0070	0.0080	0.1758	0.0280	0.4137	0.0016
15	16	7.5	6.39	2.0770	0.0363	0.0349	0.0012	0.2191	0.0040	0.0048	0.1149	0.0183	0.2704	0.0012
16	17	8	6.815	1.8862	0.0329	0.0340	0.0012	0.2132	0.0045	0.0054	0.1336	0.0213	0.3143	0.0012
17	18	8.5	7.235	1.8173	0.0317	0.0297	0.0009	0.1863	0.0064	0.0076	0.2180	0.0347	0.5129	0.0009
18	19	9	7.66	1.5167	0.0265	0.0290	0.0008	0.1821	0.0054	0.0065	0.1869	0.0297	0.4397	0.0008
19	20	9.5	8.065	1.5075	0.0263	0.0248	0.0006	0.1554	0.0034	0.0040	0.1377	0.0219	0.3239	0.0006
20	21	10	8.505	1.3217	0.0231	0.0242	0.0006	0.1518	0.0042	0.0049	0.1756	0.0279	0.4132	0.0006
21	22	10.5	8.925	1.2647	0.0221	0.0213	0.0005	0.1336	0.0035	0.0043	0.1670	0.0266	0.3930	0.0005
22	23	11	9.335	1.1184	0.0195	0.0205	0.0004	0.1288	0.0031	0.0036	0.1507	0.0240	0.3547	0.0004
23	24	11.5	9.775	1.0878	0.0190	0.0186	0.0003	0.1168	0.0018	0.0021	0.0971	0.0154	0.2284	0.0003
24	25	12	10.19	1.0149	0.0177	0.0176	0.0003	0.1103	0.0028	0.0033	0.1602	0.0255	0.3769	0.0003
25	26	12.5	10.62	0.9267	0.0162	0.0156	0.0002	0.0979	0.0042	0.0049	0.2711	0.0431	0.6379	0.0002
26	27	13	11.05	0.7739	0.0135	0.0137	0.0002	0.0857	0.0050	0.0057	0.3734	0.0593	0.8787	0.0002
27	28	13.5	11.5	0.6379	0.0111	0.0130	0.0002	0.0818	0.0009	0.0011	0.0719	0.0114	0.1691	0.0002
28	29	14	11.91	0.7202	0.0126	0.0105	0.0001	0.0660	0.0012	0.0015	0.1163	0.0185	0.2737	0.0001
29	30	14.5	0.43	10.3220	0.1802	0.1749	0.0306	1.0987	0.0345	0.0404	0.1981	0.0315	0.4668	0.0306
30	31	15	0.855	9.0296	0.1576	0.1626	0.0264	1.0217	0.0351	0.0413	0.2165	0.0344	0.5102	0.0265
31	32	15.5	1.28	8.3123	0.1451	0.1428	0.0204	0.8973	0.0295	0.0344	0.2076	0.0330	0.4892	0.0204
32	33	16	1.715	7.3365	0.1280	0.1329	0.0177	0.8353	0.0243	0.0285	0.1829	0.0291	0.4310	0.0177
33	34	16.5	2.13	6.9227	0.1208	0.1170	0.0137	0.7350	0.0221	0.0263	0.1896	0.0302	0.4467	0.0137
34	35	17	2.555	6.0695	0.1059	0.1113	0.0124	0.6992	0.0191	0.0227	0.1719	0.0274	0.4051	0.0124
35	36	17.5	2.97	5.8293	0.1017	0.0976	0.0095	0.6135	0.0166	0.0195	0.1703	0.0271	0.4013	0.0095
36	37	18	3.405	5.1189	0.0893	0.0931	0.0087	0.5847	0.0174	0.0199	0.1870	0.0297	0.4406	0.0087
37	38	18.5	3.84	4.8351	0.0844	0.0832	0.0069	0.5229	0.0122	0.0146	0.1473	0.0234	0.3470	0.0069
38	2	0.5	4.245	4.4179	0.0771	0.0782	0.0061	0.4911	0.0124	0.0147	0.1595	0.0254	0.3758	0.0061
39	3	1	4.685	4.1222	0.0719	0.0714	0.0051	0.4486	0.0114	0.0136	0.1604	0.0255	0.3780	0.0051
40	4	1.5	5.085	3.7632	0.0657	0.0669	0.0045	0.4203	0.0101	0.0120	0.1516	0.0241	0.3571	0.0045
41	5	2	5.53	3.5425	0.0618	0.0603	0.0036	0.3786	0.0109	0.0124	0.1806	0.0287	0.4256	0.0036
42	6	2.5	5.96	3.1413	0.0548	0.0573	0.0033	0.3602	0.0090	0.0105	0.1576	0.0251	0.3713	0.0033
43	7	3	6.39	3.0260	0.0528	0.0504	0.0025	0.3169	0.0088	0.0104	0.1744	0.0278	0.4110	0.0025
44	8	3.5	6.805	2.6385	0.0461	0.0492	0.0024	0.3090	0.0073	0.0085	0.1479	0.0235	0.3485	0.0024
45	9	4	7.24	2.6100	0.0456	0.0426	0.0018	0.2679	0.0068	0.0081	0.1608	0.0256	0.3788	0.0018
46	10	4.5	7.65	2.2467	0.0392	0.0421	0.0018	0.2643	0.0070	0.0084	0.1664	0.0265	0.3920	0.0018
47	11	5	8.075	2.2100	0.0386	0.0362	0.0013	0.2274	0.0060	0.0070	0.1671	0.0266	0.3938	0.0013
48	12	5.5	8.51	1.9009	0.0332	0.0355	0.0013	0.2231	0.0061	0.0072	0.1733	0.0276	0.4083	0.0013
49	13	6	8.925	1.8584	0.0324	0.0308	0.0010	0.1937	0.0047	0.0057	0.1529	0.0243	0.3602	0.0010
50	14	6.5	9.33	1.6314	0.0285	0.0304	0.0009	0.1910	0.0041	0.0048	0.1342	0.0214	0.3163	0.0009
51	15	7	9.77	1.6249	0.0284	0.0263	0.0007	0.1650	0.0044	0.0050	0.1693	0.0269	0.3989	0.0007
52	16	7.5	10.22	1.3773	0.0240	0.0259	0.0007	0.1626	0.0050	0.0057	0.1921	0.0306	0.4527	0.0007
53	17	8	10.64	1.3409	0.0234	0.0227	0.0005	0.1424	0.0027	0.0033	0.1212	0.0193	0.2856	0.0005
54	18	8.5	11.04	1.2201	0.0213	0.0222	0.0005	0.1394	0.0024	0.0030	0.1102	0.0175	0.2595	0.0005
55	19	9	11.47	1.2010	0.0210	0.0197	0.0004	0.1237	0.0032	0.0037	0.1630	0.0259	0.3842	0.0004
56	20	9.5	0.45	16.8749	0.2945	0.3003	0.0902	1.8817	0.0960	0.1123	0.3224	0.0512	0.7576	0.0904
57	21	10	0.855	14.4559	0.2523	0.2586	0.0669	1.6202	0.0719	0.0866	0.2799	0.0445	0.6576	0.0670
58	22	10.5	1.28	12.7556	0.2226	0.2245	0.0504	1.4065	0.0557	0.0655	0.2492	0.0396	0.5856	0.0505
59	23	11	1.705	11.2668	0.1966	0.1999	0.0400	1.2528	0.0454	0.0537	0.2280	0.0363	0.5356	0.0400
60	24	11.5	2.125	10.1555	0.1772	0.1769	0.0313	1.1087	0.0394	0.0466	0.2237	0.0356	0.5256	0.0313
61	25	12	2.55	9.0084	0.1572	0.1602	0.0257	1.0037	0.0341	0.0401	0.2138	0.0340	0.5023	0.0257
62	26	12.5	2.975	8.2008	0.1431	0.1426	0.0203	0.8936	0.0292	0.0342	0.2057	0.0327	0.4834	0.0204
63	27	13	3.405	7.3333	0.1280	0.1315	0.0173	0.8239	0.0233	0.0274	0.1776	0.0283	0.4173	0.0173
64	28	13.5	3.825	6.8663	0.1198	0.1169	0.0137	0.7326	0.0221	0.0264	0.1900	0.0302	0.4465	0.0137
65	29	14	4.245	6.0643	0.1058	0.1105	0.0122	0.6923	0.0187	0.0219	0.1697	0.0270	0.3988	0.0122
66	30	14.5	4.68	5.7945	0.1011	0.0975	0.0095	0.6110	0.0167	0.0196	0.1714	0.0273	0.4027	0.0095
67	31	15	5.095	5.1093	0.0892	0.0934	0.0087	0.5852	0.0155	0.0183	0.1661	0.0264	0.3904	0.0087
68	32	15.5	5.525	4.9075	0.0857	0.0832	0.0069	0.5211	0.0120	0.0141	0.1446	0.0230	0.3399	0.0069
69	33	16	5.945	4.4212	0.0772	0.0786	0.0062	0.4928	0.0140	0.0162	0.1788	0.0284	0.4200	0.0062
70	34	16.5	6.39	4.1042	0.0716	0.0713	0.0051	0.4465	0.0118	0.0138	0.1662	0.0264	0.3905	0.0051
71	35	17	6.8	3.7443	0.0654	0.0659	0.0043	0.4129	0.0115	0.0137	0.1744	0.0277	0.4098	0.0043
72	2	0	7.225	3.4473	0.0602	0.0600	0.0036	0.3762	0.0106	0.0126	0.1776	0.0283	0.4174	0.0036
73	3	0.5	7.645	3.1349	0.0547	0.0559	0.0031	0.3502	0.0086	0.0100	0.1534	0.0244	0.3604	0.0031
74	4	1	8.08	2.9572	0.0516	0.0502	0.0025	0.3145	0.0091	0.0106	0.1809	0.0288	0.4250	0.0025
75	5	1.5	8.5	2.6162	0.0457	0.0473	0.0022	0.2963	0.0086	0.0101	0.1833	0.0292	0.4307	0.0022
76	6	2	8.935	2.4619	0.0430	0.0414	0.0017	0.2597	0.0084	0.0098	0.2046	0.0325	0.4807	0.0017
77	7	2.5	9.365	2.1322	0.0372	0.0394	0.0015	0.2466	0.0072	0.0085	0.1844	0.0293	0.4332	0.0015
78	8	3	9.785	2.0474	0.0357	0.0339	0.0012	0.2127	0.0065	0.0079	0.1933	0.0308	0.4543	0.0012
79	9	3.5	10.2	1.7574	0.0307	0.0322	0.0010	0.2019	0.0070	0.0083	0.2194	0.0349	0.5155	0.0010
80	10	4	10.63	1.6441	0.0287	0.0286	0.0008	0.1792	0.0041	0.0048	0.1449	0.0231	0.3405	0.0008
81	11	4.5	11.07	1.5203	0.0265	0.0262	0.0007	0.1642	0.0050	0.0058	0.1905	0.0303	0.4476	0.0007
82	12	5	11.49	1.3589	0.0237	0.0244	0.0006	0.1529	0.0043	0.0051	0.1753	0.0279	0.4120	0.0006

H.2 Appendix H con't T1bk0df2

grouped	s/n	n (cycle)	t (s)	θi (deg)	θi (rad)	θm (rad)	$(\theta m)^2$	$X_{=16.0m/3.Tn}$ (rad/s)	δθ (rad)	θvel (rad/s)	δi (-)	ζi (-)	Pe	Xhm
	1	0	0	7.2048	0.1257									
1	2	0.5	0.485	6.3920	0.1116	0.1159	0.0134	0.7085	0.0197	0.0217	0.1706	0.0271	0.3912	0.0134
2	3	1	0.91	6.0747	0.1060	0.1039	0.0108	0.6354	0.0153	0.0178	0.1473	0.0234	0.3378	0.0108
3	4	1.5	1.345	5.5163	0.0963	0.0989	0.0098	0.6049	0.0142	0.0160	0.1435	0.0228	0.3291	0.0098
4	5	2	1.795	5.2625	0.0918	0.0901	0.0081	0.5512	0.0123	0.0139	0.1362	0.0217	0.3124	0.0081
5	6	2.5	2.23	4.8137	0.0840	0.0861	0.0074	0.5262	0.0116	0.0134	0.1346	0.0214	0.3087	0.0074
6	7	3	2.66	4.5996	0.0803	0.0782	0.0061	0.4781	0.0116	0.0137	0.1489	0.0237	0.3415	0.0061
7	8	3.5	3.08	4.1476	0.0724	0.0747	0.0056	0.4568	0.0111	0.0130	0.1491	0.0237	0.3420	0.0056
8	9	4	3.515	3.9623	0.0692	0.0679	0.0046	0.4152	0.0090	0.0102	0.1321	0.0210	0.3028	0.0046
9	10	4.5	3.96	3.6345	0.0634	0.0650	0.0042	0.3974	0.0083	0.0095	0.1279	0.0204	0.2933	0.0042
10	11	5	4.39	3.4865	0.0609	0.0597	0.0036	0.3648	0.0075	0.0086	0.1266	0.0201	0.2903	0.0036
11	12	5.5	4.835	3.2022	0.0559	0.0569	0.0032	0.3479	0.0079	0.0091	0.1387	0.0221	0.3181	0.0032
12	13	6	5.255	3.0349	0.0530	0.0524	0.0027	0.3203	0.0070	0.0082	0.1339	0.0213	0.3071	0.0027
13	14	6.5	5.685	2.8008	0.0489	0.0496	0.0025	0.3031	0.0068	0.0077	0.1372	0.0218	0.3146	0.0025
14	15	7	6.135	2.6457	0.0462	0.0466	0.0022	0.2847	0.0046	0.0053	0.0997	0.0159	0.2285	0.0022
15	16	7.5	6.555	2.5352	0.0442	0.0434	0.0019	0.2652	0.0056	0.0064	0.1291	0.0205	0.2960	0.0019
16	17	8	7.01	2.3253	0.0406	0.0419	0.0018	0.2561	0.0047	0.0054	0.1131	0.0180	0.2592	0.0018
17	18	8.5	7.43	2.2641	0.0395	0.0387	0.0015	0.2366	0.0038	0.0044	0.0971	0.0155	0.2227	0.0015
18	19	9	7.87	2.1101	0.0368	0.0375	0.0014	0.2293	0.0040	0.0046	0.1071	0.0170	0.2456	0.0014
19	20	9.5	8.3	2.0342	0.0355	0.0344	0.0012	0.2101	0.0049	0.0056	0.1438	0.0229	0.3297	0.0012
20	21	10	8.75	1.8274	0.0319	0.0329	0.0011	0.2012	0.0052	0.0058	0.1584	0.0252	0.3632	0.0011
21	22	10.5	9.195	1.7361	0.0303	0.0300	0.0009	0.1832	0.0039	0.0045	0.1290	0.0205	0.2957	0.0009
22	23	11	9.61	1.6063	0.0280	0.0287	0.0008	0.1754	0.0032	0.0037	0.1130	0.0180	0.2591	0.0008
23	24	11.5	10.07	1.5506	0.0271	0.0268	0.0007	0.1637	0.0025	0.0029	0.0946	0.0151	0.2170	0.0007
24	25	12	10.48	1.4613	0.0255	0.0257	0.0007	0.1572	0.0027	0.0032	0.1050	0.0167	0.2406	0.0007
25	26	12.5	10.91	1.3961	0.0244	0.0241	0.0006	0.1473	0.0028	0.0033	0.1174	0.0187	0.2692	0.0006
26	27	13	11.34	1.2994	0.0227	0.0233	0.0005	0.1427	0.0020	0.0023	0.0876	0.0139	0.2008	0.0005
27	28	13.5	11.785	1.2790	0.0223	0.0212	0.0005	0.1299	0.0029	0.0033	0.1356	0.0216	0.3108	0.0005
28	29	14	0.43	11.3818	0.1986	0.1973	0.0389	1.2114	0.0345	0.0396	0.1751	0.0278	0.4030	0.0390
29	30	14.5	0.87	10.3196	0.1801	0.1812	0.0328	1.1122	0.0349	0.0399	0.1934	0.0308	0.4452	0.0329
30	31	15	1.305	9.3804	0.1637	0.1644	0.0270	1.0092	0.0314	0.0361	0.1915	0.0305	0.4409	0.0271
31	32	15.5	1.74	8.5209	0.1487	0.1498	0.0224	0.9195	0.0279	0.0320	0.1865	0.0297	0.4294	0.0225
32	33	16	2.175	7.7842	0.1359	0.1391	0.0193	0.8539	0.0192	0.0224	0.1384	0.0220	0.3187	0.0194
33	34	16.5	2.6	7.4193	0.1295	0.1267	0.0161	0.7777	0.0183	0.0211	0.1450	0.0231	0.3338	0.0161
34	35	17	3.045	6.7336	0.1175	0.1200	0.0144	0.7368	0.0189	0.0216	0.1579	0.0251	0.3635	0.0144
35	36	17.5	3.475	6.3355	0.1106	0.1092	0.0119	0.6705	0.0166	0.0192	0.1522	0.0242	0.3504	0.0119
36	37	18	3.91	5.7829	0.1009	0.1040	0.0108	0.6384	0.0131	0.0151	0.1265	0.0201	0.2911	0.0108
37	38	18.5	4.345	5.5830	0.0974	0.0940	0.0088	0.5773	0.0138	0.0160	0.1468	0.0234	0.3379	0.0088
38	2	0.5	4.77	4.9933	0.0872	0.0907	0.0082	0.5569	0.0134	0.0155	0.1483	0.0236	0.3415	0.0082
39	3	1	5.21	4.8133	0.0840	0.0813	0.0066	0.4989	0.0118	0.0133	0.1448	0.0230	0.3334	0.0066
40	4	1.5	5.655	4.3201	0.0754	0.0783	0.0061	0.4809	0.0113	0.0132	0.1451	0.0231	0.3340	0.0061
41	5	2	6.07	4.1632	0.0727	0.0714	0.0051	0.4381	0.0081	0.0094	0.1130	0.0180	0.2601	0.0051
42	6	2.5	6.51	3.8585	0.0673	0.0678	0.0046	0.4164	0.0096	0.0109	0.1424	0.0227	0.3278	0.0046
43	7	3	6.955	3.6107	0.0630	0.0632	0.0040	0.3881	0.0082	0.0093	0.1303	0.0207	0.2999	0.0040
44	8	3.5	7.39	3.3872	0.0591	0.0592	0.0035	0.3635	0.0076	0.0088	0.1285	0.0204	0.2957	0.0035
45	9	4	7.815	3.1754	0.0554	0.0557	0.0031	0.3417	0.0069	0.0080	0.1243	0.0198	0.2862	0.0031
46	10	4.5	8.25	2.9912	0.0522	0.0523	0.0027	0.3208	0.0063	0.0072	0.1212	0.0193	0.2790	0.0027
47	11	5	8.695	2.8130	0.0491	0.0491	0.0024	0.3012	0.0063	0.0071	0.1281	0.0204	0.2948	0.0024
48	12	5.5	9.135	2.6316	0.0459	0.0461	0.0021	0.2832	0.0059	0.0068	0.1286	0.0205	0.2961	0.0021
49	13	6	9.565	2.4735	0.0432	0.0430	0.0019	0.2641	0.0058	0.0068	0.1355	0.0216	0.3120	0.0019
50	14	6.5	9.99	2.2981	0.0401	0.0410	0.0017	0.2516	0.0044	0.0051	0.1068	0.0170	0.2457	0.0017
51	15	7	10.43	2.2230	0.0388	0.0371	0.0014	0.2275	0.0061	0.0068	0.1651	0.0263	0.3801	0.0014
52	16	7.5	10.885	1.9483	0.0340	0.0363	0.0013	0.2230	0.0050	0.0057	0.1367	0.0217	0.3146	0.0013
53	17	8	11.295	1.9391	0.0338	0.0322	0.0010	0.1974	0.0037	0.0045	0.1154	0.0184	0.2656	0.0010
54	18	8.5	11.705	1.7359	0.0303	0.0317	0.0010	0.1948	0.0042	0.0048	0.1335	0.0212	0.3074	0.0010
55	19	9	0.47	15.8137	0.2760	0.2873	0.0826	1.7575	0.0894	0.0988	0.3136	0.0499	0.7194	0.0827
56	20	9.5	0.905	13.9019	0.2426	0.2464	0.0607	1.5072	0.0592	0.0684	0.2414	0.0384	0.5537	0.0608
57	21	10	1.335	12.4223	0.2168	0.2192	0.0480	1.3406	0.0469	0.0546	0.2150	0.0342	0.4931	0.0481
58	22	10.5	1.765	11.2128	0.1957	0.1987	0.0395	1.2156	0.0362	0.0418	0.1825	0.0290	0.4186	0.0395
59	23	11	2.2	10.3500	0.1806	0.1784	0.0318	1.0915	0.0345	0.0395	0.1941	0.0309	0.4452	0.0319
60	24	11.5	2.64	9.2345	0.1612	0.1653	0.0273	1.0114	0.0306	0.0354	0.1856	0.0295	0.4257	0.0274
61	25	12	3.065	8.5969	0.1500	0.1494	0.0223	0.9139	0.0235	0.0270	0.1578	0.0251	0.3620	0.0223
62	26	12.5	3.51	7.8865	0.1376	0.1385	0.0192	0.8471	0.0231	0.0264	0.1672	0.0266	0.3834	0.0192
63	27	13	3.94	7.2735	0.1269	0.1283	0.0165	0.7846	0.0188	0.0217	0.1465	0.0233	0.3361	0.0165
64	28	13.5	4.375	6.8115	0.1189	0.1184	0.0140	0.7240	0.0172	0.0196	0.1454	0.0231	0.3335	0.0140
65	29	14	4.815	6.2894	0.1098	0.1105	0.0122	0.6760	0.0167	0.0194	0.1518	0.0242	0.3482	0.0122
66	30	14.5	5.24	5.8520	0.1021	0.1028	0.0106	0.6287	0.0140	0.0163	0.1361	0.0217	0.3122	0.0106
67	31	15	5.67	5.4891	0.0958	0.0948	0.0090	0.5796	0.0148	0.0172	0.1561	0.0248	0.3580	0.0090
68	32	15.5	6.1	5.0065	0.0874	0.0897	0.0080	0.5484	0.0123	0.0140	0.1373	0.0219	0.3150	0.0080
69	33	16	6.55	4.7848	0.0835	0.0817	0.0067	0.4996	0.0114	0.0130	0.1400	0.0223	0.3211	0.0067
70	34	16.5	6.98	4.3525	0.0760	0.0788	0.0062	0.4822	0.0094	0.0108	0.1188	0.0189	0.2724	0.0062
71	35	17	7.415	4.2490	0.0742	0.0706	0.0050	0.4316	0.0108	0.0124	0.1535	0.0244	0.3522	0.0050
72	2	0	7.85	3.7330	0.0652	0.0696	0.0049	0.4260	0.0090	0.0104	0.1297	0.0206	0.2975	0.0049
73	3	0.5	8.285	3.7321	0.0651	0.0610	0.0037	0.3734	0.0082	0.0095	0.1350	0.0215	0.3096	0.0037
74	4	1	8.72	3.2616	0.0569	0.0610	0.0037	0.3733	0.0082	0.0095	0.1351	0.0215	0.3099	0.0037
75	5	1.5	9.155	3.2604	0.0569	0.0544	0.0030	0.3329	0.0050	0.0059	0.0922	0.0147	0.2114	0.0030
76	6	2	9.57	2.9745	0.0519	0.0537	0.0029	0.3285	0.0064	0.0073	0.1195	0.0190	0.2741	0.0029
77	7	2.5	10.03	2.8931	0.0505	0.0488	0.0024	0.2982	0.0063	0.0071	0.1298	0.0207	0.2978	0.0024
78	8	3	10.465	2.6123	0.0456	0.0470	0.0022	0.2878	0.0069	0.0079	0.1469	0.0234	0.3369	0.0022
79	9	3.5	10.905	2.4979	0.0436	0.0424	0.0018	0.2595	0.0063	0.0073	0.1498	0.0238	0.3436	0.0018
80	10	4	11.335	2.2489	0.0392	0.0410	0.0017	0.2505	0.0053	0.0062	0.1293	0.0206	0.2965	0.0017
81	11	4.5	11.76	2.1950	0.0383	0.0371	0.0014	0.2269	0.0043	0.0049	0.1159	0.0185	0.2660	0.0014

H.3 :T1bk1df1

grouped	s/n	n (cycle)	t (s)	θi (deg)	θi (rad)	θm (rad)	$(\theta m)^2$	X =16.0m/3.Tn (rad/s)	δθ (rad)	θvel (rad/s)	δi (-)	ζi (-)	Pe	Xhm
	1	0	0	5.8109	0.1014									
1	2	0.5	0.405	5.1692	0.0902	0.0887	0.0079	0.5419	0.0255	0.0298	0.2897	0.0461	0.6639	0.0079
2	3	1	0.855	4.3495	0.0759	0.0748	0.0056	0.4570	0.0309	0.0347	0.4190	0.0665	0.9601	0.0056
3	4	1.5	1.295	3.4000	0.0593	0.0625	0.0039	0.3821	0.0268	0.0303	0.4351	0.0691	0.9971	0.0039
4	5	2	1.74	2.8151	0.0491	0.0494	0.0024	0.3020	0.0198	0.0223	0.4070	0.0646	0.9328	0.0025
5	6	2.5	2.185	2.2631	0.0395	0.0425	0.0018	0.2596	0.0133	0.0151	0.3158	0.0502	0.7238	0.0018
6	7	3	2.62	2.0527	0.0358	0.0354	0.0013	0.2163	0.0082	0.0098	0.2329	0.0370	0.5337	0.0013
7	8	3.5	3.025	1.7929	0.0313	0.0319	0.0010	0.1950	0.0078	0.0089	0.2463	0.0392	0.5644	0.0010
8	9	4	3.495	1.6046	0.0280	0.0281	0.0008	0.1720	0.0063	0.0069	0.2250	0.0358	0.5158	0.0008
9	10	4.5	3.935	1.4316	0.0250	0.0245	0.0006	0.1499	0.0069	0.0079	0.2852	0.0453	0.6535	0.0006
10	11	5	4.37	1.2065	0.0211	0.0223	0.0005	0.1364	0.0053	0.0060	0.2393	0.0381	0.5485	0.0005
11	12	5.5	4.815	1.1269	0.0197	0.0190	0.0004	0.1161	0.0041	0.0047	0.2176	0.0346	0.4987	0.0004
12	13	6	5.255	0.9705	0.0169	0.0174	0.0003	0.1066	0.0045	0.0051	0.2575	0.0410	0.5902	0.0003
13	14	6.5	5.695	0.8711	0.0152	0.0151	0.0002	0.0925	0.0036	0.0041	0.2392	0.0380	0.5481	0.0002
14	15	7	6.125	0.7641	0.0133	0.0135	0.0002	0.0828	0.0033	0.0039	0.2465	0.0392	0.5650	0.0002
15	16	7.5	6.55	0.6807	0.0119	0.0122	0.0001	0.0745	0.0023	0.0026	0.1891	0.0301	0.4333	0.0001
16	17	8	7.015	0.6325	0.0110	0.0112	0.0001	0.0687	0.0013	0.0015	0.1154	0.0184	0.2646	0.0001
17	18	8.5	7.425	0.6065	0.0106	0.0105	0.0001	0.0642	0.0011	0.0013	0.1032	0.0164	0.2366	0.0001
18	19	9	7.855	0.5704	0.0100	0.0101	0.0001	0.0617	0.0010	0.0011	0.0959	0.0153	0.2198	0.0001
19	20	9.5	8.325	0.5510	0.0096	0.0093	0.0001	0.0571	0.0012	0.0014	0.1311	0.0209	0.3005	0.0001
20	21	10	8.75	0.5003	0.0087	0.0087	0.0001	0.0533	0.0018	0.0021	0.2080	0.0331	0.4768	0.0001
21	22	10.5	9.185	0.4475	0.0078	0.0079	0.0001	0.0483	0.0017	0.0019	0.2104	0.0335	0.4821	0.0001
22	23	11	9.635	0.4054	0.0071	0.0072	0.0001	0.0438	0.0013	0.0015	0.1795	0.0286	0.4114	0.0001
23	24	11.5	10.07	0.3740	0.0065	0.0067	0.0000	0.0411	0.0007	0.0008	0.1032	0.0164	0.2364	0.0000
24	25	12	10.51	0.3657	0.0064	0.0060	0.0000	0.0369	0.0010	0.0011	0.1598	0.0254	0.3663	0.0000
25	26	12.5	10.98	0.3188	0.0056	0.0056	0.0000	0.0342	0.0016	0.0019	0.2814	0.0447	0.6449	0.0000
26	27	13	11.345	0.2760	0.0048	0.0049	0.0000	0.0302	0.0013	0.0015	0.2555	0.0406	0.5856	0.0000
27	28	13.5	11.825	0.2469	0.0043	0.0045	0.0000	0.0273	0.0007	0.0008	0.1607	0.0256	0.3684	0.0000
28	29	14	0.42	10.2394	0.1787	0.1779	0.0316	1.0785	0.0836	0.0967	0.4792	0.0760	1.0896	0.0318
29	30	14.5	0.865	7.7950	0.1360	0.1389	0.0193	0.8424	0.0795	0.0889	0.5889	0.0933	1.3391	0.0195
30	31	15	1.315	5.6821	0.0992	0.1064	0.0113	0.6449	0.0594	0.0653	0.5736	0.0909	1.3042	0.0114
31	32	15.5	1.775	4.3925	0.0767	0.0797	0.0064	0.4835	0.0389	0.0427	0.4972	0.0789	1.1304	0.0064
32	33	16	2.225	3.4561	0.0603	0.0638	0.0041	0.3867	0.0258	0.0291	0.4098	0.0651	0.9318	0.0041
33	34	16.5	2.66	2.9156	0.0509	0.0514	0.0026	0.3118	0.0178	0.0206	0.3494	0.0555	0.7945	0.0027
34	35	17	3.09	2.4369	0.0425	0.0444	0.0020	0.2691	0.0130	0.0149	0.2951	0.0469	0.6709	0.0020
35	36	17.5	3.535	2.1706	0.0379	0.0375	0.0014	0.2272	0.0101	0.0114	0.2718	0.0432	0.6180	0.0014
36	37	18	3.975	1.8570	0.0324	0.0339	0.0011	0.2056	0.0080	0.0091	0.2356	0.0375	0.5356	0.0012
37	38	18.5	4.405	1.7150	0.0299	0.0290	0.0008	0.1761	0.0067	0.0074	0.2333	0.0371	0.5304	0.0008
38	2	0.5	4.89	1.4706	0.0257	0.0269	0.0007	0.1633	0.0060	0.0066	0.2234	0.0355	0.5079	0.0007
39	3	1	5.315	1.3717	0.0239	0.0231	0.0005	0.1402	0.0051	0.0060	0.2203	0.0350	0.5008	0.0005
40	4	1.5	5.74	1.1799	0.0206	0.0210	0.0004	0.1275	0.0058	0.0067	0.2793	0.0444	0.6350	0.0004
41	5	2	6.18	1.0375	0.0181	0.0186	0.0003	0.1129	0.0039	0.0046	0.2120	0.0337	0.4821	0.0003
42	6	2.5	6.595	0.9545	0.0167	0.0166	0.0003	0.1005	0.0031	0.0035	0.1846	0.0294	0.4197	0.0003
43	7	3	7.06	0.8626	0.0151	0.0156	0.0002	0.0944	0.0022	0.0025	0.1412	0.0225	0.3209	0.0002
44	8	3.5	7.46	0.8288	0.0145	0.0133	0.0002	0.0805	0.0035	0.0041	0.2685	0.0427	0.6104	0.0002
45	9	4	7.93	0.6595	0.0115	0.0130	0.0002	0.0787	0.0030	0.0033	0.2308	0.0367	0.5249	0.0002
46	10	4.5	8.36	0.6580	0.0115	0.0106	0.0001	0.0643	0.0018	0.0020	0.1719	0.0274	0.3909	0.0001
47	11	5	8.825	0.5553	0.0097	0.0105	0.0001	0.0636	0.0020	0.0024	0.1913	0.0304	0.4350	0.0001
48	12	5.5	9.2	0.5434	0.0095	0.0090	0.0001	0.0544	0.0015	0.0016	0.1625	0.0259	0.3695	0.0001
49	13	6	9.71	0.4720	0.0082	0.0086	0.0001	0.0520	0.0018	0.0020	0.2124	0.0338	0.4830	0.0001
50	14	6.5	10.13	0.4394	0.0077	0.0076	0.0001	0.0460	0.0013	0.0015	0.1734	0.0276	0.3942	0.0001
51	15	7	10.565	0.3969	0.0069	0.0070	0.0000	0.0423	0.0014	0.0016	0.1998	0.0318	0.4542	0.0000
52	16	7.5	11	0.3598	0.0063	0.0063	0.0000	0.0381	0.0013	0.0015	0.2048	0.0326	0.4657	0.0000
53	17	8	11.435	0.3234	0.0056	0.0058	0.0000	0.0353	0.0009	0.0010	0.1606	0.0255	0.3651	0.0000
54	18	8.5	11.91	0.3065	0.0053	0.0054	0.0000	0.0329	0.0004	0.0005	0.0782	0.0124	0.1778	0.0000
55	19	9	0.495	13.7490	0.2400	0.2521	0.0635	1.5158	0.1569	0.1660	0.6437	0.1019	1.4515	0.0641
56	20	9.5	0.945	9.9488	0.1736	0.1815	0.0329	1.0912	0.1170	0.1300	0.6686	0.1058	1.5076	0.0333
57	21	10	1.395	7.0454	0.1230	0.1311	0.0172	0.7886	0.0850	0.0944	0.6723	0.1064	1.5161	0.0174
58	22	10.5	1.845	5.0790	0.0886	0.0969	0.0094	0.5829	0.0521	0.0579	0.5507	0.0873	1.2419	0.0095
59	23	11	2.295	4.0619	0.0709	0.0770	0.0059	0.4630	0.0233	0.0257	0.3048	0.0484	0.6873	0.0059
60	24	11.5	2.75	3.7447	0.0654	0.0609	0.0037	0.3662	0.0200	0.0223	0.3313	0.0527	0.7470	0.0037
61	25	12	3.19	2.9165	0.0509	0.0552	0.0030	0.3317	0.0204	0.0232	0.3737	0.0594	0.8427	0.0031
62	26	12.5	3.63	2.5770	0.0450	0.0446	0.0020	0.2681	0.0126	0.0144	0.2852	0.0453	0.6430	0.0020
63	27	13	4.07	2.1929	0.0383	0.0367	0.0013	0.2209	0.0165	0.0186	0.4564	0.0724	1.0292	0.0014
64	28	13.5	4.515	1.6327	0.0285	0.0330	0.0011	0.1987	0.0105	0.0122	0.3197	0.0508	0.7208	0.0011
65	29	14	4.93	1.5929	0.0278	0.0255	0.0007	0.1533	0.0060	0.0068	0.2362	0.0376	0.5325	0.0007
66	30	14.5	5.395	1.2892	0.0225	0.0247	0.0006	0.1486	0.0062	0.0069	0.2511	0.0399	0.5662	0.0006
67	31	15	5.83	1.2392	0.0216	0.0203	0.0004	0.1222	0.0044	0.0050	0.2156	0.0343	0.4862	0.0004
68	32	15.5	6.275	1.0392	0.0181	0.0197	0.0004	0.1187	0.0038	0.0043	0.1923	0.0306	0.4337	0.0004
69	33	16	6.715	1.0224	0.0178	0.0168	0.0003	0.1012	0.0026	0.0031	0.1558	0.0248	0.3513	0.0003
70	34	16.5	7.12	0.8893	0.0155	0.0164	0.0003	0.0988	0.0028	0.0031	0.1715	0.0273	0.3868	0.0003
71	35	17	7.615	0.8612	0.0150	0.0142	0.0002	0.0852	0.0027	0.0031	0.1902	0.0303	0.4290	0.0002
72	2	0	8	0.7352	0.0128	0.0133	0.0002	0.0797	0.0036	0.0044	0.2694	0.0428	0.6076	0.0002
73	3	0.5	8.425	0.6578	0.0115	0.0118	0.0001	0.0711	0.0020	0.0023	0.1709	0.0272	0.3854	0.0001
74	4	1	8.87	0.6197	0.0108	0.0103	0.0001	0.0619	0.0024	0.0027	0.2309	0.0367	0.5208	0.0001
75	5	1.5	9.31	0.5222	0.0091	0.0097	0.0001	0.0583	0.0023	0.0026	0.2341	0.0372	0.5279	0.0001
76	6	2	9.75	0.4904	0.0086	0.0083	0.0001	0.0501	0.0015	0.0018	0.1864	0.0297	0.4203	0.0001
77	7	2.5	10.18	0.4334	0.0076	0.0077	0.0001	0.0461	0.0018	0.0020	0.2321	0.0369	0.5235	0.0001
78	8	3	10.645	0.3888	0.0068	0.0067	0.0000	0.0403	0.0017	0.0019	0.2599	0.0413	0.5860	0.0000
79	9	3.5	11.105	0.3342	0.0058	0.0059	0.0000	0.0357	0.0017	0.0019	0.2890	0.0459	0.6516	0.0000
80	10	4	11.53	0.2912	0.0051	0.0052	0.0000	0.0310	0.0014	0.0016	0.2649	0.0421	0.5972	0.0000

H.4 :T1bk1df2

grouped	s/n	n	t	θi	θi	θm	$(\theta m)^2$	$X_{=16.0m/3.Tn}$	δθ (rad)	θvel	δi	ζi	Pe	Xhm
		cycle	(s)	(deg)	(rad)	(rad)		(rad/s)	(rad)	(rad/s)	(-)	(-)		
	1	0	0	10.3058	0.1799									
1	2	0.5	0.475	8.2108	0.1433	0.1474	0.0217	0.8773	0.0649	0.0694	0.4478	0.0711	0.9994	0.0218
2	3	1	0.935	6.5857	0.1149	0.1155	0.0134	0.6877	0.0555	0.0603	0.4900	0.0778	1.0936	0.0134
3	4	1.5	1.395	5.0301	0.0878	0.0915	0.0084	0.5443	0.0470	0.0525	0.5255	0.0833	1.1727	0.0084
4	5	2	1.83	3.8940	0.0680	0.0717	0.0051	0.4269	0.0321	0.0355	0.4557	0.0723	1.0169	0.0052
5	6	2.5	2.3	3.1892	0.0557	0.0583	0.0034	0.3472	0.0192	0.0212	0.3330	0.0529	0.7432	0.0034
6	7	3	2.74	2.7911	0.0487	0.0474	0.0022	0.2821	0.0165	0.0186	0.3525	0.0560	0.7868	0.0023
7	8	3.5	3.19	2.2417	0.0391	0.0430	0.0018	0.2557	0.0115	0.0128	0.2692	0.0428	0.6007	0.0018
8	9	4	3.635	2.1325	0.0372	0.0348	0.0012	0.2071	0.0086	0.0096	0.2494	0.0397	0.5567	0.0012
9	10	4.5	4.09	1.7469	0.0305	0.0331	0.0011	0.1968	0.0083	0.0094	0.2519	0.0401	0.5621	0.0011
10	11	5	4.515	1.6577	0.0289	0.0274	0.0008	0.1632	0.0061	0.0069	0.2248	0.0358	0.5017	0.0008
11	12	5.5	4.98	1.3952	0.0244	0.0258	0.0007	0.1533	0.0064	0.0069	0.2482	0.0395	0.5538	0.0007
12	13	6	5.435	1.2934	0.0226	0.0221	0.0005	0.1315	0.0045	0.0051	0.2042	0.0325	0.4558	0.0005
13	14	6.5	5.87	1.1375	0.0199	0.0201	0.0004	0.1194	0.0050	0.0059	0.2510	0.0399	0.5601	0.0004
14	15	7	6.285	1.0063	0.0176	0.0182	0.0003	0.1081	0.0034	0.0037	0.1869	0.0297	0.4171	0.0003
15	16	7.5	6.79	0.9436	0.0165	0.0157	0.0002	0.0932	0.0038	0.0042	0.2438	0.0388	0.5440	0.0002
16	17	8	7.2	0.7886	0.0138	0.0150	0.0002	0.0894	0.0029	0.0034	0.1921	0.0306	0.4287	0.0002
17	18	8.5	7.63	0.7787	0.0136	0.0126	0.0002	0.0749	0.0024	0.0026	0.1889	0.0301	0.4216	0.0002
18	19	9	8.103	0.6529	0.0114	0.0123	0.0002	0.0732	0.0026	0.0029	0.2120	0.0337	0.4730	0.0002
19	20	9.5	8.535	0.6299	0.0110	0.0101	0.0001	0.0601	0.0026	0.0030	0.2598	0.0413	0.5798	0.0001
20	21	10	8.98	0.5035	0.0088	0.0097	0.0001	0.0577	0.0026	0.0029	0.2707	0.0430	0.6041	0.0001
21	22	10.5	9.42	0.4806	0.0084	0.0082	0.0001	0.0490	0.0011	0.0012	0.1340	0.0213	0.2991	0.0001
22	23	11	9.9	0.4403	0.0077	0.0076	0.0001	0.0450	0.0017	0.0018	0.2216	0.0352	0.4945	0.0001
23	24	11.5	10.36	0.3851	0.0067	0.0072	0.0001	0.0426	0.0011	0.0012	0.1498	0.0238	0.3342	0.0001
24	25	12	10.81	0.3791	0.0066	0.0064	0.0000	0.0378	0.0007	0.0008	0.1152	0.0183	0.2572	0.0000
25	26	12.5	11.25	0.3431	0.0060	0.0063	0.0000	0.0373	0.0007	0.0008	0.1122	0.0178	0.2503	0.0000
26	27	13	11.65	0.3389	0.0059	0.0059	0.0000	0.0353	0.0001	0.0001	0.0187	0.0030	0.0418	0.0000
27	28	13.5	12.13	0.3368	0.0059	0.0058	0.0000	0.0345	0.0002	0.0003	0.0421	0.0067	0.0940	0.0000
28	29	14	0.455	12.0813	0.2109	0.2190	0.0480	1.2972	0.1314	0.1421	0.6190	0.0980	1.3750	0.0484
29	30	14.5	0.925	8.7834	0.1533	0.1612	0.0260	0.9547	0.0994	0.1080	0.6373	0.1009	1.4156	0.0262
30	31	15	1.375	6.3875	0.1115	0.1162	0.0135	0.6882	0.0742	0.0816	0.6619	0.1048	1.4704	0.0136
31	32	15.5	1.835	4.5309	0.0791	0.0920	0.0085	0.5448	0.0390	0.0422	0.4307	0.0684	0.9567	0.0085
32	33	16	2.3	4.1522	0.0725	0.0688	0.0047	0.4074	0.0206	0.0224	0.3015	0.0479	0.6698	0.0047
33	34	16.5	2.755	3.3514	0.0585	0.0614	0.0038	0.3634	0.0222	0.0247	0.3664	0.0582	0.8138	0.0038
34	35	17	3.2	2.8785	0.0502	0.0504	0.0025	0.2986	0.0162	0.0181	0.3233	0.0514	0.7182	0.0025
35	36	17.5	3.65	2.4256	0.0423	0.0440	0.0019	0.2605	0.0125	0.0138	0.2868	0.0456	0.6370	0.0019
36	37	18	4.11	2.1609	0.0377	0.0372	0.0014	0.2201	0.0104	0.0114	0.2807	0.0446	0.6236	0.0014
37	38	18.5	4.56	1.8319	0.0320	0.0334	0.0011	0.1981	0.0085	0.0095	0.2570	0.0409	0.5709	0.0011
38	2	0.5	5.01	1.6711	0.0292	0.0288	0.0008	0.1706	0.0063	0.0072	0.2210	0.0351	0.4909	0.0008
39	3	1	5.445	1.4687	0.0256	0.0259	0.0007	0.1535	0.0065	0.0074	0.2529	0.0402	0.5617	0.0007
40	4	1.5	5.89	1.2978	0.0227	0.0225	0.0005	0.1333	0.0063	0.0070	0.2800	0.0445	0.6219	0.0005
41	5	2	6.34	1.1100	0.0194	0.0210	0.0004	0.1244	0.0033	0.0036	0.1569	0.0250	0.3486	0.0004
42	6	2.5	6.8	1.1093	0.0194	0.0180	0.0003	0.1067	0.0027	0.0032	0.1518	0.0242	0.3372	0.0003
43	7	3	7.2	0.9537	0.0166	0.0172	0.0003	0.1020	0.0043	0.0049	0.2502	0.0398	0.5557	0.0003
44	8	3.5	7.68	0.8638	0.0151	0.0147	0.0002	0.0872	0.0039	0.0041	0.2634	0.0419	0.5851	0.0002
45	9	4	8.13	0.7328	0.0128	0.0137	0.0002	0.0811	0.0028	0.0031	0.2026	0.0322	0.4499	0.0002
46	10	4.5	8.585	0.7054	0.0123	0.0123	0.0002	0.0730	0.0009	0.0010	0.0765	0.0122	0.1700	0.0002
47	11	5	9.035	0.6788	0.0118	0.0112	0.0001	0.0664	0.0022	0.0025	0.1967	0.0313	0.4368	0.0001
48	12	5.5	9.455	0.5795	0.0101	0.0110	0.0001	0.0650	0.0018	0.0021	0.1599	0.0254	0.3551	0.0001
49	13	6	9.87	0.5785	0.0101	0.0097	0.0001	0.0575	0.0008	0.0009	0.0825	0.0131	0.1833	0.0001
50	14	6.5	10.35	0.5336	0.0093	0.0094	0.0001	0.0557	0.0014	0.0015	0.1486	0.0236	0.3300	0.0001
51	15	7	10.81	0.4987	0.0087	0.0087	0.0001	0.0515	0.0012	0.0014	0.1410	0.0224	0.3132	0.0001
52	16	7.5	11.25	0.4634	0.0081	0.0082	0.0001	0.0488	0.0009	0.0010	0.1138	0.0181	0.2529	0.0001
53	17	8	11.71	0.4450	0.0078	0.0078	0.0001	0.0459	0.0007	0.0008	0.0860	0.0137	0.1911	0.0001
54	18	8.5	12.12	0.4252	0.0074	0.0076	0.0001	0.0449	0.0004	0.0004	0.0481	0.0077	0.1068	0.0001
55	19	9	0.43	15.0812	0.2632	0.2667	0.0711	1.5859	0.1594	0.1771	0.6165	0.0977	1.3748	0.0718
56	20	9.5	0.9	10.7144	0.1870	0.1970	0.0388	1.1714	0.1324	0.1439	0.6993	0.1106	1.5594	0.0392
57	21	10	1.35	7.4941	0.1308	0.1416	0.0201	0.8421	0.0908	0.0992	0.6644	0.1052	1.4816	0.0203
58	22	10.5	1.815	5.5132	0.0962	0.1027	0.0106	0.6108	0.0562	0.0604	0.5611	0.0889	1.2511	0.0106
59	23	11	2.28	4.2761	0.0746	0.0804	0.0065	0.4779	0.0317	0.0352	0.3997	0.0635	0.8912	0.0065
60	24	11.5	2.715	3.6968	0.0645	0.0633	0.0040	0.3766	0.0226	0.0252	0.3606	0.0573	0.8041	0.0040
61	25	12	3.175	2.9815	0.0520	0.0547	0.0030	0.3253	0.0196	0.0213	0.3630	0.0577	0.8094	0.0030
62	26	12.5	3.635	2.5715	0.0449	0.0453	0.0021	0.2695	0.0134	0.0147	0.2984	0.0474	0.6654	0.0021
63	27	13	4.09	2.2122	0.0386	0.0403	0.0016	0.2395	0.0092	0.0104	0.2294	0.0365	0.5114	0.0016
64	28	13.5	4.52	2.0444	0.0357	0.0341	0.0012	0.2026	0.0091	0.0101	0.2675	0.0425	0.5964	0.0012
65	29	14	4.985	1.6931	0.0295	0.0310	0.0010	0.1843	0.0094	0.0103	0.3043	0.0484	0.6786	0.0010
66	30	14.5	5.425	1.5080	0.0263	0.0266	0.0007	0.1582	0.0059	0.0067	0.2222	0.0353	0.4955	0.0007
67	31	15	5.87	1.3557	0.0237	0.0234	0.0005	0.1391	0.0059	0.0064	0.2520	0.0401	0.5619	0.0005
68	32	15.5	6.335	1.1721	0.0205	0.0212	0.0005	0.1263	0.0049	0.0054	0.2294	0.0365	0.5115	0.0005
69	33	16	6.76	1.0778	0.0188	0.0182	0.0003	0.1080	0.0046	0.0052	0.2536	0.0403	0.5656	0.0003
70	34	16.5	7.22	0.9095	0.0159	0.0164	0.0003	0.0975	0.0048	0.0053	0.2956	0.0470	0.6591	0.0003
71	35	17	7.66	0.8020	0.0140	0.0143	0.0002	0.0849	0.0032	0.0037	0.2238	0.0356	0.4991	0.0002
72	2	0	8.07	0.7271	0.0127	0.0125	0.0002	0.0743	0.0030	0.0034	0.2403	0.0382	0.5358	0.0002
73	3	0.5	8.55	0.6307	0.0110	0.0116	0.0001	0.0692	0.0021	0.0022	0.1811	0.0288	0.4038	0.0001
74	4	1	9.02	0.6067	0.0106	0.0106	0.0001	0.0633	0.0007	0.0008	0.0678	0.0108	0.1512	0.0001
75	5	1.5	9.455	0.5894	0.0103	0.0094	0.0001	0.0561	0.0023	0.0026	0.2440	0.0388	0.5442	0.0001
76	6	2	9.905	0.4753	0.0083	0.0091	0.0001	0.0541	0.0024	0.0026	0.2621	0.0417	0.5844	0.0001
77	7	2.5	10.35	0.4535	0.0079	0.0080	0.0001	0.0476	0.0006	0.0006	0.0740	0.0118	0.1650	0.0001
78	8	3	10.83	0.4414	0.0077	0.0077	0.0001	0.0460	0.0004	0.0004	0.0471	0.0075	0.1051	0.0001
79	9	3.5	11.21	0.4326	0.0076	0.0071	0.0001	0.0422	0.0012	0.0014	0.1706	0.0271	0.3805	0.0001
80	10	4	11.66	0.3722	0.0065	0.0065	0.0000	0.0384	0.0022	0.0025	0.3433	0.0546	0.7656	0.0000

H.5 : T1bk2df1

grouped	s/n	n (cycle)	t (s)	θi (deg)	θi (rad)	θm (rad)	$(\theta m)^2$	$X_{=16.0m/3.Tn}$ (rad/s)	δθ (rad)	θvel (rad/s)	δi (-)	ζi (-)	Pe	Xhm
	1	0	0	8.0767	0.1410									
1	2	0.5	0.415	7.2402	0.1264	0.1222	0.0149	0.7443	0.0375	0.0434	0.3095	0.0492	0.7069	0.0150
2	3	1	0.865	5.9267	0.1034	0.1061	0.0113	0.6464	0.0405	0.0452	0.3862	0.0614	0.8821	0.0113
3	4	1.5	1.31	4.9206	0.0859	0.0880	0.0077	0.5358	0.0309	0.0354	0.3555	0.0565	0.8120	0.0078
4	5	2	1.74	4.1535	0.0725	0.0745	0.0056	0.4540	0.0227	0.0258	0.3065	0.0487	0.7001	0.0056
5	6	2.5	2.19	3.6214	0.0632	0.0631	0.0040	0.3844	0.0187	0.0209	0.2992	0.0476	0.6833	0.0040
6	7	3	2.635	3.0795	0.0537	0.0559	0.0031	0.3402	0.0147	0.0168	0.2644	0.0420	0.6039	0.0031
7	8	3.5	3.065	2.7801	0.0485	0.0504	0.0025	0.3071	0.0067	0.0077	0.1322	0.0210	0.3019	0.0025
8	9	4	3.5	2.6982	0.0471	0.0442	0.0020	0.2695	0.0086	0.0097	0.1939	0.0308	0.4429	0.0020
9	10	4.5	3.945	2.2900	0.0400	0.0393	0.0015	0.2391	0.0157	0.0174	0.4045	0.0642	0.9238	0.0015
10	11	5	4.4	1.8006	0.0314	0.0351	0.0012	0.2136	0.0098	0.0112	0.2807	0.0446	0.6412	0.0012
11	12	5.5	4.82	1.7295	0.0302	0.0287	0.0008	0.1748	0.0054	0.0064	0.1904	0.0303	0.4349	0.0008
12	13	6	5.255	1.4884	0.0260	0.0277	0.0008	0.1690	0.0049	0.0055	0.1762	0.0280	0.4024	0.0008
13	14	6.5	5.7	1.4501	0.0253	0.0253	0.0006	0.1539	0.0014	0.0016	0.0566	0.0090	0.1294	0.0006
14	15	7	6.135	1.4065	0.0245	0.0231	0.0005	0.1405	0.0045	0.0050	0.1944	0.0309	0.4439	0.0005
15	16	7.5	6.595	1.1940	0.0208	0.0216	0.0005	0.1313	0.0060	0.0068	0.2789	0.0444	0.6371	0.0005
16	17	8	7.01	1.0641	0.0186	0.0193	0.0004	0.1178	0.0030	0.0035	0.1552	0.0247	0.3545	0.0004
17	18	8.5	7.445	1.0223	0.0178	0.0180	0.0003	0.1094	0.0012	0.0014	0.0676	0.0108	0.1543	0.0003
18	19	9	7.87	0.9946	0.0174	0.0165	0.0003	0.1006	0.0026	0.0031	0.1605	0.0255	0.3666	0.0003
19	20	9.5	8.3	0.8707	0.0152	0.0156	0.0002	0.0949	0.0036	0.0040	0.2289	0.0364	0.5228	0.0002
20	21	10	8.76	0.7911	0.0138	0.0134	0.0002	0.0817	0.0036	0.0040	0.2671	0.0425	0.6101	0.0002
21	22	10.5	9.18	0.6666	0.0116	0.0122	0.0001	0.0745	0.0032	0.0037	0.2605	0.0414	0.5950	0.0001
22	23	11	9.61	0.6097	0.0106	0.0104	0.0001	0.0631	0.0025	0.0028	0.2472	0.0393	0.5647	0.0001
23	24	11.5	10.075	0.5206	0.0091	0.0098	0.0001	0.0595	0.0018	0.0020	0.1801	0.0286	0.4112	0.0001
24	25	12	10.49	0.5092	0.0089	0.0087	0.0001	0.0531	0.0007	0.0008	0.0837	0.0133	0.1912	0.0001
25	26	12.5	10.94	0.4788	0.0084	0.0085	0.0001	0.0517	0.0008	0.0009	0.0952	0.0152	0.2175	0.0001
26	27	13	11.375	0.4630	0.0081	0.0075	0.0001	0.0455	0.0018	0.0020	0.2365	0.0376	0.5402	0.0001
27	28	13.5	11.8	0.3780	0.0066	0.0071	0.0001	0.0431	0.0020	0.0023	0.2866	0.0456	0.6545	0.0001
28	29	14	12.245	0.3476	0.0061	0.0063	0.0000	0.0381	0.0007	0.0008	0.1087	0.0173	0.2482	0.0000
29	30	14.5	12.705	0.3390	0.0059	0.0058	0.0000	0.0353	0.0005	0.0006	0.0920	0.0146	0.2101	0.0000
30	31	15	0.42	9.8983	0.1728	0.1724	0.0297	1.0475	0.0680	0.0777	0.3995	0.0635	0.9102	0.0298
31	32	15.5	0.875	7.9304	0.1384	0.1414	0.0200	0.8589	0.0628	0.0706	0.4518	0.0717	1.0295	0.0201
32	33	16	1.31	6.3000	0.1100	0.1126	0.0127	0.6842	0.0516	0.0590	0.4666	0.0741	1.0630	0.0127
33	34	16.5	1.75	4.9736	0.0868	0.0920	0.0085	0.5590	0.0359	0.0410	0.3954	0.0628	0.9008	0.0085
34	35	17	2.185	4.2426	0.0740	0.0752	0.0057	0.4572	0.0231	0.0263	0.3099	0.0493	0.7061	0.0057
35	36	17.5	2.63	3.6483	0.0637	0.0645	0.0042	0.3918	0.0191	0.0215	0.2990	0.0475	0.6812	0.0042
36	37	18	3.075	3.1463	0.0549	0.0565	0.0032	0.3435	0.0143	0.0161	0.2538	0.0404	0.5782	0.0032
37	38	18.5	3.515	2.8306	0.0494	0.0486	0.0024	0.2952	0.0127	0.0146	0.2621	0.0417	0.5973	0.0024
38	2	0.5	3.94	2.4208	0.0423	0.0447	0.0020	0.2714	0.0095	0.0108	0.2126	0.0338	0.4844	0.0020
39	3	1	4.39	2.2885	0.0399	0.0381	0.0015	0.2315	0.0083	0.0092	0.2191	0.0349	0.4993	0.0015
40	4	1.5	4.845	1.9444	0.0339	0.0364	0.0013	0.2212	0.0071	0.0083	0.1944	0.0309	0.4429	0.0013
41	5	2	5.245	1.8842	0.0329	0.0307	0.0009	0.1866	0.0065	0.0074	0.2110	0.0336	0.4808	0.0009
42	6	2.5	5.715	1.5745	0.0275	0.0297	0.0009	0.1805	0.0063	0.0070	0.2142	0.0341	0.4880	0.0009
43	7	3	6.155	1.5209	0.0265	0.0244	0.0006	0.1484	0.0061	0.0069	0.2513	0.0400	0.5726	0.0006
44	8	3.5	6.595	1.2246	0.0214	0.0238	0.0006	0.1446	0.0055	0.0063	0.2318	0.0369	0.5282	0.0006
45	9	4	7.025	1.2062	0.0211	0.0196	0.0004	0.1191	0.0035	0.0041	0.1811	0.0288	0.4127	0.0004
46	10	4.5	7.45	1.0217	0.0178	0.0192	0.0004	0.1168	0.0037	0.0043	0.1906	0.0303	0.4342	0.0004
47	11	5	7.875	0.9969	0.0174	0.0169	0.0003	0.1030	0.0018	0.0020	0.1049	0.0167	0.2390	0.0003
48	12	5.5	8.335	0.9200	0.0161	0.0160	0.0003	0.0974	0.0028	0.0032	0.1722	0.0274	0.3924	0.0003
49	13	6	8.74	0.8392	0.0146	0.0152	0.0002	0.0925	0.0017	0.0019	0.1094	0.0174	0.2493	0.0002
50	14	6.5	9.2	0.8246	0.0144	0.0136	0.0002	0.0828	0.0020	0.0022	0.1504	0.0239	0.3427	0.0002
51	15	7	9.67	0.7220	0.0126	0.0127	0.0002	0.0774	0.0033	0.0037	0.2623	0.0417	0.5977	0.0002
52	16	7.5	10.105	0.6344	0.0111	0.0115	0.0001	0.0699	0.0022	0.0025	0.1904	0.0303	0.4338	0.0001
53	17	8	10.56	0.5969	0.0104	0.0099	0.0001	0.0604	0.0023	0.0028	0.2299	0.0366	0.5237	0.0001
54	18	8.5	10.92	0.5041	0.0088	0.0088	0.0001	0.0534	0.0033	0.0038	0.3759	0.0597	0.8565	0.0001
55	19	9	11.415	0.4098	0.0072	0.0078	0.0001	0.0475	0.0020	0.0021	0.2519	0.0401	0.5740	0.0001
56	20	9.5	0.415	15.6894	0.2738	0.2736	0.0748	1.6594	0.1386	0.1631	0.5180	0.0822	1.1782	0.0754
57	21	10	0.85	11.7031	0.2043	0.2103	0.0442	1.2757	0.1270	0.1419	0.6235	0.0987	1.4183	0.0446
58	22	10.5	1.31	8.4106	0.1468	0.1617	0.0261	0.9809	0.0851	0.0951	0.5389	0.0855	1.2259	0.0263
59	23	11	1.745	6.8274	0.1192	0.1192	0.0142	0.7229	0.0552	0.0631	0.4720	0.0749	1.0738	0.0143
60	24	11.5	2.185	5.2459	0.0916	0.1001	0.0100	0.6072	0.0381	0.0436	0.3855	0.0612	0.8769	0.0101
61	25	12	2.62	4.6433	0.0810	0.0787	0.0062	0.4771	0.0258	0.0295	0.3312	0.0526	0.7533	0.0062
62	26	12.5	3.06	3.7670	0.0657	0.0719	0.0052	0.4359	0.0184	0.0210	0.2571	0.0409	0.5849	0.0052
63	27	13	3.495	3.5905	0.0627	0.0577	0.0033	0.3500	0.0161	0.0184	0.2806	0.0446	0.6383	0.0033
64	28	13.5	3.935	2.8454	0.0497	0.0555	0.0031	0.3365	0.0144	0.0160	0.2606	0.0414	0.5928	0.0031
65	29	14	4.395	2.7668	0.0483	0.0460	0.0021	0.2793	0.0072	0.0081	0.1575	0.0251	0.3584	0.0021
66	30	14.5	4.83	2.4306	0.0424	0.0430	0.0018	0.2607	0.0106	0.0123	0.2486	0.0395	0.5656	0.0018
67	31	15	5.26	2.1578	0.0377	0.0386	0.0015	0.2344	0.0076	0.0086	0.1965	0.0313	0.4469	0.0015
68	32	15.5	5.705	1.9971	0.0349	0.0332	0.0011	0.2016	0.0089	0.0102	0.2680	0.0426	0.6097	0.0011
69	33	16	6.125	1.6504	0.0288	0.0313	0.0010	0.1901	0.0070	0.0080	0.2253	0.0358	0.5124	0.0010
70	34	16.5	6.585	1.5943	0.0278	0.0260	0.0007	0.1578	0.0056	0.0062	0.2152	0.0342	0.4895	0.0007
71	35	17	7.02	1.3309	0.0232	0.0254	0.0006	0.1538	0.0049	0.0056	0.1958	0.0311	0.4454	0.0006
72	2	0	7.475	1.3108	0.0229	0.0217	0.0005	0.1315	0.0031	0.0035	0.1426	0.0227	0.3244	0.0005
73	3	0.5	7.905	1.1540	0.0201	0.0212	0.0005	0.1288	0.0033	0.0037	0.1550	0.0247	0.3526	0.0005
74	4	1	8.355	1.1226	0.0196	0.0186	0.0003	0.1126	0.0032	0.0037	0.1710	0.0272	0.3890	0.0003
75	5	1.5	8.765	0.9726	0.0170	0.0181	0.0003	0.1100	0.0029	0.0033	0.1604	0.0255	0.3649	0.0003
76	6	2	9.225	0.9562	0.0167	0.0161	0.0003	0.0978	0.0017	0.0019	0.1064	0.0169	0.2421	0.0003
77	7	2.5	9.66	0.8744	0.0153	0.0154	0.0002	0.0932	0.0027	0.0031	0.1735	0.0276	0.3947	0.0002
78	8	3	10.09	0.8039	0.0140	0.0128	0.0002	0.0777	0.0049	0.0058	0.3884	0.0617	0.8835	0.0002
79	9	3.5	10.505	0.5930	0.0103	0.0113	0.0001	0.0686	0.0055	0.0062	0.4920	0.0781	1.1191	0.0001
80	10	4	10.975	0.4915	0.0086	0.0093	0.0001	0.0562	0.0022	0.0024	0.2365	0.0376	0.5380	0.0001
81	11	4.5	11.43	0.4681	0.0082	0.0080	0.0001	0.0487	0.0011	0.0012	0.1362	0.0217	0.3099	0.0001
82	12	5	11.87	0.4289	0.0075	0.0073	0.0001	0.0442	0.0018	0.0022	0.2460	0.0391	0.5596	0.0001
83	13	5.5	12.24	0.3660	0.0064	0.0067	0.0000	0.0409	0.0015	0.0017	0.2207	0.0351	0.5019	0.0000

H.6 :T1bk2df2

grouped	s/n	n (cycle)	t (s)	θi (deg)	θi (rad)	θm (rad)	$(\theta m)^2$	X =16.0m/3.Tn (rad/s)	δθ (rad)	θvel (rad/s)	δi (-)	ζi (-)	Pe	Xhm
	1	0	0	6.4209	0.1121									
1	2	0.5	0.44	5.7071	0.0996	0.0985	0.0097	0.6007	0.0271	0.0308	0.2772	0.0441	0.6340	0.0097
2	3	1	0.88	4.8664	0.0849	0.0849	0.0072	0.5180	0.0293	0.0333	0.3489	0.0554	0.7979	0.0072
3	4	1.5	1.32	4.0262	0.0703	0.0726	0.0053	0.4428	0.0247	0.0280	0.3430	0.0545	0.7845	0.0053
4	5	2	1.76	3.4533	0.0603	0.0615	0.0038	0.3749	0.0176	0.0201	0.2879	0.0458	0.6585	0.0038
5	6	2.5	2.195	3.0189	0.0527	0.0525	0.0028	0.3199	0.0156	0.0179	0.2999	0.0477	0.6858	0.0028
6	7	3	2.63	2.5586	0.0447	0.0461	0.0021	0.2809	0.0132	0.0151	0.2896	0.0460	0.6624	0.0021
7	8	3.5	3.075	2.2598	0.0394	0.0394	0.0016	0.2401	0.0106	0.0118	0.2701	0.0429	0.6176	0.0016
8	9	4	3.525	1.9530	0.0341	0.0364	0.0013	0.2221	0.0061	0.0069	0.1666	0.0265	0.3809	0.0013
9	10	4.5	3.95	1.9131	0.0334	0.0317	0.0010	0.1934	0.0047	0.0055	0.1498	0.0238	0.3426	0.0010
10	11	5	4.385	1.6813	0.0293	0.0288	0.0008	0.1754	0.0092	0.0103	0.3242	0.0515	0.7413	0.0008
11	12	5.5	4.845	1.3834	0.0241	0.0255	0.0006	0.1554	0.0077	0.0087	0.3049	0.0485	0.6974	0.0007
12	13	6	5.275	1.2394	0.0216	0.0229	0.0005	0.1394	0.0026	0.0029	0.1122	0.0179	0.2567	0.0005
13	14	6.5	5.715	1.2365	0.0216	0.0212	0.0004	0.1294	0.0008	0.0010	0.0396	0.0063	0.0905	0.0004
14	15	7	6.13	1.1913	0.0208	0.0201	0.0004	0.1225	0.0030	0.0036	0.1490	0.0237	0.3408	0.0004
15	16	7.5	6.555	1.0653	0.0186	0.0190	0.0004	0.1161	0.0035	0.0039	0.1857	0.0295	0.4248	0.0004
16	17	8	7.035	0.9894	0.0173	0.0172	0.0003	0.1050	0.0028	0.0030	0.1602	0.0255	0.3664	0.0003
17	18	8.5	7.46	0.9076	0.0158	0.0151	0.0002	0.0922	0.0043	0.0048	0.2850	0.0453	0.6518	0.0002
18	19	9	7.925	0.7440	0.0130	0.0142	0.0002	0.0864	0.0033	0.0038	0.2371	0.0377	0.5422	0.0002
19	20	9.5	8.345	0.7160	0.0125	0.0124	0.0002	0.0757	0.0012	0.0014	0.0931	0.0148	0.2129	0.0002
20	21	10	8.765	0.6779	0.0118	0.0116	0.0001	0.0710	0.0017	0.0020	0.1458	0.0232	0.3333	0.0001
21	22	10.5	9.205	0.6189	0.0108	0.0109	0.0001	0.0664	0.0019	0.0022	0.1751	0.0279	0.4004	0.0001
22	23	11	9.62	0.5690	0.0099	0.0090	0.0001	0.0549	0.0036	0.0040	0.4045	0.0642	0.9251	0.0001
23	24	11.5	10.1	0.4130	0.0072	0.0074	0.0001	0.0449	0.0051	0.0060	0.7305	0.1155	1.6707	0.0001
24	25	12	10.49	0.2741	0.0048	0.0059	0.0000	0.0360	0.0026	0.0032	0.4478	0.0711	1.0241	0.0000
25	26	12.5	10.92	0.2639	0.0046	0.0040	0.0000	0.0242	0.0016	0.0018	0.4169	0.0662	0.9534	0.0000
26	27	13	11.38	0.1806	0.0032	0.0036	0.0000	0.0222	0.0019	0.0022	0.5496	0.0871	1.2569	0.0000
27	28	13.5	11.83	0.1523	0.0027	0.0027	0.0000	0.0162	0.0010	0.0011	0.3768	0.0599	0.8617	0.0000
28	29	14	0.445	9.2041	0.1606	0.1652	0.0273	1.0024	0.0723	0.0817	0.4447	0.0706	1.0121	0.0274
29	30	14.5	0.885	7.3940	0.1290	0.1332	0.0177	0.8083	0.0549	0.0624	0.4181	0.0664	0.9516	0.0178
30	31	15	1.325	6.0588	0.1057	0.1065	0.0113	0.6464	0.0451	0.0518	0.4294	0.0682	0.9772	0.0114
31	32	15.5	1.755	4.8127	0.0840	0.0907	0.0082	0.5504	0.0301	0.0344	0.3351	0.0533	0.7626	0.0082
32	33	16	2.2	4.3335	0.0756	0.0721	0.0052	0.4377	0.0238	0.0267	0.3323	0.0528	0.7563	0.0052
33	34	16.5	2.645	3.4519	0.0602	0.0663	0.0044	0.4023	0.0187	0.0213	0.2835	0.0451	0.6451	0.0044
34	35	17	3.075	3.2639	0.0570	0.0539	0.0029	0.3272	0.0127	0.0143	0.2357	0.0375	0.5364	0.0029
35	36	17.5	3.53	2.7270	0.0476	0.0512	0.0026	0.3107	0.0115	0.0130	0.2265	0.0360	0.5154	0.0026
36	37	18	3.96	2.6025	0.0454	0.0427	0.0018	0.2590	0.0098	0.0115	0.2316	0.0368	0.5271	0.0018
37	38	18.5	4.385	2.1632	0.0378	0.0414	0.0017	0.2513	0.0080	0.0091	0.1941	0.0309	0.4417	0.0017
38	2	0.5	4.84	2.1433	0.0374	0.0345	0.0012	0.2094	0.0065	0.0073	0.1884	0.0300	0.4288	0.0012
39	3	1	5.27	1.7916	0.0313	0.0338	0.0011	0.2050	0.0073	0.0081	0.2156	0.0343	0.4908	0.0011
40	4	1.5	5.735	1.7276	0.0302	0.0287	0.0008	0.1745	0.0050	0.0057	0.1759	0.0280	0.4002	0.0008
41	5	2	6.155	1.5027	0.0262	0.0270	0.0007	0.1641	0.0062	0.0071	0.2307	0.0367	0.5249	0.0007
42	6	2.5	6.615	1.3717	0.0239	0.0246	0.0006	0.1491	0.0033	0.0038	0.1355	0.0216	0.3083	0.0006
43	7	3	7.02	1.3123	0.0229	0.0226	0.0005	0.1373	0.0026	0.0031	0.1170	0.0186	0.2662	0.0005
44	8	3.5	7.465	1.2203	0.0213	0.0215	0.0005	0.1306	0.0028	0.0030	0.1285	0.0204	0.2924	0.0005
45	9	4	7.93	1.1541	0.0201	0.0186	0.0003	0.1132	0.0053	0.0059	0.2860	0.0455	0.6508	0.0003
46	10	4.5	8.37	0.9168	0.0160	0.0165	0.0003	0.1001	0.0073	0.0086	0.4488	0.0712	1.0214	0.0003
47	11	5	8.775	0.7368	0.0129	0.0144	0.0002	0.0874	0.0032	0.0038	0.2225	0.0354	0.5064	0.0002
48	12	5.5	9.21	0.7339	0.0128	0.0114	0.0001	0.0689	0.0030	0.0034	0.2655	0.0422	0.6043	0.0001
49	13	6	9.645	0.5649	0.0099	0.0106	0.0001	0.0645	0.0044	0.0047	0.4164	0.0661	0.9476	0.0001
50	14	6.5	10.13	0.4839	0.0084	0.0089	0.0001	0.0538	0.0020	0.0022	0.2257	0.0359	0.5137	0.0001
51	15	7	10.57	0.4508	0.0079	0.0075	0.0001	0.0456	0.0018	0.0021	0.2470	0.0393	0.5620	0.0001
52	16	7.5	11.01	0.3780	0.0066	0.0070	0.0000	0.0425	0.0017	0.0020	0.2463	0.0392	0.5604	0.0000
53	17	8	11.43	0.3524	0.0062	0.0056	0.0000	0.0342	0.0019	0.0023	0.3451	0.0548	0.7853	0.0000
54	18	8.5	11.85	0.2677	0.0047	0.0055	0.0000	0.0334	0.0013	0.0015	0.2367	0.0376	0.5386	0.0000
55	19	9	0.415	15.3427	0.2678	0.2546	0.0648	1.5514	0.1185	0.1378	0.4741	0.0752	1.0832	0.0652
56	20	9.5	0.86	11.1949	0.1954	0.2085	0.0435	1.2701	0.1186	0.1356	0.5852	0.0927	1.3371	0.0438
57	21	10	1.29	8.5455	0.1491	0.1558	0.0243	0.9489	0.0793	0.0896	0.5203	0.0825	1.1888	0.0244
58	22	10.5	1.745	6.6533	0.1161	0.1223	0.0150	0.7454	0.0536	0.0596	0.4454	0.0707	1.0176	0.0150
59	23	11	2.19	5.4741	0.0955	0.0967	0.0093	0.5889	0.0389	0.0440	0.4084	0.0649	0.9330	0.0094
60	24	11.5	2.63	4.4227	0.0772	0.0823	0.0068	0.5017	0.0264	0.0302	0.3234	0.0514	0.7388	0.0068
61	25	12	3.065	3.9616	0.0691	0.0675	0.0045	0.4110	0.0195	0.0224	0.2907	0.0462	0.6643	0.0046
62	26	12.5	3.5	3.3069	0.0577	0.0611	0.0037	0.3723	0.0161	0.0186	0.2648	0.0421	0.6051	0.0037
63	27	13	3.93	3.0399	0.0531	0.0504	0.0025	0.3070	0.0147	0.0167	0.2929	0.0466	0.6691	0.0025
64	28	13.5	4.38	2.4674	0.0431	0.0476	0.0023	0.2902	0.0109	0.0121	0.2288	0.0364	0.5228	0.0023
65	29	14	4.825	2.4181	0.0422	0.0390	0.0015	0.2378	0.0081	0.0092	0.2070	0.0329	0.4730	0.0015
66	30	14.5	5.255	2.0060	0.0350	0.0375	0.0014	0.2282	0.0095	0.0110	0.2551	0.0406	0.5828	0.0014
67	31	15	5.69	1.8737	0.0327	0.0324	0.0010	0.1972	0.0053	0.0058	0.1636	0.0260	0.3738	0.0010
68	32	15.5	6.16	1.7032	0.0297	0.0293	0.0009	0.1784	0.0068	0.0075	0.2341	0.0372	0.5349	0.0009
69	33	16	6.6	1.4826	0.0259	0.0269	0.0007	0.1638	0.0057	0.0067	0.2128	0.0339	0.4862	0.0007
70	34	16.5	7.015	1.3767	0.0240	0.0234	0.0005	0.1425	0.0050	0.0057	0.2127	0.0338	0.4859	0.0005
71	35	17	7.465	1.1985	0.0209	0.0218	0.0005	0.1327	0.0045	0.0050	0.2065	0.0328	0.4718	0.0005
72	2	0	7.91	1.1199	0.0195	0.0193	0.0004	0.1177	0.0032	0.0036	0.1663	0.0265	0.3799	0.0004
73	3	0.5	8.345	1.0149	0.0177	0.0177	0.0003	0.1081	0.0036	0.0041	0.2033	0.0323	0.4646	0.0003
74	4	1	8.78	0.9138	0.0159	0.0166	0.0003	0.1010	0.0023	0.0026	0.1383	0.0220	0.3160	0.0003
75	5	1.5	9.235	0.8838	0.0154	0.0146	0.0002	0.0889	0.0027	0.0031	0.1856	0.0295	0.4242	0.0002
76	6	2	9.655	0.7590	0.0132	0.0140	0.0002	0.0855	0.0028	0.0032	0.1986	0.0316	0.4537	0.0002
77	7	2.5	10.11	0.7247	0.0126	0.0128	0.0002	0.0781	0.0008	0.0009	0.0659	0.0105	0.1505	0.0002
78	8	3	10.59	0.7106	0.0124	0.0113	0.0001	0.0686	0.0028	0.0032	0.2493	0.0396	0.5695	0.0001
79	9	3.5	10.98	0.5648	0.0099	0.0108	0.0001	0.0656	0.0033	0.0041	0.3056	0.0486	0.6983	0.0001
80	10	4	11.38	0.5235	0.0091	0.0093	0.0001	0.0567	0.0011	0.0013	0.1179	0.0188	0.2693	0.0001
81	11	4.5	11.84	0.5020	0.0088	0.0069	0.0000	0.0423	0.0044	0.0048	0.6557	0.1038	1.4982	0.0000

H.7 : T1bk0df3

grouped	s/n	n (cycle)	t (s)	θi (deg)	θi (rad)	θm (rad)	$(\theta m)^2$	$\dot{X}_{-16.0m/3.Tn}$ (rad/s)	δθ (rad)	θvel (rad/s)	δi (-)	ζi (-)	Pe	Xhm
	1	0	0	6.1935	0.1081									
1	2	0.5	0.47	5.9953	0.1046	0.0996	0.0099	0.5373	0.0170	0.0173	0.1711	0.0272	0.3460	0.0099
2	3	1	0.985	5.2197	0.0911	0.0979	0.0096	0.5280	0.0135	0.0138	0.1385	0.0220	0.2801	0.0096
3	4	1.5	1.45	5.2201	0.0911	0.0870	0.0076	0.4691	0.0083	0.0087	0.0953	0.0152	0.1928	0.0076
4	5	2	1.935	4.7451	0.0828	0.0847	0.0072	0.4568	0.0129	0.0129	0.1522	0.0242	0.3078	0.0072
5	6	2.5	2.445	4.4833	0.0782	0.0776	0.0060	0.4188	0.0104	0.0106	0.1336	0.0213	0.2703	0.0060
6	7	3	2.91	4.1515	0.0725	0.0733	0.0054	0.3953	0.0100	0.0101	0.1361	0.0217	0.2753	0.0054
7	8	3.5	3.43	3.9129	0.0683	0.0687	0.0047	0.3705	0.0075	0.0074	0.1099	0.0175	0.2224	0.0047
8	9	4	3.935	3.7193	0.0649	0.0645	0.0042	0.3479	0.0076	0.0077	0.1178	0.0187	0.2382	0.0042
9	10	4.5	4.41	3.4783	0.0607	0.0600	0.0036	0.3234	0.0099	0.0104	0.1656	0.0264	0.3351	0.0036
10	11	5	4.89	3.1516	0.0550	0.0582	0.0034	0.3140	0.0050	0.0050	0.0859	0.0137	0.1738	0.0034
11	12	5.5	5.405	3.1919	0.0557	0.0523	0.0027	0.2820	0.0055	0.0051	0.1048	0.0167	0.2121	0.0027
12	13	6	5.955	2.8379	0.0495	0.0528	0.0028	0.2846	0.0059	0.0061	0.1122	0.0179	0.2269	0.0028
13	14	6.5	6.38	2.8531	0.0498	0.0478	0.0023	0.2578	0.0035	0.0036	0.0732	0.0116	0.1481	0.0023
14	15	7	6.915	2.6376	0.0460	0.0474	0.0022	0.2555	0.0049	0.0050	0.1030	0.0164	0.2084	0.0022
15	16	7.5	7.35	2.5738	0.0449	0.0449	0.0020	0.2423	0.0022	0.0024	0.0494	0.0079	0.1000	0.0020
16	17	8	7.835	2.5104	0.0438	0.0432	0.0019	0.2328	0.0035	0.0036	0.0817	0.0130	0.1652	0.0019
17	18	8.5	8.335	2.3719	0.0414	0.0433	0.0019	0.2336	0.0010	0.0010	0.0232	0.0037	0.0469	0.0019
18	19	9	8.865	2.4528	0.0428	0.0397	0.0016	0.2142	0.0034	0.0033	0.0848	0.0135	0.1715	0.0016
19	20	9.5	9.36	2.1791	0.0380	0.0387	0.0015	0.2089	0.0082	0.0079	0.2122	0.0338	0.4292	0.0015
20	21	10	9.9	1.9839	0.0346	0.0366	0.0013	0.1976	0.0028	0.0029	0.0763	0.0121	0.1543	0.0013
21	22	10.5	10.33	2.0192	0.0352	0.0340	0.0012	0.1833	0.0013	0.0014	0.0380	0.0061	0.0769	0.0012
22	23	11	10.855	1.9098	0.0333	0.0335	0.0011	0.1809	0.0034	0.0035	0.1015	0.0162	0.2054	0.0011
23	24	11.5	11.3	1.8242	0.0318	0.0312	0.0010	0.1683	0.0043	0.0044	0.1370	0.0218	0.2771	0.0010
24	25	12	11.82	1.6654	0.0291	0.0310	0.0010	0.1673	0.0017	0.0016	0.0537	0.0086	0.1087	0.0010
25	26	12.5	12.34	1.7287	0.0302	0.0263	0.0007	0.1416	0.0056	0.0061	0.2148	0.0342	0.4345	0.0007
26	27	13	12.745	1.3435	0.0234	0.0292	0.0009	0.1574	0.0020	0.0021	0.0677	0.0108	0.1370	0.0009
27	28	13.5	13.275	1.6156	0.0282	0.0224	0.0005	0.1210	0.0020	0.0018	0.0908	0.0145	0.1837	0.0005
28	29	14	13.87	1.2269	0.0214	0.0274	0.0008	0.1481	0.0015	0.0015	0.0546	0.0087	0.1105	0.0008
29	30	14.5	14.28	1.5297	0.0267	0.0202	0.0004	0.1088	0.0025	0.0024	0.1234	0.0196	0.2496	0.0004
30	31	15	14.895	1.0845	0.0189	0.0252	0.0006	0.1360	0.0030	0.0031	0.1185	0.0188	0.2396	0.0006
31	32	15.5	15.24	1.3588	0.0237	0.0189	0.0004	0.1020	0.0000	0.0000	0.0015	0.0002	0.0030	0.0004
32	33	16	15.85	1.0828	0.0189	0.0231	0.0005	0.1247	0.0012	0.0011	0.0513	0.0082	0.1037	0.0005
33	34	16.5	16.275	1.2909	0.0225	0.0183	0.0003	0.0989	0.0011	0.0012	0.0626	0.0100	0.1267	0.0003
34	35	17	16.81	1.0171	0.0178	0.0222	0.0005	0.1200	0.0006	0.0006	0.0258	0.0041	0.0522	0.0005
35	36	17.5	17.27	1.2580	0.0220	0.0169	0.0003	0.0913	0.0017	0.0020	0.0981	0.0156	0.1984	0.0003
36	37	18	17.655	0.9221	0.0161	0.0208	0.0004	0.1122	0.0023	0.0024	0.1112	0.0177	0.2249	0.0004
37	38	18.5	18.245	1.1256	0.0196	0.0145	0.0002	0.0785	0.0031	0.0025	0.2138	0.0340	0.4325	0.0002
38	2	0.5	18.87	0.7446	0.0130	0.0176	0.0003	0.0948	0.0041	0.0039	0.2358	0.0375	0.4770	0.0003
39	3	1	19.3	0.8892	0.0155	0.0129	0.0002	0.0697	0.0002	0.0002	0.0126	0.0020	0.0255	0.0002
40	4	1.5	19.79	0.7353	0.0128	0.0155	0.0002	0.0834	0.0001	0.0001	0.0082	0.0013	0.0166	0.0002
41	5	2	20.21	0.8819	0.0154	0.0125	0.0002	0.0677	0.0006	0.0006	0.0457	0.0073	0.0925	0.0002
42	6	2.5	20.76	0.7024	0.0123	0.0147	0.0002	0.0795	0.0013	0.0013	0.0889	0.0141	0.1798	0.0002
43	7	3	21.215	0.8069	0.0141	0.0122	0.0001	0.0660	0.0000	0.0000	0.0025	0.0004	0.0050	0.0001
44	8	3.5	21.67	0.7007	0.0122	0.0134	0.0002	0.0724	0.0013	0.0013	0.0990	0.0158	0.2002	0.0002
45	9	4	22.225	0.7309	0.0128	0.0112	0.0001	0.0603	0.0021	0.0021	0.1869	0.0297	0.3780	0.0001
46	10	4.5	22.67	0.5812	0.0101	0.0114	0.0001	0.0614	0.0027	0.0028	0.2417	0.0384	0.4890	0.0001
47	11	5	23.195	0.5739	0.0100	0.0099	0.0001	0.0532	0.0006	0.0006	0.0586	0.0093	0.1185	0.0001
48	12	5.5	23.66	0.5482	0.0096	0.0093	0.0001	0.0501	0.0014	0.0015	0.1556	0.0247	0.3147	0.0001
49	13	6	24.17	0.4913	0.0086	0.0095	0.0001	0.0511	0.0002	0.0002	0.0181	0.0029	0.0366	0.0001
50	14	6.5	24.62	0.5383	0.0094	0.0085	0.0001	0.0459	0.0001	0.0001	0.0161	0.0026	0.0325	0.0001
51	15	7	25.265	0.4834	0.0084	0.0082	0.0001	0.0443	0.0024	0.0023	0.2891	0.0460	0.5849	0.0001
52	16	7.5	25.64	0.4032	0.0070	0.0083	0.0001	0.0447	0.0003	0.0003	0.0361	0.0057	0.0729	0.0001
53	17	8	0.48	12.5362	0.2188	0.2098	0.0440	1.1342	0.0482	0.0487	0.2308	0.0367	0.4678	0.0441
54	18	8.5	0.99	10.6401	0.1857	0.1958	0.0383	1.0583	0.0461	0.0475	0.2364	0.0376	0.4793	0.0384
55	19	9	1.45	9.8966	0.1727	0.1706	0.0291	0.9220	0.0303	0.0308	0.1781	0.0283	0.3611	0.0291
56	20	9.5	1.975	8.9039	0.1554	0.1611	0.0259	0.8707	0.0233	0.0239	0.1450	0.0231	0.2940	0.0260
57	21	10	2.425	8.5604	0.1494	0.1406	0.0198	0.7602	0.0296	0.0299	0.2110	0.0336	0.4278	0.0198
58	22	10.5	2.965	7.2099	0.1258	0.1388	0.0193	0.7504	0.0212	0.0215	0.1530	0.0244	0.3102	0.0193
59	23	11	3.41	7.3457	0.1282	0.1209	0.0146	0.6536	0.0099	0.0104	0.0816	0.0130	0.1653	0.0146
60	24	11.5	3.915	6.6453	0.1160	0.1203	0.0145	0.6502	0.0159	0.0161	0.1321	0.0210	0.2677	0.0145
61	25	12	4.395	6.4368	0.1123	0.1082	0.0117	0.5847	0.0156	0.0158	0.1448	0.0230	0.2935	0.0117
62	26	12.5	4.905	5.7495	0.1003	0.1058	0.0112	0.5720	0.0131	0.0130	0.1238	0.0197	0.2509	0.0112
63	27	13	5.405	5.6874	0.0993	0.0956	0.0091	0.5168	0.0095	0.0096	0.0994	0.0158	0.2016	0.0091
64	28	13.5	5.89	5.2053	0.0908	0.0957	0.0092	0.5172	0.0072	0.0075	0.0751	0.0120	0.1523	0.0092
65	29	14	6.365	5.2758	0.0921	0.0856	0.0073	0.4628	0.0105	0.0103	0.1227	0.0195	0.2487	0.0073
66	30	14.5	6.91	4.6044	0.0804	0.0816	0.0067	0.4413	0.0209	0.0213	0.2571	0.0409	0.5213	0.0067
67	31	15	7.345	4.0795	0.0712	0.0761	0.0058	0.4112	0.0086	0.0087	0.1130	0.0180	0.2290	0.0058
68	32	15.5	7.895	4.1126	0.0718	0.0683	0.0047	0.3694	0.0057	0.0057	0.0839	0.0134	0.1701	0.0047
69	33	16	8.35	3.7512	0.0655	0.0668	0.0045	0.3611	0.0100	0.0101	0.1495	0.0238	0.3030	0.0045
70	34	16.5	8.885	3.5415	0.0618	0.0608	0.0037	0.3284	0.0094	0.0096	0.1557	0.0248	0.3156	0.0037
71	35	17	9.33	3.2104	0.0560	0.0592	0.0035	0.3198	0.0053	0.0054	0.0899	0.0143	0.1822	0.0035
72	2	0	9.87	3.2371	0.0565	0.0531	0.0028	0.2869	0.0059	0.0059	0.1119	0.0178	0.2268	0.0028
73	3	0.5	10.33	2.8706	0.0501	0.0520	0.0027	0.2813	0.0089	0.0088	0.1722	0.0274	0.3491	0.0027
74	4	1	10.89	2.7249	0.0476	0.0476	0.0023	0.2573	0.0050	0.0051	0.1051	0.0167	0.2130	0.0023
75	5	1.5	11.305	2.5843	0.0451	0.0462	0.0021	0.2500	0.0026	0.0028	0.0570	0.0091	0.1155	0.0021
76	6	2	11.845	2.5740	0.0449	0.0429	0.0018	0.2318	0.0044	0.0046	0.1038	0.0165	0.2104	0.0018
77	7	2.5	12.27	2.3296	0.0407	0.0447	0.0020	0.2414	0.0005	0.0005	0.0120	0.0019	0.0243	0.0020
78	8	3	12.83	2.5433	0.0444	0.0382	0.0015	0.2064	0.0049	0.0049	0.1296	0.0206	0.2627	0.0015
79	9	3.5	13.275	2.0464	0.0357	0.0430	0.0018	0.2323	0.0028	0.0030	0.0656	0.0104	0.1331	0.0018
80	10	4	13.785	2.3817	0.0416	0.0340	0.0012	0.1837	0.0035	0.0034	0.1019	0.0162	0.2065	0.0012
81	11	4.5	14.29	1.8482	0.0323	0.0396	0.0016	0.2139	0.0040	0.0042	0.1014	0.0161	0.2055	0.0016
82	12	5	14.74	2.1521	0.0376	0.0311	0.0010	0.1683	0.0023	0.0023	0.0726	0.0116	0.1473	0.0010
83	13	5.5	15.255	1.7187	0.0300	0.0354	0.0013	0.1916	0.0042	0.0042	0.1196	0.0190	0.2425	0.0013
84	14	6	15.74	1.9095	0.0333	0.0296	0.0009	0.1600	0.0008	0.0008	0.0273	0.0043	0.0554	0.0009
85	15	6.5	16.265	1.6724	0.0292	0.0326	0.0011	0.1763	0.0014	0.0015	0.0439	0.0070	0.0889	0.0011
86	16	7	16.71	1.8275	0.0319	0.0280	0.0008	0.1511	0.0025	0.0025	0.0884	0.0141	0.1792	0.0008
87	17	7.5	17.245	1.5309	0.0267	0.0304	0.0009	0.1645	0.0029	0.0029	0.0969	0.0154	0.1965	0.0009
88	18	8	17.72	1.6587	0.0289	0.0265	0.0007	0.1434	0.0004	0.0004	0.0138	0.0022	0.0280	0.0007
89	19	8.5	18.205	1.5099	0.0264	0.0284	0.0008	0.1534	0.0011	0.0012	0.0398	0.0063	0.0806	0.0008
90	20	9	18.69	1.5940	0.0278	0.0251	0.0006	0.1357	0.0025	0.0026	0.0997	0.0159	0.2020	0.0006
91	21	9.5	19.175	1.3667	0.0239	0.0276	0.0008	0.1493	0.0004	0.0004	0.0148	0.0024	0.0300	0.0008
92	22	10	19.695	1.5706	0.0274	0.0238	0.0006	0.1285	0.0001	0.0001	0.0062	0.0010	0.0126	0.0006
93	23	10.5	20.18	1.3582	0.0237	0.0262	0.0007	0.1417	0.0024	0.0025	0.0918	0.0146	0.1860	0.0007
94	24	11	20.665	1.4329	0.0250	0.0236	0.0006	0.1278	0.0001	0.0001	0.0060	0.0010	0.0123	0.0006
95	25	11.5	21.15	1.3500	0.0236	0.0238	0.0006	0.1289	0.0023	0.0024	0.0973	0.0155	0.1973	0.0006
96	26	12	21.635	1.3000	0.0227	0.0222	0.0005	0.1198	0.0028	0.0028	0.1258	0.0200	0.2550	0.0005
97	27	12.5	22.15	1.1904	0.0208	0.0209	0.0004	0.1132	0.0035	0.0034	0.1681	0.0267	0.3407	0.0004
98	28	13	22.68	1.0989	0.0192	0.0205	0.0004	0.1110	0.0005	0.0005	0.0245	0.0039	0.0497	0.0004
99	29	13.5	23.13	1.1616	0.0203	0.0191	0.0004	0.1034	0.0001	0.0001	0.0058	0.0009	0.0118	0.0004
100	30	14	23.655	1.0925	0.0191	0.0190	0.0004	0.1029	0.0025	0.0025	0.1312	0.0209	0.2660	0.0004
101	31	14.5	24.135	1.0188	0.0178	0.0176	0.0003	0.0952	0.0029	0.0029	0.1649	0.0262	0.3343	0.0003
102	1	0.5	0.455	17.6380	0.3078	0.2968	0.0881	1.6043	0.0932	0.0961	0.3167	0.0503	0.6419	0.0883
103	1	1	0.97	14.3363	0.2502	0.2677	0.0717	1.4468	0.0803	0.0828	0.3024	0.0481	0.6129	0.0718

H.8 : T1bk1df3

grouped	s/n	n (cycle)	t (s)	θi (deg)	θi (rad)	θm (rad)	$(\theta m)^2$	X =16.0m/3.Tn (rad/s)	δθ (rad)	θvel (rad/s)	δi (-)	ζi (-)	Pe	Xhm
	1	0	0	8.8836	0.1550									
1	2	0.5	0.47	7.6918	0.1342	0.1333	0.0178	0.7072	0.0435	0.0424	0.3290	0.0523	0.6544	0.0178
2	3	1	1.025	6.3934	0.1116	0.1143	0.0131	0.6064	0.0399	0.0387	0.3524	0.0560	0.7011	0.0131
3	4	1.5	1.5	5.4072	0.0944	0.0973	0.0095	0.5163	0.0285	0.0289	0.2951	0.0469	0.5869	0.0095
4	5	2	2.01	4.7598	0.0831	0.0851	0.0072	0.4513	0.0186	0.0180	0.2195	0.0349	0.4367	0.0072
5	6	2.5	2.535	4.3414	0.0758	0.0753	0.0057	0.3994	0.0156	0.0155	0.2073	0.0330	0.4124	0.0057
6	7	3	3.015	3.8686	0.0675	0.0677	0.0046	0.3589	0.0162	0.0164	0.2410	0.0383	0.4794	0.0046
7	8	3.5	3.525	3.4117	0.0595	0.0618	0.0038	0.3277	0.0115	0.0114	0.1868	0.0297	0.3716	0.0038
8	9	4	4.025	3.2094	0.0560	0.0540	0.0029	0.2866	0.0110	0.0109	0.2048	0.0326	0.4075	0.0029
9	10	4.5	4.535	2.7798	0.0485	0.0513	0.0026	0.2719	0.0095	0.0090	0.1865	0.0297	0.3709	0.0026
10	11	5	5.085	2.6635	0.0465	0.0445	0.0020	0.2360	0.0081	0.0079	0.1815	0.0289	0.3610	0.0020
11	12	5.5	5.56	2.3184	0.0405	0.0422	0.0018	0.2237	0.0086	0.0086	0.2050	0.0326	0.4078	0.0018
12	13	6	6.085	2.1698	0.0379	0.0379	0.0014	0.2009	0.0052	0.0051	0.1372	0.0218	0.2729	0.0014
13	14	6.5	6.57	2.0211	0.0353	0.0348	0.0012	0.1846	0.0061	0.0063	0.1768	0.0281	0.3518	0.0012
14	15	7	7.055	1.8181	0.0317	0.0317	0.0010	0.1683	0.0071	0.0070	0.2243	0.0357	0.4462	0.0010
15	16	7.5	7.58	1.6150	0.0282	0.0292	0.0009	0.1550	0.0050	0.0048	0.1717	0.0273	0.3416	0.0009
16	17	8	8.095	1.5312	0.0267	0.0246	0.0006	0.1307	0.0071	0.0070	0.2896	0.0460	0.5760	0.0006
17	18	8.5	8.59	1.2090	0.0211	0.0233	0.0005	0.1236	0.0068	0.0070	0.2961	0.0471	0.5890	0.0005
18	19	9	9.08	1.1388	0.0199	0.0199	0.0004	0.1054	0.0025	0.0026	0.1235	0.0196	0.2456	0.0004
19	20	9.5	9.53	1.0686	0.0186	0.0186	0.0003	0.0988	0.0025	0.0024	0.1350	0.0215	0.2686	0.0003
20	21	10	10.11	0.9950	0.0174	0.0174	0.0003	0.0921	0.0026	0.0024	0.1482	0.0236	0.2949	0.0003
21	22	10.5	10.62	0.9214	0.0161	0.0168	0.0003	0.0890	0.0012	0.0012	0.0697	0.0111	0.1387	0.0003
22	23	11	11.1	0.9279	0.0162	0.0159	0.0003	0.0841	0.0005	0.0005	0.0285	0.0045	0.0566	0.0003
23	24	11.5	11.61	0.8955	0.0156	0.0156	0.0002	0.0825	0.0013	0.0013	0.0823	0.0131	0.1636	0.0002
24	25	12	12.1	0.8547	0.0149	0.0149	0.0002	0.0791	0.0014	0.0014	0.0956	0.0152	0.1903	0.0002
25	26	12.5	12.61	0.8138	0.0142	0.0145	0.0002	0.0771	0.0008	0.0008	0.0523	0.0083	0.1041	0.0002
26	27	13	13.09	0.8111	0.0142	0.0142	0.0002	0.0751	0.0001	0.0001	0.0068	0.0011	0.0134	0.0002
27	28	13.5	13.66	0.8083	0.0141	0.0141	0.0002	0.0749	0.0001	0.0001	0.0057	0.0009	0.0113	0.0002
28	29	14	14.12	0.8065	0.0141	0.0141	0.0002	0.0747	0.0001	0.0001	0.0046	0.0007	0.0091	0.0002
29	30	14.5	14.66	0.8047	0.0140	0.0140	0.0002	0.0743	0.0002	0.0002	0.0111	0.0018	0.0221	0.0002
30	31	15	15.12	0.7976	0.0139	0.0139	0.0002	0.0737	0.0003	0.0003	0.0213	0.0034	0.0424	0.0002
31	32	15.5	15.56	0.7877	0.0137	0.0130	0.0002	0.0690	0.0018	0.0018	0.1399	0.0223	0.2782	0.0002
32	33	16	16.13	0.6935	0.0121	0.0128	0.0002	0.0679	0.0019	0.0019	0.1473	0.0234	0.2931	0.0002
33	34	16.5	16.56	0.6798	0.0119	0.0119	0.0001	0.0629	0.0005	0.0005	0.0402	0.0064	0.0800	0.0001
34	35	17	17.16	0.6661	0.0116	0.0107	0.0001	0.0565	0.0024	0.0023	0.2287	0.0364	0.4549	0.0001
35	36	17.5	17.61	0.5408	0.0094	0.0100	0.0001	0.0528	0.0033	0.0035	0.3390	0.0539	0.6743	0.0001
36	37	18	18.11	0.4746	0.0083	0.0083	0.0001	0.0439	0.0023	0.0023	0.2809	0.0447	0.5587	0.0001
37	38	18.5	18.6	0.4084	0.0071	0.0073	0.0001	0.0387	0.0020	0.0019	0.2696	0.0429	0.5362	0.0001
38	2	0.5	0.47	11.3648	0.1984	0.2012	0.0405	1.0726	0.0744	0.0744	0.3739	0.0594	0.7474	0.0406
39	3	1	1	9.3986	0.1640	0.1678	0.0282	0.8945	0.0611	0.0596	0.3680	0.0585	0.7356	0.0283
40	4	1.5	1.495	7.8658	0.1373	0.1390	0.0193	0.7407	0.0501	0.0501	0.3648	0.0580	0.7292	0.0194
41	5	2	2	6.5258	0.1139	0.1171	0.0137	0.6240	0.0404	0.0389	0.3490	0.0555	0.6975	0.0137
42	6	2.5	2.535	5.5486	0.0968	0.1010	0.0102	0.5383	0.0258	0.0248	0.2568	0.0408	0.5134	0.0102
43	7	3	3.04	5.0476	0.0881	0.0873	0.0076	0.4652	0.0192	0.0189	0.2203	0.0350	0.4404	0.0076
44	8	3.5	3.55	4.4514	0.0777	0.0798	0.0064	0.4254	0.0166	0.0166	0.2087	0.0332	0.4172	0.0064
45	9	4	4.04	4.0967	0.0715	0.0703	0.0049	0.3746	0.0148	0.0149	0.2115	0.0336	0.4228	0.0049
46	10	4.5	4.545	3.6027	0.0629	0.0645	0.0042	0.3440	0.0139	0.0137	0.2168	0.0345	0.4333	0.0042
47	11	5	5.055	3.2983	0.0576	0.0560	0.0031	0.2987	0.0137	0.0135	0.2450	0.0390	0.4898	0.0031
48	12	5.5	5.56	2.8198	0.0492	0.0515	0.0026	0.2743	0.0122	0.0119	0.2381	0.0379	0.4759	0.0027
49	13	6	6.08	2.5994	0.0454	0.0447	0.0020	0.2384	0.0090	0.0089	0.2019	0.0321	0.4035	0.0020
50	14	6.5	6.575	2.3044	0.0402	0.0411	0.0017	0.2189	0.0086	0.0085	0.2106	0.0335	0.4209	0.0017
51	15	7	7.095	2.1059	0.0368	0.0368	0.0014	0.1959	0.0069	0.0071	0.1891	0.0301	0.3779	0.0014
52	16	7.5	7.555	1.9074	0.0333	0.0341	0.0012	0.1818	0.0053	0.0051	0.1553	0.0247	0.3105	0.0012
53	17	8	8.125	1.8029	0.0315	0.0315	0.0010	0.1677	0.0036	0.0036	0.1161	0.0185	0.2320	0.0010
54	18	8.5	8.575	1.6984	0.0296	0.0303	0.0009	0.1617	0.0023	0.0023	0.0746	0.0119	0.1491	0.0009
55	19	9	9.09	1.6733	0.0292	0.0292	0.0009	0.1557	0.0009	0.0009	0.0300	0.0048	0.0600	0.0009
56	20	9.5	9.6	1.6482	0.0288	0.0272	0.0007	0.1449	0.0040	0.0038	0.1482	0.0236	0.2962	0.0007
57	21	10	10.16	1.4428	0.0252	0.0256	0.0007	0.1365	0.0063	0.0063	0.2474	0.0393	0.4944	0.0007
58	22	10.5	10.61	1.2870	0.0225	0.0234	0.0005	0.1247	0.0036	0.0037	0.1530	0.0243	0.3058	0.0005
59	23	11	11.13	1.2381	0.0216	0.0203	0.0004	0.1084	0.0042	0.0043	0.2091	0.0333	0.4180	0.0004
60	24	11.5	11.59	1.0441	0.0182	0.0189	0.0004	0.1008	0.0054	0.0053	0.2877	0.0457	0.5750	0.0004
61	25	12	12.14	0.9286	0.0162	0.0165	0.0003	0.0877	0.0035	0.0033	0.2148	0.0342	0.4294	0.0003
62	26	12.5	12.65	0.8423	0.0147	0.0136	0.0002	0.0726	0.0052	0.0054	0.3860	0.0613	0.7716	0.0002
63	27	13	13.1	0.6312	0.0110	0.0129	0.0002	0.0687	0.0036	0.0038	0.2843	0.0452	0.5683	0.0002
64	28	13.5	13.61	0.6338	0.0111	0.0101	0.0001	0.0540	0.0018	0.0017	0.1752	0.0279	0.3501	0.0001
65	29	14	14.13	0.5298	0.0092	0.0103	0.0001	0.0548	0.0016	0.0017	0.1516	0.0241	0.3030	0.0001
66	30	14.5	14.52	0.5447	0.0095	0.0088	0.0001	0.0470	0.0009	0.0008	0.0968	0.0154	0.1936	0.0001
67	31	15	15.16	0.4809	0.0084	0.0094	0.0001	0.0503	0.0001	0.0001	0.0156	0.0025	0.0312	0.0001
68	32	15.5	15.53	0.5363	0.0094	0.0077	0.0001	0.0412	0.0013	0.0014	0.1742	0.0277	0.3483	0.0001
69	33	16	16.14	0.4040	0.0071	0.0076	0.0001	0.0408	0.0034	0.0032	0.4556	0.0723	0.9106	0.0001
70	34	16.5	16.59	0.3400	0.0059	0.0059	0.0000	0.0316	0.0022	0.0021	0.3807	0.0605	0.7610	0.0000
71	35	17	17.18	0.2761	0.0048	0.0057	0.0000	0.0302	0.0005	0.0006	0.0966	0.0154	0.1931	0.0000
72	2	0	0.465	16.3575	0.2855	0.2862	0.0819	1.5124	0.1478	0.1508	0.5286	0.0838	1.0476	0.0825
73	3	0.5	0.98	12.1602	0.2122	0.2262	0.0512	1.1955	0.1186	0.1146	0.5368	0.0851	1.0638	0.0515
74	4	1	1.5	9.5633	0.1669	0.1792	0.0321	0.9469	0.0661	0.0652	0.3735	0.0593	0.7402	0.0322
75	5	1.5	1.995	8.3706	0.1461	0.1457	0.0212	0.7699	0.0425	0.0425	0.2938	0.0467	0.5822	0.0213
76	6	2	2.5	7.1289	0.1244	0.1266	0.0160	0.6690	0.0390	0.0382	0.3106	0.0494	0.6157	0.0161
77	7	2.5	3.015	6.1354	0.1071	0.1088	0.0118	0.5751	0.0312	0.0302	0.2891	0.0460	0.5729	0.0119
78	8	3	3.535	5.3393	0.0932	0.0941	0.0089	0.4972	0.0260	0.0254	0.2782	0.0442	0.5514	0.0089
79	9	3.5	4.04	4.6454	0.0811	0.0830	0.0069	0.4385	0.0204	0.0201	0.2476	0.0394	0.4908	0.0069
80	10	4	4.55	4.1681	0.0727	0.0749	0.0056	0.3958	0.0124	0.0120	0.1658	0.0264	0.3287	0.0056

Appendix I :Algorithm and damping coefficient estimates for the main techniques compared

s/no	Damping method/parameter estimates												
	Hyperbolic Model				Faltinsen			Modified Hyperbolic model					
	T1Bk0df1												
Optim. meth	β_{bL}	β_{bs}	α	R^2	β_1	β_2	R^2	β_{bL}	β_{bT}	β_{bS}	α	α 1	R^2
LVM	0.0762	0.02498	6.136	0.5505	0.3504	0.1482	0.2643	0.3893	0.3869	0.02491	0.7145	29.43	0.5512
TRSreg	0.0762	0.02498	6.136	0.5505	0.3504	0.1482	0.2643	0.03353	0.1048	0.02364	99.67	100.3	0.3341
G-N	0.423929	0.026004	0.423929	-	0.3504	0.1482	0.2643	0.08051	0.029499	0.02715	366.96	6.225	-
	T1Bk0df2												
Optim. meth	β_{bL}	β_{bs}	α	R^2	β_1	β_2	R^2	β_{bL}	β_{bT}	β_{bS}	α	α 1	R^2
LVM	1.223	0.0194	0.274	0.794	0.229	0.1924	0.7304	1.372	0.0196	0.01931	95.56	0.24	0.7942
TRSreg	0.1198	0.01957	3.133	0.7902	0.229	0.1924	0.7304	0.1019	0.02517	0.01817	96.91	1.483	0.794
G-N	0.3479	0.019473	0.746167	-	0.22904	0.1924	0.730	0.08868	0.02701	0.08119	8363.12	5.7744	-
	T1Bk1df1												
Optim. meth	**β_{bL}**	**β_{bs}**	**α**	**R^2**	**β_1**	**β_2**	**R^2**	**β_{bL}**	**β_{bT}**	**β_{bS}**	**α**	**α 1**	**R^2**
LVM	0.09526	0.03092	121.6	0.7746	0.4063	0.9616	0.7316	0.09833	0.04355	0.02732	956.8	78.73	0.7833
TRSreg	0.09531	0.03093	121.6	0.7746	0.4063	0.9616	0.7316	0.09832	0.04353	0.02732	958.4	78.8	0.7833
G-N	0.096	0.023	117.773	-	0.4146	0.9466	0.7415	0.0938	0.04455	0.02934	712.89	77.2426	-
	T1Bk1df2												
Optim.meth	**β_{bL}**	**β_{bs}**	**α**	**R^2**	**β_1**	**β_2**	**R^2**	**β_{bL}**	**β_{bT}**	**β_{bS}**	**α**	**α 1**	**R^2**
LVM	0.09648	0.02726	124.3	0.8058	0.3535	0.9936	0.7532	0.0989	0.03353	0.002707	11520	95.46	0.8607
TRSreg	0.09651	0.02727	124.1	0.8058	0.3535	0.9936	0.7532	0.0989	0.03354	0.002739	11490	95.42	0.8607
G-N	0.09676	0.027875	120.831	-	0.3608	0.9819	0.7575	0.09955	0.03472	0.01461	6586.34	90.682	-

I.1 Appendix I con't

s/no	Damping method/parameter estimates												
	Hyperbolic Model				Faltinsen			Modified Hyperbolic model					
	T1Bk2df1												
Optim. meth	**β_{bL}**	**β_{bs}**	**α**	**R^2**	**β_1**	**β_2**	**R^2**	**β_{bL}**	**β_{bT}**	**β_{bS}**	**α**	**α 1**	**R^2**
LVM	0.08441	0.0311	58.39	0.5813	0.3958	0.6459	0.5453	0.08807	0.05418	0.03082	99.75	33	0.5831
TRSreg	0.08441	0.0311	58.39	0.5813	0.3958	0.6459	0.5453	0.08816	0.05548	0.03083	96.56	32.04	0.5618
G-N	0.0844	0.0311	58.3675	-	0.3958	0.6459	0.5453	0.08812	0.0544	0.0308	99.4434	32.7343	-
	T1Bk2df2												
Optim. meth	**β_{bL}**	**β_{bs}**	**α**	**R^2**	**β_1**	**β_2**	**R^2**	**β_{bL}**	**β_{bT}**	**β_{bS}**	**α**	**α 1**	**R^2**
LVM	0.08463 0.08024	0.03713 0.02895	44.91 74.18	0.2385 0.6479	0.4975	0.4872	0.1915	0.08052 0.08303	0.03809	0.02705	331.2	51.73	0.681
TRSreg	0.08453 0.8023	0.03713 0.02895	45.11 74.22	0.2385 0.6479	0.4975	0.4872	0.1915	0.08052 0.083202	0.03877	0.02808	266.7	51.33	0.6521
G-N	0.085207	0.038466	41.3611	-	0.5198	0.443	0.1755	0.082725	0.041112	0.031073	126.472	52.2352	-
B1df1	T1Bk0df3												
Optim. meth	**β_{bL}**	**β_{bs}**	**α**	**R^2**	**β_1**	**β_2**	**R^2**	**β_{bL}**	**β_{bT}**	**β_{bS}**	**α**	**α 1**	**R^2**
LVM	0.06609 0.06195	0.01507 0.01465	10.01 11.41	0.2757 0.2908	0.1555 0.148	0.2379 0.2505	0.2465 0.2738	0.07887 0.2443	0.0163 0.01766	0.01422 0.01031	172.7 230	7.253 1.74	0.2924 0.5205
TRSreg	0.06609 0.06195	0.01507 0.01465	10.01 11.41	0.2757 0.2908	0.1555 0.148	0.2379 0.2505	0.2465 0.2738	0.03292 0.09348	0.07162 0.01687	0.01393 0.01004	62.11 298.8	69.59 5.587	0.2477 0.5213
G-N	0.0661	0.0151	10.0065	-	0.1555	0.2379	0.2465	0.0776383	0.0038611 2	0.0103135	312.592	5.8569	-
	T1Bk1df3												
Optim.meth	**β_{bL}**	**β_{bs}**	**α**	**R^2**	**β_1**	**β_2**	**R^2**	**β_{bL}**	**β_{bT}**	**β_{bS}**	**α**	**α 1**	**R^2**
LVM	0.09726	0.02544	20.42	0.4748	0.2628	0.5313	0.4509	0.1085 0.1072	0.03745 0.03481	0.0247 0.02075	94.56 195.8	12.14 12.99	0.4803 0.6616
TRSreg	0.09729	0.02544	20.41	0.4748	0.2628	0.5316	0.4509	0.1082 0.1072	0.03712 0.03483	0.02471 0.02076	95.94 195.2	12.27 12.97	0.4803 0.6616
G-N	0.097251	0.025443	20.4289	-	0.2628	0.5316	0.4509	0.10851	0.03754	0.02470	93.846	12.1077	-

Appendix J Coefficients obtained by Regression model for (Oliveira and Fernandes, 2012 and enhanced data set)

optimized coefficients for enhanced data						coefficients from Oliveira and Fernandez data					
ζ_L		ζ_s		α		ζ_L		ζ_s		α	
a0	-0.46	**b0**	0.0818	**c0**	-312	**a0**	2.6981	**b0**	0.7896	**c0**	5011.024
a1	-1.388	**b1**	0.177	**c1**	-1238	**a1**	7.6353	**b1**	2.1778	**c1**	11403.79
a2	1.264	**b2**	-0.147	**c2**	674	**a2**	-8.6424	**b2**	-2.4099	**c2**	-15529.1
a3	0.479	**b3**	-0.0826	**c3**	451	**a3**	-1.5981	**b3**	-0.4936	**c3**	-3211.97
a4	-0.461	**b4**	0.098	**c4**	-279	**a4**	1.9743	**b4**	0.601	**c4**	4228.756
a5	0.0442	**b5**	-0.00809	**c5**	37.5	**a5**	-0.174	**b5**	-0.0521	**c5**	-324.291
a6	-0.0506	**b6**	0.00724	**c6**	-44.1	**a6**	0.2182	**b6**	0.0633	**c6**	399.9839
a7	-0.01424	**b7**	0.00278	**c7**	-16.6	**a7**	0.0388	**b7**	0.0122	**c7**	85.58
a8	0.01681	**b8**	-0.00319	**c8**	16.3	**a8**	-0.0479	**b8**	-0.0151	**c8**	-108.738
a9	43.9	**b9**	-1	**c9**	12587	**a9**	-379.4189	**b9**	-107.16	**c9**	-534021
a10	-33	**b10**	-4.9	**c10**	2984	**a10**	447.7458	**b10**	121.3886	**c10**	695851.5
a11	-15.52	**b11**	0.87	**c11**	-7394	**a11**	90.3568	**b11**	26.376	**c11**	147005.2
a12	14.15	**b12**	0.51	**c12**	4399	**a12**	-110.6087	**b12**	-31.129	**c12**	-185891
a13	-1.561	**b13**	0.203	**c13**	-1063	**a13**	8.6285	**b13**	2.5192	**c13**	14470.44
a14	1.618	**b14**	-0.115	**c14**	914	**a14**	-10.9427	**b14**	-3.064	**c14**	-18114.1
a15	0.489	**b15**	-0.0702	**c15**	493	**a15**	-2.0915	**b15**	-0.6267	**c15**	-3859.88
a16	-0.000112	**b16**	0.000418	**c16**	3.39	**a16**	-0.0058	**b16**	-0.0011	**c16**	6.9821

Appendix K Regression model estimate of damping coefficients using only data from (Oliveira and Fernandes, 2012; 1—1 to 2--20) and enhanced data with experiment data set; T1bk0-T1bk1

													oliveira and Fernandez						Enhanced data set					
	input (dimensionalized)					input (non-dimensionalized)				output (measured)			predicted			error			predicted			error		
CASE	B(m)	T(m)	b_{bk}(m)	L_{bk}(m)	Tn (s)	T/B	b_{bk}/B	L_{bk}/B	gT_n^2/B	ζ_L	ζ_s	α	ζ_L	ζ_s	α	$\zeta_{L\ er}$	$\zeta_{s\ er}$	$\alpha_{\ er}$	ζ_L	ζ_s	α	$\zeta_{L\ er}$	$\zeta_{s\ er}$	$\alpha_{\ er}$
1--1	54.5	21	0	0	15.52	0.385	0	0	43.31	0.0515	0.012	3.488	0.0486	0.0114	3.0173	5.699	5.127	13.487	0.047	0.02	10.18	8.62	67.926	191.96
1--2	54.5	21	0.8	67.5	23.518	0.385	0.015	1.2385	99.46	0.0825	0.021	44.39	0.0702	0.0178	17.896	14.86	15.93	59.685	0.076	0.018	4.573	7.35	15.277	89.698
1--3	54.5	21	0.8	67.5	15.496	0.385	0.015	1.2385	43.18	0.0832	0.021	36.56	0.0742	0.0228	55.972	10.84	8.032	53.081	0.075	0.021	45.39	9.83	0.2106	24.129
1--4	54.5	8	0.8	67.5	21.636	0.147	0.015	1.2385	84.18	0.1268	0.03	176.3	0.1196	0.024	155.72	5.663	20.91	11.662	0.131	0.028	133.8	3.56	9.201	24.105
1--5	54.5	8	0.8	67.5	14.728	0.147	0.015	1.2385	39	0.1121	0.027	103.4	0.1049	0.0269	157.6	6.389	1.298	52.451	0.099	0.024	158.6	11.3	11.291	53.385
1--6	54.5	14.7	0.8	67.5	22.041	0.27	0.015	1.2385	87.36	0.1103	0.02	35.19	0.1051	0.0232	76.757	4.672	16.55	118.13	0.104	0.022	65	5.57	12.405	84.72
1--7	54.5	14.7	0.8	67.5	15.233	0.27	0.015	1.2385	41.73	0.0995	0.024	30.52	0.0887	0.0246	106.75	10.88	1.731	249.74	0.088	0.023	100.6	11.8	5.8179	229.52
1--8	54.5	21	1.2	67.5	15.6	0.385	0.022	1.2385	43.76	0.0844	0.032	65.79	0.0825	0.0271	76.813	2.205	15.83	16.76	0.084	0.026	67.98	0.85	20.56	3.3384
1--9	54.5	8	1.2	67.5	19.251	0.147	0.022	1.2385	66.64	0.1332	0.037	262.8	0.1287	0.0347	219.57	3.366	6.13	16.44	0.136	0.036	219.2	2.28	1.7734	16.565
1--10	54.5	8	1.2	67.5	14.672	0.147	0.022	1.2385	38.71	0.1219	0.037	244	0.1112	0.0329	193.51	8.755	11.44	20.679	0.103	0.032	194.3	15.2	14.087	20.351
1--11	54.5	14.7	1.2	67.5	22.444	0.27	0.022	1.2385	90.58	0.1062	0.035	112	0.0935	0.0336	175.3	11.98	4.734	56.507	0.114	0.041	166.9	7.7	15.182	49.025
1--12	54.5	14.7	1.2	67.5	15.038	0.27	0.022	1.2385	40.66	0.0903	0.036	99.31	0.0931	0.0288	139.3	3.063	19.47	40.27	0.095	0.029	132.1	4.99	20.036	33.005
1--13	54.5	21	1.8	67.5	15.665	0.385	0.033	1.2385	44.13	0.0962	0.032	218.7	0.0944	0.0337	109.83	1.884	7.143	49.781	0.096	0.033	103.5	0.12	3.9765	52.66
1--14	54.5	8	1.8	67.5	14.643	0.147	0.033	1.2385	38.56	0.1179	0.041	294.2	0.1209	0.0417	246.7	2.518	2.95	16.151	0.109	0.043	247.1	7.23	6.9896	16.026
1--15	54.5	14.7	1.8	67.5	14.597	0.27	0.033	1.2385	38.31	0.1099	0.045	110.9	0.0955	0.0333	187.69	13.12	25.19	69.235	0.105	0.036	174.7	4.63	18.324	57.549
2--1	54.5	21	1	127.2	15.604	0.385	0.018	2.3339	43.78	0.0598	0.017	44.99	0.0495	0.0122	19.278	17.26	29.38	57.149	0.067	0.019	20.57	12.5	11.154	54.28
2--2	54.5	14.7	1	127.2	15.179	0.27	0.018	2.3339	41.43	0.0745	0.018	43.74	0.07	0.0177	95.469	5.973	1.099	118.27	0.073	0.023	96.66	2.34	27.949	120.99
2--3	54.5	8	1	127.2	15.424	0.147	0.018	2.3339	42.78	0.0913	0.025	153.1	0.0849	0.0208	147.24	6.973	16.97	3.8251	0.08	0.027	163.4	12.1	7.2899	6.7257
2--4	57.35	16	1	130	13.583	0.279	0.017	2.2668	31.53	0.073	0.024	94.58	0.0699	0.0205	146.38	4.202	14.21	54.767	0.072	0.022	132.2	1.94	6.3515	39.726
2--5	57.35	16	3	130	14.064	0.279	0.052	2.2668	33.8	0.108	0.029	188.5	0.1047	0.0298	235.52	3.053	3.137	24.922	0.1	0.028	257	7.43	2.5788	36.293
2--6	54.52	23.78	1.5	227	21.134	0.436	0.028	4.1636	80.28	0.1353	0.022	138.7	0.1029	0.0205	146.9	23.94	8.099	5.9115	0.119	0.02	137	12.3	10.614	1.19
2--7	54.52	16.62	1.5	227	20.887	0.305	0.028	4.1636	78.42	0.1135	0.023	203.2	0.1114	0.0167	181.83	1.85	26.29	10.524	0.129	0.022	175.7	13.5	0.9269	13.546
2--8	54.52	11.27	1.5	227	20.724	0.207	0.028	4.1636	77.2	0.154	0.025	219	0.1235	0.0163	227.72	19.78	35.41	3.9653	0.139	0.024	221.3	9.85	6.6529	1.0202
2--9	56	15.136	0	0	12.663	0.27	0	0	28.06	0.049	0.018	121.7	0.0513	0.0178	97.417	4.62	2.074	19.98	0.065	0.016	57.96	33.2	11.464	52.389
2--10	56	15.136	1.2	99.2	12.808	0.27	0.021	1.7714	28.71	0.0626	0.02	212.5	0.0623	0.0205	167.69	0.483	2.977	21.07	0.082	0.025	152.4	30.4	26.368	28.285
2--11	56	15.136	1.5	99.2	12.81	0.27	0.027	1.7714	28.72	0.0682	0.023	179.9	0.0614	0.0208	188.95	10.03	8.925	5.0061	0.085	0.027	166.3	24.2	17.768	7.5614
2--12	56	15.136	1.8	99.2	12.803	0.27	0.032	1.7714	28.69	0.0693	0.021	210.6	0.0602	0.021	210.39	13.14	0.54	0.118	0.088	0.029	180.3	26.5	35.319	14.378
2--13	56	15.136	1.2	162.75	12.7956	0.27	0.021	2.9063	28.65	0.072	0.022	197	0.0642	0.0181	170.95	10.8	16.84	13.206	0.066	0.02	178.1	8.25	9.8031	9.5978
2--14	56	15.136	1.5	162.75	12.8334	0.27	0.027	2.9063	28.82	0.0725	0.022	219	0.0634	0.0179	194.02	12.51	17.05	11.389	0.065	0.019	191.9	10.3	9.7503	12.355
2--15	56	15.136	1.8	162.75	12.813	0.27	0.032	2.9063	28.73	0.0729	0.024	219	0.0612	0.0174	219.03	16.06	26.68	0.0164	0.064	0.019	206.9	12.6	18.682	5.5109
2--16	56	15.136	1.2	162.75	13.975	0.27	0.021	2.9063	34.18	0.0591	0.018	178.4	0.0768	0.0193	134.12	29.91	6.738	24.829	0.067	0.02	146.8	14.2	9.1652	17.694
2--17	56	15.136	1.2	99.2	13.1256	0.27	0.021	1.7714	30.15	0.0586	0.019	169.7	0.0665	0.0213	161.45	13.49	9.637	4.8497	0.082	0.025	148.5	40.3	29.622	12.483
2--18	56	15.136	1.5	99.2	13.057	0.27	0.027	1.7714	29.83	0.0583	0.02	181.9	0.0664	0.0219	184.07	13.97	8.925	1.2015	0.085	0.027	164.6	46.6	33.828	9.5298
2--19	56	15.136	1.2	162.75	13.085	0.27	0.021	2.9063	29.96	0.0665	0.022	178.4	0.0677	0.0185	161.56	1.864	16.98	9.4193	0.066	0.02	170.3	0.14	11.898	4.4996
2--20	56	15.136	1.5	162.75	13.144	0.27	0.027	2.9063	30.23	0.0697	0.022	193.8	0.0726	0.0196	183.82	4.197	11.92	5.1635	0.067	0.019	186.6	4.27	13.434	3.7074
T1bk0df1	38.4	12.16	0	0	9.616652	0.317	0	0	23.6	0.0762	0.025	6.136	-0.267	-0.064	302.08	450.1	356	4823.1	0.071	0.024	32.54	6.91	3.1034	430.37
T1bk0df2	38.4	16	0	0	9.85453	0.417	0	0	24.78	0.1223	0.019	0.274	-0.795	-0.208	1101	750.2	1170	401723	0.108	0.03	17.41	11.5	52.513	6253
T1bk1df1	38.4	12.16	1.2528	60.16	9.953163	0.317	0.033	1.5667	25.28	0.0953	0.031	121.6	-0.008	0.0025	196.71	108.4	91.94	61.767	0.092	0.029	151.7	3.39	6.7925	24.715
T1bk1df2	38.4	16	1.2528	60.16	10.15768	0.417	0.033	1.5667	26.33	0.0965	0.027	124.3	-0.099	-0.025	128.58	203	191.2	3.447	0.097	0.027	91.03	0.37	2.7439	26.765
T1bk2df1	38.4	12.16	0.6264	60.16	9.92844	0.317	0.016	1.5667	25.16	0.0844	0.031	58.39	0.0594	0.0223	190.27	29.67	28.4	225.85	0.073	0.025	123.4	13.4	18.096	111.32
T1bk2df2	38.4	16	0.6264	60.16	9.913736	0.417	0.016	1.5667	25.08	0.0802	0.029	74.18	0.0675	0.028	252.54	15.82	3.435	240.44	0.058	0.028	75.95	27.7	4.6067	2.3845
T1bk0df3	38.4	17.92	0	0	11.16619	0.467	0	0	31.82	0.062	0.047	11.41	-0.693	-0.181	962.74	1218	488.8	8337.7	0.079	0.034	21.66	26.8	26.588	89.814
T1bk1df3	38.4	17.92	1.2528	60.16	11.40229	0.467	0.033	1.5667	33.18	0.0973	0.025	20.42	-0.063	-0.015	57.385	165.2	160.6	181.02	0.09	0.027	38.31	7.84	4.3357	87.62

Appendix L Calibrations of various roll damping estimation techniques for T1bk1df2a2 data set.

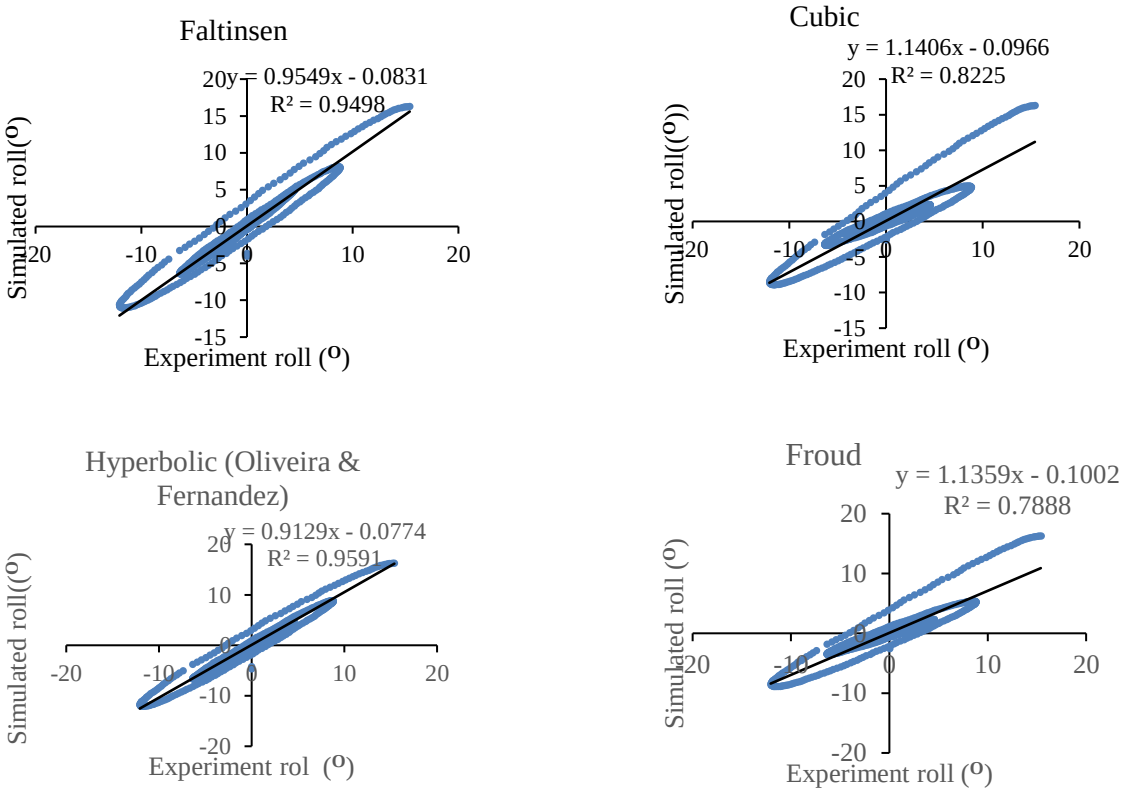

Appendix M Spectra shapes and contour plots for case 16;

M.1 BS+JSG

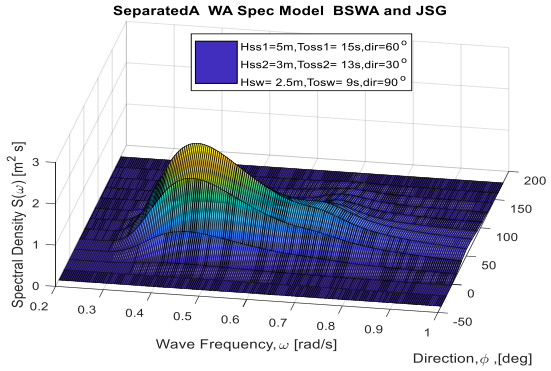

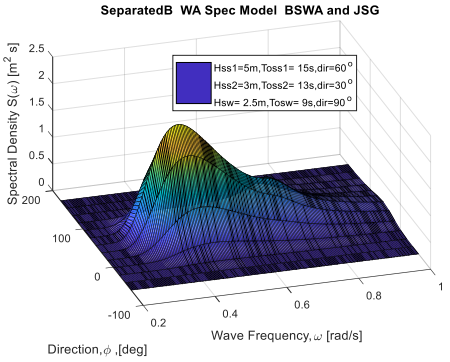

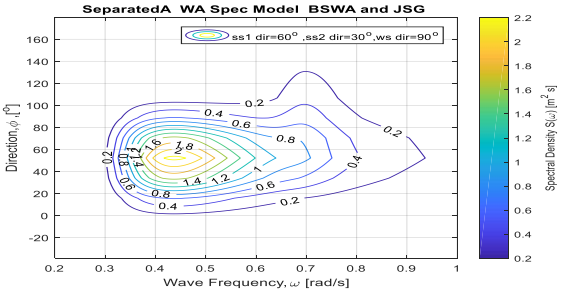

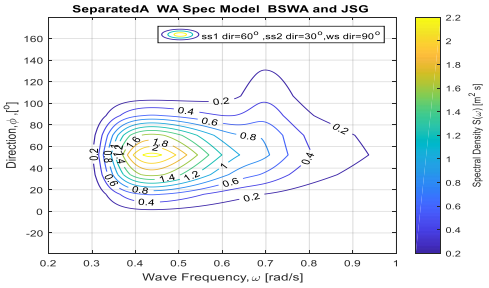

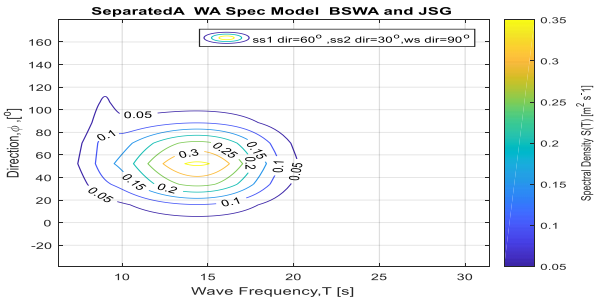

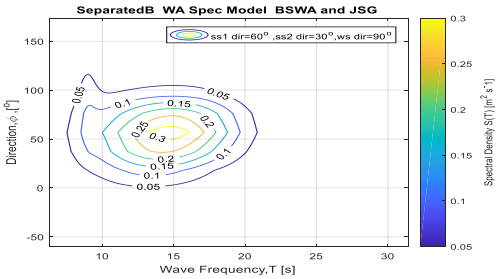

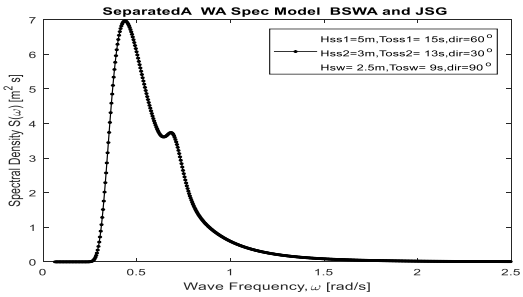

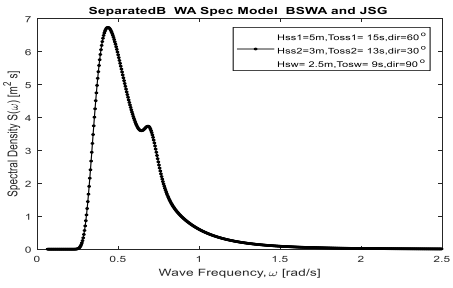

M.2 LogN+JSG

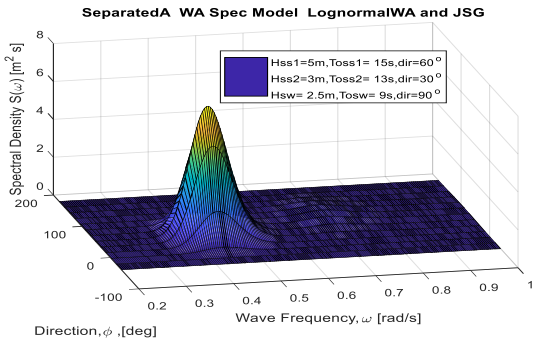
SeparatedA WA Spec Model LognormalWA and JSG
Hss1=5m,Toss1= 15s,dir=60°
Hss2=3m,Toss2= 13s,dir=30°
Hsw= 2.5m,Tosw= 9s,dir=90°
Spectral Density S(ω) [m² s]
Direction,ϕ ,[deg]
Wave Frequency, ω [rad/s]

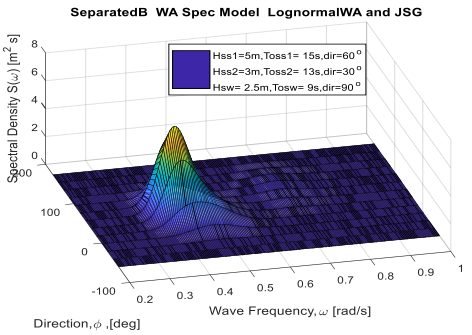
SeparatedB WA Spec Model LognormalWA and JSG
Hss1=5m,Toss1= 15s,dir=60°
Hss2=3m,Toss2= 13s,dir=30°
Hsw= 2.5m,Tosw= 9s,dir=90°
Spectral Density S(ω) [m² s]
Direction,ϕ ,[deg]
Wave Frequency, ω [rad/s]

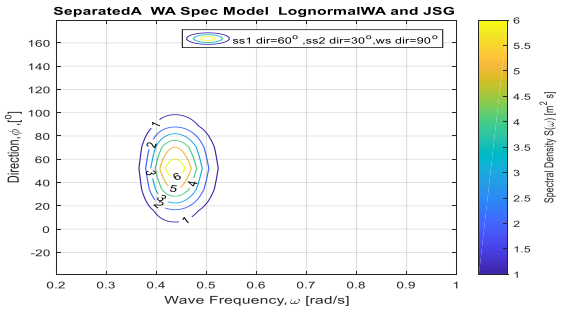
SeparatedA WA Spec Model LognormalWA and JSG
ss1 dir=60° ,ss2 dir=30°,ws dir=90°
Direction,ϕ ,[°]
Wave Frequency, ω [rad/s]
Spectral Density S(ω) [m² s]

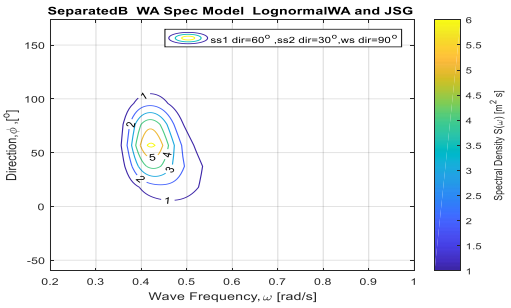
SeparatedB WA Spec Model LognormalWA and JSG
ss1 dir=60° ,ss2 dir=30°,ws dir=90°
Direction,ϕ ,[°]
Wave Frequency, ω [rad/s]
Spectral Density S(ω) [m² s]

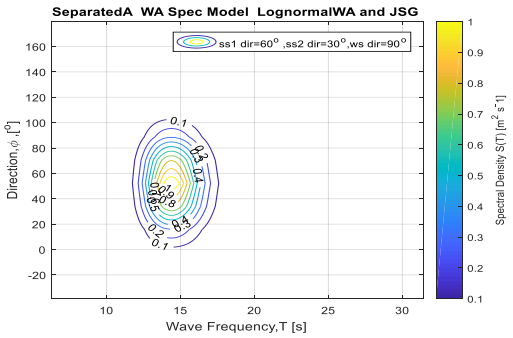
SeparatedA WA Spec Model LognormalWA and JSG
ss1 dir=60° ,ss2 dir=30°,ws dir=90°
Direction,ϕ ,[°]
Wave Frequency,T [s]
Spectral Density S(T) [m² s^-1]

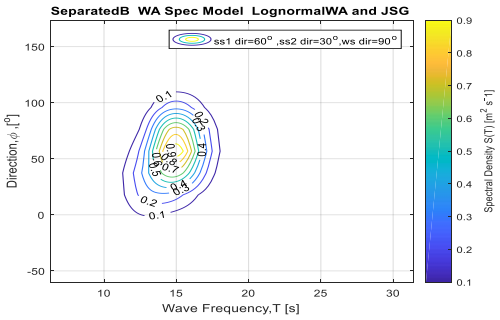
SeparatedB WA Spec Model LognormalWA and JSG
ss1 dir=60° ,ss2 dir=30°,ws dir=90°
Direction,ϕ ,[°]
Wave Frequency,T [s]
Spectral Density S(T) [m² s^-1]

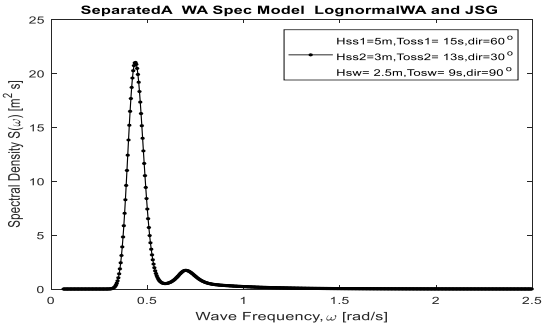
SeparatedA WA Spec Model LognormalWA and JSG
Hss1=5m,Toss1= 15s,dir=60°
Hss2=3m,Toss2= 13s,dir=30°
Hsw= 2.5m,Tosw= 9s,dir=90°
Spectral Density S(ω) [m² s]
Wave Frequency, ω [rad/s]

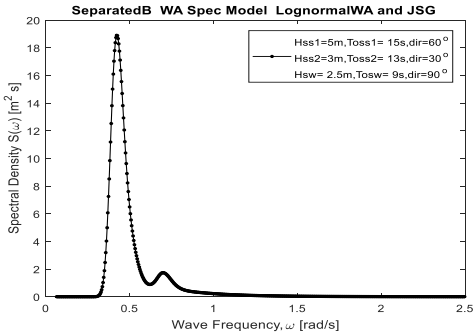
SeparatedB WA Spec Model LognormalWA and JSG
Hss1=5m,Toss1= 15s,dir=60°
Hss2=3m,Toss2= 13s,dir=30°
Hsw= 2.5m,Tosw= 9s,dir=90°
Spectral Density S(ω) [m² s]
Wave Frequency, ω [rad/s]

M.3 Ochu-Hubble+JSG

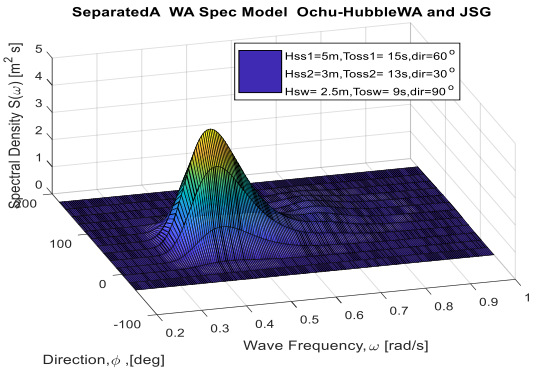

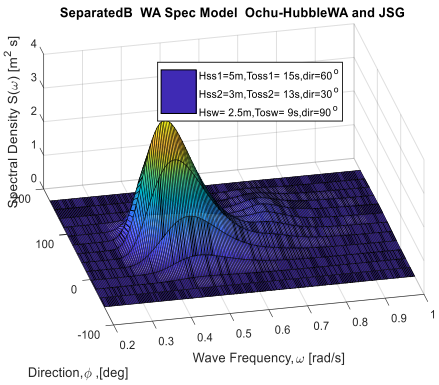

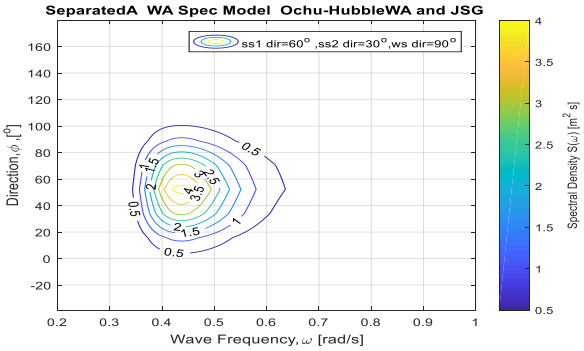

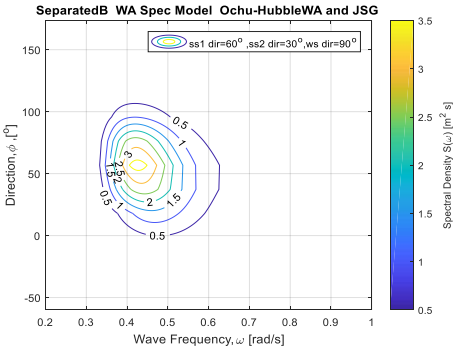

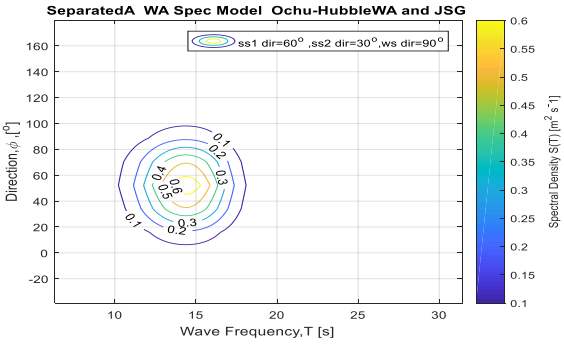

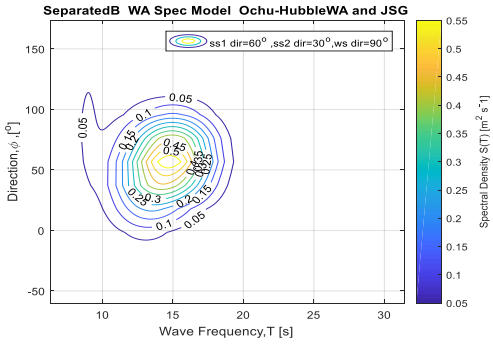

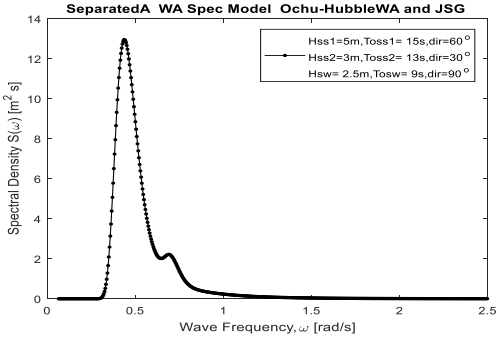

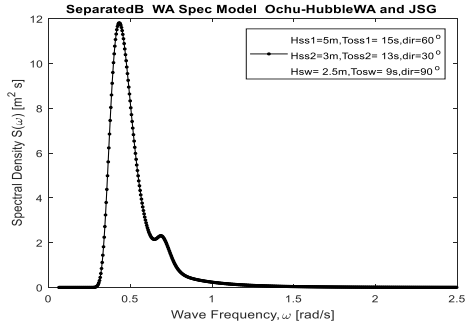

Appendix N Reconstructed data from OCIMF for VLCC to estimate Wind force coefficient.

		Cxw		Cyw		Cyw	
s/no	angle	Ballasted	Fully loaded	Ballasted	Fully loaded	Ballasted	Fully loaded
1	180	-0.87	-0.96	0	0	0	0
2	175	-0.81	-0.935	0.06	0.04	0.014	-0.004
3	170	-0.75	-0.9005	0.13	0.09	0.024	-0.008
4	165	-0.67	-0.86	0.215	0.145	0.034	-0.012
5	160	-0.61	-0.825	0.325	0.195	0.042	-0.018
6	155	-0.53	-0.78	0.43	0.25	0.048	-0.025
7	150	-0.46	-0.73	0.525	0.31	0.054	-0.034
8	145	-0.37	-0.67	0.6	0.37	0.058	-0.042
9	140	-0.265	-0.62	0.67	0.43	0.062	-0.051
10	135	-0.15	-0.55	0.73	0.5	0.063	-0.059
11	130	-0.005	-0.48	0.8	0.55	0.063	-0.066
12	125	0.14	-0.41	0.85	0.6	0.062	-0.074
13	120	0.29	-0.33	0.89	0.63	0.058	-0.082
14	115	0.4	-0.26	0.93	0.66	0.048	-0.088
15	110	0.46	-0.2	0.96	0.68	0.038	-0.094
16	105	0.5	-0.13	0.98	0.7	0.022	-0.1
17	100	0.48	-0.07	0.99	0.715	0.005	-0.103
18	95	0.39	-0.01	1	0.72	-0.016	-0.108
19	90	0.28	0.04	0.99	0.725	-0.036	-0.113
20	85	0.17	0.09	0.97	0.725	-0.063	-0.12
21	80	0.1	0.13	0.955	0.72	-0.082	-0.126
22	75	0.13	0.17	0.92	0.71	-0.098	-0.136
23	70	0.18	0.2	0.885	0.7	-0.114	-0.148
24	65	0.225	0.245	0.84	0.69	-0.124	-0.158
25	60	0.28	0.29	0.79	0.68	-0.134	-0.164
26	55	0.33	0.33	0.73	0.66	-0.144	-0.166
27	50	0.365	0.38	0.685	0.625	-0.148	-0.168
28	45	0.42	0.45	0.63	0.59	-0.152	-0.165
29	40	0.46	0.51	0.575	0.54	-0.154	-0.162
30	35	0.51	0.58	0.51	0.49	-0.15	-0.155
31	30	0.55	0.65	0.44	0.425	-0.143	-0.145
32	25	0.585	0.7	0.38	0.36	-0.126	-0.126
33	20	0.61	0.74	0.31	0.28	-0.106	-0.106
34	15	0.625	0.76	0.25	0.2	-0.084	-0.084
35	10	0.63	0.77	0.175	0.125	-0.055	-0.055
36	5	0.625	0.76	0.08	0.05	-0.028	-0.028
37	0	0.61	0.75	0	0	0	0

N.1 Appendix Table N1: Values of optimized fitted coefficients for current

Fourier				Sum of sines			
CXw							
Coefficients (with 95% confidence bounds):							
a0	-0.0456	(-0.06303,	-0.02816)	a1	2.047	(-23.39,	27.49)
a1	0.6909	(0.6372,	0.7446)	b1	0.02858	(-0.003252	0.0604)
b1	0.3724	(0.3077,	0.4371)	c1	0.6664	(-1.873,	3.205)
a2	0.1245	(0.08667,	0.1623)	a2	1.478	(-24.04,	27)
b2	-0.131	(-0.1554,	-0.1066)	b2	0.03303	(-0.001464	0.06752)
w	0.02234	(0.02133,	0.02335)	c2	3.464	(0.9001,	6.029)
Goodness of fit:							
SSE:	0.01226				0.01677		
R^2	: 0.999				0.9986		
Adjusted R^2	0.9988				0.9984		
RMSE:	0.01989				0.02326		
Cyw							
a1	0.7453	(0.7329, 0.7578)		a0	0.316	(0.2745, 0.3575)	
b1	0.01761	(0.01737, 0.01785)		a1	-0.2851	(-0.3273, -0.2429)	
c1	0.03887	(0.01209, 0.06565)		b1	0.3612	(0.2913, 0.4311)	
				a2	-0.01208	(-0.01488, -0.009285)	
				b2	0.03903	(0.02166, 0.0564)	
				a3	-0.02547	(-0.03216, -0.01877)	
				b3	0.007289	(-0.003533, 0.01811)	
				w	0.02569	(0.02364, 0.02774)	
SSE:	0.01915				0.000582		
R^2	0.9914				0.9997		
Adjusted R^2	0.9909				0.9997		
RMSE:	0.02373				0.004481		
CXYw							
a0	-0.03514	(-0.04408, -0.0262)		a1	0.1699	(-0.03639, 0.3763)	
a1	0.01575	(0.009576, 0.02192)		b1	0.01986	(0.008949, 0.03077)	
b1	-0.1071	(-0.1171, -0.09715)		c1	2.895	(1.231, 4.559)	
a2	0.01691	(0.009202, 0.02462)		a2	0.07425	(-0.13, 0.2785)	
b2	-0.04423	(-0.05459, -0.03387)		b2	0.03388	(0.01095, 0.05682)	
a3	0.001946	(-0.004661, 0.008554)		c2	-2.379	(-5.835, 1.078)	
b3	-0.02061	(-0.02826, -0.01297)		a3	0.01245	(0.001423, 0.02348)	
w	0.02114	(0.01915, 0.02312)		b3	0.07029	(0.05549, 0.0851)	
				c3	2.246	(0.6374, 3.855)	
SSE:	9.30E-05				8.64E-05		
R^2	0.9992				0.9992		
Adjusted R^2	0.999				0.999		
RMSE:	0.001791				0.001756		

Appendix O Reconstructed data from OCIMF for VLCC to estimate Current force Coefficient.

		Cxc		Cyw		Cyw	
s/no	angle	Ballasted	Fully loaded	Ballasted	Fully loaded	Ballasted	Fully loaded
1	180		-0.034		0		0
2	175		-0.033		0.04		0.01
3	170		-0.032		0.07		0.0175
4	165		-0.031		0.12		0.0275
5	160		-0.03		0.16		0.035
6	155		-0.026		0.2		0.04
7	150		-0.022		0.25		0.045
8	145		-0.016		0.29		0.05
9	140		-0.008		0.33		0.0525
10	135		0.003		0.37		0.05
11	130		0.016		0.4		0.0475
12	125		0.028		0.44		0.045
13	120		0.04		0.48		0.0425
14	115		0.043		0.51		0.035
15	110		0.042		0.54		0.025
16	105		0.04		0.56		0.02
17	100		0.036		0.58		0.01
18	95		0.026		0.6		-0.01
19	90		0.018		0.6		-0.0175
20	85		0.01		0.59		-0.025
21	80		0.004		0.58		-0.035
22	75		0		0.56		-0.0475
23	70		-0.004		0.54		-0.0575
24	65		-0.006		0.51		-0.065
25	60		-0.006		0.48		-0.07
26	55		-0.004		0.46		-0.0775
27	50		0		0.42		-0.08
28	45		0.006		0.38		-0.0825
29	40		0.014		0.34		-0.08
30	35		0.022		0.28		-0.0775
31	30		0.03		0.24		-0.075
32	25		0.036		0.2		-0.065
33	20		0.04		0.16		-0.0575
34	15		0.043		0.12		-0.0475
35	10		0.044		0.08		-0.035
36	5		0.046		0.04		-0.02
37	0		0.047		0		0

O.1 Appendix Table Q1: Values of optimized fitted coefficients for current

Fourier				Sum of sines			
CXc							
Coefficients (with 95% confidence bounds):							
a0	0.01077	(0.002398, 0.01914)		a1	0.01983	(-0.04609, 0.08575)	
a1	0.01152	(-0.0702, 0.09324)		b1	0.06979	(0.02821, 0.1114)	
b1	0.01516	(-0.01445, 0.04476)		c1	0.2569	(-3.245, 3.759)	
a2	0.02679	(-0.07949, 0.1331)		a2	0.0447	(-0.6303, 0.7197)	
b2	-0.009452	(-0.1599, 0.141)		b2	0.01686	(-0.01703, 0.05074)	
a3	-0.00509	(-0.02422, 0.01404)		c2	1.267	(-2.13, 4.664)	
b3	0.007008	(-0.09286, 0.1069)		a3	0.02921	(-0.4951, 0.5536)	
w	0.02567	(-0.003894, 0.05523)		b3	0.03328	(-0.2421, 0.3087)	
				c3	-2.938	(-25.95, 20.08)	
Goodness of fit:							
SSE:	0.0002559				0.000271		
R^2	0.99				0.9894		
Adjusted	0.9876				0.9864		
RMSE:	0.00297				0.003113		
Cyc							
a1	0.5696	(0.5595, 0.5796)		a0	0.2539	(0.2397, 0.268)	
b1	0.01813	(0.01788, 0.01837)		a1	-0.2462	(-0.2556, -0.2368)	
c1	-0.05778	(-0.0848, -0.03075)		b1	0.2268	(0.2, 0.2537)	
				w	0.02669	(0.02584, 0.02754)	
SSE:	0.01234				0.001471		
R^2	0.9912				0.9989		
Adjusted	0.9907				0.9989		
RMSE:	0.01905				0.006676		
CXYc							
a0	0.02784	(0.009771, 0.0459)		a1	0.1054	(-0.01955,	0.2303)
a1	0.02419	(0.003827, 0.04455)		b1	0.03103	(0.02527,	0.0368)
b1	-0.06731	(-0.1009, -0.03377)		c1	-2.545	(-3.254,	-1.836)
a2	-0.05451	(-0.08817, -0.02085)		a2	0.05627	(-0.06316,	0.1757)
b2	-0.0766	(-0.08182, -0.07138)		b2	0.02386	(0.01793,	0.02979)
w	0.01509	(0.0137, 0.01649)		c2	-4.484	(-5.878,	-3.09)
SSE:	0.0001126				0.000134		
R^2	0.9986				0.9984		
Adjusted	0.9984				0.9981		
RMSE:	0.001906				0.002077		

Appendix P : Numerical schemes adopted in solving the equation of motion

P.1 Runge-Kutta 4th Order

$$kg1 = dt1 * (Xivel(:, tnm));$$

$$kf1 = dt1 * (M\backslash(F(:, t) - B * Xivel(:, tnm) - C * Xi(:, tnm)));$$

$$t2 = tnb(tnm) + 0.5 * dt1;\ X2 = Xi(:, tnm) + 0.5 * kg1;$$

$$y2 = Xivel(:, tnm) + 0.5 * kf1;$$

$$kg2 = dt1 * (y2);$$

$$kf2 = dt1 * (M\backslash(F(:, t) - B * y2 - C * X2))\ ;$$

$$t3 = tnb(tnm) + 0.5 * dt1;\ X3 = Xi(:, tnm) + 0.5 * kg2;$$

$$y3 = Xivel(:, tnm) + 0.5 * kf2;$$

$$kg3 = dt1 * (y3);$$

$$kf3 = dt1 * (M\backslash(F(:, t) - B * y3 - C * X3));$$

$$t4 = tnb(tnm) + dt1;\ X4 = Xi(:, tnm) + kg3;$$

$$y4 = Xivel(:, tnm) + kf3;$$

$$kg4 = dt1 * (y4);$$

$$kf4 = dt1 * (M\backslash(F(:, t) - B * y4 - C * X4));$$

Variable approximations

$$Xi(:, tnm + 1) = Xi(:, tnm) + 1/6 * (kg1 + 2 * kg2 + 2 * kg3 + kg4);$$

$$Xivel(:, tnm + 1) = Xivel(:, tnm) + 1/6 * (kf1 + 2 * kf2 + 2 * kf3 + kf4);$$

P.2 Runge-Kutta Cashkarp

This is a multistep method, used for efficiency in computational time.

The first four terms are compute to kick start the process (using RGK4)

if tnm<=3

$$kg1 = (Xivel(:, tnm));$$

$$kf1 = M\backslash(F(:, t) - B * Xivel(:, tnm) - C * Xi(:, tnm));$$

$$t2 = tnb(tnm) + 0.2 * dt1;\ X2 = Xi(:, tnm) + 0.2 * dt1 * kg1;$$

$$y2 = Xivel(:, tnm) + 0.2 * dt1 * kf1;$$

$$kg2 = (y2);$$

$$kf2 = M\backslash(F(:, t) - B * y2 - C * X2);$$

$$t3 = tnb(tnm) + (3/10) * dt1;\ X3 = Xi(:, tnm) + (3/40) * dt1 * kg1 + (9/40) * dt1 * kg2;$$

$$y3 = Xivel(:, tnm) + (3/40) * dt1 * kf1 + (9/40) * dt1 * kf2;$$

$$kg3 = (y3);$$

$$kf3 = M\backslash(F(:, t) - B * y3 - C * X3);$$

$$t4 = tnb(tnm) + (3/5) * dt1;\ X4 = Xi(:, tnm) + (3/10) * dt1 * kg1 - (9/10) * dt1 * kg2 + (6/5) * dt1 * kg3;$$

$$y4 = Xivel(:, tnm) + (3/10) * dt1 * kf1 - (9/10) * dt1 * kf2 + (6/5) * dt1 * kf3;$$

$$kg4 = (y4);$$

$$kf4 = M\backslash(F(:, t) - B * y4 - C * X4);$$

$$t5 = tnb(tnm) + dt1;\ X5 = Xi(:, tnm) - (11/54) * dt1 * kg1 + (5/2) * dt1 * kg2 - (70/27) * dt1 * kg3 + (35/27) * dt1 * kg4;$$

$$y5 = Xivel(:, tnm) - (11/54) * dt1 * kf1 + (5/2) * dt1 * kf2 - (70/27) * dt1 * kf3 + (35/27) * dt1 * kf4;$$

$$kg5 = (y5);$$

$$kf5 = M\backslash(F(:, t) - B * y5 - C * X5);$$

$$t6 = tnb(tnm) + (7/8) * dt1;\ X6 = Xi(:, tnm) + (1613/55296) * dt1 * kg1 + (175/512) * dt1 * kg2 - (575/13824) * dt1 * kg3 + (44275/110592) * dt1 * kg4 + (253/4096) * dt1 * kg5;$$

$$y6 = Xivel(:, tnm) + (1613/55296) * dt1 * kf1 + (175/512) * dt1 * kf2 - (575/13824) * dt1 * kf3 + (44275/110592) * dt1 * kf4 + (253/4096) * dt1 * kf5;$$

$$kg6 = (y6);$$

$$kf6 = M\backslash(F(:, t) - B * y6 - C * X6);$$

Estimate the first 4 starter values for the Predictor/Corrector Method using RGK4

$$Xi(:, tnm + 1) = Xi(:, tnm) + dt1 * ((2825/27648) * kg1 + (18575/48384) * kg3 + (13525/55296) * kg4 + (277/14336) * kg5 + (1/4) * kg6);$$

$$Xivel(:, tnm + 1) = Xivel(:, tnm) + dt1 * ((2825/27648) * kf1 + (18575/48384) * kf3 + (13525/55296) * kf4 + (277/14336) * kf5 + (1/4) * kf6);$$

Commence the Multistep routine

if tnm > 3

Change Routine to Adams Bassfort (PREDICTOR) and Adams Moulton (CORRECTOR)

PREDICTOR

$$lg1 = dt1 * (Xivel(:, tnm));$$

$$lf1 = dt1 * (M\backslash(F(:, t) - B * Xivel(:, tnm) - C * Xi(:, tnm)));$$

$$t2 = tnb(tnm - 1);\ X2 = Xi(:, tnm - 1);$$

$$y2 = Xivel(:, tnm - 1);$$

$$lg2 = dt1 * (y2);$$

$$lf2 = dt1 * (M\backslash(F(:, t) - B * y2 - C * X2));$$

$$t3 = tnb(tnm - 2);\ X3 = Xi(:, tnm - 2);$$

$$y3 = Xivel(:, tnm - 2);$$

$$lg3 = dt1 * (y3);$$

$$lf3 = dt1 * (M\backslash(F(:, t) - B * y3 - C * X3));$$

$$t4 = tnb(tnm - 3);\ X4 = Xi(:, tnm - 3);$$

$$y4 = Xivel(:, tnm - 3);$$

$$lg4 = dt1 * (y4);$$

$$lf4 = dt1 * (M\backslash(F(:, t) - B * y4 - C * X4));$$

$$Xipred(:, tnm + 1) = Xi(:, tnm) + 1/24 * (55 * lg1 - 59 * lg2 + 37 * lg3 - 9 * lg4);$$

$$Xivelpred(:, tnm+1) = Xivel(:, tnm) + 1/24 * (55 * lf1 - 59 * lf2 + 37 * lf3 - 9 * lf4);$$

CORECTOR

$$mg1 = dt1 * (Xivelpred(:, tnm+1));$$

$$mf1 = dt1 * (M\backslash(F(:, t) - B * Xivelpred(:, tnm+1) - C * Xipred(:, tnm+1)));$$

$$Xicor(:, tnm+1) = Xi(:, tnm) + 1/24 * (9 * mg1 + 19 * lg2 - 5 * lg3 + lg4);$$

$$Xivelcor(:, tnm+1) = Xivel(:, tnm) + 1/24 * (9 * mf1 + 19 * lf2 - 5 * lf3 + lf4);$$

$$Xi(:, tnm+1) = Xicor(:, tnm+1);$$

$$Xivel(:, tnm+1) = Xivelcor(:, tnm+1);$$

Logical control to convert any 'NAN' computation to the immediate past value before next iteration this argument is justified since time step is a small duration

for $ii = 1{:}n$

$$Xi(ii, tnm+1) = Xi(ii, tnm+1 - isnan(Xi(ii, tnm+1)));$$

$$Xivel(ii, tnm+1) = Xivel(ii, tnm+1 - isnan(Xivel(ii, tnm+1)));$$

$$Xiaccl(ii, tnm+1) = Xiaccl(ii, tnm+1 - isnan(Xiaccl(ii, tnm+1)));$$

New solutions, stored in X, Xvel, Xaccl and used as the new initial conditions (Xi, Xivel, Xiaccl) for next time step iteration

$$\left.\begin{array}{l} X(:, t+1) = Xi(:, tnm+1) \\ Xvel(:, t+1) = Xivel(:, tnm+1) \\ XAccl(:, t+1) = Xiaccl(:, tnm \end{array}\right\}$$

P.3 Newmark-Beta 7 coefficient

Two types of computing acceleration are considered

i. Average

$gama = 1/2 ; beta = 1/4 ;$

ii. Linear

$gama = 1/2 ; beta = 1/6 ;$

Constants used in Newmark's Integration

$$a0 = 1/(beta * dt1\text{^}2); \quad a1 = gama/(beta * dt1);$$

$$a2 = 1/(beta * dt1); \quad a3 = 1/(2 * gama) - 1;$$

$$a4 = (gama/beta) - 1; \quad a5 = (gama/beta - 2) * dt1/2;$$

$$a6 = dt1 * (1 - gama); \quad a7 = gama * dt1;$$

$Ccap = C + a1 * B + a0 * M ;$ % Effective C (stiffness Matrix)

$aM = a0 * Xi(:, tnm) + a2 * Xivel(:, tnm) + a3 * Xiaccl(:, tnm);$

$aB = a1 * Xi(:, tnm) + a4 * Xivel(:, tnm) + a5 * Xiaccl(:, tnm);$

$CapF = F(:, t) + M * aM + B * aB;$ % use current value of force and moment computed

$Xi(:, tnm + 1) = (Ccap \backslash CapF);$

$Xiaccl(:, tnm + 1) = a0 * (Xi(:, tnm + 1) - Xi(:, tnm)) - a2 * Xivel(:, tnm) - a3 * Xiaccl(:, tnm);$

$Xivel(:, tnm + 1) = Xivel(:, tnm) + a6 * Xiaccl(:, tnm) + a7 * Xiaccl(:, tnm + 1);$

Appendix Q：Mathematical procedure used by Sesam in solving the hydrodynamic problem

Q.1 First order exciting forces in Irregular seas using the 3D diffraction radiation problem

Solving first order forces in irregular sea involves the solution of first order forces in regular longcrested sea formulations. This is currently done by the solution of the 3D diffraction-radiation problem of the floating body. The source density distribution method is a good approach to solving this boundary value problem on Rankine panels to estimate the potentials. The resulting solution are then converted to irregular seas by the superposition theory for different regular wave stream, and also introduction of the directional spread for shortcrested formulation. In formulating the Linear Boundary value problem (Robert, 1989; MAESTRO manual; Faltinsen, 1998; Newman,1977; Shin et al 2003 ;Hewlett 1997 and Ke et al,2012,) were consulted.

Using the standard seakeeping notation of the ship fixed Coordinate System (CS) of figure Q.1

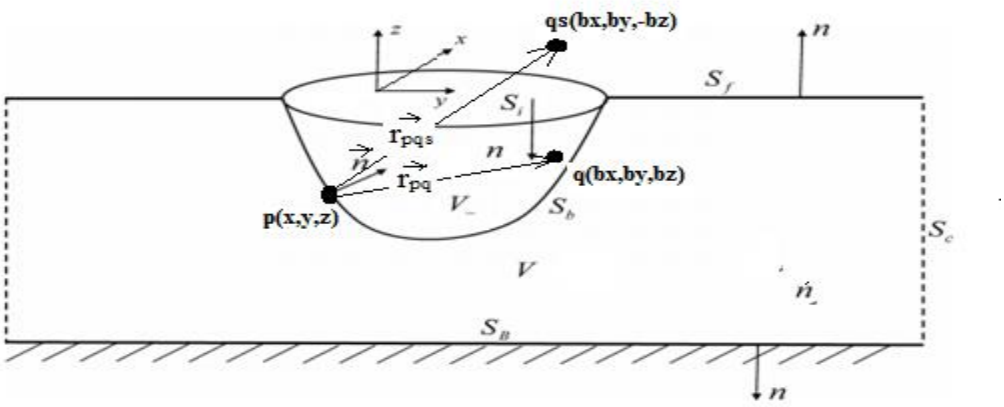

Figure Q.1 The CS and boundaries for the structure in fluid environment

The total velocity potential ψ is solved base on the Potential theory assumption,

Where;

$$\nabla\psi = iv_x + jv_y + kv_z \qquad \text{(Q.1)}$$

v_x, v_y and v_z are the component fluid velocities (i.e. $v = \nabla\psi$) .

For a potential flow,

The fluid is considered Irrotational, i.e.

Vorticity =$\vartheta = \nabla \times v = 0$ (Q.2)

Obeys the Laplace or continuity condition: $\nabla^2 . \psi = 0$ Q.3)

The total potential is then written as a combination of two other potential components

$\psi = \Phi + \varphi$ (Q.4)

The double body potential can then be written as

$\Phi = -Ux + \emptyset$ (Q.5)

Subject to the following boundary conditions (BC) in-line with the potential flow assumption

Laplace condition: $\nabla^2 . \Phi = 0$ (Q.6)

Free surface condition: $\frac{\partial \Phi}{\partial z} = 0$ (Q.7)

Body surface, impermeability condition: $\frac{\partial \Phi}{\partial n} = 0$ (Q.8)

With:

$\emptyset$ been the steady potential of a source density distribution over the body surface ***'S_b'***

$\vec{n} = (n_x, n_y, n_z)$, at point p(x, y, z) in space of the ship fixed CS.

The potential at point p, as a result of a unit source located at a point $q(b_x, b_y, b_z)$ on the ship body is expressed using the green function G which satisfies the Laplace condition.

$G^*{}_{pq} = \frac{1}{\vec{r}_{pq}}$ (Q.9)

$\vec{r}_{pq}$ is the distance between p and q. With $q_s(b_x, b_y, -b_z)$ as the symmetry image of point $q(b_x, b_y, b_z)$ about the water plane. The potential at point p, due to a unit source located at q_s is

$$G^*_{pq_s} = \frac{1}{\vec{r}_{pq_s}} \quad \text{(Q.10)}$$

The parameter $\frac{1}{\vec{r}_{pq_s}}$ is referred to as elementary singularity.

The potential at point p due to source density distribution (σ_p) on the body can then be computed as

$$\emptyset(x,y,z) = \oiint_S \; G_{p,q}\, \sigma_q dS \quad \text{(Q.11)}$$

Where the double body Green function is:

$$G_{p,q} = G^*_{pq} + G^*_{pq_s} = \frac{1}{\vec{r}_{pq}} + \frac{1}{\vec{r}_{pq_s}} \quad \text{(Q.12)}$$

From BC of equation 5.19,

The integral form of the source density can be expressed as equation Q.13, and solved for σ_p.

$$2\pi.\sigma_p + \oiint_S \; \frac{\partial G_{p,q}}{\partial n}.\sigma_q \, ds = n_x U = 0 \quad (for\ U = O) \quad \text{(Q.13)}$$

Substituting the solution of σ_p obtained from equation Q.13, into equation Q.11 and differentiating partially w.r.t. to the desired axis, the velocity components at any point of the flow p(x,y,z) can be thus computed from equation Q.14,

$$\nabla\emptyset(x,y,z) = \oiint_S \; \nabla G_{p,q}\, \sigma_p dS \quad \text{(Q.14)}$$

The Unsteady part of the total potential can be analysed by the superposition of the potential due to Froude-Krylov (undisturbed incoming wave stream), diffraction stream and the radiated wave stream. Thus ;

$$\varphi = \varphi_o + \varphi_7 + \sum_{i=1}^{6} \varphi_i \quad \text{(Q.15)}$$

Equation Q.15 can be written w.r.t. to the incident wave amplitude **ζ_o,** which is measured, based on the earth fixed axis CS and varies with time t.

$$\varphi = [\zeta_o(\varphi_o + \varphi_7) + \sum_{i=1}^{6} \varphi_i]e^{i\omega t} \quad \text{(Q.16)}$$

Equation Q.16 is a combination of a space dependent term and a time-varying harmonic term.

The angular velocity terms are expressed as

$$\omega_e = \omega - U.k.cos\mu \quad \text{(Q.17)}$$

$$k = \frac{\omega^2}{g} \quad \text{(Q.18)}$$

For the FPSO at the station (zero speed),

$U = 0\,, \quad \rightarrow \omega_e = \omega.$

The incident wave velocity potential for a first order approximation wave, in infinite deep water can be written as

$$\varphi_0 = i\frac{g}{\omega}e^{k(z-txcos\mu-tysin\mu)} \quad \text{(Q.19)}$$

The velocities at any point can then be computed by differentiating equation Q.19 w.r.t to desired axis, thus:

$$u_x = \frac{\partial\varphi_0}{\partial x} \quad \text{(Q.20)}$$

$$u_y = \frac{\partial\varphi_0}{\partial y} \quad \text{(Q.21)}$$

$$u_z = \frac{\partial\varphi_0}{\partial z} \quad \text{(Q.22)}$$

The acceleration components can be obtained by further differentiating equation Q.22

$$a_{x=}\dot{u}_x = \frac{du_x}{dt} = \frac{d}{dt}\left(\frac{\partial\varphi_0}{\partial x}\right) \quad \text{(Q.23)}$$

$$a_{y=}\dot{u}_y = \frac{du_y}{dt} = \frac{d}{dt}\left(\frac{\partial\varphi_0}{\partial y}\right) \quad \text{(Q.24)}$$

$$a_{z=}\dot{u}_z = \frac{du_z}{dt} = \frac{d}{dt}\left(\frac{\partial\varphi_0}{\partial z}\right) \quad \text{(Q.25)}$$

Q.1.1 Radiation Force computation

The radiation force is obtained by solving the Radiation potential φ_i problem. Each of the radiation potential φ_i for the six components (i=1-6) are subjected to the following boundary conditions according to the potential flow assumption as well;

Laplace or continuity condition: $\nabla^2.\varphi_i = 0$ (Q.26)

Free surface condition: $\frac{\partial \varphi_i}{\partial z} - k\varphi_i = 0$ (Q.27)

Body surface condition1: $\frac{\partial \varphi_i}{\partial n} = i\omega.n_i + m_i$ (Q.28)

Body surface, impermeability condition: $\frac{\partial \varphi_i}{\partial n} = 0$ (Q.29)

Note that:

$\vec{n} = (n_1, n_2, n_3)$, (normal vector translation along axis) (Q.30)

$\vec{r} = (x, y, z)$ (Displacement vector or any point in space within x,y,z in CS) (Q.31)

$(n_4, n_5, n_6) = \vec{r} \times \vec{n}$ (Normal to plane of rotation about the axis) (Q.32)

$(m_1, m_2, m_3) = -(\vec{n}.\nabla)\nabla\Phi$ (P.33)

$(m_4, m_5, m_6) = -(\vec{n}.\nabla)(\vec{r} \times \nabla\Phi)$ (Q.34)

Similar to equation 5.24

$2\pi.\sigma_{i(p)} + \oiint_S \frac{\partial G_{p,q}}{\partial n}.\sigma_{i(q)} ds = i\omega.n_i + m_i$ (for i=1-6) (Q.35)

The green function is similarly obtained as:

$G_{p,q} = \frac{1}{\vec{r}_{pq}} + \frac{1}{\vec{r}_{pq_s}} + kF(\boldsymbol{X}, \boldsymbol{Y}) - 2\pi.ike^{-\boldsymbol{Y}}.J_0(\boldsymbol{X})$ (Q.36)

Some of the parameters, the radius (R) and displacement vector components ($\vec{x}, \vec{y}$) on the horizontal plane are represented below in absolute and non-dimensionalised forms as

$R = \left[(x - b_x)^2 + \left(y - b_y\right)^2\right]^{1/2}$ (Q.37)

$\boldsymbol{X} = kR$ (Non-dimensionalised radius) (Q.38)

$\boldsymbol{Y} = k(z + b_z)$ (Non-dimensionalised vertical displacement vector) (Q.39)

$$F(\boldsymbol{X}, \boldsymbol{Y}) = \pi e^{-\boldsymbol{Y}}.[H_0(\boldsymbol{X}) + Y_0(\boldsymbol{X})] - 2e^{-\boldsymbol{Y}} \int_0^{\boldsymbol{Y}} \frac{e^{-t}}{(\boldsymbol{X}^2 + t^2)^{1/2}}\, dt \quad \text{(Q.40)}$$

See (Newman 1963) for specific expressions of equation P.40 for small and large values of the $(\boldsymbol{X}/\boldsymbol{Y})$.

J_0, Y_0, H_0 simply connote the zero order Bessel function of first and second kind and the zero order Struve function respectively which can be written in their integral forms and then substituted into equation Q.40 and Q.36. The resulting modified equation Q.40 is numerically integrated using the self-adaptive Simpson's integral.

With $G_{p,q}$ *and* $\sigma_{i(q)}$ known, from solving equation P.31 for all *i=1-6*, the radiation velocity potential for all 'i' can be obtained in a similar way as equation. Q.41, thus:

$$\varphi_i(x, y, z) = \oiint_S G_{p,q}\, \sigma_{i(q)} dS \qquad (for\ i = 1 - 6) \quad \text{(Q.41)}$$

Then the associated velocity and acceleration components at any point p(x, y, z) can be determined by differentiating equation Q.41 as it was done in equation Q.14.

$$\nabla\varphi_i(x, y, z) = \oiint_S \nabla G_{p,q}\, \sigma_{i(q)} dS \qquad (for\ i = 1 - 6) \quad \text{(Q.42)}$$

Q.1.2 Added mass, Damping and Restoring coefficients

The Added mass(A_{ij}) and potential damping (B_{ij}) coefficients are calculated from the radiation potential (φ_j). They are frequency and speed dependent and associated with the first pressure term obtained from the total pressure as shown in equation. Q.43

The total Pressure (unsteady and steady) can then be estimated using the Bernoulli's principle. With the velocities computed from above, the total pressure is computed as

$$P = \rho(\psi_t + \tfrac{1}{2}\nabla\psi.\nabla\psi - \tfrac{1}{2}U^2 + gz) \quad \text{(Q.43)}$$

Expanding and separating the unsteady (Pu) and the steady (Ps) pressure fields yields:

Recall that $\psi = \Phi + \varphi$; then'

$$P_U = -\rho(\varphi_t + \nabla\Phi.\nabla\varphi - \rho\left[(\vec{\boldsymbol{a}}.\nabla)(\frac{\nabla\Phi.\nabla\Phi}{2} + gz)\right] \quad \text{(Q.44)}$$

$$P_S = -\rho\left[\frac{\nabla\Phi.\nabla\Phi}{2} - \frac{1}{2}U^2 + gz\right] \quad \text{(Q.45)}$$

Where,

$$\vec{\boldsymbol{a}} = \vec{\zeta}_T + \vec{\Omega} \times \vec{r} \quad \text{(Q.46)}$$

$$\vec{\zeta}_T = (\xi_1, \xi_2, \xi), \quad \text{(RAO of translational motions)} \quad \text{(Q.47)}$$

$$\vec{\Omega} = (\xi_4, \xi_5, \xi_6) \quad \text{(RAO of rotational motions)} \quad \text{(Q.48)}$$

The added mass, damping and restoring coefficients are thus obtained as shown below;

$$A_{ij}(\omega) = -\frac{\rho}{\omega^2}\,.\,\mathrm{Re}\left\{\iint_B \left[i\omega\varphi_j + \nabla\Phi.\nabla\varphi_j\right] n_i\, ds\right\} \quad for\ \ i,j = 1-6 \quad \text{(Q.49a)}$$

$$\boldsymbol{A_{ij}} = A_{ij}(\omega) + \frac{1}{\omega}\int_0^\infty \boldsymbol{K_{ij}}(\boldsymbol{t})sin(\omega t)dt \quad \text{(Q.49b)}$$

The retardation function is computed with the knowledge of the frequency dependent damping as;

$$B_{ij}(\omega) = -\frac{\rho}{\omega^2}\,.\,\mathrm{Im}\left\{\iint_B \left[i\omega\varphi_j + \nabla\Phi.\nabla\varphi_j\right] n_i\, ds\right\} \quad for\ \ i,j = 1-6 \quad \text{(Q.50a)}$$

$$\boldsymbol{B_{ij}} = B_{ij}(\omega) - \int_0^\infty \boldsymbol{K_{ij}}(\boldsymbol{t})cos(\omega t)dt \quad \text{(Q.50b)}$$

The retardation function is computed with the knowledge of the frequency dependent damping using equation Q.51

$$\boldsymbol{K_{ij}} = \frac{2}{\pi}\int_0^\infty B_{ij}(\omega)cos(\omega t)d\omega \quad \text{(Q.51)}$$

The restoring or hydrostatic coefficient and force/moments are calculated by integration of the incident hydrostatic pressure over the wetted surface of the hull.

$$C_{ij} = \rho\,.\iint_B \left[(\vec{\boldsymbol{a}}.\nabla)(\frac{\nabla\Phi.\nabla\Phi}{2} + gz)\right] n_i\, ds \quad for\ \ i,j = 1-6 \quad \text{(Q.52)}$$

With the calculation of the frequency dependent terms from equation Q.49, Q.50, the frequency independent terms ($\boldsymbol{A_{ij}}, \boldsymbol{B_{ij}}$) in the time domain model of the equation of motion are computed according to equation Q. 49b and Q.50b and the equation of motion solved appropriately.

The radiation force is then obtained from the equation below

$$\boldsymbol{F}_{radw\,i} = -A_{ij}.\ddot{x}_j - B_{ij}.\dot{x}_j - C_{ij}.x_j \qquad \text{(Q.53)}$$

Q.1.3 Froude Krylov Force computation

The Froude-Krylov excitation is due to the incident wave potentials as earlier illustrated in equation Q.19. It is calculated by the direct integration of the incident wave pressure over the wetted surface area of hull.

$$\boldsymbol{F}_{ifk} = \rho\,.\iint_B [i\omega(\varphi_o) + \nabla\Phi.\nabla(\varphi_0)]\,n_i\,ds \quad for\ \ i,j = 1-6 \qquad \text{(Q.54)}$$

Q.1.4 Diffraction Force computation

The diffraction potential (φ_7) problem is first solved, φ_7 is subjected to the following BC similar to the radiation potential problem

Laplace condition: $\nabla^2.\varphi_7 = 0$ (in volume) (Q.55)

Free surface condition (z=0; plane of undisturbed free surface):

$$\frac{\partial^2\varphi_7}{\partial t^2} + g\frac{\partial\varphi_{e7}}{\partial z} = 0, \quad \text{(e=1-6)} \qquad \text{(Q.56)}$$

Free surface condition (z=0, t=0); $\varphi_7 - \frac{\partial\varphi_7}{\partial t} = 0$ (Q.57)

Body surface condition: $\frac{\partial(\varphi_7+\varphi_0)}{\partial n} = 0$ (Q.58)

Body surface, impermeability condition: $\frac{\partial\varphi_7}{\partial n} = 0$ (Q.59)

With

$$\varphi_0 = Re.\frac{g}{2\pi}\int_{-\infty}^{\infty}\frac{i}{\omega}e^{kz-ik(x\cos\mu+y\sin\mu)+i\omega t}\,d\omega_e \qquad \text{(Q.60)}$$

The corresponding diffraction potential Source density on body surface is obtained as

$$2\pi.\sigma_{7(p)} + \oiint_S \frac{\partial G_{p,q}}{\partial n}.\sigma_{7(q)}\, ds = \frac{\partial \varphi_0}{\partial n} \qquad \text{(Q.61)}$$

Using the Green function technique of equation Q.36 -Q.49, the boundary value problem can be solved and solutions for the diffraction velocity potential and velocity components obtained as

$$\varphi_7(x,y,z) = \oiint_s \; G_{p,q}\, \sigma_{7(q)} dS \qquad \text{(Q.62)}$$

$$\nabla\varphi_7(x,y,z) = \oiint_s \; \nabla G_{p,q}\, \sigma_{7(q)} dS \qquad \text{(Q.63)}$$

The diffraction force is then written as

$$\boldsymbol{F}_{idf} = \rho\,.\iint_B \left[i\omega(\varphi_7) + \nabla\Phi.\nabla(\varphi_7)\right] n_i\, ds \quad for\;\; i,j = 1-6 \qquad \text{(Q.64)}$$

The procedure above are then followed to expand the solutions for an irregular sea condition by the inclusion of the multiple regular frequencies and perhaps the directional spread for the shortcrested formulation. Haven obtained the parameters needed to define the equation of motion as expressed in equation 5.1, with the other components added as static components if required, the equation of motion is then adequately solved.

Q.1.5 First Order motions in Irregular seas

Irregular sea motions are solved from the knowledge of regular sea formations. With the potential problem solved for the regular wave formulations and the excitation forces obtained. The equation of motion is solved in frequency or time domain to obtain the motion complex response amplitude operator (RAO), that is the square of the transfer function $Z_k(\omega,\theta)$ or the response time series respectively. For regular wave stream the body motion amplitude is linearly related to the wave amplitude through $Z_k(\omega,\theta)$. Generally, the spectrum of the k^{th} motion mode is related to the incident wave spectrum by the equation below

$$S_{\xi k}(\omega) = \int_{-\pi}^{\pi} |Z_k(\omega,\theta)|^2 . S_\zeta(\omega,\theta).d\theta \qquad \text{(Q.65)}$$

For a given mode of motion, the significant value ($\xi_{k.1/3}$) is extracted from the area under the motion spectrum or its variance (mo) as;

$$\xi_{k.1/3} = 4 * \sqrt{mo} \quad \text{(Q.66)}$$

Where

$$mo = \int_0^\infty S_{\xi k}(\omega) \quad \text{(Q.67)}$$

Another significant extraction apart from the various moments used in the evaluation of the different periods describing the motion mode, is the reduction factor R_F. This is used in the estimation of the degree of over or under approximation of responses when the ideal longcrested formulation is used against the shortcrested sea state representation.

$$R_{Fk}(\omega) = \frac{\int_0^\infty \int_{-\pi}^{\pi} |Z_k(\omega,\theta)|^2 . S_\zeta(\omega,\theta) . d\theta d\omega}{\int_0^\infty |Z_k(\omega)|^2 . S_\zeta(\omega) . d\omega} \quad \text{(Q.68)}$$

It is worthy of note that for a longcrested sea state, the wave propagate in a single direction and thus justifies its exclusion from the transfer function in the denominator of equation (Q.69).

Frequency domain estimates are less accurate compared to time domain, due to poor capture and inclusion of possible non-linearities in motions. It is also interesting to note that the motion time series obtained from the time domain approach are easily converted to frequency domain via the Fourier transformation technique and vis a vis.

Based on the response spectrum of equation Q.58, the short-term response statistics are evaluated. The method limitations are that the equations of motion are linear which leads to linear excitation. It is also true that linear assumption is employed in the random process theory in interpreting the solution. Thus, for some nonlinear effects like damping, drag and excitation , unsteady geometry, horizontal restoring forces and surface elevation cannot be conveniently accommodated in it. However, in many cases these nonlinearities can be satisfactorily linearized for analyses of more moderate environmental conditions where linearization gives acceptable results. This study is based on a moderate environment as obtained in the West African region, and thus justifies the use of linear principles in the forgoing estimations.

Q.1.6 Second Order Forces

In addition to the first order motions mentioned above, the body, also experiences slow drift forces in the surge, sway and yaw modes. For a regular wave, with the handicapped assumption of zero mean body displacement, these forces cannot be easily estimated. Thus, use is made of the near and far field (momentum theory) approaches fundamentally presented by (Pinkster, 1976) and (Maruo,1960) respectively in dealing with these forces/motions. The in depth analysis of procedure are found in their works. The summary of equations used by Pinkster are stated below for the drift forces (surge and sway) and moment (yaw).

$$\overline{F_1} = -0.5\rho g.\int_{-\pi}^{\pi}[\overline{\zeta^2}\,cos\beta.R.d\beta] + \int_{-h}^{0}\int_{-\pi}^{\pi}\left[\left(\overline{u_R^2} - \overline{u_R^2} - \overline{u_R^2}\right)cos\beta - 2.\overline{u_R u_\beta.sin\beta}\right].R.d\beta dz \quad \text{(Q.69)}$$

$$\overline{F_2} = -0.5\rho g.\int_{-\pi}^{\pi}[\overline{\zeta^2}\,sin\beta.R.d\beta] + \int_{-h}^{0}\int_{-\pi}^{\pi}\left[\left(\overline{u_R^2} - \overline{u_R^2} - \overline{u_R^2}\right)sin\beta - 2.\overline{u_R u_\beta.cos\beta}\right].R.d\beta dz \quad \text{(Q.70)}$$

$$\overline{F_6} = -\rho.\int_{-h}^{0}\int_{-\pi}^{\pi}\left[.\overline{u_R u_\beta}\right].R.d\beta dz \quad \text{(Q.71)}$$

Where $\overline{\zeta^2}$ is the mean square water surface elevation on the radiation water surface at a depth of h.

$u_R, u_\beta\ and\ u_z$ are radial and tangential fluid components. All these parameters were evaluated based on the first order potential on the cylindrical CS (x=Rcosβ,y=Rsinβ and z=z). Equations Q.62 to Q.64 approximates the drift forces as linearly proportional to the square of the incident wave amplitude. This however does not hold through for irregular seas, because of the unsteady nature of the forces.

The mean drift force/moment in vertical motion modes (pitch, roll and heave) are calculated by integrating the 2nd order mean wave pressure over the wetted surface of the structure. This usually requires a finer mesh of the structure geometry. The vertical mean drift force is usually only of interest for structures with small water plane area (e.g. semisubmersible) having natural periods in heave and pitch well above peak period of the

wave spectrum. Thus, may be insignificant for large volume structures like the FPSO (DNV-RP-C205,2008).

Even though the mean wave drift force and moments are of second order, they depend on first order quantities majorly. They can therefore be predicted from a linear analysis and their accuracy is dependent on the accurate prediction of the first order motions.

In random seas, drift forces become unsteady, other non-linear methods are then required for its analysis

Q.1.7 Time and Frequency domain representations of Second Order Forces

An idea foundationally introduced by (Voltera,1930) in which the drift force is expanded and truncated at second order using the Taylor series has found robust application in this area.

In time domain: For a longcrested wave train,

$$F_{dr}(t) = F^1(t) + F^2(t) \quad \text{(Q.72)}$$

Where

$$F^1(t) = \int_{\infty}^{-\infty} h_1(\tau).\zeta(t-\tau).d\tau \quad \text{(Q.73)}$$

$$F^2(t) = \int_{\infty}^{-\infty} h_2(\tau_1,\tau_2).\zeta(t-\tau_1).\zeta(t-\tau_2).d\tau_1.d\tau_2 \quad \text{(Q.74)}$$

τ, τ_1, τ_2 are time shifts and $h_1(\tau)\ and\ h_2(\tau_1,\tau_2)$ are the first and second-order impulse response function respectively.

With the first order drift obtained from linear principles already described, the transfer function ($H^{(2)}$) for the second order drift force called the quadratic transfer function (QTF) is so obtained as;

$$H^{(2)}(\omega_i,\omega_j) = \int_{-\infty}^{\infty}\int_{-\infty}^{\infty} h_2(\tau_1,\tau_2).\exp\left(-i\left(\omega_i\tau_1+\omega_j\tau_1\right)\right).d\tau_1.d\tau_2 \quad \text{(Q.75)}$$

ω_i, ω_j are sets of frequency bins within the wave frequency domain.

Inversely,

$$h_2(\tau_1,\tau_2) = \frac{1}{4\pi}\int_{-\infty}^{\infty}\int_{-\infty}^{\infty} H^{(2)}(\omega_i,\omega_j).\exp\left(-i\left(\omega_i\tau_1+\omega_j\tau_1\right)\right).d\omega_i.d\omega_j \quad \text{(Q.76)}$$

The application of the symmetric assumption for the QTF, results in the formulation of the second order drift force for a regular wave as;

$$F^2(t) = \frac{\zeta_1^2}{2}\left\{Re\left[H^{(2)}(\omega,-\omega)\right] + Re\left[H^{(2)}(\omega,\omega).\exp(2i\omega t)\right]\right\} \quad \text{(Q.77)}$$

And generally, for a random sea,

$$F^2(t) = Re\left[\frac{\zeta_i^2}{2}H^{(2)}(\omega_i,-\omega_i) + \frac{\zeta_j^2}{2}H^{(2)}\left(\omega_j,-\omega_j\right)\right] + Re\left[\frac{\zeta_i^2}{2}H^{(2)}(\omega_i,\omega_i)\exp(2i(\omega_i t + \varepsilon_i) + \frac{\zeta_j^2}{2}H^{(2)}\left(\omega_j,\omega_j\right)\exp(2i\left(\omega_j t + \varepsilon_j\right)\right] + \zeta_i.\zeta_j.Re\left[H^{(2)}\left(\omega_i,\omega_j\right)\exp(i\left(\omega_i + \omega_j\right)t + i(\varepsilon_i + \varepsilon_j)\right) + H^{(2)}\left(\omega_j,-\omega_j\right)\exp(i\left(\omega_i - \omega_j\right)t + i(\varepsilon_i - \varepsilon_j))\right] \quad \text{(Q.78)}$$

The equation above is composed of three major drift force contributing phenomenon; contribution from sum frequency (high frequency) from individual wave trains, difference frequencies and the mean frequency components.

The equation Q.71 can be reduced to account for the mean and slowly varying components of the second order drift force as

$$\tilde{F}^2(t) = \sum_{i=1}^{N}\sum_{j=1}^{N}\zeta_i.\zeta_j\left\{P_{ij}.\cos\left[\left(\omega_i - \omega_j\right)t + \left(\varepsilon_i - \varepsilon_j\right)\right] + Q_{ij}.\sin\left[\left(\omega_i - \omega_j\right)t + \left(\varepsilon_i - \varepsilon_j\right)\right]\right\} \quad \text{(Q.79)}$$

Where

$$P_{ij} = 0.5\mathrm{Re}[H^{(2)}\left(\omega_i,-\omega_j\right)] \quad \text{(Q.80)}$$

$$Q_{ij} = -0.5\mathrm{Im}[H^{(2)}\left(\omega_i,-\omega_j\right)] \quad \text{(Q.81)}$$

The full QTF for regular wave can be re-written as a complete complex variable;

$$T_{ij} = P_{ij} + iQ_{ij} \quad \text{(Q.82)}$$

$$\left\{\begin{matrix} T_{ij} = T\left(\omega_i,\omega_j\right) \\ P_{ij} = P\left(\omega_i,\omega_j\right) \\ Q_{ij} = Q\left(\omega_i,\omega_j\right) \end{matrix}\right\} \quad \text{(Q.82)}$$

The mean second order drift force is obtained as:

$$\overline{F^2(t)} = \sum_{i=1}^{N}\zeta_i^2.P_{ii} \quad \text{(Q.83)}$$

With the time domain representation established, the Frequency domain approach focuses on the representation of the drift force as a spectrum. According to (Nea, 1974), the spectrum density of the low frequency component can be written as;

$$S_{F^2}(\omega) = 8\int_{-\infty}^{\infty}|T(\omega',\omega+\omega')|^2.S_\zeta(\omega').S_\zeta(\omega+\omega').d\omega' \quad \text{(Q.84)}$$

The mean second order drift force is obtained as:

$$\overline{F^2(t)} = 2\int_0^\infty S_{F^2}(\omega).d\omega \quad \text{(Q.85)}$$

It becomes more complicated to transfer these formulations to include directionality that is for a generalized short crested sea state. However, the work of (Hasselmann, 1966) was

generous enough to demystify these representations. The summary equations both in time and frequency domain are captured below, with the QTF

$$T_{ij}^{*} = P_{ij}^{*} + iQ_{ij}^{*} \quad \text{(Q.87)}$$

Where

$$\begin{Bmatrix} T_{ij}^{*} = T\left(\omega_i, \omega_j, \theta_i, \theta_j\right) \\ P_{ij}^{*} = P\left(\omega_i, \omega_j, \theta_i, \theta_j\right) \\ Q_{ij}^{*} = Q\left(\omega_i, \omega_j, \theta_i, \theta_j\right) \end{Bmatrix} \quad \text{(Q.88)}$$

Similar to equation Q.82, appropriate substitution of the expressions of equation Q.74 gives the mean and varying drift force for a shortcrested sea;

$$\tilde{F}^2(t) = \zeta_i^2 . T_{ij}^{*} + \zeta_j^2 . T_{jj}^{*} + 2.\zeta_j\zeta_i . \mathrm{Re}\left[T_{ij}^{*} . exp\left\{ i\left(\left(\omega_i - \omega_j\right)t - \left(\varepsilon_i - \varepsilon_j\right)\right)\right\}\right] \text{(Q.89)}$$

The mean drift force for irregular short crested is given as equation 5.91 below

$$\overline{F^2(t)} = \zeta_i^2 P_{ii}^{*} + \zeta_2^2 P_{jj}^{*} + 2\zeta_j\zeta_i[P_{ij}^{*}\cos\left(\varepsilon_i - \varepsilon_j\right) + Q_{ij}^{*}\sin\left(\varepsilon_i - \varepsilon_j\right)] \quad \text{(Q.90)}$$

For a regular short crested sea, $(\omega_i = \omega_j)$.

Because of the tedious computational time required to estimate the full QTF, the Newman (Newman, 1974) approximation is used to satisfactorily estimate the QTF for second order horizontal motions for structures like the FPSO. This however, is not recommended for structures like spar in which drift force play significant roles in determining the vertical motions. The approximation relies on the fact that the off diagonal elements in the matrix of the full QTF can be represented by only the diagonal elements thus;

$$H^{(2)}\left(\omega_i, \omega_j\right) \cong 0.5 * \left[H^{(2)}(\omega_i, \omega_i) + H^{(2)}\left(\omega_j, \omega_j\right)\right] \quad \text{(Q.91)}$$

Appendix R：Motion time history (Displacement) for case a1(T3bk1df2hs3q2)

Appendix Figure R1: T3bk1df2hs3q2 for Surge (a) Experiment (b) Sesam (c) Code

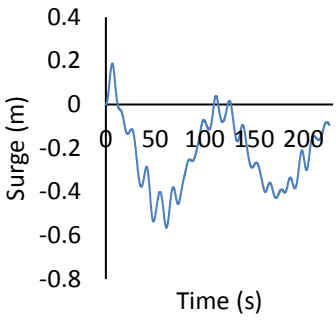

(a)

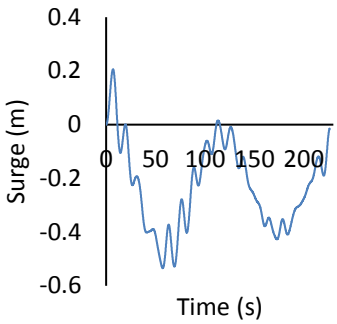

(b)

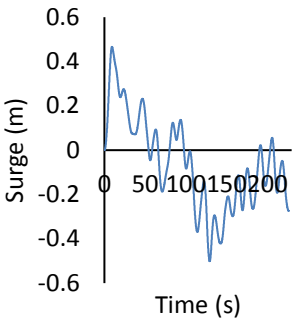

(c)

Appendix Figure R2: T3bk1df2hs3q2 for Sway (a) Experiment (b) Sesam (c) Code

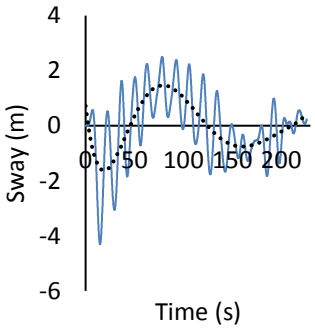

(a)

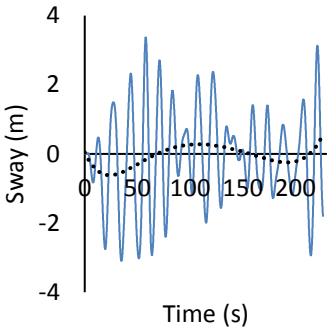

(b)

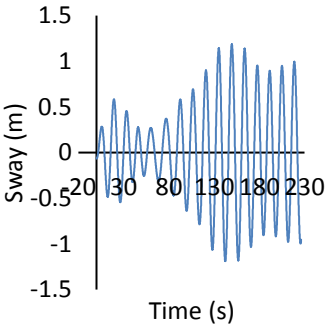

(c)

Appendix Figure R3: T3bk1df2hs3q2 for Heave (a) Experiment (b) Sesam (c) Code

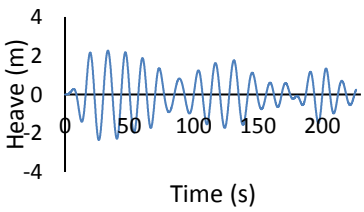

(a)

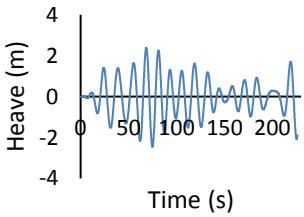

(b)

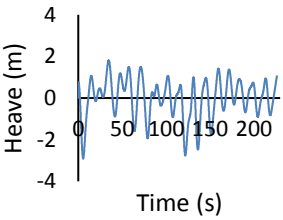

(c)

Appendix Figure R4: T3bk1df2hs3q2 for Pitch (a) Experiment (b) Sesam (c) Code

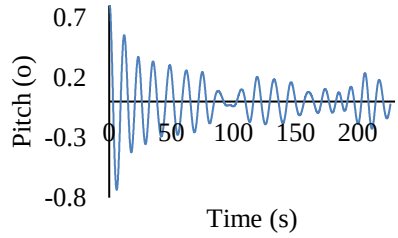

(a)

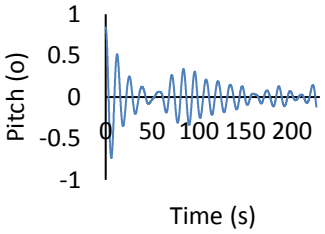

(b)

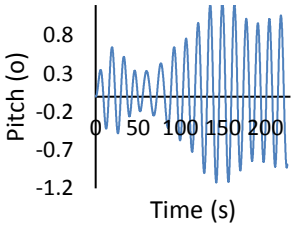

(c)

Appendix Figure R5: T3bk1df2hs3q2 for Yaw (a) Experiment (b) Sesam (c) Code

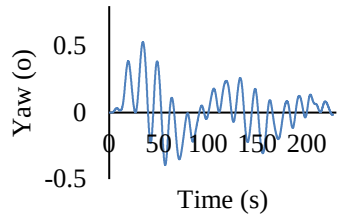

(a)

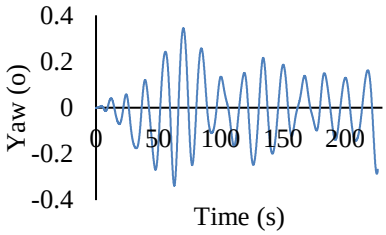

(b)

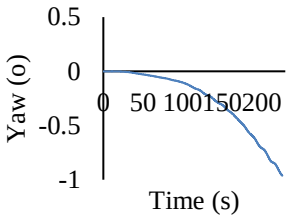

(c)

Appendix S : Statistical Evaluation of motion time history

S.1 Appendix Table S1: Statistical Evaluation of motion amplitude time history for case a1 (T3bk1df2hs1q2)

		Translational (m)			Rotational (deg)			
		Surge	**Sway**	**Heave**	**Pitch**	**Yaw**	**Roll**	**Elevation**
Experiment	std	0.1597	0.4362	0.2659	0.2344	0.0208	0.2570	0.4455
	sig. val	0.6390	1.7449	1.0636	0.9378	0.0832	1.0350	1.7821
	mean	-0.2306	-0.1492	-0.0018	0.0007	-0.0020	-0.0027	0.0023
	max	0.2088	0.8386	0.5505	0.7659	0.0487	0.8170	1.1421
	min	-0.4897	-1.4397	-0.5775	-0.7291	-0.0637	-0.9110	-1.0499
	range	0.6985	2.2782	1.1280	1.4950	0.1124	1.7280	2.1920
Sesam	std	0.1656	0.4584	0.3247	0.2803	0.0210	0.2993	0.5070
	sig. val	0.6625	1.8337	1.2990	1.1212	0.0840	1.1962	2.0280
	mean	-0.2320	0.1236	-0.0018	0.0001	0.0006	-0.0035	0.0027
	max	0.2057	1.0481	0.7643	1.0099	0.0490	0.7425	1.4389
	min	-0.5003	-0.8642	-0.7787	-0.8788	-0.0411	-0.8008	-1.3251
	range	0.7060	1.9123	1.5430	1.8886	0.0901	1.5432	2.7640
Code	std	0.1876	0.4958	0.2993	0.3046	0.0204	0.2231	0.4804
	sig. val	0.7505	1.9833	1.1970	1.2182	0.0814	0.8934	1.9218
	mean	-0.1274	0.4322	-0.0592	0.0000	-0.0198	-0.0071	1.2288
	max	0.3917	1.6643	0.5534	0.6865	0.0003	0.7213	-1.4747
	min	-0.4863	-0.3330	-0.8167	-0.7156	-0.0625	-0.0713	2.7035
	range	0.8780	1.9973	1.3701	1.4021	0.0627	1.4333	2.7035

S.2 Appendix Figure S1: Chart representation of Statistical Evaluation of motion amplitude time history for case a1 (T3bk1df2hs1q2)

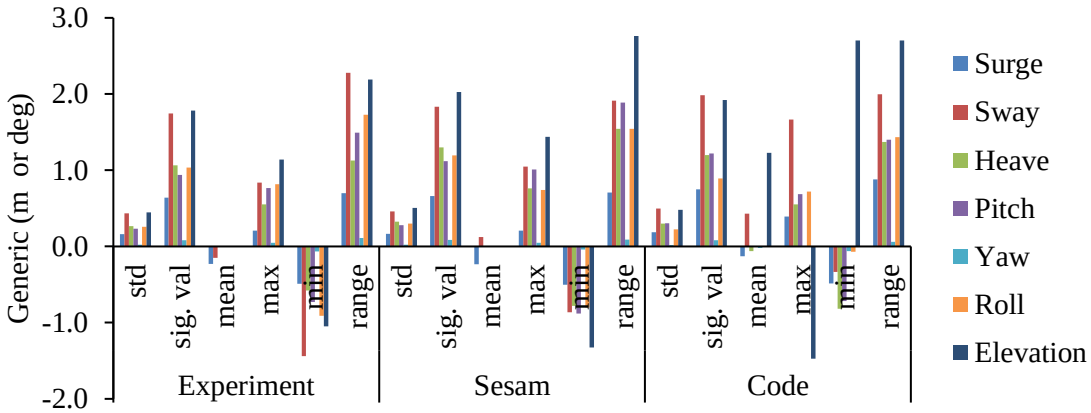

S.3 Appendix Table S2: Statistical Evaluation of motion amplitude time history for case a2 (T3bk1df2hs3q2)

		Surge	Sway	Heave	Pitch	Yaw	Roll	Elevation
Experiment	std	0.1654	1.3676	0.9847	0.1922	0.1693	3.8328	1.4108
	sig. val	0.6615	5.4704	3.9386	0.7688	0.6773	15.3311	5.6432
	mean	-0.2311	-0.0386	0.7472	0.0000	0.0222	-0.0060	-0.0120
	max	0.1873	2.4852	2.3762	0.8422	0.5295	10.4890	3.1405
	min	-0.5640	-4.3001	-2.4416	-0.7351	-0.3939	-10.1744	-3.6433
	range	0.7512	6.7852	4.8178	1.5774	0.9234	20.6635	6.7838
Sesam	std	0.1612	1.3718	0.9466	0.1792	0.1324	4.0444	1.2327
	sig. val	0.6447	5.4873	3.7863	0.7168	0.5296	16.1762	4.9308
	mean	0.1354	1.0880	0.7472	0.1250	0.1074	0.0311	0.9724
	max	0.2061	3.3610	2.3762	0.8398	0.3434	9.5035	2.8092
	min	-0.5341	-3.0940	-2.4416	-0.7331	-0.3368	-9.3447	-3.8310
	range	0.7402	6.4550	4.8178	1.5728	0.6802	18.8482	6.6402
Code	std	0.1507	1.2170	0.9680	0.1794	0.1786	3.5224	1.1703
	sig. val	0.6029	4.8679	3.8720	0.7175	0.7144	14.0873	4.7681
	mean	-0.0600	0.0000	-0.0093	0.0276	-0.2636	-0.3962	-0.0100
	max	0.4659	2.4519	2.2611	0.5264	0.0003	11.3142	2.8102
	min	-0.5008	-2.4599	-2.3480	-0.4729	-0.9626	-11.4783	-2.7368
	range	0.9667	4.9118	4.6091	0.9993	0.9629	22.7974	5.5470

S.4 Appendix Table S2: Chart representation of Statistical Evaluation of motion amplitude time history for case a2 (T3bk1df2hs3q2)